

**A STUDY OF EFFECTS OF WIND ENERGY ON POWER SYSTEM STABILITY
AND QUALITY USING PROBABILISTIC METHODS**

**MR. PANOM PARINYA
ID: 52920003**

**A THESIS SUBMITTED AS A PART OF THE REQUIREMENTS
FOR THE DEGREE OF DOCTOR OF PHILOSOPHY
IN ENERGY TECHNOLOGY**

**THE JOINT GRADUATE SCHOOL OF ENERGY AND ENVIRONMENT
AT KING MONGKUT'S UNIVERSITY OF TECHNOLOGY THONBURI**

1ST SEMESTER 2014

COPYRIGHT OF THE JOINT GRADUATE SCHOOL OF ENERGY AND ENVIRONMENT

A Study of Effects of Wind Energy on Power System Stability and
Quality using Probabilistic Methods

Mr. Panom Parinya
ID: 52920003

A Thesis Submitted as a Part of the Requirements
for the Degree of Doctor of Philosophy
in Energy Technology

The Joint Graduate School of Energy and Environment
at King Mongkut's University of Technology Thonburi

1st Semester 2014

Thesis Committee

 (Dr. Krissanapong Kirtikara)	Advisor
 (Asst. Prof. Dr. Anawach Sangswang)	Co-Advisor (if any)
 (Professor. Dr. R.H.B. Exell)	Member
 (Dr. Dusadee Sukawat)	Member
 (Dr. Dhirayut Chenvidhya)	Member
 (Asst. Prof. Dr. Sumate Naetiladdanon)	Member
 (Prof. Dr.-Ing Christoph Menke)	External Examiner

Thesis Title: A Study of Effects of Wind Energy on Power System Stability and Quality using Probabilistic Methods

Student's name, organization and telephone/fax numbers/email

Mr. Panom Parinya

The Joint Graduate School of Energy and Environment (JGSEE)

King Mongkut's University of Technology Thonburi (KMUTT)

126 Pracha Uthit Rd., Bangmod, Tungkru, Bangkok 10140 Thailand

Telephone: 0-8160-20484

Email: panom_parinya@yahoo.com

Supervisor's name, organization and telephone/fax numbers/email

Dr. Krissanapong Kirtikara

King Mongkut's University of Technology Thonburi (KMUTT)

126 Pracha Uthit Rd., Bangmod, Tungkru, Bangkok 10140 Thailand

Telephone: 0-2470-8020

Email: ikrikara@kmutt.ac.th

Topic: A Study of Effects of Wind Energy on Power System Stability and Quality using Probabilistic Methods

Name of student: Mr. Panom Parinya

Student ID: 52920003

Name of Supervisor: Dr. Krissanapong Kirtikara

ABSTRACT

This study quantitatively assesses the effects of stochastic wind energy on power quality and stability of a power system using both stochastic and probabilistic methods. The stability analysis method is newly developed in this thesis basing on the theory of stochastic stability and is called the stochastic stability index (*SSI*). To compute *SSI*, several processes have to be done consisting of the determination of steady state variables, estimation of well-defined energy function, and formulation of stochastic differential equations. Energy function method, basing on Lyapunov's theory, is used to determine the region of attraction of stable equilibrium points and the critical values of energy. The wind power is modeled using aggregated doubly-fed induction generator (DFIG) and squirrel cage induction generator (SCIG) wind turbines.

The stochastic stability index (*SSI*) can quantify the effects of increasing wind power and its noise intensity on power system stability. When the stochastic wind power increase, *SSI* will decrease and the system is less stable, especially, when there is exchanged power to or from an infinite bus. The results of *SSI* are corresponded to the results of the simulation. If apply white noise for wind power, when wind power increase 50%, 100%, and 150%, the *SSI* decrease about 56%, 75%, and 84%, respectively, comparing with base case. However, the percentage of decreasing of *SSI* when apply colored noise are larger than when apply white noise.

To maintain the synchronization of the system, the wind power generation should be limited at an appropriate value for a given noise intensity. This index gives an alternative analysis for power system stability by stochastically incorporating wind power. This stochastic stability analysis method can analyze the nonlinear and stochastic power system stability with less time and computational effort.

Keywords: stochastic stability index; small signal stability; energy function method; Lyapunov's stability; theory of stochastic stability; deterministic method

ACKNOWLEDGEMENTS

First of all, I would like to express my deepest gratitude to my advisor, Dr. Krissanapong Kirtikara, who gave me a great chance as a great teacher and truly inspired me in both working and learning. I truly appreciate my co-advisor, Asst. Prof. Dr. Anawach Sangswang, who empathize with students by intelligent suggestions and discussion. I would like to express my thankfulness to all committees for their valuable time and comments. I also would like to thank Dr. Dhirayut Chenvidhya who is both my committee and my boss who give kindness and opportunity.

Furthermore, I sincerely thank the CSSC (CES Solar Cells Testing Center) staff for their support and sympathy. I also truly appreciate my best friend for her heartwarming care and always gregarious. For most important, I deeply express my appreciation to father and mother for their understanding and caring with bountiful mind.

I also acknowledge the financial and facilities support from the CSSC, the Joint Graduate School of Energy and Environment, and King Mongkut's University of Technology Thonburi.

CONTENTS

CHAPTER	TITLE	PAGE
	ABSTRACT	i
	ACKNOWLEDGEMENT	ii
	CONTENTS	iii
	LIST OF TABLES	vi
	LIST OF FIGURES	x
	LIST OF ABBREVIATIONS	xxvii
1	INTRODUCTION	
	1.1 Rational and Problem Statement	1
	1.2 Literature Review	5
	1.3 Research Objectives	34
2	THEORIES	
	2.1 The Power System	35
	2.2 Power System Stability Classification	44
	2.3 Small Signal Stability	46
	2.4 Transient stability	51
	2.5 Voltage Stability	60
	2.6 Frequency Stability	70
	2.7 Wind Power	73
	2.8 Probabilistic Methods for the Power System	91
	2.9 Energy Function Methods	110
3	METHODOLOGY PART 1	
	3.1 The Characteristics of Wind Power	120
	3.2 The Characteristics of Power System Incorporating Wind Power	123

CONTENTS (Cont')

CHAPTER	TITLE	PAGE
3.3	A study of Effects of Wind Power on Small Signal Stability using Eigenvalue Method	132
3.4	A Study of Effects of Wind Power on Small Signal Stability using Stochastic Stability Method: The Mean First Passage Time (MFPT)	138
3.5	A Study of Effects of Wind Power on Small Signal Stability using New Stochastic Stability Method	140
3.6	A Study of Effects of Wind Power on Voltage Stability using New Stochastic Stability Method	142
3.7	A Study of Effects of Wind Power on Voltage Variation using Probabilistic Method	144
4	METHODOLOGY PART 2	
4.1	Power System Modeling	146
4.2	Power System Simulation	170
4.3	Noise Modeling and Stochastic Differential Equations Formulation	186
4.4	Well-defined Energy Function Formulation	192
4.5	Critical Energy Estimation	211
4.6	Eigenvalues Determination	211
4.7	Mean First Passage Time (MFPT) Determination	220
4.8	Stochastic Stability Index (SSI) Determination	226
5	RESULTS AND DISCUSSION PART 1	
5.1	The characteristics of wind speed and wind power	264
5.2	The characteristics of power system incorporating wind power	294

CONTENTS (Cont')

CHAPTER	TITLE	PAGE
	5.3 A study of effects of wind power on the small signal stability using eigenvalue method	332
	5.4 A study of effects of wind power on the small signal stability using stochastic stability method: the mean first passage time (MFPT)	342
6	RESULTS AND DISCUSSION PART 2	
	6.1 The Study of Effects of Wind Power on the Small Signal Stability using New Stochastic Stability Method	350
	6.2 The Study of Effects of Wind Power on the Voltage Stability using New Stochastic Stability Method	382
	6.3 The Study of Effects of Wind Power on Voltage Variation using Probabilistic Method	391
7	CONCLUSION AND FUTURE WORK	
	7.1 Conclusions	396
	7.2 Future Studies	402
	REFERENCES	403
	APPENDIX	411

LIST OF TABLES

TABLE	TITLE	PAGE
1.1	Major problems of power quality from wind power integration	18
1.2	Interesting issues of power system stability and quality incorporating wind power	21
1.3	Deterministic indices and analytical methods of power system stability	32
1.4	Probabilistic indices and analytical methods of power system stability	33
2.1	Eigenvalues with time variation and phase portrait	52
2.2	Comparison between explicit and implicit methods	58
2.3	Wind turbine types by speed and power control	80
2.4	Unstable equilibrium points formulation	116
3.1	Testing conditions for the study of probability distribution of wind power	123
3.2	Testing conditions for the study of characteristics of the power system incorporating wind power	131
3.3	System Parameters and Constants	132
3.4	The computation conditions of induction machine (SCIG) parameters	134
3.5	The computational conditions of induction machine (DFIG) parameters	136
3.6	Testing conditions for the study of the effects of wind power to multi-machine power test systems	138
3.7	System Parameters and Constants for TMIB	142
3.8	Power flow and noise conditions for SSS analysis of TMIB	142
3.9	Power flow and noise conditions for VS analysis of TMIB	144
3.10	Testing conditions for a study of effects of wind power to load voltage	145
3.11	Testing conditions for a study of effects of various noises to load voltage	145

LIST OF TABLES (Cont')

TABLE	TITLE	PAGE
4.1	The slope (k_a) and offset (c_a) of the linear relationship between internal phase angle of voltage behind transient reactance and phase angle of terminal voltage during the time 0.3 – 2.0 seconds	153
4.2	The slope (k_a) and offset (c_a) of the linear relationship between internal phase angle (δ') and angle of internal voltage (δ) of DFIG	161
4.3	System data of FMPS test system	184
4.4	Parameters of four machine power system	185
5.1	Testing conditions for the study of probability distribution of wind power	277
5.2	Testing conditions for power-load characteristic analysis	299
5.3	Testing conditions for power-angle characteristic analysis	304
5.4	Testing conditions for the study of characteristics of the power system incorporating wind power	311
5.5	Energy of the test system at interested unstable equilibrium points	322
5.6	Variables at stable equilibrium point of the test system with different wind speed	324
5.7	Share of generating power from synchronous generator, infinite bus generator, and wind turbine generator at different wind speed	324
5.8	The critical value at different wind speed	325
5.9	System Parameters and Constants	330
5.10	The testing conditions of SCIG wind turbine for SMIB power system	333
5.11	The results of eigenvalue analysis of SCIG wind turbine	335
5.12	The parameters of DFIG wind turbine under different conditions	337

LIST OF TABLES (Cont')

TABLE	TITLE	PAGE
5.13	The results of eigenvalue computations of DFIG wind turbine	337
5.14	The results of eigenvalue computation for DFIG when V_{rq} depends partly on x_w	338
5.15	The results of eigenvalue computation for DFIG when V_{rq} not depends on x_w & y_w	338
5.16	Testing conditions and steady state values of speed and angle	341
5.17	The results of eigenvalue analysis for six testing conditions	341
5.18	The participation factors	342
5.19	MFPT at different wind speed and noise intensity	346
5.20	The results of MFPT implementation	348
6.1	Testing conditions and results of exit times compared with <i>DSE</i>	354
6.2	Contribution of Lu components	355
6.3	System Parameters and Constants for TMIB	361
6.4	Testing conditions for DFIG wind turbine with white noise model	365
6.5	Critical energy of the test system with DFIG wind turbine and white noise model	365
6.6	The exit time (seconds) of six different conditions from the simulation	368
6.7	Testing conditions for DFIG wind turbine with colored noise model	373
6.8	Critical energy of the test system with DFIG wind turbine and colored noise model when $X_{14} = 0.6$	373
6.9	Critical energy of the test system with DFIG wind turbine and colored noise model when $X_{14} = 0.5$	374
6.10	The testing conditions and results of simulation to investigate Lu	380

LIST OF TABLES (Cont')

TABLE	TITLE	PAGE
6.11	The exit time (seconds) of six different conditions for DFIG WT with colored noise	382
6.12	Testing conditions for voltage stability analysis	386
6.13	Critical energy of the test system for voltage stability analysis	387
6.14	The exit times (ET) and <i>SSI</i> for DFIG wind turbine with colored noise	391
6.15	The statistical results of voltage on load bus	392
6.16	The testing conditions for the effects of various noise conditions on load voltage	393

LIST OF FIGURES

FIGURE	TITLE	PAGE
1.1	Cumulative wind power capacity growth and annual growth	3
1.2	Development of small signal stability problems (gray), wind power problems (red) and probabilistic methods (blue) for analyzing	4
1.3	Wind speed spectrum model of Van der Hoven [Burton et. al., Wind Energy Handbook]	5
1.4	Wind speed spectrum at 3 areas of Palmyra island by Hwang	6
1.5	Real power output (kW) variation (left) and power spectral density (PSD, kW.Hz ^{-1/2}) (right) of the power output from 10 turbines wind farm	6
1.6	Power spectral density of Remolinos wind farm at low wind speed	7
1.7	Power spectral density of Borja wind farm operating around 6 m/s	7
1.8	The decomposition of fast wind power variation	8
1.9	Power of aggregated wind turbines in case of 1WT, 30WTs, 150WTs, and 300WTs	9
1.10	Histogram and fit Beta distribution (left) and hourly power change (right) of aggregated wind power plants in BPA, ERCOT, and Midwest ISO	10
1.11	Power spectral density of power output of 500kW wind turbine	11
1.12	The 4-machine power system	13
1.13	Root loci of eigenvalues	13
1.14	P-V curve with three power factors	15
1.15	Q-V curve with different P	15
1.16	P-V curve of power system with and without wind power	16
1.17	P-V curve of power system, including wind farm, at different wind speeds with normal and contingency situations	16
1.18	P-V curve of power system with SVC and Capacitor bank compensator	17

LIST OF FIGURES (Cont')

FIGURE	TITLE	PAGE
1.19	Frequency deviation with constant P and V control	18
1.20	Frequency deviation with P and frequency dependent V control	18
1.21	Test system with 2 generators (G1 and G2), variation of wind speed with noise, P and Q of G1, G2 with small amount of wind power, and with large amount of wind power	19
1.22	Reactive power and voltage without reactive power compensation	20
1.23	Reactive power and voltage with reactive power compensation	20
1.24	Active power and frequency without reactive power compensation	20
1.25	Active power and frequency with reactive power compensation	20
1.26	Power spectral density of power from 225kW pitch controlled wind turbine	21
1.27	Complex plane of eigenvalues	24
1.28	Probability of instability vs load	24
1.29	Variation of MFPT with wind power of low noise intensity	28
1.30	Variation of MFPT with wind power of high noise intensity	28
1.31	The 4-bus system one-line diagram	28
1.32	Variation of MFPT with loads of 2 scaled noise intensity levels	28
1.33	Schematic diagram and generation/load data of the 6 bus power system model	29
1.34	$\ln \tau$ vs. p.u. load increase (6 bus power system) with the same (left) and with different (right) load fluctuation intensity levels (ϵ) for P and Q of buses 1, 2, and 3	29
1.35	Daily time varying load pattern	31
1.36	Probability distribution of voltage at 2 a.m.	31
1.37	Probability distribution of voltage at 2 p.m.	31
2.1	Structure of the power system	36
2.2	Current induces magnetic flux on solenoid	37
2.3	Schematic diagram of a three-phase synchronous machine	38

LIST OF FIGURES (Cont')

FIGURE	TITLE	PAGE
2.4	Stator and rotor circuit of a synchronous machine	39
2.5	Schematic diagram of two-winding transformer	42
2.6	Transmission line circuit diagram	43
2.7	Schematic diagram of Π -equivalent circuit	44
2.8	Classification of Power system stability	45
2.9	Block diagram representing state variables vector	48
2.10	Basic circuit diagram for SSS problem	49
2.11	One-line diagram of power system with 1 generator connected to an infinite bus through transmission lines 1 and 2	53
2.12	Power-rotor angle curve describing equal-area criterion	55
2.13	Potential energy-rotor angle curve	59
2.14	Circuit diagram of the power system with transmission and load impedance	61
2.15	Current, voltage, and power curves at receiving end with line and load impedance	62
2.16	The P - V characteristics with different power factor (pf)	63
2.17	The Q - V characteristics with different powers	65
2.18	P - V characteristics (left) and root loci plot of eigenvalue (right)	70
2.19	The over-generated Island diagram	71
2.20	The under-generated Island diagram	72
2.21	Power curve (left) and C_p curve (right) of Suzlon S64 wind turbine	74
2.22	Hourly wind speed (m/s) (left) and wind power (kW) (right) for 1000 hours	75
2.23	Example of velocity duration of wind over one year	76
2.24	Example of distribution function of wind speed	77
2.25	Example of frequency function of wind speed	77
2.26	Power duration curve (left) and Velocity duration curve (right)	78

LIST OF FIGURES (Cont')

FIGURE	TITLE	PAGE
2.27	Energy production (shaded area) from multiplication between power (kW) and velocity duration (hours)	78
2.28	Schematic diagram of wind power model	81
2.29	Schematic diagram of wind turbine model	83
2.30	Circuit diagram of typical radial power network including WTGs	88
2.31	Circuit diagram of power network including WTGs at the j^{th} node	88
2.32	The P - f characteristics of wind power system	90
2.33	The potential energy-rotor angle curve for PEBS method	114
3.1	The methods to study the characteristics of wind speed	121
3.2	The processes to study the characteristics of wind power	121
3.3	The method to study on the characteristics of power system incorporating wind power	123
3.4	The method to study the characteristics of the energy of the power system	124
3.5	Schematic diagram and Phasor diagram of SMIB	125
3.6	Circuit diagram of the power system with transmission and load impedance	127
3.7	SMIB including internal sources of small signal	129
3.8	SMIB including wind power and dynamic load	130
3.9	Test power system including wind power and load	131
3.10	Block diagram representing state space equation of the SCIG wind turbine	133
3.11	Single machine infinite bus power system	134
3.12	Block diagram representing state space equation of the DFIG wind turbine	135
3.13	Single machine infinite bus power system for DFIG WT	135
3.14	Process to study effects of wind power using SSI	141
3.15	The two machine infinite bus power system (TMIB)	142

LIST OF FIGURES (Cont')

FIGURE	TITLE	PAGE
4.1	Single-line (left) and phasor (right) diagrams of induction generator	150
4.2	Single-line diagram of power test system in PSCAD	152
4.3	The relationship between internal phase angle (IntA) and angle of internal voltage (AoIV) and phase angle of terminal voltage (PHA)	153
4.4	Single machine infinite bus power system for wind power modeling	154
4.5	Single-line (left) and phasor (right) diagrams of induction generator	159
4.6	Variation of internal phase angle (Deltai, δ') and angle of internal voltage (Delta, δ) and angle of stator voltage (PAdfig, θ_v) when wind power is 1.0 p.u.	160
4.7	The relationship between internal phase angle (Deltai, δ') and angle of internal voltage (Delta, δ) and angle of stator voltage (PAdfig, θ_v) when vary wind power (WP)	160
4.8	Linear relationship between k_a (left) and c_a (right) with DFIG wind power	162
4.9	Single-line (left) and phasor (right) diagrams of synchronous generator	163
4.10	Block of synchronous generator model in PSCAD	171
4.11	Block of SCIG model in PSCAD	173
4.12	Equivalent circuit of SCIG in PSCAD	174
4.13	Torque-Slip Characteristics	174
4.14	Variation of starting torque with rotor resistance	174
4.15	Variation of torque and stator current with slip	174
4.16	Performance curves of 3-phase squirrel cage induction generator	174
4.17	Schematics of nominal PI section (left) and coupled PI section (right) models	175
4.18	Tline and TLine components	176
4.19	The conductor geometry method	176
4.20	Bergeron, Frequency Dependent (Mode and Phase) models and options	176

LIST OF FIGURES (Cont')

FIGURE	TITLE	PAGE
4.21	Example of 3-phase 3-limb transformer schematic	177
4.22	AC exciters (top), DC exciters (middle), and Static exciters (bottom) in PSCAD	177
4.23	Hydro and steam turbine and governor model descriptions in PSCAD	178
4.24	Hydro turbine (top), hydro governor (middle), steam turbine (middle), steam governor (bottom) models with input and output in PSCAD	179
4.25	Fixed P and Q load and passive R, X_L , and X_C load model	179
4.26	Transfer function of wind turbine governor model	181
4.27	Schematic of wind source, turbine and governor model	181
4.28	Single machine infinite bus (SMIB) system including wind power and load	182
4.29	Four machine power system (FMPS) including wind power and load	184
4.30	Block diagram representing state space equation of the SCIG wind turbine	213
4.31	Block diagram representing state space equation of the DFIG wind turbine	215
4.32	Test power system including wind power and load for SSI	228
4.33	Test power system including wind power and load for DFIG WT	233
5.1	PSD of wind speed data from BKT1 station with frequency range of 0 - 8.3 mHz (left) and 0 - 0.14mHz (right)	265
5.2	PSD of wind speed data from CHMP1 station with frequency range of 0 - 8.3 mHz (left) and 0 - 0.18 mHz (right)	265
5.3	Hourly average (left) and monthly average (right) of wind speed of BKT1	266
5.4	Hourly average (left) and monthly average (right) of wind speed of CHMP1 station	266
5.5	Distribution of wind speed (left) and standard deviation (right) of 1-min data of 130,000 samples at CHMP1 station at 90m-height	267
5.6	Hypothesis test of every second wind speed data	268

LIST OF FIGURES (Cont')

FIGURE	TITLE	PAGE
5.7	Hypothesis test of every minute wind speed data	269
5.8	Hypothesis test of every hour wind speed data	269
5.9	Wind speed at 90m heights of BKT1 station with second (left) and minute (right) time scale	270
5.10	Wind speed (left) and its standard deviation (right) at 90m heights of CHMP1 station	270
5.11	PSD (left) and histogram (right) of 1-sec wind speed at 90m heights of BKT1 station for 2,000 samples	271
5.12	Noise wind speed 1-sec data 2,000 samples (left) and its histogram (right)	271
5.13	Wind speed distribution (left) and turbulence or noise wind speed distribution (right) of 1-min data for 26,000 samples at CHMP1 station (upper) and BKT1 station (lower)	272
5.14	Example of gust wind speed of 1-min data for 10,000 minutes at BKT1 station (left) and CHMP1 station (right)	272
5.15	Wind speed (left) and its standard deviation (right) of 1-min data for 10,000 minutes at BKT1 station (upper) and CHMP1 station (lower)	273
5.16	Hourly average wind speed (left) and calculated wind power (right) at the coastal site in the South of Thailand	274
5.17	Histogram of 7,000 hours wind speed (left) and calculated wind power (right) at the coastal site in the South of Thailand	275
5.18	Hourly average wind speed (left) and calculated wind power (right) at BKT1 station	275
5.19	Hourly average wind speed (left) and calculated wind power (right) at BKT1 station	276
5.20	PSD of 800 hours wind speed (left) and calculated wind power (right) at BKT1 station	276
5.21	Hypothesis test of hourly averaged wind power	277
5.22	One-line diagram of test system of case A1	278

LIST OF FIGURES (Cont')

FIGURE	TITLE	PAGE
5.23	Wind speed (left) and wind power (right) of case A1 (WS1 and WP1 use Cparam = 5, WS2 and WP2 use Cparam = 10)	278
5.24	Histogram of wind speed (left) and wind power (right) of case A1 (Cparam = 5)	278
5.25	Histogram of wind speed (left) and wind power (right) of case A1 (Cparam = 10)	279
5.26	One-line diagram of test system of case A2	279
5.27	Wind speed (left) and wind power (right) of case A2 (WS1 and WP1 from WTG1, WS2 and WP2 from WTG2)	280
5.28	Histogram of wind speed (left) and wind power (right) of case A2 (from WTG1)	280
5.29	Histogram of wind speed (left) and wind power (right) of case A2 (from WTG2)	280
5.30	One-line diagram of test system of case A3	281
5.31	Sample of wind speed (left) and wind power (right) of case A3	281
5.32	Histogram of wind power of WTG1 (left) and total wind power (right) of case A3	282
5.33	PSD of wind power of WTG1 (left) and total wind power (right) of case A3	282
5.34	One-line diagram of test system of case A4	283
5.35	Wind speed (left) and different wind speeds (WS2-WS1) (right) of case A4	283
5.36	Histogram of wind speed (left) and different wind speeds (WS2-WS1) (right) of case A4	284
5.37	Histogram of wind power of WTG2 (left) and different wind powers (WP2-WP1) (right) of case A4	284
5.38	Normal probability plot of different wind speeds (WS2-WS1) (left) and different wind power (WP2-WP1) (right) of case A4	284
5.39	One-line diagram of test system of case A5	285

LIST OF FIGURES (Cont')

FIGURE	TITLE	PAGE
5.40	Histogram of wind powers for the case wind speed, $k = 6\text{m/s}$ (upper left), 9m/s (upper right), and 10m/s (lower)	286
5.41	Histogram of different wind powers (WP2-WP1) for the case wind speed, $k = 6\text{m/s}$ (upper left), 9m/s (upper right), and 10m/s (lower)	286
5.42	Normal probability plot of different wind powers (WP2-WP1) for the case of wind speed, $k = 6\text{m/s}$ (upper left), 9m/s (upper right), and 10m/s (lower)	287
5.43	Different wind speed (WS2-WS1) for all k	287
5.44	One-line diagram of test system of case A6	288
5.45	Wind speed (left) and wind power (right) of case A6 (WS1 and WP1 use $C_{\text{param}} = 5$, WS2 and WP2 use $C_{\text{param}} = 10$)	288
5.46	Histogram of wind speed of case A6 for $C_{\text{param}} = 5$ (left) and $C_{\text{param}} = 10$ (right)	289
5.47	Histogram of wind power of case A6 for the case $C_{\text{param}} = 5$ (left) and $C_{\text{param}} = 10$ (right)	289
5.48	One-line diagram of test system of case A7	290
5.49	Noise wind speed (left) and noise wind power (right) of WTG2 of case A7	290
5.50	Histogram of noise wind speed (left) and wind power (right) of WTG2 of case A7	290
5.51	Normal probability plot of noise wind speed (left) and noise wind power (right) of WTG2 of case A7	291
5.52	Single line diagram of SMIB with DFIG wind turbine	292
5.53	The variation of wind power (left) and its power spectral density (right) when varying bandwidth (upper), scaling factor (middle), and noise intensity (lower)	292
5.54	The normal curve of wind power when varying bandwidth (left), scaling factor (middle), and noise intensity (right)	293

LIST OF FIGURES (Cont')

FIGURE	TITLE	PAGE
5.55	The data distribution of wind power when varying bandwidth (upper), scaling factor (middle), and noise intensity (lower)	293
5.56	The variation (left) and data distribution (right) of wind power	294
5.57	The variation (left) and normal curve (right) of angle and speed deviation (-slip)	294
5.58	The data distribution of angle (left) and speed deviation or –slip (right)	294
5.59	Schematic diagram of SMIB and equations	295
5.60	Active power-angle characteristics of SMIB system when varying voltage	295
5.61	Reactive power-angle characteristics of SMIB system when varying voltage	296
5.62	Active power-angle characteristics of SMIB system when varying total impedance	296
5.63	Reactive power-angle characteristics of SMIB system when varying total impedance	297
5.64	Reactive power-voltage characteristics of SMIB system with varying active power	298
5.65	Reactive power-voltage characteristics of SMIB system with varying line reactance	298
5.66	Phasor diagram, circuit diagram, and equations of power test system	299
5.67	Active power-load characteristics when varying Theta and fix Phi	300
5.68	Reactive power-load characteristics when varying Theta and fix Phi	300
5.69	Active power-load characteristics when varying Phi and fix Theta –Phi	301
5.70	Reactive power-load characteristics when varying Phi and fix Theta –Phi	301
5.71	Voltage-Load characteristics when fix Phi varying Theta-Phi (left) and when fix Theta-Phi varies Phi (right)	302
5.72	One line diagram and testing equations of SMIB power system	302

LIST OF FIGURES (Cont')

FIGURE	TITLE	PAGE
5.73	Block diagram (left) and function representing power-angle equation (right) of active (upper) and reactive power (lower)	303
5.74	Electrical power (p.u.) and power angle (rad) of the case 1 (upper left) to case 3 (upper right) and case 4 (lower left) to case 6 (lower right).	304
5.75	Active Power-angle characteristics for case 1 (upper left) to case 3 (upper right) and from case 4 (lower left) to case 6 (lower right).	305
5.76	Reactive Power-angle characteristics for case 1 (upper left) to case 3 (upper right), and from case 4 (lower left) to case 6 (lower right)	305
5.77	Schematic diagram and one line diagram of power test system connecting to an infinite bus and including wind power and load	306
5.78	Wind speed 10m/s constant	307
5.79	Wind speed 10m/s + ramp 1m/s4Hz	307
5.80	Power angle of constant wind	307
5.81	Power angle of case small signal	307
5.82	Rotor speed of constant wind	308
5.83	Rotor speed of case small signal	308
5.84	Active power of constant wind	308
5.85	Active power of case small signal	308
5.86	Reactive power of constant wind	308
5.87	Reactive power of case small signal	308
5.88	Voltage of constant wind	309
5.89	Voltage of case small signal	309
5.90	Test power system including wind power and load	310
5.91	Wind turbine model in PSCAD	310
5.92	The power angle and rotor speed for base case and PSD of power angle (black) and rotor speed (blue) for base case in dB/Hz	311
5.93	The power angle of generator for Case B2 in degrees and the rotor speed of generator for Case B2 in per unit	312

LIST OF FIGURES (Cont')

FIGURE	TITLE	PAGE
5.94	The power angle of generator for Case B3 in degrees and the rotor speed of the generator for Case B3 per unit	312
5.95	The wind power (left) of Case B4 (case1) compared with Case B5 (case2) and its PSD (right)	314
5.96	The power angle of synchronous generator of Case B4 (case1) compared with Case B5 (case2, left) and its PSD of Case B4 compare with Case B5 (right)	314
5.97	The rotor speed of synchronous generator of Case B4 (case1) compared with Case B5 (case2, left) and its PSD of Case B4 compare with Case B5 (right)	314
5.98	The wind power (left) and its PSD (right) of Case B6 (case 3) and Case B7 (case 4)	315
5.99	The power angle of synchronous generator of Case B6 (case 3) compared with Case B7 (case 4, left) and its PSD of Case B6 compare with Case B7 (right)	316
5.100	The rotor speed of synchronous generator of Case B6 (case 3) compared with Case B7 (case 4, left) and its PSD of Case B6 compare with Case B7 (right)	316
5.101	Wind speed (m/s) of the cases B8 – B11	318
5.102	Wind power (per unit) of the cases B8 – B11	319
5.103	Power angle (degrees) of synchronous generator of the cases B8 – B11	320
5.104	Rotor speed (per unit) of synchronous generator of the cases B8 – B11	321
5.105	Total energy of the test system	323
5.106	Phase portrait plot of voltage phase angle (x-axis) and rotor speed (y-axis)	323
5.107	Block diagrams of wind speed model, including normal random noise wind speed	326

LIST OF FIGURES (Cont')

FIGURE	TITLE	PAGE
5.108	Total energy (upper left), wind speed (lower left), and phase portrait plot (right) of synchronous generator when the standard deviation of wind speed is 0.5	327
5.109	Total energy (upper left), wind speed (lower left), and phase portrait plot (right) of synchronous generator when standard deviation of wind speed is 1.0	327
5.110	Total energy (upper left), wind speed (lower left), and phase portrait plot of synchronous generator (upper right) and phase portrait plot of wind turbine generator (lower right) when standard deviation of wind speed is 2.0	327
5.111	Total energy (upper left), wind speed (lower left), and phase portrait plot of synchronous generator (upper right) and phase portrait plot of wind turbine generator (lower right) for the case sampling frequency of wind speed is 0.5Hz	328
5.112	Total energy (upper left), wind speed (lower left), and phase portrait plot of synchronous generator (upper right) and phase portrait plot of wind turbine generator (lower right) for the case sampling frequency of wind speed is 2.0 Hz	328
5.113	Total energy (upper left), wind speed (lower left), and phase portrait plot of synchronous generator (upper right) and phase portrait plot of wind turbine generator (lower right) for the case sampling frequency of wind speed is 0.1 Hz	329
5.114	Wind power variation (left) and its distribution (right) of 4 trials of simulation	331
5.115	Angular speed (left) of generator no.1-2 and phase angle (right) of bus no. 2-4 of stochastic system simulation during 60 seconds of trial no.1	331
5.116	Example of wind power variation during 3600 seconds (left) and its distribution (right) of simulation trial no.1	331

LIST OF FIGURES (Cont')

FIGURE	TITLE	PAGE
5.117	Power spectral density of wind power variation during 3600 seconds of trial no.1	332
5.118	Block diagram representing state space equation of the SCIG wind turbine	333
5.119	Single machine infinite bus power system	333
5.120	Results of simulation case 1. (base case) : Speed (left), angle (middle), and phase protrait of speed (y-axis) and angle (x-axis)	334
5.121	Results of simulation case 2. (reduce stator voltage of SCIG) : Speed (left), angle (middle), and phase protrait of speed (y-axis) and angle (x-axis)	334
5.122	Results of simulation case 3. (increase reference voltage) : Speed (left), angle (middle), and phase protrait of speed (y-axis) and angle (x-axis)	334
5.123	Results of simulation case 4. (increase transmission reactance) : Speed (left), angle (middle), and phase protrait of speed (y-axis) and angle (x-axis)	334
5.124	Results of simulation case 5. (increase stator reactance of SCIG) : Speed (left), angle (middle), and phase protrait of speed (y-axis) and angle (x-axis).	335
5.125	Block diagram representing state space equation of the DFIG wind turbine	336
5.126	Two-machine infinite bus power system including wind power and load	340
5.127	Log-scale of MFPT at different wind speeds and noise intensity	345
5.128	Distribution of wind speed (left) and noise intensity (right) of wind speed	347
5.129	Distribution of wind power (left) and noise intensity (right) of wind power	348

LIST OF FIGURES (Cont')

FIGURE	TITLE	PAGE
5.130	Relationship between wind speed and noise intensity of wind power using wind data of Chumporn wind monitoring station in the South of Thailand	349
6.1	Test power system including wind power and load for <i>DSE</i>	351
6.2	<i>DSE</i> compared with noise intensity of wind power (α_3) at different wind powers (P_{m3} , p.u.) when frequency dependent coefficient, $c_k = 0.025$	353
6.3	Energy of the test system under 4 test conditions C1 – C4	354
6.4	Phase portraits of slip-angle (left) and energy-angle (right) of IG wind turbine when noise intensity increase from 0.2 (upper) to 0.4 (lower)	354
6.5	Single machine infinite bus power test system including wind power and load	356
6.6	The relationship of <i>DSE</i> and the noise intensity of the power load when wind power is fixed (left) and noise intensity of wind power when power load is fixed (right)	359
6.7	Phase portraits of slip-angle (left) and energy-angle (right) of IG wind turbine when noise intensity increase from 0.2 (upper) to 0.4 (lower) with constant load	359
6.8	Test power system including wind power and load for DFIG WT	361
6.9	Phase portrait of speed (x-axis)-angle (y-axis) of G3 of Case2 (left) and Case3 (right) when noise intensity is 0.4 and 0.8, respectively	366
6.10	The results of Lu' computation with increasing noise intensity compared among 6 testing conditions for DFIG wind turbine with white noise model	367
6.11	The relation of SSI (seconds) and noise intensity compared among 6 testing conditions for DFIG wind turbines with white noise model	367
6.12	The results of Lu' computation with increasing noise intensity under 6 testing conditions for DFIG wind turbine with colored noise model	375

LIST OF FIGURES (Cont')

FIGURE	TITLE	PAGE
6.13	The log-scale SSI (y-axis, seconds) with increasing of noise intensity (x-axis) under 6 testing conditions for DFIG wind turbine with colored noise model	375
6.14	The variation of mechanical wind power during 600 seconds of simulation	376
6.15	The variation of phase angle of G2 (PA Syn.Gen.), G3 (PA DFIG), and load (PA Load) during 600 seconds of simulation (left) and 311 – 323 seconds (right).	376
6.16	The variation of angular speed of G2 (Speed Syn.Gen.) and G3 (Speed DFIG) during 307 – 319 seconds (left) and 306 – 316 seconds (right).	377
6.17	The phase portrait of phase angle and angular speed of G2 (left) and G3 (right) during 0 – 318 seconds	377
6.18	The energy of the power system during 600 seconds of simulation (left) and 302 – 320 seconds (right).	378
6.19	The derivative of stochastic energy of the power system (LU) during 600 seconds of simulation (left) and 308 – 323 seconds (right).	378
6.20	The derivative of deterministic energy of the power system (pU) during 600 seconds of simulation (left) and 310 – 329 seconds (right).	379
6.21	Data distribution of Lu for the cases C1 – C3 (left) and Case 1 – Case 6 (right)	380
6.22	The variation (left) and data distribution (right) of Lu for the cases C1 (upper), C2 (middle), and C3 (lower)	381
6.23	The results of Lu computation with increasing noise intensity comparing between 6 testing conditions for voltage stability analysis	387
6.24	The results of SSI computation with increasing noise intensity (0-1.0) comparing between 6 testing conditions for voltage stability analysis	388
6.25	The results of SSI computation with increasing noise intensity (0.6-1.0) comparing between 6 testing conditions for voltage stability analysis	388
6.26	Active power (y-axis, left) and reactive power (y-axis, right).	389

LIST OF FIGURES (Cont')

FIGURE	TITLE	PAGE
6.27	Phase angle (y-axis, left) and angular speed (y-axis, right)	389
6.28	Relative energy (y-axis, left) and derivative of stochastic energy or LU (y-axis, right).	390
6.29	Voltage (upper) and reactive power (lower) at load bus	390
6.30	The average (left) and standard deviation (right) of voltage on load bus	392
6.31	The data distributions of wind power, active and reactive power loads, and wind speed for the cases T1 – T5	394
6.32	The data distribution of voltage for the cases T1 – T5 (left) and All 1 (right)	395
6.33	The data distribution of voltage for the cases T1 – T5 (left) and cases All 1 – All 2 (right)	395

LIST OF ABBREVIATIONS

Abbreviations	Full Meaning
AGC	Automatic Generation Control
BCU	Boundary Controlling Unstable Equilibrium Point Method
BW	Bandwidth
CCT	Critical Clearing Time
CDF	Cumulative Distribution Function
CFD	Computational Fluid Dynamic
DAE	Differential and Algebra Equation
DFIG	Doubly-Fed Induction Generator
DSE	Derivative of Stochastic Energy
EMC	Electromagnetic Compatibility Standard
EMTDC	Electromagnetic Transients including DC
ESD	Electrostatic Discharge
FMPS	Four-Machine Power System
FSFC	Full Scale Frequency Converter
FSIG	Fixed Speed Induction Generator
GGD	Generalized Gaussian Distribution
GWEC	Global Wind Energy Council
HB	Hopf Bifurcation
IEC	International Electrotechnical Commission
IG	Induction Generator
KE	Kinetic Energy
LCOP	Locus of Critical Operating Point
MCS	Monte Carlo Simulation
MFPT	Mean First Passage Time
NI	Noise Intensity
NR	Newton-Raphson Method
PDF	Probability Distribution Function

LIST OF ABBREVIATIONS (Cont')

Abbreviations	Full Meaning
PE	Potential Energy
PEBS	Potential Energy Boundary Surface
PMF	Probability Mass Function
PMSG	Permanent Magnet Synchronous Generator
PQ	Power Quality
PS	Power System Stability
PSCAD	Power System Computer Aided Design
PSD	Power Spectral Density
PSFC	Partial Scale Frequency Converter
SCIG	Squirrel Cage Induction Generator
SDE	Stochastic Differential Equation
SMIB	Single Machine Infinite Bus
SNB	Saddle-Node Bifurcation
SSI	Stochastic Stability Index
SSS	Small Signal Stability
SVC	Static Var Compensator
SVS	Static Var Systems
TEF	Transient Energy Function
THD	Total Harmonic Distortion
TMIB	Two Machines Infinite Bus
u.e.p.	unstable equilibrium point
VS	Voltage Stability
WRIG	Wound Rotor Induction Generator
WSS	Wind Speed Spectrum
WT	Wind Turbine
WTG	Wind Turbine Generator

CHAPTER 1

INTRODUCTION

Energy and environmental problems have encouraged people to increase their awareness of energy consumption that is friendlier to the environment. This leads to more interest in renewable and clean energy, especially solar and wind energy.

Long-term RE development, especially wind power, requires the power system to be able to support RE efficiently in terms of physical structure and performance. This requires an understanding on constraints relating to characteristics of wind power and other RE sources.

In order to increase wind power penetration, the power system stability and power quality must first be studied for grid interconnection standardization, for grid performance improvement and for basic knowledge for long-term planning of RE development.

1.1 Rationale and Problem Statement

Power system stability (PS) is the ability of the power system to maintain or control the system (synchronization, voltage, and frequency) within an equilibrium operating condition after subjection to small and large disturbances. This ability depends on characteristics of generators, loads, transmission system, and control system. PS includes phenomena with period range from several seconds to several minutes. These phenomena are, for example, the loss of synchronization, and loss control of voltage and frequency after subject to disturbances such as transient fault, loss of generator, loss of transmission line, suddenly increase of load, and small perturbation as a noise.

Power quality (PQ) concerns the quality or characteristics of voltage, current, frequency, and power that may harm the electrical equipment of customers. It is influenced by relationship between generation, transmission, and power consumption. Voltage variation, Frequency variation, and wave form distortion are general issues of PQ which period range from millisecond to several minutes.

Wind power affects both PS and PQ since it generates random and fluctuating signals to the power system. As the generated power fluctuate, system responses to the disturbances possibly vary significantly and result in power system instability and/or poor power quality.

The study of the effects of wind power on a power system previous was based on these deterministic methods for which all operating conditions and network topology are explicitly determined. The stochastic characteristics of winds, varied by space and time, can cause the large variation and unpredictable of power output. Since the nature of wind power generation, load, and disturbances in the power system are stochastic, the classical deterministic methods, which rely on steady characteristics assumptions, cannot be used realistically. Furthermore, the larger systems lead to higher degrees of complexity of solutions with many uncertainties. Since the wind power has become very much larger than the last two decades, the more complexity and severity affecting to the power system can be found frequently.

Accordingly, the probabilistic methods are the most relevant tools to overcome the realistic and dynamics conditions of a system. Even though, the probabilistic methods have been used to study the power system stability and reliability problems more than two decades, the understanding in the influencing of the random wind power still far from the real situations.

Therefore, this research aims to develop the suitable probabilistic methods to assess the effects of wind power on power quality and stability of the power system, which incorporates the stochastic characteristics of winds.

The impact of wind energy generation on power systems becomes a more serious issue according to an increase of wind energy penetration in many countries to close to the conventional acceptable level of 20% [60]. The cumulative wind power capacity grew 21% per year on average since 2004 to reach about 318 GW at the end of 2013 [24] and the most market share of wind turbine technology is Doubly-Fed Induction Generator (DFIG) at about 54.8% [64]. Wind power is the third ranking of renewable energy of the world and increase with the rate of about 25% per year. At the end of 2013, the cumulative installed capacity of wind power was about 318 GW, starting from 1995.

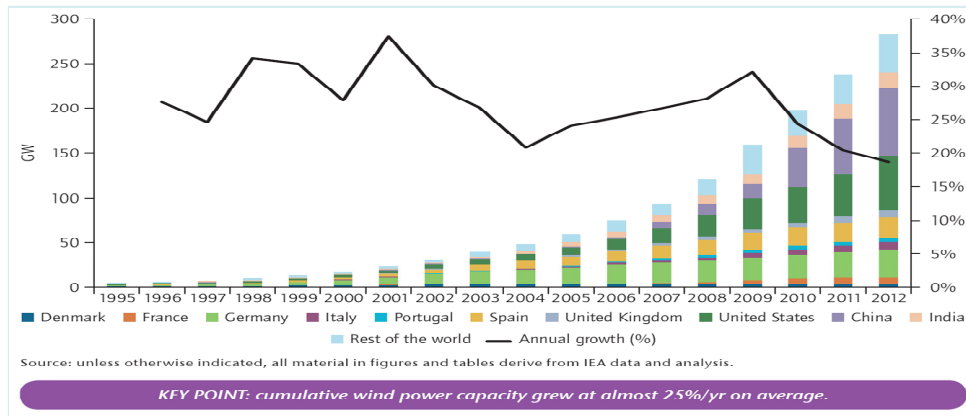


Figure 1.1 Cumulative wind power capacity growth and annual growth [24]

In the late 1990s, transient voltage stability and the dynamic behavior of induction generator during disturbances were the first that be focused on [49]. Later, International Electrotechnical Commission (IEC) published the first edition of technical standard on assessment of power quality from wind turbine in 2001 (IEC 61400-21, 2008).

In North Germany, there is high risk of grid instability due to 3-phase fault of transmission line if 3,000 MW of wind power fail. Therefore, on 1st of April in 2006, new grid interconnection regulations were published requiring fault-ride-through to deal with this problem. [29]

The same as Spain, before, Spanish's requirement is that wind turbine (WT) had to disconnect when subject to voltage dip. This caused large amount of wind power cascading decrease for 500MW, 400MW, and 1,000MW for 6 hours on 19th March in 2007. This results in high risk of grid instability and therefore, new grid code required voltage dip fault-ride-through to avoid this problem. [29]

In China, PS and PQ are already a problem because of weak inter-regional interconnections, causing power shortages. This leading many existing wind farms to be left unconnected and unused. For example, 10GW wind project at Jiu Quan in Gansu is the biggest problem which wind farm located too far from load center.(www.atimes.com, 16th Jan., 2010).

In USA, on Tuesday, 26th of February in 2008, the loss of wind power caused Texas grid operator when to the state of emergency and cut service to some large customer for 90MW. In this case, wind power fell from 1,700MW to 300MW cause grid frequency suddenly dropped and followed by blackout (www.reuters.com : Wed, 27th Feb 2008).

In 2008, the IEC published a new edition of IEC 61400-21 with advanced technical standards for assessment of power quality of wind power. This standard is an assessment procedure that considers phenomena, for example, voltage fluctuation during both continuous and switching operation, harmonics and interharmonics, response to voltage drop, active power ramp rate limitation, reactive power capability, grid protection, and reconnection time after grid fault. These phenomena depend on local characteristics of the power system. Therefore, different country with different structure of power system leads to dissimilar regulation for the unlike problems concerning.

Motivation of regulations involving impacts of wind power still be an issue of interesting more and more since the power system is more complex while renewable such as wind power is random and almost unpredictable. However, the standardization of PS assessment cannot be easily prepared due to many reasons, including the different characteristics of the power system, uncertainty of the analyzing methods, and uncertainty of many variables concerning the power system.

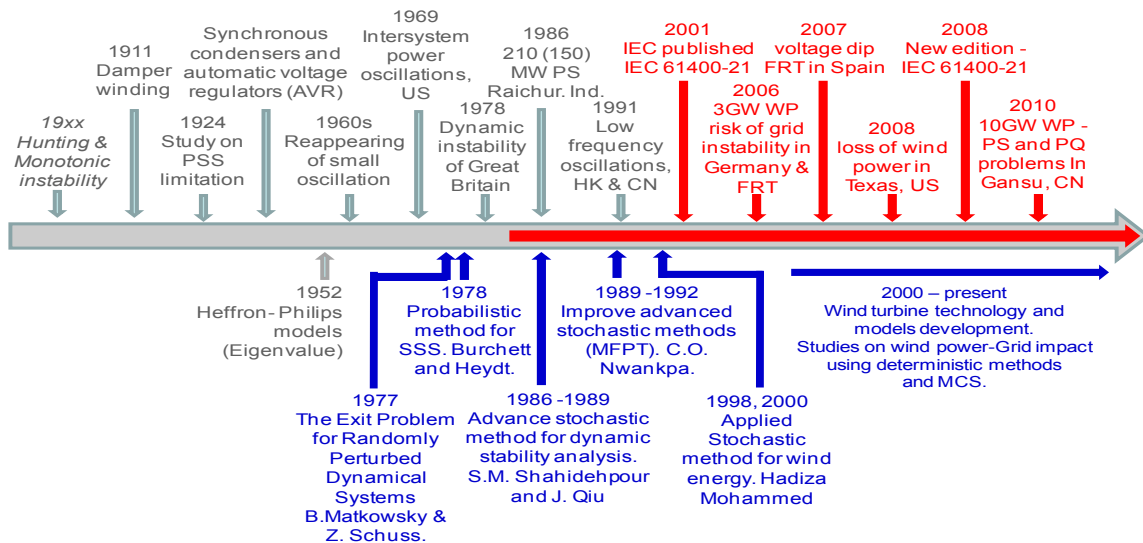


Figure 1.2 Development of small signal stability problems (gray), wind power problems (red) and probabilistic methods (blue) for analyzing

In summary, while wind power has increased continuously, more serious power system problems occur. For example, low frequency oscillation occurred in HK and CN in 1991. In 2001, IEC 61400-21 standard was published to counteract the growth of wind power. In 2006, risk of grid stability in Germany occurred with the 3GW wind power. In 2007, voltage dip fault-ride-through regulation has been applied in Spain. In 2008, loss of wind power happened in Texas, US and followed by new edition of IEC 61400-21. In

2010, power system stability and power quality problems had occurred in Gansu, CN with 10GW wind power.

1.2 Literature Review

1.2.1 Characteristics of Wind Power

The dynamics of wind speed consists of two main components, the slow variation component with spectral ranges between 10 hours and several months, and the turbulence components with spectral ranges between 1 second and 10 minutes as represented in the figure below [68].

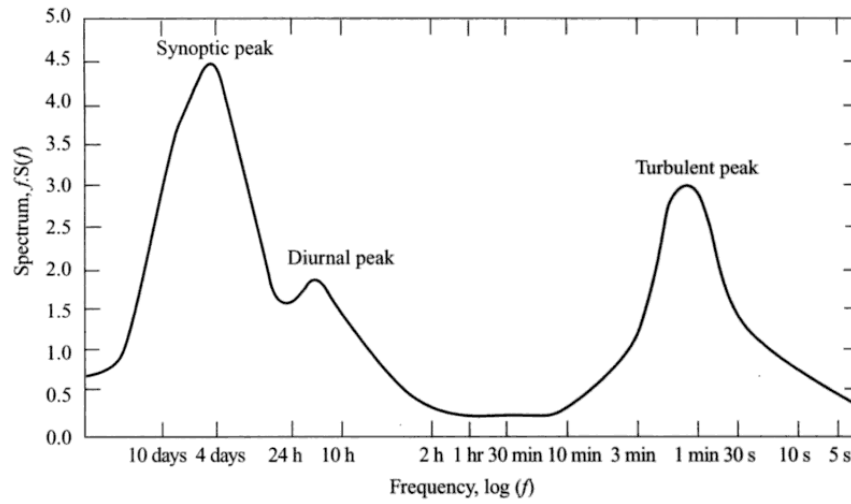


Figure 1.3 Wind speed spectrum model of Van der Hoven

In the figure above, over a large frequency range (0.007 to 900 cycles/hr) of wind speed spectrum (WSS) at Brookhaven, Van der Hoven [32] found that the 2 main phenomena influencing WSS were synoptic scale, and turbulence (micro-scale dynamics). The Meso-scale dynamics, such as diurnal effect, had less influence in this area.

The other studies about wind speed spectrum are from H. J. Hwang (1969), Jay Apt (2007), and Joaquín Mur-Amada and Ángel A. Bayod-Rújula (2007). Hwang found that at Palmyra Island as represented in Figure 1.4, WSS at 3 sites are notably different. Synoptic scale dynamics is, clearly, the most influence for Barren Island, and Causeway as shown in below figure. For Army site, synoptic scale dynamics has less influence to wind speed. For conclusion, the different location can cause vastly difference of wind speed spectrum.

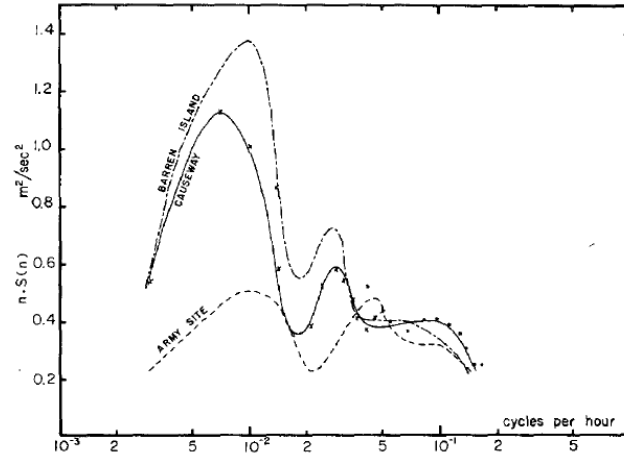


Figure 1.4 Wind speed spectrum at 3 areas of Palmyra Island by Hwang

Jay Apt used 1-s and 1-h time resolution wind data to construct the power spectrum of wind, as presented in Figure 1.5. The left figure represents the real power output (kW) of the 10-turbine wind farm for ten days at 1 sec resolution. The right figure presents power spectral density of the power output from the same wind farm at 1-h and 1-s resolutions. For highly fluctuate wind power, log-scale of power spectral density (PSD) has linear relationship with log-scale frequency during about 0.00001 - 0.5 Hz.

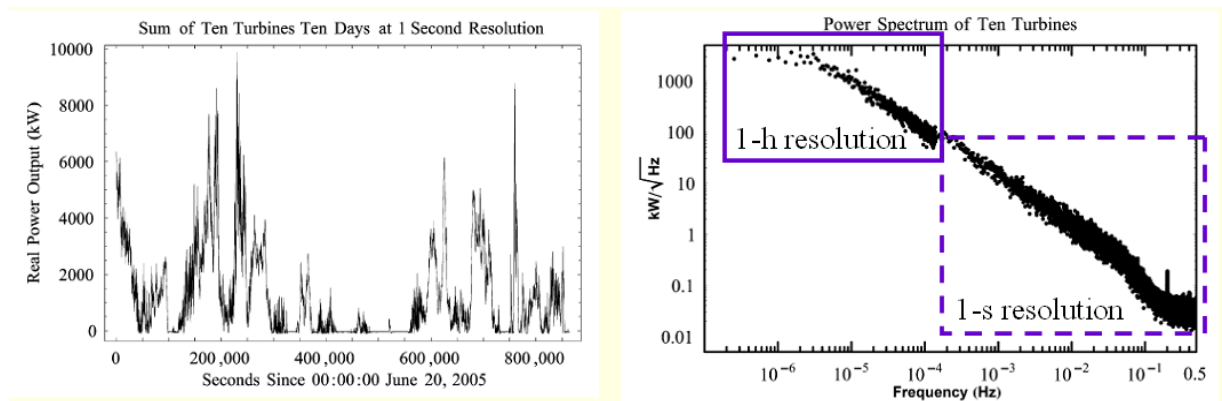


Figure 1.5 Real power output (kW) variation (left) and power spectral density (PSD, $\text{kW} \cdot \text{Hz}^{-1/2}$) (right) of the power output from 10-turbine wind farm

Amada and Rújula presented the power spectral density of 10.98 MW Remolinos wind farm operating at low winds and 16.2 MW Borja wind farm operating around 6 m/s in Aragon of Spain. In this study, the linear relationship between log-scale PSD and log-scale frequency can extent up to about 1Hz at low wind speed and 2Hz at high wind speed. At about 1 - 2 Hz, fluctuated PSD occur due to 3p (3 times of rotor speed) or tower shadow noise. The low wind speed cause PSD trend to keep constant and then fall at frequency

higher than 2Hz. For the high wind speed, log-scale PSD decrease continuously when log-scale frequency decrease at frequency higher than 2Hz. [38].

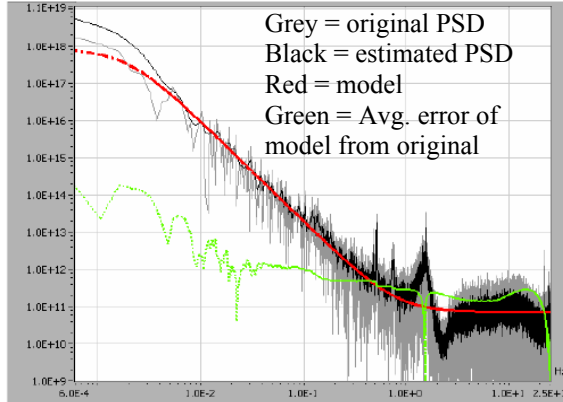


Figure 1.6 Power spectral density of Remolinos wind farm at low wind speed

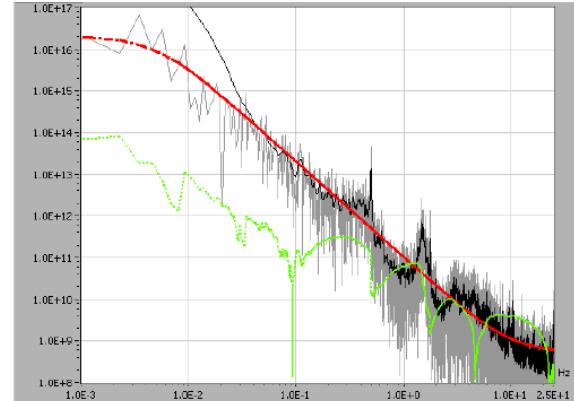


Figure 1.7 Power spectral density of Borja wind farm operating around 6 m/s.

For conclusion, at about 0.00001 - 1 Hz, log-scale PSD of wind power has a linear relationship with log-scale frequency. About 1 - 2 Hz, wind power is influenced by tower shadow noise or 3p noise. Higher than 2Hz, the low wind speed cause PSD trend to keep constant and then fall. Synoptic scale dynamics most influences wind speed followed by micro-scale dynamics. Wind speed spectrums at different locations are vastly different.

The slow variation wind component is influenced by the diurnal and seasonal or synoptic meteorological effects and can be modeled statistically using Weibull or Rayleigh distributions. The turbulence component can be modeled as a zero average random process [32].

Consequently, the wind power variation can be composed of the slow variation and fast variation components. The slow variation of wind power is influenced by the slow variation component of wind speed. The fast variation is influenced by the turbulence of wind speed and the dynamics of wind turbine. The measurement of wind power reveals the decomposition of fast wind power variation, which consist of low frequency (frequencies up to 0.5Hz) relating to the turbulence wind speed and the high frequency (frequencies above 0.5Hz) power variation relating to the dynamics of wind turbine, as represented in Figure 1.8 [49].

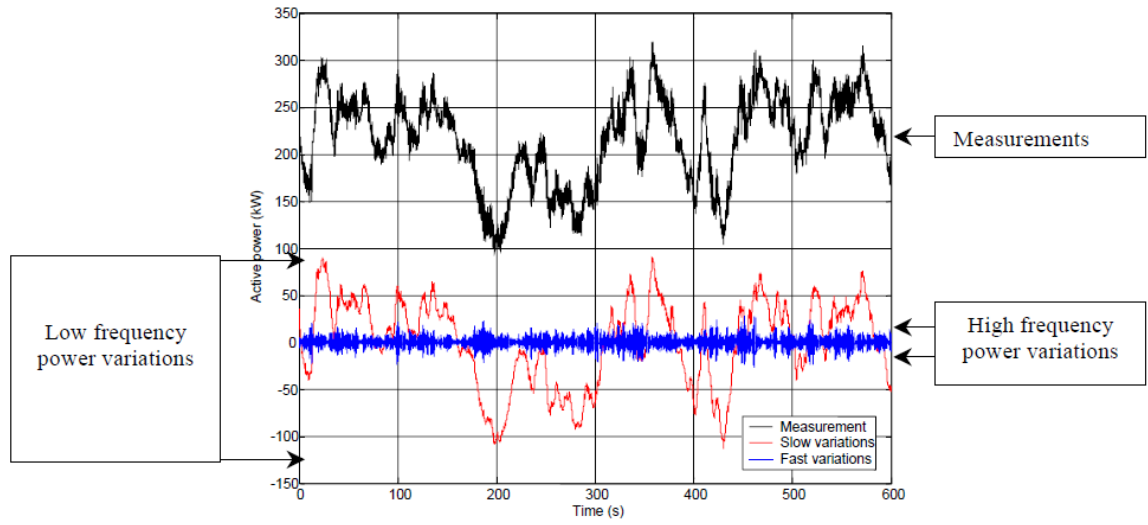


Figure 1.8 The decomposition of fast wind power variation.

The contribution of low frequency power variation is about 16 – 22% of rated capacity, while of high frequency power variation is only about $\pm 2\%$ [49]. In this study, the wind power modeling for the study of power system stability can reasonably neglect the effects of high frequency power variation. Therefore, the mechanical power input (P_m) of wind turbine can be modeled as follows

$$P_m = P_{ms} + P_{mf} = P_{ms} + P_{ml} + P_{mh} \quad \text{Eq. 1-1}$$

Where P_{ms} is slow variation wind power, P_{mf} is fast variation wind power, P_{ml} is low frequency wind power variation, and P_{mh} is high frequency wind power variation.

1) The aggregated wind power

Many previous studies concluded that the aggregation of many wind turbines can cause power to be smoother due to wind power fluctuation being compensated among each other, as shown in Figure 1.9 [49].

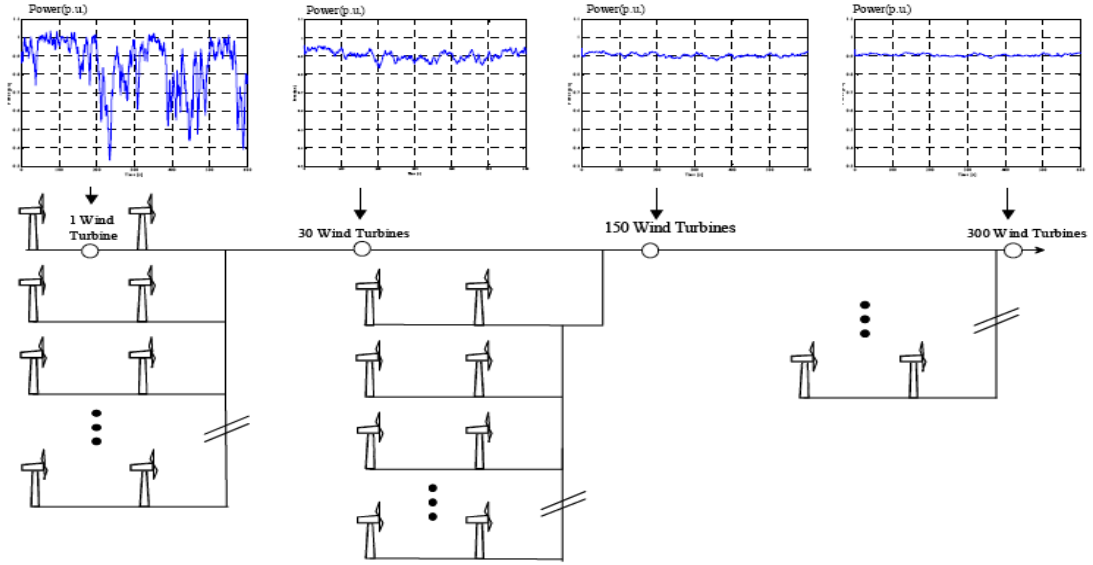


Figure 1.9 Power of aggregated wind turbines in case of 1WT, 30WTs, 150WTs, and 300WTs

Many individual wind turbines when connected together may be represented by one large turbine and called aggregated wind turbine. Each turbine produces wind power exhibiting random behavior with known and unknown probability distributions. Ideally, from the property of convolution, the random effects when summarize can reasonably be modeled using zero-mean Gaussian distributed white noise [41]. The data distribution of power output of aggregated wind turbines will close to Gaussian or Normal distribution.

In practice, many previous studies have shown that the wind power distribution of wind power plants are not a type of Gaussian distribution [41][55][48][69]. The wind power distribution may be approximated by Beta distribution, kernel estimator, or mixture three Gaussian distribution. The wind power deviation distribution is, however, may be approximated by Laplace distribution. Examples of wind power distribution for wind power plants in different location and the wind power deviation distribution are shown in Figure 1.10.

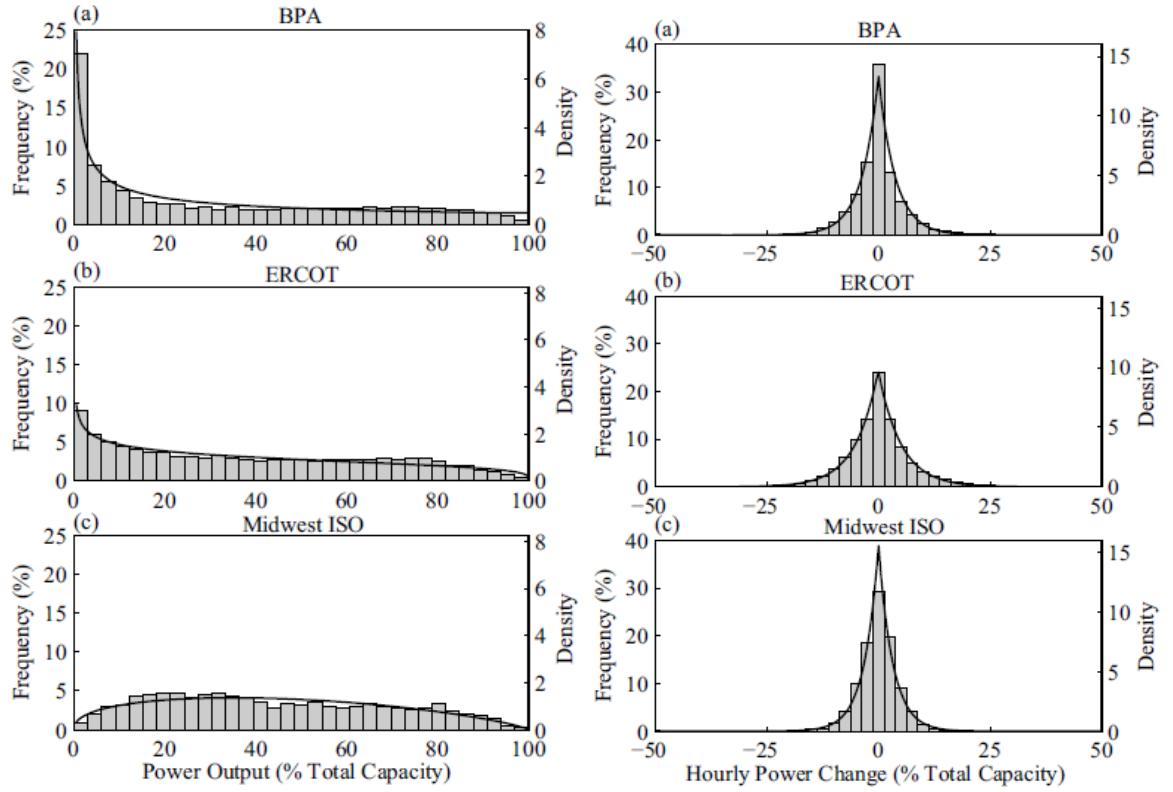


Figure 1.10 Histogram and fit Beta distribution (left) and hourly power change (right) of aggregated wind power plants in BPA, ERCOT, and Midwest ISO.

The wind power distribution of wind farm depends on many factors, especially, geographical diversity, wind speed distribution, wind turbine performance, turbulence of wind speed, etc. In Figure 1.10, the power distribution of Midwest ISO power plant seems close to normal distribution more than the other two plants due to the larger geographical diversity of wind turbines in Midwest ISO power plant comparing with the others [41].

Therefore, the slow variation component of wind power can be approximated by a Normal distribution when the geographical diversity is large enough. For the fast variation component, such as an hourly variation wind power or less, the zero mean Laplace distribution is more accurate than Normal distribution.

2) The colored noise of wind power

In Figure 1.11, the power spectral density of wind power reveals the finite ranges of wind power spectrum [49]. Therefore, the colored noise (limit spectrum) should be used for stochastic wind power modeling more realistic than white noise. From previous topic, the slow variation wind power distribution is not a type of zero mean Gaussian distribution but can be approximated using non-zero mean Beta distribution. Unfortunately, the non-zero mean data distribution is not defined in the theory of stochastic differential equations. To

apply for the study of stochastic stability analysis, following assumptions are made basing on the relaxed conditions for the theory of stochastic differential equation.

- a) The slow variation of wind power (when the fast variation part is filtered out) is long enough so that the wind power can be assumed as a constant within a definite period. For example, wind power is constant for at least 10 hours or 36,000 seconds.
- b) The fast variation of wind power (when the slow variation part is filtered out) is zero-mean data distribution and can be approximated using colored noise. The low frequency component is dominant while the high frequency component has very low contribution compared with the low frequency component and the slow variation component.

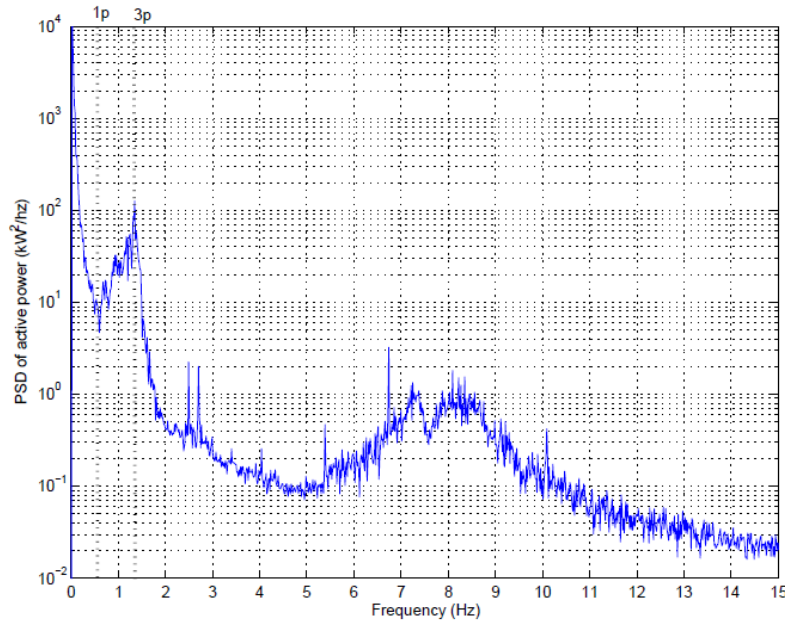


Figure 1.11 Power spectral density of power output of 500kW wind turbine

From Eq. 1-1, when high frequency component is neglected, the mechanical wind power of aggregated wind turbines can be represented as follows

$$P_m = P_{ms} + P_{ml} = P_{ms} (1 + \alpha_w v_w) \quad \text{Eq. 1-2}$$

$$p v_w = -\varepsilon_w v_w + \gamma_w \varepsilon_w p W \quad \text{Eq. 1-3}$$

Where $P_{ml} = \alpha P_{ms} v_w$, v_w represents colored noise applying to wind power, α_w and ε_w are noise intensity and bandwidth of low frequency component of wind power, γ_w is scaling factor depending on application.

From measurement by Pedro, the noise intensity of low frequency component of wind power between 0.1 – 0.2 is reasonably assumed. The bandwidth, when increased will cause the colored noise act close to a white noise. From Figure 1.11, the bandwidth of PSD of wind power in the model should not be larger than 20 Hz.

1.2.2 Impacts of wind power on the power system stability (PS)

The instability of the power system occurs when the power system cannot regain a state of operating equilibrium after facing a physical disturbance. This can be determined as the ability of synchronous machines, most of electrical machine type of generation, in the power system to keep synchronization that is called rotor angle stability. Rotor angle stability can be affected by the small, but continuous disturbances, and the large disturbances. The small and continuous disturbances may be considered using a linear relationship between the influencing small signals and the rotor angle and can be called *small signal stability*.

For the large disturbances, a nonlinear relationship between the influencing disturbances and the rotor angle of the power system always occur under transient situation and can be called *transient stability*.

The other major types of power system stability are voltage and frequency stability. It is the ability of the power system to control and stabilize the voltage and frequency under any situations. Instability of voltage caused from the negative relationship between reactive power and voltage after critical balance of load and generation and then the system lose control finally. Instability of frequency caused from unbalance between generation and load for a long time.

1) Impact on small signal stability (SSS)

Small signal stability (SSS), for the case of instability, is evaluated by the positive eigenvalue which enlarge the state variables to diverge until the system loss control. These eigenvalues are influenced by the designed parameters of the power system, for example, damping and synchronizing coefficients of generator, base rotor electrical speed, base frequency, inertia constant, field circuit inductance and resistance, and mutual inductance.

J.L. Rueda and F. Shewarega (2009) had studied the impacts of wind power on SSS of 4-machine systems with 2652.5 MW of initial value (Figure 1.12). Total load demand is 2,734 MW, with 967MW of L1 and 1,767MW of L2. Wind power plant totally 750 MW (with 215.7 MW of initial value) with 150 DFIG wind generators (5MW each) were set to replace G3 synchronous generators. There are 3 cases of this scenario: first, base case

without wind power (with O in figure); second, 85% of G3 power generation is replaced by wind power (with \square in figure); and third, G3 is fully replaced by wind power (with Δ in figure). Eigenvalues were computed with damping ratio lines as shown in the next figure.

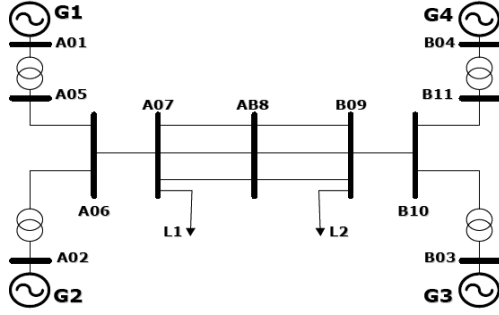


Figure 1.12 The 4-machine power system

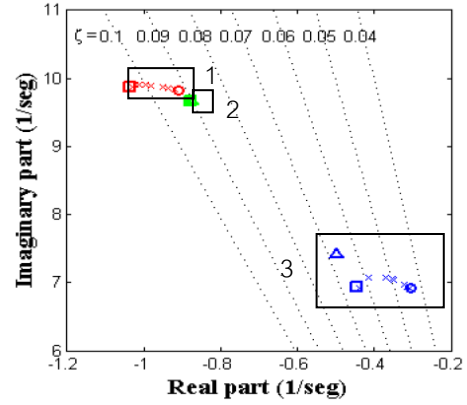


Figure 1.13 Root loci of eigenvalues

In Figure 1.13, eigenvalues are classified into 3 groups within 3 rectangular boxes. Group 1 (oscillation of G3 or G4 to the rest of system) represent local mode of oscillation with high load demand (L2 at bus B09), group 2 (oscillation of G1 or G2 to the rest of system) represent local mode of oscillation with low load demand in distant area (L1 at bus A07) and group 3 represent inter-area mode of oscillation (oscillation between area 1 with G3, G4 and area 2 with G1, G2).

The larger wind power penetration replacing G3 (path from O \gg \square \gg Δ) causes ζ (and λ) larger with negative or stability increase for local mode of oscillation with high load demand and inter-area mode. Fully replace of wind power (G3 is switched off) occur only for inter-area mode with path change obviously. For this case, ζ has no change significantly, but ω increase with insufficient damping, and thus, increasing system swing. However, local mode of oscillation with low load demand in distant area has no significant influence by wind power.

For wind power with random variations, it can be concluded that SSS can become significant depending on location of wind turbine, stress of the system (loading factor), and amount of conventional generation that replaced by wind power. Installation of Doubly-Fed Induction Generator (DFIG) wind power plant within the highly load area to replace large amount of conventional generation can improve SSS significantly.

Practically, the impact of variations in wind power on SSS or dynamic stability cannot be analyzed using eigenvalue methods. The cumulative effect of random variation of wind power can finally cause the system away off an equilibrium region and thus instability [28]. Dynamic stability cannot easily be characterized using eigenvalue method (as presented above) since the variation of mechanical input cannot directly affect to root of $(sI - A)^{-1}$ matrix. Therefore, a study of dynamic stability needs other suitable methods that can incorporate random variation effects of wind power.

2) Impact on transient stability

The most frequent transient phenomenon in a power system is a short circuit fault. During a fault, power and voltage may suddenly drop close to zero. Unbalance between mechanical power of generator (P_m) and electrical power of the system (P_e) can cause transient instability that can be described using swing equation of power system as follow.

$$\frac{d\omega_r}{dt} = \frac{d^2\delta}{dt^2} = \frac{\omega_0}{2H} [P_m - P_e] \quad \text{Eq. 1-4}$$

$$\omega_r = d\delta/dt \quad \text{Eq. 1-5}$$

where $P_e = (E_s E_B \sin \delta) / X_T$, is called *power-angle relationship*, ω_r is rotor electrical speed, δ is rotor angle, ω_0 is base rotor speed, and H is inertia constant of generator.

In Equation 1-3, the mechanical power of a generator is larger than the electrical power of a power system, and thus, causes acceleration of state variables, such as rotor electrical speed and angle. If faulted line is cleared (by open circuit) within a proper time, state variables may become stable finally but if not, instability may occur. Numerical simulation method always be used to compute time variation of δ and ω_r after subject to faults with different clearing time. The clearing time of protection devices that can make δ first enlarge and out of equilibrium is called Critical Clearing Time (CCT). CCT is used indirectly to quantify transient stability. The larger CCT means system is more stable due to practical clearing time may never reach that CCT.

The transient stability of an induction generator wind turbine strongly depends on pitch control systems. The quicker response of pitch control, the faster converge to stable condition. However, dynamics behavior of wind generators (with power 0.5 p.u.) does not have so significant effect on transient stability of conventional synchronous generators (with power 1.0 p.u.) [39].

Furthermore, transient stability is influenced by the location of wind farms, types of generators, and wind power penetration. Wind power can improve transient stability for some bus, while can cause poorer transient stability for the other bus. Variable speed scheme of DFIG wind turbine can have better transient stability than fixed speed scheme of IG because DFIG can better control reactive power. However, transient stability decrease when penetration of wind power increase [19].

3) Impact on voltage stability

Voltage instability occurs when a system cannot control voltage by the normal compensation of reactive power. This situation happens when load is too high, reactive power is limited, and/or under other contingencies such as loss of transmission line. Practically, voltage collapse (suddenly large drop of voltage) can possibly be found before voltage instability. P-V curve and Q-V curve usually are used to explain the operating condition and state of voltage stability as shown in the next figures.

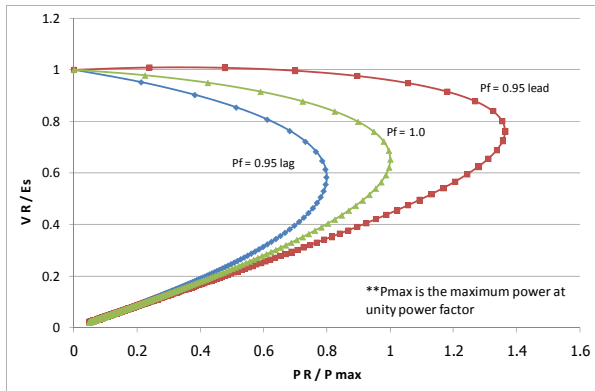


Figure 1.14 P-V curve with three power factors

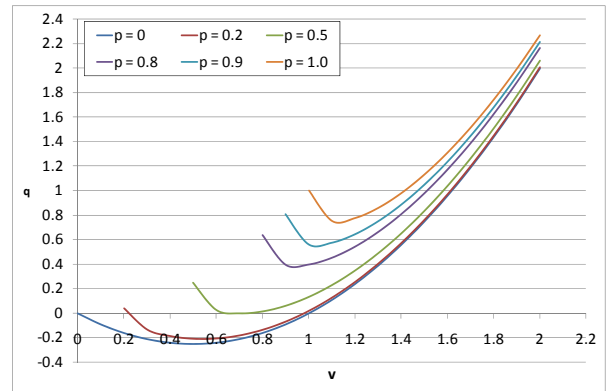


Figure 1.15 Q-V curve with different P

For voltage stability indicators under static conditions, V-Q sensitivity and roots of Q-V modal sensitivity are always considered. For dynamic condition, bifurcation concept is applied to explain characteristic of the case one value of P or Q have 2 operating points of V. The saddle-node bifurcation (SNB or point of collapse) and hopf bifurcation (HB) are specified to explain the state of operation. SNB is the point when eigenvalue of system matrix is zero while HB occur when complex conjugate eigenvalue cross imaginary axis.

The operating point at SNB is the point of maximum power at the receiving end on the P-V curve while HB may or may not occur on the P-V curve before reaching SNB. At SNB, voltage decreases vastly (or voltage collapse), V-Q sensitivity become negative,

increase Q cause aggressively drops of voltage, system loss control finally. At the point HB, voltage swings corresponding to imaginary part of eigenvalue.

The induction generator of a wind turbine usually consumes reactive power from the power system, reducing capability of the system to control voltage and reduce voltage stability (as shown in Figure 1.16). Increasing of internal parameters, such as impedance of step-up transformer and transmission line, can also increase voltage stability. Moreover, the better wind potential, the more loadability (ability to handle load without voltage instability) as shown in Figure 1.17. However, using Static var compensator (SVC) instead of capacitor bank cannot improve loadability or even SNB but can increase HB that reduces the swing of voltage as shown in Figure 1.18 [76].

Conversely, this last result contrasts with Youjie's study. Even though both cases use DFIG for simulation, Youjie found that SVC can improve loadability and SNB. Furthermore, SVC can reduce active and reactive power loss in the line and can improve voltage stability at the bus [71].

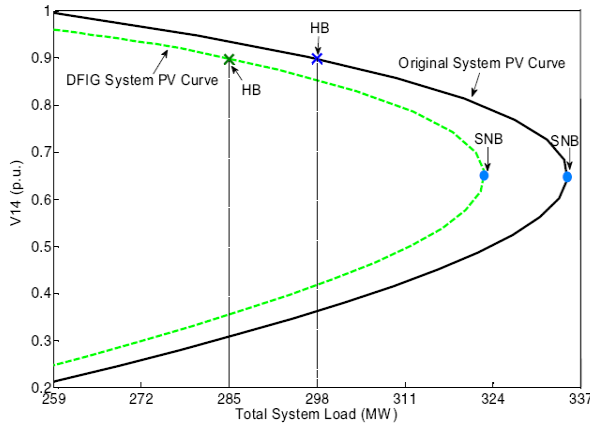


Figure 1.16 P-V curve of power system with and without wind power

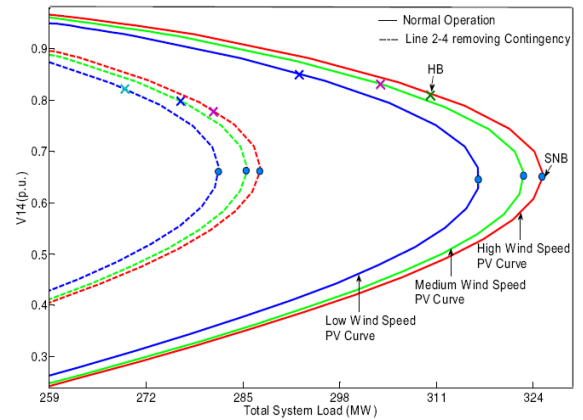


Figure 1.17 P-V curve of power system, including wind farm, at different wind speeds with normal and contingency situations.

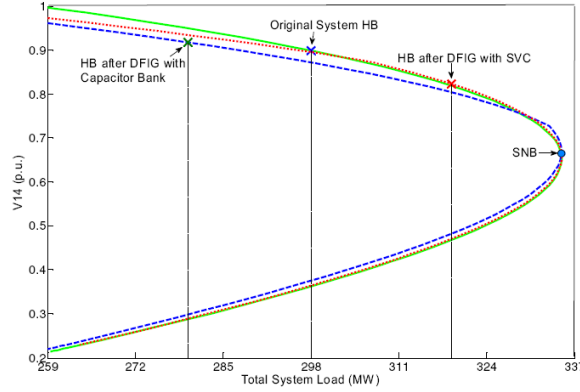


Figure 1.18 P-V curve of power system with SVC and Capacitor bank compensator

4) Impact on frequency stability

The imbalance between the mechanical power of the generator and the electrical power of the system can cause the acceleration of rotor electrical speed that affects electrical frequency directly. Therefore, frequency stability depends on ability of generator to generate power for load demand. Frequency drop when system loss of generation and then frequency instability can occur. This large disturbance may cause cascading outage due to load shedding regulation or in worst case, may be cause cascading desynchronization of generators.

Frequency stability incorporating wind power depends on both wind power penetration and control schemes of active, reactive power and voltage. For example, after 2.5% loss of generation, larger penetrations of wind power cause the frequency to drop faster with a finite time. In the case of DFIG wind generator with constant P and V control, frequency of larger penetration wind power exponentially drops until becoming stable and keeps decreasing until lower than less penetration wind power, as shown in Figure 1.19. For the case with P and frequency dependent V control, frequency drop slightly and suddenly regain to stable value as shown in Figure 1.20. However, this latter case of control scheme leads to larger voltage drop especially near a wind farm [31].

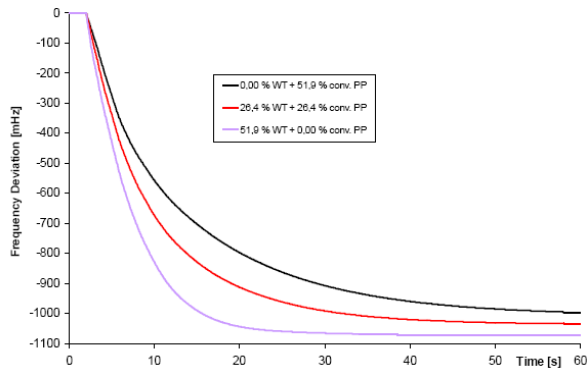


Figure 1.19 Frequency deviation with constant P and V control

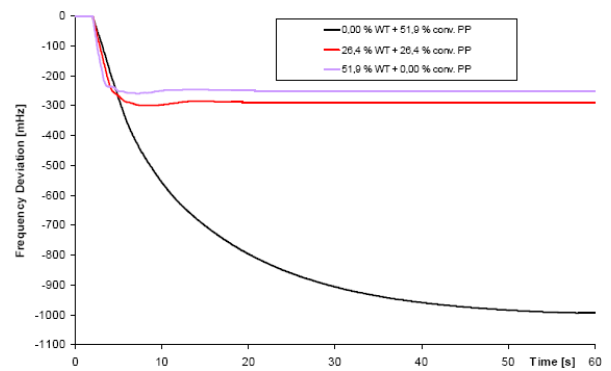


Figure 1.20 Frequency deviation with P and frequency dependent V control

1.2.3 Impacts of wind power on power quality

For PQ problems, over/under voltage, over/under frequency, flicker, harmonics, protection error, and over current could be issues of interest. Problem and causes of these issues are listed in Table 1.1 [49].

Table 1.1 Major problems of power quality from wind power integration

No.	Problems	Causes
1	Steady state voltage rise	Wind speed variation
2	Over-current	Peaks of wind speed
3	Protection error action	Peaks of wind speed
4	Flicker during continuous operation	Dynamic operation of wind turbines
5	Flicker during switching operations	Switching/start up operation of generators
6	Harmonics	Power electronic converters
7	Voltage drop	In rush current due to switching operations of generators

Wind power fluctuates with wind speed, which causes the more reactive power absorbed by wind farm when there is larger variation of wind speed and with greater wind power penetration. Furthermore, the effect of random wind speed (noise including gust and ramp) has more effect on fluctuation of P and Q for larger wind power penetration, as shown in Figure 1.21 [66].

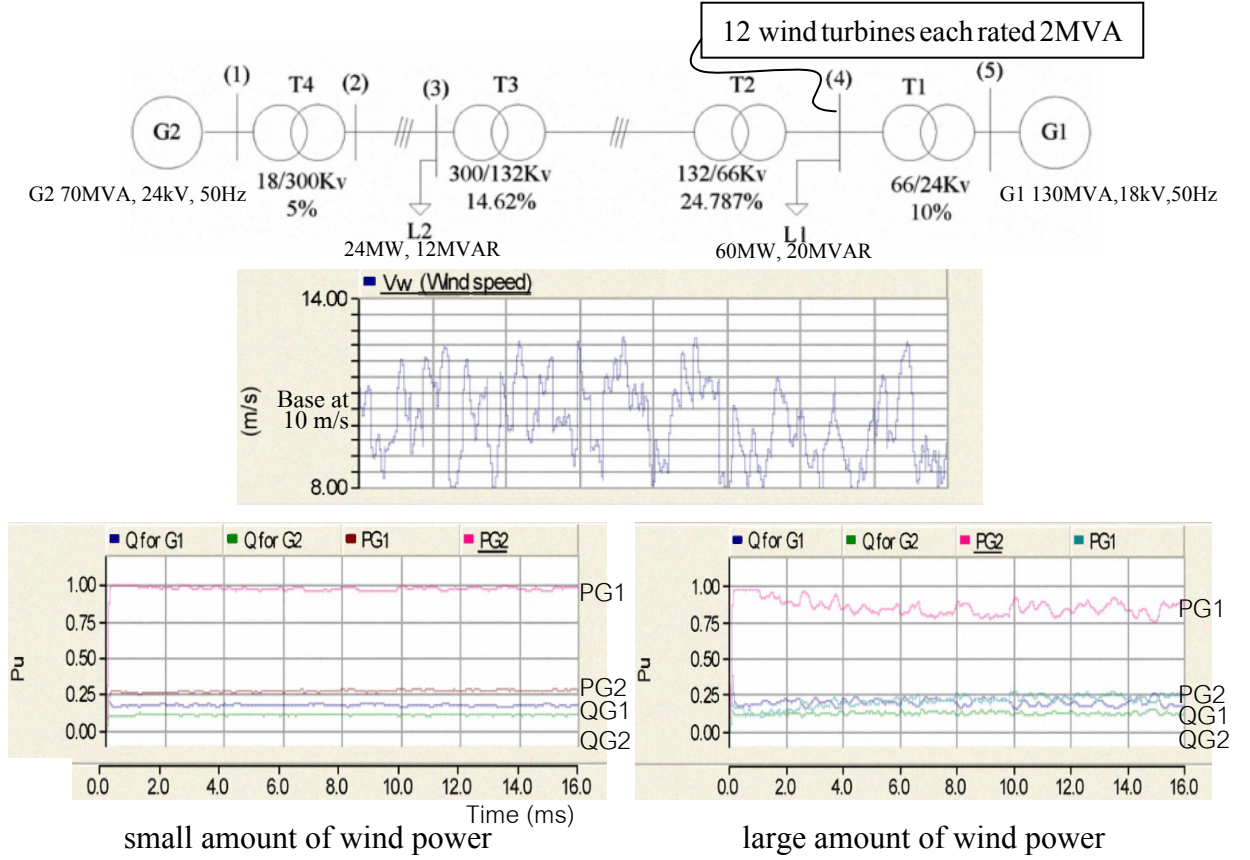


Figure 1.21 Test system with 2 generators (G1 and G2), variation of wind speed with noise, P and Q of G1, G2 with small amount of wind power, and with large amount of wind power.

Aggregation of wind farm (separated into many groups) with proper distance and time shifts between each group can cause reduce flicker and 3p noise (3 times of rotor frequency), and can make P, Q, and V smoother [36].

Later, Muljadi et al. also studied the other aspects concerning PQ in a wind power plant. From the results (as shown in Figures 1.22 – 1.25), they concluded that voltage varied with reactive power and reactive power compensation can improve voltage quality. Frequency varied with derivative of active power, and reactive power compensation cannot improve frequency quality. Self-excitation can occur when capacitor provide reactive power to induction generator during off-grid [20].

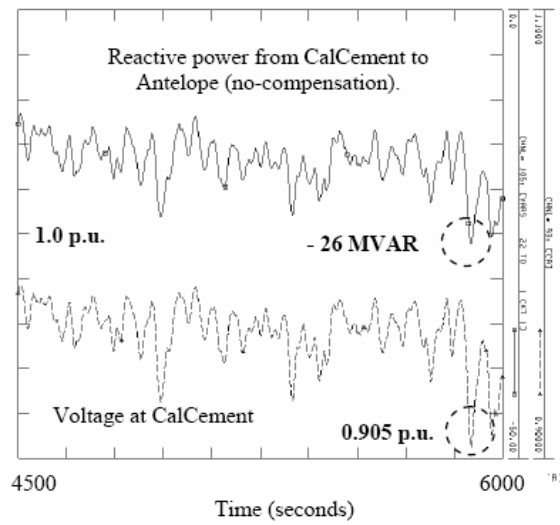


Figure 1.22 Reactive power and voltage without reactive power compensation

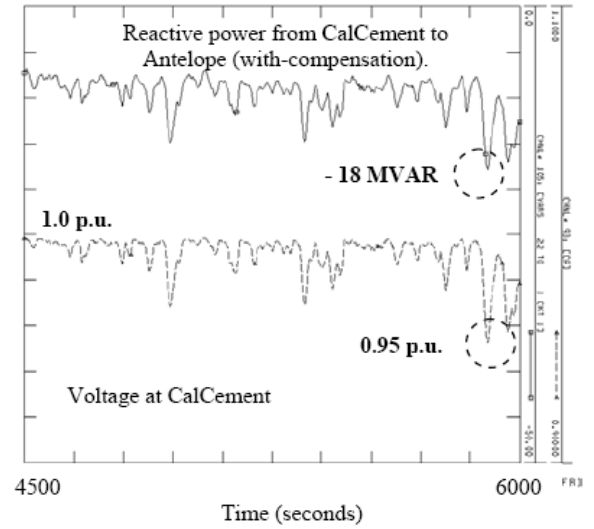


Figure 1.23 Reactive power and voltage with reactive power compensation

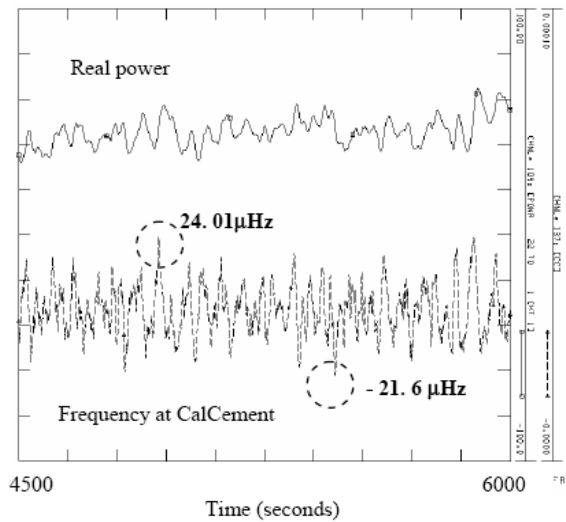


Figure 1.24 Active power and frequency without reactive power compensation

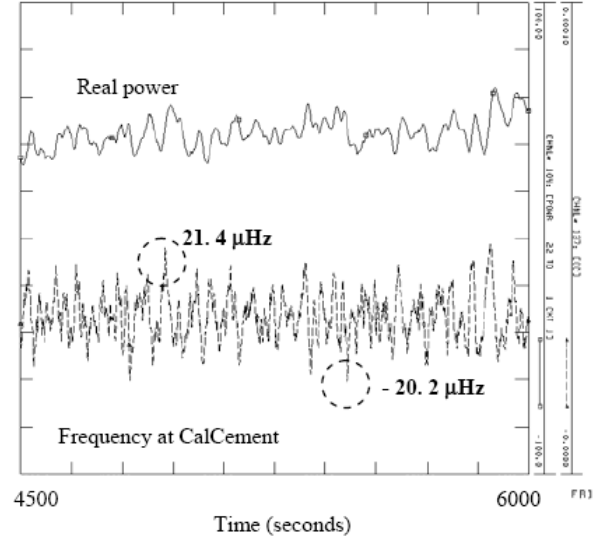


Figure 1.25 Active power and frequency with reactive power compensation

Moreover, the main flicker contributions from wind turbines comes from the 3p power variations (at the frequency of 2.1Hz) which is related to rotational turbulence and the 1p power variation (approximately 0.7Hz) is related to the rotor speed variation. In the frequency of 8.4Hz, corresponding to 12p, a small power spectral density (PSD) is related to the flexible aero elastic part of the wind turbine in addition to the induction generator, as shown in Figure 1.26 [49].

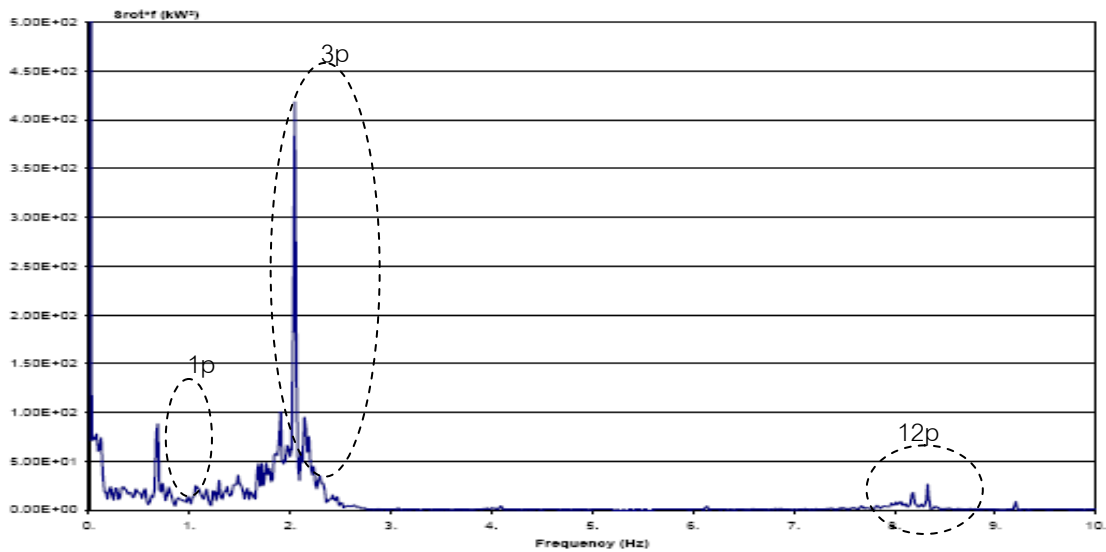


Figure 1.26 Power spectral density of power from 225kW pitch controlled wind turbine

For conclusion, interesting issues involving PS and PQ when incorporating wind power, are presented as follows.

Table 1.2 Interesting issues of power system stability and quality incorporating wind power

Power system stability	Causes
Transient instability	loss of wind , voltage drop, or line fault
Dynamics instability	cumulative effect from random variation of wind power
Voltage instability or voltage collapse	random variation of wind power during critical operating point (bifurcation)
Frequency instability	loss of loadability (critical imbalance between load and generation) during random variations of wind power
Power Quality	Causes
Voltage variation and Over/Under voltage	Variation of reactive wind power relating to variation of reactive power compensation of the power system
Frequency variation and Over/Under frequency	Variation of active wind power (relating to variation of load)
Flicker during continuous operation	Variation of mechanical power of wind turbine relating to turbulence of wind and dynamic response of turbine
Flicker during switching operation	Variation of scale, occurrence, and duration when start up and/or switching of wind power

1.2.4 Deterministic methods for power system stability and power quality analysis

Effects of wind energy on power system stability (PS) and power quality (PQ) have been studied by many authors using methods generally based on deterministic approaches. Deterministic method analyze PS by solving Differential and Algebra Equations (DAE) of power system both static and dynamic system based on generator model, network system model, load characteristics equations, and control system model.

For deterministic methods, all operating conditions and network topology are explicitly determined with the dynamic response to time-variation of generation of input and dynamic (or static) state variables. Classical small signal stability, transient stability, and voltage stability, generally based on deterministic method, are well explained in *Power System Stability and Control* by P. Kundur (1998).

Some of these classical methods are Dynamics numerical method, Equal-area criterion, Direct method, Eigenvalue analysis, Q-V modal analysis and V-Q sensitivity analysis. Examples of deterministic methods for PS analysis are presented in Chapter 2.

Moreover, voltage stability analysis method is later improved considerably and well described by Claudio A. Canizares (1995, 1998, and 2003) . He clearly describes voltage stability and voltage collapse base on bifurcation theory, optimization technique, and reduction load flow Jacobian. Furthermore, they had developed many useful voltage stability indicators such as Saddle-node bifurcation (SNB), Hopf bifurcation (HB), and Linear performance index (linear relationship between Eigenvalue index or HB and loading factor).

However, deterministic methods require enormous exact information to compute highly accurate results, which is impossible under the realistic random nature of power systems. The power system concerning many uncertainties from, for example, load varying, random occurrence of faults, dispatching of transmission line, operating of control system, and variation of generation such as renewable sources especially wind power. Spectrum of uncertainty varies from very low frequency (0-0.1 Hz) to high frequency (up to 3kHz) with small and large scale that affect to operating condition differently.

To incorporate the real random nature of the complex power system, probabilistic methods were developed and applied to studying the effects of randomly fluctuating variables. These random variables are, for example, fault type, fault location, fault occurrence, load factor, power generation, availability of equipments, impedance of

transmission line due to dispatching, impedance of overall network system, and operating condition.

1.2.5 Probabilistic methods for power system stability and power quality analysis

1) Classical probability method for small signal (dynamic) stability analysis

Originally, well-known probabilistic methods for small signal (or dynamic) stability (SSS) were discussed by Burchett and Heydt (1978). They evaluated SSS based on classical eigenvalues analysis method for the linearized system state matrix. Uncertainty (with mean and covariance) of system parameters, such as rotor angle and mechanical damping coefficient, and with sensitivity to eigenvalues was determined to compute uncertainty of eigenvalues. Probabilistic method was applied to compute the probability that all eigenvalues have negative real part which remains in the stable region. This approach can save more calculation time than deterministic approach while can accurately describe uncertainty of stability statistically. For this study, state space equation in vector form are reformed to be,

$$\Delta \dot{X} = A \Delta X \quad \text{Eq. 1-6}$$

To compute the unknown uncertainty of the eigenvalues from the known uncertainty of the state variables, sensitivity analysis was determined from this equation:

$$\Delta \lambda_i = S_{ij} \Delta z_j \quad \text{Eq. 1-7}$$

Where λ_i is i^{th} eigenvalues, z_j is j^{th} system parameter and $S_{ij} = \partial \lambda_i / \partial z_j$ is sensitivity of i^{th} eigenvalues to j^{th} system parameter. $\partial \lambda_i / \partial z_j$ can be computed from the scalar product of matrix A, and the right and left eigenvectors as follows.

$$S_{ij} = \frac{\partial \lambda_i}{\partial z_j} = \frac{\left\langle \frac{\partial A}{\partial z_j} w_i, v_i \right\rangle}{\langle w_i, v_i \rangle} \quad \text{Eq. 1-8}$$

Where w_i, v_i are the i^{th} left and right eigenvector, respectively, corresponding to the i^{th} eigenvalues.

If Δz_j are known multivariate random variables, therefore, by chain rule, $\Delta \lambda_i$ also are multivariate random variables. Theoretically, properties of multivariate random variable are used to calculate uncertainty of eigenvalues in matrix form as follow

$$\text{Mean} (\Delta \lambda) = 0 \quad \text{Eq. 1-9}$$

$$\text{Covariance} (\Delta \lambda) = \text{Real} (S) . \text{Covariance} (\Delta z) . \text{Real} (S^t) \quad \text{Eq. 1-10}$$

To compute the probability of instability that all eigenvalues have no negative real parts, zero mean (\mathbf{M}) and covariance matrix of multivariate random variables, $\text{cov}(\Delta\lambda) = \mathbf{C}$, are used in the probability density function (PDF) of the multivariate random variables, that is

$$\mathbf{f}_{\mathbf{X}}(\mathbf{X}) = \frac{1}{((2\pi)^n \det(\mathbf{C}))^{1/2}} \exp(-0.5(\mathbf{X} - \mathbf{M})' \mathbf{C}^{-1} (\mathbf{X} - \mathbf{M})) \quad \text{Eq. 1-11}$$

The probability that all eigenvalues have no negative real parts is

$$\mathbf{P}\{x_1 \geq u_1, x_2 \geq u_2, \dots, x_n \geq u_n\} = \mathbf{P}\{\mathbf{X} \geq \mathbf{U}\} = \int_{u_n}^{\infty} \dots \int_{u_2}^{\infty} \int_{u_1}^{\infty} \mathbf{f}_{\mathbf{X}}(\mathbf{X}) dx_1 dx_2 \dots dx_n \quad \text{Eq. 1-12}$$

This form of probability can be computed using the *Generalized Tetrachoric Series* method as described by R.C. Burchett and Heydt. The results of eigenvalues ($\lambda_i = A^{-1}w_i A$) with uncertainty (mean and standard deviation) and probability of instability are presented in next figure. Standard deviations of eigenvalues are computed from covariance matrix as stated before ($\text{Std}(\lambda_i) = \sqrt{c_{ii}}$).

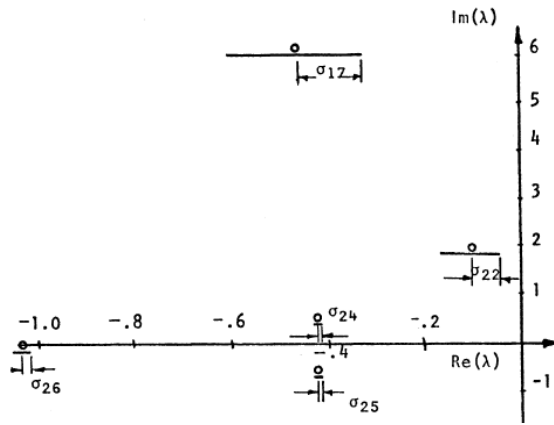


Figure 1.27 Complex plane of eigenvalues

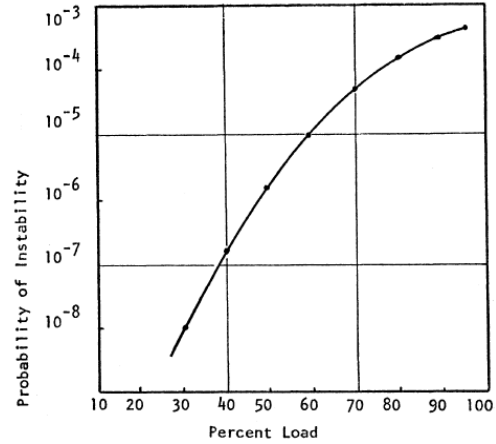


Figure 1.28 Probability of instability vs load

From the above right figure, since the rotor angle is influenced by the load, increasing the loading factor causes the eigenvalues (corresponding to rotor angle) to move from negative to close zero. This will increase the probability of the instability as a result.

2) Stochastic differential equation for dynamic stability analysis

Even though, the classical technique as presented above, has higher statistical accuracy than deterministic methods, it cannot be properly used when considering the effects of random variations of state variables and overall network parameters. This is due

to the differential equations is linearized to consider only steady system state matrix and eigenvalue could be computed without respect to fluctuation of state variables.

Theoretically, given any dynamical system that is continuously perturbed by a zero-mean Gaussian distributed noise, the probability that a given stable operating point will eventually leave its stability region in finite time is essentially one, independent of the magnitude of the noise and excluding any control actions [7]. Therefore, the cumulative effect of random variations can finally cause the system to be away off an equilibrium region and thus unstable. Dynamic stability cannot easily be characterized using eigenvalue method (as presented above) since the variation of mechanical input or load cannot directly affect to eigenvalue matrix. Therefore, study on dynamic stability need the other suitable methods which can incorporate random variation effect of wind power.

Advanced methods for dynamic stability analysis that account for the stochastic nature of random variables was clearly explained by S.M. Shahidehpour and J. Qiu (1986 and 1989) and later improved with many applications by C.O. Nwankpa et al. (1989, 1991, and 1992). For this method, Mean First Passage Time (MFPT) is introduced to be as stability indicator based on theory of Stochastic Differential Equation (SDE). Cumulative effect of random fluctuation of system variables can continuously push the system until exit the stable region within finite time. Since there are many values of exit time vary randomly, MFPT is the average of the first time exiting stable region of the system. When the system is perturbed by stochastic variation, the perturbed differential equation becomes

$$d\mathbf{X}(t)=g(\mathbf{X})dt + \sqrt{\varepsilon}\sigma dw(t) \quad \text{Eq. 1-13}$$

Where $\mathbf{X}(t)$ is the state variables matrix, $g(\mathbf{X})$ is the bounded function matrix, $\varepsilon \neq 0$ is a small real parameter, σ is the diffusion matrix, $w(t)$ is the n-dimensional Weiner process (Brownian motion).

For the exit problem, $\tau(x)$ is the mean first exit time (MFPT) when x exits from the boundary of the domain of attraction, while at time 0, $x \in \Omega$. $\tau(x)$ is determined from the solution of the boundary value problem as follows [61]:

$$\begin{aligned} L(\tau(x)) &= -1 \quad \text{for } x \in \Omega & \tau(x) &= 0 \quad \text{for } x \in \hat{\Omega} \\ L &\equiv \varepsilon \sum_{i,j=1}^n a_{i,j}(x) \frac{\partial^2}{\partial x_i \partial x_j} + \sum_{i=1}^n g_i(x) \frac{\partial}{\partial x_i} \end{aligned} \quad \text{Eq. 1-14}$$

For the power system, the Weiner process ($w(t)$) can be considered to be white noise for the idealization or colored noise depending on the characteristics of the perturbed variables and the complexity of the solution.

The white noise (ξ) has properties, as follows

- mean of $\xi(t) = E(\xi) = 0$
- power spectral density is constant for infinite bandwidth
- normally has Gaussian distribution with $N(0, \sigma^2)$

The colored noise (υ) has various properties, for example:

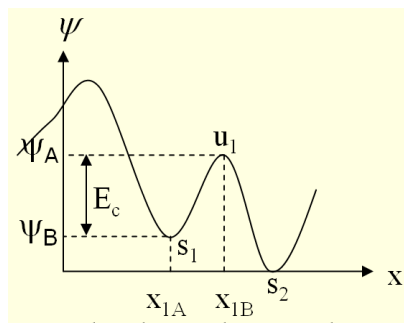
- $E(\xi) \neq \text{or} = 0$
- power spectral density is a function of $f^{-2}, f^{-1}, f^0, f^1, f^2$, or others with a finite bandwidth (word *color* means at the different range of frequency)
- not necessary to have Gaussian distribution with $N(0, \sigma^2)$

Realistically, colored noise is generally found in the nature of the power system.

For the power system with white noise perturbation, *Langevin equation* is applied as follows:

$$\dot{x}_1 = x_2 \quad \text{and} \quad \dot{x}_2 = -\beta x_2 - \psi'(x_1) + \sqrt{\varepsilon} \sigma \dot{\xi} \quad \text{Eq. 1-15}$$

Where $x(t)$ is state variables, β is coefficient related to σ , $\varepsilon \neq 0$ is magnitude of perturbation (noise intensity), σ is coefficient of perturbed variables, $\xi(t)$ is white noise, and $\psi(x)$ is system potential. When $\varepsilon = 0$, therefore, ψ with respect to x_1 is presented in below figure



For above figure, s_1 and s_2 are stable points while u_1 is unstable. This figure can be well described by the energy function method. Therefore, energy function method can be used as an boundary condition to determine $\tau(x)$ which is bounded by the critical energy ($E_c = \psi_A - \psi_B$) [61].

For the power system with colored noise perturbation, the *Orstein-Uhlenbeck process* is applied as follows [9]:

$$\dot{x}_k = -\dot{\psi}(x_k) + v_k \quad \text{and} \quad \dot{v}_k = -\alpha v + \sqrt{\varepsilon} \sigma \alpha \dot{\xi} \quad \text{Eq. 1-16}$$

Where x_k is state variables at bus k , α is bandwidth of noise, $\varepsilon \neq 0$ is noise intensity, σ is perturbed variable coefficient, v_k is colored noise, ξ is white noise, $\psi(x)$ is system potential.

Equations of colored noise are added into the system with known bandwidth and intensity. State space equation will be used to determine energy function $E = f(x_k)$. After that, find critical energy (E_c) from $\tau(x)$ can be determined from the solution of boundary value problem which is a function of ψ , ε , α , β , x_A , and x_B . Process to compute $\tau(x)$ is well described by Anawach Sangswang (2003).

The SDE method adds a perturbation part to the conventional differential equation and can be solved only by special calculus for the SDE problem. For example, the swing equation added by the perturbation of wind power generation is as follows:

$$\frac{d\omega_r}{dt} = \frac{1}{2H} [P_m(1 + \gamma \dot{w}) - P_e] \quad \text{Eq. 1-17}$$

Where ω_r is rotor electrical speed, H is inertia constant, P_m is mechanical power input of wind turbine, P_e electrical power of the system, γ is noise intensity (standard deviation divide by mean value), and \dot{w} is white Gaussian (white) noise (random noise with constant power spectral density (PSD) and normal distribution).

Furthermore, noise with selective filter (colored noise) can be stated instead of white noise due to the nature of some variables for which PSD is not constant for wide range.

Hadiza and C.O. Nwankpa (1998 and 2000) have applied this method to incorporate stochastic random of wind power. They found that MFPT decreases with increasing of wind power, noise intensity and loading factor, as shown in Figures 1.29 – 1.32.

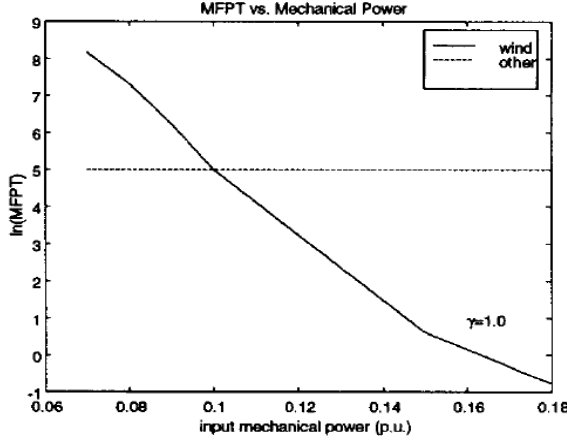


Figure 1.29 Variation of MFPT with wind power of low noise intensity

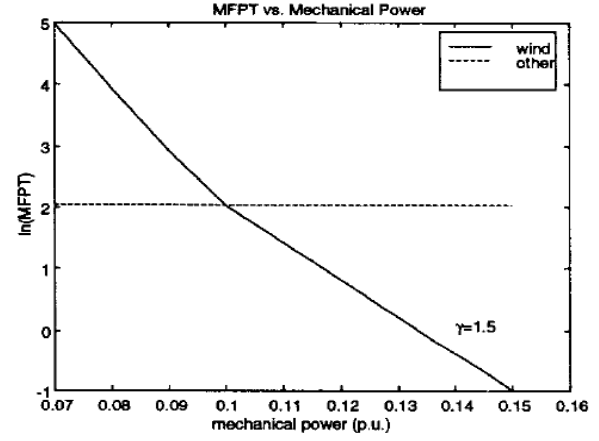


Figure 1.30 Variation of MFPT with wind power of high noise intensity

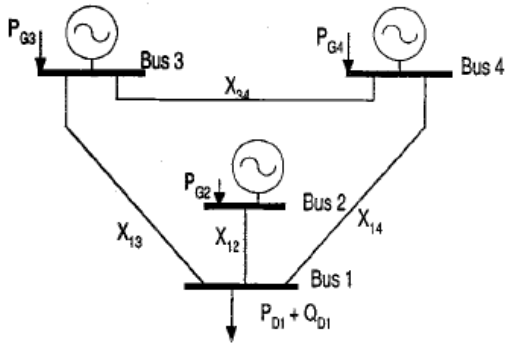


Figure 1.31 The 4-bus system one-line diagram

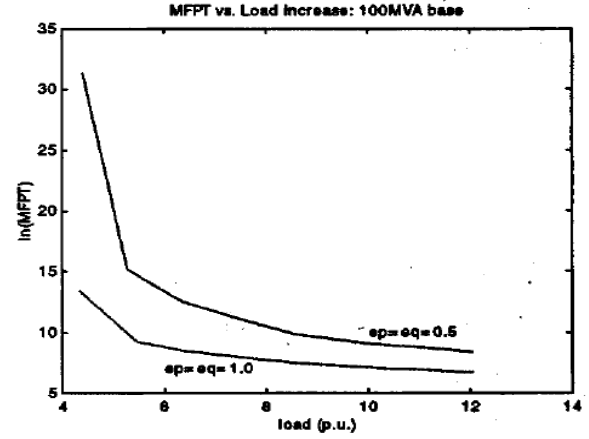


Figure 1.32 Variation of MFPT with loads of 2 scaled noise intensity levels

3) Stochastic differential equation method for voltage stability analysis

SDE is also applied to study voltage stability using stochastic voltage collapse indicator or MFPT. This concept is based on the structure-preserving model for load bus and equation of motion of generator as follows [12]:

$$\dot{V}_k = -\psi_{lk}^Q(V_k, \theta_k) + \sqrt{\varepsilon_k^Q} \sigma \dot{\xi}_k \quad \text{Eq. 1-18}$$

$$\dot{\theta}_k = -\psi_{lk}^P(V_k, \theta_k, \omega_{ref}) + \sqrt{\varepsilon_k^P} \sigma \dot{\xi}_k \quad \text{Eq. 1-19}$$

$$\dot{\theta}_j = \omega_j - \omega_{ref} \quad \text{Eq. 1-20}$$

$$\dot{\omega}_i = -\beta \omega_i - \psi_i(P_{mi}, P_{ei}) \quad \text{Eq. 1-21}$$

Where ε is noise intensity for P and Q at load bus k , $\psi(x)$ is system potential for equation of P and Q and for swing equation, V and θ are bus voltage and scaled rotor angle, and ω is angular speed of machine i , bus k , reference.

Then the energy function (E) is determined from the system potential function (ψ). Since E is known, E_C can be computed to determine $MFPT$ for voltage stability as follows

$$MFPT \approx \frac{A(E_C)}{\beta} \cdot e^{E_C/(h\varepsilon)} \quad \text{Eq. 1-22}$$

Where $A(E_C)$ is a function of E_C , h is weighted constant for ε^P and ε^Q .

Two cases the same and the different load fluctuation intensity levels (ε_l), when the load is increased, are presented in Figures 1.33 – 1.34.

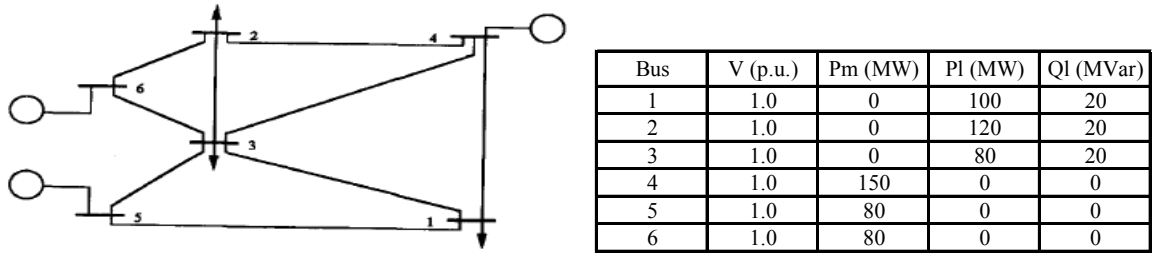


Figure 1.33 Schematic diagram and generation/load data of the 6 bus power system model

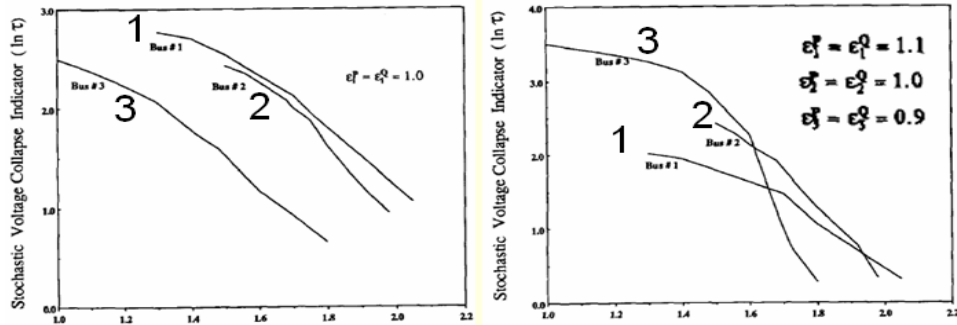


Figure 1.34 $\ln \tau$ vs. p.u. load increase (6 bus power system) with the same (left) and with different (right) load fluctuation intensity levels (ε) for P and Q of buses 1, 2, and 3

Figures 1.33 and 1.34 show that the same $\varepsilon_l=1.0$, Bus#3 has the poorest voltage stability while Bus#1 and Bus#2 are better. For the different ε_l , Bus#3 (with smallest ε_l) seem to have highest voltage stability at load less than 1.6 p.u., but after that become poorest.

However, wind speed varied with space and time results in different PSD of wind power over a finite range of frequency. Therefore, noise intensity and bandwidth will be different depend on location, time, wind turbine technology, and wind farm design. Noise intensity and bandwidth including wind power in earlier studies still lack of the details and need more information for several aspects such as

- It is true or not that only noise intensity and bandwidth parameters are enough for studying various PSD characteristics of wind power?
- If enough, how to determine noise intensity and bandwidth with different ranges of frequency and different related factors. But if not, what else?
- How to apply SDE with colored noise to analyze the dynamics and voltage stability incorporating wind power?
- How to determine energy functions of SDE applied to the problem of power quality, especially, voltage variation, frequency variation and flicker?

4) Probability method for transient stability analysis

Transient stability using the probability method was well collected and described by R. Billinton and P.R.S. Kuruganty (1979, 1980, and 1981). They computed the probability of stability by consider probability distribution function (PDF) of involving aspects for example, fault location, fault type, fault clearing time, machine inertia, and system reactance. This method even though not complicate to deal with, but require vary much of information to accurately compute PDF of involving aspects.

Lastly, Sherif O. Faried, R. Billinton and P.R.S. Kuruganty (2009 and 2010) applied this method to evaluate the transient stability of power system incorporating wind farms. The first study, they considered uncertainty from type of fault, location of fault, fault impedance, fault location, fault clearing process, system load, and spring constant of wind turbine. One year later, they studied the similar aspects with different type of fault, location of fault, fault impedance, operating condition, reclosing time, and spring constant of wind turbine. They found that, weather wind can improve transient stability or not, it depends on location of connection. Increasing of wind power penetration can possibly increase of transient stability.

1.2.6 Probabilistic methods for power quality analysis

For probabilistic methods for power quality analysis, only voltage (V) fluctuation, frequency (Fr) fluctuation, and flicker (Fl) problems are considered. The V, Fr, and Fl under acceptable ranges with upper (UL) and lower limits (LL) are reported in the IEEE and Grid Codes of many countries. Therefore, we need to know PDF of V, Fr, and Fl of the power system to determine probability of V, Fr, and Fl be within the range UL and LL. There are 2 ways to determine PDF of V, Fr, and Fl, first is based on convolution of independent random variables with known PDF for the linearized equation, second is based

on Monte Carlo simulation (MCS) with known PDF of random variables for differential equation.

The first method is based on assumptions that may be far from the real situation, while the second method, even though accuracy and realization is better, requires much computational time [22].

A Monte Carlo simulation can compute the random state variables from the differential equations. Monte Carlo simulation will randomly generate sample values with known probability distribution function and solve the differential equations iteratively. Number of calculation normally should large enough (May be more than 1,000 iterations) for statistical reason of accuracy. Therefore, large spend of computational time and effort. However, advantages of probabilistic methods still be attractive for improvement the understanding of PS and PQ incorporating wind power.

MCS is the method used to compute PDF of output unknown variables by generating (or sampling) input random variables with known PDF. Since MCS has high probabilistic accuracy and highly acceptable, therefore, this thesis will use Monte Carlo simulation method to analyze voltage fluctuation, frequency fluctuation and flicker.

Examples of probability distributions of voltage with load varying at different times by sampling P, Q (from mean and variance data) at each node and switched capacitor (from probability distribution) at each hour are presented in Figures 1.35 – 1.37 [14].

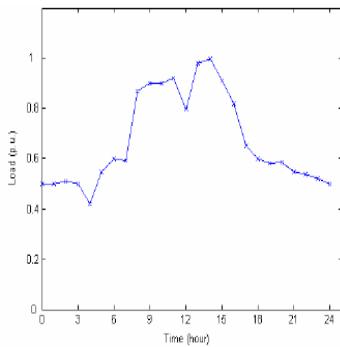


Figure 1.35 Daily time varying load pattern

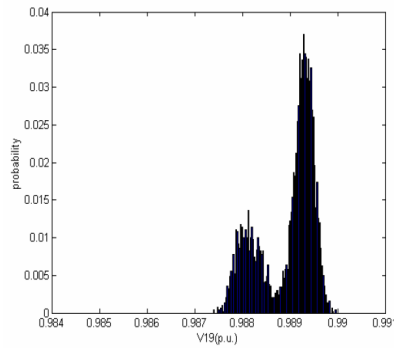


Figure 1.36 Probability distribution of voltage at 2 a.m.

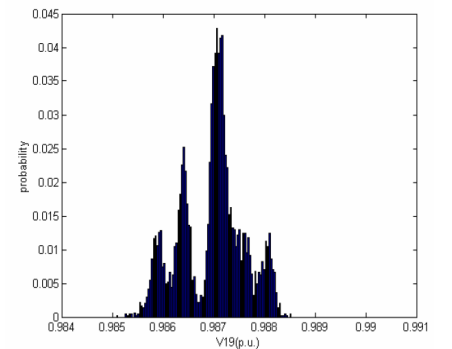


Table37 Probability distribution of voltage at 2 p.m.

1.2.7 Conclusions of Literature Review

For power system stability, the major impacts of wind power to power system are dynamic stability and voltage stability due to the continuous random fluctuation of wind power causing cumulative effects on the system performance, especially the voltage and

synchronization. Transient stability, even though important, occurs infrequently. For frequency stability, instability can occur when large amount of wind power loss during high load demand. If wind potential is low to medium, therefore, small amount wind power loss can cause small possibility of frequency instability.

For dynamic and voltage stability, MFPT is a proper indicator to quantify the level of stability based on SDE theory. Previous studies are not given details of the wind speed, wind power or any different technology influencing stability of the power system. Therefore, it is a challenge for any future research to apply this method for a study of Effects of wind energy on power system stability with more details of wind characteristics, random fluctuate wind power, and the others concerning factors.

For power quality problems, random variations of wind power lead to variations of active and reactive power, and cause frequency and voltage fluctuations, respectively. The theory of SDE even though, can compute MFPT but cannot easily calculate system parameters with uncertainty. However, if deterministic variables with known PDF can be specified, therefore, PDF of non-deterministic variables can be computed using analytical probabilistic method or Monte Carlo simulation method.

Power system stability indicators and analytical methods for deterministic and probabilistic methods are summarized in Table 1.3.

Table 1.3 Deterministic indices and analytical methods of power system stability

Disturbance	Type of stability	Stability indices	Analyzing methods
Large disturbances	Voltage stability	Voltage drop or rise with duration	Dynamics numerical method
	Transient stability	Area under power curve	Equal-area criterion
		Critical clearing time (CCT), and angle	Dynamics numerical method
		Critical energy (CE) of instability	Direct method
	Frequency stability	Frequency drop or rise with duration	Dynamics numerical method
Small disturbances	Small signal (Dynamics)	Eigenvalue of system characteristics matrix	Eigenvalue , Eigenvector analysis with linearized model
	Voltage stability	V - Q sensitivity	Newton-Raphson iterative method
		Eigenvalue of Q - V modal sensitivity	Eigenvalue , Eigenvector analysis
		Point of Collapse	Bifurcation analysis

Table 1.4 Probabilistic indices and analytical methods of power system stability

Disturbance	Type of stability	Stability indices	Analyzing methods
Large disturbances	Voltage stability	-	-
	Transient stability	$P(CT < CCT)$ (line fault)	1) Equal area criterion 2) Dynamics simulation
	Frequency stability	-	-
Small disturbances	Dynamics stability (small signal stability)	$P(\lambda < 0)$ of linearized system	Eigenvalue analysis with multivariate random variables
		MFPT	Stochastic differential equation
	Voltage stability (Voltage collapse)	Stochastic voltage collapse indicator	Stochastic differential equation

Generally, the deterministic method, called eigenvalue analysis, is used for the study of small signal stability of the power system incorporating wind power, for example, the studies of Thomas Ackermann (2005), T.R. Ayodele et al. (2010) and J.L. Rueda and F. Shewarega (2009). However, this method uses the linearization technique to approximate nonlinear characteristics of the system and lose key information as a result. Even though, there are many attempts to include the probabilistic characteristics in the SSS analysis, such as in [54], [75], and [62] but these studies still based on linearization eigenvalue analysis method.

Another probabilistic method, such as Monte Carlo Simulation (MCS), has been applied to study the nonlinear and random characteristics of the power system, for example in R. Billinton and W. Li (1994) and Z. Xu et al. (2005), but it consumes much time and computational resources. Alternatively, the stochastic techniques, such as in [11], [2], and [28], have been developed and applied for power system stability analysis using stochastic stability theory of exit time [74]. However, these techniques are based on the simplified (quadratic) energy function which is not proper for induction generator of wind turbine.

Recently, there is an alternative technique to study the effects of wind power using stochastic stability analysis method [47]. This technique can characterize a nonlinear power system including stochastic wind power while consumes less time and computational resource. Nevertheless, that paper used the simplified induction generator (IG) wind turbine in the model which is not the major share of the market and may miss the significant effects due to the different technology.

Therefore, this paper aims to study the effects of DFIG wind turbines on the stability of the power system using the stochastic stability analysis method.

1.3 Research Objectives

To quantitatively assess the effects of wind energy on the power quality and the stability of the power system using probabilistic methods to incorporate the stochastic characteristics of wind power.

Scope of Thesis

- 1) The probabilistic methods were developed for the purpose of assessing the effect of wind power on power quality and stability of the power system to incorporate the stochastic characteristics of winds.
- 2) The designed power system is based on the standard test system as a main part and with case study of Thailand as addition.
- 3) The wind power system models have been selected from suitable published studies. Fixed Speed Induction Generator (FSIG) and Doubly-Fed Induction Generator (DFIG) will be used in this research.
- 4) For power system stability analysis, dynamic stability and voltage stability are the major parts of interest for this study. The theory of Stochastic Differential Equations will be applied for power system stability analysis.
- 5) For power quality, over/under magnitude from fluctuations of voltage and frequency are the major part of interest for this research. Monte Carlo simulation and analytical probabilistic method were used for power quality analysis.

CHAPTER 2

THEORIES

From the objectives and scopes of thesis, to design the methodology for the study, it is necessary to understand the theoretical background of the power system stability, the power quality, the wind power characteristics, and the probabilistic methods. This chapter reviews these theoretical backgrounds, which are

The Power System: Consists of (1) the generator model, (2) the transformer model, and (3) the transmission line model.

Power System Stability Classification: Consists of (1) Rotor angle stability, (2) Small signal instability, (3) Transient stability, (4) Voltage stability, and (5) Frequency stability.

Wind Power: Consists of (1) Estimation of wind power, (2) Probability distribution of wind,

(3) Wind turbine technology, (4) Wind Turbine Type and Classification, (5) Wind power models, and (6) Wind Power and Power quality.

Probabilistic Methods for the Power System: Consists of (1) Random variables, (2) Stochastic processes, (3) Stochastic differential equation, and (4) Monte Carlo simulation.

Energy Function Methods: Consists of (1) Lyapunov's theory of stability, (2) Modeling aspects for stability problems, (3) Potential energy boundary surface (PEBS) method, and (4) Boundary controlling unstable equilibrium point (BCU) method (5) Critical energy estimation, and (6) Well-defined energy function formulation using the first integral method.

2.1 The Power System

Structure of the power system, which is represented in Figure 2.1, consists of

- **Generation Unit:** the generator (synchronous and/or induction generators), which converts kinetic energy into electric potential energy.
- **Transmission Unit:** the electrical network, which transfers energy from the generation unit to the distribution unit. It includes transformers, electrical wires, and electrical control and protection equipment.

- **Distribution Unit:** the electrical network which receives energy from the transmission unit and distributes to its customers. It includes transformers, electrical wires, and electrical control and protection equipment.

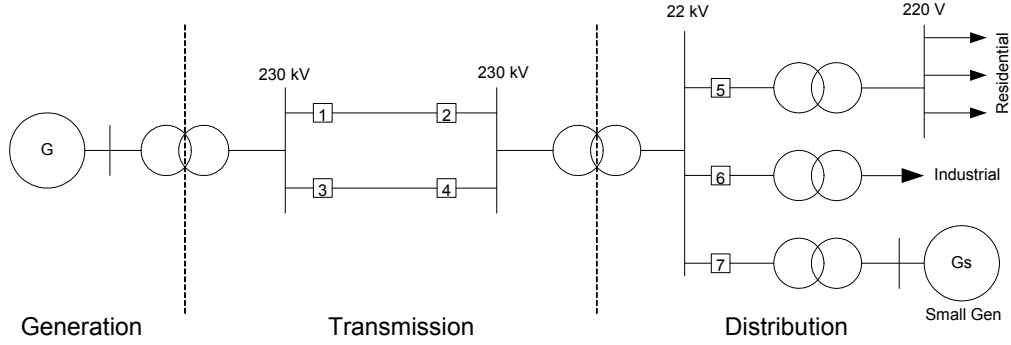


Figure 2.1 Structure of the power system

The main components focused on the study of power system stability, are the generator, transformer, and transmission line. The model of each component is described below.

2.1.1 Generator Model

The principle of the generator is based on the magnetic theory of Maxwell, which explains the relation between the magnetic field and the electric field as follows.

$\Delta \cdot B = 0$	B is magnetic flux density
$\Delta \cdot D = \rho$	D is electric field flux density
$\Delta \times H = J + \frac{\partial D}{\partial t}$	ρ is charge distribution
$\Delta \times \varepsilon = -\frac{\partial B}{\partial t}$	H is magnetic field intensity
Ampere's law $\oint H \cdot dl = \int_s J da = Ni$	J is current density
Faraday's law $\oint \varepsilon \cdot dl = -\int_s \frac{\partial B}{\partial t} \cdot da$	ε is electric field intensity
	l is length path of H
	i is current
	a is cross section area (s)
	N is turns of coil

From Ampere's law, moving charges induce magnetomotive force ($mmf = Ni$)

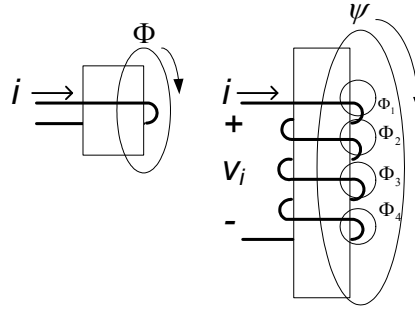


Figure 2.2 Current induces magnetic flux on solenoid

Where magnetic flux $\int_s B da = \Phi$ and for N turns of coil, total magnetic flux (flux linkage) is

$$\psi = \Phi_1 + \Phi_2 + \Phi_3 + \Phi_4 = N\Phi \quad \text{Eq. 2-1}$$

From Faraday's law, variation of magnetic flux induces electric field with induced voltage, v_i as follows:

$$v_i = \frac{d\psi}{dt} \quad \text{Eq. 2-2}$$

Flux linkage can be presented in terms of inductance L and current i as follows:

$$\psi = Li \quad \text{Eq. 2-3}$$

Maxwell's equations and Eqs. 2-1 – 2-3 are used to explain the characteristics of the generator and transformer in the following sections.

The generator transforms kinetic energy into electromagnetic energy. The rotating turbine causes magnetic field on field circuit (on the rotor or stator) to vary periodically. By Faraday's law, variation of magnetic flux induces electric field and voltage on armature circuit. The different type of generator depends on the design of rotor and stator corresponding to source of magnetic field and armature circuit.

The two types of generators discussed are synchronous generators, and asynchronous or induction generators.

2.1.1.1 Synchronous generators

For synchronous generators, the electrical frequency is synchronized with the mechanical rate of rotation of the generator.

$$n_s = \frac{120f}{p} \quad \text{Eq. 2-4}$$

Where f is electrical frequency (Hz), n_s is mechanical speed (or synchronous speed) of magnetic field (rpm), and p is number of poles.

The generator consists of two main parts, the field and the armature. The dc current is supplied to the field winding on the rotor and induces a magnetic field which N pole for d-axis and its quadrature is q-axis. The three phases system corresponds to the a-a', b-b', and c-c' armature windings. Axis of phase a is 90° with the a-a' winding while axis of phase b and c is 120° counterclockwise shift and clockwise shift, respectively and be presented in below figure. [52]

The dc current is from an external source or from a special circuit on the rotor shaft. The external source supplies dc current through slip ring or brushes which suitable for small machine since it is cost effective even though require maintenance and cause voltage drop on brushes. The special circuit, or called *brushless exciter*, consists of exciter field on the stator and exciter armature on the rotor. Rotating of rotor induces ac current on exciter armature which is converted to be dc current by 3 phase rectifier and then supply for the main field circuit on the rotor. The power supplied to an exciter field is from an external power source or from a permanent magnet circuit.

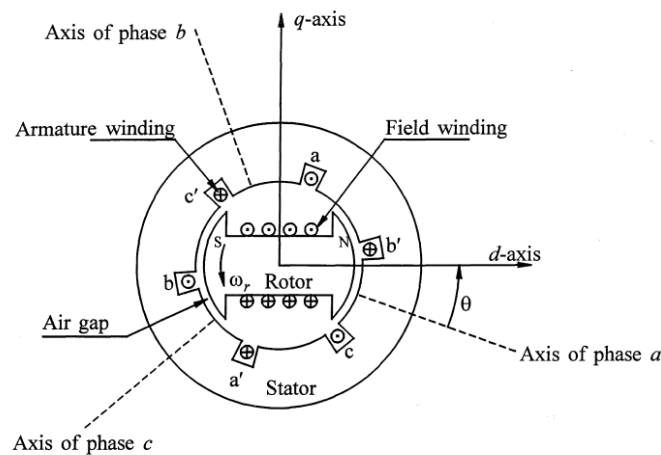


Figure 2.3 Schematic diagram of a three-phase synchronous machine

There are two rotor structures, depending on the operating speed. For low rotational speeds, such as wind turbines and hydraulic turbines, a salient pole rotor with a large number of poles is required to achieve the rated frequency. For the high speed such as steam or gas turbines, a round rotor (non-salient) with 2 or 4 poles is required.

The salient pole rotor always has damper windings or *amortisseurs* at the end ring to damp out speed oscillations and eddy current losses. Non-salient pole rotors, even

though without damper windings but a solid steel rotor, offers paths for eddy currents that affect amortisseur currents equivalently.

Therefore, the rotor circuits consist of a d-axis field circuit and d, q-axis amortisseur circuits. The stator circuits consist of a, b, c phase windings. However, for calculating convenience, the a, b, c phase winding can be presented in d and q-axis using d-q-0 transformation function. Stator and rotor circuit of a synchronous machine are presented in next figure [52].

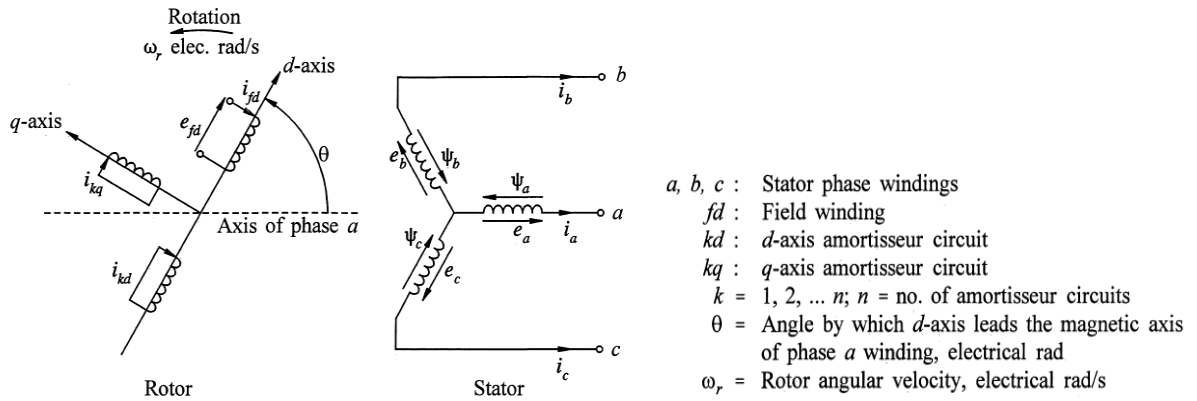


Figure 2.4 Stator and rotor circuit of a synchronous machine [52]

For the per unit system, the electrical equations of synchronous generator are presented as follows [52].

Per unit inductance L

$$\left. \begin{aligned} L_{afd} &= L_{fda} = L_{akd} = L_{kda} = L_{ad} \\ L_{akq} &= L_{kqa} = L_{aq} \\ L_{fkd} &= L_{kdf} \end{aligned} \right\}$$

Eq. 2-5

Per unit stator voltage equations

$$\left. \begin{aligned} v_d &= \dot{\psi}_d - \psi_q \omega_r - R_a i_d \\ v_q &= \dot{\psi}_q + \psi_d \omega_r - R_a i_q \\ v_0 &= \dot{\psi}_0 - R_a i_0 \end{aligned} \right\}$$

Eq. 2-7

Per unit air-gap torque

$$T_e = \psi_d i_q - \psi_q i_d \quad \text{Eq. 2-6}$$

Per unit rotor voltage equations

$$\left. \begin{aligned} v_{fd} &= \dot{\psi}_{fd} + R_{fd} i_{fd} \\ 0 &= \dot{\psi}_{1d} + R_{1d} i_{1d} \\ 0 &= \dot{\psi}_{1q} + R_{1q} i_{1q} \\ 0 &= \dot{\psi}_{2q} + R_{2q} i_{2q} \end{aligned} \right\}$$

Eq. 2-8

Per unit stator flux linkage equations

$$\left. \begin{aligned} \psi_d &= -(L_{ad} + L_l)i_d + L_{ad}i_{fd} + L_{ad}i_{1d} \\ \psi_q &= -(L_{aq} + L_l)i_q + L_{aq}i_{1q} + L_{aq}i_{2q} \\ \psi_0 &= -L_0i_0 \end{aligned} \right\} \text{Eq. 2-9}$$

Per unit rotor flux linkage equations

$$\left. \begin{aligned} \psi_{fd} &= L_{ffd}i_{fd} + L_{f1d}i_{1d} - L_{ad}i_d \\ \psi_{1d} &= L_{f1d}i_{fd} + L_{11d}i_{1d} - L_{ad}i_d \\ \psi_{1q} &= L_{11q}i_{1q} + L_{aq}i_{2q} - L_{aq}i_q \\ \psi_{2q} &= L_{aq}i_{1q} + L_{22q}i_{2q} - L_{aq}i_q \end{aligned} \right\} \text{Eq. 2-10}$$

Where fd is for field circuit d-axis, $1d$ is for amortisseur circuit no. 1 in d-axis, $1q$ and $2q$ are for amortisseur circuits no. 1 and no. 2 in q-axis, ffd is for the value of field circuit, $f1d$ is for the value between field and $1d$ circuit, and $11d$ and $22q$ are for the values of $1d$ and $2q$ circuit.

2.1.1.2 Induction (or Asynchronous) generators

For induction generators, alternating current is supplied to the stator winding, which induces alternating current in the rotor winding. This is the same as a concept of transformer. There are two main types of induction generator: (1) the squirrel cage induction generator (SCIG), and (2) the wound rotor induction generator (WRIG). For SCIG, the conducting bars at both end of rotor are shorted circuit and look like a cage. For WRIG, a rotor winding with terminals are brought out to slip rings for external connection.

First, the 3-phase current in the stator winding produces a rotating magnetic field in the air gap of the machine. The rotating magnetic field induces voltage in conductor bars of rotor. The induced voltage produces rotor current which interact with magnetic field in the air gap to produces torque. The rotor starts to rotate in the direction of magnetic field. If rotational speed of rotor (n) is less than synchronous speed (n_s), then the motor mode is applied with speed n . If $n > n_s$, the generator mode is applied. But if $n = n_s$, then there will be no torque and no induced current.

The rotational speed of the rotor (n) is always expressed in the form of a fraction of the synchronous speed or called *slip* (s) as follows:

$$s = \frac{n_s - n}{n_s} \quad \text{Eq. 2-11}$$

Where $n_s = 120f/p$.

System equations of induction generator consist of at least the voltage equations, flux linkage equations, and torque equations.

For example, per unit voltage equations of a squirrel cage induction generator (SCIG) in the d-q (direct-quadrature) reference frame, is as follows [67]:

$$\left. \begin{aligned} u_{ds} &= -R_s i_{ds} - \omega_s \psi_{qs} + \frac{d\psi_{ds}}{dt} \\ u_{qs} &= -R_s i_{qs} + \omega_s \psi_{ds} + \frac{d\psi_{qs}}{dt} \\ u_{dr} &= 0 = -R_r i_{dr} - s\omega_s \psi_{qr} + \frac{d\psi_{dr}}{dt} \\ u_{qr} &= 0 = -R_r i_{qr} + \omega_s \psi_{dr} + \frac{d\psi_{qr}}{dt} \end{aligned} \right\} \quad \text{Eq. 2-12}$$

Where u is voltage, subscript s and r are for stator and rotor, R is the resistance, i is the current, ω_s is the synchronous speed, ψ is the flux, and s is the slip.

The slip, s , is defined as follows

$$s = 1 - \frac{p}{2} \frac{\omega_m}{\omega_s} \quad \text{Eq. 2-13}$$

Where p is the number of poles and ω_m is angular frequency of generator rotor.

The flux linkages can be determined as follows

$$\left. \begin{aligned} \psi_{ds} &= -(L_{s\sigma} + L_m)i_{ds} - L_m i_{dr} \\ \psi_{qs} &= -(L_{s\sigma} + L_m)i_{qs} - L_m i_{qr} \\ \psi_{dr} &= -(L_{r\sigma} + L_m)i_{dr} - L_m i_{ds} \\ \psi_{qr} &= -(L_{r\sigma} + L_m)i_{qr} - L_m i_{qs} \end{aligned} \right\} \quad \text{Eq. 2-14}$$

Where L is the inductance and subscript σ and m are leakage and mutual, respectively.

The electrical torque is $T_e = \psi_{qr} i_{dr} - \psi_{dr} i_{qr}$ Eq. 2-15

The equation of motion is $\frac{d\omega_m}{dt} = \frac{1}{2H_m} (T_m - T_e)$ Eq. 2-16

The equation of active (P) and reactive power (Q) consumed are as follows

$$\left. \begin{aligned} P_s &= u_{ds} i_{ds} + u_{qs} i_{qs} \\ Q_s &= u_{qs} i_{ds} - u_{ds} i_{qs} \end{aligned} \right\} \quad \text{Eq. 2-17}$$

2.1.2 Transformer Model

From Ampere's law, the moving charge induces magnetomotive force ($mmf = Ni$). For a two-winding transformer, the input current of primary winding induces magnetic fluxes which consist of mutual flux Φ_m linking between primary and secondary winding, leakage flux Φ_{L1} and Φ_{L2} linking only primary and secondary circuit, respectively.

In case of ideal transformer, there are no losses, no leakage fluxes, and magnetic core has infinite permeability. The physical power transformer is close to the ideal with

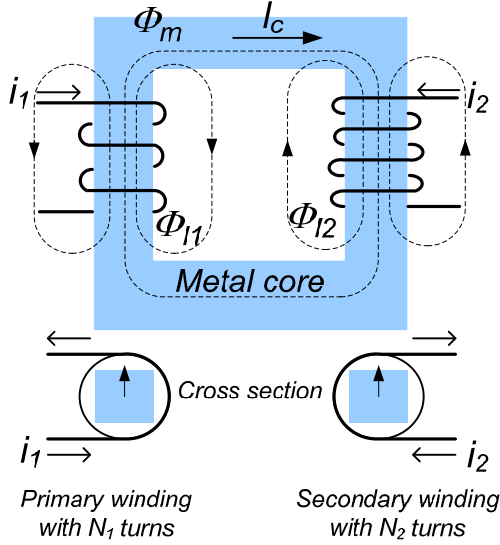
losses about 0.5% of rating, leakage fluxes about 5% of the mutual flux, and high permeability of special alloy steels.

If an ideal transformer is assumed, the flux linkages (λ) are as follows:

$$\text{For primary winding} \quad \lambda_1 = N_1(\Phi_m + \Phi_{L1}) = N_1\Phi_m \quad \text{Eq. 2-18}$$

$$\text{For secondary winding} \quad \lambda_2 = N_2(\Phi_m + \Phi_{L2}) = N_2\Phi_m \quad \text{Eq. 2-19}$$

The schematic diagram of a two-winding transformer is presented in the next figure.



$$\oint H \cdot dl = Hl = Ni \quad \text{Eq. 2-20}$$

$$B = \mu H = \mu_r \mu_0 H \quad \text{Eq. 2-21}$$

$$\int_s B da = \Phi \quad \text{or} \quad BA = \Phi \quad \text{Eq. 2-22}$$

$$\oint H_c \cdot dl = H_c l_c = N_1 i_1 + N_2 i_2 \quad \text{Eq. 2-23}$$

Figure 2.5 Schematic diagram of two-winding transformer

Where l_c is the path length along the metal core, l_g is the path length across air gap, H_c is magnetic field intensity along l_c , H_g is magnetic field intensity along l_g , R_c and R_g are reluctances.

Variation of linkage flux (mutual flux) induces the terminal voltages (v) as follows:

$$\text{For primary winding} \quad v_1 = \frac{d\lambda_1}{dt} = N_1 \frac{d\Phi_m}{dt} \quad \text{Eq. 2-24}$$

$$\text{For secondary winding} \quad v_2 = \frac{d\lambda_2}{dt} = N_2 \frac{d\Phi_m}{dt} \quad \text{Eq. 2-25}$$

The voltage gain $v_2 / v_1 = N_2 / N_1 = n$ is called *transformer turns ratio*.

For an ideal transformer in the above figure, the primary and secondary magnetomotive forces (mmfs) are added to yield the total magnetomotive force as follows:

$$F = \Phi_m \frac{l_c}{\mu_c A_c} = N_1 i_1 + N_2 i_2 = \Phi_m \mathfrak{R}_c = mmf \quad \text{Eq. 2-26}$$

where \mathfrak{R}_c is the reluctance of the core.

For the ideal transformer, the core has infinite permeability, thus the reluctance is zero. Consequently, $i_2 / i_1 = -N_1 / N_2 = -1/n = -a$. If i_2 is assumed with the opposite direction, therefore, $i_2 / i_1 = N_1 / N_2 = 1/n = a$.

2.1.3 Transmission Line Model

Transmission line can be represented in terms of phasor and impedance as follows:

$$z = r + j\omega l = \text{series impedance per meter}$$

$$y = g + j\omega c = \text{shunt admittance per meter to neutral}$$

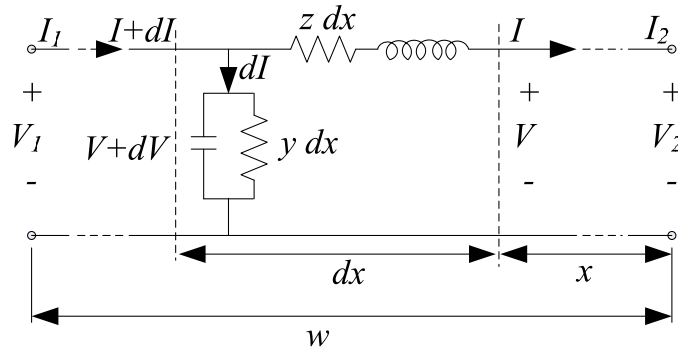


Figure 2.6 Transmission line circuit diagram

Applying Kirchhoff's voltage law and current law to the above figure yields

$$\begin{aligned} dV &= I(z dx) \\ dI &= (V + dV)y dx \approx V(y dx) \end{aligned} \quad \text{Eq. 2-27}$$

Since the product of the derivative part dV is neglected, the first-order linear differential equations are

$$\frac{dV}{dx} = Iz, \quad \frac{dI}{dx} = Vy \quad \text{Eq. 2-28}$$

The second order linear differential equations are

$$\frac{d^2 V}{dx^2} = yzV, \quad \frac{d^2 I}{dx^2} = yzI = u^2 I \quad \text{Eq. 2-29}$$

where $u = (yz)^{0.5}$ is called the *propagation constant*.

For the lumped-circuit equivalent, a Π -equivalent is assumed with parameters A, B, C, and D from the equations as follows:

$$V_1 = AV_2 + BI_2$$

$$I_1 = CV_2 + DI_2$$

where $(z/y)^{0.5} = Z_c$, $A = \cosh uw$, $B = Z_c \sinh uw$, $C = \sinh uw / Z_c$, $D = \cosh uw$.

The diagram of a Π -equivalent circuit and corresponding equations are presented as follows.

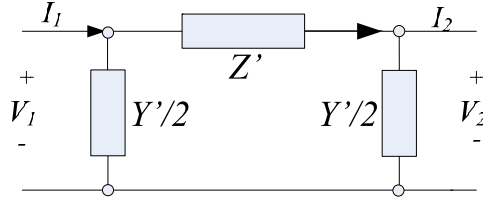


Figure 2.7 Schematic diagram of Π -equivalent circuit

Therefore:
$$V_1 = V_2 + Z' \left(I_2 + \frac{Y'}{2} V_2 \right) = \left(1 + \frac{Z'Y'}{2} \right) V_2 + Z'I_2 \quad \text{Eq. 2-30}$$

$$I_1 = \frac{Y'}{2} V_1 + \frac{Y'}{2} V_2 + I_2 = Y' \left(1 + \frac{Z'Y'}{4} \right) V_2 + \left(1 + \frac{Z'Y'}{2} \right) I_2 \quad \text{Eq. 2-31}$$

where

$$A = 1 + \frac{Z'Y'}{2}, \quad B = Z', \quad C = Y' \left(1 + \frac{Z'Y'}{4} \right), \quad D = 1 + \frac{Z'Y'}{2} \quad \text{Eq. 2-32}$$

Therefore, B is determined as follows:

$$Z' = Z_c \sinh uw = \sqrt{\frac{z}{y}} \sinh uw = zw \frac{\sinh uw}{uw} = Z \frac{\sinh uw}{uw} \quad \text{Eq. 2-33}$$

where $Z = zw$, and A is determined as:

$$A = 1 + \frac{Z'Y'}{2} = \cosh uw \quad \text{Eq. 2-34}$$

$$\frac{Y'}{2} = \frac{\cosh uw - 1}{Z_c \sinh uw} = \frac{1}{Z_c} \tanh \frac{uw}{2} = \frac{Y}{2} \frac{\tanh(uw/2)}{(uw/2)} \quad \text{Eq. 2-35}$$

where $Y = yw$. For $uw \ll 1$, $\tanh(uw/2) / (uw/2) \approx 1$, therefore, $Y'/2 = Y/2$.

2.2 Power System Stability Classification

Power system stability can be classified by the affected state variables, the scale of disturbance, and the duration of phenomena as represented in the following figure.

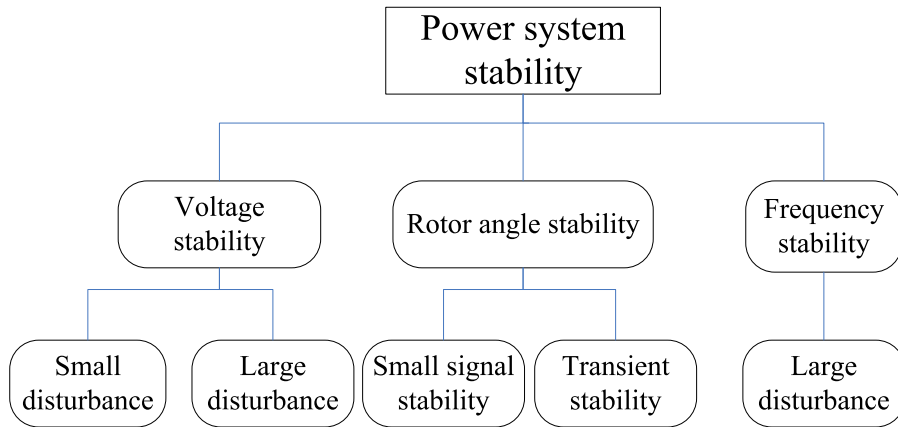


Figure 2.8 Classification of power system stability

Rotor angle stability is the ability of the power system to control the synchronization of generators or to control the rotor angle of generators when disturbed by transient and small signal.

The small signal instability is the cumulative effect on the steady state system due to the small but continuous perturbation of the input parameters and the responsive characteristic of the system which can push the state parameters (such as rotor angle of generator) and/or output parameters (such as voltage and current output of generator) away from the operating point until system lost control (or desynchronizations).

Transient stability is the ability of the power system to maintain the synchronization of generators or to balance the mechanical torque and electromagnetic torque after subjection to large and instant disturbance of voltage, current, and power.

Voltage stability is the ability of the power system to maintain or control voltage during normal operation and at given initial conditions, after subjection to disturbances. It depends on the ability to restore equilibrium between load demand and supply of the power system. The result may be voltage progressive drop or rise and finally loss of load in some areas. Voltage stability is concerned with load stability while rotor angle stability is concerned with generator stability.

Frequency stability is the ability of the power system to maintain or control frequency, during normal operation and at given initial conditions, after subjection to disturbances. The characteristics time of frequency stability range from several second corresponding to the response of devices such as generators control and protection, to several minutes corresponding to the response of devices such as prime mover systems and load voltage regulators. Frequency stability is classified as large disturbance with long-term stability

due to the characteristic time of the overall islanding is range from seconds to several minutes.

2.3 Small Signal Stability

Small disturbances, if they occur continuously, can cause the generator to lose synchronization, limit of power transfer on the transmission system, and highly stress the mechanical shaft. The effects of small disturbance on the power system are explained as follows:

- Loss of synchronization from steady increase and/or diverging oscillation of rotor angle

For under-loaded conditions, the small and continuous disturbance causes the rotor angle to swing continuously. If the damping torque is insufficient, the rotor angle will swing or oscillate with increasing of amplitude and finally uncontrollable or unstable.

For overloaded conditions, the small and continuous disturbance causes the rotor angle to increase continuously. If synchronizing torque is insufficient, the rotor angle will increase continuously and finally unstable.

These two conditions are the major effects of the small disturbance on the power system. However, the case underloaded condition can be found mainly under normal operating condition.

- Limit the power transfer of the transmission system

For machine with damper winding, the damping torque coefficient decrease with increasing power and rotor angle. Therefore, to avoid small signal instability, the power cannot be generated at maximum value. Furthermore, the larger impedance of transmission line causes the power-angle relationship move to the left with smaller maximum value. If small signal occur in such case, more power transfer is limited to avoid the instability situation.

- Increase stress on the mechanical shaft

Under mechanical dynamic condition, the larger number of shaft mass cause an increasing of swing amplitude of shaft. If fluctuating small signal resonance with natural frequency of multi-mass shaft, highly stress can be formed on the shaft and finally can harm the shaft.

Sources and involving factors of small disturbance

Sources and involving factors of small disturbances can be considered as external and internal sources/factors. For example:

External sources/factors:

- Load variation
- Variation of other fluctuating power sources
- Multi-machine synchronization and interaction

Internal sources/factors

- Response of turbine governor
- Response of excitation voltage system control
- Damper winding
- Effect of rotor flux linkage variation on the electrical power generation

The small signal instability is the cumulative effect on the steady-state system due to the small, but continuous perturbation of the input parameters and the responsive characteristic of the system, which can push the state parameters (such as rotor angle of generator) and/or output parameters (such as voltage and current output of generator) away from the operating point until the system loses control (or desynchronizations) finally.

This cumulative effect can cause oscillation or non-oscillation of state parameters (rotor angle) depending on synchronizing force and damping on force characteristics of the system. Insufficient of synchronizing torque can lead to oscillation of rotor angle while insufficient of damping torque can cause the divergence of rotor angle from operating point.

The input parameters are, for example, mechanical torque of generator, voltage sources and/or current sources. The state parameters are, for example, rotor angle (δ), rotational speed of rotor (ω_r), flux linkage of field circuit (Ψ_{fd}), controlled voltage of excitation system, and controlled voltage of power stabilizer. The output parameters are, for example, voltage, current, active and reactive power.

To understand the responsive characteristics of the steady state system, the linearized state space equations will be represented in the following forms.

$$\dot{X}=AX + BU \quad \text{Eq. 2-36}$$

$$Y=CX + DU \quad \text{Eq. 2-37}$$

Using Laplace transformations, Eqs. 2-36 and 2-37 become

$$sX(s) = AX(s) + BU(s) \text{ and } X(s) = (sI - A)^{-1}BU(s) \quad \text{Eq. 2-38}$$

$$Y(s) = CX(s) + DU(s) \text{ and } Y(s) = [C(sI - A)^{-1}B + D]U(s) \quad \text{Eq. 2-39}$$

Or: $X(s) / U(s) = A'(s) = (sI - A)^{-1}B \quad \text{Eq. 2-40}$

$$Y(s) / U(s) = T(s) = C(sI - A)^{-1}B + D \quad \text{Eq. 2-41}$$

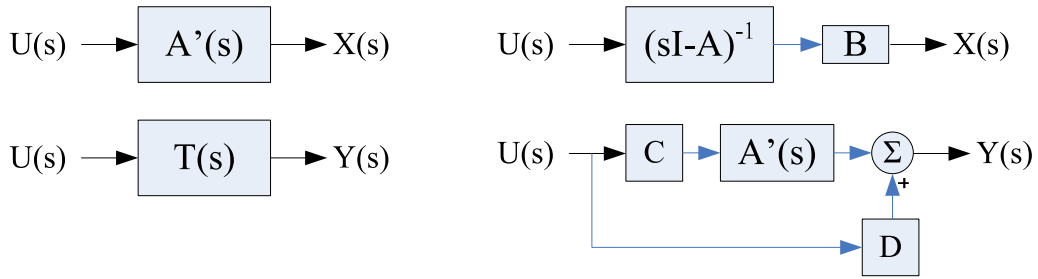


Figure 2.9 Block diagram representing state variables vector

2.3.1 Small signal stability analysis

To analyze the characteristics of the steady state stability, the linearized state space equations are represented in the following forms.

$$\Delta \dot{\mathbf{x}} = \mathbf{A}\Delta \mathbf{x} + \mathbf{B}\Delta \mathbf{u} \quad \text{Eq. 2-42}$$

$$\Delta \mathbf{y} = \mathbf{C}\Delta \mathbf{x} + \mathbf{D}\Delta \mathbf{u} \quad \text{Eq. 2-43}$$

Using Laplace transformations, Eqs. 2-42 and 2-43 become

$$s\Delta \mathbf{x}(s) = \mathbf{A}\Delta \mathbf{x}(s) + \mathbf{B}\Delta \mathbf{u}(s) \text{ and } \Delta \mathbf{x}(s) = (s\mathbf{I} - \mathbf{A})^{-1}\mathbf{B}\Delta \mathbf{u}(s) \quad \text{Eq. 2-44}$$

$$\Delta \mathbf{y}(s) = \mathbf{C}\Delta \mathbf{x}(s) + \mathbf{D}\Delta \mathbf{u}(s) \text{ and } \Delta \mathbf{y}(s) = [C(s\mathbf{I} - \mathbf{A})^{-1}\mathbf{B} + \mathbf{D}]\Delta \mathbf{u}(s) \quad \text{Eq. 2-45}$$

or $\frac{\Delta \mathbf{x}(s)}{\Delta \mathbf{u}(s)} = \mathbf{A}'(s) = (s\mathbf{I} - \mathbf{A})^{-1}\mathbf{B} \quad \text{Eq. 2-46}$

$$\frac{\Delta \mathbf{y}(s)}{\Delta \mathbf{u}(s)} = \mathbf{T}(s) = \mathbf{C}(s\mathbf{I} - \mathbf{A})^{-1}\mathbf{B} + \mathbf{D} \quad \text{Eq. 2-47}$$

For small signal stability analysis using the eigenvalue method:

- 1) Identify state, input, and output parameters
- 2) Identify state space equations in form of $\Delta \dot{\mathbf{x}} = \mathbf{A}\Delta \mathbf{x} + \mathbf{B}\Delta \mathbf{u}$ and/or $\Delta \mathbf{y} = \mathbf{C}\Delta \mathbf{x} + \mathbf{D}\Delta \mathbf{u}$
- 3) Use Laplace transformations to rearrange to $\Delta \mathbf{x}(s) = (s\mathbf{I} - \mathbf{A})^{-1}\mathbf{B}\Delta \mathbf{u}(s)$ and/or

$$\Delta \mathbf{y}(s) = [C(s\mathbf{I} - \mathbf{A})^{-1}\mathbf{B} + \mathbf{D}]\Delta \mathbf{u}(s)$$

- 4) Identify characteristic functions from $\det(s\mathbf{I} - \mathbf{A}) = 0$
- 5) Find s from characteristic functions and s is called eigenvalues (in case zero input, $sX = AX$ similar to $\lambda X = AX$).
- 6) Find ζ , ω_n , σ , and ω . Synchronizing and damping characteristics of the system depend on these parameters.
- 7) Interpret the results. The system is unstable if
 - $\zeta^2 < 1$, $s = \sigma \pm j\omega$, and $\sigma > 0$ is the case of oscillation with undamped
 - $\zeta^2 > 1$, and $s = \sigma \pm \omega > 0$ is the case of undamped without oscillation
- 8) Interpret the results, the system is stable with oscillation if
 - $\zeta^2 \approx 0$, $\sigma \approx 0$, and $s = \pm j\omega$ is the case of oscillation only
 - $\zeta^2 < 1$, and $s = \sigma \pm j\omega$ is the case of oscillation with damped
- 9) If the system is unstable or oscillated, improve the system by adjusting the parameters of \mathbf{A} .

Example of small signal stability analysis of a simple circuit is represented by the basic circuit diagram in Figure 2.10:

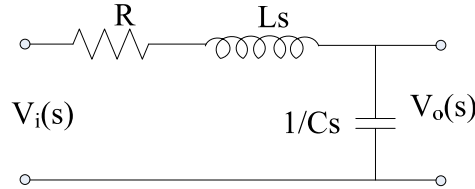


Figure 2.10 Basic circuit diagram for SSS problem

The system equation is represented by using Laplace transformations (for comparison) as follows:

$$\frac{Y(s)}{U(s)} = T(s) = \frac{V_o(s)}{V_i(s)} = \frac{1/Cs}{(R + Ls) + 1/Cs} = \frac{1/LC}{s^2 + Rs/L + 1/LC} \quad \text{Eq. 2-48}$$

For time domain equation:

$$\text{Voltage loop:} \quad V_C = V_o = V_i - V_R - V_L \quad \text{Eq. 2-49}$$

$$i_L = i_C = i_R = i = C dV_o/dt \quad \text{Eq. 2-50}$$

$$V_L = L di_L/dt = LC d^2V_o/dt^2 \quad \text{Eq. 2-51}$$

$$V_R = Ri = RC dV_o/dt \quad \text{Eq. 2-52}$$

Set differential equation: $V_i = LC \frac{dV_o^2}{dt^2} + RC \frac{dV_o}{dt} + V_o$ Eq. 2-53

To compare with the state space equation, if $u = V_i$, $x_1 = y = V_o$, and $\dot{x}_1 = x_2 = dV_o/dt$

$$u = LC\dot{x}_2 + RCx_2 + x_1 \quad \text{or} \quad \dot{x}_2 = -\frac{Rx_2}{L} - \frac{x_1}{LC} + \frac{u}{LC} \quad \text{Eq. 2-54}$$

$$\dot{X} = AX + BU \quad \text{or} \quad \begin{bmatrix} \dot{x}_1 \\ \dot{x}_2 \end{bmatrix} = \begin{bmatrix} 0 & 1 \\ -1/LC & -R/L \end{bmatrix} \begin{bmatrix} x_1 \\ x_2 \end{bmatrix} + \begin{bmatrix} 0 \\ 1/LC \end{bmatrix} u \quad \text{Eq. 2-55}$$

$$Y = CX + DU \quad \text{or} \quad y = \begin{bmatrix} 1 & 0 \end{bmatrix} \begin{bmatrix} x_1 \\ x_2 \end{bmatrix} + 0u \quad \text{Eq. 2-56}$$

Using Laplace transformations for state space equation:

$$X(s) = (sI - A)^{-1}BU(s) \quad \text{or} \quad X(s) = \begin{bmatrix} s & -1 \\ 1/LC & s + R/L \end{bmatrix}^{-1} \begin{bmatrix} 0 \\ 1/LC \end{bmatrix} U(s) \quad \text{Eq. 2-57}$$

$$Y(s) = [C(sI - A)^{-1}B + D]U(s) \quad \text{or} \quad Y(s) = \begin{bmatrix} 1 & 0 \end{bmatrix} \begin{bmatrix} s & -1 \\ 1/LC & s + R/L \end{bmatrix}^{-1} \begin{bmatrix} 0 \\ 1/LC \end{bmatrix} U(s) \quad \text{Eq. 2-58}$$

$$X(s) = \left(\frac{1}{s^2 + sR/L + 1/LC} \right) \begin{bmatrix} s + R/L & 1 \\ -1/LC & s \end{bmatrix} \begin{bmatrix} 0 \\ 1/LC \end{bmatrix} U(s) \quad \text{Eq. 2-59}$$

$$Y(s) = \left(\frac{1}{s^2 + sR/L + 1/LC} \right) \begin{bmatrix} 1 & 0 \end{bmatrix} \begin{bmatrix} s + R/L & 1 \\ -1/LC & s \end{bmatrix} \begin{bmatrix} 0 \\ 1/LC \end{bmatrix} U(s) \quad \text{Eq. 2-60}$$

$$X(s) = \left(\frac{1/LC}{s^2 + sR/L + 1/LC} \right) \begin{bmatrix} 1 \\ s \end{bmatrix} U(s) \quad \text{Eq. 2-61}$$

$$Y(s) = \left(\frac{1/LC}{s^2 + sR/L + 1/LC} \right) U(s) \quad \text{Eq. 2-62}$$

From the term in the brackets in Eq. 2-6, replacing with the damping ratio (ζ), natural frequency (ω_n) and represent in the form:

$$\frac{\omega_n^2}{s^2 + 2\zeta\omega_n s + \omega_n^2} \quad \text{where } \omega_n = 1/\sqrt{LC}, \text{ and } \zeta = \frac{R}{2L\omega_n}$$

The term $\det(sI - A)$ will become the characterized equation of the system:

$$\text{Therefore:} \quad s^2 + 2\zeta\omega_n s + \omega_n^2 = 0 \quad \text{Eq. 2-63}$$

$$\text{Identify } s: \quad s = \frac{-\zeta\omega_n \pm \sqrt{(2\zeta\omega_n)^2 - 4\omega_n^2}}{2} \quad \text{or} \quad s = -\zeta\omega_n \pm \omega_n\sqrt{\zeta^2 - 1} \quad \text{Eq. 2-64}$$

If $\zeta^2 > 1$, $R > 2L/\sqrt{LC}$, therefore $s = \sigma \pm \omega$ where $\sigma = -\zeta\omega_n$ and $\omega = \omega_n\sqrt{\zeta^2 - 1}$

If $\zeta^2 = 1$, $R = 2L/\sqrt{LC}$, therefore $(s - \sigma)^2 = 0$ where $\sigma = -\omega_n$ and $\omega = 0$

If $\zeta^2 < 1$, $R < 2L/\sqrt{LC}$, therefore $s = \sigma \pm j\omega$ where $\sigma = -\zeta\omega_n$ and $\omega = \omega_n\sqrt{1 - \zeta^2}$

If $\zeta^2 \approx 0$, $R \ll 2L/\sqrt{LC}$, therefore $s = \pm j\omega$ where $\sigma \approx 0$ and $\omega = \omega_n$

$$\text{where } \sigma = -R/2L \quad \text{and} \quad \omega = \frac{1}{2L}\sqrt{R^2 - \frac{2}{C}} \quad \text{for } \zeta^2 > 1,$$

$$\text{and} \quad \omega = \frac{1}{2L}\sqrt{\frac{2}{C} - R^2} \quad \text{for } \zeta^2 < 1$$

$$(s - \sigma + j\omega)(s - \sigma - j\omega) = s^2 - 2\sigma s + \sigma^2 + \omega^2 = 0 \quad \text{and} \quad \omega_n^2 = \sigma^2 + \omega^2$$

Assume $V_i(s)$ is $1/s$ that is called the step function, thus:

$$V_o(s) = V_i(s)T(s) = \frac{1}{s} \frac{\sigma^2 + \omega^2}{(s - \sigma + j\omega)(s - \sigma - j\omega)} = \frac{k_1}{s} + \frac{k_2}{s - \sigma + j\omega} + \frac{k_3}{s - \sigma - j\omega} \quad \text{Eq. 2-65}$$

With inverse Laplace transformation, the above equation becomes:

$$V_o(t) = k_1 + k_2 e^{(\sigma + j\omega)t} + k_3 e^{(\sigma - j\omega)t} \quad \text{Eq. 2-66}$$

Term k_1 is force response and terms $k_2 e^{(\sigma + j\omega)t}$ and $k_3 e^{(\sigma - j\omega)t}$ are natural responses.

Example of eigenvalues and phase portraits are represented in Table 2.1.

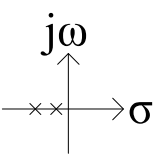
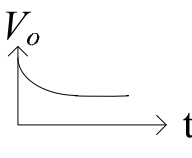
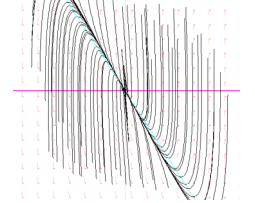
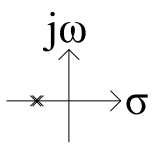
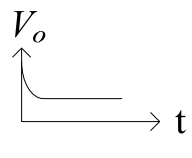
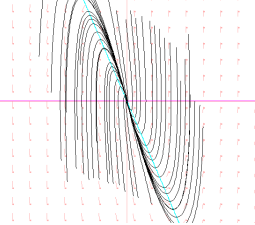
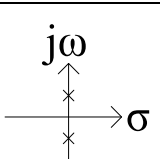
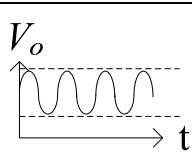
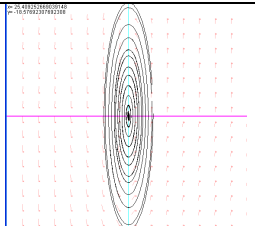
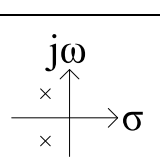
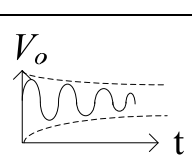
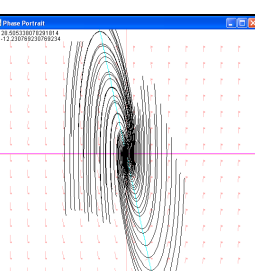
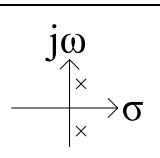
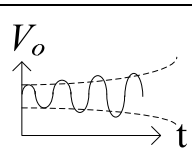
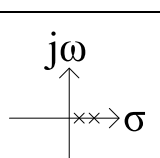
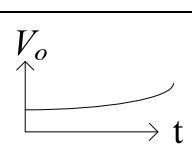
2.4 Transient stability

Transient stability is the ability of the power system to maintain the synchronization of the generators, or to balance the mechanical and electromagnetic torques after subjection to large and instantaneous disturbances of voltage, current, and power.

Factors influencing transient stability are, for example,

- Percentage of generated power of generator
- Fault location and type
- The fault-clearing time
- Post-fault transmission system reactance

Table 2.1 Eigenvalues with time variation and phase portraits.

Conditions	Complex number diagram	Time variation	Phase portrait $L=0.1, C=0.4,$ $2L/\sqrt{LC}=1$
$\zeta^2 > 1,$ $R > 2L/\sqrt{LC},$ $s = \sigma \pm \omega < 0$ $R = 1.5$		 Stable node	
$\zeta^2 = 1,$ $R = 2L/\sqrt{LC},$ $(s - \sigma)^2 = 0, \sigma < 0$ $R = 1$		 Stable node	
$\zeta^2 \approx 0, R \ll 2L/\sqrt{LC}$ $s = \pm j\omega, \sigma \approx 0,$ $\omega \approx \omega_n \approx 1/\sqrt{LC}$ $R = 0$		 Cycle	
$\zeta^2 < 1, R < 2L/\sqrt{LC},$ $s = \sigma \pm j\omega, \sigma < 0$ $R = 0.5$		 Stable spiral	
$\zeta^2 < 1, R < 2L/\sqrt{LC},$ $s = \sigma \pm j\omega, \sigma > 0$		 Unstable	Not applicable in this case
$\zeta^2 > 1,$ $R > 2L/\sqrt{LC},$ $s = \sigma \pm \omega > 0$		 Unstable	Not applicable in this case

- The generator reactance (Lower reactance increases peak power and reduces initial rotor angle)
- The generator inertia. The higher inertia the slower response and cause a reduce of kinetic energy gained during fault
- The generator internal voltage which depends on the field excitation
- The infinite bus voltage

There are 3 methods for transient stability analysis to be represented in this topic. First is an *Equal-area criterion*, second is the *Dynamics system numerical method* and third is the *Direct method*.

2.4.1 Equal-area criterion

Accelerating torque (or torque caused by differences between mechanical and electromagnetic torques) can cause the variations in rotor speed and rotor angle. In a per unit system, an electromagnetic torque is equal to and can be replaced by electrical power. The relationship between electrical power and rotor angle (Ex. $P_e = E_s E_B \sin \delta / X_T$) is called a *power-angle relationship*, is used to describe the equal-area criterion method. The next figure shows examples of power-angle relationships from the classical model of generator connecting with an infinite bus.

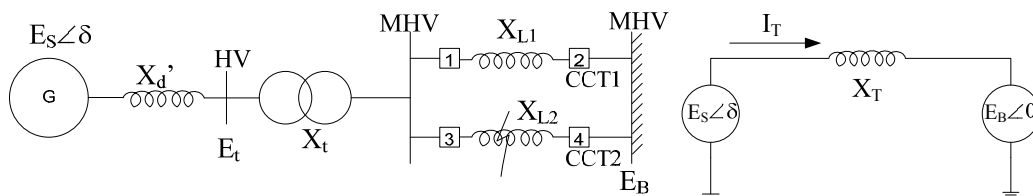


Figure 2.11 One-line diagram of power system with 1 generator connected to an infinite bus through Transmission lines 1 and 2

- 1) Initially, at an equilibrium point (Point 1), mechanical and electrical power is equal, and therefore, the rotor angle is not varied. The power-angle relationship is curve C1.
- 2) Later, if there is a disturbance in the system, for example, a short circuit to ground of transmission line, and then cause the electrical power to fall under the equilibrium point while mechanical power still remain. Since fraction of power lose to the ground, power maximum decreases and then the power-angle relationship is now curve C2.

- 3) At that time, operating point is Point 2, power (P_m) and energy of generator is more than of the power system (curve C2) and tries to transfer energy to the power system.
- 4) During transfer electrical power and rotor angle increase continuously through curve C2 from Point 2 to 3.
- 5) Immediately after disturbance, the protection system clears the short-circuited line within some specific time (t_{c1} or t_{c2}). This stop the loss of power to the ground and then power and impedance of the power system increase immediately to larger than mechanical power. The power-angle relationship is now curve C3.
- 6) At this time, operating point is Point 4, the power of the generator is less than that of the power system. Rotor speed decreases.
- 7) Subsequently, an inertia effects (rotor speed decrease while rotor angle still increase with retard) causes rotor angle and electrical power to increase until reach the maximum point (Point 5) at specific time (t_m).
- 8) At this point, there are two situations possible to occur subsequently.
 - First, clearing time is fast enough to allow area A1 to be equal to A2, or energy transfer to be equal to energy transfer from the power system. Electrical power and rotor angle return and decrease continuously to reach equilibrium point again (Point 6). This is called *Stable* case as shown in the upper figure.
 - Or second, clearing time is too late and causes area A1 to be larger than A2, and the power system loses synchronism due to electrical power and rotor angle overshoot and diverse continuously. This is called *Unstable* case as shown in the figure below.

There are two situations depend on characteristics of the power system, and configuration and/or clearing time of the protection system.

The area between the mechanical and electrical power of the generator during a range of rotor angle variation represents the energy transfer between the generator and the power system. If the area before and after clearing time is equal, an energy transfer to the power system is equal to the energy that the power system can absorb after fault clearing. This situation causes the power system to reach equilibrium point and stable after

disturbance. Conversely, if areas are not equal, the power system is unstable and lost synchronism finally. This method is then called *Equal-area criterion*.

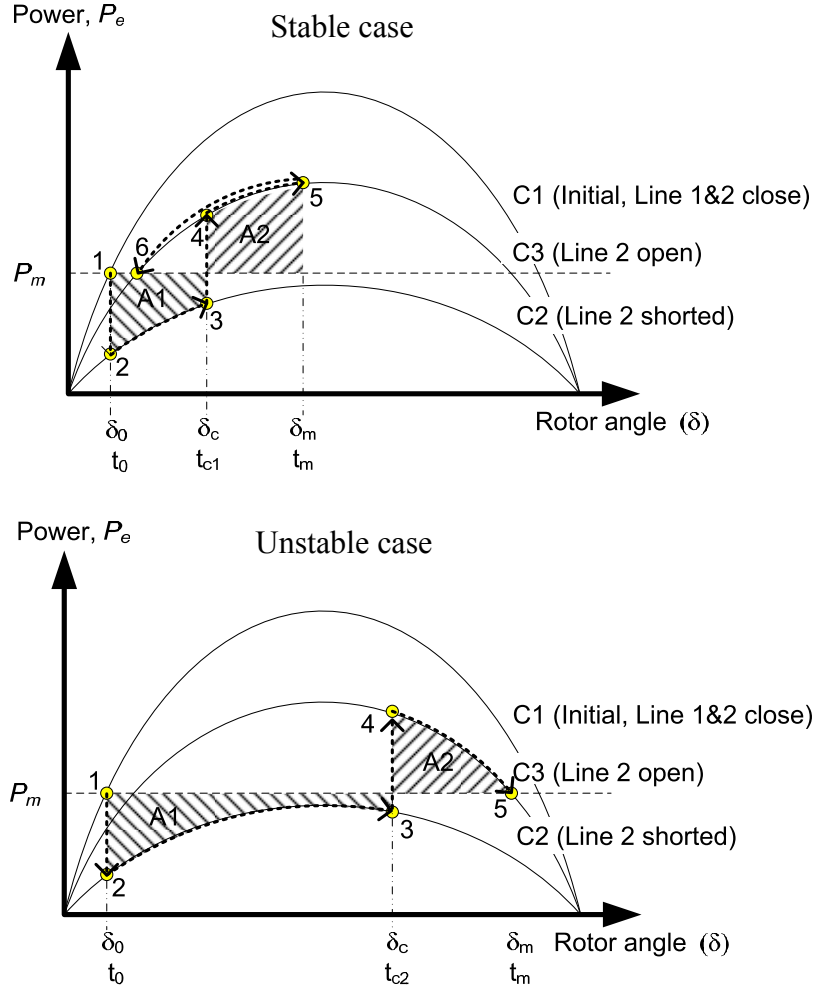


Figure 2.12 Power-rotor angle curve describing equal-area criterion

An *equal-area criterion* can be described by the following relationship:

From swing equation of motion ($\Delta\omega_r = d\delta/dt$):

$$\frac{d\Delta\omega_r}{dt} = \frac{d^2\delta}{dt^2} = \frac{\omega_0}{2H} [P_m - P_e] \quad \text{Eq. 2-67}$$

$$\text{Multiply by } \frac{2d\delta}{dt}, \quad \frac{2d\delta}{dt} \frac{d^2\delta}{dt^2} = \frac{\omega_0}{2H} [P_m - P_e] \frac{2d\delta}{dt} \quad \text{Eq. 2-68}$$

$$\text{Reform the above equation,} \quad \frac{d}{dt} \left(\frac{d\delta}{dt} \right)^2 = \frac{\omega_0}{H} [P_m - P_e] \frac{d\delta}{dt} \quad \text{Eq. 2-69}$$

Integrate both sides,

$$\left(\frac{d\delta}{dt}\right)^2 = \int \frac{\omega_0}{H} [P_m - P_e] d\delta \quad \text{Eq. 2-70}$$

For the stable case, the rotor angle is constant or $\frac{d\delta}{dt} = 0$, therefore:

$$\frac{\omega_0}{H} \int_{\delta_o}^{\delta_m} [P_m - P_e] d\delta = 0 \quad \text{Eq. 2-71}$$

Therefore, areas under $P_m - P_e$ curve is the integral over the range from δ_o to δ_m . It can be considered to be 2 ranges, which are, range from δ_o to δ_c and range from δ_c to δ_m .

$$\int_{\delta_o}^{\delta_c} [P_m - P_e] d\delta = A1, \quad \int_{\delta_c}^{\delta_m} [P_e - P_m] d\delta = A2 \quad \text{Eq. 2-72}$$

For the stable case, $A1 = A2$, therefore:

$$\int_{\delta_o}^{\delta_c} [P_m - P_e] d\delta - \int_{\delta_c}^{\delta_m} [P_e - P_m] d\delta = 0 \quad \text{Eq. 2-73}$$

$$\int_{\delta_o}^{\delta_c} [P_m - P_e] d\delta = \int_{\delta_c}^{\delta_m} [P_e - P_m] d\delta \quad \text{Eq. 2-74}$$

Areas $A1$ and $A2$ are considered as the energy transfer of the generator to and from the power system, respectively. If energy transfers to the power system before clearing time equal to the energy that the power system can absorb after clearing time, then, the system is stable.

2.4.2 Numerical methods

Since state space equations of the power system contain nonlinear ordinary differential equations with many state variables and inputs, analytical solutions cannot be used without difficulty. Numerical methods are the useful technique to solve this kind of problems with the help of computer programming. Ordinary differential equations of the power system are generally in the form:

$$\frac{dX}{dt} = f(X, t)$$

For example:

$$\frac{d\Delta\omega_r}{dt} = \frac{d^2\delta}{dt^2} = \frac{\omega_0}{2H} [P_m - P_e] \quad \text{and} \quad \frac{d\bar{\delta}}{dt} = \omega_0 \Delta\bar{\omega}_r \quad \text{Eq. 2-75}$$

For any state variable x :

$$\frac{dx}{dt} = f(x, t) \quad \text{where } x_i = x \text{ at } t = t_0 + i\Delta t \quad \text{Eq. 2-76}$$

By using Taylor's series expansion:

$$x_{i+1} = x_i + \Delta t \left(\frac{dx}{dt} \Big|_{x=x_i} \right) + \frac{\Delta t^2}{2!} \left(\frac{d^2x}{dt^2} \Big|_{x=x_i} \right) + \dots + \frac{\Delta t^n}{n!} \left(\frac{d^n x}{dt^n} \Big|_{x=x_i} \right) + \dots \quad \text{Eq. 2-77}$$

For the power system, the 1st order differential equation can generally be considered. The 2 types of numerical methods, which are *explicit* and *implicit* methods, are used for power system analysis. These methods can be truncated from Taylor's series expansion.

2.4.2.1 Explicit numerical methods

Explicit numerical methods predict the unknown values at the time step $t_1 = t_0 + \Delta t$ entirely with the known values at time step t_0 (or initial values). Examples of classical explicit numerical methods are Euler method, Modified Euler method (Huen method, Predictor-corrector methods, Adams-Bashforth methods, Milne methods, and Hamming methods), and Runge-Kutta methods.

Euler method $x_{i+1} = x_i + \Delta t \cdot f(x_i, t_i)$

Modified Euler's method $x_{i+1}^p = x_i + \Delta t \cdot f(x_i, t_i)$ and $x_{i+1}^c = x_i + \frac{\Delta t}{2} \cdot [f(x_i, t_i) + f(x_{i+1}^p, t_{i+1})]$

Runge-Kutta methods $x_{i+1} = x_i + (k_1 + 2k_2 + 2k_3 + k_4)/6$

$$k_1 = \Delta t \cdot f(x_i, t_i), \quad k_2 = \Delta t \cdot f\left(x_i + \frac{k_1}{2}, t_i + \frac{\Delta t}{2}\right),$$

$$k_3 = \Delta t \cdot f\left(x_i + \frac{k_2}{2}, t_i + \frac{\Delta t}{2}\right), \quad k_4 = \Delta t \cdot f(x_i + k_3, t_i + \Delta t)$$

2.4.2.2 Implicit numerical methods

Implicit numerical methods predict the unknown values at the time step $t_i = t_0 + i\Delta t$ and not explicitly with the known values at time step t_0 (initial values), but also with the known values at time step t_n (boundary values) and the set of unknown values at the time step before t_n .

Therefore, this is a kind of algebraic linear system of equations and could be solved using the method for example, Gauss elimination. Implicit numerical methods give higher

numerical stability (due to being limited by boundary values) but are much more complex and difficult to process than explicit methods. For example:

1-step Backward Euler method $x_{i+1} = x_i + \Delta t \cdot f(x_{i+1}, t_{i+1})$

1-step Trapezoidal method $x_{i+1} = x_i + \frac{\Delta t}{2} \cdot [f(x_i, t_i) + f(x_{i+1}, t_{i+1})]$

1-step Leapfrog method $x_{i+1} = x_{i-1} + 2\Delta t \cdot f(x_i, t_i)$

2-step Leapfrog method $3x_{i+1} - 4x_i + x_{i-1} = 2\Delta t \cdot f(x_{i+1}, t_{i+1})$

Table 2.2 Comparison between explicit and implicit methods

	Explicit methods	Implicit methods
Advantage	+ Easier to process and program	+ Higher numerical stability due to being limited by boundary values.
		+ Larger Δt and fewer time step
Disadvantage	In some case, Δt must be very small which can result in long running time.	Much more complex and difficult to process.
		Algebraic linear system of equations (Matrix) require more computer time per time step
		Larger Δt result in larger truncation errors, especially for transient problems.

Therefore, in the case of transients, explicit numerical methods are more suitable than implicit methods. This is because implicit methods can cause larger error of transients.

2.4.3 Direct method

Parameters from both equal-area criterion and numerical methods do not directly measure the level of stability of the power system. They just estimate the state of stability. Therefore, new method with direct measure of how significant of stability of the power

system should be developed. By this reason, the direct method can be used to quantify the level of stability directly.

Since rotor angle instability from transient causes are due to imbalances between mechanical and electrical torque, there are imbalances between the kinetic energy gain from generator and potential energy transfer from power system when subject to disturbances. The direct method measure minimum energy needed to make the system unstable is called *critical energy*. This method can be described as follows.

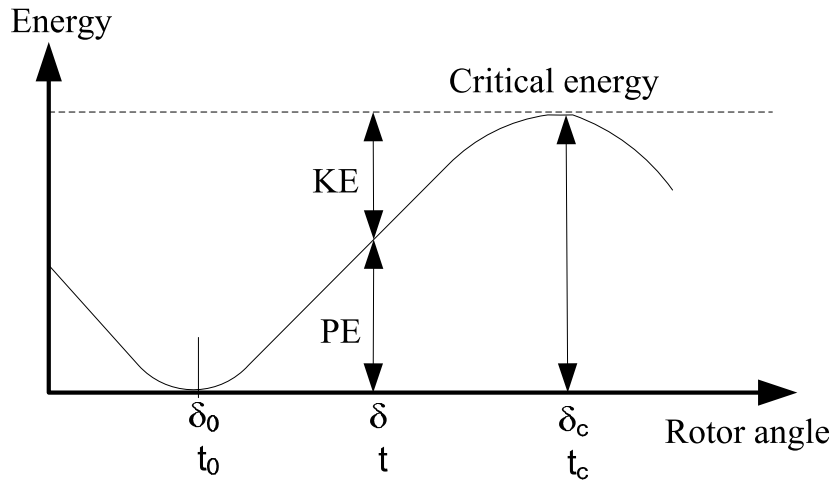


Figure 2.13 Potential energy-rotor angle curve

At a pre-fault state, the rotor angle is δ_0 , which is at a state equilibrium point. During the fault state, electrical power is zero and the power system gain power and kinetic energy (KE) from generator. The rotor angle and potential energy (PE) of generator increase continuously until faults are cleared.

If potential energy is less or equal critical energy (with rotor angle δ_c), the systems will rollback with decreasing of rotor angle and potential energy to reach state equilibrium point again. However, if potential energy is larger than critical energy, the generator loss synchronism and instability state occur.

Even though direct methods are vulnerable to numerical problems, this method needs sophisticate and robust solutions. This can make the method slower than the time domain numerical methods.

2.5 Voltage Stability

2.5.1 Definition of voltage stability and voltage collapse

The ability of the power system to maintain or control voltage during normal operation and at a given initial condition after subjection to disturbances depends on the ability to restore equilibrium between load demand and supply of the power system. The result may be voltage progressive drop or rise and finally loss of load in some areas.

Voltage stability is concerned with load stability while rotor angle stability is concerned with generator stability.

Voltage stability parameters or indices

- 1) Voltage drop or rise and duration (Dynamics analysis)
- 2) $V-Q$ sensitivity (Static analysis)
- 3) Eigenvalues of $Q-V$ modal (Static analysis)

Factors influencing voltage stability

- Load factors, for example, over load demand
- Network factors, for example, weak network power line, loss of transmission line, control system/devices error or damage after fault
- Generation factors, for example, loss of generators, generation control error

Classification of voltage stability

- 1) Small disturbance voltage stability

Voltage stability following the small disturbances which post-disturbance equilibrium voltage can be either close to the pre-disturbance values for stable cases or progressive decrease (or increase) for unstable cases.

- 2) Large disturbance voltage stability

Voltage stability normally involves large disturbances, including sudden increase, in load or power transfer. The instability is almost always a periodic decrease in voltage.

2.5.2 Power system characteristics influencing voltage stability

2.5.2.1 Transmission system and load characteristics

The transmission system and load characteristics can be described using the following figure and equations. For simple power circuit, the system consists of voltage source (E_S) at terminal of generator, line impedance (Z_{LN}), and load impedance (Z_{LD}). At

the terminal of load, voltage (V_R), active power (P_R), and reactive power (Q_R), are characterized as follows.

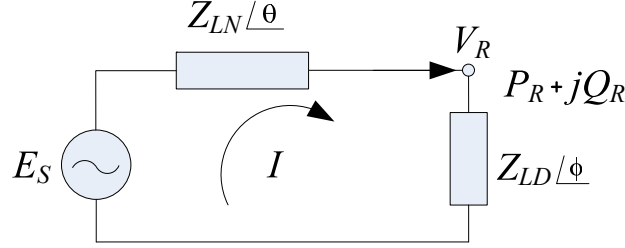


Figure 2.14 Circuit diagram of the power system with transmission and load impedance

$$Z_{LN} = |Z_{LN}| \cos \theta + j |Z_{LN}| \sin \theta \quad \text{Eq. 2-78}$$

$$Z_{LD} = |Z_{LD}| \cos \phi + j |Z_{LD}| \sin \phi \quad \text{Eq. 2-79}$$

$$I = \frac{E_S}{Z_{LN} + Z_{LD}} = \frac{E_S}{(|Z_{LN}| \cos \theta + |Z_{LD}| \cos \phi) + j(|Z_{LN}| \sin \theta + |Z_{LD}| \sin \phi)} \quad \text{Eq. 2-80}$$

$$I = \frac{1}{\sqrt{F}} \frac{E_S}{Z_{LN}} = \frac{1}{\sqrt{F}} I_{sc} \quad , \quad V_R = \frac{E_S}{\sqrt{F}} \frac{Z_{LD}}{Z_{LN}} \quad \text{Eq. 2-81}$$

where

$$F = 1 + \left(\frac{Z_{LD}}{Z_{LN}} \right)^2 + 2 \left(\frac{Z_{LD}}{Z_{LN}} \right) \cos(\theta - \phi) \quad \text{Eq. 2-82}$$

$$P_R = V_R I \cos \phi = \frac{Z_{LD}}{F} \frac{E_S^2}{Z_{LN}^2} \cos \phi \quad \text{Eq. 2-83}$$

When

$$Z_{LD} = Z_{LN}, \text{ then } P_R = P_{\max}, \quad V_R = E_S / \sqrt{2 + 2 \cos(\theta - \phi)}, \quad I = E_S / (Z_{LN} \sqrt{2 + 2 \cos(\theta - \phi)})$$

$$P_{\max} = V_R I \cos \phi = \frac{E_S}{\sqrt{F_{P_{\max}}}} \frac{E_S}{Z_{LN} \sqrt{F_{P_{\max}}}} \cos \phi = \frac{E_S^2 \cos \phi}{Z_{LN} (2 + 2 \cos(\theta - \phi))} \quad \text{Eq. 2-84}$$

$$\frac{P_R}{P_{\max}} = \frac{Z_{LD}}{F} \frac{E_S^2}{Z_{LN}^2} \left(\frac{Z_{LN} (2 + 2 \cos(\theta - \phi))}{E_S^2 \cos \phi} \right) \cos \phi = \frac{1}{F} \frac{Z_{LD}}{Z_{LN}} (2 + 2 \cos(\theta - \phi)) \quad \text{Eq. 2-85}$$

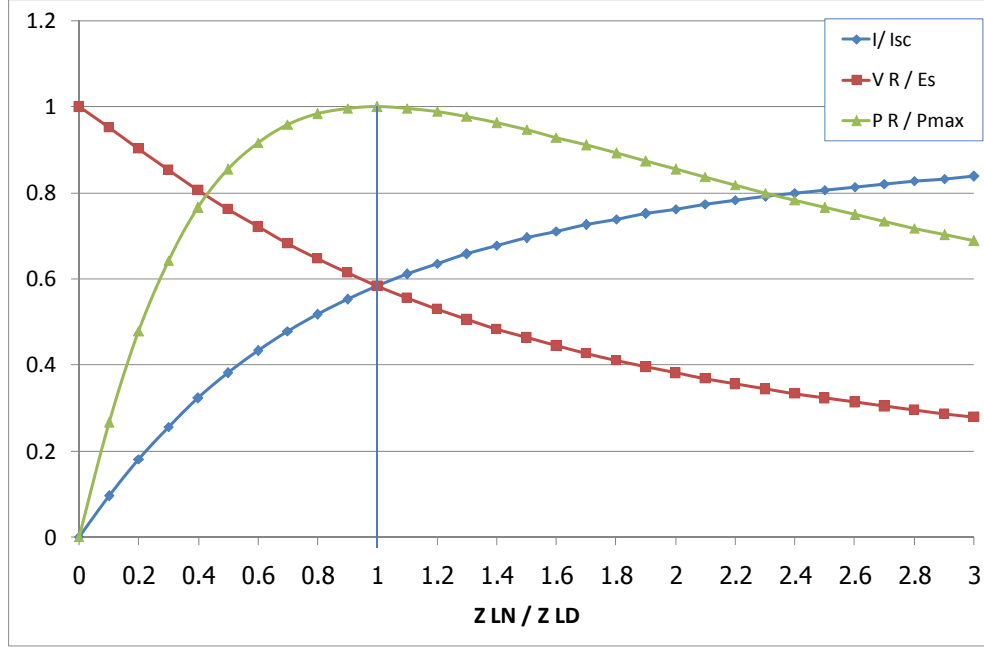


Figure 2.15 Current, voltage, and power curves at receiving end with line and load impedance

From the above figure:

- 1) $Z_{LD} > Z_{LN}$, normal or stable conditions.

Load impedance is higher than line impedance. Increasing of load (reduce Z_{LD}) causes active power, reactive power and current increase. Contradictory, load increase cause voltage decrease whereas enlarge voltage drop along the power line. Voltage can be controlled by increase or decrease reactive power. For example, in case over voltage, operator can increase reactive power to reduce voltage by change tap of substation transformers.

- 2) $Z_{LD} = Z_{LN}$, critical condition.

Load impedance is equal to line impedance. This situation causes power to reach the maximum point and be the critical operating point.

- 3) $Z_{LD} < Z_{LN}$, unstable condition or instability.

Load impedance is less than line impedance due to loading over or loss of transmission line. Increasing of load cause decreasing of active and reactive power. Voltage in this situation cannot be controlled by regulating reactive power normally and lost control finally. This is unstable condition or voltage instability which caused from large disturbance of transmission system characteristics.

If consider power factor variation, the P - V characteristics is represented as follows.

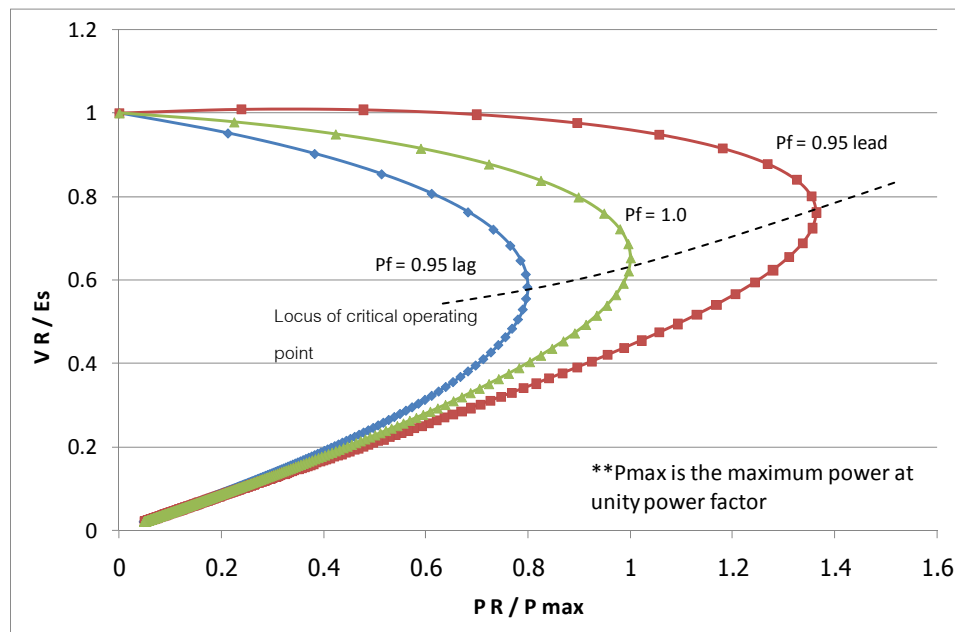


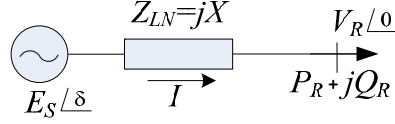
Figure 2.16 the P - V characteristics with different power factor (pf)

In the above figure, normal operating points are the points above the locus of the critical operating point line. The 3 solid curves represent P - V characteristics at the different power factor or different reactive power. The line of locus of critical operating point increases with an increasing of power factor from negative (lag) to be positive (lead) value.

The characteristics of transmission systems depend on the characteristics of load and line impedance, and the flow of active and reactive power, which can impact the stability of voltage as explained above. Therefore, the principal causes of voltage instability are

- Load is too high
- Loss of transmission line
- Voltage sources are too far from load center
- Voltage sources are too low
- Insufficient reactive power compensation

Considering Q - V characteristics, the power angle relationship is concerned and characterized. A Q - V characteristic is helpful for understanding relationship between voltage control and reactive power. Assume the power system with line impedance Z_{LN} is X (R is very small), as shown in the figure below.



$$S_R = P_R + jQ_R = V_R I = V_R \left(\frac{E_S \angle \delta - V_R \angle 0}{jX} \right) = V_R \left(\frac{E_S \cos \delta + jE_S \sin \delta - V_R}{jX} \right) \quad \text{Eq. 2-86}$$

$$S_R = \frac{E_S V_R \sin \delta}{X} + j \left(\frac{E_S V_R \cos \delta}{X} - \frac{V_R^2}{X} \right) \quad \text{Eq. 2-87}$$

If $I^2 X$ loss is neglected, therefore,

$$P_R = P_S = \frac{E_S V_R \sin \delta}{X} \quad \text{Eq. 2-88}$$

$$Q_R = \frac{E_S V_R \cos \delta}{X} - \frac{V_R^2}{X} \quad \text{Eq. 2-89}$$

If normalized power is equal to short circuit power, $Q_n = P_n = \frac{E_S^2}{X}$ and $v = \frac{V_R}{E_S}$, therefore,

$$p = \frac{P_R}{P_n} = \frac{V_R}{E_S} \sin \delta = v \sin \delta \quad \text{Eq. 2-90}$$

$$q = \frac{Q_R}{Q_n} = \frac{V_R}{E_S} \cos \delta - \left(\frac{V_R}{E_S} \right)^2 = v \cos \delta - v^2 \quad \text{Eq. 2-91}$$

If p is specified, for example $p = 0, 0.2, 0.5, 0.8, 0.9$, and 1.0 , therefore

$$q = v \cos \left(\sin^{-1} \left(\frac{p}{v} \right) \right) - v^2 \quad \text{Eq. 2-92}$$

In Figure 2.17, the stable operating condition occurs on the right side of the locus of the critical operating point while unstable case occurs on the left side. Under stable operating condition, voltage increase with increasing of reactive power. Moreover, the operating point depends on Q - V characteristics of capacitor bank which vary between a designed range by using automatic switching. At high load power, for example $p = 1.0$, out of range of capacitor bank can be expected. Therefore, operating point never reach when load power is too high.

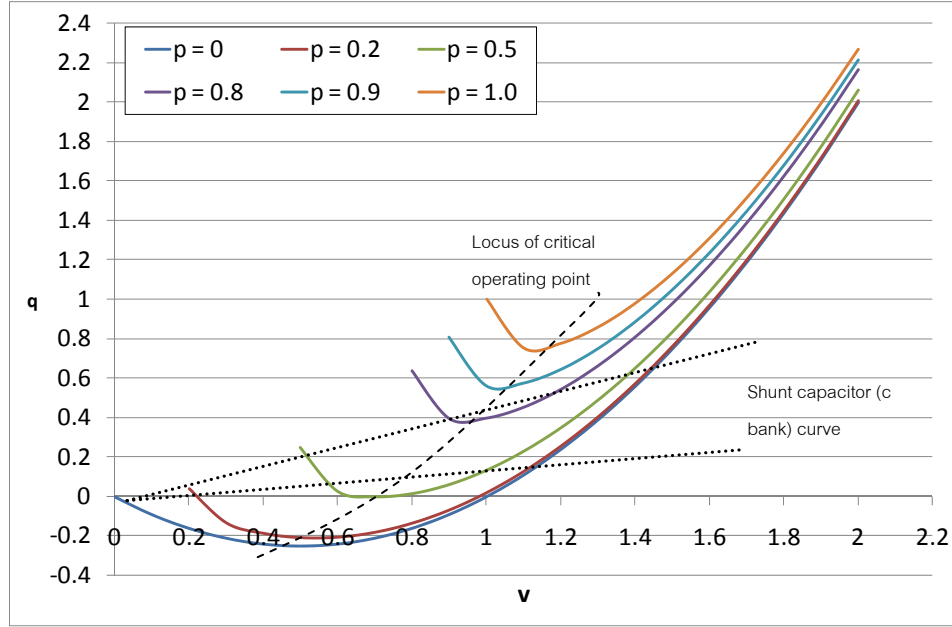


Figure 2.17 The Q - V characteristics with different powers

2.5.3 Voltage stability analysis

Power system elements influencing voltage stability are, for example, loads, generators, excitation control of generator, static var systems (SVSs), automatic generation control (AGC), and protection and control devices. These elements have significant impact on voltage stability and have to be modeled. There are mainly 2 analysis methods to be used, which are dynamic and static analysis.

2.5.3.1 Dynamic analysis

Dynamics analysis method is time-domain variation simulation similar to transient stability analysis. Therefore:

the general form of first order differential equations is

$$\dot{\mathbf{x}} = \mathbf{f}(\mathbf{x}, \mathbf{V}) \quad \text{Eq. 2-93}$$

and the general form of the algebraic equations is

$$\mathbf{I}(\mathbf{x}, \mathbf{V}) = \mathbf{Y}_N \mathbf{V} \quad \text{Eq. 2-94}$$

The initial conditions (\mathbf{x}_0 and \mathbf{V}_0) are known, where \mathbf{x} is state vector of the system, \mathbf{V} is bus voltage vector, \mathbf{I} is current injection vector, and \mathbf{Y}_N is network node admittance matrix.

Differential equations can be solved using iterative numerical methods (such as Newton-Raphson) while algebraic equation can be solved using power flow analysis methods. Step-by-step processes for solving these equations are as follows.

For the first step, specify initial values of variables of generator unit, transmission network, load devices and control unit, such as excitation systems and then set an equation $\dot{\mathbf{x}} = \mathbf{f}(\mathbf{x}, \mathbf{V})$. At this time, the steady state is assumed. The state variables are constant and $\dot{\mathbf{x}} = \mathbf{f}(\mathbf{x}, \mathbf{V}) = 0$.

2nd step: set equation $\mathbf{I}(\mathbf{x}, \mathbf{V}) = \mathbf{Y}_N \mathbf{V}$ and use previous state variables (x_1) to compute next step current and voltage (I_1 and V_1).

3rd step: use V_1 and x_1 to replace in $\dot{\mathbf{x}} = \mathbf{f}(\mathbf{x}, \mathbf{V})$ and then solve this equation to find x_2 . To solve this problem, explicit or implicit numerical methods could be used.

4th step: repeat 2nd and 3rd steps using new state variables.

The overall system equations are provided for differential and algebraic equations and can be described similar to transient stability analysis. However, characteristics of reactive compensating and voltage control devices are added to model in this case.

2.5.3.2 Static analysis

For static analysis, the derivatives of the state variables are assumed to be zero for each time frame. The power system characteristics are captured at various time frames along the considered time-domain.

Therefore, overall system equations can be reduced to be only algebraic equations and can be solved using power flow analysis methods. Mainly, 2 static analysis methods are described, which are V - Q sensitivity analysis and Q - V modal analysis.

1) V - Q sensitivity analysis

V - Q sensitivity analysis method is based on the Newton-Raphson (NR) iterative method for power flow analysis. The *Jacobian* of NR method is considered to be sensitivity between V and Q . To specify *Jacobian*, the network equation in terms of node admittance equation is first identified as follows.

$$\hat{I}_i = \sum_{k=1}^n \hat{Y}_{ik} \hat{V}_k \quad \text{Eq. 2-95}$$

For node i ,

$$\hat{S}_i = P_i + jQ_i = \hat{V}_i \hat{I}_i^* \quad \text{Eq. 2-96}$$

Substitute \hat{I}_i , yield

$$P_i + jQ_i = \hat{V}_i \sum_{k=1}^n \hat{Y}_{ik}^* \hat{V}_k^* \quad \text{Eq. 2-97}$$

Where $\hat{V}_i \hat{V}_k^* = V_i V_k (\cos \theta_i + j \sin \theta_i)(\cos \theta_k - j \sin \theta_k) = V_i V_k (\cos(\theta_i - \theta_k) + j \sin(\theta_i - \theta_k))$

and $\hat{Y}_{ik}^* = A_{ik} - jB_{ik}$.

Therefore, P and Q are functions of V and θ that can be presented as follows.

$$P_i = V_i \sum_{k=1}^n V_k (A_{ik} \cos(\theta_i - \theta_k) + B_{ik} \sin(\theta_i - \theta_k)) \quad \text{Eq. 2-98}$$

$$Q_i = V_i \sum_{k=1}^n V_k (A_{ik} \sin(\theta_i - \theta_k) - B_{ik} \cos(\theta_i - \theta_k)) \quad \text{Eq. 2-99}$$

$$P_i^{kn} - P_i = \Delta P_i = \sum_{k=1}^n \frac{\partial P_i}{\partial \theta_k} \Delta \theta_k + \sum_{k=1}^n \frac{\partial P_i}{\partial V_k} \Delta V_k \quad \text{Eq. 2-100}$$

$$Q_i^{kn} - Q_i = \Delta Q_i = \sum_{k=1}^n \frac{\partial Q_i}{\partial \theta_k} \Delta \theta_k + \sum_{k=1}^n \frac{\partial Q_i}{\partial V_k} \Delta V_k \quad \text{Eq. 2-101}$$

$$\begin{bmatrix} \Delta P_i \\ \Delta Q_i \end{bmatrix} = \sum_{k=1}^n \begin{bmatrix} \frac{\partial P_i}{\partial \theta_k} & \frac{\partial P_i}{\partial V_k} \\ \frac{\partial Q_i}{\partial \theta_k} & \frac{\partial Q_i}{\partial V_k} \end{bmatrix} \begin{bmatrix} \Delta \theta_k \\ \Delta V_k \end{bmatrix} \quad \text{Eq. 2-102}$$

For the power system with m nodes, or $i = 1$ to m , therefore:

$$\begin{bmatrix} \Delta P_1 \\ \vdots \\ \Delta P_m \\ \Delta Q_1 \\ \vdots \\ \Delta Q_m \end{bmatrix} = \begin{bmatrix} \frac{\partial P_1}{\partial \theta_1} & \cdots & \frac{\partial P_1}{\partial \theta_n} & \frac{\partial P_1}{\partial V_1} & \cdots & \frac{\partial P_1}{\partial V_n} \\ \vdots & \ddots & \vdots & \vdots & \ddots & \vdots \\ \frac{\partial P_m}{\partial \theta_1} & \cdots & \frac{\partial P_m}{\partial \theta_n} & \frac{\partial P_m}{\partial V_1} & \cdots & \frac{\partial P_m}{\partial V_n} \\ \frac{\partial Q_1}{\partial \theta_1} & \cdots & \frac{\partial Q_1}{\partial \theta_n} & \frac{\partial Q_1}{\partial V_1} & \cdots & \frac{\partial Q_1}{\partial V_n} \\ \vdots & \ddots & \vdots & \vdots & \ddots & \vdots \\ \frac{\partial Q_m}{\partial \theta_1} & \cdots & \frac{\partial Q_m}{\partial \theta_n} & \frac{\partial Q_m}{\partial V_1} & \cdots & \frac{\partial Q_m}{\partial V_n} \end{bmatrix} \begin{bmatrix} \Delta \theta_1 \\ \vdots \\ \Delta \theta_n \\ \Delta V_1 \\ \vdots \\ \Delta V_n \end{bmatrix} \quad \text{Eq. 2-103}$$

$$\begin{bmatrix} \Delta \mathbf{P} \\ \Delta \mathbf{Q} \end{bmatrix} = \begin{bmatrix} \frac{\partial \mathbf{P}}{\partial \boldsymbol{\theta}} & \frac{\partial \mathbf{P}}{\partial \mathbf{V}} \\ \frac{\partial \mathbf{Q}}{\partial \boldsymbol{\theta}} & \frac{\partial \mathbf{Q}}{\partial \mathbf{V}} \end{bmatrix} \begin{bmatrix} \Delta \boldsymbol{\theta} \\ \Delta \mathbf{V} \end{bmatrix} \quad \text{or} \quad \begin{bmatrix} \Delta \mathbf{P} \\ \Delta \mathbf{Q} \end{bmatrix} = \begin{bmatrix} \mathbf{J}_{P\theta} & \mathbf{J}_{PV} \\ \mathbf{J}_{Q\theta} & \mathbf{J}_{QV} \end{bmatrix} \begin{bmatrix} \Delta \boldsymbol{\theta} \\ \Delta \mathbf{V} \end{bmatrix} \quad \text{Eq. 2-104}$$

The matrix with derivative terms are Jacobian, where, $\mathbf{J}_{P\theta}$ is the relationship between \mathbf{P} and $\boldsymbol{\theta}$, \mathbf{J}_{PV} is the relationship between \mathbf{P} and \mathbf{V} , $\mathbf{J}_{Q\theta}$ is the relationship between \mathbf{Q} and $\boldsymbol{\theta}$, \mathbf{J}_{QV} is the relationship between \mathbf{Q} and \mathbf{V} .

If we consider only sensitivity between $\Delta \mathbf{Q}$ and $\Delta \mathbf{V}$, therefore, $\Delta \mathbf{P}$ can be zero, yields

$$0 = \mathbf{J}_{P\theta}\Delta\theta + \mathbf{J}_{PV}\Delta\mathbf{V} \quad \text{Eq. 2-105}$$

$$\Delta\mathbf{Q} = \mathbf{J}_{Q\theta}\Delta\theta + \mathbf{J}_{QV}\Delta\mathbf{V} \quad \text{Eq. 2-106}$$

From the above 2 equations: $\Delta\mathbf{Q} = \left(-\mathbf{J}_{Q\theta}\mathbf{J}_{P\theta}^{-1}\mathbf{J}_{PV} + \mathbf{J}_{QV}\right)\Delta\mathbf{V}$ or Eq. 2-107

$$\Delta\mathbf{Q} = \mathbf{J}_s\Delta\mathbf{V} \quad \text{Eq. 2-108}$$

\mathbf{J}_s is sensitivity between $\Delta\mathbf{Q}$ and $\Delta\mathbf{V}$ or called V - Q sensitivity. The positive \mathbf{J}_s means stable operation while negative means unstable operation. The smaller the sensitivity, the more stable is positive \mathbf{J}_s and more unstable is negative \mathbf{J}_s . Therefore, \mathbf{J}_s is used to be as indicator matrix for V - Q sensitivity analysis.

2) Q - V modal analysis (eigenvalue , eigenvector)

From the equation $\Delta\mathbf{V} = \mathbf{J}_s^{-1}\Delta\mathbf{Q}$ Eq. 2-109

If $\mathbf{J}_s^{-1} = \mathbf{w}\mathbf{\Lambda}^{-1}\mathbf{u}$, Eq. 2-110

where $\mathbf{\Lambda}^{-1}$ is diagonal eigenvalue matrix, \mathbf{w} and \mathbf{u} are left and right eigenvector, respectively.

Therefore, $\Delta\mathbf{V} = \mathbf{w}\mathbf{\Lambda}^{-1}\mathbf{u}\Delta\mathbf{Q}$ Eq. 2-111

Since $\mathbf{w}^{-1} = \mathbf{u}$, thus $\mathbf{u}\Delta\mathbf{V} = \mathbf{\Lambda}^{-1}\mathbf{u}\Delta\mathbf{Q}$ Eq. 2-112

or $\mathbf{v} = \mathbf{\Lambda}^{-1}\mathbf{q}$ Eq. 2-113

where $\mathbf{v} = \mathbf{u}\Delta\mathbf{V}$ is modal voltage variation, and $\mathbf{q} = \mathbf{u}\Delta\mathbf{Q}$ is modal reactive power variation.

For the node (or mode) i^{th} , replaces eigenvalue (λ_i) for $\mathbf{\Lambda}^{-1}$ yield

$$\mathbf{v}_i = \frac{1}{\lambda_i}\mathbf{q}_i \quad \text{Eq. 2-114}$$

λ_i is used as an indicator for the voltage stability condition. If $\lambda_i > 0$, \mathbf{v}_i increase with \mathbf{q}_i for stable operation. The larger λ_i means the more voltage stable. If $\lambda_i < 0$, \mathbf{v}_i decrease when \mathbf{q}_i increase for unstable operation. The smaller λ_i means the more voltage unstable.

V - Q sensitivity analysis and Q - V modal analysis are the fundamental important techniques for static analysis of the power system. These methods have been applied for modern voltages stability analysis as be described in later section.

2.5.4 Voltage collapse

Voltage collapse is a voltage stability problem when the voltage suddenly drops due to cascading change of the power system with the period ranging from several seconds to minutes. Voltage drop for large portion of high power system can be expected follow by local blackouts. Main cause of voltage collapse is an inability to serve for additional reactive power demand. However, for many cases, voltage collapse occurs when the power network is weak due to immediate loss of the transmission line.

Voltage collapse is influenced by many factors for example, large distance between generation and load, tap changing action of transformer during low voltage condition, poor load characteristics, and poor control and protective system characteristics.

Voltage instability always occurs after voltage collapse due to bifurcation. Voltage collapse is a nonlinear phenomenon. Therefore, nonlinear analysis methods, such as *bifurcation theory*, are applied to voltage collapse and voltage stability analysis.

Bifurcation theory characterizes the slow change of the system from a stable condition to an unstable one. There are 2 classes of bifurcation that are local and global bifurcations. Local bifurcation occurs when parameters change causes critical operating point (fixed point) change. There are several types of local bifurcation, for example, saddle-node bifurcation, transcritical bifurcation, pitchfork bifurcation, period-doubling bifurcation, and hopf bifurcation. Global bifurcation occurs when larger set of parameters, such as periodic orbit variation, collide with critical point and causes divergence from the critical point.

For voltage collapse and voltage stability, local bifurcation, especially, saddle-node and hopf bifurcations, are always of interest due their agreement with characteristics of the power system as real as possible.

Saddle-node bifurcation occurs at the critical point when stable operating conditions slowly disappear. For example, when load increase cause load impedance to decline slowly and equal to line impedance, the power reach maximum equilibrium point or critical point. Beyond this point, the system become unstable and cause losses control of voltage. This critical point is such kind of saddle-node as shown in the figure below.

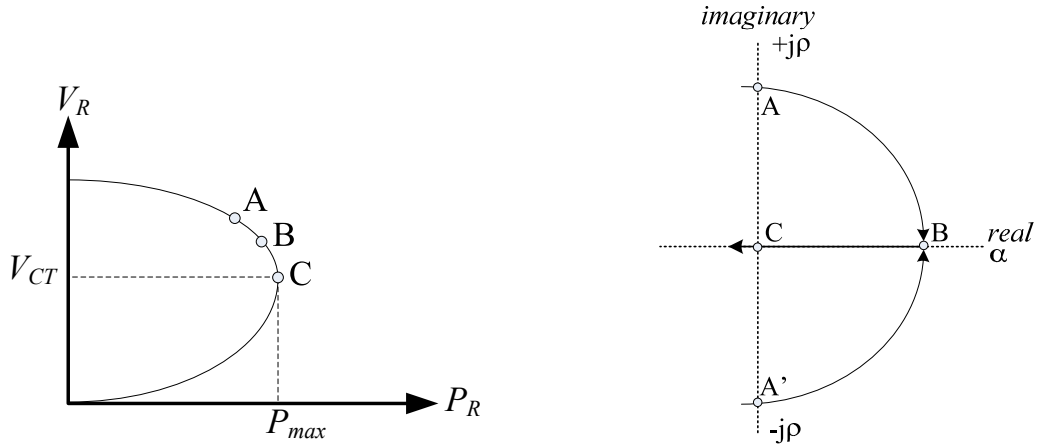


Figure 2.18 P - V characteristics (left) and root loci plot of eigenvalue (right)

In the above figure, saddle-node or critical point is point C with the maximum power P_{max} and critical voltage V_{CT} . Operating point of the system slowly changes from point B, as stable condition, to point C and after that becomes unstable. In term of eigenvalue (λ) consideration, real λ ($\lambda = \alpha$) change from positive for stable case, pass zero, and decrease further to be negative value for unstable case. This characteristic is the major interest of voltage collapse problem of local power system.

Hopf bifurcation occurs when a pair of complex conjugate eigenvalues ($\lambda = \alpha \pm j\omega$), point A and A', cross the imaginary axes of the complex plane. The consequence can be either stable oscillation or growing oscillatory unstable. This can occur when the resistance of the transmission line is significantly not zero [15].

2.6 Frequency Stability

2.6.1 Definition of frequency stability

Frequency stability is the ability of the power system to maintain or control frequency, during normal operation and at given initial conditions, after subjection to disturbances. The characteristics time of frequency stability range from several second corresponding to the response of devices such as generators control and protection, to several minutes corresponding to the response of devices such as prime mover systems and load voltage regulators.

Frequency stability is classified as large disturbance with long-term stability due to the characteristic time of the overall islanding is range from seconds to several minutes.

Factors influencing frequency stability

Frequency stability depends on the ability to restore equilibrium between loading and generation of the active power. The result may be large excursion of frequency, power, voltage, and other system variables, and result in loss of load (load shedding) in large areas.

Frequency stability mostly concerns islanding that may or may not reach an acceptable state of equilibrium and with minimum loss of load. Normally, the response of overall islanding system to the mean frequency is characterized. Frequency instability depends on, for example, poor response of control and protection equipments, or insufficient generation reserve.

2.6.2 Power system characteristics influencing frequency stability

From an islanding perspective, there are 2 possible cases of frequency instability that are, the over-frequency situation corresponding to over-generated Island, and under-frequency situation corresponding to under-generated Island.

The over-generated Island cause from, at the time of separation, the islanded area has generated power larger than area load including loss. The characteristic of islanding system depends on generation, load, loss, and generator control system.

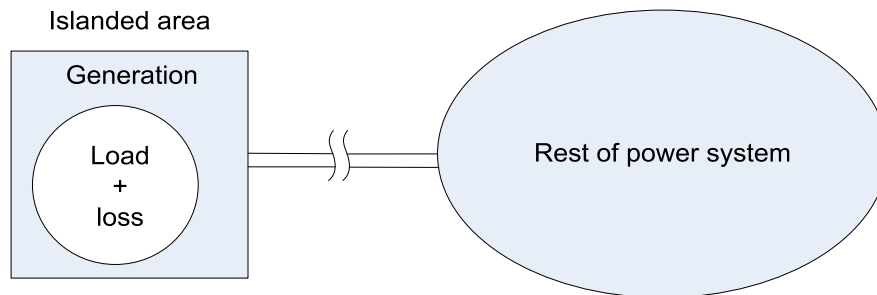


Figure 2.19 The over-generated Island diagram

For example, the over-generated cause oscillatory over-frequency for several seconds. If control system with auxiliary governor in service, an exceed frequency (or overspeed) is detected periodically. Therefore, the governor of mechanical power may be switched on-off periodically. This causes oscillatory large swing of mechanical power and other involving parameters.

The under-generated Island cause from, at the time of separation, the islanded area has generated power less than area load including loss. The characteristic of islanding system depends on generation, load, loss, and active/reactive devices.

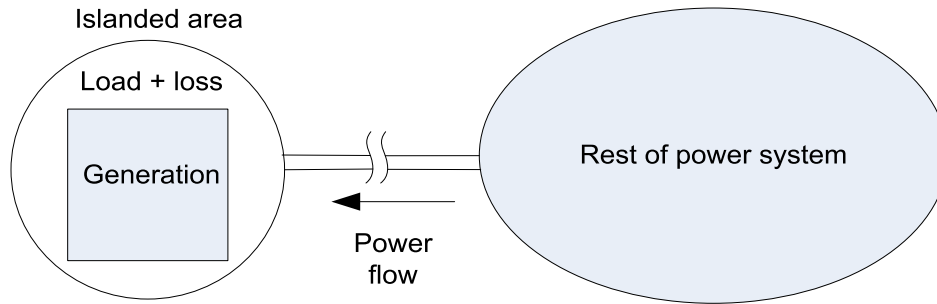


Figure 2.20 The under-generated Island diagram

For example, the under-generated cause under-frequency for several seconds. The switching sequences include load shedding relays that may reject partly area load with or without capacitor switched out. In case of capacitors are not switched out, because of surplus reactive power in the area, bus voltage increase significantly. This cause load power still high even after load shedding and generator attempt to generate power until reach the limit. This causes the frequency to drop for longer periods of time.

In the case of capacitors are switched out after load shedding, bus voltage increase but not significant. Generated power of generator is not reach the limit. The system frequency recovers to the rated value within a short time and settles after that.

2.6.3 Frequency stability analysis

Power system elements influencing frequency stability are loads, generators, excitation control of generator, governor control system, active/reactive control system, and protection and control devices. These elements are impacted to frequency stability and have to be modeled. There are mainly 2 analysis methods to be used, which are, dynamics and static analysis.

2.6.3.1 Dynamic analysis

Dynamic analysis is a time-domain variation simulation that is similar to transient and voltage stability analysis.

The general form of first order differential equations is:

$$\dot{\mathbf{x}} = \mathbf{f}(\mathbf{x}, \mathbf{V}, \omega) \quad \text{Eq. 2-115}$$

and general form of algebraic equation is

$$\mathbf{I}(\mathbf{x}, \mathbf{V}, \omega) = \mathbf{Y}_N \mathbf{V} \quad \text{Eq. 2-116}$$

Initial conditions (\mathbf{x}_0 , \mathbf{V}_0 and ω_0) are known, where \mathbf{x} is state vector of the system, \mathbf{V} is bus voltage vector, ω is rotational speed (or frequency), \mathbf{I} is current injection vector, and \mathbf{Y}_N is network node admittance matrix.

Differential equations can be solved using numerical methods while algebraic equations can be solved using power flow analysis.

The overall system equations are provided for differential and algebraic equations and can be described similar to transient stability analysis. However, characteristics of governor control system, active/reactive control devices, and protection and control devices are added to be modeled in this case.

2.7 Wind Power

2.7.1 Estimation of wind power

Wind turbines can be rotated when the air attacks the surface of the blades. Therefore, the moving air has kinetic energy to transfer to the blades as lift and drag force and then can move or rotate the rotor in the direction of net force. This kinetic energy (KE) (Wh) is

$$KE = P \times H \quad \text{Eq. 2-117}$$

Where P is the power of the wind (W) and H is the time that wind move pass the rotor (hour).

$$\text{For the power of the wind,} \quad P = \frac{1}{2} \dot{m} V^2 \quad \text{Eq. 2-118}$$

where V is velocity (m.s^{-1}), and for the air, the mass transfer is

$$\dot{m} = \rho A V \quad \text{Eq. 2-119}$$

where ρ is air density (kg.m^{-3}), A is areas of rotor swept (m^2).

Therefore, the power of the wind (W) over the rotor is

$$P = \frac{1}{2} \rho A V^3 \quad \text{Eq. 2-120}$$

It can be concluded that power of wind pass one rotor depends on the velocity cube (V^3), areas of rotor, and air density.

An extracted mechanical wind power, P_{ex} , can be calculated by

$$P_{ex} = \frac{1}{2} c_p \rho A V^3 \quad \text{Eq. 2-121}$$

where c_p is performance coefficient which depends on tip speed ratio (λ) and pitch angle (θ_p).

Generally, c_p can be estimated using information about the wind turbines from the manufacturers which already includes electrical efficiency as shown in the figure below.

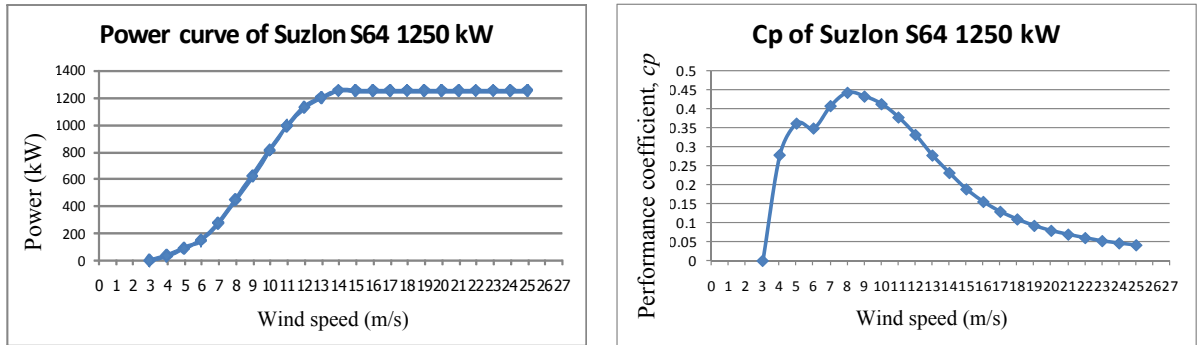


Figure 2.21 Power curve (left) and C_p curve (right) of Suzlon S64 wind turbine

For example, from the above figure, to estimate c_p , two polynomial functions will be used to fit 2 different curves. First is for the wind speed from 3 to 6 m/s, second is for the wind speed from 6 to 25 m/s.

For wind speed from 3 to 6 m/s, 3rd order polynomial can be fitted as follows.

$$c_{pa} = a_1 V^3 + a_2 V^2 + a_3 V + a_4 \quad \text{Eq. 2-122}$$

For wind speed from 6 to 25 m/s, 3rd order polynomial can be fitted as follows.

$$c_{pb} = b_1 V^3 + b_2 V^2 + b_3 V + b_4 \quad \text{Eq. 2-123}$$

Therefore, P_{ex} can be calculated using Eqs. 2-121– 2-123 and become

$$P_{ex} = \frac{1}{2} c_{pa} \rho A V^3 \quad \text{where } 3 \leq V \leq 6 \text{ m/s} \quad \text{Eq. 2-124}$$

$$P_{ex} = \frac{1}{2} c_{pb} \rho A V^3 \quad \text{where } 6 < V \leq 25 \text{ m/s} \quad \text{Eq. 2-125}$$

However, the polynomial function can be estimated differently depending on the c_p curve from the manufacturer.

If we know the time series of wind speed and c_p curve from manufacturer, then we can calculate time series of electrical wind power (P_e) using Eqs. 2-124 and 2-125 ($P_e = P_{ex}$) with the suitable range of selected wind speed. The c_{pa} and c_{pb} can be fitted using polynomial function, for example, as show in Eqs. 2-122 and 2-123. Example of electrical wind power result of calculation is shown in next figure.

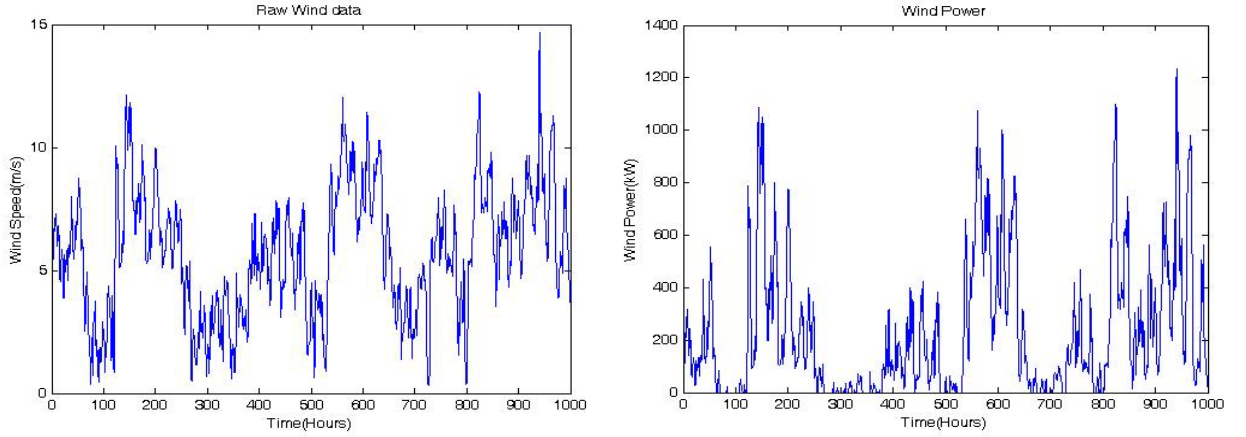


Figure 2.22 Hourly wind speed (m/s) (left) and wind power (kW) (right) for 1000 hours

In the above two figures, examples of hourly wind speed for 1000 hours are shown. The electrical wind power (P_e) is then calculated using these hourly wind speed data based on Eqs. 2-121 to 2-125. For Suzlon S64 wind turbine, A is 3,217 sq.m. and ρ is about 1.18 kg/m³ for Thailand.

2.7.2 Probability distribution of wind

The velocity duration of wind

Velocity duration of wind is the time (hours) that each level of wind velocity occurs during a period of one year, one month or one day. The Figure 2.23 is an example of frequency distribution of wind over one year.

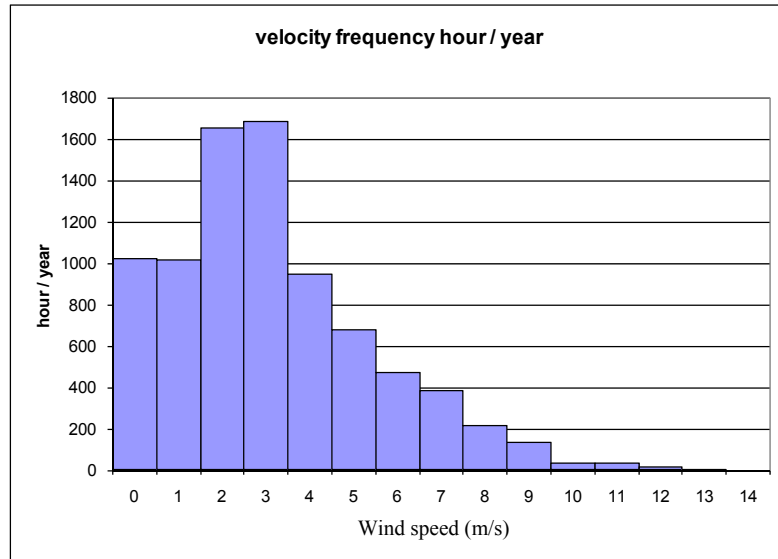


Figure 2.23 Example of velocity duration of wind over one year

Weibull distribution of wind

The distribution function (cumulative of frequency) of wind speed is expressed as:

$$F(V) = 1 - e^{-\left(\frac{V}{c}\right)^k} \quad \text{Eq. 2-126}$$

where c is the scale parameter and k is the shape parameter.

The parameter c is larger for the distribution with stronger wind. The parameter k has the value between 1.0 to 2.0 for light and fluctuating wind, and from 2.0 to 4.0 for strong and steady wind.

The frequency function of wind speed can be expressed as:

$$f(V) = \frac{k}{c} \left(\frac{V}{c}\right)^{k-1} e^{-\left(\frac{V}{c}\right)^k} \quad \text{Eq. 2-127}$$

However, to get a best fit curve of Weibull distribution, R.H.B. Exell et al. (1981) claimed that one should exclude calm winds. Figures 2.24 and 2.25 represent examples of distribution function and frequency function of wind speed, respectively.

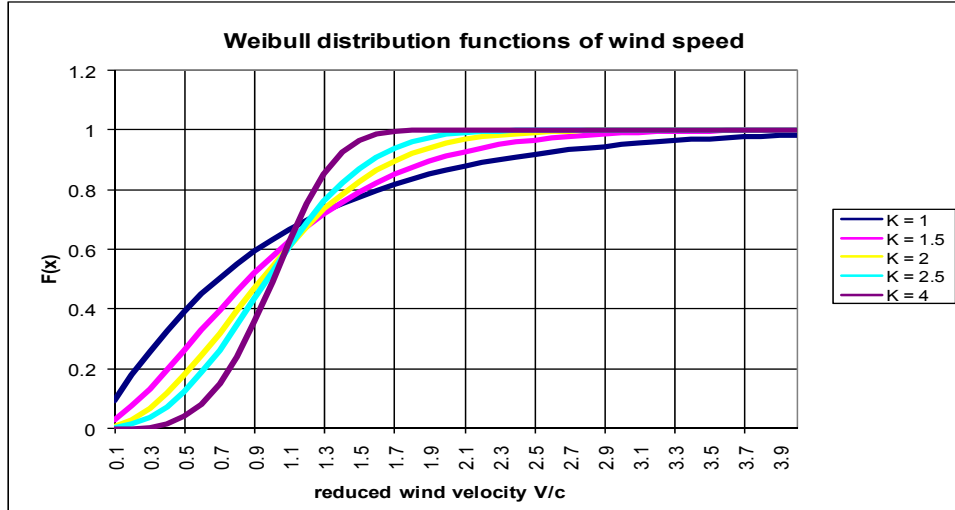


Figure 2.24 Example of distribution function of wind speed

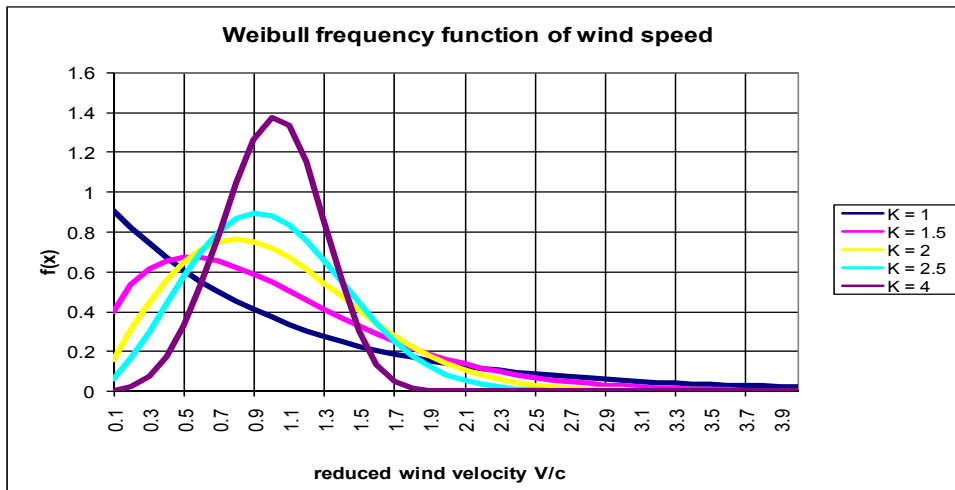


Figure 2.25 Example of frequency function of wind speed

Power Duration and Energy production estimation of Wind Turbine

From the frequency function of wind speed, we know the parameters c and k , and one specified period of time (Ex. 8760 hours), therefore we can produce a velocity duration curve as shown in Figure 2.26 (left). Commercial wind turbine generally has information of power duration curve of turbine for example as show in Figure 2.26 (right).

Since we have both the velocity and power duration curves, the energy production of that wind turbine with this wind regime can be estimated. Energy production can be calculated by integration of the multiplication between the power and duration of wind at any velocity for example as follows:

$$E = \int_{V=0}^{V=V_{\max}} P(V)h(V)dV \quad \text{Eq. 2-128}$$

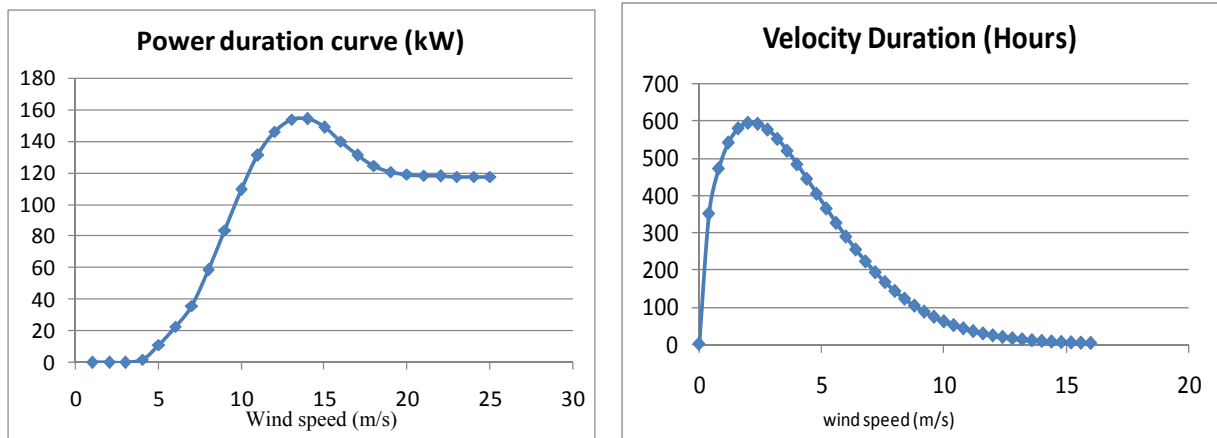


Figure 2.26 Power duration curve (left) and Velocity duration curve (right)

An example of energy production is shown in Figure 2.27.

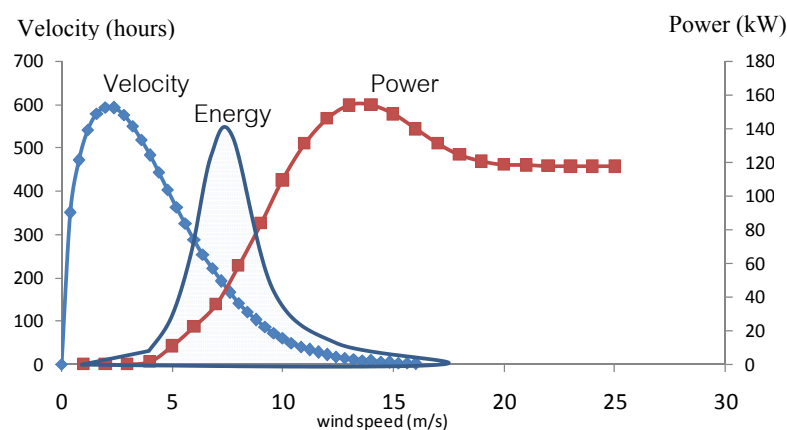


Figure 2.27 Energy production (shaded area) from multiplication between power (kW) and velocity duration (hours)

2.7.3 Wind turbine technology

2.7.3.1 Wind turbine type

There are 2 types of wind turbines based on speed control, which are:

WTS (1) Fixed-speed wind turbines

The wind turbine's rotor speed is fixed and can be controlled by *stall control*. They are normally equipped with an induction generator (squirrel cage or wound rotor) which directly connect to the grid. The fixed-speed wind turbine is simple, robust, reliable, and well-proven.

However, its disadvantages are an uncontrollable reactive power consumption, mechanical stress, and limited power quality control. In case of weak grid, power fluctuation from fixed-speed wind turbine can causes large voltage fluctuation.

WTS (2) Variable speed wind turbines

The variable speed wind turbines are designed to achieve maximum aerodynamic efficiency over a wide range of wind speeds. Therefore, the rotational speed of a wind turbine can accelerate or decelerate and tip speed ratio is fixed depending on maximum efficiency. The wind turbines are normally equipped with an induction or synchronous generator and connect to the grid through power converter. The power converter controls the generator speed, power output and voltage.

The advantages of variable speed wind turbines are increased energy capture, improved power quality, and reduced mechanical stress. The disadvantages are losses in power electronics, the use of more components, increasing cost of equipments.

There are 3 types of wind turbines base on power control, that are

WTP (1) The stall control

The stall control wind turbine is robust and cheapest when the blade angle is fixed (called passive control). The fixed blade angle is designed for the over wind speed to stall and then power losses. This is a slow aerodynamic power regulation causing less power fluctuation than fast-pitch power control.

WTP (2) The pitch control

The blades can be turned in or out to achieve the maximum power. The pitch control has advantage for the starting up and emergency stop. Power output is kept close to the rated generation. However, it causes more components with complexity. The high wind gust can cause higher power fluctuation around the rated mean power.

WTP (3) The active stall control

At low wind speed, the blades are turned the same with pitch control mechanism. At high wind speed, the blades are fixed with the angle that can cause stall effect to limit the power output. This active stall control can reduce power fluctuation at high wind speed unlike in the case of pitch control.

From the concepts of speed control and power control, wind turbines can be classified as presented in the table below.

2.7.3.2 Wind turbine classification

Typically, 4 conceptual types of wind turbines are presented in the table below [67].

Table 2.3 Wind turbine types by speed and power control

Speed control		Power control		
		Stall	Pitch	Active stall
Fixed speed	Type A	Type A0	Type A1	Type A2
Variable speed	Type B	-	Type B1	-
	Type C	-	Type C1	-
	Type D	-	Type D1	-

Type A wind turbines (fixed speed with stall control, pitch control, and active stall control) are directly connected to the grid with an asynchronous squirrel cage induction generator (SCIG). Between SCIG and transformer always has capacitor bank (C-bank) to compensate reactive power drawing from the grid. Before C-bank, soft-starter is used for smoother connecting to the grid.

Type B wind turbines (limited variable speed with pitch control) with an asynchronous wound rotor induction generator (WRIG) are directly connected to the grid through soft-starter, C-bank, and transformer. Additional important equipment is variable rotor resistance connecting to the rotor of WRIG which can be controlled by optically controlled converter. Therefore, the power output is controlled through variable rotor resistance.

Type C wind turbines (Variable speed with partial scale frequency converter), with a slip ring WRIG directly connected to the grid and parallel with partial scale frequency converter (PSFC) which are known as doubly fed induction generator (DFIG). The partial scale frequency converter (PSFC), parallel to the line between WRIG and transformer, is designed for reactive power compensation, the smoother grid connection and grid protection. Generally, the frequency or speed range of PSFC is -40% to +30% of the synchronous speed.

Type D wind turbines (Variable speed with full scale frequency converter) with the generator connected to the grid through full scale frequency converter (FSFC). FSFC is designed for reactive power compensation, the smoother grid connection and grid

protection. The generator can be excited electrically by wound rotor synchronous generator (WRSG), WRIG, or by permanent magnet synchronous generator (PMSG).

In 2002, Type C wind turbines had the most shares of 47% of total installed wind power follow by Type A wind turbines with 28% shares and type D 20% shares. [67.]

2.7.4 Wind power models

For wind power modeling, the 3 main models are wind speed model, wind turbine model or wind farm model, and grid system model.

If a wind farm is considered instead of an individual wind turbine, the wind farm model which consists of wind turbine model and wind power integration model are studied.

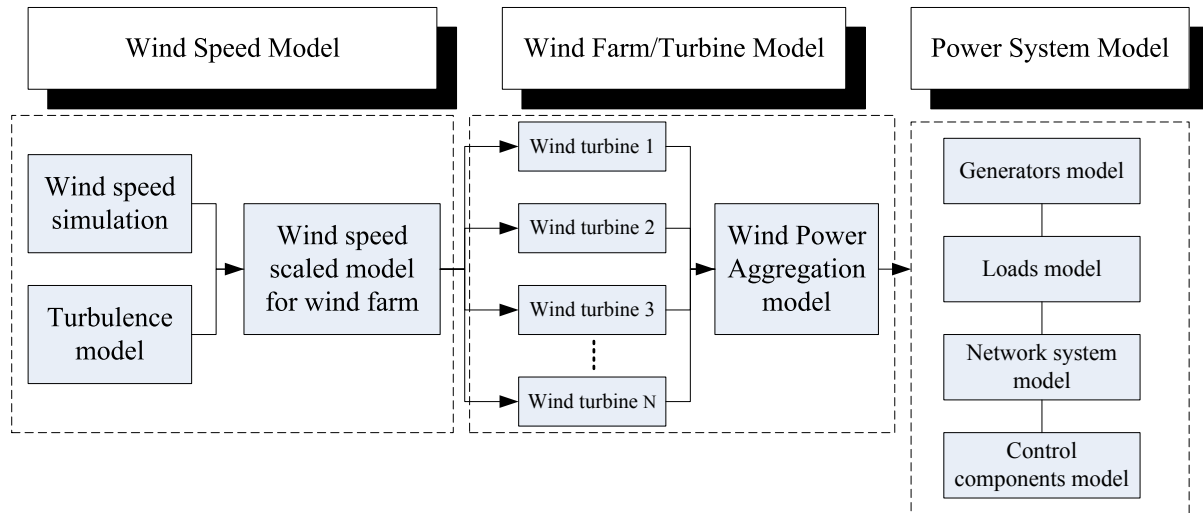


Figure 2.28 Schematic diagram of wind power model

2.7.4.1 Wind speed model

The main proposed of wind speed model is to generate wind speed for each wind turbine. The complex of topography and surrounding obstacles including nearby wind turbines causes turbulence of wind and result in complication of the modeling.

The 3 main parts of the wind speed model are wind speed simulation, turbulence model, and wind speed scaled model for wind farm.

The wind speed simulation will simulate wind speed value, for example, constant value, time varying value, ramp, sinusoid, etc., as the main part of wind speed in the case of not having the measured wind data. Straightforward wind speed simulation will not consider the physical phenomena while the complicated one applies physical phenomena of winds using mathematical model. These mathematical functions are such as conservation

of mass, conservation of momentum or motion and conservation of heat. The sophisticated mathematical modeling bases on the *Navier-Stokes Equations* that is to simulate steady or unsteady (time varying) wind speed.

The turbulence is a complicated part that is caused by topographical effects and from aerodynamic of wind turbine itself and among each other. The mathematical model for topographical effect turbulence is called *turbulence closure model* which higher order of wind speed deviation are considered. The more details are well explained in *An Introduction to Boundary Meteorology* by Roland Stull.

The turbine generated (aerodynamic of wind turbine) turbulence, or *wake effect*, can be modeled using analytical methods such as velocity deficit model, and numerical methods such as eddy viscosity model and computational fluid dynamic (CFD) aeroelastic model (from website: www.windpro.com).

The wind speed scaled model integrates the wind speed simulation and turbulence model to generate wind speeds at each wind turbine rotor position in the wind farm. This can be called a *park scaled model*, which are, for example, Mann simulation method, real cross spectral method, and complex cross spectral method [51].

2.7.4.2 Wind farm/turbine model

For a wind farm model, the wind power aggregation model is used to approximate the power output of a wind farm with reduced computational time and complications. There are 3 cases of aggregation model, that are, (1) Aggregated wind farm model, (2) Grouped wind farm model, and (3) Detailed wind farm model.

Aggregated wind farm models assume the same wind speed and same wind turbine parameters for all wind turbines. Therefore, only one wind turbine is modeled and then the power output of wind farm is the multiply by N turbines [49].

Grouped wind farm models assume the same wind speed but different wind turbine parameters for wind turbines with the different type. Therefore, each group of wind turbine is modeled differently.

Detailed wind farms compute power from individual wind turbine with different wind speed and parameters. This method has higher accuracy than the previous two methods but require much of computational time and complication.

The wind turbine model consists of many sub-models such as rotor model, mechanical shaft model, generator model, and power converter model depending on type

of wind turbine as be presented in next figure. Furthermore, the converter model, the main control system and pitch control system are also considered for some types of wind turbine.

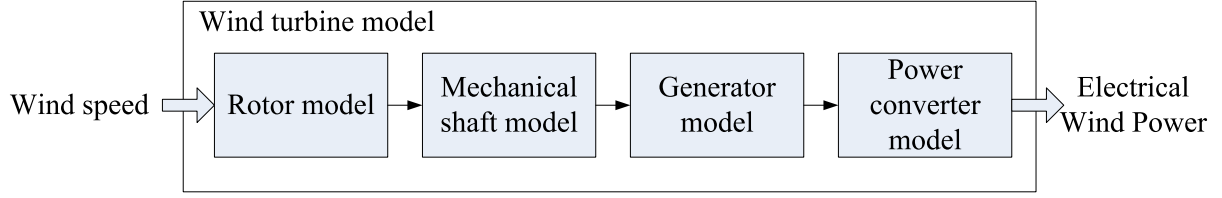


Figure 2.29 Schematic diagram of wind turbine model

The rotor model transforms kinetic energy from wind to mechanical power. Therefore, the mechanical power output of a rotor depends on wind speed (V_{ws}), air density (ρ), area of rotor (A_r), the blade angle (β), and the rotational speed of the wind turbine (ω_{wt}).

$$P_{me} = f_{Pm}(\omega_{wt}, V_{ws}, \beta) \quad \text{Eq. 2-129}$$

$$P_{me} = \frac{1}{2} \rho A c_p(\lambda, \beta) V_{ws}^3 \quad \text{Eq. 2-130}$$

The power efficiency coefficient (C_p) depends on tip speed ratio (λ), and β .

The tip speed ratio is a function of ω_{wt} , V_{ws} , and turbine radius (R) as follows

$$\lambda = \frac{\omega_{wt} R}{V_{ws}} \quad \text{Eq. 2-131}$$

The C_p can be represented in various models, for example, constant power with constant C_p , function and polynomial approximation, table representation, and blade element momentum method (BEM) and aeroelastic code. [67]

The moment of inertia of a wind rotor is about 90% of total moment, while the rotor generator is about 6-8% and remaining parts of the drive train are about 2-4%.

The mechanical shaft (or drive train of wind turbine) can be modeled using equations of mass motion. A set of the first order differential equations for i^{th} mass model is formed as follows [73]:

$$\frac{d\delta_i}{dt} = \omega_i - \omega_{si} = \Delta\omega_i \quad \text{Eq. 2-132}$$

$$\begin{aligned} J_i \frac{d\Delta\omega_i}{dt} = & \tau_i + K_{i,i+1}(\delta_{i+1} - \delta_i) - K_{i,i-1}(\delta_i - \delta_{i-1}) \\ & + D_{i,i+1}(\Delta\omega_{i+1} - \Delta\omega_i) - D_{i,i-1}(\Delta\omega_i - \Delta\omega_{i-1}) - D_i \Delta\omega_i \end{aligned} \quad \text{Eq. 2-133}$$

Where δ_i is torsion angle of i^{th} mass (displacement of the mass), ω_i is rotational speed of i^{th} mass, ω_{si} is synchronous speed of shaft rotor, J_i is moment of inertia of i^{th} mass, τ_i is external torque applied to i^{th} mass, $K_{i,i+1}$ and $K_{i,i-1}$ are stiffness coefficients of the shaft sections between mass $(i,i+1)^{th}$ and mass $(i,i-1)^{th}$, and $D_{i,i+1}$ and $D_{i,i-1}$ are damping coefficient of the shaft sections.

The generator model of squirrel cage induction generator (SCIG) wind turbine in the d-q (direct-quadrature) reference frame, was presented already in Section 2.1.3).

The generator model of doubly fed induction generator (DFIG) wind turbine in the d-q (direct-quadrature) reference frame, the voltages in per unit are as follows [67]:

$$\left. \begin{aligned} u_{ds} &= -R_s i_{ds} + \omega_s \psi_{qs} = -R_s i_{ds} + \omega_s [(L_{s\sigma} + L_m) i_{qs} + L_m i_{qr}] \\ u_{qs} &= -R_s i_{qs} - \omega_s \psi_{ds} = -R_s i_{qs} - \omega_s [(L_{s\sigma} + L_m) i_{ds} + L_m i_{dr}] \\ u_{dr} &= -R_r i_{dr} + s \omega_s \psi_{qr} = -R_r i_{dr} + s \omega_s [(L_{r\sigma} + L_m) i_{qr} + L_m i_{qs}] \\ u_{qr} &= -R_r i_{qr} - s \omega_s \psi_{dr} = -R_r i_{qr} - s \omega_s [(L_{r\sigma} + L_m) i_{dr} - L_m i_{ds}] \end{aligned} \right\} \quad \text{Eq. 2-134}$$

The differences from SCIG wind turbine are that the rotor voltage is not zero and the derivative of flux linkages are neglected.

The equations of active (P) and reactive power (Q) are also different due to the rotor winding of generator can be adjusted. These equations are

$$\left. \begin{aligned} P &= P_s + P_r = u_{ds} i_{ds} + u_{qs} i_{qs} + u_{dr} i_{dr} + u_{qr} i_{qr} \\ Q &= Q_s + Q_r = u_{qs} i_{ds} - u_{ds} i_{qs} + u_{qr} i_{dr} - u_{dr} i_{qr} \end{aligned} \right\} \quad \text{Eq. 2-135}$$

The **power converter model** is basically modeled as a current source. u_{qr} is equal to u_t (the terminal voltage) based on the assumption that d-axis corresponds to the maximum of the stator flux. Thus, electrical torque can be computed as follows

$$T_e = \frac{L_m u_t i_{qr}}{\omega_s (L_{s\sigma} + L_m)} \quad \text{Eq. 2-136}$$

The reactive power exchanged with the grid at the stator terminals (Q_s) depends on the direct component of the rotor current. Thus, DFIG wind turbine neglects the stator resistance, and assumes that d-axis corresponds to the maximum of the stator flux. Therefore,

$$Q_s = \frac{L_m u_t i_{qr}}{(L_{s\sigma} + L_m)} - \frac{u_t^2}{\omega_s (L_{s\sigma} + L_m)} \quad \text{Eq. 2-137}$$

The total reactive power exchanged with the grid depends on both the control of the generator and the control of the grid side of converter, therefore, active and reactive power converter are

$$\left. \begin{aligned} P_c &= u_{dc} i_{dc} + u_{qc} i_{qc} \\ Q_c &= u_{qc} i_{dc} - u_{dc} i_{qc} \end{aligned} \right\} \quad \text{Eq. 2-138}$$

Where c stands for converter.

In this case, P_c is equal to P_r of DFIGURE P_r may be multiplied with the converter efficiency. Total reactive power exchanged with the grid is equal to $Q_s + Q_c$.

2.7.4.3 Power system model

The power system model is a set of nonlinear first-order differential equations and algebraic equations (DAE) expressed by

$$\begin{aligned} \dot{\mathbf{x}} &= \mathbf{f}(\mathbf{x}, \mathbf{u}, t) \\ \mathbf{g}(\mathbf{x}, \mathbf{y}, \mathbf{u}, t) &= 0 \end{aligned} \quad \text{Eq. 2-139}$$

Where \mathbf{x} , \mathbf{y} , \mathbf{u} are state, input, and output vectors of generator, generator controller, turbine, turbine controller, transformer, transformer controller, transmission line, load, motor, etc.

The linear DAE of the power system is described by

$$\begin{aligned} \Delta \dot{\mathbf{x}} &= \mathbf{A} \Delta \mathbf{x} + \mathbf{B} \Delta \mathbf{u} \\ \Delta \mathbf{y} &= \mathbf{C} \Delta \mathbf{x} + \mathbf{D} \Delta \mathbf{u} \end{aligned} \quad \text{Eq. 2-140}$$

$$\mathbf{A} = \begin{bmatrix} \frac{\partial f_1}{\partial x_1} & \dots & \frac{\partial f_1}{\partial x_n} \\ \vdots & \ddots & \vdots \\ \frac{\partial f_n}{\partial x_1} & \dots & \frac{\partial f_n}{\partial x_n} \end{bmatrix}, \mathbf{B} = \begin{bmatrix} \frac{\partial f_1}{\partial u_1} & \dots & \frac{\partial f_1}{\partial u_r} \\ \vdots & \ddots & \vdots \\ \frac{\partial f_n}{\partial u_1} & \dots & \frac{\partial f_n}{\partial u_r} \end{bmatrix},$$

$$\mathbf{C} = \begin{bmatrix} \frac{\partial g_1}{\partial x_1} & \dots & \frac{\partial g_1}{\partial x_n} \\ \vdots & \ddots & \vdots \\ \frac{\partial g_m}{\partial x_1} & \dots & \frac{\partial g_m}{\partial x_n} \end{bmatrix}, \mathbf{D} = \begin{bmatrix} \frac{\partial g_1}{\partial u_1} & \dots & \frac{\partial g_1}{\partial u_r} \\ \vdots & \ddots & \vdots \\ \frac{\partial g_m}{\partial u_1} & \dots & \frac{\partial g_m}{\partial u_r} \end{bmatrix}$$

Where \mathbf{A} , \mathbf{B} , \mathbf{C} , \mathbf{D} are state matrixes that define the proportion of the input appearing directly in the output and n , m , r are the size of state variables, number of output, and number of input variables, respectively.

2.7.5 Wind Power and Power quality

2.7.5.1 Classification of power quality

The 4 major international standards of power quality are by J. Arrillaga and N.R. Watson (2000) and Roger C. Dugan (2003) as follows:

- **IEC 61000-2-5:1995** is Electromagnetic Compatibility Standard (EMC) for
 - Low-frequency phenomena (<9kHz) (conducted voltage, frequency)
 - High-frequency phenomena (>9kHz) (Electric and mechanical field)
 - Electrostatic Discharge (ESD) phenomena
- **IEC 61000-2-1:1995** for EMC that is technical reported with conducted low-frequency (<10kHz)
- **IEEE 1159:1995** for the power system with 7 categories depending on spectral content, duration, and voltage magnitude.

(C.1) Transient with impulsive (10^{-9} , 10^{-6} , 10^{-3} sec) and oscillatory

(C.2) Short-duration variation (0.5 cycle – 1 min) (sag, swell, Interruption)

(C.3) Long-duration variation (>1min) (Interruption, over/under voltage)

(C.4) Voltage imbalance (steady state)

(C.5) Waveform distortion (d.c.offset, harmonics, inter-harmonics, noise)

(C.6) Voltage fluctuation (<25Hz)

(C.7) Power frequency variation (< 10sec)

- **EN 50160-1999** standard defining the quality of the power supplied to the consumers. 7 limits for the low voltage supply are:

(1) Voltage magnitude : 95% of 10min avg. during 1 week should be within $\pm 10\%$ of the nominal voltage ($V_n = 230V$)

(2) Voltage magnitude step : not exceed $\pm 5\%$ of V_n

(3) Voltage fluctuation : 95% of 2h long term flicker (fl) during 1 week not exceed 1. ($P_{lt} = \sqrt[3]{\sum_{i=1}^{12} P_{sti}^3 / 12}$, P_{st} is short-term flicker with 10 min averages)

(4) Harmonic distortion : voltage harmonics up to order 25th not exceeding

95% of 10 min avg. during 1 week. $THD = \sqrt{\sum_{h=2}^{40} V_h^2}$ is calculated for voltage $\leq 8\%$

(5) Voltage unbalance : 95% of ratio of – and + sequence voltage 10min avg. not exceeding 2% during 1 week.

(6) Signaling voltages : 95% of the 3s avg. during 1 day not exceeding 9% for frequency up to 500Hz, 5% for freq. 1-10 kHz, 1% for higher frequencies.

(7) Frequency : 95% of 10s avg. not outside the range 49.5 – 50.5 Hz

Power quality standard for wind power

The International Electrotechnical Commission (IEC) published the first edition of the technical standard on assessment of the power quality from wind turbines in 2001 that is *IEC 61400-21* and the latest version in 2008.

There are many important parameters in IEC 61400-21 for wind turbines (WT) that are:

- (1) Maximum permitted power, P_{mc}
- (2) Maximum measured power, P_{60} (60s average)
- (3) Maximum measured power, $P_{0.2}$ (0.2s average)
- (4) Reactive power, Q
- (5) Flicker coefficient (depend on phase angle, annual avg. wind speed)
- (6) Max. number of switching operation in 10 min, N_{10}
- (7) Max. number of switching operation in 2 h, N_{120}
- (8) Flicker step factor (depend on network impedance phase angle)
- (9) Flicker change factor (depend on network impedance phase angle)
- (10) Maximum harmonics current, I_h (only WT with converter)

However, the PQ standard on the assessment of wind farm has not yet been published.

Interesting power quality aspects incorporating wind power

Based on IEEE 1159 and IEC 61400-21, 3 interesting aspects of power quality including wind power are,

- Long-duration voltage variation (Interruption, Over/under voltage due to mismatching between wind power source and load demand)
- Voltage fluctuation (<25Hz including flicker)
- Frequency variation (< 10sec)

The other categories not directly influenced by wind power fluctuations and/or rare to occur at present. Wave form distortion is not considered here since it depends on electronics components of wind power system which beyond the scopes of thesis.

2.7.5.2 Voltage variation of wind power [73]

The variation of voltage when connected to a wind power plant depends not only on variation of wind power generation and load but structure of the power network and point of connecting have also to be considered. For example 2 types of power network with different point of wind power connecting are expressed. These are 1) typical radial power network including WTGs at terminal and 2) power network including WTGs at middle node.

The voltage variation (drop) for typical radial power network including WTGs at terminal is constructed as presented in next figure.

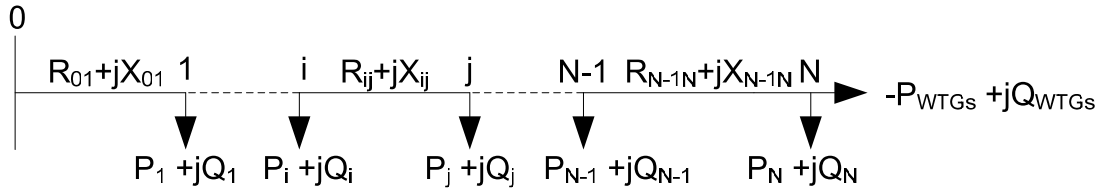


Figure 2.30 Circuit diagram of typical radial power network including WTGs

Variations of voltage, for typical radial power network, including WTGs at a terminal, as a function of active, reactive power and impedances is presented as follows.

$$\Delta V_j = \Delta V_{0j} - \Delta V_{0j}^{WTGs} = \frac{P_{WTGs} \sum_{l=0}^{j-1} R_{l,l+1} - Q_{WTGs} \sum_{l=0}^{j-1} X_{l,l+1}}{V_n} \quad \text{Eq. 2-141}$$

Where V_n is rated voltage, ΔV_{0j} is voltage drop in branches from 0 to j without WTGs.

ΔV_{0j}^{WTGs} is voltage drop with WTGs.

The voltage change in the i^{th} node for power network, including WTGs at j^{th} node is constructed, as presented in the figure below.

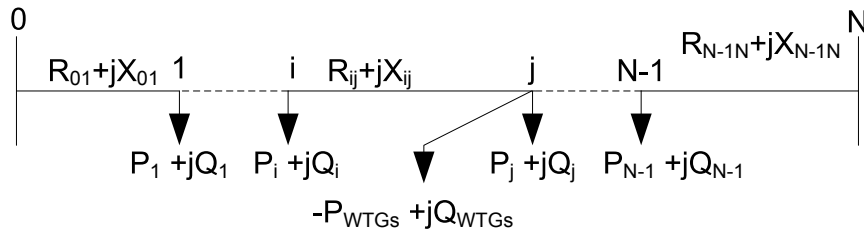


Figure 2.31 Circuit diagram of power network including WTGs at the j^{th} node

Variations of voltage for power network, including WTGs at the middle node as a function of impedances and current of WTGs is presented in the equation below.

$$\delta V_i = V_i - V_i^{WTGs} = \left(\sqrt{3} I_{WTGs} \sum_{p=0}^{i-1} Z_{p,p+1} \sum_{p=j}^{N-1} Z_{p,p+1} \right) \left(\sum_{p=0}^{N-1} Z_{p,p+1} \right)^{-1} \quad \text{Eq. 2-142}$$

Where V_i is the voltage in i^{th} node without WTGs, V_i^{WTGs} is the voltage in i^{th} node with WTGs, and I_{WTGs} is the current of WTGs.

2.7.5.3 Flicker [73]

There are 3 types of flicker according to IEC61400-12, which are:

- Flicker emission level during continuous operation for N WTGs

$$P_{st} = P_{lt} = \frac{1}{S_k} \sqrt{\sum_{i=1}^N (c_i(\psi_k, v_a) S_{ni})^2} \quad \text{Eq. 2-143}$$

- Short-term flicker emission level during switching operation for N WTGs

$$P_{st} = \frac{18}{S_k} \left(\sum_{i=1}^N N_{10i} (k_{fi}(\psi_k) S_{ni})^{3.2} \right)^{0.31} \quad \text{Eq. 2-144}$$

- Long-term flicker emission level during continuous operation for N WTGs

$$P_{lt} = \frac{8}{S_k} \left(\sum_{i=1}^N N_{120i} (k_{fi}(\psi_k) S_{ni})^{3.2} \right)^{0.31} \quad \text{Eq. 2-145}$$

Where S_k is apparent short-circuit power at PCC, S_{ni} is rated the apparent power of i^{th} wind turbine, c_i is i^{th} wind turbine flicker coefficient, ψ_k is network impedance phase angle, v_a is annual average wind speed, k_{fi} is flicker step factor, k_u is voltage change factor, N_{10i} , N_{120i} are max. number of switching operation within 10 and 120 minutes. c_i , k_{fi} , N_{10i} , N_{120i} , k_u are from measuring methods in IEC61000-21.

Relative voltage change (%) due to switching operation is

$$d = 100 \cdot k_u(\psi_k) S_n S_k^{-1} \quad \text{Eq. 2-146}$$

2.7.5.4 Frequency variation of wind power [3]

The frequency variation can be considered from two aspects, which are:

1) The frequency change considering generation characteristics

$$\frac{\Delta f}{f_n} = -R_G \frac{\Delta P_G}{P_L} = -\frac{P_L}{\sum_{i=1}^N K_i P_{mi}} \frac{\Delta P_G}{P_L} \quad \text{Eq. 2-147}$$

$$K_i = \frac{1}{R_i} = \frac{\Delta P^*}{\Delta f^*} = \frac{f_0}{P_0} \frac{P_{\max} - P_{\min}}{f_{\max} - f_{\min}} \quad \text{Eq. 2-148}$$

2) The frequency change considering system control:

$$\frac{\Delta f}{f_n} = -R_{PS} \frac{\Delta P_{PS}}{P_L} = -\frac{1}{K_{PS}} \frac{\Delta P_{PS}}{P_L} = -\frac{1}{(K_G + K_L)} \frac{\Delta P_{PS}}{P_L} \quad \text{Eq. 2-149}$$

$$\Delta P_{PS} = \Delta P_G + \Delta P_L = P_L (K_G + K_L) \Delta f / f_n \quad \text{Eq. 2-150}$$

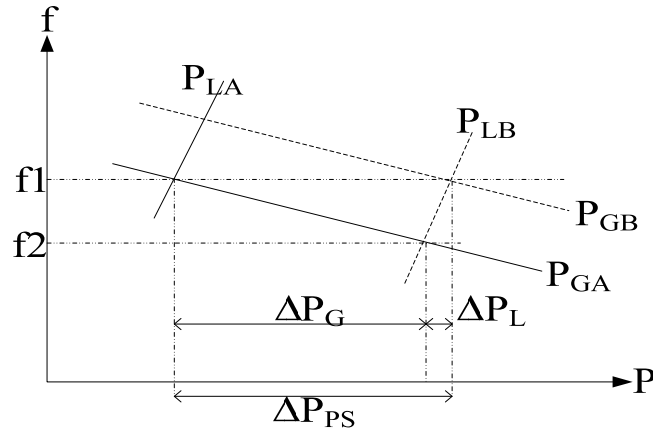


Figure 2.32 The P - f characteristics of wind power system

Where

$R_i = 1/K_i$ is *statism* or slope between rotational speed and turbine mechanical power

$R_G = 1/K_G$ is for generation

$R_L = 1/K_L$ is for load

$K_{PS} = 1/R_{PS}$ is system stiffness

P_G is power generation

P_L is power load

P_m is mechanical power generation

ΔP_{PS} is change in overall power

2.8 Probabilistic Methods for the Power System

Present and future power systems are dynamics systems that are very complicate and expected to have high reliability. Realistic operating conditions and system parameters cannot be predicted certainly due to many uncertainties from, for example, the system structure, load conditions, generation conditions, and affecting environment.

Uncertainties from unpredictable phenomena are random. Therefore, deterministic methods with high reliability cannot be used directly to deal with these problems. Normally, deterministic methods are based on worst case scenarios and ignore the variability of the important parameters of the power system. Better technique is the several cases scenario which consider several possible values of parameter or condition.

However, this is not precise enough when dealing with random variables or random processes affecting the system design and operation. Accordingly, the probabilistic methods are the most relevant tools to deal with random variables and processes of the system.

2.8.1 Random Variables

Random variable may be continuous or discrete. Important topics relating to random variables are probability distribution, cumulative distribution function, probability density function, probability mass function, Mean, Variance, and Standard Deviation of random variable, multiple random variable, and determination of distribution models.

2.8.1.1 Probability distribution

Probability distribution is the probability of the occurrence of random variable X . Probability distribution, $p(x)$ when $x \in X$ has two simple properties as follows:

For continuous random variable $0 \leq p(x) \leq 1$ and $\int_{-\infty}^{+\infty} p(x) = 1$

For discrete random variable $0 \leq p(x_i) \leq 1$ and $\sum_i p(x_i) = 1$

2.8.1.2 Cumulative distribution function

Cumulative distribution function, CDF, ($F_X(x)$) is the probability that X is less than or equal to x when $x \in X$ or

$$F_X(x) = P(X \leq x) \quad \text{Eq. 2-151}$$

- $F_X(x)$ has interval between 0 and 1
- $\lim_{x \rightarrow \infty} F_X(x) = 1$ and $\lim_{x \rightarrow -\infty} F_X(x) = 0$

- If $F_X(x)$ is discrete, then X is discrete random variable. But if $F_X(x)$ is continuous, then X is continuous random variable.

2.8.1.3 Probability density function

Considering x on the interval (a,b) on the real axis with $a < b$, the probability that X is in between the interval (a,b) is the integral of *probability density function* (PDF), $f_X(x)$, between the limit (a,b) as follows:

$$P(a < X \leq b) = \int_a^b f_X(x) dx \quad \text{Eq. 2-152}$$

Several properties involving PDF are as follows:

- $f_X(x) \geq 0$ for all x and $\int_{-\infty}^{\infty} f_X(x) dx = 1$
- $F_X(x) = \int_{-\infty}^x f(t) dt$ and $P(a \leq X \leq b) = F(b) - F(a)$
- $\frac{dF_X(x)}{dx} = f_X(x)$

2.8.1.4 Probability mass function

For a discrete random variable X , the probability mass function (PMF) is the probability that X is equal to x .

$$\text{PMF} = P(X=x) \quad \text{Eq. 2-153}$$

For the sequence of probabilities of discrete random variables ($P(X=x_i)$), CDF can be used to describe as follows:

$$F(x_i) - F(x_{i-1}) = P(X \leq x_i) - P(X \leq x_{i-1}) = P(X = x_i) \quad \text{Eq. 2-154}$$

2.8.1.5 Mean, Variance, and Standard Deviation of random variable

Mean or Expected value (Central value)

The mean or expected value of a random variable is the weighted average, while the weight is the probability of the random value.

For discrete random variables: $E(X) = \sum_i x_i p_i \quad \text{Eq. 2-155}$

For continuous random variables: $E(X) = \int_{-\infty}^{\infty} x f_X(x) dx \quad \text{Eq. 2-156}$

Variance and Standard Deviation

The expected value functions above can be applied to the function of X or $g(X)$ as follows:

For discrete random variables: $E[g(X)] = \sum_{\text{all } x_i} g(x_i) p_i$ Eq. 2-157

For continuous random variables: $E[g(X)] = \int_{-\infty}^{\infty} g(x) f_X(x) dx$ Eq. 2-158

$E[g(x)]$ is called the mathematical expectation of $g(X)$.

The variance (σ^2) of a random variable is ($\text{Var}(X)$) defined as follows:

$$\text{Var}(X) = E[(X - E(X))^2] \quad \text{Eq. 2-159}$$

If $g(X) = (X - E(X))^2$ and $E(X) = \mu_X$, therefore :

For discrete random variables: $\text{Var}(X) = \sum_{\text{all } x_i} g(x_i) p_i = \sum_{\text{all } x_i} (x_i - \mu_X)^2 p_i$ Eq. 2-160

For continuous random variables: $\text{Var}(X) = \int_{-\infty}^{\infty} (x - \mu_X)^2 f_X(x) dx = E(X^2) - \mu_X^2$ Eq. 2-161

The standard deviation (σ) of the random variable is the square root of $\text{Var}(X)$, that is:

$$\text{Std}(X) = \sqrt{\text{Var}(X)} \quad \text{Eq. 2-162}$$

For *bivariate random variable* (X, Y) , the mean, variance, and covariance are as follows:

The mean of X is $E(X) = \int_{-\infty}^{\infty} \int_{-\infty}^{\infty} x f_{XY}(x, y) dx dy$ Eq. 2-163

The variance of X is $\sigma_X = \text{Var}(X) = \int_{-\infty}^{\infty} \int_{-\infty}^{\infty} (x - \mu_X)^2 f_{XY}(x, y) dx dy$ Eq. 2-164

The covariance of X, Y is $\text{Cov}(X, Y) = E[(X - \mu_X)(Y - \mu_Y)] = E(XY) - E(X)E(Y)$ Eq. 2-165

If X and Y are independent $\text{Cov}(X, Y) = \int_{-\infty}^{\infty} (x - \mu_X) f_X(x) dx \int_{-\infty}^{\infty} (y - \mu_Y) f_Y(y) dy$ Eq. 2-166

The correlation coefficient is $\rho = \frac{\text{Cov}(X, Y)}{\sigma_X \sigma_Y}$ Eq. 2-167

2.8.1.6 Types of probability distribution

There are two main types of probability distribution, which are discrete distribution and continuous distribution.

For discrete distribution

1) The binomial distribution

The probability of exactly k occurrences in n trials in a Bernoulli sequence is the *binomial* PMF, that is:

$$P(X = k) = \binom{n}{k} p^k (1-p)^{n-k} \quad \text{Eq. 2-168}$$

Where p is probability of occurrence of an event in each trial, $\binom{n}{k} = n!/[k!(n-k)!]$ is binomial coefficient.

2) The geometric distribution

For a Bernoulli sequence, the probability that the number of trials until a specified event occurs for the first time is called *the geometric distribution* which is:

$$P(X = j) = pq^{j-1} \quad \text{Eq. 2-169}$$

Where $q=1-p$ is the probability of the nonoccurrence of an event in any of prior $(j-1)$ trials.

The mean and variance of the geometric distribution are as follows:

$$E(X) = \sum_{j=1}^{\infty} j \cdot pq^{j-1} = p(1 + 2q + 3q^2 + \dots) = p \frac{1}{(1-q)^2} = \frac{1}{p} \quad \text{Eq. 2-170}$$

$$\text{Var}(X) = \sum_j \left(j - \frac{1}{p} \right)^2 pq^{j-1} = \frac{q}{p^2} \quad \text{Eq. 2-171}$$

3) The Poisson distribution

The Poisson distribution is the probability of the occurrence of events in time and/or space assuming that a unit interval is constant and the events are all independent.

The PMF of a Poisson process (or called Poisson distribution) is:

$$P(X_t = x) = \frac{(\lambda t)^x}{x!} e^{-\lambda t} \quad \text{Eq. 2-172}$$

Where λ is the mean occurrence rate (events per unit interval) and X_t is random variable representing the number of occurrences in an interval of range t .

For continuous distribution

4) The normal distribution

The normal (or Gaussian) distribution is one of the most commonly used distributions. Its density function with a bell shape curve is:

$$f_X(x) = \frac{1}{\sqrt{2\pi\sigma^2}} e^{-\frac{(x-\mu)^2}{2\sigma^2}} \quad \text{Eq. 2-173}$$

This bell shape curve is symmetric around μ and its cumulative distribution function is:

$$F_X(x) = \int_{-\infty}^x \frac{1}{\sqrt{2\pi\sigma^2}} e^{-\frac{(y-\mu)^2}{2\sigma^2}} dy \quad \text{Eq. 2-174}$$

The normal probability density relating to normal distribution is obtained from the tables of the *standard normal distribution* (the normal distribution with zero mean and standard deviation = 1 or $N(0,1)$). The standard normal distribution is:

$$\Phi_z(z) = \frac{1}{\sqrt{2\pi}} \int_{-\infty}^z e^{-t^2/2} dt \quad \text{Eq. 2-175}$$

Where $z = (x-\mu)/\sigma$. If X has $N(\mu, \sigma)$, then CDF of random variable X is as follows:

$$F_X(x) = \Phi\left(\frac{x-\mu}{\sigma}\right) \quad \text{Eq. 2-176}$$

Therefore, the probability that X is in between a and b is:

$$P(a \leq X \leq b) = F_X(b) - F_X(a) = \Phi\left(\frac{b-\mu}{\sigma}\right) - \Phi\left(\frac{a-\mu}{\sigma}\right) \quad \text{Eq. 2-177}$$

5) The logarithmic normal distribution

If the logarithm of the random variable X has a normal distribution, then X has the *logarithmic normal distribution* (or log-normal). The PDF of X is:

$$f_X(x) = \frac{1}{\varepsilon x \sqrt{2\pi}} e^{-\frac{1}{2} \left(\frac{\ln x - \beta}{\varepsilon} \right)^2}, \quad 0 \leq x < \infty \quad \text{Eq. 2-178}$$

Where $\beta = E(\ln X)$ and $\varepsilon = \sqrt{\text{Var}(\ln X)}$ are the mean and the standard deviation of $\ln X$, respectively. The probability that X has an interval $(a, b]$ is:

$$P(a < X \leq b) = \int_a^b \frac{1}{\varepsilon x \sqrt{2\pi}} e^{-\frac{1}{2} \left(\frac{\ln x - \beta}{\varepsilon} \right)^2} dx, \quad 0 \leq x < \infty \quad \text{Eq. 2-179}$$

When considering the standard normal distribution of $\ln X$. Let $s = (\ln x - \beta)/\varepsilon$ and $dx = x \varepsilon ds$:

$$P(a < X \leq b) = \frac{1}{\sqrt{2\pi}} \int_{(\ln a - \beta)/\varepsilon}^{(\ln b - \beta)/\varepsilon} e^{-0.5s^2} ds = \Phi\left(\frac{\ln b - \beta}{\varepsilon}\right) - \Phi\left(\frac{\ln a - \beta}{\varepsilon}\right) \quad \text{Eq. 2-180}$$

6) The gamma distribution

The gamma distribution has an equation as follows:

$$f_X(x) = \frac{\lambda^\alpha}{\Gamma(\alpha)} x^{\alpha-1} e^{-\lambda x} \quad \text{Eq. 2-181}$$

Where $\alpha > 0$ and $\lambda > 0$ are the characteristic parameters of the distribution shape and $\Gamma(\alpha)$ is value of gamma function as follows:

$$\Gamma(\alpha) = \int_0^\infty x^{\alpha-1} e^{-x} dx \quad \text{and} \quad \Gamma(\alpha) = (\alpha-1)\Gamma(\alpha-1) \quad \text{Eq. 2-182}$$

Where $\mu = \alpha/\lambda$ and $\sigma^2 = \alpha/\lambda^2$.

7) The Weibull distribution

The PDF of the Weibull distribution is:

$$f_X(x) = \alpha \beta x^{\beta-1} e^{-\alpha x^\beta} \quad \alpha > 0, \beta > 0, x > 0 \quad \text{Eq. 2-183}$$

The CDF of X is from the integration of $f_X(x)$ as follows:

$$F_X(x) = \int_{-\infty}^x \alpha \beta x^{\beta-1} e^{-\alpha x^\beta} dx = 1 - e^{-\alpha x^\beta} \quad \text{Eq. 2-184}$$

Where α and β are scale and shape parameters of the Weibull distribution.

If $\beta \leq 1$, then the shape is an exponential distribution. If $\beta > 1$, then the shape is asymmetric bell. The mean and variance of Weibull distribution can be determined as follows:

$$\mu = \alpha^{-1/\beta} \Gamma(1 + 1/\beta) \quad \text{Eq. 2-185}$$

$$\sigma^2 = \alpha^{-2/\beta} \Gamma(1 + 2/\beta) - \Gamma^2(1 + 1/\beta) \quad \text{Eq. 2-186}$$

The Weibull distribution is used to determine the long-term wind speed distribution.

2.8.1.7 Multiple random variable

Before understanding multiple random variable (or multivariate random variable), the univariate and bivariate random variables are explained.

1) The univariate random variable

- There is only 1 random variable, X.
- CDF of X is $F_X(x) = P(X \leq x) = \int_{-\infty}^x f(x) dx$

2) The bivariate random variable

- There are 2 random variables, X and Y.
- Joint CDF of X and Y is $F_{XY}(x, y) = P(X \leq x, Y \leq y) = \int_{-\infty}^y \int_{-\infty}^x f_{XY}(x, y) dx dy$

Where $f_{XY}(x, y)$ is the joint PDF. To find joint PDF of X and Y, CDF and PDF of X and Y is explained as follows:

- For CDF of X: $F_X(x) = P(X \leq x, Y \leq \infty) = \int_{-\infty}^{\infty} \int_{-\infty}^x f_{XY}(x, y) dx dy$
- Therefore, PDF of X is: $f_X(x) = \frac{dF_X(x)}{dx} = \int_{-\infty}^{\infty} f_{XY}(x, y) dy$

- For CDF of Y: $F_Y(y) = P(X \leq \infty, Y \leq y) = \int_{-\infty}^{\infty} \int_{-\infty}^y f_{XY}(x, y) dy dx$
- Therefore, PDF of Y is: $f_Y(y) = \frac{dF_Y(y)}{dy} = \int_{-\infty}^{\infty} f_{XY}(x, y) dx$
- Joint PDF is: $f_{X|Y}(x|y) = \frac{f_{XY}(x, y)}{f_Y(y)}$ and $f_{Y|X}(y|x) = \frac{f_{XY}(x, y)}{f_X(x)}$
- If X and Y are independent: $f_{X|Y}(x|y) = f_X(x)$ and $f_{Y|X}(y|x) = f_Y(y)$

Therefore $f_{XY}(x, y) = f_X(x) \cdot f_Y(y)$

If X and Y have a normal distribution (*Bivariate normal random variable*), then:

$$f_X(x) = \frac{1}{\sigma_X \sqrt{2\pi}} e^{-0.5 \left(\frac{x - \mu_X}{\sigma_X} \right)^2} \quad \text{and} \quad f_Y(y) = \frac{1}{\sigma_Y \sqrt{2\pi}} e^{-0.5 \left(\frac{y - \mu_Y}{\sigma_Y} \right)^2} \quad \text{Eq. 2-187}$$

If X and Y are independent:

$$f_{XY}(x, y) = f_X(x) \cdot f_Y(y) = \frac{1}{\sigma_X \sigma_Y 2\pi} e^{\left[-0.5 \left(\frac{x - \mu_X}{\sigma_X} \right)^2 - 0.5 \left(\frac{y - \mu_Y}{\sigma_Y} \right)^2 \right]} \quad \text{Eq. 2-188}$$

If X and Y dependent,

$$\text{Joint PDF is} \quad f_{XY}(x, y) = \frac{1}{\sigma_X \sigma_Y 2\pi \sqrt{1 - \rho^2}} e^{\frac{-0.5}{(1 - \rho^2)} \left[\left(\frac{x - \mu_X}{\sigma_X} \right)^2 - 2\rho \left(\frac{x - \mu_X}{\sigma_X} \right) \left(\frac{y - \mu_Y}{\sigma_Y} \right) + \left(\frac{y - \mu_Y}{\sigma_Y} \right)^2 \right]} \quad \text{Eq. 2-189}$$

Where $\rho = \sigma_{XY} / (\sigma_X \sigma_Y)$ is the correlation coefficient, σ_{XY} is the covariance of X and Y.

3) The multivariate random variable

- There are more than 2 random variables, $U = [X_1, X_2, \dots, X_N]^T$.
- The covariance matrix of U is $\sigma_U = E((U - \mu)(U - \mu)^T) \in R^{N \times N}$

$$U = \begin{bmatrix} X_1 \\ X_2 \\ \vdots \\ X_N \end{bmatrix} \in R^N \quad \text{and} \quad E(U) = \begin{bmatrix} E(X_1) \\ E(X_2) \\ \vdots \\ E(X_N) \end{bmatrix} = \mu = \begin{bmatrix} \mu_1 \\ \mu_2 \\ \vdots \\ \mu_N \end{bmatrix} \quad \text{and} \quad \sigma_U = \begin{bmatrix} \sigma_1 \sigma_1 & \sigma_1 \sigma_2 & \cdots & \sigma_1 \sigma_N \\ \sigma_2 \sigma_1 & \sigma_2 \sigma_2 & \cdots & \sigma_2 \sigma_N \\ \vdots & \vdots & \ddots & \vdots \\ \sigma_N \sigma_1 & \sigma_N \sigma_2 & \cdots & \sigma_N \sigma_N \end{bmatrix}$$

- If U has a normal distribution, the multivariate PDF of U is

$$f(U) = \frac{1}{(2\pi)^{N/2} |\sigma_U|^{1/2}} e^{-0.5 [(U - \mu)^T \sigma_U^{-1} (U - \mu)]} \quad \text{Eq. 2-190}$$

Where σ_U is a covariance matrix and $\det(\sigma_U) = |\sigma_U|$.

2.8.1.8 Generalized tetrachoric series method for probability of multivariate random variables

To determine the probability of $X \geq K$ or $P(X \geq K)$ where X is a multivariate random variable, the integral form is first stated as follows:

$$P(X \geq K) = P(x_1 \geq k_1, x_2 \geq k_2, \dots, x_n \geq k_n) = \int_{k_n}^{\infty} \dots \int_{k_2}^{\infty} \int_{k_1}^{\infty} f_X(x_1, x_2, \dots, x_n) dx_1 dx_2 \dots dx_n \quad \text{Eq. 2-191}$$

The tetrachoric series form is:

$$P(X \geq K) = \sum_{a_1=0}^{\infty} \sum_{a_2=0}^{\infty} \dots \sum_{a_m=0}^{\infty} \left[(a_1! a_2! \dots a_m!)^{-1} (q_{p_1}^{a_1} q_{p_2}^{a_2} \dots q_{p_m}^{a_m}) (H_{r_1}(k_1) H_{r_2}(k_2) \dots H_{r_n}(k_n)) (g(k_1) g(k_2) \dots g(k_n)) \right]$$

$$\text{or } P(X \geq K) = \sum_{a_1=0}^{\infty} \sum_{a_2=0}^{\infty} \dots \sum_{a_m=0}^{\infty} \left[\prod_{i=1}^m \left(\frac{q_{p_i}^{a_i}}{a_i!} \right) \times \prod_{j=1}^n (H_{r_j}(k_j) g(k_j)) \right] \quad \text{Eq. 2-192}$$

Where $m=n(n-1)/2$, $g(x) = (2\pi)^{-0.5} \exp(-0.5x^2)$ is standard normal PDF.

$$H_{-1}(x) = (1-G(x))/g(x), \quad H_0(x) = 1, \quad H_j(x) = e^{0.5x^2} (-1)^j \left(\frac{d^j e^{-0.5x^2}}{dx^j} \right),$$

$$G(b) = \int_b^{\infty} g(x) dx.$$

$q_{p_i}^{a_i}$ can be determined step by step as follows:

Step (1): From covariance matrix of X or matrix C with dimension $n \times n$, divide row i with $(c_{ii})^{0.5}$ and divide column j with $(c_{jj})^{0.5}$. The result is matrix Q :

$$Q = \begin{bmatrix} q_{11} & q_{12} & \dots & q_{1n} \\ q_{21} & q_{22} & \dots & q_{2n} \\ \vdots & \vdots & \ddots & \vdots \\ q_{n1} & q_{n2} & \dots & q_{nn} \end{bmatrix} = \begin{bmatrix} \frac{c_{11}}{(c_{11}c_{11})^{0.5}} & \frac{c_{12}}{(c_{11}c_{22})^{0.5}} & \dots & \frac{c_{1n}}{(c_{11}c_{nn})^{0.5}} \\ \frac{c_{21}}{(c_{22}c_{11})^{0.5}} & \frac{c_{22}}{(c_{22}c_{22})^{0.5}} & \dots & \frac{c_{2n}}{(c_{22}c_{nn})^{0.5}} \\ \vdots & \vdots & \ddots & \vdots \\ \frac{c_{n1}}{(c_{nn}c_{11})^{0.5}} & \frac{c_{n2}}{(c_{nn}c_{22})^{0.5}} & \dots & \frac{c_{nn}}{(c_{nn}c_{nn})^{0.5}} \end{bmatrix}$$

Step (2): Find p_i which are numbers of row and column of Q , if $i = 1, 2, 3, \dots, m$.

$$\begin{matrix} i & 1 & 2 & \dots & n-1 & n & n+1 & \dots & 2(n-1) & 2n & 2(n+1) & \dots & m \\ \Rightarrow & 12 & 13 & \dots & 1n & 23 & 24 & \dots & 2n & 34 & 35 & \dots & n-1n \\ p_i & & & & & & & & & & & & \end{matrix}$$

Step (3) Find $q_{p_i}^{a_i}$ using p_i from Step.2) and a_i that is stated before.

r_j is defined by the summation of a_i minus 1 which, when compared to $q_{p_i}^{a_i}$ using the table below, q with row j or column j being selected.

$$\begin{array}{ccccccccccccccccc} a_i & => & a_1 & a_2 & \dots & a_{n-1} & a_n & a_{n+1} & \dots & a_{2(n-1)} & a_{2n} & a_{2(n+1)} & \dots & a_m \\ q_{p_i} & & q_{12} & q_{13} & \dots & q_{1n} & q_{23} & q_{24} & \dots & q_{2n} & q_{34} & q_{35} & \dots & q_{n-1n} \end{array}$$

For example, $r_1 = (a_1 + a_2 + \dots + a_{n-1}) - 1$, $r_2 = (a_1 + a_n + a_{n+1} + \dots + a_{2(n-1)}) - 1$

Process to find $P(X \geq K)$:

- (1) Determine n , m , and matrix Q and then start with $i = 1$ and $a_m = 0$
- (2) Define p_i and a_i and do steps (3)-(6)
- (3) Determine $q_{p_i}^{a_i}$ from (2) and (1) and then compute $\Pi (q_{p_i}^{a_i} / a_i!)$
- (4) For $j = 1$ to n , determine $g(k_j)$, r_j and $H_{r_j}(k_j)$ and then compute $\Pi H_{r_j}(k_j) \times g(k_j)$
- (5) Compute result of (3) \times (4)
- (6) $i = i + 1$, if $i > m$ go to (7) but if not return to step (2).
- (7) Increase $a_m = a_m + 1$ to infinity (practically 100) with the repeat step (1)-(6) while the sum of each step of (5) as a result
- (8) Increase $a_{m-1} = a_{m-1} + 1$ to infinity (practically 100) and repeat steps (1)-(6) while summing each step of (7) as a result
- (9) Repeat step (8) with $a_{m-2}, a_{m-3}, \dots, a_1$. The final result is $P(X \geq K)$.

2.8.1.9 Determination of distribution model using the Kolmogorov-Smirnov test

The Kolmogorov-Smirnov (K-S) test compares the selected theoretical CDF ($F(x)$) with the cumulative frequency curve of considered data ($Q_n(x)$).

The maximum difference between $F(x)$ and $Q_n(x)$ is the measure of the fit.

$$D_n = \max |F(x) - Q_n(x)| \quad \text{Eq. 2-193}$$

Since D_n is random variable, if D_n is less than the critical value D_n^α , then the distribution of considered data is fit with the selected theoretical distribution at significant level α . The probability that D_n is less than or equal to D_n^α is

$$P(D_n \leq D_n^\alpha) = 1 - \alpha \quad \text{Eq. 2-194}$$

The smaller is α , the larger is D_n^α . The larger is n , the smaller is D_n^α .

2.8.1.10 Convolution integral

If $Z = g(X, Y)$ and a unique $g^{-1}(z, y) = x$ and $g^{-1}(x, z) = y$ exist, Then the PDF of Z is:

$$f_Z(z) = \int_{-\infty}^{\infty} f_{XY}(g^{-1}, y) \left| \frac{\partial g^{-1}}{\partial z} \right| dy \quad \text{where } g^{-1}(z, y) = x = g^{-1} \text{ Eq. 2-195}$$

$$f_Z(z) = \int_{-\infty}^{\infty} f_{XY}(x, g^{-1}) \left| \frac{\partial g^{-1}}{\partial z} \right| dx \quad \text{where } g^{-1}(x, z) = y = g^{-1} \text{ Eq. 2-196}$$

If $Z = X + Y$, then, $\frac{\partial g^{-1}}{\partial z} = \frac{\partial x}{\partial z} = \frac{\partial y}{\partial z} = 1$. Thus PDF of z is:

$$f_Z(z) = \int_{-\infty}^{\infty} f_{XY}(z - y, y) dy \quad \text{Eq. 2-197}$$

Since Z is symmetric with respect to X and Y , therefore:

$$f_Z(z) = \int_{-\infty}^{\infty} f_{XY}(x, z - x) dx \quad \text{Eq. 2-198}$$

If X and Y are statistically independent:

$$f_Z(z) = \int_{-\infty}^{\infty} f_X(z - y) f_Y(y) dy \quad \text{Eq. 2-199}$$

$$f_Z(z) = \int_{-\infty}^{\infty} f_X(x) f_Y(z - x) dx \quad \text{Eq. 2-200}$$

These above two equations are called the *convolution integrals*.

2.8.2 Stochastic processes

The *stochastic process* means random functions of time. For random variables, each observation corresponds to one or more frequencies of an event occurring. For stochastic process, each observation corresponds to a function of time with the time sequence of the events.

2.8.2.1 Types of stochastic processes [58]

There are 4 categories of stochastic processes that can be analyzed using different mathematical techniques:

- Discrete values and discrete time
- Discrete values and continuous time (for example, Poisson process)
- Continuous values and discrete time
- Continuous values and continuous time (for example, Brownian motion process)

2.8.2.2 The Markov process [5]

All possible values of random variables are the state system or state space. The probability of transition from one state to another may generally depend on the prior states or the previous realization of the process. If the future state is solely influenced by the present state of the system, then the process is called a *Markov process*. If the state space is a countable set, the process is called a *Markov chain*.

For probability that is independent of the process x at the prior time before t_0 , if the process $x(t)$ is in state k_i and time t_0 , the probability that the process goes into the state k_j at time t_0+t is $P\{x(t_0+t)=k_j \mid x(t_0)=k_i\}$. If this is a Markov chain, the probability is reduced to:

$$p_{ij}(t) = P\{x(t_0+t)=k_j \mid x(t_0)=k_i\} \quad \text{Eq. 2-201}$$

If this is a homogenous Markov chain, this probability is reduced to:

$$p_{ij}(t) = P\{x(t)=k_j \mid x(t_0)=k_i\} \quad \text{Eq. 2-202}$$

For arbitrary t and s :

$$\begin{aligned} p_{ij}(t+s) &= P\{x(t+s)=k_j \mid x(0)=k_i\} \\ &= \sum_a P\{x(t+s)=k_j \mid x(t)=k_a, x(0)=k_i\} P\{x(t)=k_a \mid x(0)=k_i\} \\ &= \sum_a P\{x(t)=k_a \mid x(0)=k_i\} P\{x(t+s)=k_j \mid x(t)=k_a\} \\ p_{ij}(t+s) &= \sum_a p_{ia}(t) p_{aj}(s) \end{aligned} \quad \text{Eq. 2-203}$$

This transition probability is a continuous version of the *Chapman-Kolmogorov equation*.

If we consider the change transition probability, the *forward* and *backward Kolmogorov equations* are stated as follows:

For the *forward Kolmogorov equation*:

$$p'_{ij}(t) = \frac{p_{ij}(t+\Delta t) - p_{ij}(t)}{\Delta t} = \sum_a p_{ia}(t) \lambda_{aj} \quad i, j = 0, 1, 2, \dots \quad \text{Eq. 2-204}$$

For the *backward Kolmogorov equation*:

$$p'_{ij}(t) = \frac{p_{ij}(t+\Delta t) - p_{ij}(t)}{\Delta t} = \sum_a \lambda_{ia} p_{aj}(t) \quad i, j = 0, 1, 2, \dots \quad \text{Eq. 2-205}$$

Where $p_{ij}(0) = 0$, $i \neq j$, $p_{ii}(0) = 1$, and $\lambda_{ij} = \left. \frac{dp_{ij}(t)}{dt} \right|_{t=0}$ are the transition densities.

2.8.2.3 The Poisson process [22]

The Poisson process is a Markov process, which is a discrete value with continuous time or parameters. For the Poisson process with constant λ :

- $P_{i,j}(s,t) = P[X(t) = j \mid X(s) = i]$
- Events occurring in non-overlapping time intervals are independent of each other.
- For a very small Δt , the probabilities of occurrence of events in the interval $(t, t+\Delta t]$ are followed these two assumptions

(1) Probability of the transition to the next state is $P_{i,i+1}(t, t+\Delta t) \approx \lambda \Delta t$

(2) Probability of two or more transitions within Δt is zero, that is

$$P_{i,i}(t, t+\Delta t) \approx 1 - \lambda \Delta t$$

Let $P_n(t) = P[X(t) = n \mid X(0) = 0]$. Based on assumption (2), in general:

$$P_n(t+\Delta t) = P_{n-1}(t) \lambda \Delta t + P_n(t)(1 - \lambda \Delta t) \quad \text{Eq. 2-206}$$

$$\frac{dP_0(t)}{dt} = -\lambda P_0(t) \quad \text{Eq. 2-207}$$

$$\frac{dP_n(t)}{dt} = \lambda P_{n-1}(t) - \lambda P_n(t) \quad \text{Eq. 2-208}$$

If we assume the initial condition $P_0(0) = 1$ and $P_k(0) = 0$, $k=1, 2, 3, \dots$ for a given interval $(0, t]$, then the solution of the above linear differential equations is:

$$P_n(t) = \frac{(\lambda t)^n}{n!} e^{-\lambda t}, \quad n = 0, 1, \dots \quad \text{Eq. 2-209}$$

Instead of starting at $t=0$, the initial observation is made at $t=s$, $s>0$ which $X(s) = i$. Therefore, the probability of $(n-i)$ events in the remaining time $(t-s)$ is:

$$P_{i,s}(s, t) = \frac{[\lambda(t-s)]^{n-i}}{(n-i)!} e^{-\lambda(t-s)} \quad \text{Eq. 2-210}$$

2.8.2.4 The Brownian motion process [5]

The Brownian motion process is of continuous time and is a continuous value stochastic process. It is used to describe the movement of a particle in a liquid relating to external force and collision. The position $\mathbf{x}(t)$ of a particle is modeled as a function of second-order differential equation as follows:

$$m\mathbf{x}''(t) + f\mathbf{x}'(t) + c\mathbf{x}(t) = \mathbf{W}(t) \quad \text{Eq. 2-211}$$

where m is the mass of the particle, f is coefficient of friction, $c\mathbf{x}(t)$ is an external force, and $\mathbf{W}(t)$ is the collision force.

$\mathbf{W}(t)$ can be viewed as normal white noise with zero mean and power spectrum $S_F(\omega) = 2kTf$ where T is absolute temperature, $k = 1.37 \times 10^{-23}$ J.K is Boltzmann constant.

If restoring force $c\mathbf{x}(t)$ is not zero, the position $\mathbf{x}(t)$ approaches a stationary state with zero mean and power spectrum:

$$S_x(\omega) = \frac{2kTf}{(c - m\omega^2)^2 + f^2\omega^2} \quad \text{Eq. 2-212}$$

Its autocorrelation is:
$$R_x(\tau) = \frac{kT}{c} e^{-\alpha|\tau|} \left(\cos \beta\tau + \frac{\alpha}{\beta} \sin \beta|\tau| \right) \quad \text{Eq. 2-213}$$

For specific t , its PDF is:
$$f_x(x) = \sqrt{\frac{c}{2\pi kT}} e^{-\frac{cx^2}{2kT}} \quad \text{Eq. 2-214}$$

where $\mathbf{x}(t)$ is a normal random variable with zero mean and variance $R(0) = kT/c$.

The conditional density of $\mathbf{x}(t)$ is a normal curve with mean $a\mathbf{x}_0$ and variance P , where:

$$a = \frac{R_x(\tau)}{R_x(0)} \quad P = R_x(0)(1 - a^2) \quad \tau = t - t_0 \quad \text{Eq. 2-215}$$

If restoring force $c\mathbf{x}(t)$ is zero (for example free motion), thus:

$$m\mathbf{x}''(t) + f\mathbf{x}'(t) = \mathbf{W}(t) \quad \text{Eq. 2-216}$$

The solution of this equation is nonstationary process (since it has t in an equation).

If replace position with velocity, $\mathbf{v}(t) = \mathbf{x}'(t)$, this equation becomes:

$$m\mathbf{v}'(t) + f\mathbf{v}(t) = \mathbf{W}(t) \quad \text{Eq. 2-217}$$

This equation is called *Langevin equation*. The steady state solution of this equation is stationary process (*Ornstein-Uhlenbeck process*) with:

spectrum *Lorentzian* is
$$S_v(\omega) = \frac{2kTf}{m^2\omega^2 + f^2} \quad \text{Eq. 2-218}$$

its autocorrelation is
$$R_v(\tau) = \frac{kT}{m} e^{-\frac{f|\tau|}{m}} \quad \text{Eq. 2-219}$$

$\mathbf{v}(t)$ is a normal process with zero mean and variance kT/m , where

its PDF is
$$f_v(x) = \sqrt{\frac{m}{2\pi kT}} e^{-\frac{mv^2}{2kT}} \quad \text{Eq. 2-220}$$

The conditional density of $\mathbf{v}(t)$ is a normal with mean $a\mathbf{v}_0$ and variance P , where:

$$a = \frac{R_v(\tau)}{R_v(0)} = e^{-\frac{f\tau}{m}} \quad P = \frac{kT}{m}(1 - a^2) = \frac{kT}{m}(1 - e^{-\frac{2f\tau}{m}}) \quad \text{Eq. 2-221}$$

Its variance is
$$P = E[\mathbf{x}(t)^2] = \frac{2kT}{f} \left(t - \frac{m}{f} + \frac{m}{f} e^{-ft/m} \right) \quad \text{Eq. 2-222}$$

Therefore, $\mathbf{x}(t)$ in free motion is a nonstationary normal process with zero mean and variance P . If $t \gg m/f$, the variance P is reduced to:

$$P = E[\mathbf{x}(t)^2] \approx \frac{2kT}{f} t = 2D^2 t \quad D^2 \equiv \frac{kT}{f} \quad \text{Eq. 2-223}$$

where D is the diffusion constant.

The Brownian motion process has properties such that

For $\tau > 0$ and $X(0) = 0$, $[X(t+\tau) - X(t)]$ is a Gaussian random variable with

$$E[X(t+\tau) - X(t)] = 0$$

$$\text{Var}(X(t+\tau) - X(t)) = \alpha\tau$$

which is independent of $X(r)$ for all $r \leq t$.

The joint PDF of Brownian motion process $X(t)$ is

$$f_{X(t_1), \dots, X(t_k)}(x_1, \dots, x_k) = \prod_{n=1}^k \frac{1}{\sqrt{2\pi\alpha(t_n - t_{n-1})}} e^{\frac{-(x_n - x_{n-1})^2}{2\alpha(t_n - t_{n-1})}} \quad \text{Eq. 2-224}$$

For the *Weiner process*, $m\mathbf{x}''(t)$ of a particle in free motion is assumed to be very small compare to $f\mathbf{x}'(t)$ and can be neglected, thus:

$$f\mathbf{x}'(t) = \mathbf{W}(t) \quad \text{and} \quad \mathbf{x}(t) = \frac{1}{f} \int_0^t \mathbf{W}(\alpha) d\alpha \quad \text{Eq. 2-225}$$

Its variance is
$$P = E[\mathbf{x}(t)^2] \approx \frac{2kT}{f} t = \alpha t \quad \alpha \equiv 2D^2 \equiv \frac{2kT}{f}$$

Therefore, $\mathbf{x}(t)$ is a nonstationary normal process with PDF:

$$f_{\mathbf{x}(t)}(\mathbf{x}) = \frac{1}{\sqrt{2\pi\alpha t}} e^{\frac{-\mathbf{x}^2}{2\alpha t}} \quad \text{Eq. 2-226}$$

For the *Weiner process*, the position of a particle in free motion with negligible acceleration has the following properties

- $E[\mathbf{x}(t)] = 0$, $\text{Var}(\mathbf{x}(t)) = \alpha t$, $R_{\mathbf{x}}(t_1, t_2) = \alpha \min(t_1, t_2)$
- Independent increment
- The conditional density of $\mathbf{x}(t)$ is normal with mean $\alpha\mathbf{x}_0$ and variance P , where:

$$a = \frac{R_{\mathbf{x}}(t, t_0)}{R_{\mathbf{x}}(t_0, t_0)} = 1 \quad P = R_{\mathbf{x}}(t, t) - aR_{\mathbf{x}}(t, t_0) = \alpha t - \alpha t_0 \quad \text{Eq. 2-227}$$

- Its PDF is
$$f_{\mathbf{x}(t)}(\mathbf{x} | \mathbf{x}(t_0) = \mathbf{x}_0) = \frac{1}{\sqrt{2\pi\alpha(t-t_0)}} e^{\frac{-(\mathbf{x}-\mathbf{x}_0)^2}{2\alpha(t-t_0)}} \quad \text{Eq. 2-228}$$

2.8.2.5 Autocorrelation and autocovariance [22]

The autocorrelation function of the stochastic process $X(t)$ is

$$R_X(t, \tau) = E[X(t)X(t+\tau)]$$

The autocovariance function of the stochastic process $X(t)$ is

$$C_X(t, \tau) = \text{Cov}[X(t), X(t+\tau)]$$

For $\tau=0$, $C_X(t, t) = \text{Var}[X(t)]$

The relationship between an autocovariance and autocorrelation function is:

$$C_X(t, \tau) = R_X(t, \tau) - E[X(t)]E[X(t+\tau)]$$

2.8.2.6 The stationary process [58]

For the stationary process, the statistical properties of the process do not change with time. Therefore, the same random variable is observed at all time instants. For any time instant t and time difference τ :

$$f_{X(t)}(x) = f_{X(t+\tau)}(x) = f_X(x)$$

where $X(t) = X(t_1), X(t_2), X(t_3), \dots, X(t_m)$ for $t=t_1, t_2, t_3, \dots, t_m$ and $x = x_1, x_2, x_3, \dots, x_m$.

Stationary process is defined by the expected value, autocorrelation, and autocovariance, while a wide sense stationary process is defined only by expected value and autocorrelation as follows:

For wide sense stationary process (WSS) $X(t)$:

$$E[X(t)] = \mu_X(t) = \mu_X \quad \text{Eq. 2-229}$$

$$R_X(t, \tau) = R_X(0, \tau) = R_X(\tau) \quad \text{Eq. 2-230}$$

For a stationary process (strict sense) $X(t)$, one more property is added as follows:

$$C_X(t, \tau) = R_X(\tau) - (\mu_X)^2 = C_X(\tau) \quad \text{Eq. 2-231}$$

Therefore, a stationary process (or strict sense stationary process) is a subset of a wide sense stationary process.

The power spectrum or power spectral density (PSD) of a WSS process $\mathbf{x}(t)$, real or complex, is the Fourier transformation $S(\omega)$ of its autocorrelation $R(\tau) = E\{\mathbf{x}(t+\tau)\mathbf{x}^*(t)\}$ as follows:

$$\text{PSD is} \quad S(\omega) = \int_{-\infty}^{\infty} R(\tau) e^{-j\omega\tau} d\tau \quad \text{Eq. 2-232}$$

$$\text{Fourier inversion of PSD is} \quad R(\tau) = \frac{1}{2\pi} \int_{-\infty}^{\infty} S(\omega) e^{j\omega\tau} d\omega \quad \text{Eq. 2-233}$$

If $\mathbf{x}(t)$ is a real process, then $R(\tau)$ is real and even, and thus $S(\omega)$ is real and even. Therefore

PSD is
$$S(\omega) = \int_{-\infty}^{\infty} R(\tau) \cos(\omega\tau) d\tau = 2 \int_0^{\infty} R(\tau) \cos(\omega\tau) d\tau \quad \text{Eq. 2-234}$$

Fourier inversion of PSD is
$$R(\tau) = \frac{1}{2\pi} \int_{-\infty}^{\infty} S(\omega) \cos(\omega\tau) d\omega = \frac{1}{\pi} \int_0^{\infty} S(\omega) \cos(\omega\tau) d\omega \quad \text{Eq. 2-235}$$

The *cross-power spectrum* of two processes $\mathbf{x}(t)$ and $\mathbf{y}(t)$ is

cross-PSD is
$$S_{xy}(\omega) = \int_{-\infty}^{\infty} R_{xy}(\tau) e^{-j\omega\tau} d\tau \quad \text{Eq. 2-236}$$

Fourier inversion of *cross-PSD* is
$$R_{xy}(\tau) = \frac{1}{2\pi} \int_{-\infty}^{\infty} S_{xy}(\omega) e^{j\omega\tau} d\omega \quad \text{Eq. 2-237}$$

Where $R_{xy}(\tau) = E\{ \mathbf{x}(t+\tau) \mathbf{y}^*(t) \}$ is cross-autocorrelation.

2.8.3 Stochastic differential equation [40]

Considering the ordinary differential equation (ODE)

$$\begin{aligned} \dot{x}(t) &= f(x(t)) \quad , t > 0 \\ x(0) &= x_0 \end{aligned} \quad \text{Eq. 2-238}$$

where $\mathbf{x}(t) \in \mathbb{R}^n$ is the state of the system at time t , $f(\mathbf{x})$ is a function of \mathbf{x} for which the solution is the trajectory $\mathbf{x}(t)$.

It includes the random effects disturbing the system, ODE becomes:

$$\begin{aligned} \dot{x}(t) &= f(x(t)) + B(x(t))\xi(t), \quad t > 0 \\ x(0) &= x_0 \end{aligned} \quad \text{Eq. 2-239}$$

where $B(\mathbf{x})$ is a function of \mathbf{x} with dimension $m \times n$ and $\xi(t)$ is white noise (wide sense stationary process) with dimension m .

If $m = n$, $x_0 = 0$, and $B = I$, the solution of the above equation is the *Weiner process* or *Brownian motion* $\mathbf{w}(\cdot)$, which symbolically is

$$\dot{\mathbf{w}}(\cdot) = \xi(\cdot) \quad \text{Eq. 2-240}$$

Therefore, the white noise is the time derivative of the Wiener process.

Replace ξ with \mathbf{w} , thus:

$$\frac{d\mathbf{x}(t)}{dt} = f(\mathbf{x}(t)) + B(\mathbf{x}(t)) \frac{d\mathbf{w}(t)}{dt} \quad \text{Eq. 2-241}$$

Multiplying by dt yields

$$d\mathbf{x}(t) = f(\mathbf{x}(t))dt + B(\mathbf{x}(t))d\mathbf{w}(t) \quad \text{Eq. 2-242}$$

This equation is the *Stochastic Differential Equation* (SDE). Solve SDE to find \mathbf{x} , yield:

$$x(t) = x_0 + \int_0^t f(x(s))ds + \int_0^t B(x(s))dW \quad \text{Eq. 2-243}$$

For a *Langevin equation* problem, the model of the motion of a Brownian particle with frictional forces is as follows:

$$\dot{X} = -bX + \sigma\xi \quad \text{Eq. 2-244}$$

where X is the velocity of a particle, $b > 0$ is a coefficient of friction, σ is a diffusion coefficient. Therefore, this equation can be represented as follows

$$\begin{aligned} dX &= -bXdt + \sigma dW \\ X(0) &= X_0 \end{aligned} \quad \text{Eq. 2-245}$$

where X_0 is independent of Brownian motion (W). This is a *Langevin equation*.

$$\text{The solution is} \quad X(t) = e^{-bt} X_0 + \sigma \int_0^t e^{-b(t-s)} dW, \quad t \geq 0 \quad \text{Eq. 2-246}$$

$$\text{Its expected value is} \quad E[X(t)] = e^{-bt} E[X_0]$$

$$\text{Its variance is} \quad \text{Var}[X(t)] = e^{-2bt} \text{Var}[X_0] + \frac{\sigma^2}{2b} (1 - e^{-2bt}) \quad \text{Eq. 2-247}$$

$$\text{If } t \rightarrow \infty, \quad E[X(t)] \rightarrow 0, \quad \text{Var}[X(t)] \rightarrow \sigma^2/2b \quad \text{Eq. 2-248}$$

For the Ornstein-Uhlenbeck process problem, the motion of a Brownian particle with frictional forces becomes

$$\begin{aligned} \dot{Y} &= -bY + \sigma\xi \\ Y(0) &= Y_0, \quad \dot{Y}(0) = Y_1 \end{aligned} \quad \text{Eq. 2-249}$$

where $Y(t)$ is the position of a Brownian particle at time t , Y_0 and Y_1 are given Gaussian random variables.

Then $X = \dot{Y}$, the velocity of a particle satisfies the Langevin equation:

$$\begin{aligned} dX &= -bXdt + \sigma dW \\ X(0) &= Y_1 \end{aligned} \quad \text{Eq. 2-250}$$

$$\text{The solution of } X \text{ is} \quad X(t) = e^{-bt} Y_1 + \sigma \int_0^t e^{-b(t-s)} dW, \quad t \geq 0 \quad \text{Eq. 2-251}$$

$$\text{The solution of } Y \text{ is} \quad Y(t) = Y_0 + \int_0^t Xds \quad \text{Eq. 2-252}$$

Therefore, its mean is $E[Y(t)] = E[Y_0] + \int_0^t E[X(s)]ds = E[Y_0] + \left(\frac{1-e^{-bt}}{b}\right)E[Y_1]$ Eq. 2-253

Its variance is $\text{Var}[Y(t)] = \text{Var}[Y_0] + \frac{\sigma^2}{b^2}t + \frac{\sigma^2}{2b^3}(-3 + 4e^{-bt} - e^{-2bt})$ Eq. 2-254

The details of these solutions are described in “*An Introduction to Stochastic Differential Equations*” by Lawrence C. Evans. For higher order differential equations, a SDE solution is still not applicable due to its difficulty.

2.8.4 Monte Carlo simulation [22]

The Monte Carlo simulation is a numerical simulation applied to statistical problems with known probability distributions of random variables. It is a repeating process to generate values of random variables according to the known probability distribution. Therefore, samples from Monte Carlo simulation are (theoretically) the same with the samples from experimental observations.

2.8.4.1 Uniformly distributed random numbers

All methods to generate uniformly distributed random numbers are based on recursive calculations of residues of modulus m or $x \bmod (m)$, which returns the integer remainder when x is divided by m .

The multiplicative congruential method or power residue method, which is used most frequently at present, is stated as follows:

$$x_i = x^i \bmod m \quad \text{Eq. 2-255}$$

However, this method is not suitable for very large numbers of i , therefore, an equivalent equation can be used as follows:

$$x_i = \rho x_{i-1} \bmod m \quad \text{and} \quad u_i = x_i / m \quad \text{Eq. 2-256}$$

where ρ is a constant multiplier and u_i is a uniform CDF of x_i which $x_i = F_x^{-1}(u_i)$.

The most common choice of m is $m = r^s$, where r is the base of the number of the computer system (2, 10, 16, 64 bit) and s is the word length in the computer. Standard recommendations choose ρ to be values from $8t \pm 3$ ($t=1,2,3,\dots$).

Another recursive method is:

$$x_i = (\rho x_{i-1} + b) \bmod m \quad \text{and} \quad u_i = x_i / m \quad \text{Eq. 2-257}$$

where b is a nonnegative integer.

However, the numbers generated from these methods are really not random numbers, but *pseud-random* number. The large m causes the numbers generated uniformly distributed and statistically independent.

2.8.4.2 Random numbers with given distributions

This method requires specification of the inverse of the distribution function and called the *inverse transformation method*. For example, if u_i ($i=1,2,3,\dots$) are generated, the CDF of an exponential distribution function is

$$F_X(x) = 1 - e^{-\lambda x}, \quad x \geq 0 \quad \text{Eq. 2-258}$$

Taking then inverse of this function, thus

$$x_i = -\lambda^{-1} \ln(1-u_i) \quad \text{or} \quad x_i = -\lambda^{-1} \ln(u_i) \quad \text{Eq. 2-259}$$

since u is uniformly distributed, therefore $1-u$ is also.

2.8.4.3 Jointly distributed random numbers

If random variables $x_1, x_2, x_3, \dots, x_n$ are dependent, the joint CDF is as follows

$$F_{X_1, \dots, X_n}(x_1, \dots, x_n) = F_{X_1}(x_1) F_{X_2}(x_2 | x_1) \dots F_{X_n}(x_n | x_1, \dots, x_{n-1}) \quad \text{Eq. 2-260}$$

where $F_{X_1}(x_1)$ and $F_{X_k}(x_k | x_1, \dots, x_{k-1})$ are marginal and conditional CDF of X_1 and X_k .

If a set of uniformly distributed random numbers (u_1, u_2, \dots, u_n) is generated, then

$$x_1 = F_{x_1}^{-1}(u_1) \quad \text{Eq. 2-261}$$

$$x_2 = F_{x_2}^{-1}(u_2 | x_1) \quad \text{Eq. 2-262}$$

$$x_n = F_{x_n}^{-1}(u_n | x_1, \dots, x_{n-1}) \quad \text{Eq. 2-263}$$

This method can be used if the marginal and conditional CDFs can be inverted analytically.

2.8.5 Stochastic stability concept

The deterministic differential equation can be stated in the following form:

$$\dot{x} = f(x), \quad x(t_0) = x_0, \quad t \geq t_0 \quad \text{Eq. 2-264}$$

If there exists a positive-definite function $U(x)$ ($U(x_0) = 0$ and $U(x) > 0$ for all $x \neq x_0$) such that

$$\frac{dU(x, t)}{dt} = \frac{\partial U}{\partial t} + \sum_{i=1}^d \frac{\partial U}{\partial x_i} f_i(x, t) \leq 0 \quad \text{Eq. 2-265}$$

The equilibrium of this system is called stable. A function U which satisfies these conditions is called a *Lyapunov function*.

For probabilistic or stochastic differential equations:

$$dx = f(x, t)dt + g(x, t)dW, \quad x(t_0) = x_0, \quad t \geq t_0 \quad \text{Eq. 2-266}$$

Where $f(x, t)$ is nonlinear function, $g(x, t)$ is diffusion function, and dW is Weiner process.

If there exists a positive-definite function with continuous partial differentials, $u(x, t) = U$, such that the expectation of its differentiation is less than or equal to zero

$$E(dU) \leq 0 \quad \text{for all } t \geq t_0 \quad \text{Eq. 2-267}$$

The function $u(x, t)$ is called the Lyapunov function belonging to the particular equilibrium state of the stochastic differential equation [26].

The differentiation of U of stochastic system becomes

$$dU(x, t) = (L u(x, t)) dt + \sum_{i=1}^d \sum_{j=1}^m \frac{\partial U}{\partial x_i} u_i(x, t) g_{ij}(x, t) dW_j \quad \text{Eq. 2-268}$$

The $L u(x, t)$ is a stochastic differential operator according to Ito's sense.

$$L u(x, t) = \frac{\partial u}{\partial t} + \frac{\partial u}{\partial x} f(x, t) + \frac{1}{2} \text{Trace} \left\{ g^T(x, t) \frac{\partial^2 u}{\partial x^2} g(x, t) \right\} \quad \text{Eq. 2-269}$$

This condition can be used for stochastic system stability analysis in the sense of Lyapunov.

2.9 Energy Function Methods

The energy function method was first proposed by A.M. Lyapunov in 1892, called Lyapunov's method, which is based on the energy function representing a nonlinear dynamic system. It is the concept of energy balance which have been proved and applied for stability problems of the power system more than 40 years. Energy function method began with the application for transient stability by Magnusson and Aylett, followed by more general Lyapunov's method by Elabiad and Nagappan [50]. It was applied later for voltage stability and small signal stability from load and generation change.

For an energy function method applying for transient stability, or called *Transient Energy Function* (TEF), the system equation with 3 conditions is:

1. Initial system (Prefault) $\dot{x} = f^I(x)$, $-\infty < t \leq 0$
2. Faulted system $\dot{x} = f^F(x)$, $0 < t \leq t_{cl}$
3. Postfault system $\dot{x} = f(x)$, $t_{cl} < t$

If initial system variables are known, the faulted system and postfault system equations will be used for TEF to quantify critical energy and critical clearing times.

2.9.1 Lyapunov's Theory of Stability

For a nonlinear dynamic system, $\dot{x} = f(x)$ where $f(0) = 0$, Lyapunov suggests that if there is a positive-definite scalar function $W(x) > 0$ around the equilibrium point and the derivative $\dot{W}(x) \leq 0$, then the equilibrium is asymptotically (closely to) stable. $\dot{W}(x)$ is computed from:

$$\dot{W}(x) = \sum_{i=1}^n \frac{\partial W}{\partial x_i} \dot{x}_i = \sum_{i=1}^n \frac{\partial W}{\partial x_i} f_i(x) = \nabla \mathbf{W}^t \cdot \mathbf{f}(\mathbf{x}) \quad \text{Eq. 2-270}$$

For the power system, $W(x)$ is generally the sum of kinetic (W_{KE}) and potential (W_{PE}) energies of the postfault system. The critical value of $W(x)$ causing the system instability is called the critical energy (W_{cr}), which is different for each fault.

2.9.2 Modeling aspects for stability problems

In terms of energy perspective, $W(x) = W_{KE} + W_{PE}$. Since power is the derivative of energy, therefore, in terms of power perspective:

$$\dot{W} = \dot{W}_{KE} + \dot{W}_{PE} \quad \text{Eq. 2-271}$$

For conservative system, the increasing rate of W_{KE} is equal to the decreasing rate of W_{PE} . Therefore $\dot{W}_{KE} = -\dot{W}_{PE}$ and \dot{W} is zero.

An analogy of the equation of motion of a power system:

$$\dot{W} = 0 = \left(\frac{2H_i}{\omega_0} \frac{d^2 \delta_i}{dt^2} \right) - (P_{mi} - P_{ei}) \quad \text{or} \quad \frac{2H_i}{\omega_0} \frac{d^2 \delta_i}{dt^2} = P_{mi} - P_{ei} \quad \text{Eq. 2-272}$$

Where $i = 1, 2, \dots, m$, H_i is inertia constant of machine i , ω_0 is rated synchronous speed of machine i , δ_i is rotor angle of machine i , P_{mi} is mechanical power of machine i , and P_{ei} is electrical power of machine i .

If $E_i = |E_i| \angle \delta_i$ is the terminal voltage of machine i , and $Y_{ij} = G_{ij} + jB_{ij}$ is admittance between machine i and machine j with real part G_{ij} and imaginary part B_{ij} . Thus the electrical power of machine i relative to the other machines $j=1, 2, \dots, m$ is:

$$P_{ei} = \sum_{j=1}^m E_i E_j (G_{ij} \cos(\delta_i - \delta_j) + B_{ij} \sin(\delta_i - \delta_j)) \quad \text{Eq. 2-273}$$

$$P_{ei} = E_i^2 G_{ii} + \sum_{\substack{j=1 \\ j \neq i}}^m E_i E_j (G_{ij} \cos \delta_{ij} + B_{ij} \sin \delta_{ij}) \quad \text{Eq. 2-274}$$

Therefore,

$$\frac{2H_i}{\omega_0} \frac{d^2 \delta_i}{dt^2} = (P_{mi} - E_i^2 G_{ii}) - \sum_{\substack{j=1 \\ j \neq i}}^m E_i E_j (G_{ij} \cos \delta_{ij} + B_{ij} \sin \delta_{ij}) \quad \text{Eq. 2-275}$$

If $2H_i/\omega_0 = M_i$ and $d\delta_i/dt = \omega_i - \omega_0$, thus

$$M_i \dot{\omega}_i = (P_{mi} - E_i^2 G_{ii}) - \sum_{\substack{j=1 \\ j \neq i}}^m E_i E_j (G_{ij} \cos \delta_{ij} + B_{ij} \sin \delta_{ij}) \quad \text{Eq. 2-276}$$

In the form of a first-order differential equation (equation of motion of machine i),

$$\dot{\delta}_i = \omega_i - \omega_o \quad \text{Eq. 2-277}$$

$$M_i \dot{\omega}_i = (P_{mi} - E_i^2 G_{ii}) - \sum_{\substack{j=1 \\ j \neq i}}^m E_i E_j (G_{ij} \cos \delta_{ij} + B_{ij} \sin \delta_{ij}) \quad \text{Eq. 2-278}$$

If the center of inertia (COI) concept is applied to the above equation, then:

$$\delta_{COI} = \frac{1}{M_T} \sum_{i=1}^n M_i \delta_i \quad \text{and} \quad \omega_{COI} = \frac{1}{M_T} \sum_{i=1}^n M_i \omega_i \quad \text{Eq. 2-279}$$

$$\theta_i = \delta_i - \delta_{COI} \quad \text{and} \quad \underline{\omega}_i = \omega_i - \omega_{COI} \quad \text{Eq. 2-280}$$

where $M_T = \sum_{i=1}^m M_i$ and P_{COI} is the power at the center of inertia of the system,

$$P_{COI} = \sum_{i=1}^m (P_{mi} - P_{ei}) = \sum_{i=1}^m (P_{mi} - E_i^2 G_{ii}) - 2 \sum_{i=1}^m \sum_{j=i+1}^m E_i E_j G_{ij} \cos \theta_{ij} \quad \text{Eq. 2-281}$$

Therefore, the equation of motion becomes

$$\dot{\theta}_i = \underline{\omega}_i \quad \text{Eq. 2-282}$$

$$M_i \underline{\dot{\omega}}_i = (P_{mi} - E_i^2 G_{ii}) - \sum_{\substack{j=1 \\ j \neq i}}^m E_i E_j (G_{ij} \cos \theta_{ij} + B_{ij} \sin \theta_{ij}) - \frac{M_i}{M_T} P_{COI} \quad \text{Eq. 2-283}$$

For the faulted system:

$$M_i \underline{\dot{\omega}}_i = f_i^F(\theta) \quad \text{where } 0 < t \leq t_{cl} \quad \text{Eq. 2-284}$$

For the postfault system:

$$M_i \underline{\dot{\omega}}_i = f_i(\theta) \quad \text{where } t > t_{cl} \quad \text{Eq. 2-285}$$

If we integrate the postfault system, for θ between θ^S (rotor angle at equilibrium) and θ_i , and for ω between 0 and $\underline{\omega}_i$, then:

$$\int \dot{W} = \int \dot{W}_{KE} + \int \dot{W}_{PE} \quad \text{Eq. 2-286}$$

$$W_i(\theta, \omega) = \frac{1}{2} M_i \underline{\omega}_i^2 - \int_{\theta_i^S}^{\theta_i} f_i(\theta) d\theta_i \quad \text{Eq. 2-287}$$

$$W_i(\theta, \omega) = \frac{1}{2} M_i \omega_i^2 - \left[\int_{\theta_i^s}^{\theta_i} (P_{mi} - E_i^2 G_{ii}) d\theta - \sum_{\substack{j=1 \\ j \neq i}}^m \left(\int_{\theta_i^s}^{\theta_i} E_i E_j (G_{ij} \cos \theta_{ij} + B_{ij} \sin \theta_{ij}) d\theta \right) - \frac{M_i}{M_T} \int_{\theta_i^s}^{\theta_i} P_{COI} d\theta \right] \quad \text{Eq. 2-288}$$

This formulation process is called the first integral method. Therefore, the energy function of the power system or TEF in the COI reference frame is

$$W(\theta, \omega) = \frac{1}{2} \sum_{i=1}^m M_i \omega_i^2 - \sum_{i=1}^m \left[(P_{mi} - E_i^2 G_{ii}) (\theta_i - \theta_i^s) \right] - \sum_{i=1}^{m-1} \sum_{j=i+1}^m \left[E_i E_j B_{ij} (\cos \theta_{ij} - \cos \theta_{ij}^s) - \int_{\theta_i^s + \theta_j^s}^{\theta_i + \theta_j} E_i E_j G_{ij} \cos \theta_{ij} d(\theta_i + \theta_j) \right] \quad \text{Eq. 2-289}$$

For terms on the right,

the 1st term is a change in the rotor kinetic energy of all machines,

the 2nd term is a change in the rotor potential energy of all machines,

the 3rd term is a change in the stored magnetic energy of all branches, and

the 4th term is a change in the dissipated energy of all branches.

The 1st term is kinetic energy (W_{KE}) which depends only on the rotor speed and the 2nd, 3rd, and 4th terms are the potential energy (W_{PE}) which depends only on the rotor angle. If G is very small and close to zero, this equation is good described by Lyapunov's Method.

The system becomes unstable when energy exits some critical values, called the critical energy W_{cr} .

Generally, there are 3 methods to compute W_{cr} :

- 1) Potential Energy Boundary Surface (PEBS) method
- 2) Boundary Controlling Unstable Equilibrium Point (u.e.p.) method
- 3) Lowest Energy u.e.p. method

The Lowest Energy u.e.p. method finds the u.e.p. with the lowest value of W_{cr} of the postfault system. Since this method is not universally used and needs much computational time, it is not considered here in this report. Instead, the other two methods are described in the next topic.

2.9.3 Potential Energy Boundary Surface (PEBS) method

For the PEBS method, W_{cr} is determined as the maximum value of the potential energy components (2nd, 3rd, and 4th terms of W) of the faulted system. For the conservative system, energy (the sum of kinetic and potential energies) is a constant

depending on rotor angle and speed. The concept of the PEBS method can be described as shown in the figure below.

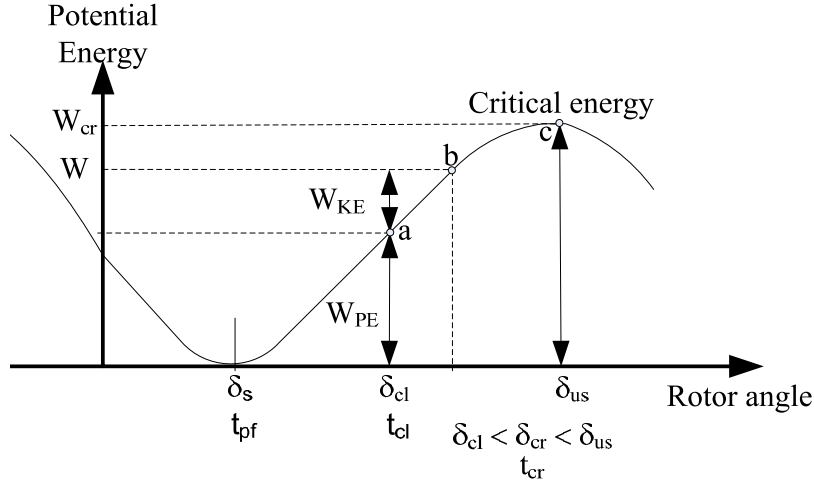


Figure 2.33 The potential energy-rotor angle curve for PEBS method

From the above figure, the postfault system has $\delta = \delta_s$ at time t_{pf} while W_{KE} and W_{PE} are zero. The system is perturbed by fault and then the fault is cleared at time t_{cl} with $\delta = \delta_{cl}$. At this time, energy W is the sum of W_{KE} and W_{PE} . If $W < W_{cr}$, thus the rotor will accelerate from point a and then start decelerating at point b . If $W > W_{cr}$, thus the rotor angle will accelerate beyond the value δ_{us} at point c and the system is unstable. If $W = W_{cr}$, the potential energy is maximum while the kinetic energy is zero and the system is nearly unstable. Therefore, $W = W_{PE} = W_{cr}$ and the clearing time is called critical clearing time (t_{cr}) with $\delta = \delta_{cr}$. W_{cr} is determined from the maximum value of W_{PE} of the faulted system.

The kinetic energy W_{KE} at time t_{cl} is considered as excess energy injected into the system. Therefore, stability of the system is the ability to absorb this excess kinetic energy.

The steps to compute critical clearing time t_{cr} are as follows

- 1) Compute δ_s and θ_s from the post fault system parameters (E, G, B)
- 2) Compute W_{PE} from the faulted system equation at each time step
- 3) Monitor if W_{PE} reach the maximum value, then $\max W_{PE} = W_{cr}$
- 4) At $W = W_{cr}$ of the faulted system, δ_{cr} and θ_{cr} are known and then t_{cr} can be estimated.

2.9.4 Boundary Controlling Unstable Equilibrium Point (BCU) method

The BCU method, is also called the exit-point method, computes the critical energy when an unstable equilibrium point (u.e.p.) is closest to the point where the faulted system function exits the region of the post fault system function. This is called *controlling u.e.p.* .

The algorithms of the BCU method are as follows:

- 1) For a contingency that involves either line switching or load/generation change, compute δ_s and θ_s of the post fault system.
- 2) Compute the controlling u.e.p.

(2.1) Integrate the faulted system equation and compute $W(\theta, \omega) = W_{KE} + W_{PE}$ at each time step. Find θ^* and time t^* when W_{PE} reaches the maximum value.

(2.2) After $\max W_{PE}$, the faulted swing equations are no longer integrated. Instead, the gradient system equations of the post fault system are used. For $t > t^*$,

$$\dot{\theta} = f(\theta), \theta(t^*) = \theta^* \quad \text{Eq.2-290}$$

The above equation is integrated and looking for the minimum of $\sum_{i=1}^m |f_i(\theta)|$.

At the first minimum, $\theta = \theta_{cus}$ is almost the controlling u.e.p close to the u.e.p (θ_{us}), and $W_{PE}(\theta_{cus})$ is approximated as W_{cr} with very little difference.

(2.3) The exact u.e.p (θ_{us}) can be computed by solving $f(\theta) = 0$ using θ_{cus} as starting point to arrive θ_{us} .

- 3) W_{cr} is determined as $W_{cr} = W(\theta_{us}, 0) = W_{PE}(\theta_{us})$

Compute t_{cr} when $W(\theta, \omega) = W_{cr}$. In the case of fault, $W(\theta, \omega)$ is from the faulted system equation and the system is stable if the fault is cleared at $t < t_{cr}$. In the case of load/generation change, $W(\theta, \omega)$ is from the post disturbance system equation and the system is stable if the $W(\theta, \omega) < W_{cr}$ for all t .

2.9.5 Critical energy estimation

The computation of critical energy needs the determination of unstable equilibrium points and stable equilibrium points. The stable equilibrium point can be calculated using the power flow solution or the simulation until reaching the steady state. For mathematical convenience, unstable equilibrium points can be estimated using the process of M. Ribberns-Pavella [43]. For the method of M. Ribberns-Pavella, unstable equilibrium points

of rotor angle, when any machine loss synchronism, can be approximated using the value $\pm\pi - x^s$ (where x^s is stable equilibrium point). Only the case of loss synchronization (unstable) of 1 machine and all machines are considered.

Table 2.4 Unstable equilibrium points formulation

Case 1 (5 sets)	Case 2 (5 sets)	Case 3 (1 set)	Case 4 (1 set)
$\mathbf{x} = \{x_1, x_2, x_3, x_4, x_5\} \times 5$ 4 of $x_i = x_i^s$ for $i=1,2, \dots, 5$ 1 of $x_k = \pi - x_k^s$ for $k = 1,2, \dots, 5$ and $(i \neq k)$	$\mathbf{x} = \{x_1, x_2, x_3, x_4, x_5\} \times 5$ 4 of $x_i = x_i^s$ for $i = 1,2, \dots, 5$ 1 of $x_k = -\pi - x_k^s$ for $k = 1,2, \dots, 5$ and $(i \neq k)$	$\mathbf{x} = \{x_1, x_2, x_3, x_4, x_5\}$ $x_i = \pi - x_i^s$ for $i = 1,2, \dots, 5$	$\mathbf{x} = \{x_1, x_2, x_3, x_4, x_5\}$ $x_i = -\pi - x_i^s$ for $i = 1,2, \dots, 5$

2.9.6 Well-defined energy function formulation using first integral method

The energy function is used in this thesis and will be applied to the study of the impact of wind power on power system stability. Energy function method, basing on Lyapunov function, is used to determine the region of attraction of stable equilibrium points and the critical values which beyond these values, system become unstable.

The cumulative effect of continuous small disturbances in the power system (such as load and wind power) can finally make the system reach critical values and become stable. An average time that the system first hit the critical boundary of region of attraction is called mean first passage time (MFPT). The mean first passage time (MFPT) is the performance index to quantify the average time a state-space trajectory takes to change from a given operating point to the boundary of its domain of attraction under the influence of small perturbations [2][9][10][11][13].

An important step for an energy function construction is to ensure that this function is a type of Lyapunov function. If then, this is called well-defined energy function which the theory of system stability of Lyapunov can be described. However, since now, there is no complete or exact solution of energy function. Carefully check an existence of energy function ($W(x_t)$) should be considered by using following conditions [9].

- I. $W(x_t) = 0$ when operating points are stable equilibrium points ($x_t = x_s$)
- II. $W(x_t) > 0$ when trajectories of operating points are within the region of attraction around equilibrium points
- III. $\dot{W}(x_t) \leq 0$ when trajectories of operating points are within the region of attraction and asymptotically move to equilibrium points

There are two methods for constructing energy functions, the two-step procedure and the first-integral method [30]. This thesis uses well-known first integral methods to formulate energy functions.

For the swing equation, the terms in the form of power balance will be integrated as an energy balance as follows:

$$M_i \dot{y}_i = P_{mi} - P_{ei} - D_i y_i \quad \text{Eq. 2-291}$$

multiply by ω_i and integrate:

$$\int_0^{y_i} M_i y_i dy_i = \int_{x_i^s}^{x_i} P_{mi} y_i dt - \int_{x_i^s}^{x_i} P_{ei} y_i dt - \int_{x_i^s}^{x_i} D_i y_i^2 dt \quad \text{Eq. 2-292}$$

$$\int_0^{y_i} M_i y_i dy_i = \int_{x_i^s}^{x_i} P_{mi} dx - \int_{x_i^s - x_j^s}^{x_i - x_j} P_{ei} dx - \int_{x_i^s}^{x_i} D_i y_i dx \quad \text{Eq. 2-293}$$

$$\frac{1}{2} M_i y_i^2 = P_{mi} (x_i - x_i^s) + \sum_{j=1}^{n+m} V_i V_j B_{ij} [\cos(x_i - x_j) - \cos(x_i^s - x_j^s)] - \int_{x_i^s}^{x_i} D_i y_i dx \quad \text{Eq. 2-294}$$

Where the left term is kinetic energy (KE) and the right terms are potential energy (PE) from mechanical power, electrical power, and damping power, respectively.

Therefore, the energy function of swing equations (W_{sw}) of an n machine system is:

$$W_{sw} = \frac{1}{2} \sum_{i=1}^n M_i y_i^2 - \sum_{i=1}^n P_{mi} (x_i - x_i^s) - \sum_{i=1}^n \sum_{j=1}^{n+m} V_i V_j B_{ij} [\cos(x_i - x_j) - \cos(x_i^s - x_j^s)] + \int_{x_i^s}^{x_i} \left(\sum_{l=1}^n D_l y_l \right) dx \quad \text{Eq. 2-295}$$

For power flow equations, in the case of active power:

$$P_{lk} = - \sum_{j=1}^{n+m} V_k V_j B_{kj} \sin(x_k - x_j) \quad \text{for } m \text{ load bus} \quad \text{Eq. 2-296}$$

multiply by dx and integrate:

$$\int_{x_k^s}^{x_k} P_{lk} dx = - \int_{x_k^s - x_j^s}^{x_k - x_j} \left(\sum_{j=1}^{n+m} V_k V_j B_{kj} \sin(x_k - x_j) \right) dx \quad \text{Eq. 2-297}$$

$$P_{lk} (x_k - x_k^s) = \sum_{j=1}^{n+m} V_k V_j B_{kj} [\cos(x_k - x_j) - \cos(x_k^s - x_j^s)] \quad \text{Eq. 2-298}$$

Therefore, the energy function of power flow equations (W_{PF}) of m load bus is:

$$W_{PF} = \sum_{k=n+1}^{n+m} P_{lk} (x_k - x_k^s) - \sum_{k=n+1}^{n+m} \sum_{j=1}^{n+m} V_k V_j B_{kj} [\cos(x_k - x_j) - \cos(x_k^s - x_j^s)] \quad \text{Eq. 2-299}$$

An energy function, $W = W_{sw} + W_{PF}$, can be computed as follows:

$$W = W_{sw} + W_{PF} = \frac{1}{2} \sum_{i=1}^n M_i y_i^2 - \sum_{i=1}^n P_{mi} (x_i - x_i^s) - \sum_{i=1}^n \sum_{j=1}^{n+m} V_i V_j B_{ij} [\cos(x_i - x_j) - \cos(x_i^s - x_j^s)] \\ + \sum_{k=n+1}^{n+m} P_{lk} (x_k - x_k^s) - \sum_{k=n+1}^{n+m} \sum_{j=1}^{n+m} V_k V_j B_{kj} [\cos(x_k - x_j) - \cos(x_k^s - x_j^s)] + \int_{x_i^s}^{x_i} \left(\sum_{i=1}^n D_i y_i \right) dx$$

Eq. 2-300

If we neglect damping terms by assuming conservative systems or lossless systems, and rearrange the above equation, the energy function is

$$W = \frac{1}{2} \sum_{i=1}^n M_i y_i^2 - \sum_{i=1}^n P_{mi} (x_i - x_i^s) + \sum_{k=n+1}^{n+m} P_{lk} (x_k - x_k^s) - \sum_{i=1}^{n+m} \sum_{j=1}^{n+m} V_i V_j B_{ij} [\cos(x_i - x_j) - \cos(x_i^s - x_j^s)]$$

Eq. 2-301

The existence of Lyapunov function candidate can be proof using three conditions as described previously:

I. $W = 0$ when operating points are the stable equilibrium points ($x_t = x_s$)

From the equation of the energy function above, if $x = x^s$, term 2nd, 3rd, and 4th on the right are exactly zero. For the first term on the right, under steady state when $x = x^s$, ω_t is nearly equal to ω_0 which $y = \omega_t - \omega_0 \approx 0$. Therefore, energy function is zero ($W = 0$) when $x = x^s$.

II. $W > 0$ when trajectories of operating points are within the region of attraction around equilibrium points

This is true in the case when $-\pi - x^s < x < \pi - x^s$ and $x \neq x^s$. The $\pi - x^s$ and $-\pi - x^s$ are unstable equilibrium points.

III. $\dot{W} \leq 0$ when trajectories of operating points are within the region of attraction and asymptotically move to stable equilibrium points

$$\dot{W} = \frac{\partial W}{\partial y} \dot{y} + \frac{\partial W}{\partial x} \dot{x} = \left[\sum M_i \dot{y}_i y_i \right] + \left[-\sum P_{mi} \dot{y}_i + \sum P_{lk} \dot{y}_i + \sum \sum V_i V_j B_{ij} \sin(x_{ij}) y_i \right] \quad \text{Eq. 2-302}$$

Placing $M_i \dot{y}_i = P_{mi} - P_{ei} - D_i y_i$ into the above equation, yields

$$\dot{W} = \left[\sum P_{mi} y_i - \sum_{i=1}^n \sum_{j=1}^{n+m} V_i V_j B_{ij} \sin(x_{ij}) y_i - \sum D_i y_i^2 \right] + \left[-\sum P_{mi} y_i + \sum P_{lk} y_i + \sum_{i=1}^{n+m} \sum_{j=1}^{n+m} V_i V_j B_{ij} \sin(x_{ij}) y_i \right]$$

Eq. 2-303

$$\dot{W} = \sum_{i=n+1}^{n+m} P_{lk} y_i + \sum_{i=n+1}^{n+m} \sum_{j=1}^{n+m} V_i V_j B_{ij} \sin(x_{ij}) y_i - \sum D_i y_i^2 \quad \text{Eq. 2-304}$$

Placing $P_{lk} = -P_{ek} = -\sum_{j=1}^{n+m} V_k V_j B_{kj} \sin(x_k - x_j)$ into the above equation, it can be seen that

$$\dot{W} = - \sum_{i=n+1}^{n+m} \sum_{j=1}^{n+m} V_i V_j B_{ij} \sin(x_{ij}) y_i + \sum_{i=n+1}^{n+m} \sum_{j=1}^{n+m} V_i V_j B_{ij} \sin(x_{ij}) y_i - \sum D_i y_i^2 \quad \text{Eq. 2-305}$$

$$\dot{W} = - \sum_{i=1}^n D_i y_i^2 \quad \text{Eq. 2-306}$$

Therefore, $\dot{W} \leq 0$ is always true in this case.

For summary, an energy function (W) of this system, when applying structure preserving models by neglecting transferred conductance terms, is a well-defined energy function that will be useful for power system stability analysis in this thesis.

CHAPTER 3

METHODOLOGY PART 1

From the objectives and scopes of thesis, the following topics are the main issues discussing in this thesis.

- The characteristics of wind power
- The characteristics of power systems incorporating wind power
- A study of effects of wind power on the small signal stability using eigenvalue methods
- A study of effects of wind power on the small signal stability using stochastic stability method: the mean first passage time (MFPT)
- A study of effects of wind power on the small signal stability using new stochastic stability methods
- A study of effects of wind power on the voltage stability using new stochastic stability methods
- A study of effects of wind power on power quality using probabilistic methods

This chapter describes the methods to study these topics.

3.1 The Characteristics of Wind Power

To study the effects of wind power on the power system requires understanding of the characteristics of wind speed and wind power in terms of statistics and probabilistic data. This topic will focus on the method to analyze the characteristics of the measured wind speed and the estimated wind power (since the measured wind power is unavailable). The wind speed data is from the monitoring station in Thailand. The wind power is calculated using the power curve of selected wind turbine. In the last section of this topic, the wind turbine models are developed and tested. These wind turbine models will be used in the stochastic stability analysis.

3.1.1 Variation of wind speed and wind power

For the study on the characteristics of wind speed, the measured wind data are separated between fast variations and slow variations. Both parts are characterized basing on time variation, frequency distribution of data, power spectral density (PSD), and standard distribution function test. It can be described using following figure.

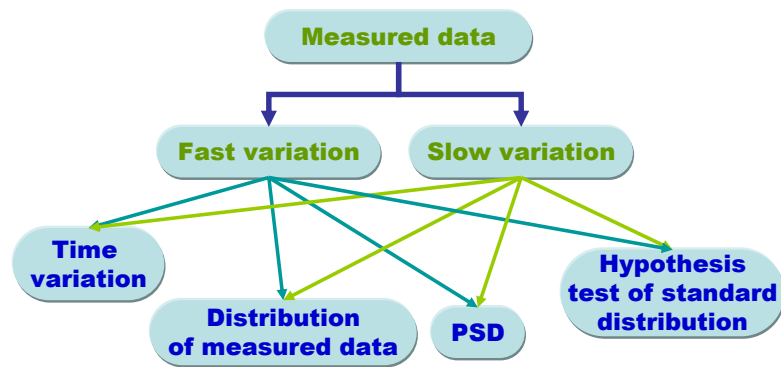


Figure 3.1 The methods to study the characteristics of wind speed

The study on the characteristics of wind power has two parts. First, the slow wind speed variation is used for wind power computation. This wind power is characterized basing on time variation, frequency distribution of data, power spectral density (PSD), and standard distribution function test as represented in below figure. Second, wind power is computed from wind speed model, wind noise model, wind power (turbine) models, and power system model which can be simulated using software PSCAD as represented in below figure.

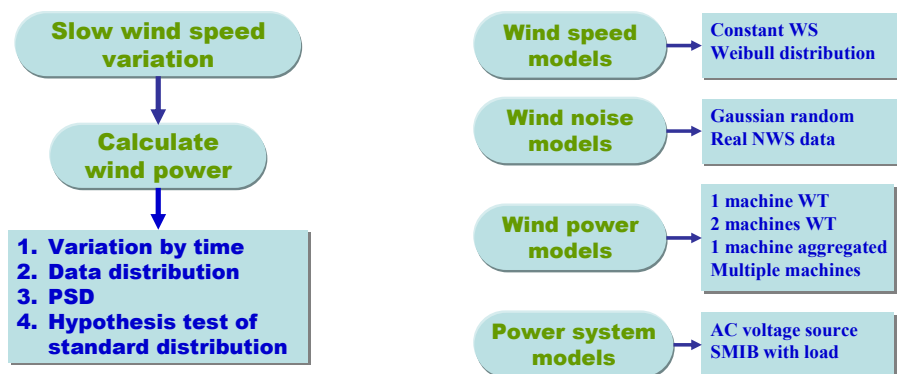


Figure 3.2 The processes to study the characteristics of wind power

Since we need to know how wind power impact to the power system stability and power quality. We assume that different characteristics of wind speed cause the difference of wind power which impact on the power system differently. Therefore, important questions are what kind of characteristics and how they affect to the power system.

There are two main types of characteristic of wind speed to be considered, which are, slow variation (slower than 10 minutes) and fast variation (faster than 10 minutes)

characteristics [42]. This thesis considers both the slow and fast variation characteristics of wind speed and wind power especially for a long term.

The characteristics of wind power are studied which consider three main affecting factors, namely, wind speed, wind farm modeling, and power system conditions. The wind turbine technology is the other important factor. However, since the measurement wind power data is not available, the simulation or modeling wind power is used instead for every cases of study.

The wind speed can be considered to have slow and fast variations, therefore, wind power in this case should be studied in term of slow and fast variations as well.

For slow variation of wind speed and without dynamic behaviors, the output wind power (P_w) is calculated using following equations:

$$P_w = \frac{1}{2} c_{p1} \rho A V^3 \quad \text{where } 3 \leq V \leq 6 \text{ m/s} \quad \text{Eq. 3-1}$$

$$P_w = \frac{1}{2} c_{p2} \rho A V^3 \quad \text{where } 6 < V \leq 25 \text{ m/s} \quad \text{Eq. 3-2}$$

For wind speed from 3 to 6 m/s, 3rd order polynomial can be fitted as follows.

$$c_{p1} = 0.016V^3 - 0.295V^2 + 1.736V - 2.994 \quad \text{Eq. 3-3}$$

For wind speed from 6 to 25 m/s, 3rd order polynomial can be fitted as follows.

$$c_{p2} = -0.004V^3 - 0.001V^2 + 0.302V - 0.909 \quad \text{Eq. 3-4}$$

where c_p data is from specification sheet of Suzlon S64 wind turbine, ρ is air density (standard air density is 1.225 kg/m³), and A is a swept area of wind turbine (for 50m diameter turbine, A is $\pi 25^2$ or about 1963.5 m²).

3.1.2 The probability distribution of wind power

The study of probability distribution characteristics of wind power can be influenced by many factors, such as, wind turbine model, power system model, wind speed model and noise model. Testing conditions are listed in Table 3.1.

Table 3.1 Testing conditions for the study of probability distribution of wind power

Case	Wind turbine model	Power system model	Wind speed model	Other conditions
A1	1x2MVA SCIG	1 AC source without load	Weibull distribution using inverse CDF	2 values of Weibull scale parameter, 100x2 runs
A2	2x2MVA SCIGs	1 AC source without load	Independent 2 wind sources with Weibull distribution	Weibull scale parameter = 10, for 10,000 runs
A3	5x10x2MVA SCIGs	1 AC source without load	Independent 5 wind sources with Weibull distribution	Weibull scale parameter = 10, 100 runs
A4	2x2MVA SCIGs	1 AC source without load	The same wind source with Weibull distribution	Add Gaussian random noise to WT2, 100 runs
A5	2x2MVA SCIGs	1 AC source without load	Constant wind speed = 6, 9, and 10 m/s for both WT	Add Gaussian random noise to WT2, 400, 1600 runs
A6	1x50x2MVA SCIG	SMIB system with load	Weibull distribution using inverse CDF	2 values of Weibull scale parameter, 200x2 runs
A7	1x50x2MVA SCIG	SMIB system with load	Weibull distribution using inverse CDF	WS noise using inverse CDF num. method, 100 runs

3.2 The Characteristics of Power System Incorporating Wind Power

To study on the characteristics of the power system incorporating wind power, the power system with different wind speed noise models is determined. There are two different wind speed noise models, the random noise model and the ramp noise model. The random noise models can be represented using different standard deviation and frequency of noise signal. The ramp noise can be differentiated using frequency of signal.

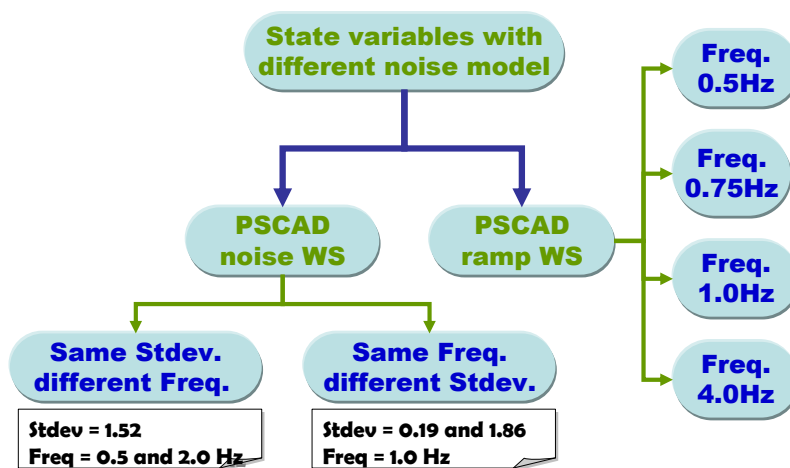


Figure 3.3 The method to study on the characteristics of power system incorporating wind power

To study the characteristics of the energy of the power system, the energy function is constructed first and then the relative energy is determined using energy function and estimated stable equilibrium points. After that, the critical energy is computed using relative energy and estimated unstable equilibrium points. This critical energy will be evaluated under different wind speed conditions. During the process, rotor speed and phase angle will be considered in form of phase portrait.

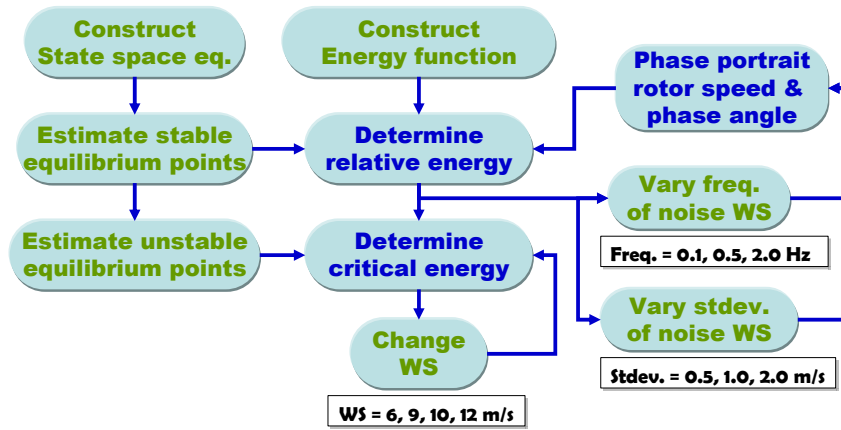


Figure 3.4 The method to study the characteristics of the energy of the power system

Finally, the stochastic variation of the state variable is considered using basic stochastic differential equations and its simulated solution. This process is the preliminary study of stochastic differential equation of the power system incorporating wind power.

The small signal stability of the power system is the ability of the system to control rotor angle and speed, and to keep normal synchronization of all generators after being perturbed by any small disturbances. Therefore, the characteristics of power and rotor angle will be analyzed using the methods representing in this topic. Since the continuous and small disturbances are mainly caused by the variation of load, therefore, the relation between power generation and load or power-load characteristics will also be analyzed.

3.2.1 Power-angle and power-load characteristics analysis

3.2.1.1 Power-angle characteristics analysis

The relationship between mechanical power output and the power angle of a synchronous generator is an important characteristics to evaluate the performance of the machine and the state of operation. Under normal or stable conditions, the power increase with increasing angle. For critical condition, the power reaches its maximum value. If the angle still increase continuously, the power become decrease and this situation is called

unstable condition. Under steady state conditions when a single machine connect to an infinite bus (SMIB), for salient pole synchronous generator (neglect internal resistance), the power-angle equation is

$$P_e = \frac{E_q E_B}{X_{Totd}} \sin \delta + \frac{E_q^2}{2} \frac{X_{Totd} - X_{Totq}}{X_{Totd} X_{Totq}} \sin 2\delta \quad \text{Eq. 3-5}$$

$$Q_e = \frac{E_q E_B X_{Totq}}{X_{Totd}} \cos \delta - \frac{E_q^2}{X_{Totd}^2} (X_{Totd} \sin^2 \delta - X_{Totq} \cos^2 \delta) \quad \text{Eq. 3-6}$$

For the round rotor machine (neglect resistance) with d- and q- axis total reactance are equal ($X_{Totd} = X_{Totq}$), the power-angle equation becomes

$$P_e = \frac{E_q E_B \sin \delta}{X_{Totd}} \quad \text{Eq. 3-7}$$

$$Q_e = \frac{E_q E_B \cos \delta}{X_{Totd}} - \frac{E_q^2}{X_{Totd}} \quad \text{Eq. 3-8}$$

Where P_e and Q_e are active and reactive electrical power output of generator, E_q is q-axis internal voltage of generator, E_B is infinite bus voltage, δ is rotor or power angle.

$$X_{Totd} = X_d + X_T + X_{TL} \quad \text{Eq. 3-9}$$

$$X_{Totq} = X_q + X_T + X_{TL} \quad \text{Eq. 3-10}$$

Where X_{Totd} and X_{Totq} are d- and q- axis total reactance of the system, X_d and X_q are d- and q- axis stator reactance, X_T is transformer reactance, and X_{TL} is transmission line reactance.

Assuming that $E_B = 1.0$ pu, and $Z_{LN} = R_{LN} + j X_{TL}$, we get the simplified equations

$$P_e = \frac{E_q \sin \delta}{X_d + X_T + Z_{LN}} = \frac{E_q \sin \delta}{Z_{Totd}} \quad \text{Eq. 3-11}$$

$$Q_e = \frac{1}{Z_{Totd}} (E_q \cos \delta - E_q^2) \quad \text{Eq. 3-12}$$

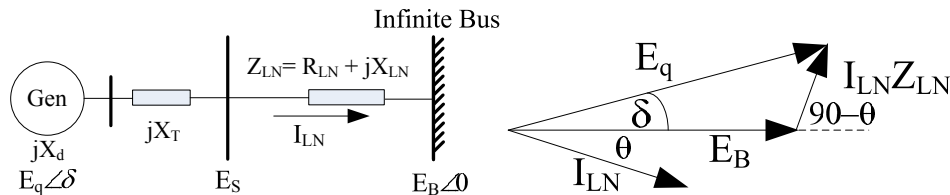


Figure 3.5 Schematic diagram and Phasor diagram of SMIB

The Eqs. 3-11, and 3-12, can be used to analyze the power-angle characteristics of the system and we can vary voltage to see how power-angle changes with voltage.

To investigate the power-angle characteristics of the generator, two assumptions should be considered. First is the active/reactive power-angle characteristic of single machine power system with voltage varying and second is the active/reactive power-angle characteristic of single machine power system with line reactance varying. Both cases use the previous equations (Eqs. 3-11, and 3-12) for modeling by using Matlab.

To analyze the power-voltage characteristics of the system, if we find δ using Eq. 3-11, we will get

$$\delta = \sin^{-1} \left(\frac{P_e Z_{Total}}{E_q} \right) \quad \text{Eq. 3-13}$$

From Eqs. 3-12 and 3-13, we can find Q_e as a function of E_q , Z_{Total} , and P_e as follows:

$$Q_e = \frac{E_q}{Z_{Total}} \cos \left(\sin^{-1} \left(\frac{P_e Z_{Total}}{E_q} \right) \right) - \frac{1}{Z_{Total}} \quad \text{Eq. 3-14}$$

Finally Eqs. 3-11 – 3-14 are used to investigate the power-voltage characteristics of the SMIB system which can be modeled using Matlab.

From the above equations, we will see that the power is related to voltage, internal impedance, transformer and line impedance, and power angle. Voltage can be controlled by increase or decrease reactive power. For example, in case over voltage, operator can decrease reactive power to reduce voltage by change tap of substation transformers.

For the voltage drop or under voltage conditions, the technique to pull up voltage is to inject reactive power by add more capacitive load into the line or to adjust power factor. If the voltage decreases to less than the critical point, it cannot be controlled by regulating reactive power normally and lost control finally. This unstable condition is called *voltage instability* caused by large and/or small disturbances in the system.

3.2.1.2 Power-load characteristic analysis

The load and transmission lines and characteristics can be described using the following figures and equations. For simple power circuit, the system consists of sending end voltage (E_s) of generator, line impedance (Z_{LN}), and load impedance (Z_{LD}). At the terminal of load, receiving end voltage (V_R), active power (P_R) of load, and reactive power (Q_R) of load, are characterized as follow.

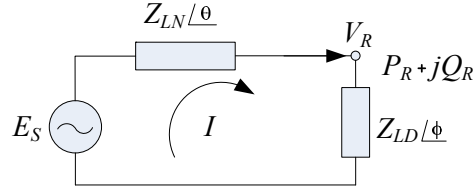


Figure 3.6 Circuit diagram of the power system with transmission and load impedance

$$Z_{LN} = |Z_{LN}| \cos \theta + j |Z_{LN}| \sin \theta \quad \text{Eq. 3-15}$$

$$Z_{LD} = |Z_{LD}| \cos \phi + j |Z_{LD}| \sin \phi \quad \text{Eq. 3-16}$$

$$I = \frac{E_S}{Z_{LN} + Z_{LD}} = \frac{E_S}{(|Z_{LN}| \cos \theta + |Z_{LD}| \cos \phi) + j(|Z_{LN}| \sin \theta + |Z_{LD}| \sin \phi)} \quad \text{Eq. 3-17}$$

$$I = \frac{1}{\sqrt{F}} \frac{E_S}{Z_{LN}} = \frac{1}{\sqrt{F}} I_{sc} \quad \text{Eq. 3-18}$$

$$V_R = \frac{E_S}{\sqrt{F}} \frac{Z_{LD}}{Z_{LN}} \quad \text{Eq. 3-19}$$

$$F = 1 + \left(\frac{Z_{LD}}{Z_{LN}} \right)^2 + 2 \left(\frac{Z_{LD}}{Z_{LN}} \right) \cos(\theta - \phi) \quad \text{Eq. 3-20}$$

$$P_R = V_R I \cos \phi = \frac{Z_{LD}}{F} \frac{E_S^2}{Z_{LN}^2} \cos \phi \quad \text{Eq. 3-21}$$

$$Q_R = V_R I \sin \phi = \frac{Z_{LD}}{F} \frac{E_S^2}{Z_{LN}^2} \sin \phi \quad \text{Eq. 3-22}$$

Find the normalized power using short circuit power, P_{sc} and Q_{sc} as follows:

$$P_{sc} = Q_{sc} = \frac{E_S^2}{Z_{LN}} \quad \text{Eq. 3-23}$$

Therefore, dividing Eqs. 3-21 and Eq. 3-22 by Eq. 3-23, we get the normalized power as:

$$P_{Rn} = \frac{P_R}{P_{sc}} = \frac{\cos \phi}{\left(\frac{Z_{LN}}{Z_{LD}} + \frac{Z_{LD}}{Z_{LN}} + 2 \cos(\theta - \phi) \right)} \quad \text{Eq. 3-24}$$

$$Q_{Rn} = \frac{Q_R}{Q_{sc}} = \frac{\sin \phi}{\left(\frac{Z_{LN}}{Z_{LD}} + \frac{Z_{LD}}{Z_{LN}} + 2 \cos(\theta - \phi) \right)} \quad \text{Eq. 3-25}$$

The Eq. 3-24, and Eq. 3-25 can be used to analyze the power-load characteristic of the system and we can expect that

1) If $Z_{LD} > Z_{LN}$ (normal or stable condition)

Load impedance is larger than line impedance. Increasing of load (or reduce Z_{LD}) causes active power, reactive power and current increase. Contradictory, load increase cause voltage decrease whereas enlarge voltage drop along the power line.

2) If $Z_{LD} = Z_{LN}$ (critical condition)

Load impedance is equal to line impedance. This situation causes power to reach maximum point and be a critical operating point.

3) If $Z_{LD} < Z_{LN}$ (unstable condition or instability)

Load impedance is less than line impedance. This causes from over load or lost of transmission line. Increasing of load decreases active and reactive power.

The load varying case assumes the relative load (or line impedance per load impedance) vary slowly and hence, has no dynamical effects. Three conditions of relative load (stable, critically stable, unstable) are assumed. This type of phenomena can occur normally in the power system.

For the simplification in power system modeling, θ always be neglected and assume 90 degrees since the line has very small resistance compare to reactance. From this assumption, the Eq. 3-24, and Eq. 3-25 become

$$P_{Rn} = \frac{\cos \phi}{\left(\frac{Z_{LN}}{Z_{LD}} + \frac{Z_{LD}}{Z_{LN}} + 2 \sin \phi \right)} \quad \text{Eq. 3-26}$$

$$Q_{Rn} = \frac{\sin \phi}{\left(\frac{Z_{LN}}{Z_{LD}} + \frac{Z_{LD}}{Z_{LN}} + 2 \sin \phi \right)} \quad \text{Eq. 3-27}$$

However, reality θ is not fixed at 90 degrees and can be changed when there is line dispatching, line improvement, and fault or disturbance on the transmission line.

3.2.2 Power-angle characteristics when applying small signals

The single machine infinite bus (SMIB) system is selected for power angle characteristic analysis, because it not complicated while representing only the relationship between electrical power and power angle in the system.

3.2.2.1 Small signal from internal sources

For the case of small signal from internal sources, the original SMIB must be modified by adding sources of small disturbances, for example, from governor, turbine,

and excitation system under operating conditions. The system consists of one synchronous machine with transformer connecting to an infinite bus through the transmission line. When the system operating under small disturbances, the power-angle characteristics of one generator can be examined using simple mathematical model.

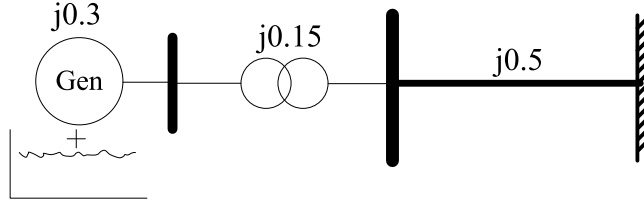


Figure 3.7 SMIB including internal sources of small signal

Assume losses of transmission line $j0.93$,

$$x_d = X_d + X_T + X_{TL} = j0.3 + j0.15 + j0.5 = j0.95 \quad \text{Eq. 3-28}$$

$$x_q = X_q + X_T + X_{TL} = j0.3 + j0.15 + j0.5 = j0.95 \quad \text{Eq. 3-29}$$

Where X_T is the transformer reactance, X_{TL} is the transmission line reactance, X_d and X_q are d- and q- axis stator reactance.

In the case of round rotor machine SMIB system, E_B is assumed constant at 1.0 p.u., therefore:

$$P_e = \frac{E_s \sin \delta}{0.95} \quad \text{and} \quad Q_e = \frac{E_s \cos \delta}{0.95} - \frac{1}{0.95} \quad \text{Eq. 3-30}$$

Therefore, P_e and Q_e strongly depend on internal voltage of generator and power angle. For convenience, the internal dynamic sources are not directly modeled, because these small signals can be included in the variation of generator voltage and power angle. Therefore, different characteristics of generator voltage and power angle will be modified to represent different kinds of external dynamic sources.

The linear or low frequency increase of power angle is due to linear or slow variation of turbine and governor. Variation of generator voltage in term of sinusoidal signal is caused from interaction of the excitation system. The band-limited white noise characteristics are caused from the stochastic nature of these small signals.

3.2.2.2 Small signal from external sources

In the case of small signals from external sources, the original SMIB must be modified by adding sources of small disturbances, for example, from dynamic load, and/or wind power under operating conditions. The system consists of one synchronous machine

with transformer connecting to an infinite bus through transmission line, adding dynamic load and wind turbine generator. When the system operating under small disturbances, the power-angle characteristics of one generator can be examined using simulation model in PSCAD.

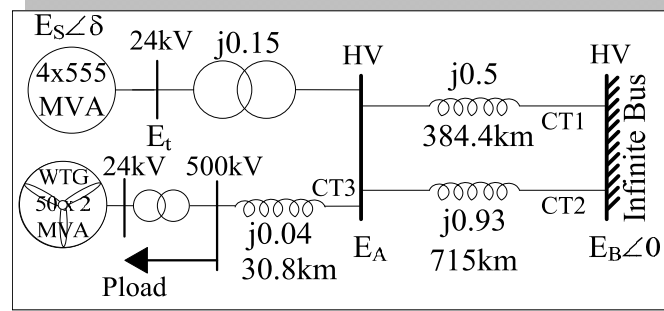


Figure 3.8 SMIB including wind power and dynamic load

There are two cases to be considered. The first is the normal case when the system operating under normal conditions reaches a steady state. The second is the case of wind power being included. The load can be set as a fix resistance load for convenience. Only small signal from wind power is considered.

3.2.3 Characteristics of the power system using simulation software

In this section, the single machine infinite bus power system is used. The power system, including fluctuating wind power, leads to higher degrees of complexity. This situation may affect the ac power system synchronization differently depending on characteristics of wind power. Therefore, the power angle and rotor speed of synchronous generator with various characteristics of wind power are investigated.

The original single machine infinite bus (SMIB) power system [52] is used for this study but with the incorporation of wind power and with additional load as presented in following figure. The software simulation for this study is PSCAD/EMTDC which suitable for analyzing dynamic characteristic of the power system (www.pscad.com).

The system voltage is 500kV with load power 50% of 2220 MVA synchronous generator. The simulation duration time is 100 seconds, which is enough for the system to reach a steady state at about 20 seconds (without wind power). The time step of the simulation is 50 micro seconds.

The synchronous generator model is an IEEE generic steam turbine model supported in PSCAD (www.pscad.com). The wind power model consists of a wind source

model and wind turbine model with pitch control. The wind source model generates mean wind speed with noise. For wind turbine model, the 50x2 MVA squirrel cage induction generator (SCIG) is used in this study. For noise wind speed (V_n) model, seven parameters are used to define its characteristics which are described in [46].

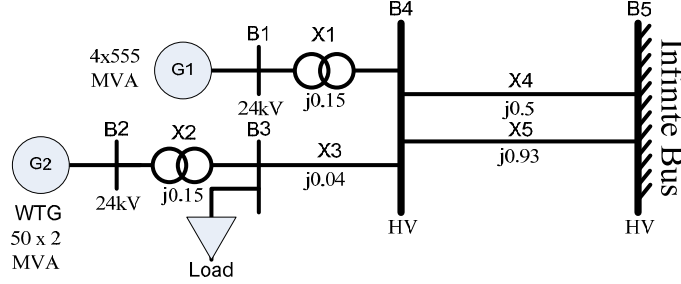


Figure 3.9 Test power system including wind power and load

Table 3.2 Testing conditions for the study of characteristics of the power system incorporating wind power

	Wind turbine	Wind speed	Noise conditions	Load	Base voltage
Case B1	No wind power	10 m/s	-	1100 MW	500 kV
Case B2	50x2MVA	10 m/s	-	1100 MW	500 kV
Case B3	50x2MVA	10 m/s	-	1100 MW	230 kV
Case B4	50x2MVA	10 m/s	Stdev 0.19 m/s, frequency 1 rad/s	1100 MW	500 kV
Case B5	50x2MVA	10 m/s	Stdev 1.86 m/s, frequency 1 rad/s	1100 MW	500 kV
Case B6	50x2MVA	10 m/s	Stdev 1.52 m/s, frequency 0.5 rad/s	1100 MW	500 kV
Case B7	50x2MVA	10 m/s	Stdev 1.52 m/s, frequency 2 rad/s	1100 MW	500 kV
Case B8	50x2MVA	10 m/s	Ramp ± 1 m/s, 0.5 Hz	1100 MW	500 kV
Case B9	50x2MVA	10 m/s	Ramp ± 1 m/s, 0.75 Hz	1100 MW	500 kV
Case B10	50x2MVA	10 m/s	Ramp ± 1 m/s, 1.0 Hz	1100 MW	500 kV
Case B11	50x2MVA	10 m/s	Ramp ± 1 m/s, 4.0 Hz	1100 MW	500 kV

For wind turbine model, the wind speed (V_w , m/s), mechanical speed of generator (ω , rad/s), and pitch angle (β , °) are input while mechanical torque (T_m) and power of turbine (P) are the output. The wind turbine has torque- ω characteristics (or equation of power coefficient) vary with V_w using standard model of wind turbine.

For synchronization system stability, important parameters to be studied are rotor speed and power angle (use power angle, δ , instead of actual rotor angle). The sources of small signal are from the different characteristics of wind speed. The 11 testing conditions with different characteristics of wind speed are represented in Table 3.2.

3.2.4 Characteristics of energy and critical energy of the power system

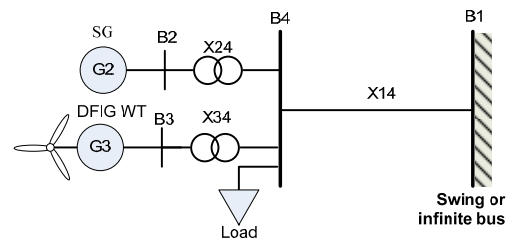
To study the characteristics of energy and the critical energy of the power system, the system dynamic equations are determined first. The steady state values of state variables can be computed from the solution of algebraic equations or using power system simulation software. The energy function can be formulated using the first integral method and applying steady state variables to compute the energy value. Finally, the critical energy can be approximated using the method of M. Ribbens-Pavella and B. Lemal (1976).

3.2.4.1 The power test system and conditions

The power test system in this paper is designed to clearly represent the effects of wind power on a nearby synchronous generator and load bus, which are connected to the infinite bus through long transmission lines. The per unit base power is 100 MVA. From the one line diagram below figure, there are aggregated synchronous generators (G2) and aggregated DFIG wind turbines (G3), connecting on bus B2 and B3, respectively. Bus B1 is an infinite bus and B4 is a load bus. The system is assumed lossless which the line resistance can be neglected. X_{14} is a line reactance (tie line) connecting between bus B1 and B4. X_{24} and X_{34} are line reactances including transformer's reactance. The electric load is a dynamic load which has c_k at about 0.05 [13]. The other values of system parameters and constants are list in Table 3.3.

Table 3.3 System Parameters and Constants

$M = 7.0$ sec	$\omega_0 = 314.2$ rad/sec	$L_m = 3.95279$ p.u.
$L_r = 0.09955$ p.u.	$L_s = 0.09241$ p.u.	$T_0 = 2.343$ p.u.
$X = 4.0$ p.u.	$X' = 0.1$ p.u.	$X_T = 0.5$ p.u.
$k_d = 0.8868$	$k_b = 7.372$	$k_a = 0.274P_m + 0.346$
$k_p = 1.0$	$k_{op} = 0.56$	$c_a = -0.022 P_m + 0.006$
$ E' = V_w = 1.05$ p.u.	$k_{c1} = 0.97396$	$k_{c2} = 1.90308$
$V_s = 1.0$ (p.u.)	$V_0 = 1.0$ (p.u.)	$k_m = 1.017$
$X_{14} = 0.75$ p.u.	$X_{24} = 0.2$ p.u.	$X_{34} = 0.2$ p.u.



3.3 A study of effects of Wind Power on Small Signal Stability using Eigenvalue Method

The eigenvalue method is the conventional and well-known method for the small signal stability analysis in the power industry.

3.3.1 Eigenvalues of single machine power system

In this section, wind power is modeled using a squirrel cage induction generator (SCIG) and doubly-fed induction generator (DFIG). The swing equation and voltage behind transient reactance are focused regarding the synchronization stability problem. The difference between synchronous generator and induction generator is the slip (s_w) which is the difference between angular speed of rotor and electrical field at stator of induction generator. Moreover, in the swing equations, damping coefficient (D) is diminished in the case of SCIG, but occurs in the case of DFIG. The state space equations for induction generator from are rewritten here:

3.3.1.1 Wind turbine with squirrel cage induction generator (SCIG)

To analyze the small signal stability of an induction generator wind turbine, the state space equation will be represented in a new form as follows.

If we represent system equations in the form of a matrix:

$$\dot{\mathbf{X}} = \mathbf{A}\mathbf{X} + \mathbf{B}\mathbf{U}$$

We will get:

$$\begin{bmatrix} \Delta \dot{x}_w \\ \Delta \dot{y}_w \end{bmatrix} = \begin{bmatrix} -K_E & \omega_0 \\ -K_S/M & -K_D/M \end{bmatrix} \begin{bmatrix} \Delta x_w \\ \Delta y_w \end{bmatrix} + \begin{bmatrix} 0 \\ 1/M \end{bmatrix} \Delta \bar{P}_{mw} \quad \text{Eq. 3-31}$$

Where $K_S = \frac{\partial \bar{P}_e}{\partial x}$ is synchronizing power coefficient, and $K_D = \frac{\partial \bar{P}_e}{\partial y}$ is damping power coefficient of induction generator.

$$K_S = \frac{\partial \bar{P}_e}{\partial x_w} = \bar{V}_w \sum_{j=1, j \neq w}^n \bar{V}_j \bar{B}_{wj} \cos(x_w^s - x_j^s) \quad \text{and} \quad K_D = \frac{\partial \bar{P}_e}{\partial y} = 0 \quad \text{Eq. 3-32}$$

$$K_E = k_b \bar{V}_{sw} k_a \cos(k_a x_w^s + c_a) \quad \text{Eq. 3-33}$$

magnitude of damping power coefficient (K_D) and synchronizing power coefficient (K_S).

Eqs. 3-32 and 3-33 can be represented using block diagram as in the following figure.

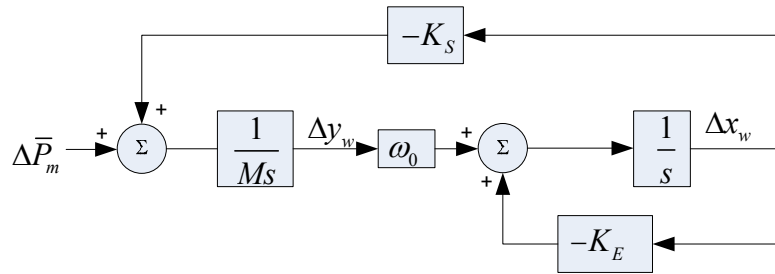


Figure 3.10 Block diagram representing state space equation of the SCIG wind turbine

Even though, induction generator has no damper circuit, its oscillation is less than synchronous generator and can improve oscillation stability of the power system when replace synchronous generator [45]. From the above figure, the flux decay effect (term with cosine function causing from varying of E') and K_s causing the negative feedback control of x_w can finally improve small signal stability of the system. This conclusion can be examined by the following simulation.

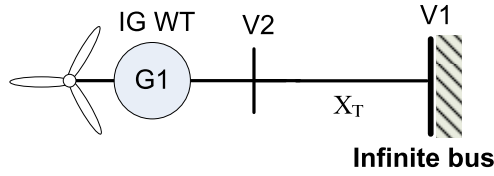


Figure 3.11 Single machine infinite bus power system

The induction machine parameters for computation are as follows [45]:

Given:

$$\begin{array}{lllll}
 M = 7.0 \text{ sec} & \omega_0 = 314.2 \text{ rad/sec} & L_m = 3.95279 \text{ p.u.} & L_r = 0.09955 \text{ p.u.} & L_s = 0.09241 \text{ p.u.} \\
 X = 4.0 \text{ p.u.} & X' = 0.2 \text{ p.u.} & T_0 = 2.343 & |E'| = V_w = 1.05 \text{ p.u.} & \eta_c = 0.95 \\
 k_d = 0.8868 & k_b = 7.372 & k_a = 0.61 & c_a = -0.05 & X_T = 0.75 \text{ p.u.}
 \end{array}$$

$$K_s = \frac{1.1\bar{V}_1}{(\bar{X}' + \bar{X}_T)} \cos(x_w^s) \quad \text{Eq. 3-34}$$

$$K_E = 4.497\bar{V}_{sw} \cos(0.61x_w^s - 0.05) \quad \text{Eq. 3-35}$$

Table 3.4 The computation conditions of induction machine (SCIG) parameters

Parameters	Case 1	Case 2	Case 3	Case 4	Case 5
Variables	Base case	Reduce V_s	Increase V_0	Increase X_T	Increase x_w
V_s (p.u.)	1.00	0.50	1.00	1.00	1.00
V_0 (p.u.)	1.0	1.0	0.5	1.0	1.0
$ X_T $ (p.u.)	0.1	0.1	0.1	0.4	0.1
x_w^s (rad)	0.3	0.3	0.3	0.3	0.6

3.3.1.2 Wind turbine with doubly-fed induction generator (DFIG)

To analyze the small signal stability of the induction generator wind turbine, the state space equation will be represented in a new form as follows.

If we represent system equations in the form of a matrix:

$$\dot{\mathbf{X}} = \mathbf{A}\mathbf{X} + \mathbf{B}\mathbf{U} \quad \text{Eq. 3-36}$$

We will get

$$\begin{bmatrix} \Delta \dot{x}_w \\ \Delta \dot{y}_w \end{bmatrix} = \begin{bmatrix} K_{E1} & K_{E2} \\ -K_S/M & -K_D/M \end{bmatrix} \begin{bmatrix} \Delta x_w \\ \Delta y_w \end{bmatrix} + \begin{bmatrix} 0 \\ 1/M \end{bmatrix} \Delta \bar{P}_{mw} \quad \text{Eq. 3-37}$$

Eq. 3-37 can be represented using a block diagram as in the following figure.

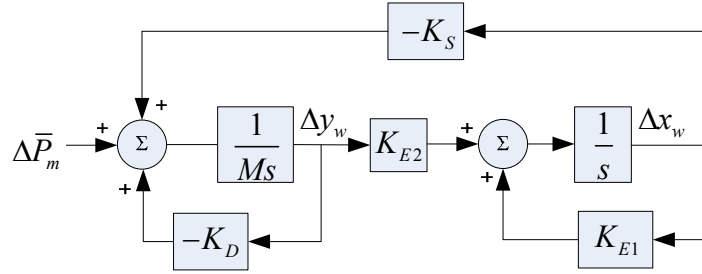


Figure 3.12 Block diagram representing state space equation of the DFIG wind turbine

Even though the induction generator has no damper circuit, its oscillation is less than that of the synchronous generator and can improve oscillation stability of the power system when replacing the synchronous generator [45]. From above figure, the flux decay effect (term with cosine function causing from varying of \mathbf{E}') and K_S causing the negative feedback control of x_w can finally improve small signal stability of the system. This conclusion can be examined by the following simulation.

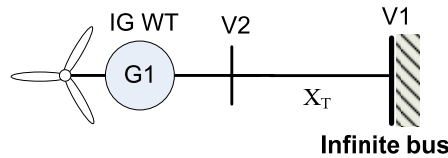


Figure 3.13 Single machine infinite bus power system for DFIG WT

The induction machine parameters for computation are as follows [45]:

Given:

$$\begin{array}{lllll}
 M = 7.0 \text{ sec} & \omega_0 = 314.2 \text{ rad/sec} & L_m = 3.95279 \text{ p.u.} & L_r = 0.09955 \text{ p.u.} & L_s = 0.09241 \text{ p.u.} \\
 X = 4.0 \text{ p.u.} & X' = 0.2 \text{ p.u.} & T_0 = 2.343 \text{ p.u.} & |E'| = V_w = 1.05 \text{ p.u.} & \eta_c = 0.95 \\
 k_d = 0.8868 & k_b = 7.372 & k_a = 0.61 & c_a = -0.05 & X_T = 0.75 \text{ p.u.} \\
 k_{vrq} = 0.0056 & k_{op} = 0.56 & k_{c1} = 0.97396 & k_{c2} = 1.90308 &
 \end{array}$$

$$\left. \begin{aligned}
 K_{E1} &= -323.45863 y_w^s \bar{V}_{sw} \sin(0.61 x_w^s - 0.05) - 4.49692 \bar{V}_{sw} \cos(0.61 x_w^s - 0.05) \\
 K_{E2} &= 42.82303 + 530.26 \bar{V}_{sw} \cos(0.61 x_w^s - 0.05) + 1.7476 \frac{(1 + y_w^s)}{\bar{V}_{sw}} \\
 K_S &= \frac{\bar{V}_w \bar{V}_0}{(\bar{X}'_w + \bar{X}_T)} \cos(x_w^s) + \frac{\bar{V}_w \bar{V}_0}{(\bar{X}'_w + \bar{X}_T)} \cos(x_w^s) y_w^s = \frac{\bar{V}_w \bar{V}_0}{(0.2 + \bar{X}_T)} \cos(x_w^s) (1 + y_w^s) \\
 K_D &= \frac{\bar{V}_w \bar{V}_0}{(0.2 + \bar{X}_T)} \sin(x_w^s)
 \end{aligned} \right\} \text{Eq. 3-38}$$

Table 3.5 The computational conditions of induction machine (DFIG) parameters

Parameters	Case1	Case2	Case3	Case4	Case5	Case6
Variables	Base case	Reduce V_s	Increase V_0	Increase X_T	Increase x_w	Increase y_w
V_s (p.u.)	1.00	0.50	1.00	1.00	1.00	1.00
V_0 (p.u.)	1.0	1.0	0.5	1.0	1.0	1.0
$ X_T $ (p.u.)	0.3	0.3	0.3	0.6	0.3	0.3
x_w^s (rad)	0.3	0.3	0.3	0.3	0.6	0.3
y_w^s (p.u.)	0.15	0.15	0.15	0.15	0.15	0.2

3.3.2 Eigenvalues of multi-machine power system including wind power

In this section, wind power is modeled using a doubly fed induction generator (DFIG), on which the swing equation and voltage behind transient reactance are focused, regarding the synchronization stability problem. The difference between the synchronous generator and the induction generator is the slip (s_w) which is the difference between angular speed of rotor and electrical field at stator of induction generator. Moreover, in the swing equations, damping coefficient (D) is diminished in case of SCIG but occur in case of DFIG.

Even though an induction generator has no damper circuit, its oscillation is less than that of the synchronous generator and can improve the oscillation stability of the power system when replace synchronous generator [45]. From above figure, the flux decay

effect (term with cosine function causing from varying of \mathbf{E}') and K_s causing the negative feedback control of x_w can finally improve small signal stability of the system. This conclusion can be examined by the following simulation.

The induction machine parameters for computation are as follows [45]:

Given:

$M_2 = M_3 = 7.0 \text{ sec}$	$\omega_0 = 314.2 \text{ rad/sec}$	$L_m = 3.95279 \text{ p.u.}$
$L_r = 0.09955 \text{ p.u.}$	$L_s = 0.09241 \text{ p.u.}$	$T_0 = 2.343 \text{ p.u.}$
$X = 4.0 \text{ p.u.}$	$X' = 0.2 \text{ p.u.}$	$X_T = 0.75 \text{ p.u.}$
$k_d = 0.8868$	$k_b = 7.372$	$k_a = 0.61$
$k_p = 1$	$k_{op} = 0.56$	$c_a = -0.05$
$ E' = V_w = 1.05 \text{ p.u.}$	$k_{c1} = 0.97396$	$k_{c2} = 1.90308$
$V_s = 1.0 \text{ (p.u.)}$	$V_0 = 1.0 \text{ (p.u.)}$	$k_m = 0.98$

If we represent the above equations in the form of a matrix:

$$\dot{\mathbf{X}} = \mathbf{A}\mathbf{X} + \mathbf{B}\mathbf{U} \quad \text{Eq. 3-39}$$

We will get:

$$\begin{bmatrix} \Delta \dot{x}_i \\ \Delta \dot{x}_w \\ \Delta \dot{x}_k \\ \Delta \dot{y}_w \\ \Delta \dot{y}_i \end{bmatrix} = \begin{bmatrix} 0 & 0 & 0 & 0 & \omega_0 \\ 0 & K_{Ew1} & K_{Ew2} & K_{Ew3} & 0 \\ -K_{Ski} & -K_{Skw} & -K_{Skk} & 0 & 0 \\ -K_{Swi} & -K_{Sww} & -K_{Sww} & -K_{Dw} & 0 \\ -K_{Sii} & -K_{Siw} & -K_{Sik} & 0 & -K_{Di} \end{bmatrix} \begin{bmatrix} \Delta x_i \\ \Delta x_w \\ \Delta x_k \\ \Delta y_w \\ \Delta y_i \end{bmatrix} + \begin{bmatrix} 0 \\ 0 \\ -\Delta \bar{P}_{lk}/c_k \\ \Delta \bar{P}_{mw}/M \\ \Delta \bar{P}_{mi}/M \end{bmatrix} \quad \text{Eq. 3-40}$$

$$\begin{bmatrix} \Delta \dot{x}_2 \\ \Delta \dot{x}_3 \\ \Delta \dot{x}_4 \\ \Delta \dot{y}_3 \\ \Delta \dot{y}_2 \end{bmatrix} = \begin{bmatrix} 0 & 0 & 0 & 0 & \omega_0 \\ 0 & K_{Ew1} & K_{Ew2} & K_{Ew3} & 0 \\ -K_{S42} & -K_{S43} & -K_{S44} & 0 & 0 \\ 0 & -K_{S33} & -K_{S34} & -K_{D3} & 0 \\ -K_{S22} & 0 & -K_{S24} & 0 & -K_{D2} \end{bmatrix} \begin{bmatrix} \Delta x_2 \\ \Delta x_3 \\ \Delta x_4 \\ \Delta y_3 \\ \Delta y_2 \end{bmatrix} + \begin{bmatrix} 0 \\ 0 \\ -\Delta \bar{P}_{l4}/c_k \\ \Delta \bar{P}_{m3}/M_3 \\ \Delta \bar{P}_{m2}/M_2 \end{bmatrix} \quad \text{Eq. 3-41}$$

The eigenvalue analysis of induction generator models of wind turbine.

From Eq. 3-41, rearranging by using the following form and taking a Laplace transformation yields:

$$\mathbf{X}(s) = (s\mathbf{I} - \mathbf{A})^{-1} \mathbf{B}\mathbf{U}(s) \quad \text{Eq. 3-42}$$

$$\begin{bmatrix} \Delta x_2(s) \\ \Delta x_3(s) \\ \Delta x_4(s) \\ \Delta y_3(s) \\ \Delta y_2(s) \end{bmatrix} = \begin{bmatrix} s & 0 & 0 & 0 & -\omega_0 \\ 0 & s - K_{Ew1} & -K_{Ew2} & -K_{Ew3} & 0 \\ K_{S42} & K_{S43} & s + K_{S44} & 0 & 0 \\ K_{S32} & K_{S33} & K_{S34} & s + K_{D3} & 0 \\ K_{S22} & K_{S23} & K_{S24} & 0 & s + K_{D2} \end{bmatrix}^{-1} \begin{bmatrix} 0 \\ 0 \\ -\Delta \bar{P}_{l4}(s)/c_k \\ \Delta \bar{P}_{m3}(s)/M \\ \Delta \bar{P}_{m2}(s)/M \end{bmatrix} \quad \text{Eq. 3-43}$$

$$(\mathbf{sI} - \mathbf{A})^{-1} = \frac{1}{\det(\mathbf{sI} - \mathbf{A})} (\mathbf{sI} - \mathbf{A})^T \quad \text{Eq. 3-44}$$

The solutions of $\det(\mathbf{sI} - \mathbf{A}) = 0$ are the eigenvalues of this state space equation, therefore:

$$\det(\mathbf{sI} - \mathbf{A}) = s(s - K_{Ew1})(s + K_{S44})(s + K_{D3})(s + K_{D2}) - \omega_0(s + K_{S44})K_{S22}K_{S33}K_{Ew3} = 0 \quad \text{Eq. 3-45}$$

Table 3.6 Testing conditions for the study of the effects of wind power on multi-machine power test systems

Variables	Case1	Case2	Case3	Case4	Case5	Case6
Load (p.u.)	4	4	4	4	4	4
P_{m3} of G_3 (p.u.)	1	1	1	0.4	0.6	0.8
P_{m2} of G_2 (p.u.)	3	4	2	3.6	3.4	3.2
$P_{\text{exchanged}}$ (P_{mG})	0	-1	1	0	0	0

3.4 A Study of Effects of Wind Power on Small Signal Stability using Stochastic Stability Method: The Mean First Passage Time (MFPT)

The mean first passage time (MFPT) is used as an index to evaluate the stability of the power system when perturbed by any small signal. This section applies the method of C.O. Nwankpa [9] to formulate the stochastic differential equations (SDE) and compute the MFPT of the power system incorporating stochastic wind power. The MFPT of stochastic power system is studied by varying noise intensities and wind speed. The measurement wind speed data in Thailand is used as an example for implementation.

The MFPT is a solution of following problem:

$$\left. \begin{aligned} \varepsilon C_1^* W \tau_0''(W) + [\varepsilon C_2 - C_3^* W] \tau_0'(W) &= -1 \\ \tau_0(W_C) &= 0, \quad \tau_0(0) < \infty \end{aligned} \right\} \quad \text{Eq. 3-46}$$

Therefore, the solution is:

$$\tau_0(0) \approx \frac{1}{C_3^*} (W_C)^{-C_2/C_1^*} \left[\int_0^{W_C} t^{(C_2/C_1^*)-1} \cdot e^{-(C_3^* t / \varepsilon_l C_1^*)} dt \right] e^{(C_3^* W_C / \varepsilon_l C_1^*)} \quad \text{Eq. 3-47}$$

$$\tau(0) \approx \frac{1}{\beta C_3^*} (W_C)^{-C_2/C_1^*} \left[\int_0^{W_C} t^{(C_2/C_1^*)-1} \cdot e^{-(C_3^* t / \varepsilon_l C_1^*)} dt \right] e^{(C_3^* W_C / \varepsilon_l C_1^*)} \quad \text{Eq. 3-48}$$

Where critical energy (W_C) computational technique is presented in the previous Progress Report II and coefficients C_1^* , C_2 , and C_3^* are stated in Appendix A.

From Sections 2.4.1 – 2.4.2 and Appendix A, MFPT can be calculated the using next process:

- (S1) Stable equilibrium points and critical energy are computed as represented in previous topics.
- (S2) Matrix **H** can be constructed using Eqs. A-3 to A-6 in Appendix A.
- (S3) Find eigenvalues and eigenvectors of matrix **H**. After matrix **H** is constructed explicitly, software *Matlab* can be used to find eigenvalues and eigenvectors.
- (S4) Construct set of matrix **D** and matrix **F** using Eqs. A-29 to A-33 in Appendix A.

These matrixes will be used in the formulation of MFPT.

- (S5) Compute C coefficient using Eqs. A-25 to A-28 in Appendix A.
- (S6) Compute MFPT using Eq. 3-48. Each step from (S1) – (S5) is done completely.
- (S7) Change conditions of wind power, such as wind speed and noise intensity and repeat (S1) – (S6) again to see the variation of MFPT.

The MFPT with different wind speeds (or wind power) and noise intensity is determined and explained in the next chapter. The case study of Thailand is examined for MFPT implementation. The testing conditions are

- Wind speed 4, 6, 8, 10, and 12 m/s
- Noise intensity varies between 0.0 – 4.0
- Wind speed data is from the 90m-height monitoring station locating in Chumporn province of Thailand, during October 2011 and May 2012.
- The wind power in this case is calculated using VESTAS V90 2000kW specification

3.5 A Study of Effects of Wind Power on Small Signal Stability using New Stochastic Stability Method

Objectives and scopes

- To develop new methods for the study of effects of stochastic wind power on power system stability using less computational effort.
- To study the effects of different wind power characteristics, wind turbine type and the exchanged power on the small signal stability of the power system using a new method.

Methods

The new method is developed based on the theory of stochastic stability. The following list are the processes to formulate stochastic stability index as a new alternative method.

- Formulate the stochastic differential equations of the power system incorporating wind power using power system dynamic equations from Sections 3.1 – 3.3.
- Find steady state values of state variables at different conditions, such as different wind power and its noise intensity, different exchange power. It can be done by using simulation software or by solving the power flow problem using Newton-Raphson's method.
- Formulate stochastic well-defined energy function as described in Sections 3.3 and 3.5
- Compute critical energy using method of Ribbens as described in Section 3.5.
- Find the derivative of mean of stochastic well-defined energy function and formulate a new stability index and compute.
- Evaluate the results of new stability index under different testing conditions

Expected results

- Steady state values of state variables at different conditions, such as different wind power and its noise intensity, different exchange power.
- Critical energy and the derivative stochastic well-defined energy of the power system with different conditions
- The new stability index with different testing conditions and the evaluation results

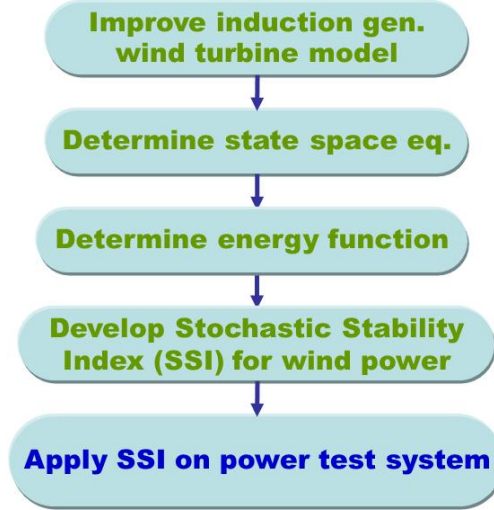


Figure 3.14 Process to study effects of wind power using SSI

Testing conditions

The power test system (details are in Section 4.2.2)

- Two machines infinite bus power system (TMIB)

The wind turbine types (details are in Section 4.1)

- Squirrel cage induction generator (SCIG)
- Doubly-fed induction generator (DFIG)

The noise model conditions (details are in Section 4.3)

- White noise wind power (normal distribution with infinite bandwidth)
- Colored noise wind power (normal distribution with limited bandwidth)

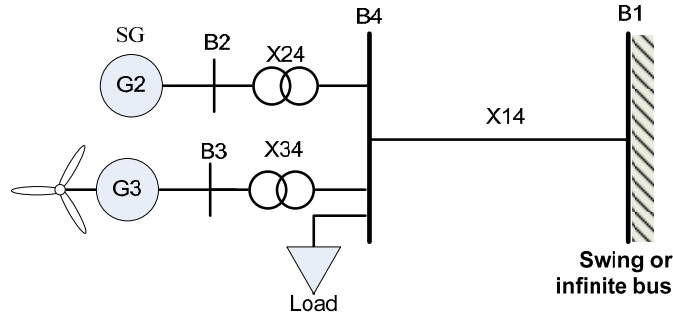
The power flow conditions

- Different wind power without exchange power to/from infinite bus
- Different exchanged power of infinite bus

In Figure 3.15, G2 is generation bus with synchronous generator (SG), G3 is wind power bus with DFIG or SCIG. X24 is reactance of lines B2-B4 including transformer, X34 is reactance of lines B3-B4 including transformer. Load bus is constant active power load. For bus 1, x_1 is a reference angle of infinite bus generator and y_1 is reference speed deviation ($\bar{\omega}_{r1} - \bar{\omega}_s \approx 0$) which is close to zero. The details of the test system is in Section 4.2.2.

Table 3.7 System Parameters and Constants for TMIB

$M = 7.0$ sec	$\omega_0 = 314.2$ rad/sec	$L_m = 3.95279$ p.u.
$L_r = 0.09955$ p.u.	$L_s = 0.09241$ p.u.	$T_0 = 2.343$ p.u.
$X = 4.0$ p.u.	$X' = 0.1$ p.u.	$X_T = 0.5$ p.u.
$k_d = 0.8868$	$k_b = 7.372$	$k_a = 0.274P_m + 0.346$
$k_p = 1.0$	$k_{op} = 0.56$	$c_a = -0.022 P_m + 0.006$
$ E' = V_w = 1.05$ p.u.	$k_{c1} = 0.97396$	$k_{c2} = 1.90308$
$V_s = 1.0$ (p.u.)	$V_0 = 1.0$ (p.u.)	$k_m = 1.017$
$X_{14} = 0.5$ p.u.	$X_{24} = 0.2$ p.u.	$X_{34} = 0.2$ p.u.

**Figure 3.15** The two machine infinite bus power system (TMIB)**Table 3.8** Power flow and noise conditions for SSS analysis of TMIB

Variables	Case 1	Case 2	Case 3	Case 4	Case 5	Case 6
Load (p.u.)	4	4	4	4	4	4
P_{m3} of G_3 (p.u.)	1	1	1	0.4	0.6	0.8
P_{m2} of G_2 (p.u.)	3	4	2	3.6	3.4	3.2
Exchange (P_{mG})	0	-1	1	0	0	0
Noise intensity, NI	0.0 – 1.0					
Bandwidth, BW	0 – 20					

3.6 A Study of Effects of Wind Power on Voltage Stability using New Stochastic Stability Method

Objectives and scopes

- To develop new methods to study the effects of stochastic wind power on power system voltage stability.
- To study the effects of different noise intensity of wind power, wind turbine type, and conditions of exchange power on the voltage stability of the power system.

Methods

- Formulate power system dynamic equations and stochastic differential equations, incorporating DFIG wind turbines, and with dynamic voltage equation at load bus.
- Find steady state values of state variables at different conditions such as different wind power and its noise intensity, different exchange power.
- Formulate stochastic well-defined energy function using DFIG WT, colored noise model, and with dynamic voltage at load bus.
- Compute critical energy using method of Ribbens.
- Formulate new voltage stability index and compute using the derivative stochastic well-defined energy function and the critical energy.
- Evaluate the results of new voltage stability index under different testing conditions.

Expected results

- Steady state values of state variables at different conditions such as different wind power and its noise intensity, different exchange power.
- Critical energy and the derivative stochastic well-defined energy of the power system with different conditions.
- The voltage stability index with different testing conditions and the evaluation results.

Testing conditions

The power test system

- Two machines infinite bus power system

The wind turbine types

- Doubly-fed induction generator (DFIG)

The noise model conditions

- Colored noise wind power

The power flow conditions

- Different wind power without exchange power to/from infinite bus
- Different exchanged power of infinite bus

Therefore, the power test system and parameters are the same as in Section 3.5.

Table 3.9 Power flow and noise conditions for VS analysis of TMIB

Variables	Case1	Case2	Case3	Case4	Case5	Case6
Load (p.u.)	4	4	4	4	4	4
P_{m3} of G_3 (p.u.)	1	1	1	0.4	0.6	0.8
P_{m2} of G_2 (p.u.)	3	3.5	2.5	3.6	3.4	3.2
Exchange (P_{mG})	0	-0.5	0.5	0	0	0
Noise intensity, NI	0.0 – 1.0					
Bandwidth, BW	0 – 20					

3.7 A Study of Effects of Wind Power on Voltage Variations using Probabilistic Method

Objectives and scopes

- To study the relation between the random wind power and voltage of the power system
- To study the effects of different noise intensity of wind power on voltage and frequency of the power system
- To study the effects of type of wind turbine on voltage of the power system

Methods

- Formulate wind power dynamics models using DFIG
- Apply MCS for the study using PSCAD and Matlab
- Run the simulation for 1000 rounds comparing between DFIG and with the different noise intensity of wind power

Expected results

- The probability distribution of wind power with different noise intensity of DFIG
- The probability distribution of voltage at load bus under different conditions

The effects of wind power on the power quality, especially voltage, will be determined using the probabilistic method called Monte Carlo Simulation (MCS). There are two main topics which will be studied: (1) the effects of wind power with stochastic noise on load voltage, and (2) the effects of various noises on load voltage. The testing conditions for these two topics are stated in the following tables.

Table 3.10 Testing conditions for a study of effects of wind power on load voltage

Variable	Case 1	Case 2	Case 3	Case 4	Case 5	Case 6
P_{Load}	4	4	4	4	4	4
P_{m3}	1.0	1.0	1.0	0.4	0.6	0.8
P_{m2}	3.0	3.5	2.5	3.6	3.4	3.2
$P_{exchange} (P_{mG})$	0.0	-0.5	0.5	0.0	0.0	0.0
NI P_{m3}	0.3, 0.6					
BW P_{m3}	1, 10					

Table 3.11 Testing conditions for a study of effects of various noises on load voltage

Variable	Case T1	Case T2	Case T3	Case T4	Case T5	All 1	All 2
P_{Load}	4	4	4	4	4	4	4
P_{mw}	1.0	1.0	1.0	1.0	1.0	1.0	1.0
P_{mi}	3.0	3.0	3.0	3.0	3.0	3.0	3.0
$P_{exchange}$	0.0	0.0	0.0	0.0	0.0	0.0	0.0
Q_{Load}	1.0	1.0	1.0	1.0	1.0	1.0	1.0
NI,BW P_{mw}	0.1,10	-	-	0.1,0.1	-	0.1,10	0.1,10
NI,BW P_{Load}	-	0.025,0.1	-	-	-	0.025,0.1	0.025,0.1
NI,BW Q_{Load}	-	-	0.1,0.1	-	-	0.1,0.1	0.1,0.1
Weibull WS	-	-	-	-	yes	yes	-

CHAPTER 4

METHODOLOGY PART 2

The methodologies in part 2 are the techniques used for the studies in Chapter 3 (Methodology Part 1). These methods are adapted from the studies in the past except the stochastic stability index which is a new developed method. The following topics are the main issues described in this chapter.

- Power system modeling
- Power system simulation
- Noise modeling and stochastic differential equations formulation
- Energy function formulation
- Critical energy estimation
- Eigenvalue determination
- Mean first passage time (MFPT) determination
- Stochastic stability index (SSI) determination

4.1 Power System Modeling

For the study of power system stability, it is reasonable to neglect dynamics occurring at stator while focus only on rotor dynamics. The swing equation is focused regarding the synchronization stability problem (for example, small disturbance around equilibrium operating point).

4.1.1 Wind power modeling using SCIG wind turbine

In this section, wind power is modeled using squirrel cage induction generator (SCIG), on which the swing equation is focused regarding the synchronization stability problem. The voltage behind transient reactance is also included. The different between synchronous generator and induction generator is the slip (s_w) which is the different between angular speed of rotor and electrical field at stator of induction generator. Moreover, in the swing equations, damping coefficient (D) is diminished for SCIG.

4.1.1.1 Relationship between rotor angle (δ) and phase angle (θ)

For three phase electrical system (abc), terminal phase voltage (v_a, v_b, v_c) can be represented as follows:

$$\left. \begin{aligned} v_a &= V_m \cos(\omega_s t + \theta) \\ v_b &= V_m \cos(\omega_s t - 2\pi/3 + \theta) \\ v_c &= V_m \cos(\omega_s t + 2\pi/3 + \theta) \end{aligned} \right\} \quad \text{Eq. 4-1}$$

For rotating reference frame, dq transformation of phase voltage is:

$$\left. \begin{aligned} v_d &= V_m \cos(\omega_s t + \theta - \alpha) \\ v_q &= V_m \sin(\omega_s t + \theta - \alpha) \end{aligned} \right\} \quad \text{Eq. 4-2}$$

Where V_m is maximum phase voltage, θ is angle of terminal voltage phasor which leads angle of reference bus voltage, α is angle which d -axis leads axis of phase a and $\alpha = \omega_r t + \theta_0$ (where θ_0 is initial angle and assumes zero).

For synchronizing reference frame, d -axis is assumed in phase with phase a . Therefore, terminal phase voltage on dq axis of synchronizing reference frame is

$$\left. \begin{aligned} v_d &= v_a = V_m \cos(\omega_s t + \theta) \\ v_q &= V_m \sin(\omega_s t + \theta) \end{aligned} \right\} \quad \text{Eq. 4-3}$$

For a synchronous machine, δ is the rotor angle or power angle, which is the same with the angle of voltage behind the transient reactance. But for an induction machine, δ is determined as the angle of voltage behind transient reactance for synchronizing reference frame and is not the rotor angle. The difference between the angle of terminal voltage and angle of voltage behind the transient reactance is called *internal phase angle* (δ') as follows:

$$\delta = \delta' + \theta \quad \text{Eq. 4-4}$$

$$\phi = \theta - \theta_c \quad \text{Eq. 4-5}$$

Where θ_c is angle of terminal current and ϕ is power factor angle which is the difference between θ and θ_c .

4.1.1.2 Electromagnetic torque under steady state conditions

The dynamical electromagnetic torque (T_g) in per unit is stated by Olimpo Anaya-Lara, et al. (2009):

$$\bar{T}_g = \frac{E'_d \bar{i}_d + E'_q \bar{i}_q}{\bar{\omega}_s} \quad \text{Eq. 4-6}$$

Where \bar{E}'_d and \bar{E}'_q are voltage behind transient reactance in d and q axis, respectively.

\bar{i}_{ds} and \bar{i}_{qs} are stator current in d and q axis, respectively.

However, if the magnetic field of rotor rotates at synchronous speed in which q-axis in-phase with voltage behind transient reactance, only q components of voltage behind transient reactance is occurred. Eq. 4-6 becomes [6]:

$$\bar{T}_g \approx E'_q \bar{i}_q \quad \text{Eq. 4-7}$$

Where $\bar{\omega}_s$ is assumed to be one.

Under steady state conditions, the electromagnetic torque (T_g) of SCIG can be expressed as follows [45]:

$$T_g = 3 \frac{p}{2} \frac{r_r}{s_w \omega_s} I_r^2 \quad \text{Eq. 4-8}$$

$$\text{Where } \mathbf{I}_r = \frac{\mathbf{V}_s}{\left(r_s + \frac{r_r}{s_w} \right) + j(X_s + X_r)} \quad \text{Eq. 4-9}$$

If we assume r_s, X_s, X_r are very much less than r_r/s_w , [73], hence:

$$I_r \approx \frac{V_s}{r_r/s_w} = \frac{V_s s_w}{r_r} \quad \text{Eq. 4-10}$$

When replacing I_r in Eq. 4-10 into Eq. 4-8, the relationship between power output and slip of SCIG can be approximated as follows:

$$T_g \approx 3 \frac{p}{2} \frac{r_r}{s_w \omega_{sw}} \left(\frac{V_s s_w}{r_r} \right)^2 = 3 \frac{p}{2} \frac{V_s^2 s_w}{r_r \omega_{sw}} \quad \text{Eq. 4-11}$$

For per unit base

$$\bar{T}_g = \bar{P}_g = \frac{T_g}{S_{base}/\omega_{sw}} = \frac{P_g}{S_{base}} \approx 3 \frac{p}{2} \frac{V_s^2 s_w}{r_r S_{base}} = 3 \frac{p}{2} \frac{\bar{V}_s^2 s_w}{\bar{r}_r} \quad \text{Eq. 4-12}$$

Where S_{base} is apparent base power and the slip (s_w) can be represented by

$$s_w = 1 - \frac{p}{2} \frac{\omega_r}{\omega_s} = 1 - \frac{\omega_r}{\omega_s} = \frac{\omega_s - \omega_r}{\omega_s} \quad [67] \quad \text{Eq. 4-13}$$

Where p is number of pole, ω_{rm} is revolution speed of rotor in mechanical radians per second, ω_{rw} is angular speed of rotor in electrical radians per second and ω_{sw} is angular speed of electrical field at stator in electrical radians per second.

4.1.1.3 Swing equation of induction generator

For swing equation (or rotor mechanic equation) of induction generator, Newton's second law is applied to the rotating machine as follows.

From $\sum F_i = ma$, F is force which is torque (T) over distance (r) from the center of rotating in Newton (N), m is mass in kilogram (kg), and a is acceleration (m/s^2). The relationship becomes:

$$\sum F_i = \frac{T_m}{r} + \left(-\frac{T_g}{r} \right) = ma = \frac{1}{r}(T_m - T_g) \quad \text{Eq. 4-14}$$

Where T_m is mechanical torque and T_g is electromagnetic torque.

We know that $a = r(d\omega_r/dt)$, replacing in the above equation yields

$$mr^2 \frac{d\omega_r}{dt} = J \frac{d\omega_r}{dt} = T_m - T_g \quad \text{Eq. 4-15}$$

Where J is moment of inertia (kg.m).

Eq. 4-15 is the rotor dynamic equation which can be explained as the relationship between torque balance and deviation of frequency (angular speed of rotor). To express it in per unit base, the inertia constant H (seconds) is proposed and rearranged.

$$H = \frac{J\omega_s^2}{2S_{base}} \text{ or } J = \frac{2HS_{base}}{\omega_s^2} \quad \text{Eq. 4-16}$$

Placing Eq. 4-16 into Eq. 4-15, we will get

$$\left(\frac{2HS_{base}}{\omega_s^2} \right) \frac{d\omega_r}{dt} = T_m - T_g \quad \text{Eq. 4-17}$$

Rearrange Eq. 4-17, yields

$$\frac{1}{\omega_s} \frac{d\omega_r}{dt} = \frac{d\bar{\omega}_r}{dt} = \frac{1}{2H} \left(\frac{T_m - T_g}{S_{base}/\omega_s} \right) \quad \text{or} \quad \frac{d\omega_r}{dt} = \frac{\omega_s}{2H} (\bar{T}_m - \bar{T}_g) \quad \text{Eq. 4-18}$$

$$\text{In per unit system} \quad \bar{T} = \frac{T}{T_{base}} = \frac{T}{S_{base}/\omega_{base}} = \frac{T\omega_{base}}{S_{base}} = \frac{P}{S_{base}} = \bar{P} \quad \text{Eq. 4-19}$$

Therefore, in per unit system, torque is equal to power.

From Eq. 4-18, we have found that [45]:

$$\frac{d}{dt} \left(\frac{\omega_r}{\omega_s} \right) = \frac{d}{dt} \bar{\omega}_r = \frac{1}{2H} (\bar{P}_m - \bar{P}_g) \quad \text{Eq. 4-20}$$

If assumes ω_s is constant or change very small, replace Eq. 4-20 into 2-27, we have found that

$$\frac{ds_w}{dt} = -\frac{1}{M} (\bar{P}_m - \bar{P}_g) \quad \text{Eq. 4-21}$$

Where $M = 2H$.

4.1.1.4 Voltage behind transient reactance of induction generator

When neglecting rotor circuit, equivalent circuit is based solely on stator voltage behind the transient reactance (E') of induction generator can be represented by following diagram.

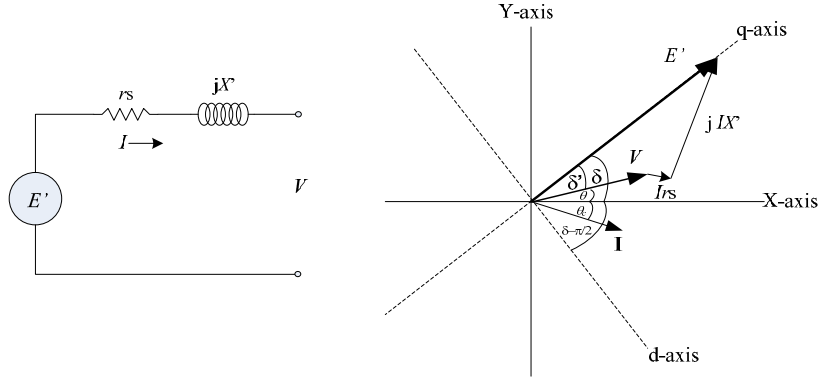


Figure 4.1 Single-line (left) and phasor (right) diagrams of induction generator

In the above figure, for system reference axis or XY-axis, it can be represented using following relationship.

$$\bar{\mathbf{E}}'_{xy} = \bar{\mathbf{E}}'_{dq} e^{j\left(\delta - \frac{\pi}{2}\right)} = \bar{E}' e^{j\delta} \quad \text{Eq. 4-22}$$

$$\bar{\mathbf{V}}_{xy} = \bar{\mathbf{V}}_{dq} e^{j\left(\delta - \frac{\pi}{2}\right)} = (\bar{V}_q - j\bar{V}_d) e^{j\delta} = \bar{V} e^{j\theta} \quad \text{Eq. 4-23}$$

$$\bar{\mathbf{I}}_{xy} = \bar{\mathbf{I}}_{dq} e^{j\left(\delta - \frac{\pi}{2}\right)} = (\bar{I}_q - j\bar{I}_d) e^{j\delta} = \bar{I} e^{j\theta_c} \quad \text{Eq. 4-24}$$

From above figure, neglecting stator resistance, for d-q reference axis (machine reference), the Kirchhoff's law can be applied and yield

$$\bar{\mathbf{E}}'_{dq} = \bar{\mathbf{V}}_{dq} + j\bar{X}\bar{\mathbf{I}}_{dq} \quad \text{or} \quad \bar{\mathbf{E}}'_{xy} = \bar{\mathbf{V}}_{xy} + j\bar{X}\bar{\mathbf{I}}_{xy} \quad \text{Eq. 4-25}$$

If we give $\bar{\mathbf{E}}'_{dq} = \bar{E}'_d + j\bar{E}'_q$, $\bar{\mathbf{V}}_{dq} = \bar{V}_d + j\bar{V}_q$ and $\bar{\mathbf{I}}_{dq} = \bar{I}_d + j\bar{I}_q$, Eq. 4-25 becomes

$$\bar{E}'_d + j\bar{E}'_q = (\bar{V}_d + j\bar{V}_q) + \bar{X}'(-\bar{I}_q + j\bar{I}_d) \quad \text{Eq. 4-26}$$

$$\bar{E}'_d = \bar{V}_d - \bar{X}'\bar{I}_q \quad \text{Eq. 4-27}$$

$$\bar{E}'_q = \bar{V}_q + \bar{X}'\bar{I}_d \quad \text{Eq. 4-28}$$

Since q-axis is in-phase with $\bar{\mathbf{E}}'$, \bar{E}'_d is assumed zero, therefore, from Eq. 4-27, $\bar{V}_d = \bar{X}'\bar{I}_q$.

Given $\bar{V}_d = \bar{V}\sin(\delta')$ and $\bar{V}_q = \bar{V}\cos(\delta')$, $\delta' = \delta - \theta$, replace into Eq. 4-27 and 4-28, yield

$$\bar{E}'_q = \bar{E}' = \bar{V}\cos(\delta') + \bar{X}'\bar{I}_d \quad \text{Eq. 4-29}$$

$$\bar{V} \sin(\delta') = \bar{X}' \bar{I}_q \quad \text{Eq. 4-30}$$

If we give $\bar{\mathbf{E}}'_{xy} = \bar{\mathbf{E}}'_x + j\bar{\mathbf{E}}'_y$, $\bar{\mathbf{V}}_{xy} = \bar{\mathbf{V}}_x + j\bar{\mathbf{V}}_y$ and $\bar{\mathbf{I}}_{xy} = \bar{\mathbf{I}}_x + j\bar{\mathbf{I}}_y$, Eq. 4-25 becomes

$$\bar{\mathbf{E}}'_x + j\bar{\mathbf{E}}'_y = (\bar{\mathbf{V}}_x + j\bar{\mathbf{V}}_y) + \bar{X}'(j\bar{\mathbf{I}}_x - \bar{\mathbf{I}}_y) \quad \text{Eq. 4-31}$$

If the stator resistance is very small and can be neglected, for induction motor in x-y reference axis (system reference), the deviation of voltage behind transient reactance (E') can be represented as follows [23]:

$$\frac{d\bar{\mathbf{E}}'_{xy}}{dt} = -\frac{1}{\bar{T}_0} [\bar{\mathbf{E}}'_{xy} - j(\bar{X} - \bar{X}')\bar{\mathbf{I}}_{xy}] - js_w\omega_s\bar{\mathbf{E}}'_{xy} \quad \text{Eq. 4-32}$$

Where T_0 is the per unit transient open circuit time constant of induction machine (seconds), X is the per unit open circuit reactance, X' is the per unit transient short circuit reactance.

For the induction generator, only the sign of the current term of the above equation is changed to be [6]:

$$\frac{d\bar{\mathbf{E}}'_{xy}}{dt} = -\frac{1}{\bar{T}_0} [\bar{\mathbf{E}}'_{xy} + j(\bar{X} - \bar{X}')\bar{\mathbf{I}}_{xy}] - js_w\omega_s\bar{\mathbf{E}}'_{xy} \quad \text{Eq. 4-33}$$

However, to represent Eq. 4-33 in the form of magnitude and angle of $\bar{\mathbf{E}}'$ separately, placing Eqs. 4-22 to 4-24 into Eq. 4-33, yields

$$e^{j\delta} \frac{d\bar{\mathbf{E}}'}{dt} + j\bar{\mathbf{E}}'e^{j\delta} \frac{d\delta}{dt} = -\frac{1}{\bar{T}_0} [\bar{\mathbf{E}}'e^{j\delta} + j(\bar{X} - \bar{X}')(\bar{\mathbf{I}}_q - j\bar{\mathbf{I}}_d)e^{j\delta}] - js_w\omega_s\bar{\mathbf{E}}'e^{j\delta} \quad \text{Eq. 4-34}$$

Divide above equation by $e^{j\delta}$,

$$\frac{d\bar{\mathbf{E}}'}{dt} + j\bar{\mathbf{E}}' \frac{d\delta}{dt} = -\frac{1}{\bar{T}_0} [\bar{\mathbf{E}}' + (\bar{X} - \bar{X}')(\bar{\mathbf{I}}_d + j\bar{\mathbf{I}}_q)] - js_w\omega_s\bar{\mathbf{E}}' \quad \text{Eq. 4-35}$$

Separate real and imaginary parts, becomes

$$\frac{d\bar{\mathbf{E}}'}{dt} = -\frac{1}{\bar{T}_0} [\bar{\mathbf{E}}' + (\bar{X} - \bar{X}')\bar{\mathbf{I}}_d] \quad \text{Eq. 4-36}$$

$$\frac{d\delta}{dt} = -\frac{(\bar{X} - \bar{X}')\bar{\mathbf{I}}_q}{\bar{T}_0\bar{\mathbf{E}}'} - s_w\omega_s \quad \text{Eq. 4-37}$$

where

$$\bar{T}_0 = \frac{\bar{L}_{rr}}{\bar{r}_r} = \frac{\bar{L}_r + \bar{L}_m}{\bar{r}_r} \quad \text{Eq. 4-38}$$

$$\bar{X} = \bar{\omega}_s \bar{L}_{ss} = \bar{\omega}_s (\bar{L}_s + \bar{L}_m) \quad \text{Eq. 4-39}$$

$$\bar{X}' = \bar{\omega}_s \left(\bar{L}_{ss} - \frac{\bar{L}_m^2}{\bar{L}_{rr}} \right) \quad \text{Eq. 4-40}$$

4.1.1.5 Relationship between internal phase angle of voltage behind transient reactance and phase angle of terminal voltage

In the SMIB model, replacing synchronous generator by induction generator, the simulation result using PSCAD can reveal the relationship between internal phase angle of voltage behind transient reactance and phase angle of terminal voltage as follows.

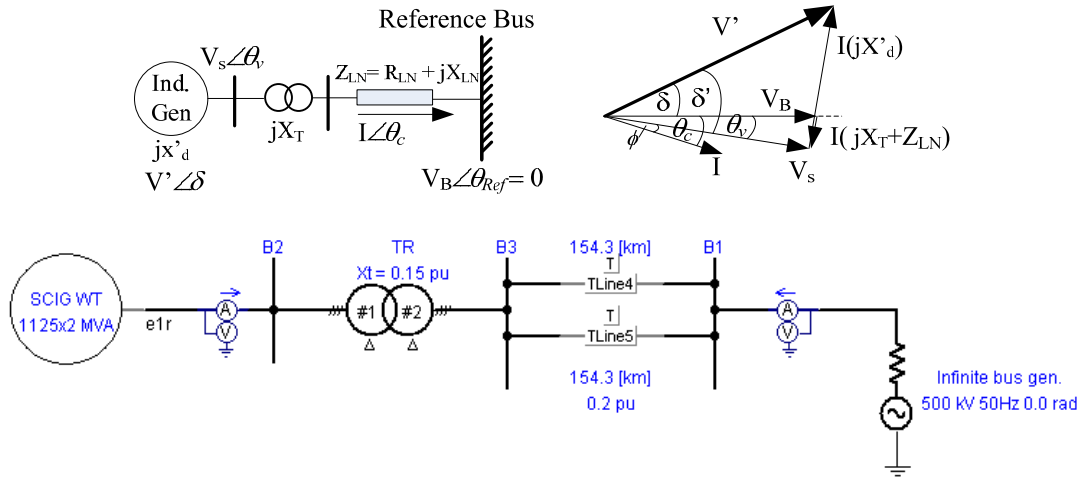


Figure 4.2 Single-line diagram of power test system in PSCAD

Where X_T is transformer reactance and X_{LN} is line reactance, wind speed is 8, 9, 10 m/s.

Assuming that $\delta' \approx k_a \delta + c_a$, from the above figure we found that $k_a > 0$. For the linear relationship between internal phase angle (IntA, δ') and angle of internal voltage (AoIV, δ) during the time 0.3 – 10.0 seconds, k_a is about 0.624 and c_a is -0.048.

From the result of simulation, k_a (positive) and c_a (negative) have small increases with increasing wind speed. This is due to an increasing wind power resulting in rotor speed deviation acceleration and finally causes an angle of voltage behind transient reactance (δ) to increase. The relationship between deviation of δ' , δ and θ are as follows

$$\delta = \delta' + \theta, \quad \delta' \approx k_a \delta + c_a \quad \text{Eq. 4-41}$$

the above equation becomes

$$\dot{\delta}' = k_a \dot{\delta} \quad \text{and} \quad \dot{\delta} = \dot{\delta}' + \dot{\theta} \quad \text{Eq. 4-42}$$

Table 4.1 The slope (k_a) and offset (c_a) of the linear relationship between internal phase angle of voltage behind transient reactance and phase angle of terminal voltage during the time 0.3 – 2.0 seconds.

Wind speed	k_a	c_a
8 m/s	0.613	-0.053
9 m/s	0.614	-0.051
10 m/s	0.622	-0.049

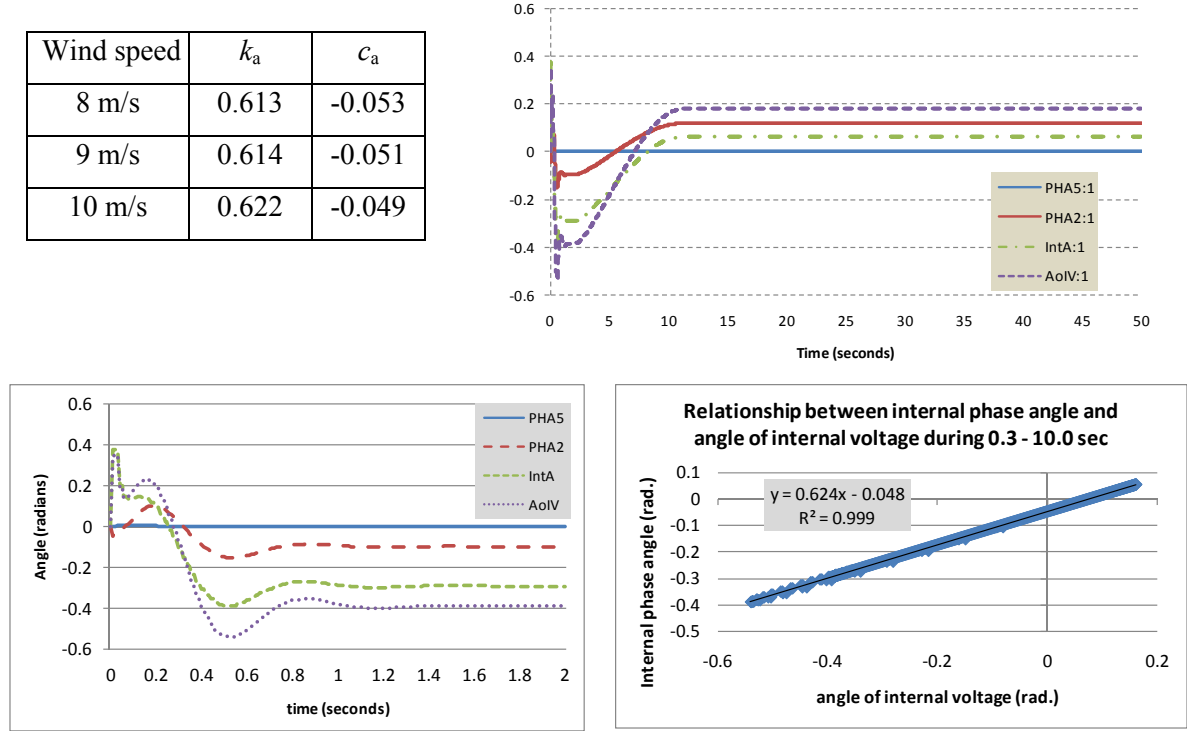


Figure 4.3 The relationship between internal phase angle (IntA, δ') and angle of internal voltage (AoIV, δ) and phase angle of terminal voltage (PHA, θ_v)

4.1.2 Wind power modeling using DFIG wind turbine

This report focuses on the variable speed wind turbine using DFIG which has the largest share in the market. The DFIG third-order model is represented for a study on the small signal stability analysis.

4.1.2.1 Steady state characteristics

If we neglect iron losses (from stator and rotor) and air gap loss, the power balance of DFIG can be represented using the following equation

$$\bar{P}_m = \bar{P}_G = \bar{P}_s + \bar{P}_r \quad \text{Eq. 4-43}$$

Where P_m is mechanical input power, P_m is power generation to the grid, P_s is electrical power on stator and P_r is electrical power on rotor (per unit).

Equation of motion:

The equation of motion (relationship between torque balance and the deviation of frequency) of DFIG is similar to the general induction generator (IG), except for the power on rotor (P_r). This equation becomes [45]:

$$\frac{d}{dt} \left(\frac{\omega_r}{\omega_s} \right) = \frac{d}{dt} \bar{\omega}_r = -\frac{d}{dt} s_w = \frac{1}{M} (\bar{P}_m - \bar{P}_s - \bar{P}_r) = \frac{1}{M} (\bar{P}_m - \bar{P}_G) \quad \text{Eq. 4-44}$$

Where ω_r and ω_s are angular speed of rotor and of electrical field at stator (electrical radians per second). P_m is mechanical input power and P_s is electrical power on stator (per unit). $M = 2H$ is inertia constant of generator (second). s_w is slip $((\omega_r - \omega_s) / \omega_s)$. The over bar represents per unit value and p is the derivative over time operator.

The P_s can be represented in the following equations:

$$\bar{P}_s \approx \bar{P}_G - \bar{P}_r = \frac{\bar{P}_G}{(1-s_w)} \quad \text{Eq. 4-45}$$

$$\bar{P}_r = \bar{I}_{rd} \bar{V}_{rd} + \bar{I}_{rq} \bar{V}_{rq} \approx -s_w \bar{P}_s \quad [45] \quad \text{Eq. 4-46}$$

$$\bar{P}_G \approx \bar{P}_{ew} = \bar{E}'_w \sum_{j=1}^n \bar{V}_j B_{wj} \sin(\delta_w - \theta_j) \quad \text{Eq. 4-47}$$

Where P_e is electrical power generation of machine, P_r is electrical power on rotor, δ is an angle of voltage behind transient reactance (E'), θ is angle of voltage (V_0) at reference point, δ' is an angle between E' and V_0 , X_T is line reactance, B_{wj} is susceptance between internal bus w and network bus j . The other variables are described below.

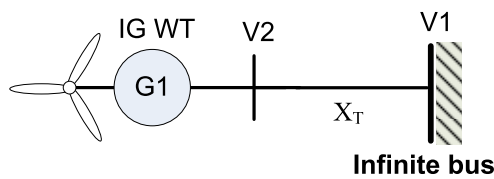


Figure 4.4 Single machine infinite bus power system for wind power modeling

For synchronous generators, the damping power decreases with increasing line reactance [44]. For SCIG, the damping power due to the current flow in the rotor circuit ($i^2 r$) is very small. For DFIG, however, its damping power may larger than that of SCIG due to the rotor voltage (V_r) which is in-phase with E' . Therefore, Eq. 4-47 is used to relate the effect of line reactance on the damping power and is replaced into Eq. 4-46, yields

$$M_w p y_w = (\bar{P}_{mw} - \bar{P}_{ew}) \quad \text{Eq. 4-48}$$

Where $y_w = -s_w$ is state variable which represent speed deviation.

4.1.2.2 Equation of voltage behind transient reactance

The deviation of voltage behind transient reactance, \mathbf{E}' , of DFIG in x-y reference axis (system reference) can be represented as follows [45]:

$$\frac{d\bar{\mathbf{E}}'_{xy}}{dt} = -\frac{1}{T_0} \left[\bar{\mathbf{E}}'_{xy} + j(\bar{X} - \bar{X}') \bar{\mathbf{I}}_{xy} \right] - js_w \omega_s \bar{\mathbf{E}}'_{xy} + j\omega_s \frac{\bar{L}_m}{\bar{L}_{rr}} \bar{\mathbf{V}}_r \quad \text{Eq. 4-49}$$

If representing Eq. 4-49 in the form of magnitude and angle separately, the new forms in d-q axis reference are

$$\frac{d\bar{E}'}{dt} = -\frac{1}{T_0} \left[\bar{E}' - (\bar{X} - \bar{X}') \bar{I}_{sd} \right] - \omega_s \frac{\bar{L}_m}{\bar{L}_{rr}} \bar{V}_{rd} \quad \text{Eq. 4-50}$$

$$\frac{d\delta}{dt} = -\frac{(\bar{X} - \bar{X}') \bar{I}_{sq}}{\bar{T}_0 \bar{E}'} - s_w \omega_s + \omega_s \frac{\bar{L}_m}{\bar{L}_{rr}} \bar{V}_{rq} \quad \text{Eq. 4-51}$$

Where \mathbf{I}_s is stator current, δ is phase angle of \mathbf{E}'_{xy} , T_0 is the transient open circuit time constant of induction machine (seconds), X is open circuit reactance, X' is transient short circuit reactance. \mathbf{V}_r , \mathbf{V}_s are rotor and stator voltage, respectively. L_m is mutual inductance and L_r (when $L_{rr} = L_r + L_m$) is rotor circuit inductance. \mathbf{E}_{xy} is assumed in-phase with q-axis and following equations are also stated:

$$\bar{\mathbf{E}}'_{xy} = \bar{\mathbf{E}}'_{dq} e^{j\left(\delta - \frac{\pi}{2}\right)} = (\bar{E}'_q - j\bar{E}'_d) e^{j\delta} = \bar{E}' e^{j\delta} \quad \text{Eq. 4-52}$$

$$\bar{\mathbf{V}}_{xy} = \bar{\mathbf{V}}_{dq} e^{j\left(\delta - \frac{\pi}{2}\right)} = (\bar{V}_q - j\bar{V}_d) e^{j\delta} = \bar{V} e^{j\theta} \quad \text{Eq. 4-53}$$

$$\bar{\mathbf{I}}_{xy} = \bar{\mathbf{I}}_{dq} e^{j\left(\delta - \frac{\pi}{2}\right)} = (\bar{I}_q - j\bar{I}_d) e^{j\delta} = \bar{I} e^{j\theta_c} \quad \text{Eq. 4-54}$$

The steady state voltage balance of stator can be represented as follows:

$$\bar{V}_{sq} = (\bar{E}'_q - \bar{I}_{sd} \bar{X}') - \bar{I}_{sq} \bar{r}_s \quad \text{Eq. 4-55}$$

$$\bar{V}_{sd} = \bar{E}'_d + \bar{I}_{sq} \bar{X}' - \bar{I}_{sd} \bar{r}_s \quad \text{Eq. 4-56}$$

$$\bar{I}_{sd} = -\frac{1}{\omega_s \bar{L}_{ss}} \bar{V}_{sq} + \frac{\bar{L}_m}{\bar{L}_{ss}} \bar{I}_{rd} \quad \text{Eq. 4-57}$$

$$\bar{I}_{sq} = \frac{\bar{L}_m}{\bar{L}_{ss}} \bar{I}_{rq} \quad \text{Eq. 4-58}$$

Assuming pE' in Eq. 4-50 and the terms with r_s in Eq. 4-55 and Eq. 4-56 are very small and can be neglected and V_r has only q-component. Replace I_{sq} from Eq. 4-56 into Eq. 4-51. Finally, Eq. 4-51 becomes

$$\frac{d\delta}{dt} = -\frac{(\bar{X} - \bar{X}')\bar{V}_{sd}}{\bar{T}_0\bar{X}'} - s_w\omega_s + \omega_s\frac{\bar{L}_m}{\bar{L}_{rr}}\frac{\bar{V}_{rq}}{\bar{E}'} \quad \text{Eq. 4-59}$$

Eq. 4-59 reveals the relationship between V_{rq} , s_w , E' , and $p\delta$ while V_{rd} in Eq. 4-50 is very small and not affect to E' . These assumptions are necessary for the following topics.

The dynamic control of this DFIG model is applied using *current-mode control technique* [45]. For the study of small signal stability, only torque and voltage control models is discussed.

From Eq. 4-56, if ω_r less than 0.7 p.u., then T_{sp} will be zero, but if ω_r is larger than 1.2 p.u., the T_{sp} will remain at 0.81 p.u. until ω_r reach the shut down speed at 1.33 p.u. which T_{sp} becomes zero, where [45]

$$\bar{T}_0 = \frac{\bar{L}_{rr}}{\omega_0\bar{r}_r} = \frac{\bar{L}_r + \bar{L}_m}{\omega_0\bar{r}_r} \quad \text{Eq. 4-60}$$

$$\bar{X} = \bar{\omega}_s\bar{L}_{ss} = \bar{\omega}_s(\bar{L}_s + \bar{L}_m) \quad \text{Eq. 4-61}$$

$$\bar{X}' = \bar{\omega}_s\left(\bar{L}_{ss} - \frac{\bar{L}_m^2}{\bar{L}_{rr}}\right) \quad \text{Eq. 4-62}$$

4.1.2.3 Torque control model

From Eq. 4-51 and Eq. 4-59, we have found that speed ($p\delta$) and terminal voltage (V_{sq}) can be controlled by adjusting V_{rq} and V_{rd} , respectively. Therefore, the torque control model has a purpose to regulate torque by adjusting V_{rq} automatically. The following equations, Eqs. 4-63 – 4-71, are used as follows:

$$\left. \begin{aligned} \bar{T}_{sp} &= K_{op}\bar{\omega}_r^2 \Big| \bar{\omega}_{cut-in} \leq \bar{\omega}_r < \bar{\omega}_{limit} \\ \bar{T}_{sp} &= 0 \quad \Big| \bar{\omega}_r < \bar{\omega}_{cut-in}, \bar{\omega}_r \geq \bar{\omega}_{shutdown} \\ \bar{T}_{sp} &= \bar{T}_{limit} \quad \Big| \bar{\omega}_r \geq \bar{\omega}_{limit} \end{aligned} \right\} \quad \text{Eq. 4-63}$$

$$\bar{I}_{rq_ref} = \bar{T}_{sp} \frac{\bar{\omega}_s\bar{L}_{ss}}{\bar{L}_m\bar{V}_{sq}} \quad \text{Eq. 4-64}$$

$$pZ_I = \bar{I}_{rq_ref} - \bar{I}_{rq} \quad \text{Eq. 4-65}$$

$$\bar{V}'_{rq} = K_P(\bar{I}_{rq_ref} - \bar{I}_{rq}) + K_I Z_I \quad \text{Eq. 4-66}$$

$$\bar{V}_{rq_c} = s_w\bar{\omega}_s(\bar{L}_{rr}\bar{I}_{rd} - \bar{L}_m\bar{I}_{sd}) \quad \text{Eq. 4-67}$$

I_{rd} can be calculated using Eq. 4-55 and Eq. 4-57 to be

$$\bar{I}_{rd} = \left(\frac{\bar{L}_{ss}}{\bar{L}_m \bar{X}'} \right) \bar{E}' + \left(\frac{1}{\bar{\omega}_s \bar{L}_m} - \frac{\bar{L}_{ss}}{\bar{L}_m \bar{X}'} \right) \bar{V}_{sq} \quad \text{Eq. 4-68}$$

I_{rq} can be calculated using Eq. 4-56 and Eq. 4-58 to be

$$\bar{I}_{rq} \approx \frac{\bar{L}_{ss}}{\bar{L}_m \bar{X}'} \bar{V}_{sd} \quad \text{Eq. 4-69}$$

where

$$\bar{V}_s = \sqrt{\bar{V}_{sd}^2 + \bar{V}_{sq}^2} \quad \text{Eq. 4-70}$$

$$\bar{V}_{rq} = \bar{V}'_{rq} + \bar{V}_{rq_c} \quad \text{Eq. 4-71}$$

Where T_{sp} is an optimum torque (set point torque, p.u.), K_{op} is an aerodynamic performance constant from manufacturer, I_{rq_ref} is q-axis rotor current reference value, V_{rq_c} is compensator value of q-axis rotor voltage, and W_1 and V'_{rq} are any variables.

Replacing I_{rd} in Eq. 4-68 and I_{sd} in Eq. 4-57 into V_{rq_c} in Eq. 4-67, we have:

$$\begin{aligned} \bar{V}_{rq_c} &= s_w \bar{\omega}_s \left[\left(\bar{L}_{rr} - \frac{\bar{L}_m^2}{\bar{L}_{ss}} \right) \bar{I}_{rd} + \frac{\bar{L}_m}{\bar{\omega}_s \bar{L}_{ss}} \bar{V}_{sq} \right] \\ &= s_w \bar{\omega}_s \left[\left(\bar{L}_{rr} - \frac{\bar{L}_m^2}{\bar{L}_{ss}} \right) \left(\frac{\bar{L}_{ss}}{\bar{L}_m \bar{X}'} \right) \bar{E}' + \left(\bar{L}_{rr} - \frac{\bar{L}_m^2}{\bar{L}_{ss}} \right) \left(\frac{1}{\bar{\omega}_s \bar{L}_m} - \frac{\bar{L}_{ss}}{\bar{L}_m \bar{X}'} \right) \bar{V}_{sq} + \frac{\bar{L}_m}{\bar{\omega}_s \bar{L}_{ss}} \bar{V}_{sq} \right] \\ &= s_w \bar{\omega}_s \left[\left(\bar{L}_{rr} - \frac{\bar{L}_m^2}{\bar{L}_{ss}} \right) \left(\frac{\bar{L}_{ss}}{\bar{L}_m \bar{X}'} \right) \bar{E}' + \left(\left(\bar{L}_{rr} - \frac{\bar{L}_m^2}{\bar{L}_{ss}} \right) \left(\frac{1}{\bar{\omega}_s \bar{L}_m} - \frac{\bar{L}_{ss}}{\bar{L}_m \bar{X}'} \right) + \frac{\bar{L}_m}{\bar{\omega}_s \bar{L}_{ss}} \right) \bar{V}_{sq} \right] \end{aligned} \quad \text{Eq. 4-72}$$

$$\text{Or} \quad \bar{V}_{rq_c} = s_w \left(k_{c1} \bar{E}' + k_{c2} \bar{V}_{sq} \right) \quad \text{Eq. 4-73}$$

Where

$$\left. \begin{aligned} k_{c1} &= \bar{\omega}_s \left(\bar{L}_{rr} - \frac{\bar{L}_m^2}{\bar{L}_{ss}} \right) \left(\frac{\bar{L}_{ss}}{\bar{L}_m \bar{X}'} \right) \\ k_{c2} &= \bar{\omega}_s \left(\left(\bar{L}_{rr} - \frac{\bar{L}_m^2}{\bar{L}_{ss}} \right) \left(\frac{1}{\bar{\omega}_s \bar{L}_m} - \frac{\bar{L}_{ss}}{\bar{L}_m \bar{X}'} \right) + \frac{\bar{L}_m}{\bar{\omega}_s \bar{L}_{ss}} \right) \end{aligned} \right\} \quad \text{Eq. 4-74}$$

The V'_{rq} in Eq. 4-66, in order to be used in the torque-speed control (PVrq) scheme, can be represented as follows:

$$\bar{V}'_{rq} = K_p \left(\frac{\bar{\omega}_s \bar{L}_{ss}}{\bar{L}_m \bar{V}_{sq}} \bar{T}_{sp} - \frac{\bar{L}_{ss}}{\bar{L}_m \bar{X}'} \bar{V}_{sd} \right) + K_I Z_I \quad \text{Eq. 4-75}$$

Where T_{sp} is the set-point torque at any generator speed (ω) and can be represented using Eq. 4-60. The function with K_p and K_I are the PI control parameters.

However, for the simulation purposes, instead of using $I'_{rq} - I_{rq}$, we can use $T_{sp} - T_s$ (the latter is per unit torque output) for the simplified control function to avoid the difficult task but still remain the same purpose. In per-unit base, T_s is equal to P_s (per unit electrical power output on stator). Therefore, we can develop a new V'_{rq} as follows

$$\bar{P}_s \approx \frac{\bar{E}'\bar{V}_s}{X'} \sin(\delta') \quad \text{and} \quad \bar{V}_{sd} = \bar{V}_s \sin(\delta'), \text{ Therefore } \frac{\bar{P}_s}{\bar{E}'} = \frac{\bar{V}_{sd}}{X'}$$

Placing the above equation into Eq. 4-75 yields

$$\bar{V}'_{rq} = K_P \left(\frac{\bar{\omega}_s \bar{L}_{ss}}{\bar{L}_m} \frac{\bar{T}_{sp}}{\bar{V}_{sq}} - \frac{L_{ss}}{L_m} \frac{\bar{P}_s}{\bar{E}'} \right) + K_I \int_0^t \left(\frac{\bar{\omega}_s \bar{L}_{ss}}{\bar{L}_m} \frac{\bar{T}_{sp}}{\bar{V}_{sq}} - \frac{L_{ss}}{L_m} \frac{\bar{P}_s}{\bar{E}'} \right) dt \quad \text{Eq. 4-76}$$

From Eq. 4-45 – 4-47, $\bar{P}_s \approx \frac{\bar{P}_e}{(1-s_w)}$ and V'_{rq} becomes

$$\begin{aligned} \bar{V}'_{rq} &= K_P \left(\frac{\bar{\omega}_s \bar{L}_{ss}}{\bar{L}_m \bar{V}_{sq}} \bar{T}_{sp} - \frac{L_{ss}}{L_m \bar{E}'} \frac{\bar{P}_e}{(1-s_w)} \right) + K_I \int_0^t \left(\frac{\bar{\omega}_s \bar{L}_{ss}}{\bar{L}_m} \frac{\bar{T}_{sp}}{\bar{V}_{sq}} - \frac{L_{ss}}{L_m \bar{E}'} \frac{\bar{P}_e}{(1-s_w)} \right) dt \\ &= k_P \left(\bar{T}_{sp} - \bar{P}'_s \right) + k_I \int_0^t \left(\bar{T}_{sp} - \bar{P}'_s \right) dt \end{aligned} \quad \text{Eq. 4-77}$$

Where K_P and K_I are constants. The parameter k_P and k_I are provided to represent the new convenient form of PI control. The \bar{P}'_s is a modified value of P_s .

$$k_P \propto \frac{\bar{L}_{ss}}{\bar{L}_m} \frac{K_P}{\bar{V}_{sq}}, \quad k_I \propto \frac{\bar{L}_{ss}}{\bar{L}_m} \frac{K_I}{\bar{V}_{sq}}, \quad \bar{P}'_s = k_m \frac{\bar{P}_e}{(1-s_w)} \quad \text{and} \quad k_m \propto \frac{L_{ss}}{L_m \bar{E}'} \quad \text{Eq. 4-78}$$

Where k_n is a constant using to adjust \bar{P}'_s to be equal to T_{sp} when reach the maximum value.

$$\bar{V}_{rq} = s_w \left(k_{c1} \bar{E}' + k_{c2} \bar{V}_{sq} \right) + k_P \left(\bar{T}_{sp} - \bar{P}'_s \right) + k_I Z'_I \quad \text{Eq. 4-79}$$

Eq. 4-79 will be used in the state space equations formulation. However, for an energy function formulation, the T_{sp} is assumed to operate under normal conditions for which rotor speed is not beyond the rated value and not less than the lower limit.

4.1.2.4 Voltage control model

The voltage control model has a purpose to regulate voltage by adjusting V_{rd} automatically. The following equations will describe voltage control and are stated as follows:

$$\bar{I}_{rd_gref} = K_{VC} (\bar{V}_{s_ref} - \bar{V}_s) \quad \text{Eq. 4-80}$$

$$\bar{I}_{rd_mref} = \bar{V}_s \left(\frac{1}{\bar{\omega}_s \bar{L}_m} \right) \quad \text{Eq. 4-81}$$

$$\bar{I}_{rd_ref} = \bar{I}_{rd_gref} + \bar{I}_{rd_mref} \quad \text{Eq. 4-82}$$

$$pW_2 = \bar{I}_{rd_ref} - \bar{I}_{rd} \quad \text{Eq. 4-83}$$

$$\bar{V}'_{rd} = K_P (\bar{I}_{rd_ref} - \bar{I}_{rd}) + K_I W_2 \quad \text{Eq. 4-84}$$

$$\bar{V}_{rd_c} = s_w \left[\left(\bar{L}_{rr} - \frac{\bar{L}_m^2}{\bar{L}_{ss}} \right) \bar{I}_{rq} \right] \quad \text{Eq. 4-85}$$

$$\bar{V}_{rd} = \bar{V}'_{rd} + \bar{V}_{rd_c} \quad \text{Eq. 4-86}$$

Where K_{VC} is a constant, I_{rd_ref} is d-axis rotor current reference value, I_{rd_mref} is a magnetizing component of generator, I_{rd_gref} is a terminal voltage control (grid) component, V_{rd_c} is compensator value of d-axis rotor voltage, W_2 and V'_{rd} are any variables.

4.1.2.5 Relationship between internal phase angle of voltage behind transient reactance and phase angle of terminal voltage

To simplify the DFIG model, the V_{sd} and V_{sq} can be represented in the form of trigonometric functions:

$$\bar{V}_{sd} = \bar{V}_s \sin \delta' = \bar{V}_s \sin (\delta - \theta_v) \quad \text{Eq. 4-87}$$

$$\bar{V}_{sq} = \bar{V}_s \cos \delta' = \bar{V}_s \cos (\delta - \theta_v) \quad \text{Eq. 4-88}$$

Where δ is angle of internal voltage or voltage behind transient reactance (E'), θ_v is angle of stator voltage (V_s) and δ' is an internal phase angle (different angle between δ and θ_v).

From the DFIG wind turbine model in PSCAD, the simulation result can reveal the relationship between δ and θ_v as follows.

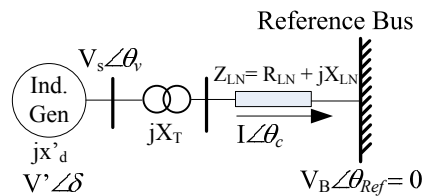


Figure 4.5 Single-line (left) and phasor (right) diagrams of induction generator

Where X_T is transformer reactance and X_{LN} is line reactance, wind speed is sinusoidal signal of magnitude 11 ± 2 m/s with period of about 6 seconds.

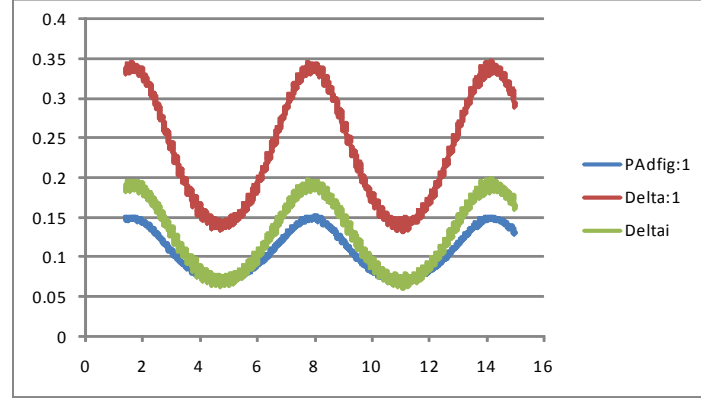


Figure 4.6 Variation of internal phase angle (Deltai, δ') and angle of internal voltage (Delta, δ) and angle of stator voltage (PAdfig, θ_v) when wind power is 1.0 p.u.

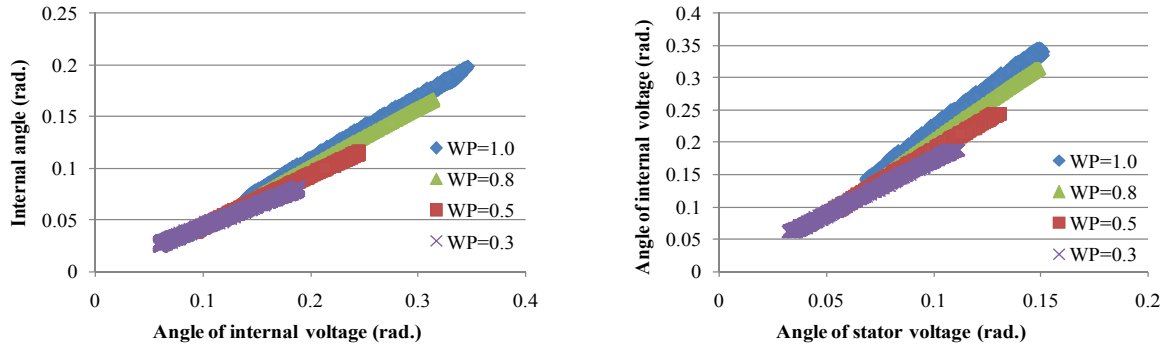


Figure 4.7 The relationship between internal phase angle (Deltai, δ'), angle of internal voltage (Delta, δ), and angle of stator voltage (PAdfig, θ_v) at four wind powers (WP)

The above figure shows the linear relationship between the internal phase angle (Deltai, δ') and angle of internal voltage (Delta, δ). We find that δ' increase with increasing δ and vice versa. The slope (k_a) and offset (c_a) of the linear relationship are computed by varying wind power and the result is shown in next table.

Table 4.2 The slope (k_a) and offset (c_a) of the linear relationship between internal phase angle ($\Delta\theta$, δ') and angle of internal voltage ($\Delta\theta$, δ) of DFIG

Wind Power (p.u.)	$\delta \approx k'_a \theta_v + c'_a$			$\delta' \approx k_a \delta + c_a$		
	k'_a	c'_a	R^2	k_a	c_a	R^2
0.3	1.698	0.002	0.996	0.413	0.0012	0.993
0.5	2.004	-0.014	0.998	0.502	-0.007	0.998
0.8	2.363	-0.034	0.998	0.577	-0.0144	0.999
1.0	2.539	-0.037	0.993	0.608	-0.0146	0.997

From the result of simulation, k_a increases while c_a decreases with increasing wind power. This is due to increasing wind power resulting in rotor speed deviation acceleration, finally causing the angle of voltage behind transient reactance (δ) to increase. The relationship between deviation of δ' , δ and θ are as follows:

$$\delta' = \delta - \theta, \quad \delta' \approx k_a \delta + c_a \quad \text{Eq. 4-89}$$

The above equation becomes

$$p\delta' = k_a p\delta \quad \text{and} \quad p\delta = p\delta' + p\theta_v \quad \text{Eq. 4-90}$$

It has to be mentioned that, in the case of a generator, δ' must not less than zero. If the angle δ is less than zero (such as when import power from the infinite bus), the Eq. 4-89 is invalid and has to be modified to let δ' not be negative. Therefore, the reference angle of DFIG wind turbines for the computation of δ' should be the phase angle of the main bus for which the branch of wind turbines is first connected. As a result, the new equation of δ' should be

$$\delta' \approx k_a |\delta - \theta_{ref}| + c_a \quad \text{Eq. 4-91}$$

Moreover, k_a and c_a can be approximated using a linear relationship with wind power (WP), as follows:

$$k_a = 0.274WP + 0.346 \quad \text{Eq. 4-92}$$

$$c_a = -0.022WP + 0.006 \quad \text{Eq. 4-93}$$

The slopes and offsets are from the simulation result using PSCAD.

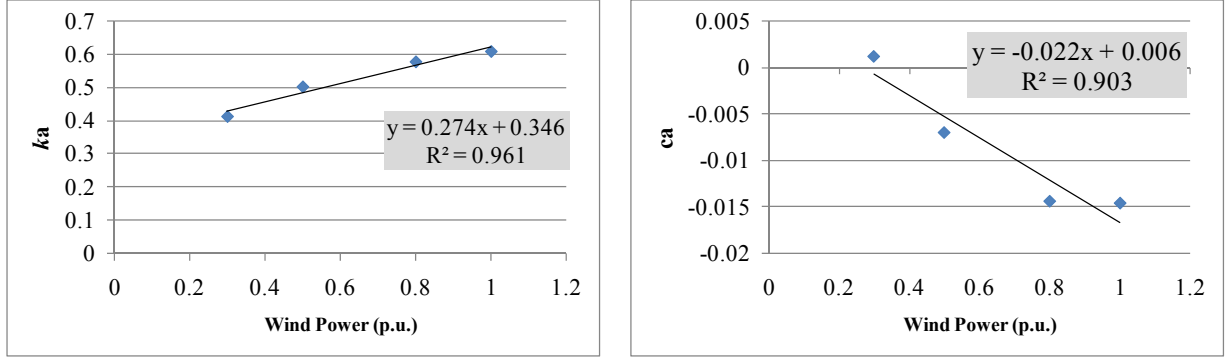


Figure 4.8 Linear relationship between k_a (left) and c_a (right) with DFIG wind power.

4.1.3 Synchronous generator modeling

For electrical models of synchronous generator for power system stability, only swing equations (equation of motion) and power flow equations are applied to represent only the synchronous stability parameters (rotor angle and speed) due to small disturbances and to reduce the complexity of solutions to focus only on the physical meaning as a concept. Therefore, for synchronous generator, the dynamics of voltage and current are neglected.

$$\delta = \omega_r t - \omega_s t + \delta_0 \quad \text{Eq. 4-94}$$

$$\frac{d\delta}{dt} = \omega_r - \omega_s = \Delta\omega_r \quad \text{Eq. 4-95}$$

$$\frac{d^2\delta}{dt^2} = \frac{d\Delta\omega_r}{dt} \quad \text{Eq. 4-96}$$

$$\frac{d\delta}{dt} = \omega_0 \Delta\bar{\omega}_r \quad [52] \quad \text{Eq. 4-97}$$

Where δ is rotor angle (electrical radians) of generator at bus i , ω_r is electrical angular velocity of rotor of generator at bus i and ω_s is synchronous speed at its rated value ($2\pi f_0$, electrical radians / second), and δ_0 is the initial rotor angle of generator at time $t=0$. The over bar represents the per unit value.

In per unit system, mechanical (and electrical) torque is equal to mechanical (and electrical) power [52].

$$\bar{T}_{mi} = \bar{P}_{mi} \text{ and } \bar{T}_{gi} = \bar{P}_{gi} = \psi_{di} \bar{I}_{qi} - \psi_{qi} \bar{I}_{di} \quad i = 1, 2, \dots, m \quad \text{Eq. 4-98}$$

Where \bar{T}_{mi} is mechanical torque and \bar{T}_{gi} is electrical torque in per unit base at bus i , ψ_{di}, ψ_{qi} are flux linkage in d- and q-axis, and $\bar{I}_{di}, \bar{I}_{qi}$ are stator current in d- and q-axis, respectively.

From the above equations, in per unit system, state space equations are [52]

$$\left. \begin{aligned} \dot{\delta}_i &= \omega_0 \Delta \bar{\omega}_{ri} \\ \frac{d\Delta \bar{\omega}_{ri}}{dt} &= -\frac{D_i}{M_i} \Delta \bar{\omega}_{ri} + \frac{1}{M_i} (\bar{P}_{mi} - \bar{P}_{gi}) \end{aligned} \right\} \quad i = 1, 2, \dots, m \quad \text{Eq. 4-99}$$

$$\left. \begin{aligned} \frac{1}{\omega_s} \frac{d\psi_{di}}{dt} &= r_s \bar{I}_{di} + \frac{\omega_{ri}}{\omega_s} \psi_{qi} + V_{di} \\ \frac{1}{\omega_s} \frac{d\psi_{qi}}{dt} &= r_s \bar{I}_{qi} - \frac{\omega_{ri}}{\omega_s} \psi_{di} + V_{qi} \end{aligned} \right\} \quad i = 1, 2, \dots, m \quad \text{Eq. 4-100}$$

Where $\bar{V}_{di}, \bar{V}_{qi}$ are stator voltage in d- and q-axis, respectively.

The simplified voltage equations on the stator circuit (two-axis model) are:

$$\bar{E}'_d + j\bar{E}'_q = (\bar{V}_d + j\bar{V}_q) + \bar{X}'(\bar{I}_q - j\bar{I}_d) \quad \text{Eq. 4-101}$$

$$\left. \begin{aligned} \bar{E}'_d &= \bar{V}_d + \bar{X}'\bar{I}_q \\ \bar{E}'_q &= \bar{V}_q - \bar{X}'\bar{I}_d \end{aligned} \right\} \quad \text{Eq. 4-102}$$

Where \bar{E}'_d, \bar{E}'_q are the voltages behind transient reactance in d- and q-axis, respectively.

This voltage equation can be shown in the figure below.

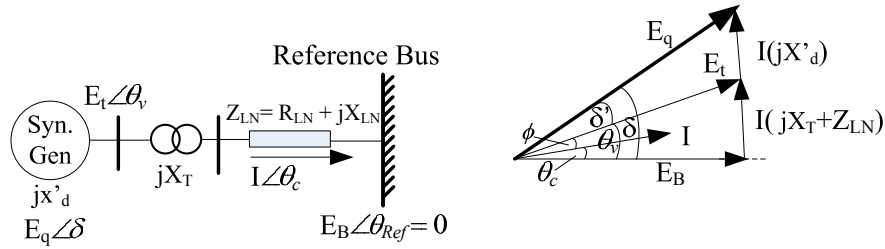


Figure 4.9 Single-line (left) and phasor (right) diagrams of synchronous generator

4.1.4 Dynamic load modeling

For a load model, static constant power load and frequency dependent load model are applied. The frequency dependent load model is used according to the assumption that real power changes nearly linear with frequency [9].

$$\dot{\theta}_k = -\frac{1}{c_i} (\bar{P}_{lk} + \bar{P}_{ek}) \quad \text{Eq. 4-103}$$

Where c_i is frequency coefficient of load bus i and θ_k is phase angle of voltage (V) at bus k .

For a static constant power load, \bar{P}_{lk} and \bar{Q}_{lk} are constant values. The power load P_{lk} can be modeled depending on voltage. For the constant impedance load, $P_{lk} = P_{lk}(V_k)^2$.

For voltage stability analysis, the voltage on the load bus can be formulated as follows: [11]

$$\dot{\bar{V}}_k = \frac{1}{\lambda_k \bar{V}_k} (-\bar{Q}_{lk} + \bar{Q}_{ek}) \quad \text{Eq. 4-104}$$

Where \bar{Q}_{lk} is reactive power load, V_k is voltage on load bus, λ_k is reciprocal of the convergence speed of the voltage magnitude to its equilibrium value.

$$\bar{Q}_{ek} = \bar{V}_k \sum_{j=1}^n \bar{V}_j \bar{B}_{kj} \cos(x_k - x_j) \quad \text{Eq. 4-105}$$

$$\bar{Q}_{lk} = \bar{Q}_0 (\bar{V}_k / \bar{V}_{0k})^{ak} \quad \text{Eq. 4-106}$$

For the constant impedance load, $ak = 2$, for constant power load, $ak = 0$, and for constant current load, $ak = 1$.

4.1.5 Network modeling

The network equations assume a structure-preserving model for which both active and reactive power neglect transferred conductance terms (terms with $G_{ij} = 0$ for simplicity in calculation but not overlook the main purpose). The network equations (per unit) can be represented as follows.

For the active power generation,

$$P_{gi} = \text{Re}[\mathbf{E}_i' \mathbf{I}_i^*] = \text{Re} \left[\mathbf{E}_i' \sum_{j=1}^n \mathbf{Y}_{ij}^* \mathbf{E}_j' \right] \quad \text{Eq. 4-107}$$

$$\text{where} \quad \mathbf{Y}_{ij} = G_{ij} + jB_{ij} = Y_{ij} e^{j\phi_{ij}} = |Y_{ij}| \angle \phi_{ij} \quad \text{Eq. 4-108}$$

Where $\bar{E}_i' e^{j\delta_i} = |\bar{E}_i'| \angle \delta_i$, $G_{ij} = |Y_{ij}| \cos \phi_{ij}$ is conductance, $B_{ij} = |Y_{ij}| \sin \phi_{ij}$ is susceptance (imaginary part of admittance) and ϕ_{ij} is angle of admittance linking between bus i and j .

If placing Eq. 4-108 into Eq 4-107, yields [44]:

$$\begin{aligned}
P_{gi} &= \operatorname{Re} \left[\sum_{j=1}^n \left(|Y_{ij}| \cos \varphi_{ij} - j |Y_{ij}| \sin \varphi_{ij} \right) \left(|\bar{E}_i'| \cos \delta_i + j |\bar{E}_i'| \sin \delta_i \right) \left(|\bar{E}_j'| \cos \delta_j - j |\bar{E}_j'| \sin \delta_j \right) \right] \\
&= \operatorname{Re} \left[\sum_{j=1}^n \left(|Y_{ij}| \cos \varphi_{ij} - j |Y_{ij}| \sin \varphi_{ij} \right) |\bar{E}_i'| |\bar{E}_j'| \left((\cos \delta_i \cos \delta_j + \sin \delta_i \sin \delta_j) + j (\sin \delta_i \cos \delta_j - \cos \delta_i \sin \delta_j) \right) \right] \\
&= \operatorname{Re} \left[\sum_{j=1}^n |\bar{E}_i'| |\bar{E}_j'| |Y_{ij}| \left((\cos \varphi_{ij} - j \sin \varphi_{ij}) (\cos (\delta_i - \delta_j) + j \sin (\delta_i - \delta_j)) \right) \right] \\
&= \sum_{j=1}^n |\bar{E}_i'| |\bar{E}_j'| |Y_{ij}| \left(\cos \varphi_{ij} \cos (\delta_i - \delta_j) + \sin \varphi_{ij} \sin (\delta_i - \delta_j) \right) \\
&= |\bar{E}_i'|^2 G_{ii} + \sum_{\substack{j=1 \\ j \neq i}}^n |\bar{E}_i'| |\bar{E}_j'| |Y_{ij}| \left(\cos \varphi_{ij} \cos (\delta_i - \delta_j) + \sin \varphi_{ij} \sin (\delta_i - \delta_j) \right) \\
&= |\bar{E}_i'|^2 G_{ii} + \sum_{\substack{j=1 \\ j \neq i}}^n |\bar{E}_i'| |\bar{E}_j'| \left(G_{ij} \cos (\delta_i - \delta_j) + B_{ij} \sin (\delta_i - \delta_j) \right) = |\bar{E}_i'|^2 G_{ii} + P_{ei}
\end{aligned}$$

Eq. 4-109

Eq. 4-109 can be used for all generator buses (both synchronous and induction generators). From this equation, assuming zero conductance, it becomes:

$$P_{gi} = P_{ei} = \sum_{\substack{j=1 \\ j \neq i}}^n |\bar{E}_i'| |\bar{E}_j'| B_{ij} \sin (\delta_i - \delta_j) \quad \text{Eq. 4-110}$$

For the load bus:

$$P_{ek} = \operatorname{Re} [\mathbf{V}_k \mathbf{I}_k^*] = \operatorname{Re} \left[\mathbf{V}_k \sum_{j=1}^n \mathbf{Y}_{kj}^* \mathbf{V}_j^* \right] \quad \text{and} \quad Q_{ek} = \operatorname{Im} [\mathbf{V}_k \mathbf{I}_k^*] = \operatorname{Im} \left[\mathbf{V}_k \sum_{j=1}^n \mathbf{Y}_{kj}^* \mathbf{V}_j^* \right] \quad \text{Eq. 4-111}$$

$$\left. \begin{aligned}
P_{ek} &= \operatorname{Re} \left[\sum_{j=1}^n |\mathbf{V}_k| |\mathbf{V}_j| |Y_{kj}| \left(\cos \varphi_{kj} - j \sin \varphi_{kj} \right) \left(\cos (\theta_k - \theta_j) + j \sin (\theta_k - \theta_j) \right) \right] \\
Q_{ek} &= \operatorname{Im} \left[\sum_{j=1}^n |\mathbf{V}_k| |\mathbf{V}_j| |Y_{kj}| \left(\cos \varphi_{kj} - j \sin \varphi_{kj} \right) \left(\cos (\theta_k - \theta_j) + j \sin (\theta_k - \theta_j) \right) \right]
\end{aligned} \right\} \quad \text{Eq. 4-112}$$

$$\left. \begin{aligned}
P_{ek} &= \sum_{j=1}^n |\mathbf{V}_k| |\mathbf{V}_j| \left(G_{kj} \cos (\theta_k - \theta_j) + B_{kj} \sin (\theta_k - \theta_j) \right) \\
Q_{ek} &= \sum_{j=1}^n |\mathbf{V}_k| |\mathbf{V}_j| \left(G_{kj} \sin (\theta_k - \theta_j) - B_{kj} \cos (\theta_k - \theta_j) \right)
\end{aligned} \right\} \quad \text{Eq. 4-113}$$

when assuming zero conductance, Eq. 4-113 becomes:

$$\left. \begin{aligned}
P_{ek} &= \sum_{j=1}^n |\mathbf{V}_k| |\mathbf{V}_j| B_{kj} \sin (\theta_k - \theta_j) \\
Q_{ek} &= - \sum_{j=1}^n |\mathbf{V}_k| |\mathbf{V}_j| B_{kj} \cos (\theta_k - \theta_j)
\end{aligned} \right\} \quad \text{Eq. 4-114}$$

4.1.6 Dynamic power system equations

The power system equations in this section are the structure-preserving model for multi-machine infinite bus power systems. Given $i = 1, \dots, (m-p)$ and $w = (m-p)+1, \dots, m$ and $k = m+1, \dots, n$. and approximate ω_s by using ω_0 . These power system equations are applied from the previous section and can be represented as follows:

4.1.6.1 For SCIG, included in the power system

$$\frac{d\delta_i}{dt} = \omega_0 \Delta \bar{\omega}_{ri} \quad \text{Eq. 4-115}$$

$$\frac{d\Delta \bar{\omega}_{ri}}{dt} = -\frac{D_i}{M_i} \Delta \bar{\omega}_{ri} + \frac{1}{M_i} (\bar{P}_{mi} - \bar{P}_{gi}) \quad \text{Eq. 4-116}$$

$$\frac{d\delta_w}{dt} = -\frac{(\bar{X}_w - \bar{X}'_w) \bar{I}_{qw}}{\bar{T}_0 \bar{E}'_w} + \omega_0 \Delta \bar{\omega}_{rw} \quad \text{Eq. 4-117}$$

$$\frac{d\Delta \bar{\omega}_{rw}}{dt} = \frac{1}{M_w} (\bar{P}_{mw} - \bar{P}_{gw}) \quad \text{Eq. 4-118}$$

$$\frac{d\bar{E}'_w}{dt} = -\frac{1}{\bar{T}_0} [\bar{E}'_w + (\bar{X}_w - \bar{X}'_w) \bar{I}_{dw}] \quad \text{Eq. 4-119}$$

$$\frac{d\theta_k}{dt} = -\frac{1}{c_k} (\bar{P}_{lk} + \bar{P}_{ek}) \quad \text{Eq. 4-120}$$

$$\bar{E}'_w = \bar{V}_w \cos(k_a \delta_w + c_a) + \bar{X}'_w \bar{I}_{dw} \quad \text{Eq. 4-121}$$

$$\bar{V}_w \sin(k_a \delta_w + c_a) = \bar{X}'_w \bar{I}_{qw} \quad \text{Eq. 4-122}$$

$$P_{gi} = \sum_{\substack{j=1 \\ j \neq i}}^n |\bar{E}'_i| |\bar{E}'_j| B_{ij} \sin(\delta_i - \delta_j) \quad \text{Eq. 4-123}$$

$$P_{gw} = \sum_{\substack{j=1 \\ j \neq w}}^n |\bar{E}'_w| |\bar{E}'_j| B_{wj} \sin(\delta_w - \delta_j) \quad \text{Eq. 4-124}$$

$$P_{ek} = \sum_{\substack{j=1 \\ j \neq k}}^n |V_k| |V_j| B_{kj} \sin(\theta_k - \theta_j) \quad \text{Eq. 4-125}$$

For reasons of simplicity and convenience in mathematical modeling, several assumptions can be made as follows:

A1) In the case of the generator bus, replace E_i and E_w by V_i and V_w , respectively. The transient reactance are included into B_{ij} and B_{wj} . Therefore, Eq. 4-123 and Eq. 4-124 become:

$$P_{gi} = \sum_{\substack{j=1 \\ j \neq i}}^n V_i V_j B_{ij} \sin(\delta_i - \delta_j) \quad \text{Eq. 4-126}$$

$$P_{gw} = \sum_{\substack{j=1 \\ j \neq w}}^n V_w V_j B_{wj} \sin(\delta_w - \delta_j) \quad \text{Eq. 4-127}$$

A.2) For the load bus, just replace angles θ_k and θ_j by δ_k and δ_j , respectively.

A.3) Generator bus no.1 can be set as a reference bus and new variables (x and y) (relative on reference bus) can be stated as follows

$$x_i = \delta_i - \delta_1, x_w = \delta_w - \delta_1, x_k = \delta_k - \delta_1, y_i = \Delta \bar{\omega}_{ri}, y_w = \Delta \bar{\omega}_{rw} \quad \text{Eq. 4-128}$$

A.4) The reference angle is assumed and therefore, the deviation of Eq. 4-128 is

$$\dot{x}_i = \dot{\delta}_i - \dot{\delta}_1 = \omega_0 (y_i - y_1), \dot{x}_w = \dot{\delta}_w - \dot{\delta}_1 = \dot{\delta}_w - \omega_0 y_1, \dot{x}_k = \dot{\delta}_k - \omega_0 y_1, \dot{y}_i = \Delta \dot{\bar{\omega}}_{ri}, \dot{y}_w = \Delta \dot{\bar{\omega}}_{rw} \quad \text{Eq. 4-129}$$

A.5) Furthermore, the deviation of magnitude of internal voltage in Eq. 4-119 is assumed to be very small and can be neglected. Furthermore, both internal voltage (E') and terminal voltage (V) are assumed to be constants of around one. Therefore, from Eq. 4-117 to Eq. 4-122, the simplified results are:

$$\frac{d\delta_w}{dt} = \omega_0 \Delta \bar{\omega}_{rw} - \frac{(\bar{X}_w - \bar{X}'_w)}{\bar{T}_0 \bar{X}'_w \bar{E}'_w} V_w \sin(k_a \delta_w + c_a) \quad \text{Eq. 4-130}$$

the results are:

$$\dot{x}_i = \omega_0 (y_i - y_1) \quad \text{Eq. 4-131}$$

$$\dot{y}_i = -\frac{D_i}{M_i} y_i + \frac{1}{M_i} (\bar{P}_{mi} - \bar{P}_{ei}) \quad \text{Eq. 4-132}$$

$$\dot{x}_w = \omega_0 (y_w - y_1) - k_b V_w \sin(k_a x_w + c_b) \quad \text{Eq. 4-133}$$

$$\dot{y}_w = \frac{1}{M} (\bar{P}_{mw} - \bar{P}_{ew}) \quad \text{Eq. 4-134}$$

$$\dot{x}_k = -\frac{1}{c_k} (\bar{P}_{lk} + \bar{P}_{ek}) - \omega_0 y_1 \quad \text{Eq. 4-135}$$

$$P_{ei} = V_i \sum_{j=1, j \neq i}^n V_j B_{ij} \sin(x_i - x_j) \quad i = 1, 2, \dots, m-p \quad \text{Eq. 4-136}$$

$$P_{ew} = V_w \sum_{j=1, j \neq w}^n V_j B_{wj} \sin(x_w - x_j) \quad w = (m-p)+1, (m-p)+2, \dots, m \quad \text{Eq. 4-137}$$

$$P_{ek} = V_k \sum_{j=1, j \neq k}^n V_j B_{kj} \sin(x_k - x_j) \quad k = m+1, m+2, \dots, n \quad \text{Eq. 4-138}$$

Where $i = 1, \dots, (m-p)$ and $w = (m-p)+1, \dots, m$ and $k = m+1, \dots, n$. $c_b = k_a \delta_1 + c_a$, k_b is normally positive with $k_b = (\bar{X}_w - \bar{X}'_w) / (\bar{T}_0 \bar{X}'_w \bar{E}'_w)$

In many cases, the mechanical power of an induction generator wind turbine can be approximated using the value of wind speed and power coefficient from the manufacturer as follows:

$$\bar{P}_{mw} \approx \frac{1}{2S_{base}} \rho c_p A V_{ws}^3 \quad \text{Eq. 4-139}$$

The ρ is air density (kg/m^3), A is the swept area of the turbine, c_p is power coefficient (provided by manufacturer), and V_{ws} is wind speed at hub height.

4.1.6.2 For DFIG, included in the power system

From the assumptions of A.1 to A.5, the power system equations incorporating DFIG become:

$$M_i p y_i = (\bar{P}_{mi} - \bar{P}_{ei}) - D_i y_i \quad \text{Eq. 4-140}$$

$$p x_i = \omega_0 (y_i - y_{coi}) \quad \text{Eq. 4-141}$$

$$M_w p y_w = (\bar{P}_{mw} - \bar{P}_{ew}) \quad \text{Eq. 4-142}$$

$$p x_w = \omega_0 (y_w - y_{coi}) - k_b \bar{V}_{sw} \sin(k_a |x_w - x_{ref}| + c_a) + \omega_0 k_d \bar{V}_{rq} \quad \text{Eq. 4-143}$$

$$p Z'_I = \bar{T}_{sp} - \bar{P}'_{sw} \quad \text{Eq. 4-144}$$

$$c_k p x_k = -(\bar{P}_{lk} + \bar{P}_{ek}) - c_k \omega_0 y_{coi} \quad \text{Eq. 4-145}$$

$$\bar{V}_{rq} = -y_w \left(k_{c1} \bar{V}_w + k_{c2} \bar{V}_{sw} \cos(k_a |x_w - \theta_{ref}| + c_a) \right) + k_p (\bar{T}_{sp} - \bar{P}'_{sw}) + k_I Z'_I \quad \text{Eq. 4-146}$$

$$\bar{P}'_{sw} = k_m \bar{P}_{ew} / (1 + y_w) \quad \text{Eq. 4-147}$$

$$\bar{T}_{sp} = k_{op} (1 + y_w)^2 \quad \text{Eq. 4-148}$$

$$\bar{P}_{ew} = \bar{V}_w \sum_{j=1, j \neq w}^n \bar{V}_j \bar{B}_{wj} \sin(x_w - x_j) \quad \text{Eq. 4-149}$$

$$\bar{P}_{ei} = \bar{V}_i \sum_{j=1, j \neq i}^n \bar{V}_j \bar{B}_{ij} \sin(x_i - x_j) \quad \text{Eq. 4-150}$$

$$\bar{P}_{ek} = \bar{V}_k \sum_{j=1, j \neq k}^n \bar{V}_j \bar{B}_{kj} \sin(x_k - x_j) \quad \text{Eq. 4-151}$$

$$k_d = \bar{L}_m / (\bar{L}_{rr} \bar{E}') \quad \text{and} \quad k_b = (\bar{X}_w - \bar{X}'_w) / (\bar{T}_0 \bar{X}'_w \bar{E}'_w) \quad \text{Eq. 4-152}$$

$$\left. \begin{aligned} k_{c1} &= \bar{\omega}_0 \left(\bar{L}_{rr} - \frac{\bar{L}_m^2}{\bar{L}_{ss}} \right) \left(\frac{\bar{L}_{ss}}{\bar{L}_m \bar{X}'} \right) \\ k_{c2} &= \bar{\omega}_0 \left(\left(\bar{L}_{rr} - \frac{\bar{L}_m^2}{\bar{L}_{ss}} \right) \left(\frac{1}{\bar{\omega}_s \bar{L}_m} - \frac{\bar{L}_{ss}}{\bar{L}_m \bar{X}'} \right) + \frac{\bar{L}_m}{\bar{\omega}_s \bar{L}_{ss}} \right) \end{aligned} \right\} \quad \text{Eq. 4-153}$$

$$k_a \approx 0.274 \bar{P}_{mw} + 0.346 \quad \text{and} \quad c_a \approx -0.022 \bar{P}_{mw} + 0.006 \quad \text{Eq. 4-154}$$

Where n is the number of network buses, w is wind power bus, k is load bus, V is terminal voltage, B_{ij} is susceptance component between bus i and j , P_{lk} is a constant power load, P_{ew} , and P_{ek} are electrical power at wind power bus and load bus, respectively. c_k is frequency dependent coefficient of load.

4.1.7 Dynamic power system equations for voltage stability analysis

For the power system incorporating DFIG wind turbines, the dynamic power system equations for voltage stability analysis are represented as follows:

$$M_i p y_i = (\bar{P}_{mi} - \bar{P}_{ei}) - D_i y_i \quad \text{Eq. 4-155}$$

$$p x_i = \omega_0 (y_i - y_{coi}) \quad \text{Eq. 4-156}$$

$$M_w p y_w = (\bar{P}_{mw} - \bar{P}_{ew}) \quad \text{Eq. 4-157}$$

$$p x_w = \omega_0 (y_w - y_{coi}) - k_b \bar{V}_{sw} \sin(k_a |x_w - x_{ref}| + c_a) + \omega_0 k_d \bar{V}_{rq} \quad \text{Eq. 4-158}$$

$$p Z'_I = \bar{T}_{sp} - \bar{P}'_{sw} \quad \text{Eq. 4-159}$$

$$c_k p x_k = -(\bar{P}_{lk} + \bar{P}_{ek}) - c_k \omega_0 y_{coi} \quad \text{Eq. 4-160}$$

$$p \bar{V}_k = (\lambda_k \bar{V}_k)^{-1} (-\bar{Q}_{lk} + \bar{Q}_{ek}) \quad \text{Eq. 4-161}$$

$$\bar{V}_{rq} = -y_w \left(k_{c1} \bar{V}_w + k_{c2} \bar{V}_{sw} \cos(k_a |x_w - \theta_{ref}| + c_a) \right) + k_p (\bar{T}_{sp} - \bar{P}'_{sw}) + k_I Z'_I \quad \text{Eq. 4-162}$$

$$\bar{P}'_{sw} = k_m \bar{P}_{ew} / (1 + y_w) \quad \text{Eq. 4-163}$$

$$\bar{T}_{sp} = k_{op} (1 + y_w)^2 \quad \text{Eq. 4-164}$$

$$\bar{P}_{ew} = \bar{V}_w \sum_{j=1, j \neq w}^n \bar{V}_j \bar{B}_{wj} \sin(x_w - x_j) \quad \text{Eq. 4-165}$$

$$\bar{P}_{ei} = \bar{V}_i \sum_{j=1, j \neq i}^n \bar{V}_j \bar{B}_{ij} \sin(x_i - x_j) \quad \text{Eq. 4-166}$$

$$\bar{P}_{ek} = \bar{V}_k \sum_{j=1, j \neq k}^n \bar{V}_j \bar{B}_{kj} \sin(x_k - x_j) \quad \text{Eq. 4-167}$$

$$\bar{Q}_{ek} = \bar{V}_k \sum_{j=1}^n \bar{V}_j \bar{B}_{kj} \cos(x_k - x_j) \quad \text{Eq. 4-168}$$

$$\bar{Q}_{lk} = \bar{Q}_0 (\bar{V}_k / \bar{V}_{0k})^{ak} \quad \text{Eq. 4-169}$$

$$k_d = \bar{L}_m / (\bar{L}_{rr} \bar{E}') \quad \text{and} \quad k_b = (\bar{X}_w - \bar{X}_w') / (\bar{T}_0 \bar{X}_w' \bar{E}_w') \quad \text{Eq. 4-170}$$

$$\left. \begin{aligned} k_{c1} &= \bar{\omega}_0 \left(\bar{L}_{rr} - \frac{\bar{L}_m^2}{\bar{L}_{ss}} \right) \left(\frac{\bar{L}_{ss}}{\bar{L}_m \bar{X}'} \right) \\ k_{c2} &= \bar{\omega}_0 \left(\left(\bar{L}_{rr} - \frac{\bar{L}_m^2}{\bar{L}_{ss}} \right) \left(\frac{1}{\bar{\omega}_s \bar{L}_m} - \frac{\bar{L}_{ss}}{\bar{L}_m \bar{X}'} \right) + \frac{\bar{L}_m}{\bar{\omega}_s \bar{L}_{ss}} \right) \end{aligned} \right\} \quad \text{Eq. 4-171}$$

$$k_a \approx 0.274 \bar{P}_{mw} + 0.346 \quad \text{and} \quad c_a \approx -0.022 \bar{P}_{mw} + 0.006 \quad \text{Eq. 4-172}$$

Where n is the number of network buses, w is wind power bus, k is load bus, V is terminal voltage, B_{ij} is susceptance component between bus i and j , P_{lk} is a constant power load, P_{ew} , and P_{ek} are electrical power at wind power bus and load bus, respectively. c_k is the frequency dependent coefficient of load. Q_0 , V_{0k} , and ak are constant reactive load, initial voltage and exponential component representing characteristic of load, respectively.

4.2 Power System Simulation

4.2.1 Power system simulation using PSCAD

In this part, an overview of PSCAD/EMTDC is given first. After that, the six main components of power system models in PSCAD/EMTDC are explained. These components are generator model, power line model, transformer model, load model, excitation system model, and turbine and governor model.

4.2.1.1 Overview of PSCAD/EMTDC

The PSCAD is the graphical user interface linking to the EMTDC (Electromagnetic Transients including DC) solution engine. The PSCAD was first known in 1988 and was first commercialized in 1994. The EMTDC was first written in 1975 to solve differential equations in a time domain based on fixed time steps.

EMTDC, which differs from many other programs, can serve all frequencies not only fundamental frequency. This tool can represents electrical circuits using steady-state equations, which represent machine mechanical dynamics using actual differential equation solutions. Its network solution is solved using LU decomposition method, which can

reduce the size of the sparse conductance matrix. Moreover, user-defined EMTDC code can be written in Fortran, C and MATLAB languages.

4.2.1.2 Generator model

PSCAD represents four rotating machine types: a Synchronous Machine, a Squirrel Cage Induction Machine, a Wound-Rotor Induction Machine and a DC Machine. This report describes only synchronous and squirrel cage induction machines because they are major parts concerning the wind power system.

1) Synchronous generator

There are two types of synchronous generator (SG), *round rotor (high speed)* represents only one damper winding and *salient pole rotor (low speed)* represents second damper winding. Mathematical models of SG are represented in the previous section.

For the simulation of rotating machines, the initialization conditions must be specified. Machine initialization in PSCAD consists of

- Initialisation for Load Flow (start with generator mode when de-energized condition is investigated),
- Starting as a Voltage Source (to shorten starting time into a steady-state condition and then can switch to a generator mode),
- Locked Rotor Operation (Rotor dynamics is disabled when applied to enhance start-up speed disregarding mechanical dynamics after switching from voltage source modes), and
- Free Running Rotor (The mechanical dynamics from torque and windage, and friction losses are considered in this case).

The following topics describe the parameters and configuration options of SG, which consists of six main parts, B1 – B6, as shown in the next figure.

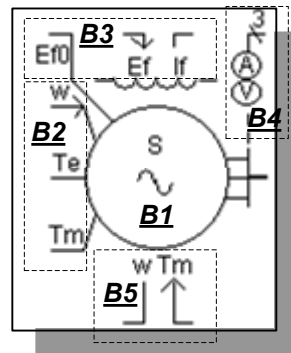


Figure 4.10 Block of synchronous generator model in PSCAD

B1 : Rotating machine parameters

- Basic data (for example rated rms V_{LN} , rated rms I_L , Base angular frequency, inertia constant, number of coherent machine)
- No. of Q-axis damper winding (one is for round rotor, two for salient pole rotor)
- Data entry format (Generator data from manufacturer provided with per unit d- and q- axis reactance and time constants, equivalent circuit data base on d- and q- axis synchronous machine equivalent circuits)
- Initial conditions (when starting as generator and as voltage source)
- Output variable name (active and reactive power, neutral voltage and current to ground, load angle, rotor mechanical angle, internal phase A angle, steady electrical torque)

B2 : Input/Output multi-mass shaft model interface

- Rotor angular speed (ω) signal from multi-mass shaft model can be a direct input with positive value
- Electrical torque (T_e) and mechanical torque (T_m) output are used for the multi-mass shaft model

B3 : Input/Output excitation system parameters

- The initial output field voltage (E_{f0})
- The input field voltage (E_f) from excitation system under operating conditions
- The output field current (I_f) to excitation system under operating conditions

B4 : Terminal voltage and current feedback parameters

- The three phase terminal voltage and current signal can be supplied to the exciter model to set the terminal constraints

B5 : Input/Output turbine and governor parameters

- Rotor angular speed (ω) signal from turbine and governor model can be as direct inputs with positive values
- Mechanical torque (T_m) outputs are used for the turbine and governor model

2) Squirrel cage induction generator (SCIG)

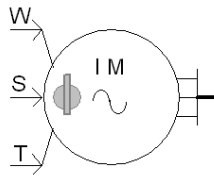


Figure 4.11 Block of SCIG model in PSCAD

The input of squirrel cage induction generator can be either from rotor angular speed (W , rad/s) signal or from mechanical torque (T , kW-rad/s) signal. The switch signal (S , speed or torque control) is used to switch between torque and speed input. Its output is single or three phase wires with electrical parameters. Configuration data are similar to rotating machine parameters of synchronous generators.

Configuration data

- Rated RMS Phase Voltage [kV] (from design)
- Rated RMS Phase Current [kA] (from design)
- Base Angular Frequency [rad/s] (from design)
- Data Generation/ Entry (as follows)
- Multi-mass Interface (when sub-synchronous oscillation is considered)
- The saturation condition can also be modeled

Data Generation/Entry

Data generation or data entry is the method of specifying the electrical components of the generator. There are 3 methods as follows:

- Typical : Specify horse power of the generator in case no other information is available.
- Explicit : Specify winding resistances, reactance, polar moment of inertia ($J=2H$), and mechanical damping in the case that information is available (recommended).
- EMTP type 40 : Specify characteristics of Torque-Slip Curves from the manufacturer, such as power factor and efficiency at rated load, slip at full load, starting current, starting torque, maximum torque, number of pole, polar moment of inertia ($J=2H$), and mechanical damping.

Internal Output Variables

When electrical outputs data are required, the names of the following variables are listed.

Real Power (+in) (p.u.)	Reactive power (+in) (p.u.)	output rotor angle (rad)
Output Mechanical Torque (p.u.)	output speed (p.u.)	Electrical Torque (p.u.)
Torque Angle (rad)	Slip Angle (rad)	

Explicit Information

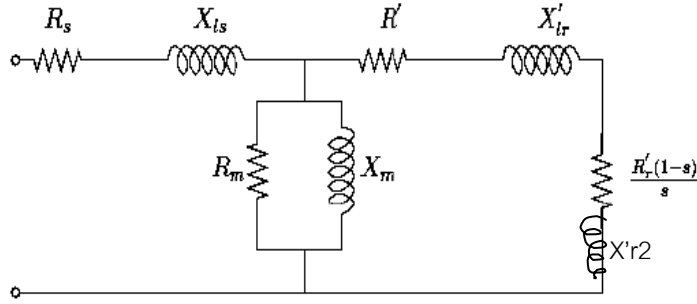


Figure 4.12 Equivalent circuit of SCIG in PSCAD

- 1) Stator Resistance (R_s)
- 2) First Cage Resistance ($R'r$)
- 3) Second Cage Resistance ($R'r(1-s)/s$)
- 4) Stator Unsaturated Leakage Reactance (X_{ls})
- 5) Unsaturated Magnetizing Reactance (X_m)
- 6) Rotor Unsaturated Mutual Reactance (X'_{lr})
- 7) Second Cage Unsaturated Reactance (X'_{r2})

EMTP type 40 Information (Example)

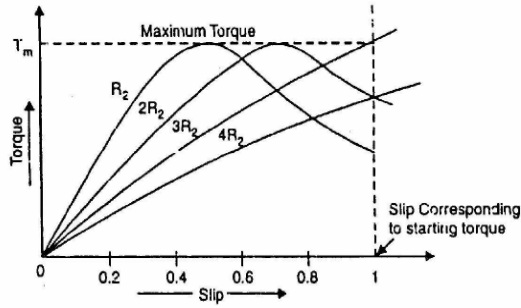


Figure 4.13 Torque-Slip Characteristics

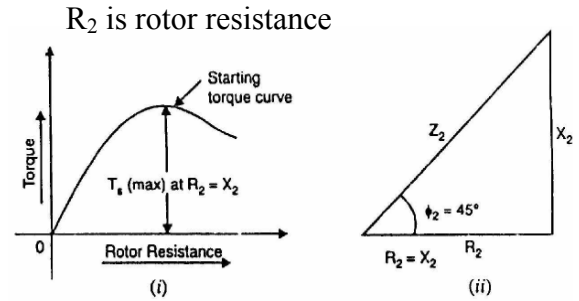


Figure 4.14 Variation of starting torque with rotor resistance

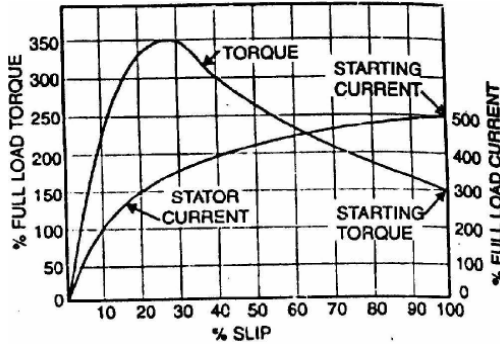


Figure 4.15 Variation of torque and stator current with slip

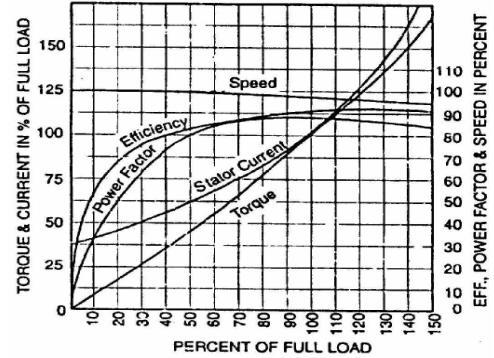


Figure 4.16 Performance curves of 3-phase squirrel cage induction generator

4.2.1.3 Transmission line model

There are two types of power line models described: the PI section model and distributed transmission line model. The underground transmission line model and mutually electrical wires are also provided, but not used in this thesis, therefore, unexplained.

1) PI section model

There are two types of PI section line model, the nominal PI section and the coupled PI section components. Nominal PI section model represents voltage measured to local ground. The coupled PI section model represents voltage, which always measured to earth (true ground).



Figure 4.17 Schematics of nominal PI section (left) and coupled PI section (right) models

2) Distributed transmission line model

The three models of distributed transmission lines are provided in PSCAD: the Bergeron model, Frequency Dependent (Mode) model, and Frequency Dependent (Phase) model, depending on increasing accuracies.

The Bergeron model represent the transmission line with lumped R, and distributed L and C components. It is useful when requiring the correct steady state impedance/admittance at fundamental frequency. This model has computational time faster than the other two.

The Frequency Dependent (Mode) model is useful for studies of behaviors involving transients or harmonics. It uses curve fitting to represent the frequency response of the line. It works very well with the transposed lines but should not be used for untransposed lines or when the multiple towers are modeled in the same right of way.

The Frequency Dependent (Phase) model represents the full range of the frequency responses of the lines. It is useful for study behaviors involving transients or harmonics. It is the most advanced time domain transmission line model and is used for most studies.

Five steps of distributed transmission line modeling are described.

Step#1: Enter a line name and numbers of conductors by double-clicking on the Tline (1) interface components. This name must be unique for this circuit.

Step#2: Double-click on the TLine (T) component and enter the same name as in STEP 1. Then enter the line length, steady state frequency and number of conductors.

Step#3: Open the TLine configuration by double-click on "Edit Configuration" or "Edit...." and then copy desired line constants components onto the sub-page.

Step#4: Select only one line model (Bergeron model, Frequency Dependent (Mode) model, Frequency Dependent (Phase) model) and give conditions.

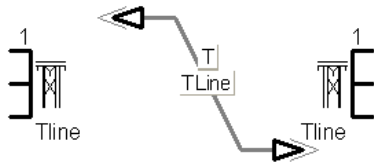


Figure 4.18 Tline and TLine components

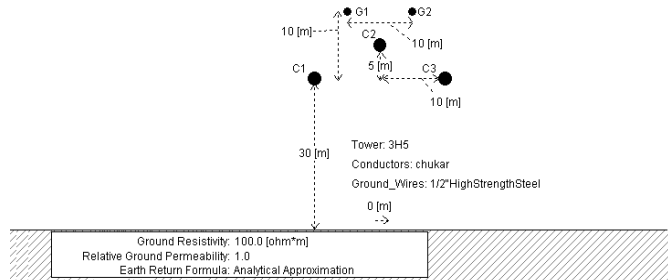


Figure 4.19 The conductor geometry method

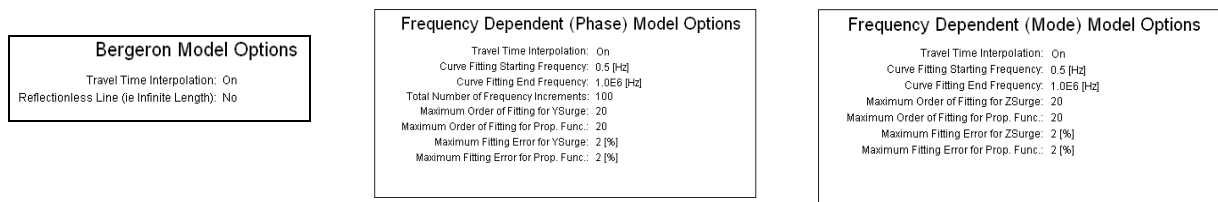
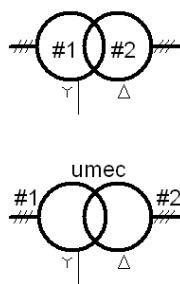


Figure 4.20 Bergeron, Frequency Dependent (Mode and Phase) models and options

Step#5: Select the data entry method. The manual entry is used only for Bergeron model by providing R , X_L , and X_C . The conductor geometry with ground and tower components methods is suitable for Frequency Dependent (Mode) model and Frequency Dependent (Phase) model.

4.2.1.4 Transformer model



The transformer models in PSCAD are 3-phase 2- winding, 3-phase 3-winding, and 3-phase 4-winding transformer models. For these models, the two different core geometries are provided, which are the Classical transformer model and the Unified Magnetic Equivalent Circuit (UMEC) transformer model. The classical model normally considers the magnetic coupling between winding of the same phase while the UMEC transformer model additionally considers the magnetic coupling between winding of different phase.

The transformer core structures which can be modeled using UMEC are, for example, single phase 4-winding, 3-phase 3-limb unit, and 3-phase 5-limb unit.

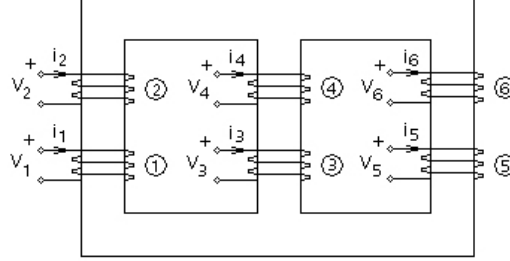
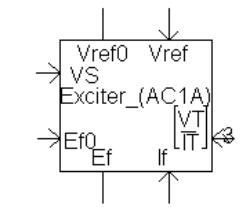


Figure 4.21 Example of 3-phase 3-limb transformer schematic



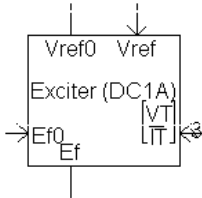
AC exciter models

Input:

V_{ref} is reference voltage
 E_{f0} is initial field voltage
 I_f is field current
 $[V_T/I_T]$ is 3-element of terminal voltage and current

Output:

V_{ref0} is initial reference voltage
 E_f is field voltage



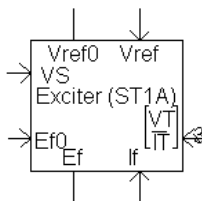
DC exciter models

Input:

V_{ref} is reference voltage
 E_{f0} is initial field voltage
 $[V_T/I_T]$ is 3-element of terminal

Output:

V_{ref0} is initial reference voltage
 E_f is field voltage



Static exciter models

Input:

V_{ref} is reference voltage
 E_{f0} is initial field voltage
 I_f is field current
 $[V_T/I_T]$ is 3-element of terminal voltage and current

Output:

V_{ref0} is initial reference voltage
 E_f is field voltage

Figure 4.22 AC exciters (top), DC exciters (middle), and Static exciters (bottom) in PSCAD.

4.2.1.5 Excitation system model

PSCAD provides 8 standard AC exciter models, 3 standard DC exciter models, and 5 standard Static exciter models. AC exciter models use an alternator, and either stationary or rotating rectifiers to produce the direct current needed for the synchronous machine field. DC exciter models use a direct current generator with a commutator as the source of excitation system power. Static exciter models have no rotating parts, but excitation power is supplied through transformers or auxiliary generator windings and rectifiers.

4.2.1.6 Turbine and Governor model

PSCAD provides 4 hydro turbine models, 4 hydro governor models, 2 steam (thermal) turbine models, and 5 steam (thermal) governor models as shown in Figure 4.23.

Hydro Turbines	Description
TUR1	Non-Elastic Water Column without Surge Tank
TUR2	Elastic Water Column without Surge Tank
TUR3	Non-Elastic Water Column with Surge Tank
TUR4	Elastic Water Column with Surge Tank

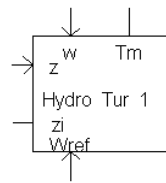
Thermal Turbines	Description
TUR1	Generic Turbine Model
TUR2	Generic Turbine Model Including IV Effect

Hydro Governors	Description
GOV1	Mechanical-Hydraulic Controls
GOV2	PID Controls including Pilot and Servo Dynamics
GOV3	Enhanced Controls for Load Rejection Studies
HGOV18	V2 Compatible Hydro Governor (HGOV18)

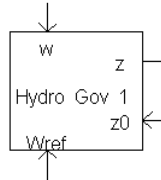
Thermal Governors	Description
GOV1	Approximate Mechanical-Hydraulic Controls
GOV2	Mechanical-Hydraulic Controls (GE)
GOV3	Electro-Hydraulic Controls (GE)
GOV4	DEH Controls (Westinghouse)
GOV5	NEI Parsons Controls

Figure 4.23 Hydro and steam turbine and governor model descriptions in PSCAD

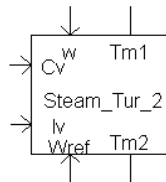
These models have inputs and outputs as follows.



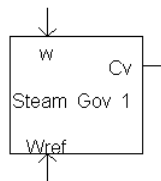
hydro turbine



hydro governor



steam turbine



steam governor

Input:

w is per-unit speed

W_{ref} is per-unit speed reference

z is gate position

Output:

T_m is mechanical torque (which is input to the Synchronous Machine)

z_i is initial gate position (which is input to the Hydro Governor for initialization)

Input:

w is per-unit speed

W_{ref} is per-unit speed reference

z_0 is gate position during initialization

Output:

z is gate position

Input:

C_v is per-unit control valve position

I_v is per-unit intercept valve position from the corresponding Thermal (Steam) Governor.

Output:

T_{m1} and T_{m2} are output from the HP and LP turbines respectively

Input:

w is per-unit speed

W_{ref} is per-unit speed reference

Output:

C_v is per-unit control valve position

Figure 4.24 Hydro turbine (top), hydro governor (upper middle), steam turbine (lower middle), steam governor (bottom) models with input and output in PSCAD

4.2.1.7 Load model

However, PSCAD represents only fixed P and Q loads and passive R, X_L , and X_C load as presented in the figure below.

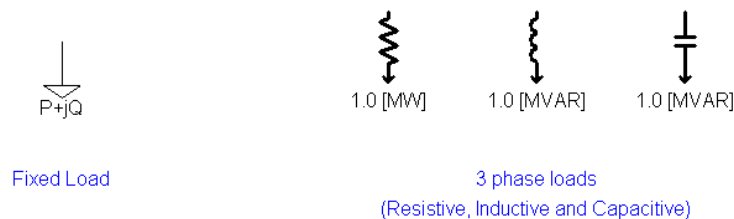


Figure 4.25 Fixed P and Q load and passive R, X_L , and X_C load model

4.2.1.8 Wind Source, Turbine and Governor model

- Wind source model

The wind source model generates wind speed with 4 different signal patterns, mean wind speed, gust wind, ramp wind, and noise wind. There are four parameters to define gust wind and ramp wind. These are the peak or maximum velocity, gust or ramp period, start time, and number of gust or ramp. The gust and ramp are described in Section 2.2.

For noise wind speed (V_n), seven parameters are defined as [46]:

Number of noise component (N): this number is a probability density function counter limit.

Noise amplitude controlling parameter ($\Delta\omega$): controlled values in range 0.5 – 2.0 .

Surface drag coefficient (c_d): the ratio between drag force and incident force (or kinetic energy) of fluid on the surface, in this case $c_d = 0.004$.

Turbulence scale (L): the length scale that the turbulence is important, and $L = 2000$ feet.

Random seed number (k): an initial number 1 – 99 using for generate N random number (ϕ) of the interval 0 to 2π .

Time interval for random generation: a new set of N random number will be generated after the end of this time .

Mean wind speed at reference height (u): this number is previously defined with internal or external conditions.

The noise wind speed is generated using the following equations.

$$V_n = 2 \left(\sum_{i=1}^N \left(\sqrt{S(\omega_i) \Delta\omega} \right) \cos(\omega_i t + \phi_i) \right) \quad \text{Eq. 4-173}$$

$$\omega_i = (i - 0.5) \Delta\omega \quad \text{Eq. 4-174}$$

$$S(\omega_i) = \frac{2c_d L^2 |\omega_i|}{\pi^2 \left[1 + \left(\frac{L \omega_i}{u \pi} \right)^2 \right]^{\frac{4}{3}}} \quad \text{or} \quad \frac{2 \times 0.004 \times 2000^2 |\omega_i|}{\pi^2 \left[1 + \left(\frac{2000 \omega_i}{u \pi} \right)^2 \right]^{\frac{4}{3}}} \quad \text{Eq. 4-175}$$

Where $S(\omega_i)$ is spectral density function at frequency ω_i .

- Wind turbine model

The wind speed (V_w , m/s), mechanical speed of generator (W , rad/s), and pitch angle (Beta, °) are input while the mechanical torque (T_m) and the power of the turbine (P) are output. The wind turbine has torque- W characteristics (or equation of power

coefficient) varies with V_w using standard model called MOD 2 wind turbine-generator system. This standard model is developed by Purdue University.

Input parameters are Rated power of the wind turbine (MVA), Rated MVA of the machine (MVA), Rated mechanical speed of the machine (rad/s), Radius of the wind turbine blades (m), Rotor blade area (m^2), Air density (kg/m^3), Efficiency of the turbine gearbox (p.u.), Gearbox speed ratio, and equation of power coefficient (MOD 2 for three-blade and MOD 5 for two-blade wind turbine).

- Wind turbine governor model

The inputs are mechanical speed of the machine (W_m , rad/s) and the power output of the machine based on the machine rating (P_g , p.u.). The output is pitch angle (β , $^\circ$).

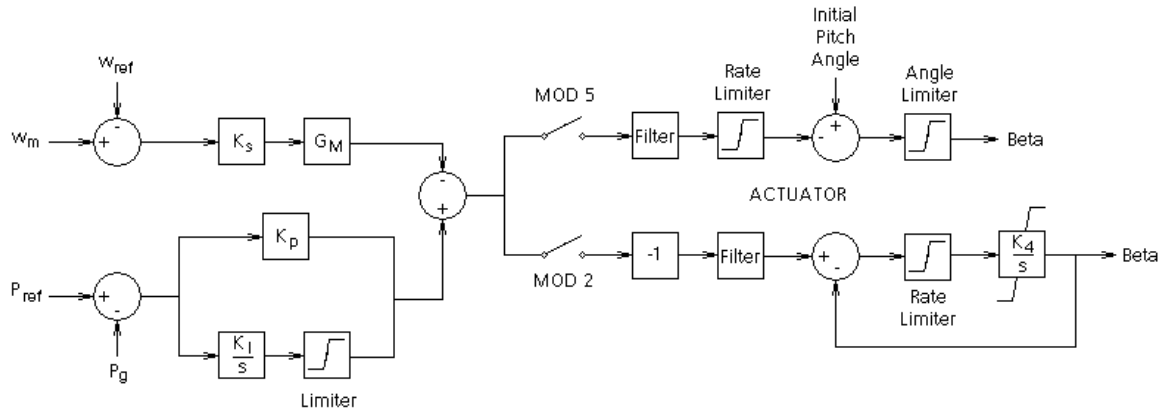


Figure 4.26 Transfer function of wind turbine governor model

Where W_{ref} is reference speed (rad/s), P_{ref} is power demand (MW), K_S is gain ($^\circ/p.u.$), K_P is proportional gain ($^\circ/p.u.$), K_I is integral gain ($^\circ/p.u.$), G_M is gain multiplier ($^\circ/p.u.$), and K_4 is blade actuator integral gain (s).

The wind speed, wind turbine, and governor models are presented in following figure.

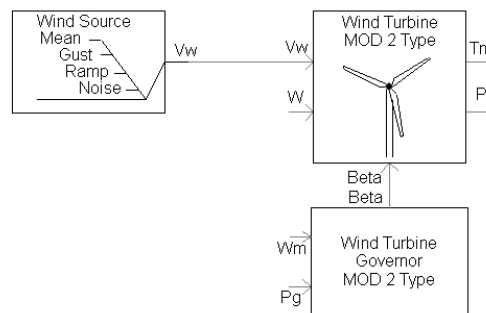


Figure 4.27 Schematic of wind source, turbine and governor model

4.2.2 The power test system

Many small signal stability studies use the test system from the Power System Stability and Control by P. Kundur (1998). These test systems can represent the stability problems with the simplicity designed by using fundamental concept and can clearly reveal the small signal stability problems. Two types of interesting test system are single machine infinite bus (SMIB) system and Four machine power system (FMPS) system.

4.2.2.1 Single Machine Infinite Bus (SMIB)

This system can represent problem of small signal disturbance using eigenvalue analysis method, for example, by P. Kundur (1998). Eigenvalue can describe the damping and oscillation characteristics of the system. The mode of oscillation involving only one machine is called local area oscillation mode. Present technology of stabilizer can control and eliminate this kind of oscillation efficiently.

The test system is used to give an example of small signal and transient stability. The single machine can represent the only local oscillation mode of generator interacting with the rest of power system (or infinite bus). The base voltage and power of the system are 24kV, 100MVA. The wind power and load buses, with line reactance 0.04 p.u., are not previously presented in the original test system.

Wind power is latter designed to have rated power of 5% of generator (Total capacity 2,000MVA). The 2MW wind turbine is selected because it has the largest share of 40% of total as by GL Garrad Hassan (one of the world's leading wind energy consultants) and posted on the Website: www.wind-energy-the-facts.org . Load power can vary to assess the power system performance.

The test system is based on SMIB test system by P. Kundur except the wind power and load of circuit CT3. This model neglects the resistance (very small part) and represents only reactance. The transmission line reactance ($x_L = j\omega L / Z_C$) is in per unit.

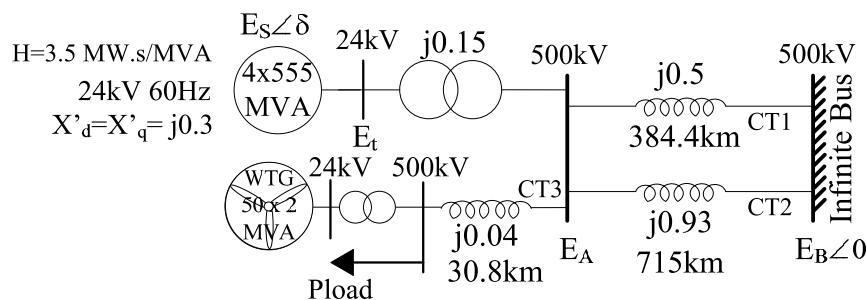


Figure 4.28 Single machine infinite bus (SMIB) system including wind power and load

The line reactance can be implied to line length using the base impedance of the system, that is, characteristic impedance $Z_c = \sqrt{z/y}$ ohms. If the line has series impedance per unit length (z) is 0.35 ohms/km and shunt admittance per unit length (y) is 4.8×10^{-6} ohms/km, therefore, Z_c is 270 about ohms. These per unit length values can be found in Matlab Simulink SimPowerSystem. The line length can be computed from

$$Z = Z_c \lambda L \quad \text{or} \quad L = \frac{Z}{Z_c} \frac{1}{\lambda} \quad \text{Eq. 4-176}$$

where Z/Z_c is per unit impedance (neglect line resistance), $\lambda = \sqrt{zy}$ is phase velocity, L is line length (km).

However, this test system will be modified to suit the objectives and scope of each section.

4.2.2.2 Four Machines Power System (FMPS)

This system can additionally represent oscillatory interaction between machine and group of machines or so called inter-area oscillation mode, for example, by P. Kundur [52]. However, it is still difficult to control and eliminate this kind of oscillation.

This test system is used to give an example of small signal and voltage stability. The generator in this case is the equivalent sum of coherency generators to have totally 4x900MVA rated group capacity. The four machines can represent the both local mode of generator and inter-area mode of oscillation interacting between area 1 and 2.

The base voltage and power of the system are 230kV, 100MVA. The active and reactive loads at buses 7 and 9 have capacitive impedance compensators, as shown in the figure below. The wind power is not previously presented in the original test system. The 180 MW wind power is latter designed to has rated power of 5% of generator (Total capacity 3,600MVA) connecting on bus 9. Load power can be varied to study the effects.

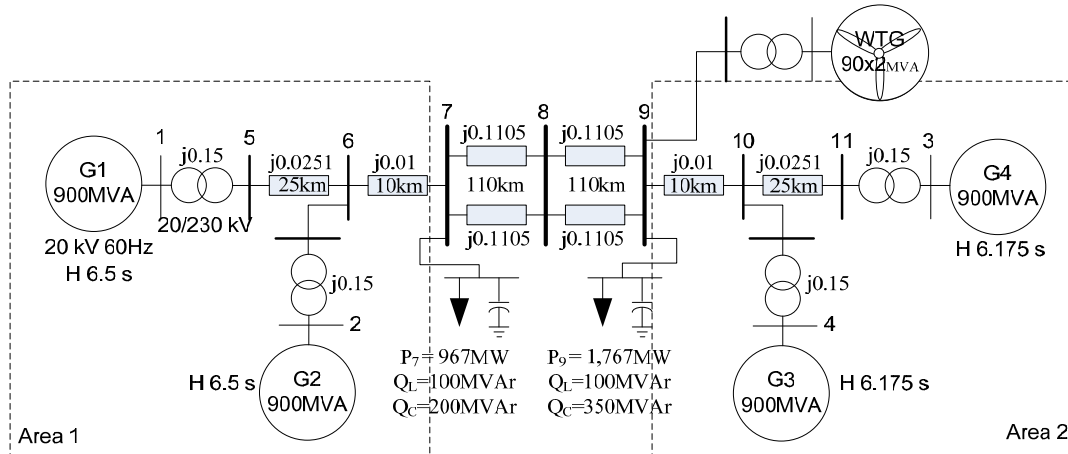


Figure 4.29 Four machine power system (FMPS) including wind power and load

The test system provides line length and r-l-c impedance per unit length. To represent line impedance in per unit value, multiply $z = r + jl$ ohms/km with the line length to result per unit impedance. In this case, resistance can be neglected. The system data are shown in next table.

Table 4.3 System data of FMPS test system

No.	System Data	Vaule	Unit
1	Line base power	100	MVA
2	Line base voltage	230	kV
3	System Frequency	60	Hz
4	The Number of Bus (Nodes): Load bus : Generators	11:2:4	-
5	Sum of the Generator Rated Capacity	3600	MVA
6	Sum of the Generator Output (Active power)	2819	MW
7	Sum of the Generator Output (Reactive power)	798	MVAr
8	Sum of the Load (Active power)	2734	MW
9	Sum of the Load (Inductive power)	200	MVAr
10	Sum of the Load (Capacitive power)	550	MVAr

Table 4.4 Parameters of four machine power system

Generator		
Generator rated capacity	900	MVA
Generator base voltage	20	kV
Step-up transformer impedance	0+j0.15	pu
Step-up transformer voltage	20/230	kV
Sum of the Generator Rated Capacity	3600	MVA
Sum of the Generator Output (Active power)	2819	MW
Sum of the Generator Output (Reactive power)	798	MVAr

Parameters	Value	Parameters	Value	Parameters	Value
Xd	1.8	Xq"	0.25	Asat	0.015
Xq	1.7	Ra	0.0025	Bsat	9.6
Xl	0.2	Td0' (s)	8	yT1	0.9
Xd'	0.3	Tq0' (s)	0.4	H (G1,G2) s	6.5
Xq'	0.55	Td0" (s)	0.03	H (G3,G4) s	6.175
Xd"	0.25	Tq0" (s)	0.05	KD	0

Transmission system		
Line base power	100	MVA
Line base voltage	230	kV
Base line impedance	529	ohm

Parameters	Value	unit
r	0.0001	pu/km
xL	0.001	pu/km
Bc	0.00175	pu/km

Load		
Sum of the Load (Active	2734	MW
Sum of the Load (Inductive	200	MVAr
Sum of the Load (Capacitive	550	MVAr

	P (MW)	QL(MVAr)	Qc(MVAr)
Load Bus7	967	100	200
Load Bus9	1767	100	350

Excitation system	KA	TA	KF	TF	TE	Aex	Bex	TR	TB
Self-excited dc exciter	20	0.055	0.125	1.8	0.36	0.0056	1.075	0.05	-
Tyristor exciter with high transient gain	200	-	-	-	-	-	-	0.01	-
Tyristor exciter with transient gain reduction (TGR)	200	1	-	-	-	-	-	0.01	10
	KA	Kstab	TW	T1	T2	T3	T4	TR	
Tyristor exciter with high transient gain and PSS	200	20	10	0.05	0.02	3	5.4	0.01	

Wind Power		
Wind Farm Rated Power	180	MW
Number of wind turbine	90	
Wind Turbine Rated Power	2	MW
Type of Wind turbine	Fixed speed	
Generator model of wind turbine	SCIG	
Wind speed mean value	3,5,10,15	m/s
Wind speed characteristics	Rayleigh	

4.3 Noise Modeling and Stochastic Differential Equations Formulation

4.3.1 SDE of the power system incorporating SCIG wind turbines

From power system equation in Section 4.1, if we apply stochastic part ($1 + \gamma_w \dot{W}$, \dot{W} is white noise, γ_w is noise intensity = standard deviation / mean value) into mechanical wind power (P_{mw}), we will get stochastic differential equations as follows

$$\dot{y}_w = \frac{1}{M_w} (P_{mw} (1 + \gamma_w \dot{W}) - P_{ew}) \quad \text{Eq. 4-177}$$

$$\dot{y}_w = \frac{1}{M_w} (P_{mw} - P_{ew}) + \frac{1}{M_w} P_{mw} \gamma_w \dot{W} \quad \text{Eq. 4-178}$$

If we use noise scaling factor (ε) for the above equation as:

$$\sqrt{\varepsilon_l} = \inf \left\{ \frac{\gamma P_{mw}}{M_w \sqrt{2\beta}} \middle| \gamma > 0 \right\} \text{ and } \sqrt{\varepsilon_w} = \frac{\gamma P_{mw}}{M_w \sqrt{2\beta \varepsilon_l}} \quad \text{Eq. 4-179}$$

Where w is wind power bus = 1, ..., g . $\beta = D_i / M_i$ is damping coefficient which is the same for all generators and is used to rescale intensity of noise.

Since D of SCIG is very small as compared to the synchronous generator, the parameter α is presented here to scale D of SCIG. Therefore, we will get the standard form of the stochastic differential equation of SCIG as:

$$\dot{y}_w = -\beta \alpha y_w + \frac{1}{M_w} (P_{mw} - P_{ew}) + \sqrt{2\beta \varepsilon_l \varepsilon_w} \dot{W} \quad \text{Eq. 4-180}$$

From Eqs. 4-131 – 4-138, if wind power is applied on one bus (bus $w=2$), the matrix form of the state space equation, including noise term, is represented as follows:

$$\frac{d}{dt} \begin{bmatrix} x_1 \\ x_2 \\ x_3 \\ x_4 \\ x_5 \\ y_1 \\ y_2 \\ y_3 \end{bmatrix} = \begin{bmatrix} y_1 - y_3 \\ \frac{P V_2^2}{2 P_{e2} R_{r2}} (y_2 - 1) - y_3 \\ 0 \\ -\frac{1}{c_4} (P_{l4} + P_{e4}) - y_3 \\ -\frac{1}{c_5} (P_{l5} + P_{e5}) - y_3 \\ -\beta y_1 + \frac{1}{M_1} (P_{m1} - P_{e1}) \\ -\beta \alpha y_2 + \frac{1}{M_2} (P_{m2} - P_{e2}) \\ -\beta y_3 + \frac{1}{M_3} (P_{m3} - P_{e3}) \end{bmatrix} + \sqrt{2\beta \varepsilon_l} \begin{bmatrix} 0 \\ 0 \\ 0 \\ 0 \\ 0 \\ 0 \\ \sqrt{\varepsilon_w} \\ 0 \end{bmatrix} \frac{dW}{dt} \quad \text{Eq. 4-181}$$

Or

$$d\mathbf{x} = f(\mathbf{x})dt + g(\mathbf{x})dW \quad \text{Eq. 4-182}$$

If we define $\phi_{l,k}(\mathbf{X}, y_3) = \frac{1}{c_k}(P_{lk} + P_{ek}) + y_3$ and $\phi_{m,i}(\mathbf{X}) = \frac{1}{M_i}(P_{mi} - P_{ei})$. Then

$$\begin{bmatrix} \dot{x}_1 \\ \dot{x}_2 \\ \dot{x}_3 \\ \dot{x}_4 \\ \dot{x}_5 \\ \dot{y}_1 \\ \dot{y}_2 \\ \dot{y}_3 \end{bmatrix} = \begin{bmatrix} y_1 - y_3 \\ y'_2 - y_3 \\ 0 \\ -\phi_{l,4}(\mathbf{X}, y_3) \\ -\phi_{l,5}(\mathbf{X}, y_3) \\ -\beta y_1 - \phi_{m,6}(\mathbf{X}) \\ -\beta \alpha y_2 - \phi_{m,7}(\mathbf{X}) \\ -\beta y_3 - \phi_{m,8}(\mathbf{X}) \end{bmatrix} + \sqrt{2\beta\epsilon_l} Q_w \dot{W} \quad \text{Eq. 4-183}$$

Where $y'_2 = a(y_2 - 1)$, $a = \frac{PV_2^2}{2P_{e2}R_{r2}}$, and Q_w is $m+n \times 1$ matrix with $q_{71} = \sqrt{\epsilon_w}$.

4.3.2 SDE of the power system incorporating DFIG wind turbines

4.3.2.1 White noise model

From the state space equation in Section 2.1, if we apply stochastic part ($1 + \alpha_w \dot{W}$, \dot{W} is white noise, α_w is noise intensity which is the standard deviation divided by mean value) into mechanical wind power (P_{mw}), we will get stochastic differential equations [74] as follows

$$\dot{y}_w = \frac{1}{M_w} (P_{mw} (1 + \alpha_w \dot{W}) - P_{ew}) \quad \text{Eq. 4-184}$$

$$\dot{y}_w = \frac{1}{M_w} (P_{mw} - P_{ew}) + \frac{1}{M_w} P_{mw} \alpha_w \dot{W} \quad \text{Eq. 4-185}$$

$$\gamma_w = \frac{P_{ms} \alpha_w}{M_w} = \sqrt{2\beta\epsilon_{lw}\epsilon_w} \quad \text{Eq. 4-186}$$

$$\sqrt{\epsilon_{lw}} = \inf \left\{ \frac{P_{ms} \alpha_w}{M_w \sqrt{2\beta}} \middle| \alpha_w > 0 \right\} \quad \text{and} \quad \sqrt{\epsilon_w} = \frac{P_{ms} \alpha_w}{M_w \sqrt{2\beta\epsilon_{lw}}} \quad \text{Eq. 4-187}$$

Where ϵ_{lw} is the noise scaling factor of wind power bus which has the lowest value and ϵ_w is the noise scaling factor of wind power bus w . β is a parameter to rescale the intensity of noise for mathematical convenience.

Furthermore, when the load fluctuation is represented, the stochastic differential equation of the dynamic load is:

$$\dot{x}_k = -\frac{1}{c_k}(\bar{P}_{l4} + \bar{P}_{e4}) - \omega_0 y_0 + \frac{1}{c_k} \alpha_k P_{lk} \dot{W} \quad \text{Eq. 4-188}$$

$$\gamma_w = \frac{1}{c_k} \alpha_k P_{lk} = \sqrt{2\beta \varepsilon_{lk} \varepsilon_k} \quad \text{Eq. 4-189}$$

$$\sqrt{\varepsilon_{lk}} = \inf \left\{ \frac{\alpha_k P_{lk}}{c_k \sqrt{2\beta}} \middle| \alpha_k > 0 \right\} \quad \text{and} \quad \sqrt{\varepsilon_k} = \frac{\alpha_k P_{lk}}{c_k \sqrt{2\beta \varepsilon_{lk}}} \quad \text{Eq. 4-190}$$

Where ε_{lk} is the noise scaling factor of load which has lowest value and ε_k is the noise scaling factor of load bus k .

Therefore, the matrix form of stochastic differential equations will become the dynamic perturbed system in a matrix form as follows:

$$\frac{d}{dt} \begin{bmatrix} x_i \\ x_w \\ x_k \\ y_i \\ y_w \end{bmatrix} = \begin{bmatrix} \omega_0 (y_i - y_0) \\ \omega_0 (y_w - y_0) + \varphi_{df}(\mathbf{V}, \mathbf{x}) \\ \varphi_k(\mathbf{V}, \mathbf{x}) \\ \varphi_i(\mathbf{V}, \mathbf{x}) - \beta_i y_i \\ \varphi_w(\mathbf{V}, \mathbf{x}) \end{bmatrix} + \begin{bmatrix} 0 \\ 0 \\ \gamma_k \\ 0 \\ \gamma_w \end{bmatrix} \frac{dW}{dt} \quad \text{Eq. 4-191}$$

$$\left. \begin{aligned} \varphi_{df}(\mathbf{V}, \mathbf{x}) &= \omega_0 k_d \bar{V}_{rq} - k_b \bar{V}_{s3} \sin(k_a (x_w - x_{ref}) + c_a) \\ \varphi_k(\mathbf{V}, \mathbf{x}) &= -\frac{1}{c_k}(\bar{P}_{lk} + \bar{P}_{ek}) - \omega_0 y_0 \\ \varphi_i(\mathbf{V}, \mathbf{x}) &= \frac{1}{M_i}(\bar{P}_{mi} - \bar{P}_{ei}) \\ \varphi_w(\mathbf{V}, \mathbf{x}) &= \frac{1}{M_w}(\bar{P}_{mw} - \bar{P}_{ew}) \end{aligned} \right\} \quad \text{Eq. 4-192}$$

where $\beta_i = D_i/M_i$. The above equation can be represented in the standard stochastic differential equation as:

$$d\mathbf{x} = f(\mathbf{x})dt + g(\mathbf{x})dW \quad \text{Eq. 4-193}$$

Where f is a nonlinear drift function, the matrix g is the diffusion function, and matrix \mathbf{x} is the state variable matrix.

4.3.2.2 Colored noise model

The colored noise represents the normal distribution signal which has limited bandwidth. From the state space equation in Section 4.1, if we apply the stochastic part into the mechanical wind power (P_{mw}), we will get stochastic differential equations [74] as follows:

$$P_{mw} = P_{ms} (1 + \alpha_w \upsilon_w) \quad \text{Eq. 4-194}$$

$$p\upsilon_w = -\psi_w \upsilon_w + \gamma_w \psi_w pW \quad \text{Eq. 4-195}$$

Where $P_{ml} = \alpha P_{ms} \upsilon$, υ_w represents colored noise applying to wind power, α_w and ψ_w are noise intensity (the standard deviation divided by mean value) and bandwidth of low frequency component of wind power. γ_w is scaling factor of wind power noise which is formulated using the method in [11] as follows:

$$\gamma_w = \frac{P_{ms} \alpha_w}{M_w} = \sqrt{2\beta \varepsilon_{lw} \varepsilon_w} \quad \text{Eq. 4-196}$$

$$\sqrt{\varepsilon_{lw}} = \inf \left\{ \frac{P_{ms} \alpha_w}{M_w \sqrt{2\beta}} \middle| \alpha_w > 0 \right\} \quad \text{and} \quad \sqrt{\varepsilon_w} = \frac{P_{ms} \alpha_w}{M_w \sqrt{2\beta \varepsilon_{lw}}} \quad \text{Eq. 4-197}$$

Where ε_{lw} is the noise scaling factor of the wind power bus that has the lowest value and ε_w is the noise scaling factor of wind power bus w . β is a parameter to rescale the intensity of noise for mathematical convenient.

For power load, when the load fluctuation is represented, the stochastic differential equation of dynamic load is

$$px_k = -\frac{1}{c_k} (\bar{P}_{lk} + \bar{P}_{ek}) - \omega_0 y_0 + \frac{1}{c_k} \bar{P}_{lk} \alpha_k \upsilon_k \quad \text{Eq. 4-198}$$

$$p\upsilon_k = -\psi_k \upsilon_k + \gamma_k \psi_k pW \quad \text{Eq. 4-199}$$

Where $P_{lk} (1 - \alpha_k \upsilon_k)$ is stochastic power load, υ_k represents colored noise applying to power load, α_k and ψ_k are noise intensity and bandwidth of power load, γ_k is scaling factor of power load which is formulated using the method in [11] as follows:

$$\gamma_k = \frac{P_{lk} \alpha_k}{c_k} = \sqrt{2\beta \varepsilon_{lk} \varepsilon_k} \quad \text{Eq. 4-200}$$

$$\sqrt{\varepsilon_{lk}} = \inf \left\{ \frac{P_{lk} \alpha_k}{c_k \sqrt{2\beta}} \middle| \alpha_k > 0 \right\} \quad \text{and} \quad \sqrt{\varepsilon_k} = \frac{P_{lk} \alpha_k}{c_k \sqrt{2\beta \varepsilon_{lk}}} \quad \text{Eq. 4-201}$$

Where ε_{lk} is the noise scaling factor of the load bus that has the lowest value and ε_k is the noise scaling factor of load bus k . β is a parameter to rescale the intensity of noise for mathematical convenient.

Furthermore, it is assumed that

$$\gamma_{wk} = \frac{\gamma_w}{\gamma_k} = \frac{\sqrt{\varepsilon_{lw} \varepsilon_w}}{\sqrt{\varepsilon_{lk} \varepsilon_k}} = \frac{\bar{P}_{wm} \alpha_w}{\bar{P}_{lk} \alpha_k} \frac{c_k}{M_w} = \bar{P}'_{wm} \frac{\alpha_w c_k}{\alpha_k M_w} \quad \text{Eq. 4-202}$$

The system equations will become the dynamic perturbed system in a matrix form as follows:

$$\frac{d}{dt} \begin{bmatrix} x_i \\ x_w \\ x_k \\ y_i \\ y_w \\ v_w \\ v_k \end{bmatrix} = \begin{bmatrix} \omega_0 (y_i - y_0) \\ \omega_0 (y_w - y_0) + \varphi_{df}(\mathbf{V}, \mathbf{x}) \\ \varphi_k(\mathbf{V}, \mathbf{x}) + \gamma_k v_k \\ \varphi_i(\mathbf{V}, \mathbf{x}) - \beta_i y_i \\ \varphi_w(\mathbf{V}, \mathbf{x}) + \gamma_k \gamma_{wk} v_w \\ -\psi_w v_w \\ -\psi_k v_k \end{bmatrix} + \gamma_k \begin{bmatrix} 0 \\ 0 \\ 0 \\ 0 \\ 0 \\ \gamma_{wk} \psi_w \\ \psi_k \end{bmatrix} \frac{dW}{dt} \quad \text{Eq. 4-203}$$

$$\left. \begin{aligned} \varphi_{df}(\mathbf{V}, \mathbf{x}) &= \omega_0 k_d \bar{V}_{rq} - k_b \bar{V}_{s3} \sin(k_a (x_w - x_{ref}) + c_a) \\ \varphi_k(\mathbf{V}, \mathbf{x}) &= -\frac{1}{c_k} (\bar{P}_{lk} + \bar{P}_{ek}) - \omega_0 y_0 \\ \varphi_i(\mathbf{V}, \mathbf{x}) &= \frac{1}{M_i} (\bar{P}_{mi} - \bar{P}_{ei}) \\ \varphi_w(\mathbf{V}, \mathbf{x}) &= \frac{1}{M_w} (\bar{P}_{mw} - \bar{P}_{ew}) \end{aligned} \right\} \quad \text{Eq. 4-204}$$

where $\beta_i = D_i/M_i$. The above equation can be represented in the standard stochastic differential equation as

$$p\mathbf{X} = \mathbf{f}(\mathbf{X}, t) + \mathbf{g}(\mathbf{X}, t) pW, \quad \mathbf{x}(t_0) = \mathbf{x}_0, \quad t \geq t_0 \quad \text{Eq. 4-205}$$

where $\mathbf{f}(\mathbf{X}, t)$ is a nonlinear drift function, $\mathbf{g}(\mathbf{X}, t)$ is a diffusion function in matrix form.

4.3.3 SDE of the power system incorporating DFIG wind turbines for voltage stability analysis

From the state space equation in Section 2.1, if we apply the stochastic part into the mechanical wind power (P_{mw}), we will get stochastic differential equations [74] as follows:

$$P_{mw} = P_{ms} (1 + \alpha_w v_w) \quad \text{Eq. 4-206}$$

$$p v_w = -\psi_w v_w + \gamma_w \psi_w pW \quad \text{Eq. 4-207}$$

Where $P_{ml} = \alpha P_{ms} v_w$, v_w represents colored noise applying to wind power, α_w and ψ_w are noise intensity (the standard deviation divided by mean value) and bandwidth of low frequency component of wind power. γ_w is scaling factor of wind power noise which is formulated using the method in [11] as follows:

$$\gamma_w = \frac{P_{ms} \alpha_w}{M_w} = \sqrt{2\beta \varepsilon_{lw} \varepsilon_w} \quad \text{Eq. 4-208}$$

$$\sqrt{\varepsilon_{lw}} = \inf \left\{ \frac{P_{ms} \alpha_w}{M_w \sqrt{2\beta}} \middle| \alpha_w > 0 \right\} \quad \text{and} \quad \sqrt{\varepsilon_w} = \frac{P_{ms} \alpha_w}{M_w \sqrt{2\beta \varepsilon_{lw}}} \quad \text{Eq. 4-209}$$

Where ε_{lw} is the noise scaling factor of wind power bus which has lowest value and ε_w is the noise scaling factor of wind power bus w . β is a parameter to rescale the intensity of noise for mathematical convenience.

For the active power load, when the load fluctuation is represented, the stochastic differential equation of the dynamic load is:

$$px_k = -\frac{1}{c_k}(\bar{P}_{lk} + \bar{P}_{ek}) - \omega_0 y_0 + \frac{1}{c_k} \bar{P}_{lk} \alpha_{pk} v_{pk} \quad \text{Eq. 4-210}$$

$$pv_{pk} = -\psi_{pk} v_{pk} + \gamma_{pk} \psi_{pk} pW \quad \text{Eq. 4-211}$$

Where P_{lk} ($1 - \alpha_{pk} v_{pk}$) is stochastic power load, v_k represents colored noise applying to power load, α_{pk} and ψ_{pk} are noise intensity and bandwidth of power load, γ_{pk} is scaling factor of power load which is formulated using the method in [11] as follows:

$$\gamma_{pk} = \frac{P_{lk} \alpha_{pk}}{c_k} = \sqrt{2\beta \varepsilon_{lpk} \varepsilon_{pk}} \quad \text{Eq. 4-212}$$

$$\sqrt{\varepsilon_{lpk}} = \inf \left\{ \frac{P_{lk} \alpha_{pk}}{c_k \sqrt{2\beta}} \middle| \alpha_{pk} > 0 \right\} \quad \text{and} \quad \sqrt{\varepsilon_{pk}} = \frac{P_{lk} \alpha_{pk}}{c_k \sqrt{2\beta \varepsilon_{lpk}}} \quad \text{Eq. 4-213}$$

Where ε_{lk} is the noise scaling factor of the load bus that has the lowest value and ε_k is the noise scaling factor of load bus k . β is a parameter to rescale the intensity of noise for mathematical convenience.

For reactive power load, when the load fluctuation is represented, the stochastic differential equation of dynamic load is:

$$p\bar{V}_k = (\lambda_k \bar{V}_k)^{-1} (-\bar{Q}_{lk} (1 - \alpha_{qk} v_{qk}) + \bar{Q}_{ek}) = \frac{1}{\lambda_k \bar{V}_k} (-\bar{Q}_{lk} + \bar{Q}_{ek}) + \frac{1}{\lambda_k \bar{V}_k} \bar{Q}_{lk} \alpha_{qk} v_{qk} \quad \text{Eq. 4-214}$$

$$pv_{qk} = -\psi_{qk} v_{qk} + \gamma_{qk} \psi_{qk} pW \quad \text{Eq. 4-215}$$

Where Q_{lk} ($1 - \alpha_{qk} v_{qk}$) is stochastic reactive power load, v_{qk} represents colored noise applying to Q_{lk} , α_{qk} and ψ_{qk} are noise intensity and bandwidth of reactive power load, γ_{qk} is scaling factor of power load using the method in [11] as follows:

$$\gamma_{qk} = \frac{Q_{lk} \alpha_{qk}}{\lambda_k V_k} = \sqrt{2\beta \varepsilon_{lqk} \varepsilon_{qk}} \quad \text{Eq. 4-216}$$

$$\sqrt{\varepsilon_{lqk}} = \inf \left\{ \frac{Q_{lk} \alpha_{qk}}{\lambda_k V_k \sqrt{2\beta}} \middle| \alpha_{qk} > 0 \right\} \quad \text{and} \quad \sqrt{\varepsilon_{qk}} = \frac{Q_{lk} \alpha_{qk}}{\lambda_k V_k \sqrt{2\beta \varepsilon_{lqk}}} \quad \text{Eq. 4-217}$$

Furthermore, it is assumed that

$$\gamma_{wpk} = \frac{\gamma_w}{\gamma_{pk}} = \frac{\sqrt{\varepsilon_{lw}\varepsilon_w}}{\sqrt{\varepsilon_{lpk}\varepsilon_{pk}}} = \frac{\bar{P}_{wm}\alpha_w}{\bar{P}_{lk}\alpha_{pk}} \frac{c_k}{M_w} = \bar{P}'_{wm} \frac{\alpha_w c_k}{\alpha_{pk} M_w} \quad \text{Eq. 4-218}$$

$$\gamma_{qpk} = \frac{\gamma_{qk}}{\gamma_{pk}} = \frac{\sqrt{\varepsilon_{lqk}\varepsilon_{qk}}}{\sqrt{\varepsilon_{lpk}\varepsilon_{pk}}} = \frac{\bar{Q}_{lk}\alpha_{qk}c_k}{\bar{P}_{lk}\alpha_{pk}\lambda_k V_k} = \bar{Q}'_{lk} \frac{\alpha_{qk}c_k}{\alpha_{pk}\lambda_k V_k} \quad \text{Eq. 4-219}$$

The system equations will become the dynamic perturbed system in a matrix form as follows:

$$\frac{d}{dt} \begin{bmatrix} x_i \\ x_w \\ x_k \\ y_i \\ y_w \\ V_k \\ v_w \\ v_{pk} \\ v_{qk} \end{bmatrix} = \begin{bmatrix} \omega_0(y_i - y_0) \\ \omega_0(y_w - y_0) + \varphi_{df}(\mathbf{V}, \mathbf{x}) \\ \varphi_{xk}(\mathbf{V}, \mathbf{x}) + \gamma_{pk}v_{pk} \\ \varphi_i(\mathbf{V}, \mathbf{x}) - \beta_i y_i \\ \varphi_w(\mathbf{V}, \mathbf{x}) + \gamma_k \gamma_{wk} v_w \\ \varphi_{vk}(\mathbf{V}, \mathbf{x}) + \gamma_{qk}v_{qk} \\ -\psi_w v_w \\ -\psi_{pk} v_{pk} \\ -\psi_{qk} v_{qk} \end{bmatrix} + \gamma_{pk} \begin{bmatrix} 0 \\ 0 \\ 0 \\ 0 \\ 0 \\ 0 \\ \gamma_{wpk}\psi_w \\ \psi_{pk} \\ \gamma_{qpk}\psi_{qk} \end{bmatrix} \frac{dW}{dt} \quad \text{Eq. 4-220}$$

$$\left. \begin{aligned} \varphi_{df}(\mathbf{V}, \mathbf{x}) &= \omega_0 k_d \bar{V}_{rq} - k_b \bar{V}_{s3} \sin(k_a(x_w - x_{ref}) + c_a) \\ \varphi_{xk}(\mathbf{V}, \mathbf{x}) &= -\frac{1}{c_k} (\bar{P}_{lk} + \bar{P}_{ek}) - \omega_0 y_0 \\ \varphi_i(\mathbf{V}, \mathbf{x}) &= \frac{1}{M_i} (\bar{P}_{mi} - \bar{P}_{ei}) \\ \varphi_w(\mathbf{V}, \mathbf{x}) &= \frac{1}{M_w} (\bar{P}_{mw} - \bar{P}_{ew}) \\ \varphi_{vk}(\mathbf{V}, \mathbf{x}) &= \frac{1}{\lambda_k \bar{V}_k} (-\bar{Q}_{lk} + \bar{Q}_{ek}) \end{aligned} \right\} \quad \text{Eq. 4-221}$$

where $\beta_i = D_i/M_i$. The above equation can be represented in the standard stochastic differential equation as:

$$p\mathbf{X} = \mathbf{f}(\mathbf{X}, t) + \mathbf{g}(\mathbf{X}, t) pW, \quad \mathbf{x}(t_0) = \mathbf{x}_0, \quad t \geq t_0 \quad \text{Eq. 4-222}$$

where $\mathbf{f}(\mathbf{X}, t)$ is a nonlinear drift function, $\mathbf{g}(\mathbf{X}, t)$ is a diffusion function in matrix form.

4.4 Well-defined Energy Function Formulation

4.4.1 Well-defined energy function preparation

The stochastic stability index is developed for the study of the impact of wind power on the power system stability. Energy function method, basing on Lyapunov's

theory, is used to determine the region of attraction of stable equilibrium points and the critical values which beyond these values, system become unstable.

The cumulative effect of continuous small disturbances on the power system (such as load and wind power) can finally make the system reach the critical values and become unstable. An important step for energy function construction is to ensure that this function is a type of Lyapunov function. If then, this is called well-defined energy function which the theory of system stability of Lyapunov can be described. However, since now, there is no complete or exact solution of energy function. Carefully checking the existence of an energy function ($W(x_t)$) should be considered by using the following conditions [9][30].

C.1 $U(x_t) = 0$ when operating points are the stable equilibrium points ($x_t = x_s$)

C.2 $\dot{U}(x_t) < 0$ when trajectories of operating points are within the region of attraction and asymptotically moving to equilibrium points

C.3 $U(x_t)$ is bounded, which means x_t is also bounded.

There are two methods to construct an energy function: the two-step procedure and the first-integral method [30]. This thesis uses well-known first integral method to construct the energy function.

To construct a well-defined energy function of the induction generator, a new method was developed in this study.

The well-defined energy function can start from the power balance equations of the power system without loss (neglect conductance terms). These equations consist of the power flow, load, and generation terms. The generation terms can be separated to be generation from synchronous generator and induction generator.

4.4.1.1 Energy function of synchronous generator

For synchronous generators, if the reference bus is an infinite bus ($y_1 = 0$), the terms of power (from equation of motion) will be integrated to be the energy balance as follows:

$$M_i \dot{y}_i = \bar{P}_{mi} - \bar{P}_{ei} - D_i y_i \quad \text{Eq. 4-223}$$

$$\text{multiply by } y_i, \quad M_i \dot{y}_i y_i = P_{mi} y_i - P_{ei} y_i - D_i y_i^2 \quad \text{Eq. 4-224}$$

Replace $y_i = \dot{x}_i / \omega_0 + y_0$ into the right side of the above equation except for the last term yields:

$$\omega_0 M_i \dot{y}_i y_i - \bar{P}_{mi} \dot{x}_i + \bar{P}_{ei} \dot{x}_i = -\omega_0 D_i y_i^2 + \omega_0 y_1 (\bar{P}_{mi} - \bar{P}_{ei}) \quad \text{Eq. 4-225}$$

The electrical power of a synchronous generator can be stated as follows

$$P_{ei} = V_i \sum_{j=1}^n V_j B_{ij} \sin(x_i - x_j) \quad \text{Eq. 4-226}$$

Placing Eq. 4-226 into Eq. 4-225, and summing all the machines, we will get

$$\sum_{i=1}^{m-p} \omega_0 M_i \dot{y}_i y_i - \sum_{i=1}^{m-p} \bar{P}_{mi} \dot{x}_i + \sum_{i=1}^{m-p} \sum_{j=1}^n V_i V_j B_{ij} \sin(x_i - x_j) \dot{x}_i = - \sum_{i=1}^{m-p} \omega_0 D_i y_i^2 + \omega_0 y_0 \left(\sum_{i=1}^{m-p} P_{mi} - \sum_{i=1}^{m-p} P_{ei} \right) \quad \text{Eq. 4-227}$$

4.4.1.2 Energy function of induction generator

For induction generator, the speed of the rotor is faster than the synchronous speed, which is called the slip. If the slip is constant, the rotor angle increases continuously with a fixed rate. Therefore, the rotor angle is generally not defined for induction generator.

Since the torque-slip characteristics of induction generator is important for the power and energy balance, the speed of rotor (and/or slip) should be state variables for the energy function instead of the angle. Consequently, the power flow equations cannot be included in the swing equations as the same with the case of synchronous generator and the energy function of power flow equations at induction generator bus is also different. This study proposes a new method to construct energy function of induction generator as follows:

1) For SCIG with colored noise, the swing equation of the induction generator is represented in the form

$$M_w \dot{y}_w = \bar{P}_{mw} (1 + \alpha_w \nu_w) - \bar{P}_{ew} \quad \text{Eq. 4-228}$$

multiply above equation by \dot{x}_w

$$\dot{x}_w = \omega_0 y_w - k_b V_{sw} \sin(k_a x_w + c_a) - \omega_0 y_0 \quad \text{Eq. 4-229}$$

Replace above \dot{x}_w into the term on the left of Eq. 4-229, yields

$$M_w y_w \omega_0 \dot{y}_w - M_w \dot{y}_w k_b V_{sw} \sin(k_a x_w + c_a) - \bar{P}_{mw} (1 + \alpha_w \nu_w) \dot{x}_w + \bar{P}_{ew} \dot{x}_w = \omega_0 y_0 M_w \dot{y}_w$$

Replace $M_w \dot{y}_w$ on the right with $P_{mw} - P_{ew}$ and multiplying above equation by dt

we will have

$$M_w y_w \omega_0 \dot{y}_w - M_w \dot{y}_w k_b V_{sw} \sin(k_a x_w + c_a) - \bar{P}_{mw} (1 + \alpha_w \nu_w) \dot{x}_w + \bar{P}_{ew} \dot{x}_w = \omega_0 y_0 (\bar{P}_{mw} - \bar{P}_{ew}) \quad \text{Eq. 4-230}$$

The electrical power of induction generator can be stated as follows

$$P_{ew} = V_w \sum_{j=1}^n V_j B_{wj} \sin(x_w - x_j) \quad \text{Eq. 4-231}$$

Replace Eq. 4-231 into Eq. 4-230, and summing all machines, we will get

$$\sum_{w=m}^m M_w y_w \omega_0 \dot{y}_w - \sum_{w=m}^m M_w \dot{y}_w k_b V_{sw} \sin(k_a x_w + c_a) - \sum_{w=m}^m \bar{P}_{mw} (1 + \alpha_w \nu_w) \dot{x}_w$$

$$+ \sum_{w=m}^m \sum_{j=1}^n V_w V_j B_{wj} \sin(x_w - x_j) \dot{x}_w = \omega_0 y_0 \left(\sum_{w=m}^m P_{mw} - \sum_{w=m}^m P_{ew} \right)$$
Eq. 4-232

For white noise model, the ν_w is zero, the above equation becomes

$$\sum_{w=m}^m M_w y_w \omega_0 \dot{y}_w - \sum_{w=m}^m M_w \dot{y}_w k_b V_{sw} \sin(k_a x_w + c_a) - \sum_{w=m}^m \bar{P}_{mw} \dot{x}_w + \sum_{w=m}^m \sum_{j=1}^n V_w V_j B_{wj} \sin(x_w - x_j) \dot{x}_w$$

$$= \omega_0 y_0 \left(\sum_{w=m}^m P_{mw} - \sum_{w=m}^m P_{ew} \right)$$
Eq. 4-233

2) For DFIG with colored noise, the swing equation of the induction generator is represented in the form

$$M_w \dot{y}_w = \bar{P}_{mw} (1 + \alpha_w \nu_w) - \bar{P}_{ew}$$
Eq. 4-234

multiplying above equation by \dot{x}_w and sum all terms of induction machines to get

$$M_w \dot{x}_w \dot{y}_w = \bar{P}_{mw} (1 + \alpha_w \nu_w) \dot{x}_w - \bar{P}_{ew} \dot{x}_w$$
Eq. 4-235

$$\dot{x}_w = \omega_0 y_w - \omega_0 y_0 - k_b \bar{V}_{sw} \sin(k_a (x_w - x_{ref}) + c_a) + \omega_0 k_d \bar{V}_{rq}$$
Eq. 4-236

Replace above \dot{x}_w into the term on the left of Eq. 4-235, yields

$$M_w y_w \omega_0 \dot{y}_w - M_w \dot{y}_w k_b V_{sw} \sin(k_a (x_w - x_{ref}) + c_a) - \bar{P}_{mw} (1 + \alpha_w \nu_w) \dot{x}_w + \bar{P}_{ew} \dot{x}_w + M_w \dot{y}_w \omega_0 k_d \bar{V}_{rq} = \omega_0 y_0 M_w \dot{y}_w$$
Eq. 4-237

Replace $M_w \dot{y}_w$ on the right with $P_{mw} - P_{ew}$ we will have

$$M_w y_w \omega_0 \dot{y}_w - M_w \dot{y}_w k_b V_{sw} \sin(k_a (x_w - x_{ref}) + c_a) - \bar{P}_{mw} (1 + \alpha_w \nu_w) \dot{x}_w + \bar{P}_{ew} \dot{x}_w + M_w \dot{y}_w \omega_0 k_d \bar{V}_{rq} = \omega_0 y_0 (\bar{P}_{mw} - \bar{P}_{ew})$$
Eq. 4-238

$$\bar{V}_{rq} (x_w, y_w) = -y_w \left(k_{c2} \bar{V}_{sw} \cos(k_a (x_w - x_{ref}) + c_a) + k_{c1} \bar{V}_w \right) + k_p k_{op} (y_w + 1)^2 - k_p \bar{P}'_{sw}$$

$$\bar{P}'_{sw} \approx k_m \bar{P}_{ew} / (1 + y_w)$$

Where $k_m = \bar{L}_m^2 / (\bar{L}_{ss} \bar{L}_{rr})$ is a constant and B_{wr} is the susceptance including transient reactance of stator and susceptance connecting between terminal of stator and the reference bus (in this case is load bus).

The electrical power of induction generator can be stated as follows

$$P_{ew} = V_w \sum_{j=1}^n V_j B_{wj} \sin(x_w - x_j)$$
Eq. 4-239

Replace Eq. 4-239 into Eq. 4-238, and summing all machines, we will get

$$\begin{aligned} & \sum_{w=m}^m M_w y_w \omega_0 \dot{y}_w - \sum_{w=m}^m M_w \dot{y}_w k_b V_{sw} \sin(k_a (x_w - x_{ref}) + c_a) - \sum_{w=m}^m \bar{P}_{mw} (1 + \alpha_w v_w) \dot{x}_w \\ & + \sum_{w=m}^m \sum_{j=1}^n V_w V_j B_{wj} \sin(x_w - x_j) \dot{x}_w + \sum_{w=m}^m M_w \omega_0 k_d \bar{V}_{rq} \dot{y}_w = \omega_0 y_0 \left(\sum_{w=m}^m P_{mw} - \sum_{w=m}^m P_{ew} \right) \end{aligned} \quad \text{Eq. 4-240}$$

For white noise model, the v_w is zero, the above equation becomes

$$\begin{aligned} & \sum_{w=m}^m M_w y_w \omega_0 \dot{y}_w - \sum_{w=m}^m M_w \dot{y}_w k_b V_{sw} \sin(k_a (x_w - x_{ref}) + c_a) - \sum_{w=m}^m \bar{P}_{mw} \dot{x}_w \\ & + \sum_{w=m}^m \sum_{j=1}^n V_w V_j B_{wj} \sin(x_w - x_j) \dot{x}_w + \sum_{w=m}^m M_w \omega_0 k_d \bar{V}_{rq} \dot{y}_w = \omega_0 y_0 \left(\sum_{w=m}^m P_{mw} - \sum_{w=m}^m P_{ew} \right) \end{aligned} \quad \text{Eq. 4-241}$$

4.4.1.3 Energy function of load [8]

1) For load equations with colored noise

The active power load is

$$c_k \dot{x}_k = -P_{lk} (1 - \alpha_{pk} v_{pk}) - P_{ek} - c_k \omega_0 y_0 \quad \text{for } m \text{ load bus} \quad \text{Eq. 4-242}$$

multiply by \dot{x}_k and sum all terms of load and rearrange to yields

$$\sum_{k=m+1}^n P_{lk} (1 - \alpha_{pk} v_{pk}) \dot{x}_k + \sum_{k=m+1}^n P_{ek} \dot{x}_k = - \sum_{k=m+1}^n c_k \dot{x}_k^2 - \sum_{k=m+1}^n c_k \omega_0 y_0 \dot{x}_k \quad \text{Eq. 4-243}$$

Where $P_{ek} = \sum_{j=1}^{n+m} V_k V_j B_{kj} \sin(x_k - x_j)$, k is load bus number

Rearrange above equation

$$\sum_{k=m+1}^n P_{lk} (1 - \alpha_{pk} v_{pk}) \dot{x}_k + \sum_{k=m+1}^n \sum_{j=1}^n V_k V_j B_{kj} \sin(x_k - x_j) \dot{x}_k = - \sum_{k=m+1}^n c_k \dot{x}_k^2 - \omega_0 y_0 \sum_{k=m+1}^n c_k \dot{x}_k \quad \text{Eq. 4-244}$$

The power load P_{lk} can be modeled depending on voltage. For the constant impedance load, $P_{lk} = P_{l0k} (V_k)^2$.

$$\begin{aligned} & \sum_{k=m+1}^n P_{l0k} V_k^2 (1 - \alpha_{pk} v_{pk}) \dot{x}_k + \sum_{k=m+1}^n \sum_{j=1}^n V_k V_j B_{kj} \sin(x_k - x_j) \dot{x}_k \\ & = - \sum_{k=m+1}^n c_k \dot{x}_k^2 - \omega_0 y_0 \sum_{k=m+1}^n c_k \dot{x}_k \end{aligned} \quad \text{Eq. 4-245}$$

For white noise model, the v_{pk} is zero, above equation become

$$\sum_{k=m+1}^n P_{l0k} V_k^2 \dot{x}_k + \sum_{k=m+1}^n \sum_{j=1}^n V_k V_j B_{kj} \sin(x_k - x_j) \dot{x}_k = - \sum_{k=m+1}^n c_k \dot{x}_k^2 - \omega_0 y_0 \sum_{k=m+1}^n c_k \dot{x}_k \quad \text{Eq. 4-246}$$

2) The voltage dynamic of load with colored noise

It can be formulated as follows:

$$\lambda_k \dot{\bar{V}}_k = (\bar{V}_k)^{-1} \left(-\bar{Q}_{lk} (1 - \alpha_{qk} v_{qk}) + \bar{Q}_{ek} \right) \quad \text{for } m \text{ load bus} \quad \text{Eq. 4-247}$$

multiply by $\dot{\bar{V}}_k$ and sum all terms of load and rearrange to yields

$$\sum_{k=m+1}^n \bar{Q}_{lk} (1 - \alpha_{qk} v_{qk}) \bar{V}_k^{-1} \dot{\bar{V}}_k - \sum_{k=m+1}^n \sum_{l=1}^n V_k V_l B_{kl} \cos(x_k - x_l) \bar{V}_k^{-1} \dot{\bar{V}}_k = - \sum_{k=m+1}^n \lambda_k \dot{\bar{V}}_k^2 \quad \text{Eq. 4-248}$$

Q_{lk} is modeled depending on voltage. For the constant impedance load, $Q_{lk} = Q_{0k}(V_k)^2$.

For white noise model, the v_{qk} is zero, above equation become

$$\sum_{k=m+1}^n \bar{Q}_{lk} \bar{V}_k^{-1} \dot{\bar{V}}_k - \sum_{k=m+1}^n \sum_{l=1}^n V_k V_l B_{kl} \cos(x_k - x_l) \bar{V}_k^{-1} \dot{\bar{V}}_k = - \sum_{k=m+1}^n \lambda_k \dot{\bar{V}}_k^2 \quad \text{Eq. 4-249}$$

4.4.1.4 Colored noise parameters

If the colored noise model is applied to both wind power and load, its derivative equations are

$$\dot{v}_w = -\psi_w v_w \quad \text{Eq. 4-250}$$

$$\dot{v}_{pk} = -\psi_{pk} v_{pk} \quad \text{Eq. 4-251}$$

$$\dot{v}_{qk} = -\psi_{qk} v_{qk} \quad \text{Eq. 4-252}$$

multiplying by $\bar{P}_{mw} \alpha_w v_w$, $\bar{P}_{l0k} \alpha_{pk} v_{pk}$ and $\bar{Q}_{0k} \alpha_{qk} v_{qk}$ to Eqs. 4-250 – 4-252, respectively,

rearranging to yield:

$$\bar{P}_{mw} \alpha_w v_w \dot{v}_w = -\bar{P}_{mw} \alpha_w \psi_w v_w^2 \quad \text{Eq. 4-253}$$

$$\bar{P}_{l0k} \alpha_{pk} v_{pk} \dot{v}_{pk} = -\bar{P}_{l0k} \alpha_{pk} \psi_{pk} v_{pk}^2 \quad \text{Eq. 4-254}$$

$$\bar{Q}_{0k} \alpha_{qk} v_{qk} \dot{v}_{qk} = -\bar{Q}_{0k} \alpha_{qk} \psi_{qk} v_{qk}^2 \quad \text{Eq. 4-255}$$

4.4.2 Well-defined energy function of the power system incorporating SCIG wind turbines

From Section 4.4.1, the involved equations are

4.4.2.1 Energy function and its derivative with white noise model

Combining and rearranging the equations in Section 4.4.1, yields

$$\begin{aligned}
& \sum_{i=1}^{m-p} \omega_0 M_i \dot{y}_i y_i - \sum_{i=1}^{m-p} P_{mi} \dot{x}_i + \sum_{i=1}^{m-p} \sum_{j=1}^n V_i V_j B_{ij} \sin(x_i - x_j) \dot{x}_i \\
& + \sum_{w=m-p+1}^m M_w y_w \omega_0 \dot{y}_w - \sum_{w=m-p+1}^m M_w \dot{y}_w k_b V_w \sin(k_a x_w + c_b) \\
& - \sum_{w=m-p+1}^m \bar{P}_{mw} \dot{x}_w + \sum_{w=m-p+1}^m \sum_{j=1}^n V_w V_j B_{wj} \sin(x_w - x_j) \dot{x}_w \\
& + \sum_{k=m+1}^n P_{lk} \dot{x}_k + \sum_{k=m+1}^n \sum_{j=1}^{n+m} V_k V_j B_{kj} \sin(x_k - x_j) \dot{x}_k \\
& = - \sum_{k=m+1}^n c_k \dot{x}_k^2 - \sum_{i=1}^{m-p} \omega_0 D_i y_i^2 + \omega_0 y_1 \left(\sum_{i=1}^{m-p} P_{mi} - \sum_{i=1}^{m-p} P_{ei} - \sum_{k=m+1}^n c_k \dot{x}_k \right)
\end{aligned} \tag{Eq. 4-256}$$

When expressing the above equation in the form of differential equation (first integral method), we will get an energy function derivation:

$$\begin{aligned}
& \left[\sum_{i=1}^{m-p} \frac{1}{2} \omega_0 M_i y_i^2 - \sum_{i=1}^{m-p} \bar{P}_{mi} x_i + \sum_{k=m+1}^n P_{lk} x_k - \sum_{w=m-p+1}^m \bar{P}_{mw} x_w \right. \\
& \left. + \sum_{w=m-p+1}^m \frac{1}{2} \omega_0 M_w y_w^2 - \sum_{w=m-p+1}^m \int_{y_{0w}}^{y_w} M_w k_b V_{sw} \sin(k_a (x_w - x_{ref}) + c_a) dy_w \right. \\
& \left. - \sum_{i=1}^{n-1} \sum_{j=i+1}^n V_i V_j B_{ij} \cos(x_i - x_j) + K \right] \\
& = - \sum_{i=1}^{m-p} \omega_0 D_i y_i^2 - \sum_{k=m+1}^n c_k \dot{x}_k^2 + \omega_0 y_0 \left(\sum_{i=1}^m P_{mi} - \sum_{j=1}^m P_{ej} - \sum_{k=m+1}^n c_k \dot{x}_k \right)
\end{aligned} \tag{Eq. 4-257}$$

The term in the bracket is the energy function of the power system (U) where a constant K is defined in which U will equal zero at the equilibrium point ($y_j = y_j^s$ and $x_j = x_j^s$), therefore:

$$K = \left\{ - \sum_{i=1}^{m-p} \frac{1}{2} \omega_0 M_i y_i^{s2} + \sum_{i=1}^{m-p} \bar{P}_{mi} x_i^s + \sum_{w=m-p+1}^m \bar{P}_{mw} x_w^s - \sum_{k=m+1}^n P_{lk} x_k^s \right. \\
\left. - \sum_{w=m-p+1}^m \frac{1}{2} \omega_0 M_w y_w^{s2} + \sum_{w=m-p+1}^m \int_{y_{0w}}^{y_w^s} \left[M_w k_b V_{sw} \sin(k_a (x_w - x_{ref}) + c_a) \right] dy_w \right. \\
\left. + \sum_{i=1}^{n-1} \sum_{j=i+1}^n V_i V_j B_{ij} \cos(x_i^s - x_j^s) \right\} \tag{Eq. 4-258}$$

The integral terms in the above equations can be approximated using the trapezoidal rule. The term with y_i^s is close to zero and can be neglected. Therefore, the energy function (U) of the power system including SCIG wind turbines with white noise can be stated as follows:

$$\begin{aligned}
U = & \frac{1}{2} \sum_{i=1}^{m-p} \omega_0 M_i y_i^2 + \frac{1}{2} \sum_{w=m-p+1}^m \omega_0 M_w (y_w^2 - y_w^{s2}) - \sum_{i=1}^{m-p} \bar{P}_{mi} (x_i - x_i^s) \\
& - \sum_{w=m-p+1}^m \bar{P}_{mw} (x_w - x_w^s) + \sum_{k=m+1}^n P_{lk} (x_k - x_k^s) \\
& - \sum_{w=m-p+1}^m \frac{1}{2} M_w k_b V_{sw} \left(\sin(k_a (x_w - x_{ref}) + c_a) + \sin(k_a (x_w^s - x_{ref}) + c_a) \right) (y_w - y_w^s) \\
& - \sum_{i=1}^{n-1} \sum_{j=i+1}^n \bar{V}_i \bar{V}_j \bar{B}_{ij} [\cos(x_i - x_j) - \cos(x_i^s - x_j^s)]
\end{aligned} \tag{Eq. 4-259}$$

The derivation of the energy function can be stated as

$$\frac{dU}{dt} = - \sum_{i=1}^{m-p} \omega_0 D_i y_i^2 - \sum_{k=m+1}^n c_k \dot{x}_k^2 + \omega_0 y_0 \left(\sum_{j=1}^m \bar{P}_{mj} - \sum_{j=1}^m \bar{P}_{ej} - \sum_{k=m+1}^n c_k \dot{x}_k \right) \tag{Eq. 4-260}$$

The last term on the right of Eq. 4-260 is diminished as proven by [9]. The derivation of the energy function is

$$\frac{dU}{dt} = - \sum_{i=1}^{m-p} \omega_0 D_i y_i^2 - \sum_{k=m+1}^n c_k \dot{x}_k^2 \tag{Eq. 4-261}$$

4.4.3 Well-defined energy function of the power system incorporating DFIG wind turbines

From Section 4.4.1, the involved equations are

4.4.3.1 Energy function and its derivative for colored noise model

Combining and rearranging the equations in Section 4.4.1 to yield:

$$\begin{aligned}
& \sum_{i=1}^{m-p} \omega_0 M_i \dot{y}_i y_i - \sum_{i=1}^{m-p} \bar{P}_{mi} \dot{x}_i + \sum_{i=1}^{m-p} \sum_{j=1}^n V_i V_j B_{ij} \sin(x_i - x_j) \dot{x}_i + \sum_{k=m+1}^n P_{lk} \dot{x}_k - \sum_{k=m+1}^n P_{lk} \alpha_k v_k \dot{x}_k \\
& + \sum_{k=m+1}^n \sum_{j=1}^{n+m} V_k V_j B_{kj} \sin(x_k - x_j) \dot{x}_k + \sum_{w=m-p+1}^m M_w y_w \omega_0 \dot{y}_w - \sum_{w=m-p+1}^m M_w \dot{y}_w k_b V_{sw} \sin(k_a (x_w - x_{ref}) + c_a) \\
& - \sum_{w=m-p+1}^m \bar{P}_{mw} \dot{x}_w - \sum_{w=m-p+1}^m \bar{P}_{mw} \alpha_w v_w \dot{x}_w + \sum_{w=m-p+1}^m \sum_{j=1}^n V_w V_j B_{wj} \sin(x_w - x_j) \dot{x}_w \\
& + \sum_{w=m-p+1}^m M_w \omega_0 k_d \bar{V}_{rq} \dot{y}_w - \sum_{w=m-p+1}^m \bar{P}_{mw} \alpha_w v_w \dot{v}_w - \sum_{k=m+1}^n \bar{P}_{lk} \alpha_k v_k \dot{v}_k \\
& = - \sum_{i=1}^{m-p} \omega_0 D_i y_i^2 - \sum_{k=m+1}^n c_k \dot{x}_k^2 + \omega_0 y_0 \left(\sum_{i=1}^{m-p} P_{mi} - \sum_{i=1}^{m-p} P_{ei} \right) + \omega_0 y_0 \left(\sum_{w=m-p+1}^m P_{mw} - \sum_{w=m-p+1}^m P_{ew} \right) \\
& - \omega_0 y_0 \sum_{k=m+1}^n c_k \dot{x}_k - \sum_{w=m-p+1}^m \frac{1}{\psi_w} \bar{P}_{mw} \alpha_w \dot{v}_w^2 - \sum_{k=m+1}^n \frac{1}{\psi_k} \bar{P}_{lk} \alpha_k \dot{v}_k^2
\end{aligned} \tag{Eq. 4-262}$$

Rearranging the above equation, we will get

$$\begin{aligned}
& \sum_{i=1}^{m-p} \omega_0 M_i y_i \dot{y}_i - \sum_{i=1}^{m-p} \bar{P}_{mi} \dot{x}_i + \sum_{k=m+1}^n P_{lk} \dot{x}_k - \sum_{\substack{w=m \\ -p+1}}^m \bar{P}_{mw} \dot{x}_w + \sum_{k=m+1}^n P_{lk} \alpha_k v_k \dot{x}_k - \sum_{\substack{w=m \\ -p+1}}^m \bar{P}_{mw} \alpha_w v_w \dot{x}_w \\
& + \sum_{\substack{w=m \\ -p+1}}^m M_w y_w \omega_0 \dot{y}_w - \sum_{\substack{w=m \\ -p+1}}^m M_w k_b V_{sw} \sin(k_a (x_w - x_{ref}) + c_a) \dot{y}_w + \sum_{\substack{w=m \\ -p+1}}^m M_w \omega_0 k_d \bar{V}_{rq} \dot{y}_w \\
& + \sum_{i=1}^{n-1} \sum_{j=i+1}^n V_i V_j B_{ij} \sin(x_i - x_j) (\dot{x}_i - \dot{x}_j) + \sum_{\substack{w=m \\ -p+1}}^m \bar{P}_{mw} \alpha_w v_w \dot{v}_w + \sum_{k=m+1}^n \bar{P}_{lk} \alpha_k v_k \dot{v}_k \\
& = - \sum_{i=1}^{m-p} \omega_0 D_i y_i^2 - \sum_{k=m+1}^n c_k \dot{x}_k^2 - \sum_{\substack{w=m \\ -p+1}}^m \frac{1}{\psi_w} \bar{P}_{mw} \alpha_w \dot{v}_w^2 - \sum_{k=m+1}^n \frac{1}{\psi_k} \bar{P}_{lk} \alpha_k \dot{v}_k^2 + \omega_0 y_0 \left(\sum_{i=1}^m P_{mi} - \sum_{j=1}^m P_{ej} - \sum_{k=m+1}^n c_k \dot{x}_k \right)
\end{aligned}$$

Eq. 4-263

When expressing the above equations in the form of differential equations (first integral method), we will get the energy function derivation

$$\begin{aligned}
& \left[\sum_{i=1}^{m-p} \frac{1}{2} \omega_0 M_i y_i^2 - \sum_{i=1}^{m-p} \bar{P}_{mi} x_i + \sum_{k=m+1}^n P_{lk} x_k - \sum_{\substack{w=m \\ -p+1}}^m \bar{P}_{mw} x_w - \sum_{k=m+1}^n \int_{x_{0k}}^{x_k} P_{lk} \alpha_k v_k dx_k - \sum_{\substack{w=m \\ -p+1}}^m \int_{x_{0w}}^{x_w} \bar{P}_{mw} \alpha_w v_w dx_w \right. \\
& \frac{d}{dt} + \sum_{\substack{w=m \\ -p+1}}^m \frac{1}{2} \omega_0 M_w y_w^2 - \sum_{\substack{w=m \\ -p+1}}^m \int_{y_{0w}}^{y_w} M_w k_b V_{sw} \sin(k_a (x_w - x_{ref}) + c_a) dy_w + \sum_{\substack{w=m \\ -p+1}}^m \int_{y_{0w}}^{y_w} M_w \omega_0 k_d \bar{V}_{rq} dy_w \\
& \left. - \sum_{i=1}^{n-1} \sum_{j=i+1}^n V_i V_j B_{ij} \cos(x_i - x_j) + \sum_{\substack{w=m \\ -p+1}}^m \frac{1}{2} \bar{P}_{mw} \alpha_w v_w^2 + \sum_{k=m+1}^n \frac{1}{2} \bar{P}_{lk} \alpha_k v_k^2 + K \right] \\
& = - \sum_{i=1}^{m-p} \omega_0 D_i y_i^2 - \sum_{k=m+1}^n c_k \dot{x}_k^2 - \sum_{\substack{w=m \\ -p+1}}^m \frac{1}{\psi_w} \bar{P}_{mw} \alpha_w \dot{v}_w^2 - \sum_{k=m+1}^n \frac{1}{\psi_k} \bar{P}_{lk} \alpha_k \dot{v}_k^2 + \omega_0 y_0 \left(\sum_{i=1}^m P_{mi} - \sum_{j=1}^m P_{ej} - \sum_{k=m+1}^n c_k \dot{x}_k \right)
\end{aligned}$$

Eq. 4-264

$$\begin{aligned}
& \left[\sum_{i=1}^{m-p} \frac{1}{2} \omega_0 M_i y_i^2 - \sum_{i=1}^{m-p} \bar{P}_{mi} x_i - \sum_{\substack{w=m \\ -p+1}}^m \bar{P}_{mw} x_w + \sum_{k=m+1}^n P_{lk} x_k - \sum_{k=m+1}^n \int_{x_{0k}}^{x_k} P_{lk} \alpha_k v_k dx_k - \sum_{\substack{w=m \\ -p+1}}^m \int_{x_{0w}}^{x_w} \bar{P}_{mw} \alpha_w v_w dx_w \right. \\
& + \sum_{\substack{w=m \\ -p+1}}^m \frac{1}{2} \omega_0 M_w y_w^2 - \sum_{\substack{w=m \\ -p+1}}^m \int_{y_{0w}}^{y_w} \left[M_w k_b V_{sw} \sin(k_a (x_w - x_{ref}) + c_a) \right] dy_w \\
& + \sum_{\substack{w=m \\ -p+1}}^m \int_{y_{0w}}^{y_w} \left[M_w \omega_0 k_d \left(k_p k_{op} (y_w + 1)^2 - k_p k_m \bar{P}_{ew} (1 + y_w)^{-1} - y_w \left(k_{c2} \bar{V}_{sw} \cos(k_a (x_w - x_{ref}) + c_a) + k_{c1} \bar{V}_w \right) \right) \right] dy_w \\
& \left. - \sum_{i=1}^{n-1} \sum_{j=i+1}^n V_i V_j B_{ij} \cos(x_i - x_j) + \sum_{\substack{w=m \\ -p+1}}^m \frac{1}{2} \bar{P}_{mw} \alpha_w v_w^2 + \sum_{k=m+1}^n \frac{1}{2} \bar{P}_{lk} \alpha_k v_k^2 + K \right] \\
& = - \sum_{i=1}^{m-p} \omega_0 D_i y_i^2 - \sum_{k=m+1}^n c_k \dot{x}_k^2 - \sum_{\substack{w=m \\ -p+1}}^m \frac{1}{\psi_w} \bar{P}_{mw} \alpha_w \dot{v}_w^2 - \sum_{k=m+1}^n \frac{1}{\psi_k} \bar{P}_{lk} \alpha_k \dot{v}_k^2 + \omega_0 y_0 \left(\sum_{i=1}^m P_{mi} - \sum_{j=1}^m P_{ej} - \sum_{k=m+1}^n c_k \dot{x}_k \right)
\end{aligned}$$

Eq. 4-265

The terms in the brackets is the energy function of the power system (U) where a constant K is defined in which U will equal to zero at equilibrium point ($y_j = y_j^s$ and $x_j = x_j^s$), therefore

$$K = \left\{ \begin{aligned} & - \sum_{i=1}^{m-p} \frac{1}{2} \omega_0 M_i y_i^{s2} + \sum_{i=1}^{m-p} \bar{P}_{mi} x_i^s + \sum_{\substack{w=m \\ -p+1}}^m \bar{P}_{mw} x_w^s - \sum_{k=m+1}^n P_{lk} x_k^s + \sum_{k=m+1}^n \int_{x_{0k}}^{x_k^s} P_{lk} \alpha_k \nu_k dx_k + \sum_{\substack{w=m \\ -p+1}}^m \int_{x_{0w}}^{x_w^s} \bar{P}_{mw} \alpha_w \nu_w dx_w \\ & - \sum_{\substack{w=m \\ -p+1}}^m \frac{1}{2} \omega_0 M_w y_w^{s2} + \sum_{\substack{w=m \\ -p+1}}^m \int_{y_{0w}}^{y_w^s} \left[M_w k_b V_{sw} \sin(k_a (x_w - x_{ref}) + c_a) \right] dy_w \\ & - \sum_{\substack{w=m \\ -p+1}}^m \int_{y_{0w}}^{y_w^s} \left[M_w \omega_0 k_d \left(k_p (k_{op} (y_w + 1)^2 - k_m \bar{P}_{ew} (1 + y_w)^{-1}) - y_w (k_{c2} \bar{V}_{sw} \cos(k_a (x_w - x_{ref}) + c_a) + k_{c1} \bar{V}_w) \right) \right] dy_w \\ & + \sum_{i=1}^{n-1} \sum_{j=i+1}^n V_i V_j B_{ij} \cos(x_i^s - x_j^s) + \sum_{\substack{w=m \\ -p+1}}^m \frac{1}{2} \bar{P}_{mw} \alpha_w \nu_w^{s2} + \sum_{k=m+1}^n \frac{1}{2} \bar{P}_{lk} \alpha_k \nu_k^{s2} \end{aligned} \right\}$$

Eq. 4-266

If ν_w does not relate to x_w , the following solution is acceptable.

$$\begin{aligned}
& - \sum_{k=m+1}^n \int_{x_{0k}}^{x_k} P_{lk} \alpha_k v_k dx_k + \sum_{k=m+1}^n \int_{x_{0k}}^{x_k^s} P_{lk} \alpha_k v_k dx_k - \sum_{w=m}^m \int_{x_{0w}}^{x_w} \bar{P}_{mw} \alpha_w v_w dx_w + \sum_{w=m}^m \int_{x_{0w}}^{x_w^s} \bar{P}_{mw} \alpha_w v_w dx_w \\
& - \sum_{w=m}^m \int_{y_{0w}}^{y_w} \left[M_w k_b V_{sw} \sin(k_a (x_w - x_{ref}) + c_a) \right] dy_w + \sum_{w=m}^m \int_{y_{0w}}^{y_w^s} \left[M_w k_b V_{sw} \sin(k_a (x_w - x_{ref}) + c_a) \right] dy_w \\
& + \sum_{w=m}^m \int_{y_{0w}}^{y_w} \left[M_w \omega_0 k_d \left(k_p k_{op} (y_w + 1)^2 - k_p k_m \bar{P}_{ew} (1 + y_w)^{-1} - y_w \left(k_{c2} \bar{V}_{sw} \cos(k_a (x_w - x_{ref}) + c_a) + k_{c1} \bar{V}_w \right) \right) \right] dy_w \\
& - \sum_{w=m}^m \int_{y_{0w}}^{y_w^s} \left[M_w \omega_0 k_d \left(k_p \left(k_{op} (y_w + 1)^2 - k_m \bar{P}_{ew} (1 + y_w)^{-1} \right) - y_w \left(k_{c2} \bar{V}_{sw} \cos(k_a (x_w - x_{ref}) + c_a) + k_{c1} \bar{V}_w \right) \right) \right] dy_w \\
& = - \sum_{k=m+1}^n \int_{x_k^s}^{x_k} P_{lk} \alpha_k v_k dx_k - \sum_{w=m}^m \int_{x_w^s}^{x_w} \bar{P}_{mw} \alpha_w v_w dx_w - \sum_{w=m}^m \int_{y_w^s}^{y_w} \left[M_w k_b V_{sw} \sin(k_a (x_w - x_{ref}) + c_a) \right] dy_w \\
& + \sum_{w=m}^m \int_{y_w^s}^{y_w} \left(M_w \omega_0 k_d k_p k_{op} (y_w + 1)^2 \right) dy_w - \sum_{w=m}^m \int_{y_w^s}^{y_w} M_w \omega_0 k_d k_p k_m \bar{P}_{ew} \frac{d(y_w + 1)}{(y_w + 1)} \\
& - \sum_{w=m}^m \int_{y_w^s}^{y_w} M_w \omega_0 k_d k_{c1} \bar{V}_w y_w dy_w - \sum_{w=m}^m \int_{y_w^s}^{y_w} M_w \omega_0 k_d k_{c2} \bar{V}_{sw} \cos(k_a (x_w - x_{ref}) + c_a) y_w dy_w \\
& = - \sum_{k=m+1}^n P_{lk} \alpha_k v_k (x_k - x_k^s) - \sum_{w=m}^m \bar{P}_{mw} \alpha_w v_w (x_w - x_w^s) \\
& - \sum_{w=m}^m \frac{1}{2} M_w k_b V_{sw} \left(\sin(k_a (x_w - x_{ref}) + c_a) + \sin(k_a (x_w^s - x_{ref}) + c_a) \right) (y_w - y_w^s) \\
& + \sum_{w=m}^m \frac{1}{3} M_w \omega_0 k_d k_p k_{op} \left((y_w + 1)^3 - (y_w^s + 1)^3 \right) - \sum_{w=m}^m \frac{1}{2} M_w \omega_0 k_d k_p k_m \left(\frac{\bar{P}_{ew}}{(y_w + 1)} + \frac{\bar{P}_{ew}^s}{(y_w^s + 1)} \right) (y_w - y_w^s) \\
& - \sum_{w=m}^m \frac{1}{2} M_w \omega_0 k_d k_{c1} \bar{V}_w (y_w^2 - y_w^{s2}) \\
& - \sum_{w=m}^m \frac{1}{2} M_w \omega_0 k_d k_{c2} \bar{V}_{sw} \left(\cos(k_a (x_w - x_{ref}) + c_a) y_w + \cos(k_a (x_w^s - x_{ref}) + c_a) y_w^s \right) (y_w - y_w^s)
\end{aligned}$$

Eq. 4-267

The integral terms in the above equation can be approximated using the trapezoidal rule. The term with y_i^s is close to zero and can be neglected. Therefore, the energy function (U) of the power system including DFIG wind turbines with colored noise can be stated as follows:

$$\begin{aligned}
U = & \frac{1}{2} \sum_{i=1}^{m-p} \omega_0 M_i y_i^2 + \frac{1}{2} \sum_{w=m-p+1}^m \omega_0 M_w (y_w^2 - y_w^{s2}) - \sum_{i=1}^{m-p} \bar{P}_{mi} (x_i - x_i^s) - \sum_{w=m-p+1}^m \bar{P}_{mw} (x_w - x_w^s) + \sum_{k=m+1}^n P_{lk} (x_k - x_k^s) \\
& - \sum_{\substack{w=m \\ -p+1}}^m \frac{1}{2} M_w k_b V_{sw} \left(\sin(k_a (x_w - x_{ref}) + c_a) + \sin(k_a (x_w^s - x_{ref}) + c_a) \right) (y_w - y_w^s) \\
& + \sum_{\substack{w=m \\ -p+1}}^m \frac{1}{3} M_w \omega_0 k_d k_p k_{op} \left((y_w + 1)^3 - (y_w^s + 1)^3 \right) \\
& - \sum_{\substack{w=m \\ -p+1}}^m \frac{1}{2} M_w \omega_0 k_d k_p k_m \left(\frac{\bar{P}_{ew}}{(y_w + 1)} + \frac{\bar{P}_{ew}^s}{(y_w^s + 1)} \right) (y_w - y_w^s) \\
& - \sum_{\substack{w=m \\ -p+1}}^m \frac{1}{2} M_w \omega_0 k_d k_{c1} \bar{V}_w (y_w^2 - y_w^{s2}) \\
& - \sum_{\substack{w=m \\ -p+1}}^m \frac{1}{2} M_w \omega_0 k_d k_{c2} \bar{V}_{sw} \left(\cos(k_a (x_w - x_{ref}) + c_a) y_w + \cos(k_a (x_w^s - x_{ref}) + c_a) y_w^s \right) (y_w - y_w^s) \\
& - \sum_{i=1}^{n-1} \sum_{j=i+1}^n \bar{V}_i \bar{V}_j \bar{B}_{ij} \left[\cos(x_i - x_j) - \cos(x_i^s - x_j^s) \right] \\
& - \sum_{\substack{w=m \\ -p+1}}^m \bar{P}_{mw} \alpha_w v_w (x_w - x_w^s) - \sum_{k=m+1}^n P_{lk} \alpha_k v_k (x_k - x_k^s) \\
& + \sum_{\substack{w=m \\ -p+1}}^m \frac{1}{2} \bar{P}_{mw} \alpha_w (v_w^2 - v_w^{s2}) + \sum_{k=m+1}^n \frac{1}{2} \bar{P}_{lk} \alpha_k (v_k^2 - v_k^{s2})
\end{aligned}$$

Eq. 4-268

The derivation of the energy function can be stated as:

$$\frac{dU}{dt} = - \sum_{i=1}^{m-p} \omega_0 D_i y_i^2 - \sum_{k=m+1}^n c_k \dot{x}_k^2 - \sum_{\substack{w=m \\ -p+1}}^m \frac{1}{\psi_w} \bar{P}_{mw} \alpha_w \dot{v}_w^2 - \sum_{k=m+1}^n \frac{1}{\psi_k} \bar{P}_{lk} \alpha_k \dot{v}_k^2 + \omega_0 y_0 \left(\sum_{j=1}^m \bar{P}_{mj} - \sum_{j=1}^m \bar{P}_{ej} - \sum_{k=m+1}^n c_k \dot{x}_k \right)$$

Eq. 4-269

The last term on the right of Eq. 4-269 is diminished as proven by [9] where j denotes both synchronous and induction generators. The derivation of the energy function is

$$\frac{dU}{dt} = - \sum_{i=1}^{m-p} \omega_0 D_i y_i^2 - \sum_{k=m+1}^n c_k \dot{x}_k^2 - \sum_{\substack{w=m \\ -p+1}}^m \frac{1}{\psi_w} \bar{P}_{mw} \alpha_w \dot{v}_w^2 - \sum_{k=m+1}^n \frac{1}{\psi_k} \bar{P}_{lk} \alpha_k \dot{v}_k^2$$

Eq. 4-270

4.4.3.2 Energy function and its derivative for the white noise model

For the white noise model, all the terms with v are zero, the well-defined energy function becomes:

$$\begin{aligned}
U = & \frac{1}{2} \sum_{i=1}^{m-p} \omega_0 M_i y_i^2 + \frac{1}{2} \sum_{w=m-p+1}^m \omega_0 M_w (y_w^2 - y_w^{s2}) - \sum_{i=1}^{m-p} \bar{P}_{mi} (x_i - x_i^s) - \sum_{w=m-p+1}^m \bar{P}_{mw} (x_w - x_w^s) + \sum_{k=m+1}^n P_{lk} (x_k - x_k^s) \\
& - \sum_{w=m-p+1}^m \frac{1}{2} M_w k_b V_{sw} \left(\sin(k_a (x_w - x_{ref}) + c_a) + \sin(k_a (x_w^s - x_{ref}) + c_a) \right) (y_w - y_w^s) \\
& + \sum_{w=m-p+1}^m \frac{1}{3} M_w \omega_0 k_d k_p k_{op} \left((y_w + 1)^3 - (y_w^s + 1)^3 \right) - \sum_{w=m-p+1}^m \frac{1}{2} M_w \omega_0 k_d k_p k_m \left(\frac{\bar{P}_{ew}}{(y_w + 1)} + \frac{\bar{P}_{ew}^s}{(y_w^s + 1)} \right) (y_w - y_w^s) \\
& - \sum_{w=m-p+1}^m \frac{1}{2} M_w \omega_0 k_d k_{c2} \bar{V}_{sw} \left(\cos(k_a (x_w - x_{ref}) + c_a) y_w + \cos(k_a (x_w^s - x_{ref}) + c_a) y_w^s \right) (y_w - y_w^s) \\
& - \sum_{w=m-p+1}^m \frac{1}{2} M_w \omega_0 k_d k_{c1} \bar{V}_w (y_w^2 - y_w^{s2}) - \sum_{i=1}^{n-1} \sum_{j=i+1}^n \bar{V}_i \bar{V}_j \bar{B}_{ij} \left[\cos(x_i - x_j) - \cos(x_i^s - x_j^s) \right]
\end{aligned}$$

Eq. 4-271

The derivation of energy for the white noise model can be stated as

$$\frac{dU}{dt} = - \sum_{i=1}^{m-p} \omega_0 D_i y_i^2 - \sum_{k=m+1}^n c_k \dot{x}_k^2$$

Eq. 4-272

4.4.4 Well-defined energy function of the power system incorporating DFIG wind turbines for voltage stability analysis

From Section 4.4.1, the equations involved in voltage stability analysis are:

4.4.4.1 Energy function and its derivative for voltage stability analysis

applying colored noise

Combining and rearranging the equations in Section 4.4.1, we will get

$$\begin{aligned}
& \sum_{i=1}^{m-p} \omega_0 M_i y_i \dot{y}_i - \sum_{i=1}^{m-p} \bar{P}_{mi} \dot{x}_i - \sum_{w=m-p+1}^m \bar{P}_{mw} (1 + \alpha_w \nu_w) \dot{x}_w \\
& + \sum_{k=m+1}^n P_{l0k} V_k^2 (1 - \alpha_{pk} \nu_{pk}) \dot{x}_k + \sum_{k=m+1}^n \bar{Q}_{0k} (1 - \alpha_{qk} \nu_{qk}) \bar{V}_k \dot{\bar{V}}_k \\
& + \sum_{w=m-p+1}^m M_w y_w \omega_0 \dot{y}_w - \sum_{w=m-p+1}^m M_w k_b V_{sw} \sin(k_a (x_w - x_{ref}) + c_a) \dot{y}_w + \sum_{w=m-p+1}^m M_w \omega_0 k_d \bar{V}_{rq} \dot{y}_w \\
& + \sum_{i=1}^{n-1} \sum_{j=i+1}^n V_i V_j B_{ij} \sin(x_i - x_j) (\dot{x}_i - \dot{x}_j) - \sum_{k=m+1}^n \sum_{l=1}^n \bar{V}_l B_{kl} \cos(x_k - x_l) \dot{\bar{V}}_k \\
& + \sum_{w=m-p+1}^m \bar{P}_{mw} \alpha_w \nu_w \dot{\nu}_w + \sum_{k=m+1}^n \bar{P}_{l0k} \alpha_{pk} \nu_{pk} \dot{\nu}_{pk} + \sum_{k=m+1}^n \bar{Q}_{0k} \alpha_{qk} \nu_{qk} \dot{\nu}_{qk} \\
& = - \sum_{i=1}^{m-p} \omega_0 D_i y_i^2 - \sum_{k=m+1}^n c_k \dot{x}_k^2 - \sum_{k=m+1}^n \lambda_k \dot{\bar{V}}_k^2 - \sum_{w=m-p+1}^m \frac{1}{\psi_w} \bar{P}_{mw} \alpha_w \dot{\nu}_w^2 - \sum_{k=m+1}^n \frac{1}{\psi_{pk}} \bar{P}_{l0k} \alpha_{pk} \dot{\nu}_{pk}^2 \\
& - \sum_{k=m+1}^n \frac{1}{\psi_{qk}} \bar{Q}_{0k} \alpha_{qk} \dot{\nu}_{qk}^2 + \omega_0 y_0 \left(\sum_{i=1}^m P_{mi} - \sum_{j=1}^m P_{ej} - \sum_{k=m+1}^n c_k \dot{x}_k \right)
\end{aligned}$$

Eq. 4-273

If given

$$\begin{aligned}
 F_1 &= \sum_{i=1}^{n-1} \sum_{j=i+1}^n V_i V_j B_{ij} \sin(x_i - x_j) (\dot{x}_i - \dot{x}_j) \\
 F_1 &= F_{1A} + F_{1B} + F_{1C} = \sum_{i=1}^{m-1} \sum_{l=i+1}^m V_i V_l B_{il} \sin(x_i - x_l) (\dot{x}_i - \dot{x}_l) \\
 &\quad + \sum_{i=1}^{m-1} \sum_{k=m+1}^n V_i V_k B_{ik} \sin(x_i - x_k) (\dot{x}_i - \dot{x}_k) \\
 &\quad + \sum_{k=m+1}^{n-1} \sum_{l=k+1}^n V_k V_l B_{kl} \sin(x_k - x_l) (\dot{x}_k - \dot{x}_l)
 \end{aligned} \tag{Eq. 4-274}$$

$$\begin{aligned}
 F_2 &= \sum_{k=m+1}^n \sum_{l=1}^n \bar{V}_l B_{kl} \cos(x_k - x_l) \dot{\bar{V}}_k \\
 F_2 &= F_{2B} + F_{2C} + F_{2D} + F_{2E} = \sum_{i=1}^{m-1} \sum_{k=m+1}^n \bar{V}_i B_{ik} \cos(x_i - x_k) \dot{\bar{V}}_k \\
 &\quad + \sum_{k=m+1}^{n-1} \sum_{l=k+1}^n \bar{V}_l B_{kl} \cos(x_k - x_l) \dot{\bar{V}}_k \\
 &\quad + \sum_{l=m+2}^n \sum_{k=m+1}^{l-1} \bar{V}_k B_{kl} \cos(x_k - x_l) \dot{\bar{V}}_l + \sum_{k=m+1}^n B_{kk} \bar{V}_k \dot{\bar{V}}_k
 \end{aligned} \tag{Eq. 4-275}$$

$$\begin{aligned}
 \dot{F}_{3B} &= -F_{1B} + F_{2B} = \frac{d}{dt} \sum_{i=1}^{m-1} \sum_{k=m+1}^n \bar{V}_i \bar{V}_k B_{ik} \cos(x_i - x_k) \\
 &= \left(\begin{aligned} & - \sum_{i=1}^{m-1} \sum_{k=m+1}^n V_i V_k B_{ik} \sin(x_i - x_k) (\dot{x}_i - \dot{x}_k) \\ & + \sum_{i=1}^{m-1} \sum_{k=m+1}^n \bar{V}_i B_{ik} \cos(x_i - x_k) \dot{\bar{V}}_k \end{aligned} \right)
 \end{aligned} \tag{Eq. 4-276}$$

$$\begin{aligned}
 \dot{F}_{3C} &= -F_{1C} + F_{2C} + F_{2D} = \frac{d}{dt} \sum_{k=m+1}^{n-1} \sum_{l=k+1}^n \bar{V}_l \bar{V}_k B_{kl} \cos(x_k - x_l) \\
 &= \left(\begin{aligned} & - \sum_{k=m+1}^{n-1} \sum_{l=k+1}^n V_k V_l B_{kl} \sin(x_k - x_l) (\dot{x}_k - \dot{x}_l) \\ & + \sum_{k=m+1}^{n-1} \sum_{l=k+1}^n \bar{V}_l B_{kl} \cos(x_k - x_l) \dot{\bar{V}}_k \\ & + \sum_{l=m+1}^n \sum_{\substack{k=m+1 \\ l \neq k}}^{l-1} \bar{V}_k B_{kl} \cos(x_k - x_l) \dot{\bar{V}}_l \end{aligned} \right)
 \end{aligned} \tag{Eq. 4-277}$$

Therefore

$$\begin{aligned}
F_1 - F_2 &= -(F_2 - F_1) = - \left(\sum_{k=m+1}^n \sum_{l=1}^n \bar{V}_l B_{kl} \cos(x_k - x_l) \dot{\bar{V}}_k \right. \\
&\quad \left. - \sum_{i=1}^{n-1} \sum_{j=i+1}^n V_i V_j B_{ij} \sin(x_i - x_j) (\dot{x}_i - \dot{x}_j) \right) \\
&= -(F_{2B} + F_{2C} + F_{2D} + F_{2E} - F_{1A} - F_{1B} - F_{1C}) \quad \text{Eq. 4-278} \\
&= -(\dot{F}_{3B} + \dot{F}_{3C} + F_{2E} - F_{1A})
\end{aligned}$$

When expressing the above equations in the form of differential equations (first integral method), we will get the energy function derivation

$$\begin{aligned}
&\left[\sum_{i=1}^{m-p} \frac{1}{2} \omega_0 M_i y_i^2 - \sum_{i=1}^{m-p} \bar{P}_{mi} x_i - \sum_{\substack{w=m \\ -p+1}}^m \bar{P}_{mw} x_w + \sum_{k=m+1}^n \frac{1}{2} \bar{Q}_{0k} \bar{V}_k^2 + \sum_{\substack{w=m \\ -p+1}}^m \frac{1}{2} \omega_0 M_w y_w^2 \right. \\
&\quad - \sum_{\substack{w=m \\ -p+1}}^m \int_0^{x_w} \bar{P}_{mw} \alpha_w v_w dx_w + \sum_{k=m+1}^n \int_0^{x_k} P_{l0k} \bar{V}_k^2 (1 - \alpha_{pk} v_{pk}) dx_k - \sum_{k=m+1}^n \int_0^{\bar{V}_k} \bar{Q}_{0k} \alpha_{qk} v_{qk} \bar{V}_k d\bar{V}_k \\
&\quad - \sum_{\substack{w=m \\ -p+1}}^m \int_0^{y_w} M_w k_b V_{sw} \sin(k_a (x_w - x_{ref}) + c_a) dy_w + \sum_{\substack{w=m \\ -p+1}}^m \int_0^{y_w} M_w \omega_0 k_d \bar{V}_{rq} dy_w \\
&\quad - \sum_{i=1}^{m-1} \sum_{k=m+1}^n \bar{V}_i \bar{V}_k B_{ik} \cos(x_i - x_k) - \sum_{k=m+1}^{n-1} \sum_{l=k+1}^n \bar{V}_l \bar{V}_k B_{kl} \cos(x_k - x_l) \\
&\quad - \sum_{i=1}^{m-1} \sum_{l=i+1}^m V_i V_l B_{ij} \cos(x_i - x_j) - \sum_{k=m+1}^n \frac{1}{2} B_{kk} \bar{V}_k^2 \\
&\quad \left. + \sum_{\substack{w=m \\ -p+1}}^m \frac{1}{2} \bar{P}_{mw} \alpha_w v_w^2 + \sum_{k=m+1}^n \frac{1}{2} \bar{P}_{l0k} \alpha_{pk} v_{pk}^2 + \sum_{k=m+1}^n \frac{1}{2} \bar{Q}_{0k} \alpha_{qk} v_{qk}^2 + K \right] \\
&= - \sum_{i=1}^{m-p} \omega_0 D_i y_i^2 - \sum_{k=m+1}^n c_k \dot{x}_k^2 - \sum_{k=m+1}^n \lambda_k \dot{\bar{V}}_k^2 - \sum_{\substack{w=m \\ -p+1}}^m \frac{1}{\psi_w} \bar{P}_{mw} \alpha_w \dot{v}_w^2 - \sum_{k=m+1}^n \frac{1}{\psi_{pk}} \bar{P}_{l0k} \alpha_{pk} \dot{v}_{pk}^2 \quad \text{Eq. 4-279} \\
&\quad - \sum_{k=m+1}^n \frac{1}{\psi_{qk}} \bar{Q}_{0k} \alpha_{qk} \dot{v}_{qk}^2 + \omega_0 y_0 \left(\sum_{i=1}^m P_{mi} - \sum_{j=1}^m P_{ej} - \sum_{k=m+1}^n c_k \dot{x}_k \right)
\end{aligned}$$

Where

$$\begin{aligned}
& \left[\sum_{i=1}^{m-p} \frac{1}{2} \omega_0 M_i y_i^2 - \sum_{i=1}^{m-p} \bar{P}_{mi} x_i - \sum_{\substack{w=m \\ -p+1}}^m \bar{P}_{mw} x_w + \sum_{k=m+1}^n \frac{1}{2} \bar{Q}_{0k} \bar{V}_k^2 + \sum_{\substack{w=m \\ -p+1}}^m \frac{1}{2} \omega_0 M_w y_w^2 \right. \\
& - \sum_{\substack{w=m \\ -p+1}}^m \int_0^{x_w} \bar{P}_{mw} \alpha_w v_w dx_w - \sum_{k=m+1}^n \int_0^{x_k} P_{l0k} \bar{V}_k^2 (1 - \alpha_{pk} v_{pk}) dx_k - \sum_{k=m+1}^n \int_0^{\bar{V}_k} \bar{Q}_{0k} \alpha_{qk} v_{qk} \bar{V}_k d\bar{V}_k \\
& - \sum_{\substack{w=m \\ -p+1}}^m \int_0^{y_w} \left[M_w k_b V_{sw} \sin(k_a (x_w - x_{ref}) + c_a) \right] dy_w \\
& \left. + \sum_{\substack{w=m \\ -p+1}}^m \int_0^{y_w} \left[M_w \omega_0 k_d \left(k_p k_{op} (y_w + 1)^2 - k_p k_m \bar{P}_{ew} (1 - y_w) - y_w \left(k_{c2} \bar{V}_{sw} \cos(k_a (x_w - x_{ref}) + c_a) + k_{c1} \bar{V}_w \right) \right) \right] dy_w \right. \\
& - \sum_{i=1}^{m-1} \sum_{k=m+1}^n \bar{V}_i \bar{V}_k B_{ik} \cos(x_i - x_k) - \sum_{k=m+1}^{n-1} \sum_{l=k+1}^n \bar{V}_l \bar{V}_k B_{kl} \cos(x_k - x_l) \\
& - \sum_{i=1}^{m-1} \sum_{l=i+1}^m V_i V_l B_{ij} \cos(x_i - x_j) - \sum_{k=m+1}^n \frac{1}{2} B_{kk} \bar{V}_k^2 \\
& \left. + \sum_{\substack{w=m \\ -p+1}}^m \frac{1}{2} \bar{P}_{mw} \alpha_w v_w^2 + \sum_{k=m+1}^n \frac{1}{2} \bar{P}_{l0k} \alpha_{pk} v_{pk}^2 + \sum_{k=m+1}^n \frac{1}{2} \alpha_{qk} \bar{Q}_{0k} v_{qk}^2 + K \right] \\
& = - \sum_{i=1}^{m-p} \omega_0 D_i y_i^2 - \sum_{k=m+1}^n c_k \dot{x}_k^2 - \sum_{k=m+1}^n \lambda_k \dot{\bar{V}}_k^2 - \sum_{\substack{w=m \\ -p+1}}^m \frac{1}{\psi_w} \bar{P}_{mw} \alpha_w \dot{v}_w^2 - \sum_{k=m+1}^n \frac{1}{\psi_k} \bar{P}_{l0k} \alpha_{pk} \dot{v}_{pk}^2 - \sum_{k=m+1}^n \frac{1}{\psi_k} \bar{Q}_{0k} \alpha_{qk} \dot{v}_{qk}^2 \\
& + \omega_0 y_0 \left(\sum_{i=1}^m P_{mi} - \sum_{j=1}^m P_{ej} - \sum_{k=m+1}^n c_k \dot{x}_k \right)
\end{aligned}$$

Eq. 4-280

The terms in the brackets are the energy functions of the power system (U) where a constant K is defined in which U will equal to zero at the equilibrium point ($y_j = y_j^s$ and $x_j = x_j^s$), therefore

$$K = \left\{ \begin{aligned} & - \sum_{i=1}^{m-p} \frac{1}{2} \omega_0 M_i y_i^{s^2} + \sum_{i=1}^{m-p} \bar{P}_{mi} x_i^s + \sum_{\substack{w=m \\ -p+1}}^m \bar{P}_{mw} x_w^s - \sum_{k=m+1}^n \frac{1}{2} \bar{Q}_{0k} \bar{V}_k^{s^2} - \sum_{\substack{w=m \\ -p+1}}^m \frac{1}{2} \omega_0 M_w y_w^{s^2} \\ & + \sum_{\substack{w=m \\ -p+1}}^m \int_0^{x_w^s} \bar{P}_{mw} \alpha_w v_w dx_w - \sum_{k=m+1}^n \int_0^{x_k^s} P_{l0k} \bar{V}_k^2 (1 - \alpha_{pk} v_{pk}) dx_k + \sum_{k=m+1}^n \int_0^{\bar{V}_k^s} \bar{Q}_{0k} \alpha_{qk} v_{qk} \bar{V}_k d\bar{V}_k \\ & + \sum_{\substack{w=m \\ -p+1}}^m \int_0^{y_w^s} \left[M_w k_b V_{sw} \sin(k_a (x_w - x_{ref}) + c_a) \right] dy_w \\ & - \sum_{\substack{w=m \\ -p+1}}^m \int_0^{y_w^s} \left[M_w \omega_0 k_d \left(k_p (k_{op} (y_w + 1) - k_m \bar{P}_{ew} (1 - y_w)) - y_w (k_{c2} \bar{V}_{sw} \cos(k_a (x_w - x_{ref}) + c_a) + k_{c1} \bar{V}_w) \right) \right] dy_w \\ & + \sum_{i=1}^{m-1} \sum_{k=m+1}^n \bar{V}_i \bar{V}_k^s B_{ik} \cos(x_i^s - x_k^s) + \sum_{k=m+1}^{n-1} \sum_{l=k+1}^n \bar{V}_l \bar{V}_k^s B_{kl} \cos(x_k^s - x_l^s) \\ & + \sum_{i=1}^{m-1} \sum_{l=i+1}^m V_i V_j B_{ij} \cos(x_i^s - x_j^s) + \sum_{k=m+1}^n \frac{1}{2} B_{kk} \bar{V}_k^{s^2} - \sum_{\substack{w=m \\ -p+1}}^m \frac{1}{2} \bar{P}_{mw} \alpha_w v_w^{s^2} - \sum_{k=m+1}^n \frac{1}{2} \bar{P}_{l0k} \alpha_{pk} v_{pk}^{s^2} - \sum_{k=m+1}^n \frac{1}{2} \alpha_{qk} \bar{Q}_{0k} v_{qk}^{s^2} \end{aligned} \right\}$$

Eq. 4-281

The integral terms in the above equation can be approximated using the trapezoidal rule. The term with y_i^s is close to zero and can be neglected. Therefore, the energy function (U) can be stated as follows:

$$\begin{aligned}
U = & \frac{1}{2} \sum_{i=1}^{m-p} \omega_0 M_i y_i^2 + \frac{1}{2} \sum_{w=m-p+1}^m \omega_0 M_w (y_w^2 - y_w^{s2}) - \sum_{i=1}^{m-p} \bar{P}_{mi} (x_i - x_i^s) - \sum_{w=m-p+1}^m \bar{P}_{mw} (1 + \alpha_w v_w) (x_w - x_w^s) \\
& + \sum_{k=m+1}^n \frac{1}{2} P_{l0k} (\bar{V}_k^2 + \bar{V}_k^{s2}) (1 - \alpha_{pk} v_{pk}) (x_k - x_k^s) + \sum_{k=m+1}^n \frac{1}{2} \bar{Q}_{0k} (1 - \alpha_{qk} v_{qk}) (\bar{V}_k^2 - \bar{V}_k^{s2}) \\
& + \sum_{w=m-p+1}^m \frac{1}{3} M_w \omega_0 k_d k_p k_{op} \left((y_w + 1)^3 - (y_w^s + 1)^3 \right) \\
& - \sum_{w=m-p+1}^m \frac{1}{2} M_w k_b V_{sw} \left(\sin(k_a (x_w - x_{ref}) + c_a) + \sin(k_a (x_w^s - x_{ref}^s) + c_a) \right) (y_w - y_w^s) \\
& - \sum_{w=m-p+1}^m \frac{1}{2} M_w \omega_0 k_d k_p k_m \left(\frac{\bar{P}_{ew}}{(y_w + 1)} + \frac{\bar{P}_{ew}^s}{(y_w^s + 1)} \right) (y_w - y_w^s) - \sum_{w=m-p+1}^m \frac{1}{2} M_w \omega_0 k_d k_{cl} \bar{V}_w (y_w^2 - y_w^{s2}) \\
& - \sum_{w=m-p+1}^m \frac{1}{2} M_w \omega_0 k_d k_{c2} \bar{V}_{sw} \left(\cos(k_a (x_w - x_{ref}) + c_a) y_w + \cos(k_a (x_w^s - x_{ref}^s) + c_a) y_w^s \right) (y_w - y_w^s) \\
& + \sum_{w=m-p+1}^m \frac{1}{2} \bar{P}_{mw} \alpha_w (v_w^2 - v_w^{s2}) + \sum_{k=m+1}^n \frac{1}{2} \bar{P}_{l0k} \alpha_{pk} (v_{pk}^2 - v_{pk}^{s2}) + \sum_{k=m+1}^n \frac{1}{2} \bar{Q}_{0k} \alpha_{qk} (v_{qk}^2 - v_{qk}^{s2}) \\
& - \sum_{i=1}^m \sum_{k=m+1}^n \bar{V}_i B_{ik} \left(\bar{V}_k \cos(x_i - x_k) - \bar{V}_k^s \cos(x_i^s - x_k^s) \right) \\
& - \sum_{k=m+1}^{n-1} \sum_{l=k+1}^n B_{kl} \left(\bar{V}_l \bar{V}_k \cos(x_k - x_l) - \bar{V}_l^s \bar{V}_k^s \cos(x_k^s - x_l^s) \right) \\
& - \sum_{i=1}^{m-1} \sum_{j=i+1}^m V_i V_j B_{ij} \left(\cos(x_i - x_j) - \cos(x_i^s - x_j^s) \right) - \sum_{k=m+1}^n \frac{1}{2} B_{kk} (\bar{V}_k^2 - \bar{V}_k^{s2})
\end{aligned}$$

Eq. 4-282

The derivation of the energy function can be stated as

$$\begin{aligned}
\frac{dU}{dt} = & - \sum_{i=1}^{m-p} \omega_0 D_i y_i^2 - \sum_{k=m+1}^n c_k \dot{x}_k^2 - \sum_{k=m+1}^n \lambda_k \dot{\bar{V}}_k^2 - \sum_{w=m-p+1}^m \frac{1}{\psi_w} \bar{P}_{mw} \alpha_w \dot{v}_w^2 - \sum_{k=m+1}^n \frac{1}{\psi_k} \bar{P}_{l0k} \alpha_{pk} \dot{v}_{pk}^2 \\
& - \sum_{k=m+1}^n \frac{1}{\psi_k} \bar{Q}_{0k} \alpha_{qk} \dot{v}_{qk}^2 + \omega_0 y_0 \left(\sum_{i=1}^m P_{mi} - \sum_{j=1}^m P_{ej} - \sum_{k=m+1}^n c_k \dot{x}_k \right)
\end{aligned}$$

Eq. 4-283

The last term on the right of Eq. 4-283 is diminished as proven by C.O. Nwankpa where j denotes both synchronous and induction generators. The derivation of the energy function is

$$\frac{dU}{dt} = - \sum_{i=1}^{m-p} \omega_0 D_i y_i^2 - \sum_{k=m+1}^n c_k \dot{x}_k^2 - \sum_{k=m+1}^n \lambda_k \dot{\bar{V}}_k^2 - \sum_{w=m-p+1}^m \frac{1}{\psi_w} \bar{P}_{mw} \alpha_w \dot{v}_w^2 - \sum_{k=m+1}^n \frac{1}{\psi_k} \bar{P}_{l0k} \alpha_{pk} \dot{v}_{pk}^2 - \sum_{k=m+1}^n \frac{1}{\psi_k} \bar{Q}_{0k} \alpha_{qk} \dot{v}_{qk}^2$$

Eq. 4-284

4.4.5 Existence of Lyapunov function candidate

From Sections 4.4.2 – 4.4.4, three conditions are needed for well-defined energy function to be suitable for power system stability analysis are

I. $\dot{U} = 0$ when operating points are at the stable equilibrium points

From Eq. 4-282, if $x = x^s$, $y_i = 0$ and $y_w = y_w^s$, every term is exactly zero, which is defined already using K_{sg} , K_{ig} and K_{PF} . Therefore, energy function is zero ($U = 0$) when reach stable equilibrium state.

II. $\dot{U} \leq 0$ (negative-definite) when trajectories of operating points are within the region of attraction and asymptotically move to stable equilibrium points

$$\dot{U} = -\sum_{i=1}^{m-p} \omega_0 D_i y_i^2 - \sum_{k=m+1}^n c_k \dot{x}_k^2 - \sum_{k=m+1}^n \lambda_k \dot{\bar{V}}_k^2 - \sum_{\substack{w=m \\ -p+1}}^m \frac{1}{\psi_w} \bar{P}_{mw} \alpha_w \dot{v}_w^2 - \sum_{k=m+1}^n \frac{1}{\psi_k} \bar{P}_{l0k} \alpha_{pk} \dot{v}_{pk}^2 - \sum_{k=m+1}^n \frac{1}{\psi_k} \bar{Q}_{0k} \alpha_{qk} \dot{v}_{qk}^2$$

Eq. 4-285

In normal operations when U is not larger than the critical energy, D_i , c_k and P_{sw} are normally positive. Since y_i^2 , y_w^2 and \dot{x}_k^2 are always greater than or equal to zero, therefore, the term terms on the right are negative except at the stable equilibrium points (which \dot{U} is zero). Consequently, \dot{U} is negative-definite and is satisfied for this case. Therefore, the energy of this system is always dissipated [8]. The disturbance can cause the energy of the system to increase which, if not larger than critical energy, the energy will decrease until reaching zero at steady state condition. However, if energy increases to reach critical value, sign of D_i or c_k or P_{sw} can be changed, the energy become increase continuously which means the system is unstable.

III. $U(x_i)$ is bounded which means x_i are also bounded.

From the function of U , it always bounded whenever state variables are not approach to infinity (or U is not larger than critical energy) and vice versa. Since $U = 0$ at the stable equilibrium points and $\dot{U} < 0$ for the other operating points, it can be concluded that the energy of the system is bounded and state variables x_i are also bounded [30].

For summary, an energy function (U) of this system, when apply structure-preserving model by neglecting transferred conductance terms, is an acceptable well-defined energy function in the sense of Hsiao-Dong Chiang (2011) and can be used for the voltage stability analysis.

4.5 Critical Energy Estimation

The critical energy is used in this study to evaluate the limit of the power system to gain energy when perturbed by any disturbances. For convenience, it can be estimated using method of M. Ribbens-Pavella and B. Lemal (1976) which requires the determination of energy function, stable equilibrium points, and unstable equilibrium points. Energy function can be determined using methods in Section 4.4 . The stable equilibrium points can be determined using the power system simulation software or by solving the power flow problems. Basing on power-angle characteristic of generator, unstable equilibrium points of angle can be approximated using the value $\pm\pi - x^s$ where x^s is the stable equilibrium point.

Four cases of approximation of unstable equilibrium points are represented as follows:

Case 1: For m machines, only one machine is loss of synchronization and its angle of internal voltage is approximated by $\pi - x^s$ where x^s is the stable equilibrium point before unstable. Therefore, Case 1 has totally m sub-cases.

Case 2: For m machines, only one machine is loss of synchronization and its angle of internal voltage is approximated by $-\pi - x^s$. Therefore, Case 2 has totally m sub-cases.

Case 3: For m machines, all machines are loss of synchronization and their angles of internal voltage are approximated by $\pi - x^s$. Therefore, Case 3 has no sub-cases.

Case 4: For m machines, all machines are loss of synchronization and their angles of internal voltage are approximated by $-\pi - x^s$. Therefore, Case 4 has no sub-cases.

These unstable equilibrium points are called *interested unstable equilibrium points*. When replace these stable equilibrium points and interested unstable equilibrium points of Case 1-4 into the well-defined energy function, totally $2 \times m + 2$ values of energy of the system will be determined. The lowest energy from $2 \times m + 2$ values is used as a critical energy.

4.6 Eigenvalues Determination

4.6.1 Eigenvalues of single machine power system

The eigenvalue method is the conventional and well-known method for the small signal stability analysis in power industry. For the system equations in this section, wind power is modeled using squirrel cage induction generator (SCIG) and doubly-fed induction

generator (DFIG). The swing equation and voltage behind the transient reactance are focused regarding the synchronization stability problem.

4.6.1.1 Squirrel cage induction generator (SCIG) wind turbine

To analyze the small signal stability of a SCIG wind turbine, the linearization of the system equations is formulated as follows:

$$px_w = \omega_0 (y_w - y_1) - k_b \bar{V}_s \sin(k_a x'_w + c_a) \quad \text{Eq. 4-286}$$

$$M_w py_w = (\bar{P}_{mw} - \bar{P}_{ew}) \quad \text{Eq. 4-287}$$

$$\bar{P}_{ew} = \frac{\bar{V}_w \bar{V}_0}{(\bar{X}'_w + \bar{X}_T)} \sin(x'_w) \quad \text{Eq. 4-288}$$

$$k_b = (\bar{X}_w - \bar{X}'_w) / (\bar{T}_0 \bar{X}'_w \bar{E}'_w) \quad \text{Eq. 4-289}$$

$$\bar{T}_0 = \frac{\bar{L}_{rr}}{\omega_0 \bar{r}_r} = \frac{\bar{L}_r + \bar{L}_m}{\omega_0 \bar{r}_r} \quad \text{Eq. 4-290}$$

$$\bar{X} = \bar{\omega}_s \bar{L}_{ss} = \bar{\omega}_s (\bar{L}_s + \bar{L}_m) \quad \text{Eq. 4-291}$$

$$\bar{X}' = \bar{\omega}_s \left(\bar{L}_{ss} - \frac{\bar{L}_m^2}{\bar{L}_{rr}} \right) \quad \text{Eq. 4-292}$$

Where $x'_w = x_w - x_{ref}$, x_{ref} is the reference angle. For example, an angle of infinite bus voltage. In the following details, x'_w will be replaced by only x_w .

Linearization of Eq. 4-286 and Eq. 4-287 are represented in the form:

$$\frac{d\Delta x_w}{dt} = \omega_0 \Delta y_w - k_b \bar{V}_{sw} k_a \cos(k_a x_w^s + c_a) \Delta x_w \quad \text{Eq. 4-293}$$

$$\frac{d\Delta y_w}{dt} = \frac{1}{M} (\Delta \bar{P}_{mw} - \Delta \bar{P}_{ew}) = \frac{1}{M} \Delta \bar{P}_{mw} - K_S \Delta x_w - K_D \Delta y_w \quad \text{Eq. 4-294}$$

If we represent the above equations in the form of matrix:

$$\dot{\mathbf{X}} = \mathbf{A}\mathbf{X} + \mathbf{B}\mathbf{U}$$

We will get

$$\begin{bmatrix} \Delta \dot{x}_w \\ \Delta \dot{y}_w \end{bmatrix} = \begin{bmatrix} -K_E & \omega_0 \\ -K_S & -K_D \end{bmatrix} \begin{bmatrix} \Delta x_w \\ \Delta y_w \end{bmatrix} + \begin{bmatrix} 0 \\ 1/M \end{bmatrix} \Delta \bar{P}_{mw} \quad \text{Eq. 4-295}$$

Where K_S is synchronizing power coefficient, and K_D is damping power coefficient of induction generator.

$$K_S = \frac{1}{M} \frac{\partial \bar{P}_e}{\partial x_w} = \frac{1}{M} \bar{V}_w \sum_{j=1, j \neq w}^n \bar{V}_j \bar{B}_{wj} \cos(x_w^s - x_j^s) \quad \text{and} \quad K_D = \frac{1}{M} \frac{\partial \bar{P}_e}{\partial y} \approx 0 \quad \text{Eq. 4-296}$$

$$K_E = k_b \bar{V}_{sw} k_a \cos(k_a x_w^s + c_a) \quad \text{Eq. 4-297}$$

magnitude of damping power coefficient (K_D) and synchronizing power coefficient (K_S).

Eq. 4-296 and Eq. 4-297 can be represented using block diagrams as in the following figure.

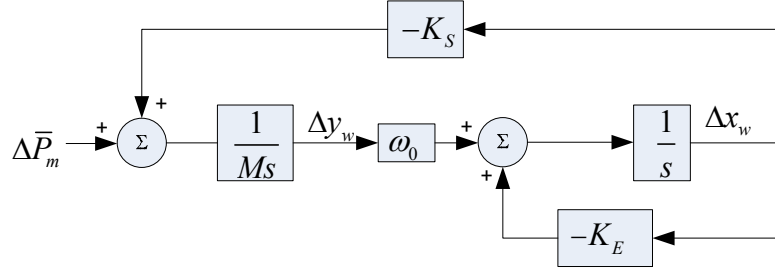


Figure 4.30 Block diagram representing state space equation of the SCIG wind turbine

Take Laplace transformation, yields

$$\mathbf{X}(s) = (s\mathbf{I} - \mathbf{A})^{-1} \mathbf{B} \mathbf{U}(s) \quad \text{or}$$

$$\begin{bmatrix} \Delta x_w(s) \\ \Delta y_w(s) \end{bmatrix} = \begin{bmatrix} s + K_E & -\omega_0 \\ K_S & s \end{bmatrix}^{-1} \begin{bmatrix} 0 \\ 1/M \end{bmatrix} \Delta \bar{P}_m(s) \quad \text{Eq. 4-298}$$

$$\mathbf{X}(s) = \left(\frac{1}{s^2 + sK_E + \omega_0 K_S} \right) \begin{bmatrix} s & \omega_0 \\ -K_S & s + K_E \end{bmatrix} \begin{bmatrix} 0 \\ 1/M \end{bmatrix} \Delta \bar{P}_m(s) \quad \text{Eq. 4-299}$$

$$\mathbf{X}(s) = \left(\frac{1}{s^2 + sK_E + \omega_0 K_S} \right) \begin{bmatrix} \omega_0/M \\ (s + K_E)/M \end{bmatrix} \Delta \bar{P}_m(s) \quad \text{Eq. 4-300}$$

The determinant of matrix $(s\mathbf{I} - \mathbf{A})$ can be used to find eigenvalues using the following equation

$$\det(s\mathbf{I} - \mathbf{A}) = s^2 + sK_E + \omega_0 K_S = 0 \quad \text{Eq. 4-301}$$

Eq. 4-301 is called the characteristic equation of this state space equation and can be represented in the following form

$$s^2 + 2\zeta\omega_n s + \omega_n^2 = 0 \quad \text{Eq. 4-302}$$

where ζ is damping ratio and ω_n is natural frequency.

$$\omega_n = \sqrt{\omega_0 K_S} \quad \text{and} \quad \zeta = \frac{K_E}{2\omega_n} \quad \text{Eq. 4-303}$$

$$\text{Identify } s, \quad s = \frac{-2\zeta\omega_n \pm \sqrt{(2\zeta\omega_n)^2 - 4\omega_n^2}}{2} \quad \text{or} \quad s = -\zeta\omega_n \pm \omega_n \sqrt{\zeta^2 - 1} \quad \text{Eq. 4-304}$$

$$\begin{aligned}
\text{If } \zeta^2 > 1, K_E > 2\omega_n, \text{ therefore } & s = \sigma \pm \omega \quad \text{where } \sigma = -\zeta\omega_n \text{ and } \omega = \omega_n\sqrt{\zeta^2 - 1} \\
\text{If } \zeta^2 = 1, K_E = 2\omega_n, \text{ therefore } & (s - \sigma)^2 = 0 \quad \text{where } \sigma = -\omega_n \text{ and } \omega = 0 \\
\text{If } \zeta^2 < 1, K_E < 2\omega_n, \text{ therefore } & s = \sigma \pm j\omega \quad \text{where } \sigma = -\zeta\omega_n \text{ and } \omega = \omega_n\sqrt{1 - \zeta^2} \\
\text{If } \zeta^2 \approx 0, K_E \ll 2\omega_n, \text{ therefore } & s = \pm j\omega \quad \text{where } \sigma \approx 0 \text{ and } \omega = \omega_n
\end{aligned}$$

4.6.1.2 Wind turbine with doubly-fed induction generator (DFIG)

To analyze the small signal stability of the DFIG wind turbine, the linearization of the system equations is represented as follows.

$$px_w = \omega_0 (y_w - y_0) - k_b \bar{V}_{sw} \sin(k_a x'_w + c_a) + \omega_0 k_d \bar{V}_{rq} \quad \text{Eq. 4-305}$$

$$M_w py_w = (\bar{P}_{mw} - \bar{P}_{ew}) \quad \text{Eq. 4-306}$$

$$\bar{P}_{ew} = \frac{\bar{V}_w \bar{V}_0}{(\bar{X}'_w + \bar{X}_T)} \sin(x'_w) \quad \text{Eq. 4-307}$$

$$\bar{V}_{rq} = -y_w (k_{c1} \bar{V}_w + k_{c2} \bar{V}_{sw} \cos(k_a x'_w + c_a)) + k_p (\bar{T}_{sp} - \bar{P}'_{sw}) \quad \text{Eq. 4-308}$$

$$\bar{P}'_{sw} = k_m \bar{P}_{ew} / (1 + y_w) \quad \text{Eq. 4-309}$$

$$\bar{T}_{sp} = k_{op} (1 + y_w)^2 \quad \text{Eq. 4-310}$$

$$k_d = \bar{L}_m / (\bar{L}_{rr} \bar{E}') \quad \text{and} \quad k_b = (\bar{X}_w - \bar{X}'_w) / (\bar{T}_0 \bar{X}'_w \bar{E}'_w) \quad \text{Eq. 4-311}$$

$$\left. \begin{aligned} k_{c1} &= \bar{\omega}_0 \left(\bar{L}_{rr} - \frac{\bar{L}_m^2}{\bar{L}_{ss}} \right) \left(\frac{\bar{L}_{ss}}{\bar{L}_m \bar{X}'} \right) \\ k_{c2} &= \bar{\omega}_0 \left(\left(\bar{L}_{rr} - \frac{\bar{L}_m^2}{\bar{L}_{ss}} \right) \left(\frac{1}{\bar{\omega}_s \bar{L}_m} - \frac{\bar{L}_{ss}}{\bar{L}_m \bar{X}'} \right) + \frac{\bar{L}_m}{\bar{\omega}_s \bar{L}_{ss}} \right) \end{aligned} \right\} \quad \text{Eq. 4-312}$$

$$k_a \approx 0.274 \bar{P}_{mw} + 0.346 \quad \text{and} \quad c_a \approx -0.022 \bar{P}_{mw} + 0.006 \quad \text{Eq. 4-313}$$

Where $x'_w = x_w - \theta_{ref}$, θ_{ref} is the reference angle. For example, an angle of infinite bus voltage. In the following details, x'_w will be replaced by only x_w .

Linearization of Eq. 4-305 and Eq. 4-306 are represented in the form

$$\frac{d\Delta x_w}{dt} = \left(\omega_0 k_d \frac{\partial \bar{V}_{rq}}{\partial x_w} - k_b \bar{V}_{sw} k_a \cos(k_a x_w + c_a) \right) \Delta x_w + \left(\omega_0 + \omega_0 k_d \frac{\partial \bar{V}_{rq}}{\partial y_w} \right) \Delta y_w = K_{E1} \Delta x_w + K_{E2} \Delta y_w \quad \text{Eq. 4-314}$$

$$\frac{d\Delta y_w}{dt} = \frac{1}{M} \Delta \bar{P}_{mw} - \frac{1}{M} \frac{\partial \bar{P}_{ew}}{\partial x_w} \Delta x_w - \frac{1}{M} \frac{\partial \bar{P}_{ew}}{\partial y_w} \Delta y_w = \frac{1}{M} \Delta \bar{P}_{mw} - K_S \Delta x_w - K_D \Delta y_w \quad \text{Eq. 4-315}$$

Where K_S is synchronizing power coefficient, K_D is damping power coefficient of DFIGURE

$$K_{E1} = \omega_0 k_d \frac{\partial \bar{V}_{rq}}{\partial x_w} - k_b \bar{V}_{sw} k_a \cos(k_a x_w^s + c_a) \quad \text{Eq. 4-316}$$

$$K_{E2} = \omega_0 + \omega_0 k_d \frac{\partial \bar{V}_{rq}}{\partial y_w} \quad \text{Eq. 4-317}$$

$$K_S = \frac{1}{M} \frac{\partial \bar{P}_{ew}}{\partial x_w} = \frac{1}{M} \frac{\bar{V}_w \bar{V}_0}{(\bar{X}'_w + \bar{X}_T)} \cos(x_w^s) \quad \text{Eq. 4-318}$$

$$K_D = \frac{1}{M} \frac{\partial \bar{P}_{ew}}{\partial y_w} \approx 0 \quad \text{Eq. 4-319}$$

$$\frac{\partial \bar{V}_{rq}}{\partial x_w} = y_w k_{c2} k_a \bar{V}_{sw} \sin(k_a x_w + c_a) - \frac{k_p k_m \bar{V}_w \bar{V}_0}{(\bar{X}'_w + \bar{X}_T)(1 + y_w)} \cos(x_w) \quad \text{Eq. 4-320}$$

$$\begin{aligned} \frac{\partial \bar{V}_{rq}}{\partial y_w} = & -\left(k_{c1} \bar{V}_w + k_{c2} \bar{V}_{sw} \cos(k_a x_w + c_a)\right) + 2k_p k_{op} (1 + y_w) \\ & + k_p k_m \frac{\bar{V}_w \bar{V}_0 \sin(x_w)}{(\bar{X}'_w + \bar{X}_T)(1 + y_w)^2} \end{aligned} \quad \text{Eq. 4-321}$$

If we represent the above equations in the form of a matrix,

$$\dot{\mathbf{X}} = \mathbf{A}\mathbf{X} + \mathbf{B}\mathbf{U}$$

We will get

$$\begin{bmatrix} \Delta \dot{x}_w \\ \Delta \dot{y}_w \end{bmatrix} = \begin{bmatrix} K_{E1} & K_{E2} \\ -K_S & -K_D \end{bmatrix} \begin{bmatrix} \Delta x_w \\ \Delta y_w \end{bmatrix} + \begin{bmatrix} 0 \\ 1/M \end{bmatrix} \Delta \bar{P}_{mw} \quad \text{Eq. 4-322}$$

Eq. 4-322 can be represented using block diagram as in the following figure.

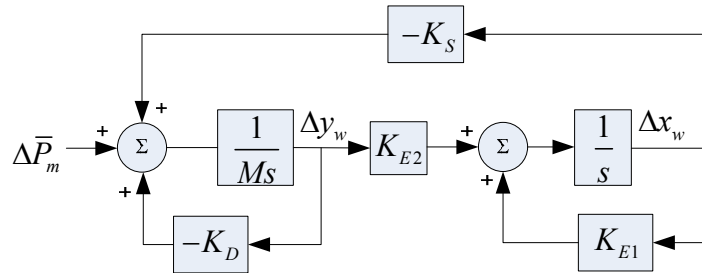


Figure 4.31 Block diagram representing state space equation of the DFIG wind turbine

From Eq. 4-322, rearranging using the following form and taking Laplace transformation, yields

$$\mathbf{X}(s) = (s\mathbf{I} - \mathbf{A})^{-1} \mathbf{B}\mathbf{U}(s) \quad \text{or}$$

$$\begin{bmatrix} \Delta x_w(s) \\ \Delta y_w(s) \end{bmatrix} = \begin{bmatrix} s - K_{E1} & -K_{E2} \\ K_S & s + K_D \end{bmatrix}^{-1} \begin{bmatrix} 0 \\ \Delta \bar{P}_{mw}(s)/M \end{bmatrix} \quad \text{Eq. 4-323}$$

$$(\mathbf{sI} - \mathbf{A})^{-1} = \frac{1}{\det(\mathbf{sI} - \mathbf{A})} (\mathbf{sI} - \mathbf{A})^T \quad \text{Eq. 4-324}$$

The solutions of $\det(\mathbf{sI} - \mathbf{A}) = 0$ are the eigenvalues of this state space equation, therefore

$$\det(\mathbf{sI} - \mathbf{A}) = (s - K_{E1})(s + K_D) + K_S K_{E2} = 0 \quad \text{Eq. 4-325}$$

4.6.2 Eigenvalue method for multi-machine power system including wind power

4.6.2.1 Power system equations

In this section, wind power is modeled using a doubly fed induction generator (DFIG) which the swing equation and voltage behind transient reactance are focused regarding the synchronization stability problem. The system equations are rewritten as follows:

$$px_i = \omega_0 (y_i - y_0) \quad \text{Eq. 4-326}$$

$$px_w = \omega_0 (y_w - y_0) - k_b \bar{V}_{sw} \sin(k_a |x_w - x_{ref}| + c_a) + \omega_0 k_d \bar{V}_{rq} \quad \text{Eq. 4-327}$$

$$c_k px_k = -(\bar{P}_{lk} + \bar{P}_{ek}) - c_k \omega_0 y_0 \quad \text{Eq. 4-328}$$

$$M_i py_i = (\bar{P}_{mi} - \bar{P}_{ei}) - D_i y_i \quad \text{Eq. 4-329}$$

$$M_w py_w = (\bar{P}_{mw} - \bar{P}_{ew}) - D_w y_w \quad \text{Eq. 4-330}$$

$$pZ'_I = \bar{T}_{sp} - \bar{P}'_{sw} \quad \text{Eq. 4-331}$$

$$\bar{V}_{rq} = -y_w \left(k_{c1} \bar{V}_w + k_{c2} \bar{V}_{sw} \cos(k_a |x_w - \theta_{ref}| + c_a) \right) + k_p (\bar{T}_{sp} - \bar{P}'_{sw}) + k_I Z'_I \quad \text{Eq. 4-332}$$

$$\bar{P}'_{sw} = k_m \bar{P}_{ew} / (1 + y_w) \quad \text{Eq. 4-333}$$

$$\bar{T}_{sp} = k_{op} (1 + y_w)^2 \quad \text{Eq. 4-334}$$

$$\bar{P}_{ew} = \bar{V}_w \sum_{j=1, j \neq w}^n \bar{V}_j \bar{B}_{wj} \sin(x_w - x_j) \quad \text{Eq. 4-335}$$

$$\bar{P}_{ei} = \bar{V}_i \sum_{j=1, j \neq i}^n \bar{V}_j \bar{B}_{ij} \sin(x_i - x_j) \quad \text{Eq. 4-336}$$

$$\bar{P}_{ek} = \bar{V}_k \sum_{j=1, j \neq k}^n \bar{V}_j \bar{B}_{kj} \sin(x_k - x_j) \quad \text{Eq. 4-337}$$

$$k_d = \bar{L}_m / (\bar{L}_{rr} \bar{E}') \text{ and } k_b = (\bar{X}_w - \bar{X}'_w) / (\bar{T}_0 \bar{X}'_w \bar{E}') \quad \text{Eq. 4-338}$$

$$\left. \begin{aligned} k_{c1} &= \bar{\omega}_0 \left(\bar{L}_{rr} - \frac{\bar{L}_m^2}{\bar{L}_{ss}} \right) \left(\frac{\bar{L}_{ss}}{\bar{L}_m \bar{X}'} \right) \\ k_{c2} &= \bar{\omega}_0 \left(\left(\bar{L}_{rr} - \frac{\bar{L}_m^2}{\bar{L}_{ss}} \right) \left(\frac{1}{\bar{\omega}_s \bar{L}_m} - \frac{\bar{L}_{ss}}{\bar{L}_m \bar{X}'} \right) + \frac{\bar{L}_m}{\bar{\omega}_s \bar{L}_{ss}} \right) \end{aligned} \right\} \quad \text{Eq. 4-339}$$

$$k_a \approx 0.274 \bar{P}_{mw} + 0.346 \quad \text{and} \quad c_a \approx -0.022 \bar{P}_{mw} + 0.006 \quad \text{Eq. 4-340}$$

$$\bar{T}_0 = \frac{\bar{L}_{rr}}{\omega_0 \bar{r}_r} = \frac{\bar{L}_r + \bar{L}_m}{\omega_0 \bar{r}_r}, \quad \bar{X} = \bar{\omega}_0 \bar{L}_{ss} = \bar{\omega}_0 (\bar{L}_s + \bar{L}_m), \quad \bar{X}' = \bar{\omega}_0 \left(\bar{L}_{ss} - \frac{\bar{L}_m^2}{\bar{L}_{rr}} \right) \quad \text{Eq. 4-341}$$

However, the k_1 in Eq. 4-332 is very small compared with the other terms. Therefore, $k_1 Z_1$ is neglected for convenient.

4.6.2.2 Linearization of power system equations

To analyze the small signal stability of the power system, including induction generator wind turbine, the state space equation will be represented in a new form as follows.

Linearization of Eq. 4-326 to Eq. 4-330 are represented in the following form

$$\frac{d\Delta x_i}{dt} = \omega_0 \Delta y_i \quad \text{Eq. 4-342}$$

$$\begin{aligned} \frac{d\Delta x_w}{dt} &= \omega_0 \Delta y_w - k_b \bar{V}_{sw} k_a \cos(k_a (x_w - x_{ref}) + c_a) \Delta x_w + \omega_0 k_d \frac{\partial \bar{V}_{rq}}{\partial x_{ref}} \Delta x_{ref} \\ &+ k_b \bar{V}_{sw} k_a \cos(k_a (x_w - x_{ref}) + c_a) \Delta x_{ref} + \omega_0 k_d \frac{\partial \bar{V}_{rq}}{\partial y_w} \Delta y_w + \omega_0 k_d \frac{\partial \bar{V}_{rq}}{\partial x_w} \Delta x_w \end{aligned} \quad \text{Eq. 4-343}$$

$$\frac{d\Delta x_k}{dt} = -\frac{1}{c_k} \left(\Delta \bar{P}_{lk} + \frac{\partial \bar{P}_{ek}}{\partial x_k} \Delta x_k + \frac{\partial \bar{P}_{ek}}{\partial x_i} \Delta x_i + \frac{\partial \bar{P}_{ek}}{\partial x_w} \Delta x_w \right) \quad \text{Eq. 4-344}$$

$$\frac{d\Delta y_i}{dt} = \frac{1}{M_i} \left(\Delta \bar{P}_{mi} - \frac{\partial \bar{P}_{ei}}{\partial x_i} \Delta x_i - \frac{\partial \bar{P}_{ei}}{\partial x_w} \Delta x_w - \frac{\partial \bar{P}_{ei}}{\partial x_k} \Delta x_k \right) - \frac{D_i}{M_i} \Delta y_i \quad \text{Eq. 4-345}$$

$$\frac{d\Delta y_w}{dt} = \frac{1}{M} \left(\Delta \bar{P}_{mw} - \frac{\partial \bar{P}_{ew}}{\partial x_w} \Delta x_w - \frac{\partial \bar{P}_{ew}}{\partial x_i} \Delta x_i - \frac{\partial \bar{P}_{ew}}{\partial x_k} \Delta x_k \right) - \frac{D_w}{M_w} \Delta y_w \quad \text{Eq. 4-346}$$

Where $\partial \bar{V}_{rq} / \partial x_{ref} \approx 0$. K_S is synchronizing power coefficient.

From Eq. 4-343 and Eq. 4-346, we can represent in the following form

$$\begin{aligned}
\frac{d\Delta x_w}{dt} &= \left(\omega_0 k_d \frac{\partial \bar{V}_{rq}}{\partial x_w} - k_b \bar{V}_{sw} k_a \cos(k_a (x_w - x_{ref}) + c_a) \right) \Delta x_w \\
&+ \left(\omega_0 k_d \frac{\partial \bar{V}_{rq}}{\partial x_{ref}} + k_b \bar{V}_{sw} k_a \cos(k_a (x_w - x_{ref}) + c_a) \right) \Delta x_{ref} \\
&+ \left(\omega_0 + \omega_0 k_d \frac{\partial \bar{V}_{rq}}{\partial y_w} \right) \Delta y_w = K_{Ew1} \Delta x_w + K_{Ew2} \Delta x_{ref} + K_{Ew3} \Delta y_w
\end{aligned} \tag{Eq. 4-347}$$

$$\begin{aligned}
\frac{d\Delta x_k}{dt} &= -\frac{1}{c_k} \left(\Delta \bar{P}_{lk} + \frac{\partial \bar{P}_{ek}}{\partial x_k} \Delta x_k + \frac{\partial \bar{P}_{ek}}{\partial x_i} \Delta x_i + \frac{\partial \bar{P}_{ek}}{\partial x_w} \Delta x_w \right) \\
&= -\frac{1}{c_k} \Delta \bar{P}_{lk} - K_{Skk} \Delta x_k - K_{Ski} \Delta x_i - K_{Skw} \Delta x_w
\end{aligned} \tag{Eq. 4-348}$$

$$\begin{aligned}
\frac{d\Delta y_i}{dt} &= \frac{1}{M_i} \left(\Delta \bar{P}_{mi} - \frac{\partial \bar{P}_{ei}}{\partial x_i} \Delta x_i - \frac{\partial \bar{P}_{ei}}{\partial x_k} \Delta x_k - \frac{\partial \bar{P}_{ei}}{\partial x_w} \Delta x_w \right) - \frac{D_i}{M_i} \Delta y_i \\
&= \frac{1}{M_i} \Delta \bar{P}_{mi} - K_{Sii} \Delta x_i - K_{Sik} \Delta x_k - K_{Siw} \Delta x_w - K_{Di} \Delta y_i
\end{aligned} \tag{Eq. 4-349}$$

$$\begin{aligned}
\frac{d\Delta y_w}{dt} &= \frac{1}{M} \Delta \bar{P}_{mw} - \frac{1}{M} \frac{\partial \bar{P}_{ew}}{\partial x_w} \Delta x_w - \frac{1}{M} \frac{\partial \bar{P}_{ew}}{\partial x_i} \Delta x_i - \frac{1}{M} \frac{\partial \bar{P}_{ew}}{\partial x_k} \Delta x_k - \frac{D_w}{M_w} \Delta y_w \\
&= \frac{1}{M} \Delta \bar{P}_{mw} - K_{Sww} \Delta x_w - K_{Swk} \Delta x_k - K_{Swi} \Delta x_i - K_{Dw} \Delta y_i
\end{aligned} \tag{Eq. 4-350}$$

$$K_{Ew1} = \omega_0 k_d \frac{\partial \bar{V}_{rq}}{\partial x_w} - k_b k_a \bar{V}_{sw} \cos(k_a (x_w - x_{ref}) + c_a) \tag{Eq. 4-351}$$

$$K_{Ew2} = \omega_0 k_d \frac{\partial \bar{V}_{rq}}{\partial x_{ref}} + k_b k_a \bar{V}_{sw} \cos(k_a (x_w - x_{ref}) + c_a) \tag{Eq. 4-352}$$

$$K_{Ew3} = \omega_0 + \omega_0 k_d \frac{\partial \bar{V}_{rq}}{\partial y_w} \tag{Eq. 4-353}$$

$$\frac{\partial \bar{V}_{rq}}{\partial x_w} = k_a k_{c2} \bar{V}_{sw} \sin(k_a (x_w - x_{ref}) + c_a) y_w - k_p k_m \frac{\partial \bar{P}_{ew}}{\partial x_w} \frac{1}{(1 + y_w)} \tag{Eq. 4-354}$$

$$\frac{\partial \bar{V}_{rq}}{\partial x_{ref}} = -k_a k_{c2} \bar{V}_{sw} \sin(k_a (x_w - x_{ref}) + c_a) y_w + k_p k_m \frac{\partial \bar{P}_{ew}}{\partial x_{ref}} \frac{1}{(1 + y_w)} \tag{Eq. 4-355}$$

$$\frac{\partial \bar{V}_{rq}}{\partial y_w} = 2k_p k_{op} (y_w + 1) - (k_{c1} \bar{V}_w + k_{c2} \bar{V}_{sw} \cos(k_a (x_w - x_{ref}) + c_a)) + k_p k_m \bar{P}_{ew} \frac{1}{(1 + y_w)^2} \tag{Eq. 4-356}$$

$$K_{Sww} = \frac{1}{M_w} \frac{\partial \bar{P}_{ew}}{\partial x_w} = \frac{1}{M_w} \bar{V}_w \sum \bar{V}_j \bar{B}_{wj} \cos(x_w - x_j) \tag{Eq. 4-357}$$

$$K_{Swi} = \frac{1}{M_w} \frac{\partial \bar{P}_{ew}}{\partial x_i} = -\frac{1}{M_w} \bar{V}_w \sum \bar{V}_i \bar{B}_{wi} \cos(x_w - x_i) \tag{Eq. 4-358}$$

$$K_{Swk} = \frac{1}{M_w} \frac{\partial \bar{P}_{ew}}{\partial x_k} = -\frac{1}{M_w} \bar{V}_w \sum \bar{V}_k \bar{B}_{wk} \cos(x_w - x_k) \quad \text{Eq. 4-359}$$

$$K_{Sii} = \frac{1}{M_i} \frac{\partial \bar{P}_{ei}}{\partial x_i} = \frac{1}{M_i} \bar{V}_i \sum \bar{V}_j \bar{B}_{ij} \cos(x_i - x_j) \quad \text{Eq. 4-360}$$

$$K_{Siw} = \frac{1}{M_i} \frac{\partial \bar{P}_{ei}}{\partial x_w} = -\frac{1}{M_i} \bar{V}_i \sum \bar{V}_w \bar{B}_{iw} \cos(x_i - x_w) \quad \text{Eq. 4-361}$$

$$K_{Sik} = \frac{1}{M_i} \frac{\partial \bar{P}_{ei}}{\partial x_k} = -\frac{1}{M_i} \bar{V}_i \sum \bar{V}_k \bar{B}_{ik} \cos(x_i - x_k) \quad \text{Eq. 4-362}$$

$$K_{Skk} = \frac{1}{c_k} \frac{\partial \bar{P}_{ek}}{\partial x_k} = \frac{1}{c_k} \bar{V}_k \sum \bar{V}_j \bar{B}_{kj} \cos(x_k - x_j) \quad \text{Eq. 4-363}$$

$$K_{Ski} = \frac{1}{c_k} \frac{\partial \bar{P}_{ek}}{\partial x_i} = -\frac{1}{c_k} \bar{V}_k \sum \bar{V}_i \bar{B}_{ki} \cos(x_k - x_i) \quad \text{Eq. 4-364}$$

$$K_{Skw} = \frac{1}{c_k} \frac{\partial \bar{P}_{ek}}{\partial x_w} = -\frac{1}{c_k} \bar{V}_k \sum \bar{V}_w \bar{B}_{kw} \cos(x_k - x_w) \quad \text{Eq. 4-365}$$

4.6.2.3 Eigenvalue computation

If we represent the above equations in the form of the matrix,

$$\dot{\mathbf{X}} = \mathbf{A}\mathbf{X} + \mathbf{B}\mathbf{U} \quad \text{Eq. 4-366}$$

We will get

$$\begin{bmatrix} \Delta \dot{x}_i \\ \Delta \dot{x}_w \\ \Delta \dot{x}_k \\ \Delta \dot{y}_w \\ \Delta \dot{y}_i \end{bmatrix} = \begin{bmatrix} 0 & 0 & 0 & 0 & \omega_0 \\ 0 & K_{Ew1} & K_{Ew2} & K_{Ew3} & 0 \\ -K_{Ski} & -K_{Skw} & -K_{Skk} & 0 & 0 \\ -K_{Swi} & -K_{Sww} & -K_{Swk} & -K_{Dw} & 0 \\ -K_{Sii} & -K_{Siw} & -K_{Sik} & 0 & -K_{Di} \end{bmatrix} \begin{bmatrix} \Delta x_i \\ \Delta x_w \\ \Delta x_k \\ \Delta y_w \\ \Delta y_i \end{bmatrix} + \begin{bmatrix} 0 \\ 0 \\ -\Delta \bar{P}_{lk}/c_k \\ \Delta \bar{P}_{mw}/M \\ \Delta \bar{P}_{mi}/M \end{bmatrix} \quad \text{Eq. 4-367}$$

From Eq. 4-367, rearranging and taking Laplace transformation, yields

$$\mathbf{X}(s) = (s\mathbf{I} - \mathbf{A})^{-1} \mathbf{B}\mathbf{U}(s) \quad \text{or}$$

$$\begin{bmatrix} \Delta x_i(s) \\ \Delta x_w(s) \\ \Delta x_k(s) \\ \Delta y_w(s) \\ \Delta y_i(s) \end{bmatrix} = \begin{bmatrix} s & 0 & 0 & 0 & -\omega_0 \\ 0 & s - K_{Ew1} & -K_{Ew2} & -K_{Ew3} & 0 \\ K_{Ski} & K_{Skw} & s + K_{Skk} & 0 & 0 \\ K_{Swi} & K_{Sww} & K_{Swk} & s + K_{Dw} & 0 \\ K_{Sii} & K_{Siw} & K_{Sik} & 0 & s + K_{Di} \end{bmatrix}^{-1} \begin{bmatrix} 0 \\ 0 \\ -\Delta \bar{P}_{lk}(s)/c_k \\ \Delta \bar{P}_{mw}(s)/M \\ \Delta \bar{P}_{mi}(s)/M \end{bmatrix} \quad \text{Eq. 4-368}$$

$$(s\mathbf{I} - \mathbf{A})^{-1} = \frac{1}{\det(s\mathbf{I} - \mathbf{A})} (s\mathbf{I} - \mathbf{A})^T \quad \text{Eq. 4-369}$$

The solutions of $\det(s\mathbf{I} - \mathbf{A}) = 0$ are the eigenvalues of this state space equation, therefore

$$\det(s\mathbf{I} - \mathbf{A}) = s(s - K_{Ew1})(s + K_{Skk})(s + K_{Dw})(s + K_{Di}) - \omega_0(s + K_{Skk})K_{Sii}K_{Sww}K_{Ew3} = 0$$

Eq. 4-370

4.7 Mean First Passage Time (MFPT) Determination

The mean first passage time (MFPT) is used as an index to evaluate the stability of the power system when perturbed by any small signal. This section applies methods of [9] to formulate the stochastic differential equations (SDE) and compute MFPT of power system incorporating stochastic wind power.

4.7.1 Formation of stochastic differential equations

From the state space equation in Section 4.1.7, if we apply stochastic part ($1 + \gamma_w \dot{W}$, \dot{W} is white noise, γ_w is noise intensity = standard deviation / mean value) into mechanical wind power (P_{mw}), we will get stochastic differential equations as follows:

$$\dot{y}_w = \frac{1}{M_w} (P_{mw} (1 + \gamma_w \dot{W}) - P_{ew}) \quad \text{Eq. 4-371}$$

$$\dot{y}_w = \frac{1}{M_w} (P_{mw} - P_{ew}) + \frac{1}{M_w} P_{mw} \gamma_w \dot{W} \quad \text{Eq. 4-372}$$

If we use noise scaling factor (ε) for the above equation as:

$$\sqrt{\varepsilon_l} = \inf \left\{ \frac{\gamma P_{mw}}{M_w \sqrt{2\beta}} \middle| \gamma > 0 \right\} \text{ and } \sqrt{\varepsilon_w} = \frac{\gamma P_{mw}}{M_w \sqrt{2\beta \varepsilon_l}} g \quad \text{Eq. 4-373}$$

Where w represent wind power bus = 1, ... , and $\beta = D_i/M_i$ is the same for all generators and use to rescale intensity of noise. Since D of SCIG is very small comparing with synchronous generator, the parameter α is presented here to scale D of SCIG. Therefore, we will get standard form of stochastic differential equation of SCIG as:

$$\dot{y}_w = -\beta \alpha y_w + \frac{1}{M_w} (P_{mw} - P_{ew}) + \sqrt{2\beta \varepsilon_l \varepsilon_w} \dot{W} \quad \text{Eq. 4-374}$$

From Eqs. 4-131 – 4-138, if wind power is applied on one bus (bus $w=2$), the matrix form of the state space equation, including the noise term is represented as follows:

$$\begin{bmatrix} \dot{x}_1 \\ \dot{x}_2 \\ \dot{x}_3 \\ \dot{x}_4 \\ \dot{x}_5 \\ \dot{y}_1 \\ \dot{y}_2 \\ \dot{y}_3 \end{bmatrix} = \begin{bmatrix} y_1 - y_3 \\ \frac{pV_2^2}{2P_{e2}R_{r2}}(y_2 - 1) - y_3 \\ 0 \\ -\frac{1}{c_4}(P_{l4} + P_{e4}) - y_3 \\ -\frac{1}{c_5}(P_{l5} + P_{e5}) - y_3 \\ -\beta y_1 + \frac{1}{M_1}(P_{m1} - P_{e1}) \\ -\beta \alpha y_2 + \frac{1}{M_2}(P_{m2} - P_{e2}) \\ -\beta y_3 + \frac{1}{M_3}(P_{m3} - P_{e3}) \end{bmatrix} + \sqrt{2\beta\epsilon_l} \begin{bmatrix} 0 \\ 0 \\ 0 \\ 0 \\ 0 \\ 0 \\ \sqrt{\epsilon_w} \\ 0 \end{bmatrix} \dot{W} \quad \text{Eq. 4-375}$$

If we set $\phi_{l,k}(\mathbf{X}, y_3) = \frac{1}{c_k}(P_{lk} + P_{ek}) + y_3$ and $\phi_{m,i}(\mathbf{X}) = \frac{1}{M_i}(P_{mi} - P_{ei})$. Then

$$\begin{bmatrix} \dot{x}_1 \\ \dot{x}_2 \\ \dot{x}_3 \\ \dot{x}_4 \\ \dot{x}_5 \\ \dot{y}_1 \\ \dot{y}_2 \\ \dot{y}_3 \end{bmatrix} = \begin{bmatrix} y_1 - y_3 \\ y'_2 - y_3 \\ 0 \\ -\phi_{l,4}(\mathbf{X}, y_3) \\ -\phi_{l,5}(\mathbf{X}, y_3) \\ -\beta y_1 - \phi_{m,6}(\mathbf{X}) \\ -\beta \alpha y_2 - \phi_{m,7}(\mathbf{X}) \\ -\beta y_3 - \phi_{m,8}(\mathbf{X}) \end{bmatrix} + \sqrt{2\beta\epsilon_l} Q_w \dot{W} \quad \text{Eq. 4-376}$$

Where $y'_2 = a(y_2 - 1)$, $a = \frac{pV_2^2}{2P_{e2}R_{r2}}$, and Q_w is $m+n \times 1$ matrix with $q_{71} = \sqrt{\epsilon_w}$.

4.7.2 Asymptotic solution to MFPT

The MFPT (τ) is defined as follows:

$$\tau = E\left(\inf\{t : W(\mathbf{x}(t), \mathbf{y}(t)) = W_C\} \mid \mathbf{x}(0) = \mathbf{x}, \mathbf{y}(0) = \mathbf{y}\right) \quad \text{Eq. 4-377}$$

The MFPT is known to be a solution of following boundary value problem which is based on the Backward Kolmogorov Equation (BKE).

$$\left. \begin{aligned} & \beta \varepsilon_l \varepsilon_w \frac{\partial^2 \tau}{\partial x_w^2} + (y_1 - y_3) \frac{\partial \tau}{\partial x_1} + (y_2' - y_3) \frac{\partial \tau}{\partial x_2} + (y_3 - y_3) \frac{\partial \tau}{\partial x_3} \\ & - (\phi_{l,4}(\mathbf{X}, y_3)) \frac{\partial \tau}{\partial x_4} - (\phi_{l,5}(\mathbf{X}, y_3)) \frac{\partial \tau}{\partial x_5} - (\beta y_1 + \phi_{m,6}(\mathbf{X})) \frac{\partial \tau}{\partial y_1} \\ & - (\beta \alpha y_2 + \phi_{m,7}(\mathbf{X})) \frac{\partial \tau}{\partial y_2} - (\beta y_3 + \phi_{m,8}(\mathbf{X})) \frac{\partial \tau}{\partial y_3} = -1 \quad (\mathbf{x}, \mathbf{y}) \in \Omega \\ & \tau = 0 \quad (\mathbf{x}, \mathbf{y}) \in \partial\Omega \end{aligned} \right\} \text{Eq. 4-378}$$

To solve this problem, the asymptotic method is applied. Using this method, the second order differential equation is reduced to a first order differential equation and then the asymptotic expansion of τ can be computed more easily:

Firstly, τ is expanded as a function of β

$$\tau = \frac{1}{\beta} \tau_0 + \tau_1 + \beta \tau_2 + \dots \quad \text{Eq. 4-379}$$

Replace τ in Eq. 4-379 into Eq. 4-378 while D_2 is zero for induction generator.

$$\begin{aligned} & \beta \varepsilon_l \varepsilon_w \frac{\partial^2 \left(\frac{1}{\beta} \tau_0 + \tau_1 + \beta \tau_2 + \dots \right)}{\partial x_w^2} + (y_1 - y_3) \frac{\partial \left(\frac{1}{\beta} \tau_0 + \tau_1 + \beta \tau_2 + \dots \right)}{\partial x_1} \\ & + (y_2' - y_3) \frac{\partial \left(\frac{1}{\beta} \tau_0 + \tau_1 + \beta \tau_2 + \dots \right)}{\partial x_2} - (\phi_{l,4}(\mathbf{X}, y_3)) \frac{\partial \left(\frac{1}{\beta} \tau_0 + \tau_1 + \beta \tau_2 + \dots \right)}{\partial x_4} \\ & - (\phi_{l,5}(\mathbf{X}, y_3)) \frac{\partial \left(\frac{1}{\beta} \tau_0 + \tau_1 + \beta \tau_2 + \dots \right)}{\partial x_5} - (\beta y_1 + \phi_{m,6}(\mathbf{X})) \frac{\partial \left(\frac{1}{\beta} \tau_0 + \tau_1 + \beta \tau_2 + \dots \right)}{\partial y_1} \\ & - (\beta \alpha y_2 + \phi_{m,7}(\mathbf{X})) \frac{\partial \left(\frac{1}{\beta} \tau_0 + \tau_1 + \beta \tau_2 + \dots \right)}{\partial y_2} - (\beta y_3 + \phi_{m,8}(\mathbf{X})) \frac{\partial \left(\frac{1}{\beta} \tau_0 + \tau_1 + \beta \tau_2 + \dots \right)}{\partial y_3} = -1 \end{aligned} \quad \text{Eq. 4-380}$$

For the terms with the coefficient β^1 , a homogenous first order differential equation is a result as follows:

$$\begin{aligned} L_1(\tau_0) &= (y_1 - y_3) \frac{\partial \tau_0}{\partial x_1} + (y_2' - y_3) \frac{\partial \tau_0}{\partial x_2} - (\phi_{l,4}(\mathbf{X}, y_3)) \frac{\partial \tau_0}{\partial x_4} - (\phi_{l,5}(\mathbf{X}, y_3)) \frac{\partial \tau_0}{\partial x_5} \\ & - (\phi_{m,6}(\mathbf{X})) \frac{\partial \tau_0}{\partial y_1} - (\phi_{m,7}(\mathbf{X})) \frac{\partial \tau_0}{\partial y_2} - (\phi_{m,8}(\mathbf{X})) \frac{\partial \tau_0}{\partial y_3} = 0 \end{aligned} \quad \text{Eq. 4-381}$$

From Eq. 4-381, its characteristic equations are [21]:

$$\frac{\partial \tau_0}{\partial s} = \frac{\partial \tau_0}{\partial x_1} \frac{dx_1}{ds} + \frac{\partial \tau_0}{\partial x_2} \frac{dx_2}{ds} + \frac{\partial \tau_0}{\partial x_4} \frac{dx_4}{ds} + \frac{\partial \tau_0}{\partial x_5} \frac{dx_5}{ds} + \frac{\partial \tau_0}{\partial y_1} \frac{dy_1}{ds} + \frac{\partial \tau_0}{\partial y_2} \frac{dy_2}{ds} + \frac{\partial \tau_0}{\partial y_3} \frac{dy_3}{ds} = 0 \quad \text{Eq. 4-382}$$

and

$$\left. \begin{aligned} \frac{dx_1}{ds} &= y_1 - y_3 \\ \frac{dx_2}{ds} &= y_2' - y_3 \\ \frac{dx_4}{ds} &= -\phi_{l,4}(\mathbf{X}, y_3) \\ \frac{dx_5}{ds} &= -\phi_{l,5}(\mathbf{X}, y_3) \\ \frac{dy_1}{ds} &= -\phi_{m,6}(\mathbf{X}) \\ \frac{dy_2}{ds} &= -\phi_{m,7}(\mathbf{X}) \\ \frac{dy_3}{ds} &= -\phi_{m,8}(\mathbf{X}) \end{aligned} \right\} \quad \text{Eq. 4-383}$$

We will see that Eq. 4-383 is similar to Eq. 4-376 when β is set to zero. This means that the system has no damping force of generator and has no perturbation part. The system in this case does not converge to its equilibrium points but across the surface (s) which is the solution of Eq. 4-383 .

Since the trajectories in the region of attraction following Eq. 4-376 is bounded by the critical energy (W_C) which has the same boundary of Eq. 4-383. Therefore, we can conclude that τ_0 is a function of W or

$$\tau_0 = \tau_0(W) \quad \text{Eq. 4-384}$$

Therefore, on the boundary of the surface (s) or energy contour, the τ_0 is constant.

For the terms with coefficient β^0 , an inhomogenous first order differential equation is as follows:

$$\begin{aligned} L_1(\tau_1) &= (y_1 - y_3) \frac{\partial \tau_1}{\partial x_1} + (y_2' - y_3) \frac{\partial \tau_1}{\partial x_2} - (\phi_{l,4}(\mathbf{X}, y_3)) \frac{\partial \tau_1}{\partial x_4} - (\phi_{l,5}(\mathbf{X}, y_3)) \frac{\partial \tau_1}{\partial x_5} \\ &- (\phi_{m,6}(\mathbf{X})) \frac{\partial \tau_1}{\partial y_1} - (\phi_{m,7}(\mathbf{X})) \frac{\partial \tau_1}{\partial y_2} - (\phi_{m,8}(\mathbf{X})) \frac{\partial \tau_1}{\partial y_3} = -\varepsilon_l \varepsilon_w \frac{\partial^2 \tau_0}{\partial x_2^2} + y_1 \frac{\partial \tau_0}{\partial y_1} + y_2 \alpha \frac{\partial \tau_0}{\partial y_2} + y_3 \frac{\partial \tau_0}{\partial y_3} - 1 \end{aligned} \quad \text{Eq. 4-385}$$

If the integration along time is the same with the integration along the energy contour, then the solution of the above equation is

$$\frac{1}{T(W)} \oint_W \left(\varepsilon_l \varepsilon_2 \frac{\partial^2 \tau_0}{\partial x_2^2} - y_1 \frac{\partial \tau_0}{\partial y_1} - y_2 \alpha \frac{\partial \tau_0}{\partial y_2} - y_3 \frac{\partial \tau_0}{\partial y_3} + 1 \right) ds = 0 \quad \text{Eq. 4-386}$$

Where $T(W) = \oint_W ds_c$ and s_c is the surface element in a Cartesian coordinate system. $T(W)$

is defined here to form the solvable boundary value problem.

Since τ_0 is a function of W , thus

$$\frac{\partial \tau_0}{\partial y_1} = \tau'_0(W) \frac{\partial W}{\partial y_1}, \quad \frac{\partial \tau_0}{\partial y_2} = \tau'_0(W) \frac{\partial W}{\partial y_2}, \quad \frac{\partial \tau_0}{\partial y_3} = \tau'_0(W) \frac{\partial W}{\partial y_3} \quad \text{Eq. 4-387}$$

$$\frac{\partial \tau_0}{\partial x_2} = \tau'_0(W) \frac{\partial W}{\partial x_2} \quad \text{and} \quad \frac{\partial^2 \tau_0}{\partial x_2^2} = \tau'_0(W) \frac{\partial^2 W}{\partial x_2^2} + \tau''_0(W) \left(\frac{\partial W}{\partial x_2} \right)^2 \quad \text{Eq. 4-388}$$

Substituting Eq. 4-388 and Eq. 4-387 into Eq. 4-386, yields

$$\frac{1}{T(W)} \oint_W \left(\varepsilon_l \varepsilon_2 \tau''_0(W) \left(\frac{\partial W}{\partial x_2} \right)^2 + \varepsilon_l \varepsilon_2 \tau'_0(W) \frac{\partial^2 W}{\partial x_2^2} - y_1 \tau'_0(W) \frac{\partial W}{\partial y_1} - y_2 \alpha \tau'_0(W) \frac{\partial W}{\partial y_2} - y_3 \tau'_0(W) \frac{\partial W}{\partial y_3} + 1 \right) ds_c = 0 \quad \text{Eq. 4-389}$$

Eq. 4-389 can be represented as the boundary value problem as follows

$$\begin{aligned} & \left(\frac{1}{T(W)} \oint_W \varepsilon_l \varepsilon_2 \left(\frac{\partial W}{\partial x_2} \right)^2 ds_c \right) \tau''_0(W) \\ & + \left(\frac{1}{T(W)} \oint_W \left(\varepsilon_l \varepsilon_2 \frac{\partial^2 W}{\partial x_2^2} - y_1 \frac{\partial W}{\partial y_1} - y_2 \alpha \frac{\partial W}{\partial y_2} - y_3 \frac{\partial W}{\partial y_3} \right) ds_c \right) \tau'_0(W) = -1 \\ & \tau_0(W_c) = 0, \quad \tau_0(0) < \infty \end{aligned} \quad \text{Eq. 4-390}$$

or

$$\left. \begin{aligned} & \varepsilon_l C_1(W) \tau''_0(W) + [\varepsilon_l C_2(W) - C_3(W)] \tau'_0(W) = -1 \\ & \tau_0(W_c) = 0, \quad \tau_0(0) < \infty \end{aligned} \right\} \quad \text{Eq. 4-391}$$

Where

$$\left. \begin{aligned} C_1(W) &= \frac{1}{T(W)} \oint_W \varepsilon_l \varepsilon_2 \left(\frac{\partial W}{\partial x_2} \right)^2 ds_c \\ C_2(W) &= \frac{1}{T(W)} \oint_W \varepsilon_l \varepsilon_2 \frac{\partial^2 W}{\partial x_2^2} ds_c \\ C_3(W) &= \frac{1}{T(W)} \oint_W \left(y_1 \frac{\partial W}{\partial y_1} + y_2 \alpha \frac{\partial W}{\partial y_2} + y_3 \frac{\partial W}{\partial y_3} \right) ds_c \end{aligned} \right\} \quad \text{Eq. 4-392}$$

Since the energy function cannot be used directly for the solution of the problem in Eq. 4-391, thus an approximate energy function based on the ellipsoidal surface is represented instead. This takes [9]

$$W = \sum_{i=1}^{n+m-1} \sum_{j=i+1}^{n+m} \left[\frac{1}{2} \frac{M_i M_j}{M_T} (y_i - y_j)^2 + \frac{1}{2} \cos(x_i^s - x_j^s) V_i V_j B_{ij} (z_i - z_j)^2 \right] \quad \text{Eq. 4-393}$$

where $M_T = \sum_{i=1}^n M_i$ and $z_i = x_i - x_i^s$ if $i = 1, 2, \dots, n+m$

This form of energy function can be used to find coefficients C_1^* , C_2 , C_3^* which are occur in the MFPT solution as follows:

$$\left. \begin{aligned} \varepsilon C_1^* W \tau_0''(W) + [\varepsilon C_2 - C_3^* W] \tau_0'(W) &= -1 \\ \tau_0(W_C) &= 0, \quad \tau_0(0) < \infty \end{aligned} \right\} \quad \text{Eq. 4-394}$$

$$\tau_0(0) \approx \frac{1}{C_3^*} (W_C)^{-C_2/C_1^*} \left[\int_0^{W_C} t^{(C_2/C_1^*)-1} \cdot e^{-(C_3^* t / \varepsilon_l C_1^*)} dt \right] e^{(C_3^* W_C / \varepsilon_l C_1^*)} \quad \text{Eq. 4-395}$$

$$\tau(0) \approx \frac{1}{\beta C_3^*} (W_C)^{-C_2/C_1^*} \left[\int_0^{W_C} t^{(C_2/C_1^*)-1} \cdot e^{-(C_3^* t / \varepsilon_l C_1^*)} dt \right] e^{(C_3^* W_C / \varepsilon_l C_1^*)} \quad \text{Eq. 4-396}$$

Where critical energy (W_C) computation technique is presented in the previous Progress Report II and coefficients C_1^* , C_2 , and C_3^* are stated in Appendix A.

4.7.3 Computation of MFPT

From Sections 4.7.1 – 4.7.2 and Appendix A, MFPT can be calculated using the next process

- (S1) Stable equilibrium points and critical energy are computed as represented in the previous topics.
- (S2) Matrix **H** can be constructed using Eqs. A-3 to A-6 in Appendix A.
- (S3) Find eigenvalues and eigenvectors of matrix **H**. After matrix **H** is constructed explicitly, software *Matlab* can possibly be used to find eigenvalues and eigenvectors.
- (S4) Construct set of matrix **D** and matrix **F** using e Eqs. A-29 to A-33 in Appendix A. These matrixes will be used in the formulation of MFPT.
- (S5) Compute C coefficient using Eqs. A-25 to A-28 in Appendix A.

(S6) Compute MFPT using Eq. 4-396. Every steps from (S1) – (S5) is done completely.

(S7) Change conditions of wind power, such as wind speed and noise intensity and repeat (S1) – (S6) again to see the variation of MFPT.

4.8 Stochastic Stability Index (SSI) Determination

The new method is developed in this study based on the theory of stochastic stability. The following list is the processes to formulate stochastic stability index as a new method.

P1. Formulate the stochastic differential equations of the power system incorporating wind power using power system dynamic equations from Sections 4.1 – 4.3.

P2. Find steady state values of state variables at different conditions such as different wind power and its noise intensity, different exchange power. It can be done by using simulation software or by solving the power flow problem using Newton-Raphson's method.

P3. Formulate stochastic well-defined energy function which is described in Sections 4.3 and 4.5

P4. Compute critical energy using method of Ribbens which is described in Section 4.5

P5. Find the derivative of mean of stochastic well-defined energy function and formulate a new stability index and compute.

P6. Evaluate the results of new stability index under different testing conditions.

Since the processes P1 to P4 are described in the previous Sections 4.1 – 4.5, this section will give the detail of how to formulate the derivative of stochastic well-defined energy function or the derivative of stochastic energy (*DSE*).

For deterministic differential equation,

$$\dot{x} = f(x) \quad , x(t_0) = x_0 \quad , t \geq t_0 \quad \text{Eq. 4-397}$$

If there exists a positive-definite function $U(x)$ ($U(x_0) = 0$ and $U(x) > 0$ for all $x \neq x_0$) such that

$$\frac{dU(x,t)}{dt} = \frac{\partial U}{\partial t} + \sum_{i=1}^d \frac{\partial U}{\partial x_i} f_i(x,t) \leq 0 \quad \text{Eq. 4-398}$$

The equilibrium of this system is called stable. A function U which satisfies these conditions is called the *Lyapunov function*.

For probabilistic or stochastic differential equations,

$$dx = f(x, t)dt + g(x, t)dW, \quad x(t_0) = x_0, \quad t \geq t_0 \quad \text{Eq. 4-399}$$

Where $f(x, t)$ is nonlinear function, $g(x, t)$ is diffusion function, and dW is Wiener process.

If there exists a positive-definite function with continuous partial differentials, $u(x, t) = U$, such that the expectation of its differentiation less than or equal to zero.

$$E(dU) \leq 0 \quad \text{for all } t \geq t_0 \quad \text{Eq. 4-400}$$

This condition will be used for a stochastic system stability analysis in the sense of Lyapunov. The function $u(x, t)$ is called the Lyapunov function belonging to the particular equilibrium state of the stochastic differential equation [26].

The differentiation of U of the stochastic system becomes:

$$dU(x, t) = (Lu(x, t))dt + \sum_{i=1}^d \sum_{j=1}^m \frac{\partial U}{\partial x_i} u_i(x, t) g_{ij}(x, t) dW_j \quad \text{Eq. 4-401}$$

The $Lu(x, t)$ is a stochastic differential operator according to Ito's sense.

$$Lu(x, t) = \frac{\partial u}{\partial t} + \frac{\partial u}{\partial x} f(x, t) + \frac{1}{2} \text{Trace} \left\{ g^T(x, t) \frac{\partial^2 u}{\partial x^2} g(x, t) \right\} \quad \text{Eq. 4-402}$$

The stability condition $dU(x, t) \leq 0$ cannot be applied directly since the indefinite sign of the stochastic term. Therefore, the expectation of the function assumes the trajectory of x stay around equilibrium points radially. Therefore, the above stability condition becomes

$$E(dU) = E[(Lu(x, t))dt] \leq 0 \quad \text{for all } t \geq t_0 \quad \text{Eq. 4-403}$$

which finally yields the stochastic stability condition

$$Lu(x, t) \leq 0 \quad \text{for all } t \geq t_0 \quad \text{Eq. 4-404}$$

$$d \begin{bmatrix} x_1 \\ x_2 \\ x_3 \\ \vdots \\ x_n \end{bmatrix} = \begin{bmatrix} f_1(x, t) \\ f_2(x, t) \\ f_2(x, t) \\ \vdots \\ f_n(x, t) \end{bmatrix} dt + \begin{bmatrix} g_1(x, t) \\ g_2(x, t) \\ g_3(x, t) \\ \vdots \\ g_n(x, t) \end{bmatrix} dW \quad \text{Eq. 4-405}$$

$$\frac{\partial U}{\partial \mathbf{x}} \mathbf{f}(\mathbf{x}, t) = \begin{bmatrix} \frac{\partial U}{\partial x_1} & \frac{\partial U}{\partial x_2} & \dots & \frac{\partial U}{\partial x_n} \end{bmatrix} \begin{bmatrix} f_1(\mathbf{x}, t) \\ f_2(\mathbf{x}, t) \\ \vdots \\ f_n(\mathbf{x}, t) \end{bmatrix} = \sum_{i=1}^n \frac{\partial U}{\partial x_i} f_i(\mathbf{x}, t) \quad \text{Eq. 4-406}$$

$$\frac{1}{2} \text{Trace} \left\{ \mathbf{g}^T(\mathbf{x}, t) \frac{\partial^2 U}{\partial \mathbf{x}^2} \mathbf{g}(\mathbf{x}, t) \right\} = \frac{1}{2} \begin{bmatrix} g_1(\mathbf{x}, t) & g_2(\mathbf{x}, t) & \dots & g_n(\mathbf{x}, t) \end{bmatrix} \begin{bmatrix} \frac{\partial^2 U}{\partial x_1 \partial x_1} & \frac{\partial^2 U}{\partial x_1 \partial x_2} & \dots & \frac{\partial^2 U}{\partial x_1 \partial x_n} \\ \frac{\partial^2 U}{\partial x_2 \partial x_1} & \frac{\partial^2 U}{\partial x_2 \partial x_2} & \dots & \frac{\partial^2 U}{\partial x_2 \partial x_n} \\ \vdots & \vdots & \ddots & \vdots \\ \frac{\partial^2 U}{\partial x_n \partial x_1} & \frac{\partial^2 U}{\partial x_n \partial x_2} & \dots & \frac{\partial^2 U}{\partial x_n \partial x_n} \end{bmatrix} \begin{bmatrix} g_1(\mathbf{x}, t) \\ g_2(\mathbf{x}, t) \\ \vdots \\ g_n(\mathbf{x}, t) \end{bmatrix} \quad \text{Eq. 4-407}$$

$$\frac{1}{2} \text{Trace} \left\{ \mathbf{g}^T(\mathbf{x}, t) \frac{\partial^2 U}{\partial \mathbf{x}^2} \mathbf{g}(\mathbf{x}, t) \right\} = \frac{1}{2} \left[\sum_{j=1}^n \sum_{i=1}^n g_i(\mathbf{x}, t) g_j(\mathbf{x}, t) \frac{\partial^2 U}{\partial x_i \partial x_j} \right]$$

The stochastic stability condition equation becomes

$$L u(\mathbf{x}, t) = \frac{\partial U}{\partial t} + \sum_{i=1}^n \frac{\partial U}{\partial x_i} f_i(\mathbf{x}, t) + \frac{1}{2} \left[\sum_{j=1}^n \sum_{i=1}^n g_i(\mathbf{x}, t) g_j(\mathbf{x}, t) \frac{\partial^2 U}{\partial x_i \partial x_j} \right] \leq 0 \quad \text{Eq. 4-408}$$

4.8.1 The derivative of stochastic energy (DSE) for small signal stability analysis

To find the stochastic stability of the power system incorporating SCIG wind turbines, it can be started with the power test system as follows:

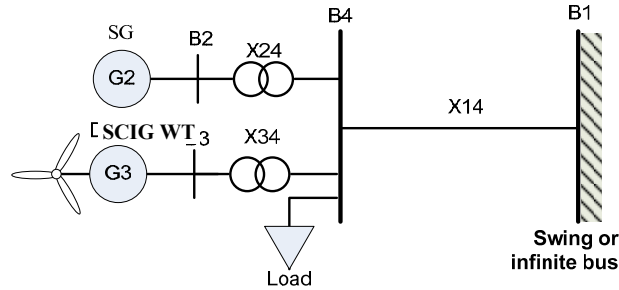


Figure 4.32 Test power system including wind power and load for *DSE* determination

For bus 1, x_1 is a reference angle of infinite bus generator and y_1 is reference speed deviation ($\bar{\omega}_{r1} - \bar{\omega}_s \approx 0$) which is close to zero. The matrix form of stochastic differential equations of the test system becomes:

$$d \begin{bmatrix} x_2 \\ x_3 \\ x_4 \\ y_2 \\ y_3 \end{bmatrix} = \begin{bmatrix} \omega_0 (y_2 - y_1) \\ \omega_0 (y_3 - y_1) - k_b V_3 \sin(k_a x_3 + c_b) \\ -\frac{1}{c_k} (\bar{P}_{l4} + \bar{P}_{e4}) - \omega_0 y_1 \\ -\frac{D_2}{M_2} y_2 + \frac{1}{M_2} (\bar{P}_{m2} - \bar{P}_{e2}) \\ \frac{1}{M_3} (\bar{P}_{m3} - \bar{P}_{e3}) \end{bmatrix} dt + \begin{bmatrix} 0 \\ 0 \\ 0 \\ 0 \\ \frac{\bar{P}_{m3}}{M_3} \alpha_3 \end{bmatrix} dW \quad \text{Eq. 4-409}$$

The next step is to find partial derivative functions of the energy function U as follows:

$$\frac{\partial U}{\partial t} = 0 \quad \text{Eq. 4-410}$$

$$\begin{aligned} \frac{\partial U}{\partial x_2} = & -P_{m2} + V_2 V_3 b_{23} \sin(x_2 - x_3) - V_1 V_2 b_{12} \sin(x_1 - x_2) \\ & + V_2 V_4 b_{24} \sin(x_2 - x_4) \end{aligned} \quad \text{Eq. 4-411}$$

$$\begin{aligned} \frac{\partial U}{\partial x_3} = & -P_{m3} - V_1 V_3 b_{13} \sin(x_1 - x_3) - V_2 V_3 b_{23} \sin(x_2 - x_3) \\ & + V_3 V_4 b_{34} \sin(x_3 - x_4) - \frac{1}{2} M_3 k_a k_b V_3 (y_3 - y_3^s) \cos(k_a x_3 + c_b) \end{aligned} \quad \text{Eq. 4-412}$$

$$\frac{\partial U}{\partial x_4} = \left(\begin{aligned} & \bar{P}_{l4} - V_1 V_4 b_{14} \sin(x_1 - x_4) - V_2 V_4 b_{24} \sin(x_2 - x_4) \\ & - V_3 V_4 b_{34} \sin(x_3 - x_4) \end{aligned} \right) = \bar{P}_{l4} + \bar{P}_{e4} \quad \text{Eq. 4-413}$$

$$\frac{\partial U}{\partial y_2} = \omega_0 M_2 y_2 \quad \text{Eq. 4-414}$$

$$\begin{aligned} \frac{\partial U}{\partial y_3} = & M_3 \left(\omega_0 (y_3 - y_1) - k_b V_3 \sin(k_a x_3 + c_b) \right) \\ & + \frac{1}{2} M_3 k_b V_3 \left(\sin(k_a x_3 + c_b) - \sin(k_a x_3^s + c_b) \right) \end{aligned} \quad \text{Eq. 4-415}$$

$$\frac{\partial^2 U}{\partial x_2^2} = V_2 V_3 b_{23} \cos(x_2 - x_3) + V_1 V_2 b_{12} \cos(x_1 - x_2) + V_2 V_4 b_{24} \cos(x_2 - x_4) \quad \text{Eq. 4-416}$$

$$\begin{aligned} \frac{\partial^2 U}{\partial x_3^2} = & V_1 V_3 b_{13} \cos(x_1 - x_3) + V_2 V_3 b_{23} \cos(x_2 - x_3) + V_3 V_4 b_{34} \cos(x_3 - x_4) \\ & + M_3 k_a^2 k_b (y_3 - y_3^s) \sin(k_a x_3 + c_b) \end{aligned} \quad \text{Eq. 4-417}$$

$$\frac{\partial^2 U}{\partial x_4^2} = V_1 V_4 b_{14} \cos(x_1 - x_4) + V_2 V_4 b_{24} \cos(x_2 - x_4) + V_3 V_4 b_{34} \cos(x_3 - x_4) \quad \text{Eq. 4-418}$$

$$\frac{\partial^2 U}{\partial y_2^2} = \omega_0 M_2 \quad \text{Eq. 4-419}$$

$$\frac{\partial^2 U}{\partial y_3^2} = M_3 \omega_0 \quad \text{Eq. 4-420}$$

$$\frac{\partial^2 U}{\partial x_2 \partial x_3} = \frac{\partial^2 U}{\partial x_3 \partial x_2} = -V_2 V_3 b_{23} \cos(x_2 - x_3) \quad \text{Eq. 4-421}$$

$$\frac{\partial^2 U}{\partial x_2 \partial x_4} = \frac{\partial^2 U}{\partial x_4 \partial x_2} = -V_2 V_4 b_{24} \cos(x_2 - x_4) \quad \text{Eq. 4-422}$$

$$\frac{\partial^2 U}{\partial x_3 \partial x_4} = \frac{\partial^2 U}{\partial x_4 \partial x_3} = -V_3 V_4 b_{34} \cos(x_3 - x_4) \quad \text{Eq. 4-423}$$

$$\frac{\partial^2 U}{\partial x_3 \partial y_3} = \frac{\partial^2 U}{\partial y_3 \partial x_3} = -\frac{1}{2} M_3 k_a k_b V_3 \cos(k_a x_3 + c_b) \quad \text{Eq. 4-424}$$

$$\frac{\partial^2 U}{\partial x_2 \partial y_2} = \frac{\partial^2 U}{\partial y_2 \partial x_2} = \frac{\partial^2 U}{\partial y_2 \partial x_3} = \frac{\partial^2 U}{\partial x_3 \partial y_2} = \frac{\partial^2 U}{\partial y_2 \partial x_4} = \frac{\partial^2 U}{\partial x_4 \partial y_2} = \frac{\partial^2 U}{\partial y_2 \partial y_3} = \frac{\partial^2 U}{\partial y_3 \partial y_2} = 0 \quad \text{Eq. 4-425}$$

Therefore, the $\frac{\partial U}{\partial \mathbf{x}} \mathbf{f}(\mathbf{x})$ is

$$\frac{\partial U}{\partial \mathbf{x}} \mathbf{f}(\mathbf{x}) = \begin{bmatrix} \frac{\partial U}{\partial x_2} & \frac{\partial U}{\partial x_3} & \frac{\partial U}{\partial x_4} & \frac{\partial U}{\partial y_2} & \frac{\partial U}{\partial y_3} \end{bmatrix} \begin{bmatrix} \omega_0 (y_2 - y_1) \\ \omega_0 (y_3 - y_1) - k_b V_3 \sin(k_a x_3 + c_b) \\ -\frac{1}{c_k} (\bar{P}_{l4} + \bar{P}_{e4}) - \omega_0 y_1 \\ -\frac{D_2}{M_2} y_2 + \frac{1}{M_2} (\bar{P}_{m2} - \bar{P}_{e2}) \\ \frac{1}{M_3} (\bar{P}_{m3} - \bar{P}_{e3}) \end{bmatrix} \quad \text{Eq. 4-426}$$

$$\begin{aligned} \frac{\partial U}{\partial \mathbf{x}} \mathbf{f}(\mathbf{x}) &= \frac{\partial U}{\partial x_2} \omega_0 (y_2 - y_1) + \frac{\partial U}{\partial x_3} (\omega_0 (y_3 - y_1) - k_b V_3 \sin(k_a x_3 + c_b)) \\ &\quad - \frac{\partial U}{\partial x_4} \frac{1}{c_k} (\bar{P}_{l4} + \bar{P}_{e4}) - \frac{\partial U}{\partial x_4} \omega_0 y_1 - \frac{\partial U}{\partial y_2} \frac{D_2}{M_2} y_2 + \frac{\partial U}{\partial y_2} \frac{1}{M_2} (\bar{P}_{m2} - \bar{P}_{e2}) \\ &\quad + \frac{\partial U}{\partial y_3} \frac{1}{M_3} (\bar{P}_{m3} - \bar{P}_{e3}) \end{aligned} \quad \text{Eq. 4-427}$$

$$\begin{aligned}
\frac{\partial U}{\partial \mathbf{x}} \mathbf{f}(\mathbf{x}) = & -\omega_0 D_2 y_2^2 - \frac{1}{c_k} (\bar{P}_{l4} + \bar{P}_{e4})^2 - \omega_0 y_1 (\bar{P}_{l4} + \bar{P}_{e4}) + \omega_0 y_1 (\bar{P}_{m2} - \bar{P}_{e2}) \\
& - \frac{1}{2} M_3 k_a k_b V_3 (y_3 - y_3^s) \cos(k_a x_3 + c_b) (\omega_0 (y_3 - y_1) - k_b V_3 \sin(k_a x_3 + c_b)) \\
& + \frac{1}{2} k_b V_3 (\bar{P}_{m3} - \bar{P}_{e3}) (\sin(k_a x_3 + c_b) - \sin(k_a x_3^s + c_b))
\end{aligned} \quad \text{Eq. 4-428}$$

The $\frac{1}{2} \text{Trace} \left\{ \mathbf{g}^T(\mathbf{x}, t) \frac{\partial^2 \mathbf{u}}{\partial \mathbf{x}^2} \mathbf{g}(\mathbf{x}, t) \right\}$ can be stated as follows:

$$\begin{aligned}
& \frac{1}{2} \text{Trace} \left\{ \mathbf{g}^T(\mathbf{x}, t) \frac{\partial^2 \mathbf{u}}{\partial \mathbf{x}^2} \mathbf{g}(\mathbf{x}, t) \right\} \\
& = \frac{1}{2} \text{Trace} \left\{ \begin{bmatrix} 0 & 0 & 0 & 0 & \frac{\bar{P}_{m3}}{M_3} \alpha_3 \end{bmatrix} \begin{bmatrix} U_{x_2 x_2} & U_{x_2 x_3} & U_{x_2 x_4} & U_{x_2 y_2} & U_{x_2 y_3} \\ U_{x_3 x_2} & U_{x_3 x_3} & U_{x_3 x_4} & U_{x_3 y_2} & U_{x_3 y_3} \\ U_{x_4 x_2} & U_{x_4 x_3} & U_{x_4 x_4} & U_{x_4 y_2} & U_{x_4 y_3} \\ U_{y_2 x_2} & U_{y_2 x_3} & U_{y_2 x_4} & U_{y_2 y_2} & U_{y_2 y_3} \\ U_{y_3 x_2} & U_{y_3 x_3} & U_{y_3 x_4} & U_{y_3 y_2} & U_{y_3 y_3} \end{bmatrix} \begin{bmatrix} 0 \\ 0 \\ 0 \\ 0 \\ \frac{\bar{P}_{m3}}{M_3} \alpha_3 \end{bmatrix} \right\} \quad \text{Eq. 4-429} \\
& = \frac{1}{2} U_{y_3 y_3} \left(\frac{\bar{P}_{m3}}{M_3} \alpha_3 \right)^2 = \frac{\omega_0}{2 M_3} (\bar{P}_{m3} \alpha_3)^2
\end{aligned}$$

Therefore, from the stochastic stability condition, $L u(\mathbf{x}, t) \leq 0$, the above equations can be summarized to have

$$\begin{aligned}
L u(\mathbf{x}, t) = & -\omega_0 D_2 y_2^2 - \frac{1}{c_k} (\bar{P}_{l4} + \bar{P}_{e4})^2 + \omega_0 y_1 [\bar{P}_{m2} - \bar{P}_{e2} - (\bar{P}_{l4} + \bar{P}_{e4})] + \frac{\omega_0}{2 M_3} (\bar{P}_{m3} \alpha_3)^2 \\
& - \frac{1}{2} M_3 k_a k_b V_3 (y_3 - y_3^s) \cos(k_a x_3 + c_b) (\omega_0 (y_3 - y_1) - k_b V_3 \sin(k_a x_3 + c_b)) \\
& + \frac{1}{2} k_b V_3 (\bar{P}_{m3} - \bar{P}_{e3}) (\sin(k_a x_3 + c_b) - \sin(k_a x_3^s + c_b)) \leq 0
\end{aligned} \quad \text{Eq. 4-430}$$

Simplifying the power balance terms to yields

$$\begin{aligned}
L u(\mathbf{x}, t) = & -\omega_0 D_2 y_2^2 - \frac{1}{c_k} (\Delta \bar{P}_4)^2 + \omega_0 y_1 (\Delta \bar{P}_2 - \Delta \bar{P}_4) + \frac{\omega_0}{2 M_3} (\bar{P}_{m3} \alpha_3)^2 \\
& - \frac{1}{2} M_3 k_a k_b V_3 (y_3 - y_3^s) \cos(k_a x_3 + c_b) [\omega_0 (y_3 - y_1) - k_b V_3 \sin(k_a x_3 + c_b)] \\
& + \frac{1}{2} k_b (\Delta \bar{P}_3) [\sin(k_a x_3 + c_b) - \sin(k_a x_3^s + c_b)] \leq 0
\end{aligned} \quad \text{Eq. 4-431}$$

Where $\Delta \bar{P}_4 = \bar{P}_{e4} - |\bar{P}_{l4}|$, $\Delta \bar{P}_2 = \bar{P}_{m2} - \bar{P}_{e2}$, $\Delta \bar{P}_3 = \bar{P}_{m3} - \bar{P}_{e3}$

This equation is the stability condition of this stochastic system, but it is still too complicated to analyze, therefore, the following two assumptions are applied

- 1) Trajectories of x_3 and y_3 are around and close to their equilibrium points.
- 2) The last two terms are very small (due to reason in 1)) when compared to the others and can be neglected.

The above condition becomes

$$L u(x, t) = -\omega_0 D_2 y_2^2 - \frac{1}{c_k} (\Delta \bar{P}_4)^2 + \omega_0 y_1 (\Delta \bar{P}_2 - \Delta \bar{P}_4) + \frac{\omega_0}{2M_3} (\bar{P}_{m3} \alpha_3)^2 \leq 0 \quad \text{Eq. 4-432}$$

This equation is the stability condition of this test system but it is not convenient for analysis. Therefore, the following assumptions are stated. The trajectories of x_3 and y_3 are around and close to their equilibrium points. The last two terms in Eq. 4-432 are very small when compare to the other terms and can be neglected. The speed deviation of SG is very small and can be neglected. Accordingly, the derivative of stochastic energy (*DSE*) can be formulated from Eq. 4-432 as follows

$$DSE \approx -\frac{1}{c_k} (\Delta \bar{P}_4)^2 + \frac{\omega_0}{2M_3} (\bar{P}_{m3} \alpha_3)^2 \quad \text{Eq. 4-433}$$

If considering the effects of fluctuations of wind power on the stability of the power system, the above equation can be represented in the form of the limitation of α_3 as

$$\begin{aligned} (\alpha_3)^2 &\leq \frac{2M_3}{\bar{P}_{m3}^2 \omega_0} \left(\frac{1}{c_k} (\Delta \bar{P}_4)^2 + \omega_0 D_2 y_2^2 - \omega_0 y_1 (\Delta \bar{P}_2 - \Delta \bar{P}_4) \right) \quad \text{or} \\ &\frac{\omega_0 (\alpha_3 \bar{P}_{m3})^2}{2M_3 \left(\frac{1}{c_k} (\Delta \bar{P}_4)^2 + \omega_0 D_2 y_2^2 - \omega_0 y_1 (\Delta \bar{P}_2 - \Delta \bar{P}_4) \right)} \leq 1 \end{aligned} \quad \text{Eq. 4-434}$$

Furthermore, if we assume a constant angle of load bus ($\dot{x}_4 = 0, P_{l4} = P_{e4}$) and $y_1 = \bar{\omega}_{r1} - \bar{\omega}_s \approx 0$, the limitation condition of α_3 is only

$$(\alpha_3)^2 \leq \frac{2M_3 D_2 y_2^2}{\bar{P}_{m3}^2} \quad \text{or} \quad \frac{(\bar{P}_{m3} \alpha_3)^2}{2M_3 D_2 y_2^2} \leq 1 \quad \text{Eq. 4-435}$$

4.8.2 The Stochastic Stability Index (SSI) for small signal stability analysis

This sub-section focuses on the study of the effects of stochastic wind power using the new stability performance index which is called the stochastic stability index (SSI). The following conditions are used to formulate SSI.

The power test system incorporating doubly-fed induction generator (*DFIG*) wind turbines is represented as follows:

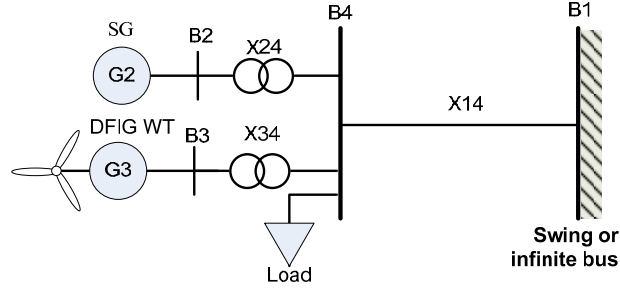


Figure 4.33 Test power system including *DFIG* wind turbine and load

For bus 1, x_1 is a reference angle of infinite bus generator and y_1 is reference speed deviation ($\bar{\omega}_{r1} - \bar{\omega}_s \approx 0$), which is close to zero.

4.8.2.1 For *DFIG* wind turbine applying Gaussian distribution white noise

1) The well-defined energy function

From the well-defined energy function of the power system including *DFIG* WT:

$$\begin{aligned}
 U = & \frac{1}{2} \omega_0 M_2 y_2^2 - \bar{P}_{m2} (x_2 - x_2^s) - \bar{P}_{m3} (x_3 - x_3^s) + \bar{P}_{l4} (x_4 - x_4^s) \\
 & + \frac{1}{2} \omega_0 M_3 (y_3^2 - y_3^{s2}) - \frac{3}{4} M_3 k_b V_{s3} \left(\sin(k_a (x_3 - x_4) + c_a) y_3 - \sin(k_a (x_3^s - x_4^s) + c_a) y_3^s \right) \\
 & + \frac{1}{3} M_3 \omega_0 k_d k_P k_{op} \left((y_3 + 1)^3 - (y_3^s + 1)^3 \right) \\
 & - \frac{1}{2} M_3 \omega_0 k_d \left[(k_{c2} \bar{V}_{s3} \cos(k_a (x_3 - x_4) + c_a) + k_{c1} \bar{V}_3) y_3^2 - (k_{c2} \bar{V}_{sw} \cos(k_a (x_3^s - x_4^s) + c_a) + k_{c1} \bar{V}_3) y_3^{s2} \right] \\
 & - \frac{1}{4} M_3 \omega_0 k_d k_P k_m \left(\bar{P}_{e3} y_3 (3 - 2y_3) - \bar{P}_{e3}^s y_3^s (3 - 2y_3^s) \right) \\
 & - \bar{V}_1 \bar{V}_4 \bar{B}_{14} (\cos(x_1 - x_4) - \cos(x_1^s - x_4^s)) \\
 & - \bar{V}_2 \bar{V}_4 \bar{B}_{24} (\cos(x_2 - x_4) - \cos(x_2^s - x_4^s)) \\
 & - \bar{V}_3 \bar{V}_4 \bar{B}_{34} (\cos(x_3 - x_4) - \cos(x_3^s - x_4^s))
 \end{aligned}$$

Eq. 4-436

2) The partial derivative components of the energy function are

$$\frac{\partial U}{\partial t} = 0$$

Eq. 4-437

$$\frac{\partial U}{\partial x_2} = -\bar{P}_{m2} + \bar{V}_2 \bar{V}_4 b_{24} \sin(x_2 - x_4) = -\bar{P}_{m2} + \bar{P}_{e2}$$

Eq. 4-438

$$\begin{aligned}
\frac{\partial U}{\partial x_3} &= -\bar{P}_{m3} + \bar{V}_3 \bar{V}_4 b_{34} \sin(x_3 - x_4) \\
&\quad + \frac{1}{2} M_3 \omega_0 k_d k_a k_{c2} \bar{V}_{s3} \sin(k_a(x_3 - x_4) + c_a) y_3^2 \\
&\quad - \frac{1}{4} M_3 \omega_0 k_d k_p k_m \bar{V}_3 \bar{V}_4 b_{34} \cos(x_3 - x_4) (3y_3 - 2y_3^2) \\
&\quad - \frac{3}{4} M_3 k_a k_b \bar{V}_{s3} \cos(k_a(x_3 - x_4) + c_a) y_3 \\
&= -\bar{P}_{m3} + \bar{P}_{e3} - f_1(x_3, x_4, y_3)
\end{aligned} \tag{Eq. 4-439}$$

$$\begin{aligned}
\frac{\partial U}{\partial x_4} &= \bar{P}_{l4} - \bar{V}_1 \bar{V}_4 b_{14} \sin(x_1 - x_4) - \bar{V}_2 \bar{V}_4 b_{24} \sin(x_2 - x_4) - \bar{V}_3 \bar{V}_4 b_{34} \sin(x_3 - x_4) \\
&\quad - \frac{1}{2} M_3 \omega_0 k_d k_a k_{c2} \bar{V}_{s3} \sin(k_a(x_3 - x_4) + c_a) y_3^2 \\
&\quad + \frac{1}{4} M_3 \omega_0 k_d k_p k_m \bar{V}_3 \bar{V}_4 b_{34} \cos(x_3 - x_4) (3y_3 - 2y_3^2) \\
&\quad + \frac{3}{4} M_3 k_a k_b \bar{V}_{s3} \cos(k_a(x_3 - x_4) + c_a) y_3 \\
&= \bar{P}_{l4} + \bar{P}_{e4} + f_1(x_3, x_4, y_3)
\end{aligned} \tag{Eq. 4-440}$$

$$\frac{\partial U}{\partial y_2} = \omega_0 M_2 y_2 \tag{Eq. 4-441}$$

$$\begin{aligned}
\frac{\partial U}{\partial y_3} &= \omega_0 M_3 y_3 + M_3 \omega_0 k_d k_p k_{op} (y_3 + 1)^2 - \frac{3}{4} M_3 k_b V_{s3} \sin(k_a(x_3 - x_4) + c_a) \\
&\quad - M_3 \omega_0 k_d (k_{c2} \bar{V}_{s3} \cos(k_a(x_3 - x_4) + c_a) + k_{c1} \bar{V}_3) y_3 \\
&\quad - \frac{1}{4} M_3 \omega_0 k_d k_p k_m \bar{V}_3 \bar{V}_4 b_{34} \sin(x_3 - x_4) (3 - 4y_3)
\end{aligned} \tag{Eq. 4-442}$$

$$\frac{\partial^2 U}{\partial x_2^2} = \bar{V}_2 \bar{V}_4 b_{24} \cos(x_2 - x_4) \tag{Eq. 4-443}$$

$$\begin{aligned}
\frac{\partial^2 U}{\partial x_3^2} &= \bar{V}_3 \bar{V}_4 b_{34} \cos(x_3 - x_4) \\
&\quad + \frac{1}{2} M_3 \omega_0 k_d k_a^2 k_{c2} \bar{V}_{s3} \cos(k_a(x_3 - x_4) + c_a) y_3^2 \\
&\quad + \frac{1}{4} M_3 \omega_0 k_d k_p k_m \bar{V}_3 \bar{V}_4 b_{34} \sin(x_3 - x_4) (3y_3 - 2y_3^2) \\
&\quad + \frac{3}{4} M_3 k_a^2 k_b \bar{V}_{s3} \sin(k_a(x_3 - x_4) + c_a) y_3
\end{aligned} \tag{Eq. 4-444}$$

$$\begin{aligned}
\frac{\partial^2 U}{\partial x_4^2} = & \bar{V}_1 \bar{V}_4 b_{14} \cos(x_1 - x_4) + \bar{V}_2 \bar{V}_4 b_{24} \cos(x_2 - x_4) + \bar{V}_3 \bar{V}_4 b_{34} \cos(x_3 - x_4) \\
& + \frac{1}{2} M_3 \omega_0 k_d k_a^2 k_{c2} \bar{V}_{s3} \cos(k_a(x_3 - x_4) + c_a) y_3^2 \\
& + \frac{1}{4} M_3 \omega_0 k_d k_P k_m \bar{V}_3 \bar{V}_4 b_{34} \sin(x_3 - x_4) (3y_3 - 2y_3^2) \\
& + \frac{3}{4} M_3 k_a^2 k_b \bar{V}_{s3} \sin(k_a(x_3 - x_4) + c_a) y_3
\end{aligned} \tag{Eq. 4-445}$$

$$\frac{\partial^2 U}{\partial y_2^2} = \omega_0 M_2 \tag{Eq. 4-446}$$

$$\begin{aligned}
\frac{\partial^2 U}{\partial y_3^2} = & \omega_0 M_3 + 2M_3 \omega_0 k_d k_P k_{op} (y_3 + 1) + M_3 \omega_0 k_d k_P k_m \bar{V}_3 \bar{V}_4 b_{34} \sin(x_3 - x_4) \\
& - M_3 \omega_0 k_d (k_{c2} \bar{V}_{s3} \cos(k_a(x_3 - x_4) + c_a) + k_{c1} \bar{V}_3)
\end{aligned} \tag{Eq. 4-447}$$

$$\frac{\partial^2 U}{\partial x_2 \partial x_3} = \frac{\partial^2 U}{\partial x_3 \partial x_2} = 0 \tag{Eq. 4-448}$$

$$\frac{\partial^2 U}{\partial x_2 \partial x_4} = \frac{\partial^2 U}{\partial x_4 \partial x_2} = -\bar{V}_2 \bar{V}_4 b_{24} \cos(x_2 - x_4) \tag{Eq. 4-449}$$

$$\begin{aligned}
\frac{\partial^2 U}{\partial x_3 \partial x_4} = & \frac{\partial^2 U}{\partial x_4 \partial x_3} = -\bar{V}_3 \bar{V}_4 b_{34} \cos(x_3 - x_4) \\
& - \frac{1}{2} M_3 \omega_0 k_d k_a^2 k_{c2} \bar{V}_{s3} \cos(k_a(x_3 - x_4) + c_a) y_3^2 \\
& - \frac{1}{4} M_3 \omega_0 k_d k_P k_m \bar{V}_3 \bar{V}_4 b_{34} \sin(x_3 - x_4) (3y_3 - 2y_3^2) \\
& - \frac{3}{4} M_3 k_a^2 k_b \bar{V}_{s3} \sin(k_a(x_3 - x_4) + c_a) y_3
\end{aligned} \tag{Eq. 4-450}$$

$$\begin{aligned}
\frac{\partial^2 U}{\partial x_3 \partial y_3} = & \frac{\partial^2 U}{\partial y_3 \partial x_3} = M_3 \omega_0 k_d k_a k_{c2} \bar{V}_{s3} \sin(k_a(x_3 - x_4) + c_a) y_3 \\
& - \frac{1}{4} M_3 \omega_0 k_d k_P k_m \bar{V}_3 \bar{V}_4 b_{34} \cos(x_3 - x_4) (3 - 4y_3) \\
& - \frac{3}{4} M_3 k_a k_b \bar{V}_{s3} \cos(k_a(x_3 - x_4) + c_a)
\end{aligned} \tag{Eq. 4-451}$$

$$\begin{aligned}
\frac{\partial^2 U}{\partial y_3 \partial x_4} = & \frac{\partial^2 U}{\partial x_4 \partial y_3} = -M_3 \omega_0 k_d k_a k_{c2} \bar{V}_{s3} \sin(k_a(x_3 - x_4) + c_a) y_3 \\
& + \frac{1}{4} M_3 \omega_0 k_d k_P k_m \bar{V}_3 \bar{V}_4 b_{34} \cos(x_3 - x_4) (3 - 4y_3) \\
& + \frac{3}{4} M_3 k_a k_b \bar{V}_{s3} \cos(k_a(x_3 - x_4) + c_a)
\end{aligned} \tag{Eq. 4-452}$$

$$\frac{\partial^2 U}{\partial x_2 \partial y_2} = \frac{\partial^2 U}{\partial y_2 \partial x_2} = \frac{\partial^2 U}{\partial y_2 \partial x_3} = \frac{\partial^2 U}{\partial x_3 \partial y_2} = \frac{\partial^2 U}{\partial y_2 \partial x_4} = \frac{\partial^2 U}{\partial x_4 \partial y_2} = \frac{\partial^2 U}{\partial y_2 \partial y_3} = \frac{\partial^2 U}{\partial y_3 \partial y_2} = 0 \quad \text{Eq. 4-453}$$

$$3) \text{ Find } \frac{\partial U}{\partial \mathbf{x}} \mathbf{f}(\mathbf{x})$$

$$\frac{\partial U}{\partial \mathbf{x}} \mathbf{f}(\mathbf{x}) = \begin{bmatrix} \frac{\partial U}{\partial x_2} & \frac{\partial U}{\partial x_3} & \frac{\partial U}{\partial x_4} & \frac{\partial U}{\partial y_2} & \frac{\partial U}{\partial y_3} \end{bmatrix} \begin{bmatrix} \omega_0 (y_2 - y_0) \\ \omega_0 (y_3 - y_0) - k_b \bar{V}_{s3} \sin(k_a |x_3 - x_4| + c_a) + \omega_0 k_d \bar{V}_{rq} \\ -\frac{1}{c_k} (\bar{P}_{l4} + \bar{P}_{e4}) - \omega_0 y_0 \\ \frac{1}{M_2} (\bar{P}_{m2} - \bar{P}_{e2}) - \frac{D_2}{M_2} y_2 \\ \frac{1}{M_3} (\bar{P}_{m3} - \bar{P}_{e3}) \end{bmatrix}$$

Eq. 4-454

$$\begin{aligned} \frac{\partial U}{\partial \mathbf{x}} \mathbf{f}(\mathbf{x}) &= \frac{\partial U}{\partial x_2} \omega_0 (y_2 - y_0) - \frac{\partial U}{\partial y_2} \frac{D_2}{M_2} y_2 + \frac{\partial U}{\partial y_3} \frac{1}{M_3} (\bar{P}_{m3} - \bar{P}_{e3}) \\ &+ \frac{\partial U}{\partial x_3} \left(\omega_0 (y_3 - y_0) - k_b \bar{V}_{s3} \sin(k_a |x_3 - x_4| + c_a) + \omega_0 k_d \bar{V}_{rq} \right) \\ &- \frac{\partial U}{\partial x_4} \frac{1}{c_k} (\bar{P}_{l4} + \bar{P}_{e4}) - \frac{\partial U}{\partial x_4} \omega_0 y_1 + \frac{\partial U}{\partial y_2} \frac{1}{M_2} (\bar{P}_{m2} - \bar{P}_{e2}) \end{aligned} \quad \text{Eq. 4-455}$$

$$\begin{aligned} \frac{\partial U}{\partial \mathbf{x}} \mathbf{f}(\mathbf{x}) &= (-\bar{P}_{m2} + \bar{P}_{e2}) \omega_0 (y_2 - y_0) \\ &+ (-\bar{P}_{m3} + \bar{P}_{e3} - f_1(x_3, x_4, y_3)) \begin{pmatrix} \omega_0 (y_3 - y_0) \\ -k_b \bar{V}_{s3} \sin(k_a |x_3 - x_4| + c_a) \\ +\omega_0 k_d \bar{V}_{rq} \end{pmatrix} \\ &- (\bar{P}_{l4} + \bar{P}_{e4} + f_1(x_3, x_4, y_3)) \frac{1}{c_k} (\bar{P}_{l4} + \bar{P}_{e4}) - (\bar{P}_{l4} + \bar{P}_{e4} + f_1(x_3, x_4, y_3)) \omega_0 y_0 \\ &+ (\omega_0 M_2 y_2) \frac{1}{M_2} (\bar{P}_{m2} - \bar{P}_{e2}) - (\omega_0 M_2 y_2) \frac{D_2}{M_2} y_2 \\ &+ \left(\begin{aligned} &\omega_0 M_3 y_3 + M_3 \omega_0 k_d k_p k_{op} (y_3 + 1)^2 - \frac{3}{4} M_3 k_b V_{s3} \sin(k_a (x_3 - x_4) + c_a) \\ &- M_3 \omega_0 k_d (k_{c2} \bar{V}_{s3} \cos(k_a (x_3 - x_4) + c_a) + k_{c1} \bar{V}_3) y_3 \\ &- \frac{1}{4} M_3 \omega_0 k_d k_p k_m \bar{V}_3 \bar{V}_4 b_{34} \sin(x_3 - x_4) (3 - 4y_3) \end{aligned} \right) \frac{1}{M_3} (\bar{P}_{m3} - \bar{P}_{e3}) \end{aligned}$$

Eq. 4-456

If y_0 is close to zero, it can be neglected,

$$\begin{aligned} \frac{\partial U}{\partial \mathbf{x}} \mathbf{f}(\mathbf{x}) = & -\frac{1}{c_k} (\bar{P}_{l4} + \bar{P}_{e4})^2 - \frac{1}{c_k} f_1(x_3, x_4, y_3) (\bar{P}_{l4} + \bar{P}_{e4}) - \omega_0 D_2 y_2^2 \\ & - \left((\bar{P}_{m3} - \bar{P}_{e3}) + f_1(x_3, x_4, y_3) \right) \begin{pmatrix} \omega_0 y_3 \\ -k_b \bar{V}_{s3} \sin(k_a |x_3 - x_4| + c_a) \\ +\omega_0 k_d \bar{V}_{rq} \end{pmatrix} \\ & + (\bar{P}_{m3} - \bar{P}_{e3}) \begin{pmatrix} \omega_0 y_3 - k_b V_{s3} \sin(k_a (x_3 - x_4) + c_a) \\ +\omega_0 k_d k_p k_{op} (y_3 + 1)^2 \\ -\omega_0 k_d k_p k_m \bar{V}_3 \bar{V}_4 b_{34} \sin(x_3 - x_4) (1 - y_3) \\ -\omega_0 k_d (k_{c2} \bar{V}_{s3} \cos(k_a (x_3 - x_4) + c_a) + k_{c1} \bar{V}_3) y_3 \\ +\frac{1}{4} k_b V_{s3} \sin(k_a (x_3 - x_4) + c_a) \\ +\omega_0 k_d k_p k_m \bar{V}_3 \bar{V}_4 b_{34} \sin(x_3 - x_4) (1 - y_3) \\ -\frac{1}{4} \omega_0 k_d k_p k_m \bar{V}_3 \bar{V}_4 b_{34} \sin(x_3 - x_4) (3 - 4y_3) \end{pmatrix} \end{aligned} \quad \text{Eq. 4-457}$$

$$\begin{aligned} \frac{\partial U}{\partial \mathbf{x}} \mathbf{f}(\mathbf{x}) = & -\frac{1}{c_k} (\bar{P}_{l4} + \bar{P}_{e4})^2 - \frac{1}{c_k} f_1(x_3, x_4, y_3) (\bar{P}_{l4} + \bar{P}_{e4}) - \omega_0 D_2 y_2^2 \\ & - f_1(x_3, x_4, y_3) \begin{pmatrix} \omega_0 y_3 \\ -k_b \bar{V}_{s3} \sin(k_a |x_3 - x_4| + c_a) \\ +\omega_0 k_d \bar{V}_{rq} \end{pmatrix} \\ & + (\bar{P}_{m3} - \bar{P}_{e3}) \begin{pmatrix} \frac{1}{4} k_b V_{s3} \sin(k_a (x_3 - x_4) + c_a) \\ +\frac{1}{4} \omega_0 k_d k_p k_m \bar{V}_3 \bar{V}_4 b_{34} \sin(x_3 - x_4) \end{pmatrix} \end{aligned} \quad \text{Eq. 4-458}$$

$$\frac{\partial U}{\partial \mathbf{x}} \mathbf{f}(\mathbf{x}) = -c_k \left(\frac{d\mathbf{x}_4}{dt} \right)^2 - \omega_0 D_2 y_2^2 - f_1(x_3, x_4, y_3) \left(\frac{d(x_3 - x_4)}{dt} \right) + f_2(x_3, x_4, y_3) \frac{dy_3}{dt} \quad \text{Eq. 4-459}$$

Where

$$\begin{aligned}
f_1(x_3, x_4, y_3) = & -\frac{1}{2} M_3 \omega_0 k_d k_a k_{c2} \bar{V}_{s3} \sin(k_a(x_3 - x_4) + c_a) y_3^2 \\
& + \frac{1}{4} M_3 \omega_0 k_d k_p k_m \bar{V}_3 \bar{V}_4 b_{34} \cos(x_3 - x_4) (3y_3 - 2y_3^2) \\
& + \frac{3}{4} M_3 k_d k_b \bar{V}_{s3} \cos(k_a(x_3 - x_4) + c_a) y_3
\end{aligned} \tag{Eq. 4-460}$$

$$\begin{aligned}
f_2(x_3, x_4, y_3) = & \frac{1}{4} M_3 k_b V_{s3} \sin(k_a(x_3 - x_4) + c_a) \\
& + \frac{1}{4} M_3 \omega_0 k_d k_p k_m \bar{V}_3 \bar{V}_4 b_{34} \sin(x_3 - x_4)
\end{aligned} \tag{Eq. 4-461}$$

$$4) \text{ Find } \frac{1}{2} \text{Trace} \left\{ \mathbf{g}^T(\mathbf{x}, t) \frac{\partial^2 \mathbf{u}}{\partial \mathbf{x}^2} \mathbf{g}(\mathbf{x}, t) \right\}$$

$$\begin{aligned}
& \frac{1}{2} \text{Trace} \left\{ \mathbf{g}^T(\mathbf{x}, t) \frac{\partial^2 \mathbf{u}}{\partial \mathbf{x}^2} \mathbf{g}(\mathbf{x}, t) \right\} \\
& = \frac{1}{2} \text{Trace} \left\{ \begin{bmatrix} 0 & 0 & 0 & 0 & \frac{P_{m3} \alpha_3}{M_3} \end{bmatrix} \begin{bmatrix} U_{x_2 x_2} & U_{x_2 x_3} & U_{x_2 x_4} & U_{x_2 y_2} & U_{x_2 y_3} \\ U_{x_3 x_2} & U_{x_3 x_3} & U_{x_3 x_4} & U_{x_3 y_2} & U_{x_3 y_3} \\ U_{x_4 x_2} & U_{x_4 x_3} & U_{x_4 x_4} & U_{x_4 y_2} & U_{x_4 y_3} \\ U_{y_2 x_2} & U_{y_2 x_3} & U_{y_2 x_4} & U_{y_2 y_2} & U_{y_2 y_3} \\ U_{y_3 x_2} & U_{y_3 x_3} & U_{y_3 x_4} & U_{y_3 y_2} & U_{y_3 y_3} \end{bmatrix} \begin{bmatrix} 0 \\ 0 \\ 0 \\ 0 \\ \frac{P_{m3} \alpha_3}{M_3} \end{bmatrix} \right\} \tag{Eq. 4-462}
\end{aligned}$$

$$\begin{aligned}
& \frac{1}{2} \text{Trace} \left\{ \mathbf{g}^T(\mathbf{x}, t) \frac{\partial^2 \mathbf{u}}{\partial \mathbf{x}^2} \mathbf{g}(\mathbf{x}, t) \right\} = U_{y_3 y_3} \left(\frac{P_{m3} \alpha_3}{M_3} \right)^2 \\
& = \frac{\omega_0}{M_3} \left(\frac{1 + 2k_d k_p k_{op} (y_3 + 1) + k_d k_p k_m \bar{V}_3 \bar{V}_4 b_{34} \sin(x_3 - x_4)}{-k_d (k_{c2} \bar{V}_{s3} \cos(k_a(x_3 - x_4) + c_a) + k_{c1} \bar{V}_3)} \right) (P_{m3} \alpha_3)^2 \\
& = f_3(x_3, x_4, y_3) (P_{m3} \alpha_3)^2
\end{aligned} \tag{Eq. 4-463}$$

Where

$$f_3(x_3, x_4, y_3) = \frac{\omega_0}{M_3} \left(\frac{1 + 2k_d k_p k_{op} (y_3 + 1) + k_d k_p k_m \bar{V}_3 \bar{V}_4 b_{34} \sin(x_3 - x_4)}{-k_d (k_{c2} \bar{V}_{s3} \cos(k_a(x_3 - x_4) + c_a) + k_{c1} \bar{V}_3)} \right) \tag{Eq. 4-464}$$

5) The derivative of well-defined energy functions

Therefore, from the stochastic stability condition, $L u(\mathbf{x}, t) \leq 0$, the above equations can be summarized to have

$$\begin{aligned}
Lu(x, t) = & -c_k \left(\frac{dx_4}{dt} \right)^2 - \omega_0 D_2 y_2^2 - f_1(x_3, x_4, y_3) \left(\frac{d(x_3 - x_4)}{dt} \right) \\
& + f_2(x_3, x_4, y_3) \frac{dy_3}{dt} + f_3(x_3, x_4, y_3) (P_{m3} \alpha_3)^2 \leq 0
\end{aligned} \tag{Eq. 4-465}$$

It can be noticed that the first two terms on the right of Lu are the same as the derivative of the energy function of the deterministic system (pU). Therefore, the Lu is the derivative of stochastic energy function and has the stability condition the same as the pU in deterministic system. However, it can definitely prove that the pU is less than or equal to zero but not for Lu . If we multiply Lu by the scaling factor $\varphi = (1/P_{lk})^2$, the Lu becomes

$$\begin{aligned}
Lu' = \varphi Lu = & -\varphi c_k \left(\frac{dx_4}{dt} \right)^2 - \varphi \omega_0 D_2 y_2^2 - \varphi f_1(x_3, x_4, y_3) \left(\frac{d(x_3 - x_4)}{dt} \right) \\
& + \varphi f_2(x_3, x_4, y_3) \frac{dy_3}{dt} + f_3(x_3, x_4, y_3) (P'_{m3} \alpha_3)^2
\end{aligned} \tag{Eq. 4-466}$$

Where $P'_{m3} = P_{m3} / P_{l4}$ is the penetration ratio of wind power compared with the load.

Conceptually, the derivative of the energy function is the rate of change of energy when perturbed by small or large disturbances. Its negative value is the stable condition in which the energy of the system is dissipative. After disturbance in such condition, this total energy will reduce and be zero when the state variable reaches its equilibrium point. In contrast, the positive value of the derivative of energy will result in an increasing of energy until beyond the critical value and the system becomes unstable.

The Lu , compared with the derivative of the deterministic energy function (pU), is possibly the same concept as pU and can be used to formulate the stochastic stability index as follows.

4.8.2.2 For *DFIG* wind turbine applying Gaussian distribution colored noise

1) The well-defined energy function

From the well-defined energy function of the power system, including DFIG WT:

$$\begin{aligned}
U = & \frac{1}{2} \omega_0 M_2 y_2^2 + \frac{1}{2} \omega_0 M_3 (y_3^2 - y_3^{s2}) - \bar{P}_{m2} (x_2 - x_2^s) - \bar{P}_{m3} (x_3 - x_3^s) + \bar{P}_{l4} (x_4 - x_4^s) \\
& - \frac{1}{2} M_3 k_b V_{s3} \left(\sin(k_a (x_3 - x_4) + c_a) + \sin(k_a (x_3^s - x_4) + c_a) \right) (y_3 - y_3^s) \\
& + \frac{1}{3} M_3 \omega_0 k_d k_p k_{op} \left((y_3 + 1)^3 - (y_3^s + 1)^3 \right) \\
& - \frac{1}{2} M_3 \omega_0 k_d k_p k_m \bar{V}_3 \bar{V}_4 \bar{B}_{34} \left(\frac{\sin(x_3 - x_4)}{(y_3 + 1)} + \frac{\sin(x_3^s - x_4^s)}{(y_3^s + 1)} \right) (y_3 - y_3^s) \\
& - \frac{1}{2} M_3 \omega_0 k_d k_{c1} \bar{V}_3 (y_3^2 - y_3^{s2}) \\
& - \frac{1}{2} M_3 \omega_0 k_d k_{c2} \bar{V}_{s3} \left(\cos(k_a (x_3 - x_4) + c_a) y_3 + \cos(k_a (x_3^s - x_4^s) + c_a) y_3^s \right) (y_3 - y_3^s) \\
& - \bar{V}_1 \bar{V}_4 \bar{B}_{14} \left(\cos(x_1 - x_4) - \cos(x_1^s - x_4^s) \right) \\
& - \bar{V}_2 \bar{V}_4 \bar{B}_{24} \left(\cos(x_2 - x_4) - \cos(x_2^s - x_4^s) \right) \\
& - \bar{V}_3 \bar{V}_4 \bar{B}_{34} \left(\cos(x_3 - x_4) - \cos(x_3^s - x_4^s) \right) \\
& - \bar{P}_{m3} \alpha_3 \nu_3 (x_3 - x_3^s) - P_{l4} \alpha_4 \nu_4 (x_4 - x_4^s) + \frac{1}{2} \bar{P}_{m3} \alpha_3 (\nu_3^2 - \nu_3^{s2}) + \frac{1}{2} \bar{P}_{l4} \alpha_4 (\nu_4^2 - \nu_4^{s2})
\end{aligned} \tag{Eq. 4-467}$$

2) The partial derivative components of the energy function are

$$\frac{\partial U}{\partial x_i} = -\bar{P}_{mi} + \bar{V}_i \sum_{j=i+1}^n \bar{V}_j \bar{B}_{ij} \sin(x_i - x_j) - \bar{V}_i \sum_{j=i-1}^1 \bar{V}_j \bar{B}_{ij} \sin(x_j - x_i) \tag{Eq. 4-468}$$

$$\begin{aligned}
\frac{\partial U}{\partial x_w} = & -\bar{P}_{mw} + \bar{V}_w \sum_{j=w+1}^n \bar{V}_j \bar{B}_{wj} \sin(x_w - x_j) - \bar{V}_w \sum_{j=w-1}^1 \bar{V}_j \bar{B}_{wj} \sin(x_j - x_w) \\
& - \frac{1}{2} M_w k_b V_{sw} k_a \cos(k_a (x_w - x_{ref}) + c_a) (y_w - y_w^s) \\
& - \frac{1}{2} M_w \omega_0 k_d k_p k_m \frac{(y_w - y_w^s)}{(y_w + 1)} \left(\bar{V}_w \sum_{j=1}^n \bar{V}_j \bar{B}_{wj} \cos(x_w - x_j) \right) \\
& + \frac{1}{2} M_w \omega_0 k_d k_{c2} \bar{V}_{sw} k_a \sin(k_a (x_w - x_{ref}) + c_a) y_w (y_w - y_w^s) - \bar{P}_{mw} \alpha_w \nu_w
\end{aligned} \tag{Eq. 4-469}$$

$$\begin{aligned}
\frac{\partial U}{\partial x_k} = & P_{lk} + \bar{V}_k \sum_{j=i+1}^n \bar{V}_j \bar{B}_{kj} \sin(x_k - x_j) - \bar{V}_k \sum_{j=i-1}^1 \bar{V}_j \bar{B}_{kj} \sin(x_j - x_k) - P_{lk} \alpha_k \nu_k \\
& + \sum_{\substack{w=m \\ -p+1}}^m \frac{1}{2} M_w k_b V_{sw} k_a \cos(k_a (x_w - x_k) + c_a) (y_w - y_w^s) \Big|_{x_k=x_{ref}} \\
& + \sum_{\substack{w=m \\ -p+1}}^m \frac{1}{2} M_w \omega_0 k_d k_p k_m \bar{V}_w \bar{V}_k \bar{B}_{wk} \cos(x_w - x_k) \frac{(y_w - y_w^s)}{(y_w + 1)} \\
& - \sum_{\substack{w=m \\ -p+1}}^m \frac{1}{2} M_w \omega_0 k_d k_{c2} \bar{V}_{sw} k_a \sin(k_a (x_w - x_k) + c_a) y_w (y_w - y_w^s) \Big|_{x_k=x_{ref}}
\end{aligned} \tag{Eq. 4-470}$$

$$\frac{\partial U}{\partial y_i} = \omega_0 M_i y_i \quad \text{Eq. 4-471}$$

$$\begin{aligned} \frac{\partial U}{\partial y_w} = & \omega_0 M_w y_w + M_w \omega_0 k_d k_p k_{op} (y_w + 1)^2 \\ & - \frac{1}{2} M_w k_b V_{sw} \left(\sin(k_a (x_w - x_{ref}) + c_a) + \sin(k_a (x_w^s - x_{ref}^s) + c_a) \right) \\ & - \frac{1}{2} M_w \omega_0 k_d k_p k_m \left(\frac{\bar{P}_{ew} (y_w^s + 1)}{(y_w + 1)^2} + \frac{\bar{P}_{ew}^s}{(y_w^s + 1)} \right) - M_w \omega_0 k_d k_{c1} \bar{V}_w y_w \\ & - \frac{1}{2} M_w \omega_0 k_d k_{c2} \bar{V}_{sw} \left(\cos(k_a (x_w - x_{ref}) + c_a) (2y_w - y_w^s) \right. \\ & \left. + \cos(k_a (x_w^s - x_{ref}^s) + c_a) y_w^s \right) \end{aligned} \quad \text{Eq. 4-472}$$

$$\frac{\partial U}{\partial v_w} = -\bar{P}_{mw} \alpha_w (x_w - x_w^s) + \bar{P}_{mw} \alpha_w v_w \quad \text{Eq. 4-473}$$

$$\frac{\partial U}{\partial v_k} = -\bar{P}_{lk} \alpha_k (x_k - x_k^s) + \bar{P}_{lk} \alpha_k v_k \quad \text{Eq. 4-474}$$

$$\frac{\partial^2 U}{\partial v_w^2} = \bar{P}_{mw} \alpha_w \quad \text{Eq. 4-475}$$

$$\frac{\partial^2 U}{\partial v_k^2} = \bar{P}_{lk} \alpha_k \quad \text{Eq. 4-476}$$

The next step is to find a partial derivative function of the energy function U as follows:

$$\frac{\partial U}{\partial t} = 0 \quad \text{Eq. 4-477}$$

$$\frac{\partial U}{\partial x_2} = -\bar{P}_{m2} + \bar{V}_2 \bar{V}_4 b_{24} \sin(x_2 - x_4) = -\bar{P}_{m2} + \bar{P}_{e2} \quad \text{Eq. 4-478}$$

$$\begin{aligned} \frac{\partial U}{\partial x_3} = & -\bar{P}_{m3} + \bar{V}_3 \bar{V}_4 b_{34} \sin(x_3 - x_4) \\ & - \frac{1}{2} M_3 k_b V_{s3} k_a \cos(k_a (x_3 - x_4) + c_a) (y_3 - y_3^s) \\ & - \frac{1}{2} M_3 \omega_0 k_d k_p k_m \bar{V}_3 \bar{V}_4 \bar{B}_{34} \cos(x_3 - x_4) (y_3 + 1)^{-1} (y_3 - y_3^s) \\ & + \frac{1}{2} M_3 \omega_0 k_d k_{c2} \bar{V}_{s3} k_a \sin(k_a (x_3 - x_4) + c_a) y_3 (y_3 - y_3^s) - \bar{P}_{m3} \alpha_3 v_3 \\ = & -\bar{P}_{m3} (1 + \alpha_3 v_3) + \bar{P}_{e3} - f_1(x_3, x_4, y_3) \end{aligned} \quad \text{Eq. 4-479}$$

$$\begin{aligned}
\frac{\partial U}{\partial x_4} &= \bar{P}_4 - \bar{V}_1 \bar{V}_4 b_{14} \sin(x_1 - x_4) - \bar{V}_2 \bar{V}_4 b_{24} \sin(x_2 - x_4) - \bar{V}_3 \bar{V}_4 b_{34} \sin(x_3 - x_4) \\
&\quad + \frac{1}{2} M_3 k_b V_{s3} k_a \cos(k_a (x_3 - x_4) + c_a) (y_3 - y_3^s) \\
&\quad + \frac{1}{2} M_3 \omega_0 k_d k_p k_m \bar{V}_3 \bar{V}_4 \bar{B}_{34} \cos(x_3 - x_4) (y_3 + 1)^{-1} (y_3 - y_3^s) \\
&\quad - \frac{1}{2} M_3 \omega_0 k_d k_{c2} \bar{V}_{s3} k_a \sin(k_a (x_3 - x_4) + c_a) y_3 (y_3 - y_3^s) - P_{l4} \alpha_4 v_4 \\
&= \bar{P}_{l4} (1 - \alpha_4 v_4) + \bar{P}_{e4} + f_1(x_3, x_4, y_3)
\end{aligned} \tag{Eq. 4-480}$$

$$\frac{\partial U}{\partial y_2} = \omega_0 M_2 y_2 \tag{Eq. 4-481}$$

$$\begin{aligned}
\frac{\partial U}{\partial y_3} &= \omega_0 M_3 y_3 - \frac{1}{2} M_3 k_b V_{s3} \left(\sin(k_a (x_3 - x_4) + c_a) + \sin(k_a (x_3^s - x_4^s) + c_a) \right) \\
&\quad + M_3 \omega_0 k_d k_p k_{op} (y_3 + 1)^2 - M_3 \omega_0 k_d k_{c1} \bar{V}_3 y_3 \\
&\quad - \frac{1}{2} M_3 \omega_0 k_d k_p k_m \bar{V}_3 \bar{V}_4 \bar{B}_{34} \left(\frac{\sin(x_3 - x_4) (y_3^s + 1)}{(y_3 + 1)^2} + \frac{\sin(x_3^s - x_4^s)}{(y_3^s + 1)} \right) \\
&\quad - \frac{1}{2} M_3 \omega_0 k_d k_{c2} \bar{V}_{s3} \left(\frac{\cos(k_a (x_3 - x_4) + c_a) (2y_3 - y_3^s)}{+ \cos(k_a (x_3^s - x_4^s) + c_a) y_3^s} \right)
\end{aligned} \tag{Eq. 4-482}$$

$$\frac{\partial U}{\partial v_3} = -\bar{P}_{m3} \alpha_3 (x_3 - x_3^s) + \bar{P}_{m3} \alpha_3 v_3 \tag{Eq. 4-483}$$

$$\frac{\partial U}{\partial v_4} = -P_{l4} \alpha_4 (x_4 - x_4^s) + \bar{P}_{l4} \alpha_4 v_4 \tag{Eq. 4-484}$$

$$\frac{\partial^2 U}{\partial x_2^2} = \bar{V}_2 \bar{V}_4 b_{24} \cos(x_2 - x_4) \tag{Eq. 4-485}$$

$$\begin{aligned}
\frac{\partial^2 U}{\partial x_3^2} &= \bar{V}_3 \bar{V}_4 b_{34} \cos(x_3 - x_4) \\
&\quad + \frac{1}{2} M_3 k_b V_{s3} k_a^2 \sin(k_a (x_3 - x_4) + c_a) (y_3 - y_3^s) \\
&\quad + \frac{1}{2} M_3 \omega_0 k_d k_p k_m \bar{V}_3 \bar{V}_4 \bar{B}_{34} \sin(x_3 - x_4) (y_3 + 1)^{-1} (y_3 - y_3^s) \\
&\quad + \frac{1}{2} M_3 \omega_0 k_d k_{c2} \bar{V}_{s3} k_a^2 \cos(k_a (x_3 - x_4) + c_a) y_3 (y_3 - y_3^s)
\end{aligned} \tag{Eq. 4-486}$$

$$\begin{aligned}
\frac{\partial^2 U}{\partial x_4^2} &= \bar{V}_1 \bar{V}_4 b_{14} \cos(x_1 - x_4) + \bar{V}_2 \bar{V}_4 b_{24} \cos(x_2 - x_4) + \bar{V}_3 \bar{V}_4 b_{34} \cos(x_3 - x_4) \\
&+ \frac{1}{2} M_3 k_b V_{s3} k_a^2 \sin(k_a (x_3 - x_4) + c_a) (y_3 - y_3^s) \\
&+ \frac{1}{2} M_3 \omega_0 k_d k_P k_m \bar{V}_3 \bar{V}_4 \bar{B}_{34} \sin(x_3 - x_4) (y_3 + 1)^{-1} (y_3 - y_3^s) \\
&+ \frac{1}{2} M_3 \omega_0 k_d k_{c2} \bar{V}_{s3} k_a^2 \cos(k_a (x_3 - x_4) + c_a) y_3 (y_3 - y_3^s)
\end{aligned} \tag{Eq. 4-487}$$

$$\frac{\partial^2 U}{\partial y_2^2} = \omega_0 M_2 \tag{Eq. 4-488}$$

$$\begin{aligned}
\frac{\partial^2 U}{\partial y_3^2} &= \omega_0 M_3 + 2M_3 \omega_0 k_d k_P k_{op} (y_3 + 1) \\
&+ M_3 \omega_0 k_d k_P k_m \bar{V}_3 \bar{V}_4 \bar{B}_{34} \sin(x_3 - x_4) \frac{(y_3^s + 1)}{(y_3 + 1)^3} \\
&- M_3 \omega_0 k_d k_{c1} \bar{V}_3 - M_3 \omega_0 k_d k_{c2} \bar{V}_{s3} \cos(k_a (x_3 - x_4) + c_a)
\end{aligned} \tag{Eq. 4-489}$$

$$\frac{\partial^2 U}{\partial v_3^2} = \bar{P}_{m3} \alpha_3 \tag{Eq. 4-490}$$

$$\frac{\partial^2 U}{\partial v_4^2} = \bar{P}_{l4} \alpha_4 \tag{Eq. 4-491}$$

$$\frac{\partial^2 U}{\partial x_2 \partial x_3} = \frac{\partial^2 U}{\partial x_3 \partial x_2} = 0 \tag{Eq. 4-492}$$

$$\frac{\partial^2 U}{\partial x_2 \partial x_4} = \frac{\partial^2 U}{\partial x_4 \partial x_2} = -\bar{V}_2 \bar{V}_4 b_{24} \cos(x_2 - x_4) \tag{Eq. 4-493}$$

$$\begin{aligned}
\frac{\partial^2 U}{\partial x_3 \partial x_4} &= \frac{\partial^2 U}{\partial x_4 \partial x_3} = -\bar{V}_3 \bar{V}_4 b_{34} \cos(x_3 - x_4) \\
&- \frac{1}{2} M_3 k_b V_{s3} k_a^2 \sin(k_a (x_3 - x_4) + c_a) (y_3 - y_3^s) \\
&- \frac{1}{2} M_3 \omega_0 k_d k_P k_m \bar{V}_3 \bar{V}_4 \bar{B}_{34} \sin(x_3 - x_4) (y_3 + 1)^{-1} (y_3 - y_3^s) \\
&- \frac{1}{2} M_3 \omega_0 k_d k_{c2} \bar{V}_{s3} k_a^2 \cos(k_a (x_3 - x_4) + c_a) y_3 (y_3 - y_3^s)
\end{aligned} \tag{Eq. 4-494}$$

$$\begin{aligned}
\frac{\partial^2 U}{\partial x_3 \partial y_3} &= \frac{\partial^2 U}{\partial y_3 \partial x_3} = \frac{1}{2} M_3 k_b V_{s3} k_a \cos(k_a (x_3 - x_4) + c_a) \\
&- \frac{1}{2} M_3 \omega_0 k_d k_P k_m \bar{V}_3 \bar{V}_4 \bar{B}_{34} \cos(x_3 - x_4) (y_3 + 1)^{-2} (y_3^s + 1) \\
&+ \frac{1}{2} M_3 \omega_0 k_d k_{c2} \bar{V}_{s3} k_a \sin(k_a (x_3 - x_4) + c_a) (2y_3 - y_3^s)
\end{aligned} \tag{Eq. 4-495}$$

$$\begin{aligned}\frac{\partial^2 U}{\partial y_3 \partial x_4} &= \frac{\partial^2 U}{\partial x_4 \partial y_3} = \frac{1}{2} M_3 k_b V_{s3} k_a \cos(k_a (x_3 - x_4) + c_a) \\ &+ \frac{1}{2} M_3 \omega_0 k_d k_p k_m \bar{V}_3 \bar{V}_4 \bar{B}_{34} \cos(x_3 - x_4) (y_3 + 1)^{-2} (y_3^s + 1)\end{aligned}\quad \text{Eq. 4-496}$$

$$\begin{aligned}& - \frac{1}{2} M_3 \omega_0 k_d k_{c2} \bar{V}_{s3} k_a \sin(k_a (x_3 - x_4) + c_a) (2y_3 - y_3^s) \\ \frac{\partial^2 U}{\partial v_3 \partial x_3} &= \frac{\partial^2 U}{\partial x_3 \partial v_3} = -\bar{P}_{m3} \alpha_3\end{aligned}\quad \text{Eq. 4-497}$$

$$\frac{\partial^2 U}{\partial v_4 \partial x_4} = \frac{\partial^2 U}{\partial x_4 \partial v_4} = -\bar{P}_{l4} \alpha_4 \quad \text{Eq. 4-498}$$

$$\frac{\partial^2 U}{\partial x_2 \partial y_2} = \frac{\partial^2 U}{\partial y_2 \partial x_2} = \frac{\partial^2 U}{\partial y_2 \partial x_3} = \frac{\partial^2 U}{\partial x_3 \partial y_2} = \frac{\partial^2 U}{\partial y_2 \partial x_4} = \frac{\partial^2 U}{\partial x_4 \partial y_2} = \frac{\partial^2 U}{\partial y_2 \partial y_3} = \frac{\partial^2 U}{\partial y_3 \partial y_2} = 0 \quad \text{Eq. 4-499}$$

3) Find $\frac{\partial U}{\partial \mathbf{x}} \mathbf{f}(\mathbf{x})$

$$\frac{\partial U}{\partial \mathbf{x}} \mathbf{f}(\mathbf{x}) = \begin{bmatrix} \frac{\partial U}{\partial x_2} & \frac{\partial U}{\partial x_3} & \frac{\partial U}{\partial x_4} & \frac{\partial U}{\partial y_2} & \frac{\partial U}{\partial y_3} & \frac{\partial U}{\partial v_3} & \frac{\partial U}{\partial v_4} \end{bmatrix} \begin{bmatrix} \omega_0 (y_2 - y_0) \\ \omega_0 (y_3 - y_0) + \varphi_{df}(\mathbf{V}, \mathbf{x}) \\ \varphi_k(\mathbf{V}, \mathbf{x}) + \bar{P}_{l4} \alpha_4 v_4 / c_k \\ \varphi_i(\mathbf{V}, \mathbf{x}) - \beta_2 y_2 \\ \varphi_w(\mathbf{V}, \mathbf{x}) + P_{m3} \alpha_3 v_3 / M_3 \\ -\psi_3 v_3 \\ -\psi_4 v_4 \end{bmatrix} \quad \text{Eq. 4-500}$$

$$\begin{aligned}\frac{\partial U}{\partial \mathbf{x}} \mathbf{f}(\mathbf{x}) &= \frac{\partial U}{\partial x_2} \omega_0 (y_2 - y_0) + \frac{\partial U}{\partial x_3} \left(\omega_0 (y_3 - y_0) - k_b \bar{V}_{s3} \sin(k_a |x_3 - x_4| + c_a) + \omega_0 k_d \bar{V}_{rq} \right) \\ &- \frac{\partial U}{\partial x_4} \frac{1}{c_k} (\bar{P}_{l4} (1 - \alpha_4 v_4) + \bar{P}_{e4}) - \frac{\partial U}{\partial x_4} \omega_0 y_1 + \frac{\partial U}{\partial y_2} \frac{1}{M_2} (\bar{P}_{m2} - \bar{P}_{e2}) - \frac{\partial U}{\partial y_2} \frac{D_2}{M_2} y_2 \\ &+ \frac{\partial U}{\partial y_3} \frac{1}{M_3} (\bar{P}_{m3} (1 + \alpha_3 v_3) - \bar{P}_{e3}) - \psi_3 v_3 \frac{\partial U}{\partial v_3} - \psi_4 v_4 \frac{\partial U}{\partial v_4}\end{aligned}$$

Eq. 4-501

$$\begin{aligned}
\frac{\partial U}{\partial \mathbf{x}} \mathbf{f}(\mathbf{x}) = & \left(-\bar{P}_{m2} + \bar{P}_{e2} \right) \omega_0 (y_2 - y_0) \\
& + \left(-\bar{P}_{m3} (1 + \alpha_3 \nu_3) + \bar{P}_{e3} - f_1(x_3, x_4, y_3) \right) \left(\begin{array}{l} \omega_0 (y_3 - y_0) \\ -k_b \bar{V}_{s3} \sin(k_a |x_3 - x_4| + c_a) \\ + \omega_0 k_d \bar{V}_{rq} \end{array} \right) \\
& - \left(\bar{P}_{l4} (1 - \alpha_4 \nu_4) + \bar{P}_{e4} + f_1(x_3, x_4, y_3) \right) \left(\frac{1}{c_k} (\bar{P}_{l4} (1 - \alpha_4 \nu_4) + \bar{P}_{e4}) - \omega_0 y_1 \right) \\
& + (\omega_0 M_2 y_2) \frac{1}{M_2} (\bar{P}_{m2} - \bar{P}_{e2}) - (\omega_0 M_2 y_2) \frac{D_2}{M_2} y_2 \\
& + \left(\begin{array}{l} \omega_0 M_3 y_3 - \frac{1}{2} M_3 k_b V_{s3} \left(\sin(k_a (x_3 - x_4) + c_a) + \sin(k_a (x_3^s - x_4^s) + c_a) \right) \\ + M_3 \omega_0 k_d k_p k_{op} (y_3 + 1)^2 - M_3 \omega_0 k_d k_{cl} \bar{V}_3 y_3 \\ - \frac{1}{2} M_3 \omega_0 k_d k_p k_m \bar{V}_3 \bar{V}_4 \bar{B}_{34} \left(\frac{\sin(x_3 - x_4)(y_3^s + 1)}{(y_3 + 1)^2} + \frac{\sin(x_3^s - x_4^s)}{(y_3^s + 1)} \right) \\ - \frac{1}{2} M_3 \omega_0 k_d k_{c2} \bar{V}_{s3} \left(\begin{array}{l} \cos(k_a (x_3 - x_4) + c_a) (2y_3 - y_3^s) \\ + \cos(k_a (x_3^s - x_4^s) + c_a) y_3^s \end{array} \right) \end{array} \right) \frac{1}{M_3} (\bar{P}_{m3} (1 + \alpha_3 \nu_3) - \bar{P}_{e3}) \\
& + \bar{P}_{m3} \alpha_3 (x_3 - x_3^s) \psi_3 \nu_3 - \bar{P}_{m3} \alpha_3 \psi_3 \nu_3^2 + P_{l4} \alpha_4 (x_4 - x_4^s) \psi_4 \nu_4 - \bar{P}_{l4} \alpha_4 \psi_4 \nu_4^2
\end{aligned}$$

Eq. 4-502

$$\begin{aligned}
f_1(x_3, x_4, y_3) = & \frac{1}{2} M_3 k_b V_{s3} k_a \cos(k_a (x_3 - x_4) + c_a) (y_3 - y_3^s) \\
& + \frac{1}{2} M_3 \omega_0 k_d k_p k_m \bar{V}_3 \bar{V}_4 \bar{B}_{34} \cos(x_3 - x_4) (y_3 + 1)^{-1} (y_3 - y_3^s) \\
& - \frac{1}{2} M_3 \omega_0 k_d k_{c2} \bar{V}_{s3} k_a \sin(k_a (x_3 - x_4) + c_a) y_3 (y_3 - y_3^s)
\end{aligned}$$

Eq. 4-503

If y_0 is close to zero, it can be neglected, and the 2 conditions are assumed differently,

- Operating points are near and around the steady state values.
- Operating points are not close to the steady state values.

For the first condition, when operating points are near and around the steady state values

$$\begin{aligned}
\frac{\partial U}{\partial \mathbf{x}} \mathbf{f}(\mathbf{x}) = & \left(-\bar{P}_{m2} + \bar{P}_{e2} \right) \omega_0 y_2 \\
& + \left(-\bar{P}_{m3} (1 + \alpha_3 v_3) + \bar{P}_{e3} - f_1(x_3, x_4, y_3) \right) \begin{pmatrix} \omega_0 y_3 \\ -k_b \bar{V}_{s3} \sin(k_a(x_3 - x_4) + c_a) \\ +\omega_0 k_d \bar{V}_{rq} \end{pmatrix} \\
& - \left(\bar{P}_{l4} (1 - \alpha_4 v_4) + \bar{P}_{e4} + f_1(x_3, x_4, y_3) \right) \left(\frac{1}{c_k} (\bar{P}_{l4} (1 - \alpha_4 v_4) + \bar{P}_{e4}) \right) \\
& + (\omega_0 M_2 y_2) \frac{1}{M_2} (\bar{P}_{m2} - \bar{P}_{e2}) - (\omega_0 M_2 y_2) \frac{D_2}{M_2} y_2 \\
& + \begin{pmatrix} \omega_0 y_3 - k_b V_{s3} \sin(k_a(x_3 - x_4) + c_a) \\ +\omega_0 k_d k_p k_{op} (y_3 + 1)^2 - \omega_0 k_d k_p k_m \bar{V}_3 \bar{V}_4 \bar{B}_{34} \sin(x_3 - x_4) (y_3 + 1)^{-1} \\ -\omega_0 k_d k_{c1} \bar{V}_3 y_3 - \omega_0 k_d k_{c2} \bar{V}_{s3} \cos(k_a(x_3 - x_4) + c_a) y_3 \end{pmatrix} \left(\bar{P}_{m3} (1 + \alpha_3 v_3) - \bar{P}_{e3} \right) \\
& + \bar{P}_{m3} \alpha_3 (x_3 - x_3^s) \psi_3 v_3 - \bar{P}_{m3} \alpha_3 \psi_3 v_3^2 + P_{l4} \alpha_4 (x_4 - x_4^s) \psi_4 v_4 - \bar{P}_{l4} \alpha_4 \psi_4 v_4^2 \\
\frac{\partial U}{\partial \mathbf{x}} \mathbf{f}(\mathbf{x}) = & -\omega_0 D_2 y_2^2 - \frac{1}{c_k} (\bar{P}_{l4} (1 - \alpha_4 v_4) + \bar{P}_{e4})^2 - \frac{1}{c_k} f_1(x_3, x_4, y_3) (\bar{P}_{l4} (1 - \alpha_4 v_4) + \bar{P}_{e4}) \\
& - f_1(x_3, x_4, y_3) \left(\omega_0 y_3 - k_b \bar{V}_{s3} \sin(k_a(x_3 - x_4) + c_a) + \omega_0 k_d \bar{V}_{rq} \right) \\
& + \bar{P}_{m3} \alpha_3 (x_3 - x_3^s) \psi_3 v_3 - \bar{P}_{m3} \alpha_3 \psi_3 v_3^2 + P_{l4} \alpha_4 (x_4 - x_4^s) \psi_4 v_4 - \bar{P}_{l4} \alpha_4 \psi_4 v_4^2
\end{aligned}$$

Eq. 4-504

$$\begin{aligned}
\frac{\partial U}{\partial \mathbf{x}} \mathbf{f}(\mathbf{x}) = & -\frac{D_2}{\omega_0} \left(\frac{d\mathbf{x}_2}{dt} \right)^2 - c_k \left(\frac{d\mathbf{x}_4}{dt} \right)^2 - \frac{1}{\psi_3} \bar{P}_{m3} \alpha_3 \left(\frac{dv_3}{dt} \right)^2 - \frac{1}{\psi_4} \bar{P}_{lk} \alpha_4 \left(\frac{dv_4}{dt} \right)^2 \\
& - f_1(x_3, x_4, y_3) \left(\frac{d(x_3 - x_4)}{dt} \right) - \bar{P}_{m3} \alpha_3 (x_3 - x_3^s) \frac{dv_3}{dt} - \bar{P}_{lk} \alpha_4 (x_4 - x_4^s) \frac{dv_4}{dt}
\end{aligned}$$

Eq. 4-505

$$4) \text{ Find } \frac{1}{2} \text{Trace} \left\{ \mathbf{g}^T(\mathbf{x}, t) \frac{\partial^2 \mathbf{u}}{\partial \mathbf{x}^2} \mathbf{g}(\mathbf{x}, t) \right\}$$

$$\frac{1}{2} \text{Trace} \left\{ \mathbf{g}^T(\mathbf{x}, t) \frac{\partial^2 \mathbf{u}}{\partial \mathbf{x}^2} \mathbf{g}(\mathbf{x}, t) \right\}$$

$$= \frac{1}{2} \text{Trace} \left\{ \begin{bmatrix} 0 & 0 & 0 & 0 & 0 & \gamma_w \psi_w & \gamma_k \psi_k \end{bmatrix} \begin{bmatrix} U_{x_2 x_2} & U_{x_2 x_3} & U_{x_2 x_4} & U_{x_2 y_2} & U_{x_2 y_3} \\ U_{x_3 x_2} & U_{x_3 x_3} & U_{x_3 x_4} & U_{x_3 y_2} & U_{x_3 y_3} \\ U_{x_4 x_2} & U_{x_4 x_3} & U_{x_4 x_4} & U_{x_4 y_2} & U_{x_4 y_3} \\ U_{y_2 x_2} & U_{y_2 x_3} & U_{y_2 x_4} & U_{y_2 y_2} & U_{y_2 y_3} \\ U_{y_3 x_2} & U_{y_3 x_3} & U_{y_3 x_4} & U_{y_3 y_2} & U_{y_3 y_3} \end{bmatrix} \begin{bmatrix} 0 \\ 0 \\ 0 \\ 0 \\ 0 \\ \gamma_w \psi_w \\ \gamma_k \psi_k \end{bmatrix} \right\}$$

Eq. 4-506

$$\frac{1}{2} \text{Trace} \left\{ \mathbf{g}^T(\mathbf{x}, t) \frac{\partial^2 \mathbf{u}}{\partial \mathbf{x}^2} \mathbf{g}(\mathbf{x}, t) \right\} = \frac{1}{2} U_{v_3 v_3} (\gamma_3 \psi_3)^2 + \frac{1}{2} U_{v_4 v_4} (\gamma_4 \psi_4)^2$$

Eq. 4-507

$$= \frac{1}{2} \bar{P}_{m3} \alpha_3 (\gamma_3 \psi_3)^2 + \frac{1}{2} \bar{P}_{l4} \alpha_4 (\gamma_4 \psi_4)^2$$

Where

$$\gamma_3 = \frac{P_{m3} \alpha_3}{M_3} = \sqrt{2\beta \varepsilon_{l3} \varepsilon_3} \quad \text{and} \quad \gamma_4 = \frac{P_{l4} \alpha_4}{c_k} = \sqrt{2\beta \varepsilon_{l4} \varepsilon_4}$$

Eq. 4-508

$$\gamma_{34} = \frac{\gamma_3}{\gamma_4} = \frac{\sqrt{\varepsilon_{l3} \varepsilon_3}}{\sqrt{\varepsilon_{l4} \varepsilon_4}} = \frac{\bar{P}_{m3} \alpha_3}{\bar{P}_{l4} \alpha_4} \frac{c_k}{M_3} = \bar{P}'_{m3} \frac{\alpha_3 c_k}{\alpha_4 M_3}$$

Eq. 4-509

$$\sqrt{\varepsilon_{l3}} = \sqrt{\varepsilon_3} = \frac{P_{m3} \alpha_3}{M_3 \sqrt{2\beta \varepsilon_{l3}}} \quad \text{and} \quad \sqrt{\varepsilon_{l4}} = \sqrt{\varepsilon_4} = \frac{P_{l4} \alpha_4}{c_k \sqrt{2\beta \varepsilon_{l4}}}$$

Eq. 4-510

5) The derivative of well-defined energy function

Therefore, from the stochastic stability condition, $L u(\mathbf{x}, t) \leq 0$, the above equations can be summarized to have

$$L u(\mathbf{x}, t) = -\frac{D_2}{\omega_0} \left(\frac{dx_2}{dt} \right)^2 - c_k \left(\frac{dx_4}{dt} \right)^2 - \frac{1}{\psi_3} \bar{P}_{m3} \alpha_3 \left(\frac{dv_3}{dt} \right)^2 - \frac{1}{\psi_4} \bar{P}_{l4} \alpha_4 \left(\frac{dv_4}{dt} \right)^2$$

$$- f_1(x_3, x_4, y_3) \left(\frac{d(x_3 - x_4)}{dt} \right) - \bar{P}_{m3} \alpha_3 (x_3 - x_3^s) \frac{dv_3}{dt} - \bar{P}_{l4} \alpha_4 (x_4 - x_4^s) \frac{dv_4}{dt}$$

$$+ \frac{1}{2} \bar{P}_{m3} \alpha_3 (\gamma_3 \psi_3)^2 + \frac{1}{2} \bar{P}_{l4} \alpha_4 (\gamma_4 \psi_4)^2 \leq 0$$

Eq. 4-511

The first four terms on the right of Eq. 4-511 are in the form of the dissipative derivative of the energy function. The last five terms on the right are additional terms that represent the variation of power on bus 3 (wind power bus) and bus 4 (load bus).

If replacing the scaling factor with $\gamma_k = \frac{P_{lk} \alpha_k}{c_k}$ and $\gamma_w = \frac{P_{ms} \alpha_w}{M_w}$

$$\begin{aligned}
L u(x, t) = & -\frac{D_2}{\omega_0} \left(\frac{dx_2}{dt} \right)^2 - c_k \left(\frac{dx_4}{dt} \right)^2 - \frac{1}{\psi_3} \bar{P}_{m3} \alpha_3 \left(\frac{dv_3}{dt} \right)^2 - \frac{1}{\psi_4} \bar{P}_{lk} \alpha_4 \left(\frac{dv_4}{dt} \right)^2 \\
& - f_1(x_3, x_4, y_3) \left(\frac{d(x_3 - x_4)}{dt} \right) - \bar{P}_{m3} \alpha_3 (x_3 - x_3^s) \frac{dv_3}{dt} - \bar{P}_{lk} \alpha_4 (x_4 - x_4^s) \frac{dv_4}{dt} \\
& + \frac{1}{2} (\bar{P}_{m3} \alpha_3)^3 \left(\frac{\psi_3}{M_3} \right)^2 + \frac{1}{2} (\bar{P}_{lk} \alpha_4)^3 \left(\frac{\psi_4}{c_k} \right)^2 \leq 0
\end{aligned}$$

Eq. 4-512

If only wind power is perturbed by stochastic wind, the load is assumed to be constant during the studied period. Eq. 4-512 becomes

$$\begin{aligned}
L u(x, t) = & -\frac{D_2}{\omega_0} \left(\frac{dx_2}{dt} \right)^2 - c_k \left(\frac{dx_4}{dt} \right)^2 - \frac{1}{\psi_3} \bar{P}_{m3} \alpha_3 \left(\frac{dv_3}{dt} \right)^2 \\
& - f_1(x_3, x_4, y_3) \left(\frac{d(x_3 - x_4)}{dt} \right) - \bar{P}_{m3} \alpha_3 (x_3 - x_3^s) \frac{dv_3}{dt} + \frac{1}{2} (\bar{P}_{m3} \alpha_3)^3 \left(\frac{\psi_3}{M_3} \right)^2 \leq 0
\end{aligned}$$

Eq. 4-513

If only the electric load is perturbed by stochastic variation, the wind power is assumed to be constant during the studied period, Eq. 4-512 becomes

$$\begin{aligned}
L u(x, t) = & -\frac{D_2}{\omega_0} \left(\frac{dx_2}{dt} \right)^2 - c_k \left(\frac{dx_4}{dt} \right)^2 - \frac{1}{\psi_4} \bar{P}_{lk} \alpha_4 \left(\frac{dv_4}{dt} \right)^2 \\
& - f_1(x_3, x_4, y_3) \left(\frac{d(x_3 - x_4)}{dt} \right) - \bar{P}_{lk} \alpha_4 (x_4 - x_4^s) \frac{dv_4}{dt} + \frac{1}{2} (\bar{P}_{lk} \alpha_4)^3 \left(\frac{\psi_4}{c_k} \right)^2 \leq 0
\end{aligned}$$

Eq. 4-514

For the condition when operating points are not close to the steady state values:

$$\begin{aligned}
\frac{\partial U}{\partial \mathbf{x}} \mathbf{f}(\mathbf{x}) = & (-\bar{P}_{m2} + \bar{P}_{e2}) \omega_0 y_2 \\
& + (-\bar{P}_{m3} (1 + \alpha_3 v_3) + \bar{P}_{e3} - f_1(x_3, x_4, y_3)) \begin{pmatrix} \omega_0 y_3 \\ -k_b \bar{V}_{s3} \sin(k_a (x_3 - x_4) + c_a) \\ + \omega_0 k_d \bar{V}_{rq} \end{pmatrix} \\
& - (\bar{P}_{l4} (1 - \alpha_4 v_4) + \bar{P}_{e4} + f_1(x_3, x_4, y_3)) \left(\frac{1}{c_k} (\bar{P}_{l4} (1 - \alpha_4 v_4) + \bar{P}_{e4}) \right) \\
& + (\omega_0 M_2 y_2) \frac{1}{M_2} (\bar{P}_{m2} - \bar{P}_{e2}) - (\omega_0 M_2 y_2) \frac{D_2}{M_2} y_2 \\
& + \begin{pmatrix} \omega_0 y_3 - k_b V_{s3} \sin(k_a (x_3 - x_4) + c_a) + \omega_0 k_d k_p k_{op} (y_3 + 1)^2 \\ - \omega_0 k_d k_{c1} \bar{V}_{s3} y_3 - \omega_0 k_d k_p k_m \bar{V}_3 \bar{V}_4 \bar{B}_{34} \frac{\sin(x_3 - x_4)}{(y_3 + 1)} \\ - \omega_0 k_d k_{c2} \bar{V}_{s3} \cos(k_a (x_3 - x_4) + c_a) y_3 \\ + \frac{1}{2} k_b V_{s3} (\sin(k_a (x_3 - x_4) + c_a) - \sin(k_a (x_3^s - x_4^s) + c_a)) \\ + \frac{1}{2} \omega_0 k_d k_p k_m \bar{V}_3 \bar{V}_4 \bar{B}_{34} \left(\frac{\sin(x_3 - x_4) (2y_3 - y_3^s + 1)}{(y_3 + 1)^2} - \frac{\sin(x_3^s - x_4^s)}{(y_3^s + 1)} \right) \\ + \frac{1}{2} \omega_0 k_d k_{c2} \bar{V}_{s3} \begin{pmatrix} \cos(k_a (x_3 - x_4) + c_a) \\ - \cos(k_a (x_3^s - x_4^s) + c_a) \end{pmatrix} y_3^s \end{pmatrix} (\bar{P}_{m3} (1 + \alpha_3 v_3) - \bar{P}_{e3}) \\
& + \bar{P}_{m3} \alpha_3 (x_3 - x_3^s) \psi_3 v_3 - \bar{P}_{m3} \alpha_3 \psi_3 v_3^2 + P_{l4} \alpha_4 (x_4 - x_4^s) \psi_4 v_4 - \bar{P}_{l4} \alpha_4 \psi_4 v_4^2
\end{aligned}$$

Eq. 4-515

$$\begin{aligned}
\frac{\partial U}{\partial \mathbf{x}} \mathbf{f}(\mathbf{x}) = & -\omega_0 D_2 y_2^2 - \frac{1}{c_k} (\bar{P}_{l4} (1 - \alpha_4 v_4) + \bar{P}_{e4})^2 - \frac{1}{c_k} f_1(x_3, x_4, y_3) (\bar{P}_{l4} (1 - \alpha_4 v_4) + \bar{P}_{e4}) \\
& - f_1(x_3, x_4, y_3) (\omega_0 y_3 - k_b \bar{V}_{s3} \sin(k_a (x_3 - x_4) + c_a) + \omega_0 k_d \bar{V}_{rq}) + f_2(x_3, x_4, y_3) (\bar{P}_{m3} (1 + \alpha_3 v_3) - \bar{P}_{e3}) \\
& + \bar{P}_{m3} \alpha_3 (x_3 - x_3^s) \psi_3 v_3 - \bar{P}_{m3} \alpha_3 \psi_3 v_3^2 + P_{l4} \alpha_4 (x_4 - x_4^s) \psi_4 v_4 - \bar{P}_{l4} \alpha_4 \psi_4 v_4^2
\end{aligned}$$

Eq. 4-516

$$\begin{aligned}
\frac{\partial U}{\partial \mathbf{x}} \mathbf{f}(\mathbf{x}) = & -\frac{D_2}{\omega_0} \left(\frac{dx_2}{dt} \right)^2 - c_k \left(\frac{dx_4}{dt} \right)^2 - \frac{1}{\psi_3} \bar{P}_{m3} \alpha_3 \left(\frac{dv_3}{dt} \right)^2 - \frac{1}{\psi_4} \bar{P}_{lk} \alpha_4 \left(\frac{dv_4}{dt} \right)^2 \\
& - f_1(x_3, x_4, y_3) \left(\frac{d(x_3 - x_4)}{dt} \right) + f_2(x_3, x_4, y_3) M_3 \frac{dy_3}{dt} - \bar{P}_{m3} \alpha_3 (x_3 - x_3^s) \frac{dv_3}{dt} - \bar{P}_{lk} \alpha_4 (x_4 - x_4^s) \frac{dv_4}{dt}
\end{aligned}$$

Eq. 4-517

The Lu of condition two, when operating points are not close to the steady state value, is

$$\begin{aligned}
Lu(x, t) = & -\frac{D_2}{\omega_0} \left(\frac{dx_2}{dt} \right)^2 - c_k \left(\frac{dx_4}{dt} \right)^2 - \frac{1}{\psi_3} \bar{P}_{m3} \alpha_3 \left(\frac{dv_3}{dt} \right)^2 - \frac{1}{\psi_4} \bar{P}_{lk} \alpha_4 \left(\frac{dv_4}{dt} \right)^2 \\
& - f_1(x_3, x_4, y_3) \left(\frac{d(x_3 - x_4)}{dt} \right) + f_2(x_3, x_4, y_3) M_3 \frac{dy_3}{dt} - \bar{P}_{m3} \alpha_3 (x_3 - x_3^s) \frac{dv_3}{dt} - \bar{P}_{lk} \alpha_4 (x_4 - x_4^s) \frac{dv_4}{dt} \\
& + \frac{1}{2} (\bar{P}_{m3} \alpha_3)^3 \left(\frac{\psi_3}{M_3} \right)^2 + \frac{1}{2} (\bar{P}_{lk} \alpha_4)^3 \left(\frac{\psi_4}{c_k} \right)^2 \leq 0
\end{aligned}$$

Eq. 4-518

$$\begin{aligned}
f_2(x_3, x_4, y_3) = & \frac{1}{2} k_b V_{s3} \left(\sin(k_a(x_3 - x_4) + c_a) - \sin(k_a(x_3^s - x_4^s) + c_a) \right) \\
& + \frac{1}{2} \omega_0 k_d k_p k_m \bar{V}_3 \bar{V}_4 \bar{B}_{34} \left(\frac{\sin(x_3 - x_4)(2y_3 - y_3^s + 1)}{(y_3 + 1)^2} - \frac{\sin(x_3^s - x_4^s)}{(y_3^s + 1)} \right) \\
& + \frac{1}{2} \omega_0 k_d k_{c2} \bar{V}_{s3} \left(\begin{array}{c} \cos(k_a(x_3 - x_4) + c_a) \\ -\cos(k_a(x_3^s - x_4^s) + c_a) \end{array} \right) y_3^s
\end{aligned}$$

Eq. 4-519

Therefore, the difference between these two conditions are the existence of the function $f_2(x, y)$. It can be noticed from Eq. 4-511, Eq. 4-512, Eq. 4-513, Eq. 4-514, and Eq. 4-518 that the first two terms on the right of Lu is the same with the derivative of the energy function of the deterministic system (pU). Comparatively, the Lu has concept similar to the derivative of stochastic energy function. However, it can definitely prove that the pU is less than or equal to zero but not for Lu . Clearly, the Lu relationship describes similar meaning of the average rate of change of energy. When Lu is negative, after disturbance, the system energy will decrease and the state variables will move toward equilibrium point. When Lu is positive, the energy may increase beyond the critical energy and the system become unstable.

Since Lu in Eq. 4-518 is quite complicated, it is assumed that the system is started from the equilibrium state in which the derivative terms are small enough and can be neglected. Therefore, Lu will be diminished by focus only on the non-derivative terms and becomes Lu' .

By dividing the critical energy (U_c) with the Lu' , the time that the energy takes to reach the critical value can be perceived. This conceptual time is then called the *Stochastic Stability Index (SSI)*. This *SSI* is improved from the previous section (*DSE*) and has the same concept with the mean first passage time (*MFPT*) which is the performance index to quantify the average time a state-space trajectory takes to change from a given operating point to the boundary of its domain of attraction (the set of all possible trajectories which

converge to equilibrium points) under the influence of small perturbations.

Compared to DSE in the previous section, Lu' is always positive while DSE can probably be positive or negative. Theoretically, without corrective action, any continuously perturbed system will surely be unstable within a definite time even under an influence of small perturbation [74]. The larger Lu means the faster the energy increases and reaches the critical value. Therefore, the Lu' is the term which has negative effect on the power system stability or can cause the system become less stable.

4.8.3 The Stochastic Stability Index (SSI) for voltage stability analysis

To study the effect of wind power on the voltage stability of the power system using SSI, the following conditions are applied.

4.8.3.1 The well-defined energy function

The energy function of the power system can be represented as follows

$$\begin{aligned}
 U = & \frac{1}{2} \omega_0 M_2 y_2^2 + \frac{1}{2} \omega_0 M_3 (y_3^2 - y_3^{s2}) - \bar{P}_{m2} (x_2 - x_2^s) - \bar{P}_{m3} (1 + \alpha_3 v_3) (x_3 - x_3^s) \\
 & + \bar{P}_{l4} (1 - \alpha_{p4} v_{p4}) (x_{p4} - x_{p4}^s) + \frac{1}{2} \bar{Q}_{04} (1 - \alpha_{q4} v_{q4}) (\bar{V}_4^2 - \bar{V}_4^{s2}) \\
 & - \frac{1}{2} M_3 k_b V_{s3} \left(\sin(k_a (x_3 - x_4) + c_a) + \sin(k_a (x_3^s - x_4^s) + c_a) \right) (y_3 - y_3^s) \\
 & + \frac{1}{3} M_3 \omega_0 k_d k_p k_{op} \left((y_3 + 1)^3 - (y_3^s + 1)^3 \right) - \frac{1}{2} M_3 \omega_0 k_d k_{c1} \bar{V}_3 (y_3^2 - y_3^{s2}) \\
 & - \frac{1}{2} M_3 \omega_0 k_d k_{c2} \bar{V}_{s3} \left(\cos(k_a (x_3 - x_4) + c_a) y_3 + \cos(k_a (x_3^s - x_4^s) + c_a) y_3^s \right) (y_3 - y_3^s) \\
 & - \frac{1}{2} M_3 \omega_0 k_d k_p k_m \left(\frac{\bar{P}_{e3}}{(y_3 + 1)} + \frac{\bar{P}_{e3}^s}{(y_3^s + 1)} \right) (y_3 - y_3^s) \\
 & + \frac{1}{2} \bar{P}_{m3} \alpha_3 (v_3^2 - v_3^{s2}) + \frac{1}{2} \bar{P}_{l4} \alpha_{p4} (v_{p4}^2 - v_{p4}^{s2}) + \frac{1}{2} \bar{Q}_{04} \alpha_{q4} (v_{q4}^2 - v_{q4}^{s2}) \\
 & - \bar{V}_1 \bar{V}_4 \bar{B}_{14} \left(\cos(x_1 - x_4) - \cos(x_1^s - x_4^s) \right) - \bar{V}_2 \bar{V}_4 \bar{B}_{24} \left(\cos(x_2 - x_4) - \cos(x_2^s - x_4^s) \right) \\
 & - \bar{V}_3 \bar{V}_4 \bar{B}_{34} \left(\cos(x_3 - x_4) - \cos(x_3^s - x_4^s) \right) - \frac{1}{2} B_{44} (\bar{V}_4^2 - \bar{V}_4^{s2})
 \end{aligned}$$

Eq. 4-520

4.8.3.2 The partial derivative components of the energy function

The partial derivatives of the energy function to state variables are:

$$\frac{\partial U}{\partial x_i} = -\bar{P}_{mi} + \bar{V}_i \sum_{k=m+1}^n B_{ik} \bar{V}_k \sin(x_i - x_k) + V_i \sum_{j=i+1}^m V_j B_{ij} \sin(x_i - x_j) + V_i \sum_{h=1}^{i-1} V_h B_{hi} \sin(x_h - x_i)$$

Eq. 4-521

$$\begin{aligned}
\frac{\partial U}{\partial x_w} = & -\bar{P}_{mw} + \bar{V}_w \sum_{j=w+1}^m \bar{V}_j \bar{B}_{wj} \sin(x_w - x_j) - \bar{V}_w \sum_{i=1}^{w-1} \bar{V}_i \bar{B}_{iw} \sin(x_i - x_w) + \bar{V}_w \sum_{k=m+1}^n \bar{V}_k \bar{B}_{wk} \sin(x_w - x_k) \\
& - \frac{1}{2} M_w k_b V_{sw} k_a \cos(k_a (x_w - x_{ref}) + c_a) (y_w - y_w^s) \\
& - \frac{1}{2} M_w \omega_0 k_d k_p k_m \frac{(y_w - y_w^s)}{(y_w + 1)} \left(\frac{\partial \bar{P}_{ew}}{\partial x_w} \right) \\
& + \frac{1}{2} M_w \omega_0 k_d k_{c2} \bar{V}_{sw} k_a \sin(k_a (x_w - x_{ref}) + c_a) y_w (y_w - y_w^s) - \bar{P}_{mw} \alpha_w \nu_w
\end{aligned}$$

Eq. 4-522

$$\begin{aligned}
\frac{\partial U}{\partial x_k} = & \frac{1}{2} P_{l0k} (\bar{V}_k^2 + \bar{V}_k^{s2}) (1 - \alpha_{pk} \nu_{pk}) \\
& + \bar{V}_k \sum_{l=k+1}^n \bar{V}_l \bar{B}_{kl} \sin(x_k - x_l) - \bar{V}_k \sum_{l=m+1}^{n-1} \bar{V}_l \bar{B}_{lk} \sin(x_l - x_k) - \bar{V}_k \sum_{i=1}^m \bar{V}_i \bar{B}_{ik} \sin(x_i - x_k) \\
& + \sum_{\substack{w=m \\ -p+1}}^m \frac{1}{2} M_w k_b V_{sw} k_a \cos(k_a (x_w - x_k) + c_a) (y_w - y_w^s) \Big|_{x_k=x_{ref}} \\
& - \frac{1}{2} M_w \omega_0 k_d k_p k_m \frac{(y_w - y_w^s)}{(y_w + 1)} \left(\frac{\partial \bar{P}_{ew}}{\partial x_k} \right) \Big|_{x_k=x_{ref}} \\
& - \sum_{\substack{w=m \\ -p+1}}^m \frac{1}{2} M_w \omega_0 k_d k_{c2} \bar{V}_{sw} k_a \sin(k_a (x_w - x_k) + c_a) y_w (y_w - y_w^s) \Big|_{x_k=x_{ref}}
\end{aligned}$$

Eq. 4-523

$$\frac{\partial U}{\partial y_i} = \omega_0 M_i y_i$$

Eq. 4-524

$$\begin{aligned}
\frac{\partial U}{\partial y_w} = & \omega_0 M_w y_w \\
& - \frac{1}{2} M_w k_b V_{sw} \left(\sin(k_a (x_w - x_{ref}) + c_a) + \sin(k_a (x_w^s - x_{ref}^s) + c_a) \right) + M_w \omega_0 k_d k_p k_{op} (y_w + 1)^2 \\
& - \frac{1}{2} M_w \omega_0 k_d k_p k_m \left(\frac{\bar{P}_{ew} (y_w^s + 1)}{(y_w + 1)^2} + \frac{\bar{P}_{ew}^s}{(y_w^s + 1)} \right) - M_w \omega_0 k_d k_{c1} \bar{V}_w y_w \\
& - \frac{1}{2} M_w \omega_0 k_d k_{c2} \bar{V}_{sw} \left(\cos(k_a (x_w - x_{ref}) + c_a) (2y_w - y_w^s) + \cos(k_a (x_w^s - x_{ref}^s) + c_a) y_w^s \right)
\end{aligned}$$

Eq. 4-525

$$\begin{aligned} \frac{\partial U}{\partial \bar{V}_k} &= P_{l0k} \bar{V}_k (1 - \alpha_{pk} \nu_{pk}) (x_k - x_k^s) + \bar{Q}_{0k} (1 - \alpha_{qk} \nu_{qk}) \bar{V}_k - \sum_{\substack{w=m \\ -p+1}}^m \frac{1}{2} M_w \omega_0 k_d k_p k_m \frac{(y_w - y_w^s)}{(y_w + 1)} \frac{\partial \bar{P}_{ew}}{\partial \bar{V}_k} \\ &- \sum_{i=1}^{m-1} \bar{V}_i B_{ik} \cos(x_i - x_k) - \sum_{l=k+1}^n B_{kl} \bar{V}_l \cos(x_k - x_l) - \sum_{l=m+1}^{k-1} B_{kl} \bar{V}_l \cos(x_l - x_k) - B_{kk} \bar{V}_k \end{aligned}$$

Eq. 4-526

$$\frac{\partial U}{\partial \nu_w} = -\bar{P}_{mw} \alpha_w (x_w - x_w^s) + \bar{P}_{mw} \alpha_w \nu_w$$

Eq. 4-527

$$\frac{\partial U}{\partial \nu_{pk}} = -\bar{P}_{lk} \alpha_{pk} (x_k - x_k^s) + \bar{P}_{lk} \alpha_{pk} \nu_{pk}$$

Eq. 4-528

$$\frac{\partial U}{\partial \nu_{qk}} = -\frac{1}{2} \bar{Q}_{0k} \alpha_{qk} (\bar{V}_k^2 - \bar{V}_k^{s2}) + \bar{Q}_{0k} \alpha_{qk} \nu_{qk}$$

Eq. 4-529

$$\frac{\partial^2 U}{\partial \nu_w^2} = \bar{P}_{mw} \alpha_w, \quad \frac{\partial^2 U}{\partial \nu_{pk}^2} = \bar{P}_{lk} \alpha_{pk}, \quad \frac{\partial^2 U}{\partial \nu_{qk}^2} = \bar{Q}_{0k} \alpha_{qk}$$

Eq. 4-530

Next step is to find partial derivative function of energy function U as follows

$$\frac{\partial U}{\partial t} = 0$$

Eq. 4-531

$$\frac{\partial U}{\partial x_2} = -\bar{P}_{m2} + \bar{V}_2 \bar{V}_4 b_{24} \sin(x_2 - x_4) = -\bar{P}_{m2} + \bar{P}_{e2}$$

Eq. 4-532

$$\begin{aligned} \frac{\partial U}{\partial x_3} &= -\bar{P}_{m3} + \bar{V}_3 \bar{V}_4 B_{34} \sin(x_3 - x_4) \\ &- \frac{1}{2} M_3 k_b V_{s3} k_a \cos(k_a (x_3 - x_4) + c_a) (y_3 - y_4^s) \\ &- \frac{1}{2} M_3 \omega_0 k_d k_p k_m \frac{(y_3 - y_3^s)}{(y_3 + 1)} (\bar{V}_3 \bar{V}_4 B_{34} \cos(x_3 - x_4)) \\ &+ \frac{1}{2} M_3 \omega_0 k_d k_{c2} \bar{V}_{s3} k_a \sin(k_a (x_3 - x_4) + c_a) y_3 (y_3 - y_3^s) - \bar{P}_{m3} \alpha_3 \nu_3 \\ &= -\bar{P}_{m3} (1 + \alpha_3 \nu_3) + \bar{P}_{e3} - f_1(x_3, x_4, y_3) \end{aligned}$$

Eq. 4-533

$$\begin{aligned}
\frac{\partial U}{\partial x_4} &= \frac{1}{2} \bar{P}_{l04} (\bar{V}_4^2 + \bar{V}_4^{s2}) (1 - \alpha_{p4} \nu_{p4}) - \bar{V}_1 \bar{V}_4 b_{14} \sin(x_1 - x_4) - \bar{V}_2 \bar{V}_4 b_{24} \sin(x_2 - x_4) - \bar{V}_3 \bar{V}_4 b_{34} \sin(x_3 - x_4) \\
&\quad + \frac{1}{2} M_3 k_b V_{s3} k_a \cos(k_a (x_3 - x_4) + c_a) (y_3 - y_4^s) \\
&\quad + \frac{1}{2} M_3 \omega_0 k_d k_p k_m \frac{(y_3 - y_3^s)}{(y_3 + 1)} (\bar{V}_3 \bar{V}_4 B_{34} \cos(x_3 - x_4)) \\
&\quad - \frac{1}{2} M_3 \omega_0 k_d k_{c2} \bar{V}_{s3} k_a \sin(k_a (x_3 - x_4) + c_a) y_3 (y_3 - y_3^s) \\
&= \bar{P}_{l4} (1 - \alpha_{p4} \nu_{p4}) + \bar{P}_{e4} + f_1(x_3, x_4, y_3)
\end{aligned}$$

Eq. 4-534

$$\frac{\partial U}{\partial y_2} = \omega_0 M_2 y_2$$

Eq. 4-535

$$\begin{aligned}
\frac{\partial U}{\partial y_3} &= \omega_0 M_3 y_3 - M_3 \omega_0 k_d k_{c1} \bar{V}_{s3} y_3 \\
&\quad - \frac{1}{2} M_3 k_b V_{s3} \left(\sin(k_a (x_3 - x_4) + c_a) + \sin(k_a (x_3^s - x_4^s) + c_a) \right) + M_3 \omega_0 k_d k_p k_{op} (y_3 + 1)^2 \\
&\quad - \frac{1}{2} M_3 \omega_0 k_d k_p k_m \bar{V}_{s3} B_{34} \left(\frac{\bar{V}_4 \sin(x_3 - x_4) (y_3^s + 1)}{(y_3 + 1)^2} + \frac{\bar{V}_4^s \sin(x_3^s - x_4^s)}{(y_3^s + 1)} \right) \\
&\quad - \frac{1}{2} M_3 \omega_0 k_d k_{c2} \bar{V}_{s3} \left(\cos(k_a (x_3 - x_4) + c_a) (2y_3 - y_3^s) + \cos(k_a (x_3^s - x_4^s) + c_a) y_3^s \right)
\end{aligned}$$

Eq. 4-536

$$\begin{aligned}
\frac{\partial U}{\partial V_4} &= \bar{Q}_{04} \bar{V}_4 - \frac{1}{2} M_3 \omega_0 k_d k_p k_m \frac{(y_3 - y_3^s)}{(y_3 + 1)} \bar{V}_3 B_{34} \sin(x_3 - x_4) - \bar{Q}_{04} \alpha_{q4} \nu_{q4} \bar{V}_4 \\
&\quad - \bar{V}_1 B_{14} \cos(x_1 - x_4) - \bar{V}_2 B_{24} \cos(x_2 - x_4) - \bar{V}_3 B_{34} \cos(x_3 - x_4) - B_{44} \bar{V}_4
\end{aligned}$$

Eq. 4-537

$$\frac{\partial U}{\partial \nu_3} = -\bar{P}_{m3} \alpha_3 (x_3 - x_3^s) + \bar{P}_{m3} \alpha_3 \nu_3$$

Eq. 4-538

$$\frac{\partial U}{\partial \nu_{p4}} = -\bar{P}_{l4} \alpha_{p4} (x_4 - x_4^s) + \bar{P}_{l4} \alpha_{p4} \nu_{p4}$$

Eq. 4-539

$$\frac{\partial U}{\partial \nu_{q4}} = -\frac{1}{2} \bar{Q}_{04} \alpha_{q4} (\bar{V}_4^2 - \bar{V}_4^{s2}) + \bar{Q}_{04} \alpha_{q4} \nu_{q4}$$

Eq. 4-540

$$\frac{\partial^2 U}{\partial \nu_3^2} = \bar{P}_{m3} \alpha_3, \quad \frac{\partial^2 U}{\partial \nu_{p4}^2} = \bar{P}_{l4} \alpha_{p4}, \quad \frac{\partial^2 U}{\partial \nu_{q4}^2} = \bar{Q}_{l4} \alpha_{q4}$$

Eq. 4-541

1) Find $\frac{\partial U}{\partial \mathbf{x}} f(\mathbf{x})$

$$\frac{\partial U}{\partial \mathbf{x}} f(\mathbf{x}) = \left[\frac{\partial U}{\partial x_2} \quad \frac{\partial U}{\partial x_3} \quad \frac{\partial U}{\partial x_4} \quad \frac{\partial U}{\partial y_2} \quad \frac{\partial U}{\partial y_3} \quad \frac{\partial U}{\partial \bar{V}_4} \quad \frac{\partial U}{\partial v_3} \quad \frac{\partial U}{\partial v_{p4}} \quad \frac{\partial U}{\partial v_{q4}} \right] \begin{bmatrix} \omega_0(y_2 - y_0) \\ \omega_0(y_3 - y_0) + \varphi_{df}(\mathbf{V}, \mathbf{x}) \\ \varphi_{xk}(\mathbf{V}, \mathbf{x}) + \bar{P}_{l4} \alpha_{p4} v_{p4} / c_k \\ \varphi_i(\mathbf{V}, \mathbf{x}) - \beta_2 y_2 \\ \varphi_w(\mathbf{V}, \mathbf{x}) + P_{m3} \alpha_3 v_3 / M_3 \\ \varphi_{vk}(\mathbf{V}, \mathbf{x}) + \bar{Q}_{l4} \alpha_{q4} v_{q4} / (\lambda_k \bar{V}_4) \\ -\psi_3 v_3 \\ -\psi_{p4} v_{p4} \\ -\psi_{q4} v_{q4} \end{bmatrix} \quad \text{Eq. 4-542}$$

$$\begin{aligned} \frac{\partial U}{\partial \mathbf{x}} f(\mathbf{x}) = & (-\bar{P}_{m2} + \bar{P}_{e2}) \omega_0(y_2 - y_0) + (-\bar{P}_{m3}(1 + \alpha_3 v_3) + \bar{P}_{e3} - f_1(x_3, x_4, y_3)) (\omega_0(y_3 - y_0) + \varphi_{df}(\mathbf{V}, \mathbf{x})) \\ & - (\bar{P}_{l4}(1 - \alpha_{p4} v_{p4}) + \bar{P}_{e4} + f_1(x_3, x_4, y_3)) (\varphi_{xk}(\mathbf{V}, \mathbf{x}) + \bar{P}_{l4} \alpha_{p4} v_{p4} / c_k) + (\omega_0 M_2 y_2) (\varphi_i(\mathbf{V}, \mathbf{x}) - \beta_2 y_2) \\ & + \left(\begin{aligned} & \omega_0 M_3 y_3 - M_3 \omega_0 k_d k_{c1} \bar{V}_3 y_3 \\ & - \frac{1}{2} M_3 k_b V_{s3} \left(\sin(k_a(x_3 - x_4) + c_a) + \sin(k_a(x_3^s - x_4^s) + c_a) \right) + M_3 \omega_0 k_d k_p k_{op} (y_3 + 1)^2 \\ & - \frac{1}{2} M_3 \omega_0 k_d k_p k_m \bar{V}_3 B_{34} \left(\frac{\bar{V}_4 \sin(x_3 - x_4) (y_3^s + 1)}{(y_3 + 1)^2} + \frac{\bar{V}_4^s \sin(x_3^s - x_4^s)}{(y_3^s + 1)} \right) \\ & - \frac{1}{2} M_3 \omega_0 k_d k_{c2} \bar{V}_{s3} \left(\frac{\cos(k_a(x_3 - x_4) + c_a) (2y_3 - y_3^s)}{+ \cos(k_a(x_3^s - x_4^s) + c_a) y_3^s} \right) \end{aligned} \right) \left(\begin{aligned} & \varphi_w(\mathbf{V}, \mathbf{x}) \\ & + \frac{P_{m3} \alpha_3 v_3}{M_3} \end{aligned} \right) \\ & + \left(\begin{aligned} & \bar{Q}_{04} \bar{V}_4 - \frac{1}{2} M_3 \omega_0 k_d k_p k_m \frac{(y_3 - y_3^s)}{(y_3 + 1)} \bar{V}_3 B_{34} \sin(x_3 - x_4) - \bar{Q}_{04} \alpha_{q4} v_{q4} \bar{V}_4 \\ & - \bar{V}_1 B_{14} \cos(x_1 - x_4) - \bar{V}_2 B_{24} \cos(x_2 - x_4) - \bar{V}_3 B_{34} \cos(x_3 - x_4) - B_{44} \bar{V}_4 \end{aligned} \right) \left(\begin{aligned} & \varphi_{vk}(\mathbf{V}, \mathbf{x}) + \frac{\bar{Q}_{l4} \alpha_{q4} v_{q4}}{\lambda_k \bar{V}_4} \end{aligned} \right) \\ & + (\bar{P}_{m3} \alpha_3 (x_3 - x_3^s) - \bar{P}_{m3} \alpha_3 v_3) \psi_3 v_3 + (\bar{P}_{l4} \alpha_{p4} (x_4 - x_4^s) - \bar{P}_{l4} \alpha_{p4} v_{p4}) \psi_{p4} v_{p4} \\ & + \left(\frac{1}{2} \bar{Q}_{04} \alpha_{q4} (\bar{V}_4^2 - \bar{V}_4^{s2}) - \bar{Q}_{04} \alpha_{q4} v_{q4} \right) \psi_{q4} v_{q4} \end{aligned}$$

Eq. 4-543

$$\begin{aligned}
\frac{\partial U}{\partial \mathbf{x}} \mathbf{f}(\mathbf{x}) = & \left(-\bar{P}_{m2} + \bar{P}_{e2} \right) \omega_0 (y_2 - y_0) \\
& - \left(\bar{P}_{m3} (1 + \alpha_3 v_3) - \bar{P}_{e3} + f_1(x_3, x_4, y_3) \right) \begin{pmatrix} \omega_0 (y_3 - y_0) \\ -k_b \bar{V}_{s3} \sin(k_a |x_3 - x_4| + c_a) \\ -\omega_0 k_d y_3 k_{c2} \bar{V}_{s3} \cos(k_a (x_3 - x_4) + c_a) - \omega_0 k_d y_3 k_{c1} \bar{V}_3 \\ + \omega_0 k_d k_p k_{op} (y_3 + 1)^2 - \omega_0 k_d k_p k_m \bar{P}_{e3} / (1 + y_3) \end{pmatrix} \\
& - \left(\bar{P}_{l4} (1 - \alpha_{p4} v_{p4}) + \bar{P}_{e4} + f_1(x_3, x_4, y_3) \right) \frac{1}{c_k} \left(\bar{P}_{l4} (1 - \alpha_{p4} v_{p4}) + \bar{P}_{e4} \right) \\
& + (\omega_0 M_2 y_2) \frac{1}{M_2} (\bar{P}_{m2} - \bar{P}_{e2}) - (\omega_0 M_2 y_2) \frac{D_2}{M_2} y_2 \\
& + \begin{pmatrix} \omega_0 M_3 y_3 - M_3 \omega_0 k_d k_{c1} \bar{V}_3 y_3 \\ -\frac{1}{2} M_3 k_b V_{s3} \left(\sin(k_a (x_3 - x_4) + c_a) + \sin(k_a (x_3^s - x_4^s) + c_a) \right) + M_3 \omega_0 k_d k_p k_{op} (y_3 + 1)^2 \\ -\frac{1}{2} M_3 \omega_0 k_d k_p k_m \bar{V}_3 B_{34} \left(\frac{\bar{V}_4 \sin(x_3 - x_4) (y_3^s + 1)}{(y_3 + 1)^2} + \frac{\bar{V}_4^s \sin(x_3^s - x_4^s)}{(y_3^s + 1)} \right) \\ -\frac{1}{2} M_3 \omega_0 k_d k_{c2} \bar{V}_{s3} \left(\cos(k_a (x_3 - x_4) + c_a) (2y_3 - y_3^s) + \cos(k_a (x_3^s - x_4^s) + c_a) y_3^s \right) \end{pmatrix} \frac{1}{M_3} \begin{pmatrix} \bar{P}_{m3} (1 + \alpha_3 v_3) \\ -\bar{P}_{e3} \end{pmatrix} \\
& - \begin{pmatrix} \bar{Q}_{04} \bar{V}_4 - \frac{1}{2} M_3 \omega_0 k_d k_p k_m \frac{(y_3 - y_3^s)}{(y_3 + 1)} \bar{V}_3 B_{34} \sin(x_3 - x_4) - \bar{Q}_{04} \alpha_{q4} v_{q4} \bar{V}_4 \\ -\bar{V}_1 B_{14} \cos(x_1 - x_4) - \bar{V}_2 B_{24} \cos(x_2 - x_4) - \bar{V}_3 B_{34} \cos(x_3 - x_4) - B_{44} \bar{V}_4 \end{pmatrix} \frac{1}{\lambda_k V_4} \begin{pmatrix} \bar{Q}_{l4} (1 - \alpha_{q4} v_{q4}) \\ -\bar{Q}_{e4} \end{pmatrix} \\
& + \left(\bar{P}_{m3} \alpha_3 (x_3 - x_3^s) - \bar{P}_{m3} \alpha_3 v_3 \right) \psi_3 v_3 + \left(\bar{P}_{l4} \alpha_{p4} (x_4 - x_4^s) - \bar{P}_{l4} \alpha_{p4} v_{p4} \right) \psi_{p4} v_{p4} \\
& + \left(\frac{1}{2} \bar{Q}_{04} \alpha_{q4} (\bar{V}_4^2 - \bar{V}_4^{s2}) - \bar{Q}_{04} \alpha_{q4} v_{q4} \right) \psi_{q4} v_{q4}
\end{aligned}$$

Eq. 4-544

If y_0 is close to zero, it can be neglected, and 2 conditions are assumed differently.

For the case when operating points are near and around the steady state values:

$$\frac{1}{2} k_b V_{s3} \begin{pmatrix} \sin(k_a (x_3 - x_4) + c_a) \\ + \sin(k_a (x_3^s - x_4^s) + c_a) \end{pmatrix} \approx k_b \bar{V}_{s3} \sin(k_a (x_3 - x_4) + c_a) \quad \text{Eq. 4-545}$$

$$\frac{1}{2}\omega_0 k_d k_p k_m \bar{V}_3 B_{34} \left(\frac{\bar{V}_4 \sin(x_3 - x_4)(y_3^s + 1)}{(y_3 + 1)^2} + \frac{\bar{V}_4^s \sin(x_3^s - x_4^s)}{(y_3^s + 1)} \right) \approx \omega_0 k_d k_p k_m \bar{P}_{e3} / (1 + y_3) \quad \text{Eq. 4-546}$$

$$\frac{1}{2}M_3 \omega_0 k_d k_{c2} \bar{V}_{s3} \left(\frac{\cos(k_a(x_3 - x_4) + c_a)(2y_3 - y_3^s)}{+\cos(k_a(x_3^s - x_4^s) + c_a)y_3^s} \right) \approx \omega_0 k_d y_3 k_{c2} \bar{V}_{s3} \cos(k_a(x_3 - x_4) + c_a) \quad \text{Eq. 4-547}$$

$$\left(\bar{Q}_{04} \bar{V}_4 - \bar{Q}_{04} \alpha_{q4} \nu_{q4} \bar{V}_4 - \frac{1}{2} M_3 \omega_0 k_d k_p k_m \frac{(y_3 - y_3^s)}{(y_3 + 1)} \bar{V}_3 B_{34} \sin(x_3 - x_4) \right. \\ \left. - \bar{V}_1 B_{14} \cos(x_1 - x_4) - \bar{V}_2 B_{24} \cos(x_2 - x_4) - \bar{V}_3 B_{34} \cos(x_3 - x_4) - B_{44} \bar{V}_4 \right) \quad \text{Eq. 4-548}$$

$$\approx \frac{1}{\bar{V}_4} \left(\bar{Q}_{l4} (1 - \alpha_{q4} \nu_{q4}) - \bar{Q}_{e4} \right) - \frac{1}{2} M_3 \omega_0 k_d k_p k_m \frac{(y_3 - y_3^s)}{(y_3 + 1)} \bar{V}_3 B_{34} \sin(x_3 - x_4)$$

If y_0 is close to zero, it can be neglected:

$$\begin{aligned}
\frac{\partial U}{\partial \mathbf{x}} \mathbf{f}(\mathbf{x}) = & \left(-\bar{P}_{m2} + \bar{P}_{e2} \right) \omega_0 (y_2 - y_0) \\
& - \left(\bar{P}_{m3} (1 + \alpha_3 \nu_3) - \bar{P}_{e3} \right) \begin{pmatrix} \omega_0 (y_3 - y_0) \\ -k_b \bar{V}_{s3} \sin(k_a |x_3 - x_4| + c_a) \\ -\omega_0 k_d y_3 k_{c2} \bar{V}_{s3} \cos(k_a (x_3 - x_4) + c_a) - \omega_0 k_d y_3 k_{c1} \bar{V}_3 \\ +\omega_0 k_d k_P k_{op} (y_3 + 1)^2 - \omega_0 k_d k_P k_m \bar{P}_{e3} / (1 + y_3) \end{pmatrix} \\
& + \left(\bar{P}_{m3} (1 + \alpha_3 \nu_3) - \bar{P}_{e3} \right) \begin{pmatrix} \omega_0 (y_3 - y_0) \\ -k_b \bar{V}_{s3} \sin(k_a |x_3 - x_4| + c_a) \\ -\omega_0 k_d y_3 k_{c2} \bar{V}_{s3} \cos(k_a (x_3 - x_4) + c_a) - \omega_0 k_d y_3 k_{c1} \bar{V}_3 \\ +\omega_0 k_d k_P k_{op} (y_3 + 1)^2 - \omega_0 k_d k_P k_m \bar{P}_{e3} / (1 + y_3) \end{pmatrix} \\
& - \left(\bar{P}_{l4} (1 - \alpha_{p4} \nu_{p4}) + \bar{P}_{e4} + f_1(x_3, x_4, y_3) \right) \frac{1}{c_k} \left(\bar{P}_{l4} (1 - \alpha_{p4} \nu_{p4}) + \bar{P}_{e4} \right) \\
& + \left(\omega_0 M_2 y_2 \right) \frac{1}{M_2} (\bar{P}_{m2} - \bar{P}_{e2}) - \left(\omega_0 M_2 y_2 \right) \frac{D_2}{M_2} y_2 + \frac{1}{\lambda_k \bar{V}_4^2} \left(\bar{Q}_{l4} (1 - \alpha_{q4} \nu_{q4}) - \bar{Q}_{e4} \right)^2 \\
& + \frac{1}{2 \lambda_k \bar{V}_4} M_3 \omega_0 k_d k_P k_m \frac{(y_3 - y_3^s)}{(y_3 + 1)} \bar{V}_3 B_{34} \sin(x_3 - x_4) \left(\bar{Q}_{l4} (1 - \alpha_{q4} \nu_{q4}) - \bar{Q}_{e4} \right) \\
& + \left(\bar{P}_{m3} \alpha_3 (x_3 - x_3^s) - \bar{P}_{m3} \alpha_3 \nu_3 \right) \psi_3 \nu_3 + \left(\bar{P}_{l4} \alpha_{p4} (x_4 - x_4^s) - \bar{P}_{l4} \alpha_{p4} \nu_{p4} \right) \psi_{p4} \nu_{p4} \\
& + \left(\frac{1}{2} \bar{Q}_{04} \alpha_{q4} (\bar{V}_4^2 - \bar{V}_4^{s2}) - \bar{Q}_{04} \alpha_{q4} \nu_{q4} \right) \psi_{q4} \nu_{q4}
\end{aligned} \tag{Eq. 4-549}$$

$$\begin{aligned}
\frac{\partial U}{\partial \mathbf{x}} \mathbf{f}(\mathbf{x}) = & -\frac{1}{c_k} \left(\bar{P}_{l4} (1 - \alpha_{q4} \nu_{q4}) + \bar{P}_{e4} \right)^2 - \frac{1}{c_k} f_1(x_3, x_4, y_3) \left(\bar{P}_{l4} (1 - \alpha_{q4} \nu_{q4}) + \bar{P}_{e4} \right) - \omega_0 D_2 y_2^2 \\
& - f_1(x_3, x_4, y_3) \begin{pmatrix} \omega_0 y_3 \\ -k_b \bar{V}_{s3} \sin(k_a |x_3 - x_4| + c_a) \\ +\omega_0 k_d \bar{V}_{rq} \end{pmatrix} + \frac{1}{\lambda_k \bar{V}_4^2} \left(\bar{Q}_{l4} (1 - \alpha_{q4} \nu_{q4}) - \bar{Q}_{e4} \right)^2 \\
& + f_3(x_3, x_4, y_3) \frac{1}{\lambda_k \bar{V}_4} \left(\bar{Q}_{l4} (1 - \alpha_{q4} \nu_{q4}) - \bar{Q}_{e4} \right) \\
& + \left(\bar{P}_{m3} \alpha_3 (x_3 - x_3^s) - \bar{P}_{m3} \alpha_3 \nu_3 \right) \psi_3 \nu_3 + \left(\bar{P}_{l4} \alpha_{p4} (x_4 - x_4^s) - \bar{P}_{l4} \alpha_{p4} \nu_{p4} \right) \psi_{p4} \nu_{p4} \\
& + \left(\frac{1}{2} \bar{Q}_{04} \alpha_{q4} (\bar{V}_4^2 - \bar{V}_4^{s2}) - \bar{Q}_{04} \alpha_{q4} \nu_{q4} \right) \psi_{q4} \nu_{q4}
\end{aligned}$$

Eq. 4-550

$$\begin{aligned}
\frac{\partial U}{\partial \mathbf{x}} f(\mathbf{x}) = & -\frac{D_2}{\omega_0} \left(\frac{dx_2}{dt} \right)^2 - c_k \left(\frac{dx_4}{dt} \right)^2 - f_1(x_3, x_4, y_3) \left(\frac{d(x_3 - x_4)}{dt} \right) - f_3(x_3, x_4, y_3) \frac{dV_4}{dt} + \lambda_k \left(\frac{d\bar{V}_4}{dt} \right)^2 \\
& - \bar{P}_{m3} \alpha_3 (x_3 - x_3^s) \frac{dv_3}{dt} - \frac{1}{\psi_3} \bar{P}_{m3} \alpha_3 \left(\frac{dv_3}{dt} \right)^2 - \bar{P}_{lk} \alpha_4 (x_4 - x_4^s) \frac{dv_{p4}}{dt} - \frac{1}{\psi_{p4}} \bar{P}_{lk} \alpha_{p4} \left(\frac{dv_{p4}}{dt} \right)^2 \\
& - \frac{1}{2} \bar{Q}_{04} \alpha_{q4} (\bar{V}_4^2 - \bar{V}_4^{s2}) \frac{dv_{q4}}{dt} - \frac{1}{\psi_{q4}} \bar{Q}_{l4} \alpha_{q4} \left(\frac{dv_{q4}}{dt} \right)^2
\end{aligned}$$

Eq. 4-551

Where

$$\begin{aligned}
f_1(x_3, x_4, y_3) = & \frac{1}{2} M_3 k_b V_{s3} k_a \cos(k_a (x_3 - x_4) + c_a) (y_3 - y_3^s) \\
& + \frac{1}{2} M_3 \omega_0 k_d k_p k_m \frac{(y_3 - y_3^s)}{(y_3 + 1)} (\bar{V}_3 \bar{V}_4 B_{34} \cos(x_3 - x_4)) \\
& - \frac{1}{2} M_3 \omega_0 k_d k_{c2} \bar{V}_{s3} k_a \sin(k_a (x_3 - x_4) + c_a) y_3 (y_3 - y_3^s)
\end{aligned}$$

Eq. 4-552

$$f_3(x_3, x_4, y_3) = \frac{1}{2} M_3 \omega_0 k_d k_p k_m \frac{(y_3 - y_3^s)}{(y_3 + 1)} \bar{V}_3 B_{34} \sin(x_3 - x_4)$$

Eq. 4-553

For the case when operating points are not close to the steady state values:

$$\begin{aligned}
& -\frac{1}{2} k_b V_{s3} \left(\frac{\sin(k_a (x_3 - x_4) + c_a)}{+ \sin(k_a (x_3^s - x_4^s) + c_a)} \right) = -k_b \bar{V}_{s3} \sin(k_a (x_3 - x_4) + c_a) \\
& + \frac{1}{2} k_b \bar{V}_{s3} \left(\sin(k_a (x_3 - x_4) + c_a) - \sin(k_a (x_3^s - x_4^s) + c_a) \right) \\
& - \frac{1}{2} \omega_0 k_d k_p k_m \bar{V}_3 B_{34} \left(\frac{\bar{V}_4 \sin(x_3 - x_4) (y_3^s + 1)}{(y_3 + 1)^2} + \frac{\bar{V}_4^s \sin(x_3^s - x_4^s)}{(y_3^s + 1)} \right) \\
& = -\omega_0 k_d k_p k_m \bar{V}_3 \bar{V}_4 \bar{B}_{34} \frac{\sin(x_3 - x_4)}{(y_3 + 1)} + \frac{1}{2} \omega_0 k_d k_p k_m \bar{V}_3 \bar{V}_4 \bar{B}_{34} \left(\frac{\sin(x_3 - x_4) (2y_3 - y_3^s + 1)}{(y_3 + 1)^2} - \frac{\sin(x_3^s - x_4^s)}{(y_3^s + 1)} \right)
\end{aligned}$$

Eq. 4-554

Eq. 4-555

$$\begin{aligned}
& -\frac{1}{2} M_3 \omega_0 k_d k_{c2} \bar{V}_{s3} \left(\frac{\cos(k_a (x_3 - x_4) + c_a) (2y_3 - y_3^s)}{+ \cos(k_a (x_3^s - x_4^s) + c_a) y_3^s} \right) \\
& = -\omega_0 k_d k_{c2} \bar{V}_{s3} \cos(k_a (x_3 - x_4) + c_a) y_3 + \frac{1}{2} \omega_0 k_d k_{c2} \bar{V}_{s3} \left(\frac{\cos(k_a (x_3 - x_4) + c_a)}{-\cos(k_a (x_3^s - x_4^s) + c_a)} \right) y_3^s
\end{aligned}$$

Eq. 4-556

$$\begin{aligned}
\frac{\partial U}{\partial \mathbf{x}} \mathbf{f}(\mathbf{x}) = & \left(-\bar{P}_{m2} + \bar{P}_{e2} \right) \omega_0 (y_2 - y_0) \\
& - \left(\bar{P}_{m3} (1 + \alpha_3 \nu_3) - \bar{P}_{e3} \right) \begin{pmatrix} \omega_0 (y_3 - y_0) \\ -k_b \bar{V}_{s3} \sin(k_a |x_3 - x_4| + c_a) \\ -\omega_0 k_d y_3 k_{c2} \bar{V}_{s3} \cos(k_a (x_3 - x_4) + c_a) - \omega_0 k_d y_3 k_{c1} \bar{V}_3 \\ +\omega_0 k_d k_p k_{op} (y_3 + 1)^2 - \omega_0 k_d k_p k_m \bar{P}_{e3} / (1 + y_3) \end{pmatrix} \\
& + \left(\bar{P}_{m3} (1 + \alpha_3 \nu_3) - \bar{P}_{e3} \right) \begin{pmatrix} \omega_0 (y_3 - y_0) \\ -k_b \bar{V}_{s3} \sin(k_a |x_3 - x_4| + c_a) \\ -\omega_0 k_d y_3 k_{c2} \bar{V}_{s3} \cos(k_a (x_3 - x_4) + c_a) - \omega_0 k_d y_3 k_{c1} \bar{V}_3 \\ +\omega_0 k_d k_p k_{op} (y_3 + 1)^2 - \omega_0 k_d k_p k_m \bar{P}_{e3} / (1 + y_3) \end{pmatrix} \\
& + \left(\bar{P}_{m3} (1 + \alpha_3 \nu_3) - \bar{P}_{e3} \right) \begin{pmatrix} \frac{1}{2} k_b V_{s3} \left(\sin(k_a (x_3 - x_4) + c_a) - \sin(k_a (x_3^s - x_4^s) + c_a) \right) \\ + \frac{1}{2} \omega_0 k_d k_p k_m \bar{V}_3 \bar{V}_4 \bar{B}_{34} \left(\frac{\sin(x_3 - x_4)(2y_3 - y_3^s + 1)}{(y_3 + 1)^2} - \frac{\sin(x_3^s - x_4^s)}{(y_3^s + 1)} \right) \\ + \frac{1}{2} \omega_0 k_d k_{c2} \bar{V}_{s3} \begin{pmatrix} \cos(k_a (x_3 - x_4) + c_a) \\ -\cos(k_a (x_3^s - x_4^s) + c_a) \end{pmatrix} y_3^s \end{pmatrix} \\
& - \left(\bar{P}_{l4} (1 - \alpha_{p4} \nu_{p4}) + \bar{P}_{e4} + f_1(x_3, x_4, y_3) \right) \frac{1}{c_k} \left(\bar{P}_{l4} (1 - \alpha_{p4} \nu_{p4}) + \bar{P}_{e4} \right) \\
& + (\omega_0 M_2 y_2) \frac{1}{M_2} (\bar{P}_{m2} - \bar{P}_{e2}) - (\omega_0 M_2 y_2) \frac{D_2}{M_2} y_2 + \frac{1}{\lambda_k \bar{V}_4^2} (\bar{Q}_{l4} (1 - \alpha_{q4} \nu_{q4}) - \bar{Q}_{e4})^2 \\
& + \frac{1}{2 \lambda_k \bar{V}_4} M_3 \omega_0 k_d k_p k_m \frac{(y_3 - y_3^s)}{(y_3 + 1)} \bar{V}_3 B_{34} \sin(x_3 - x_4) (\bar{Q}_{l4} (1 - \alpha_{q4} \nu_{q4}) - \bar{Q}_{e4}) \\
& + \left(\bar{P}_{m3} \alpha_3 (x_3 - x_3^s) - \bar{P}_{m3} \alpha_3 \nu_3 \right) \psi_3 \nu_3 + \left(\bar{P}_{l4} \alpha_{p4} (x_4 - x_4^s) - \bar{P}_{l4} \alpha_{p4} \nu_{p4} \right) \psi_{p4} \nu_{p4} \\
& + \left(\frac{1}{2} \bar{Q}_{04} \alpha_{q4} (\bar{V}_4^2 - \bar{V}_4^{s2}) - \bar{Q}_{04} \alpha_{q4} \nu_{q4} \right) \psi_{q4} \nu_{q4}
\end{aligned}$$

Eq. 4-557

$$2) \text{ Find } \frac{1}{2} \text{Trace} \left\{ \mathbf{g}^T(\mathbf{x}, t) \frac{\partial^2 \mathbf{u}}{\partial \mathbf{x}^2} \mathbf{g}(\mathbf{x}, t) \right\}$$

$$\frac{1}{2} \text{Trace} \left\{ \mathbf{g}^T(\mathbf{x}, t) \frac{\partial^2 \mathbf{u}}{\partial \mathbf{x}^2} \mathbf{g}(\mathbf{x}, t) \right\}$$

$$= \frac{1}{2} \text{Trace} \left\{ \begin{bmatrix} 0 & 0 & 0 & 0 & 0 & 0 & \gamma_w \psi_w & \gamma_{pk} \psi_{pk} & \gamma_{qk} \psi_{qk} \end{bmatrix} \begin{bmatrix} U_{x_2 x_2} & U_{x_2 x_3} & U_{x_2 x_4} & U_{x_2 y_2} & U_{x_2 y_3} \\ U_{x_3 x_2} & U_{x_3 x_3} & U_{x_3 x_4} & U_{x_3 y_2} & U_{x_3 y_3} \\ U_{x_4 x_2} & U_{x_4 x_3} & U_{x_4 x_4} & U_{x_4 y_2} & U_{x_4 y_3} \\ U_{y_2 x_2} & U_{y_2 x_3} & U_{y_2 x_4} & U_{y_2 y_2} & U_{y_2 y_3} \\ U_{y_3 x_2} & U_{y_3 x_3} & U_{y_3 x_4} & U_{y_3 y_2} & U_{y_3 y_3} \end{bmatrix} \begin{bmatrix} 0 \\ 0 \\ 0 \\ 0 \\ 0 \\ 0 \\ \gamma_w \psi_w \\ \gamma_{pk} \psi_{pk} \\ \gamma_{qk} \psi_{qk} \end{bmatrix} \right\}$$

Eq. 4-558

$$\frac{1}{2} \text{Trace} \left\{ \mathbf{g}^T(\mathbf{x}, t) \frac{\partial^2 \mathbf{u}}{\partial \mathbf{x}^2} \mathbf{g}(\mathbf{x}, t) \right\} = \frac{1}{2} U_{v_3 v_3} (\gamma_3 \psi_3)^2 + \frac{1}{2} U_{v_{p4} v_{p4}} (\gamma_{p4} \psi_{p4})^2 + \frac{1}{2} U_{v_{q4} v_{q4}} (\gamma_{q4} \psi_{q4})^2$$

$$= \frac{1}{2} \bar{P}_{m3} \alpha_3 (\gamma_3 \psi_3)^2 + \frac{1}{2} \bar{P}_{l4} \alpha_{p4} (\gamma_{p4} \psi_{p4})^2 + \frac{1}{2} \bar{Q}_{l4} \alpha_{q4} (\gamma_{q4} \psi_{q4})^2$$

Eq. 4-559

Where $\gamma_3 = \frac{P_{m3} \alpha_3}{M_3} = \sqrt{2 \beta \varepsilon_{l3} \varepsilon_3}$ Eq. 4-560

$$\gamma_{p4} = \frac{P_{l4} \alpha_{p4}}{c_k} = \sqrt{2 \beta \varepsilon_{lp4} \varepsilon_{p4}}$$
 Eq. 4-561

$$\gamma_{q4} = \frac{Q_{l4} \alpha_{q4}}{\lambda_k V_4} = \sqrt{2 \beta \varepsilon_{lq4} \varepsilon_{q4}}$$
 Eq. 4-562

$$\gamma_{3p4} = \frac{\gamma_3}{\gamma_{p4}} = \frac{\sqrt{\varepsilon_{l3} \varepsilon_3}}{\sqrt{\varepsilon_{lp4} \varepsilon_{p4}}} = \frac{\bar{P}_{m3} \alpha_3}{\bar{P}_{l4} \alpha_{p4}} \frac{c_k}{M_3} = \bar{P}'_{m3} \frac{\alpha_3 c_k}{\alpha_{p4} M_3}$$
 Eq. 4-563

$$\gamma_{qp4} = \frac{\gamma_{q4}}{\gamma_{p4}} = \frac{\sqrt{\varepsilon_{lq4} \varepsilon_{q4}}}{\sqrt{\varepsilon_{lp4} \varepsilon_{p4}}} = \frac{\bar{Q}_{l4} \alpha_{q4}}{\bar{P}_{l4} \alpha_{p4}} \frac{c_k}{\lambda_k V_4} = \bar{Q}'_{l4} \frac{\alpha_{q4} c_k}{\alpha_{p4} \lambda_k V_4}$$
 Eq. 4-564

$$\sqrt{\varepsilon_{l3}} = \sqrt{\varepsilon_3} = \frac{P_{m3} \alpha_3}{M_3 \sqrt{2 \beta \varepsilon_{l3}}}$$
 Eq. 4-565

$$\sqrt{\varepsilon_{lp4}} = \sqrt{\varepsilon_{p4}} = \frac{P_{l4} \alpha_{p4}}{c_k \sqrt{2 \beta \varepsilon_{lp4}}}$$
 Eq. 4-566

4.8.3.3 The derivative of well-defined energy function

Therefore, from the stochastic stability condition, $L u(x, t) \leq 0$, the above equations can be summarized to have:

$$\begin{aligned}
 L u(x, t) = & -\frac{D_2}{\omega_0} \left(\frac{dx_2}{dt} \right)^2 - c_k \left(\frac{dx_4}{dt} \right)^2 - \frac{1}{\psi_3} \bar{P}_{m3} \alpha_3 \left(\frac{dv_3}{dt} \right)^2 - \frac{1}{\psi_{p4}} \bar{P}_{lk} \alpha_{p4} \left(\frac{dv_{p4}}{dt} \right)^2 - \frac{1}{\psi_{q4}} \bar{Q}_{l4} \alpha_{q4} \left(\frac{dv_{q4}}{dt} \right)^2 \\
 & - f_1(x_3, x_4, y_3) \left(\frac{d(x_3 - x_4)}{dt} \right) + f_2(x_3, x_4, y_3) \frac{dy_3}{dt} - f_3(x_3, x_4, y_3) \frac{d\bar{V}_4}{dt} + \lambda_k \left(\frac{d\bar{V}_4}{dt} \right)^2 \\
 & - \bar{P}_{m3} \alpha_3 (x_3 - x_3^s) \frac{dv_3}{dt} - \bar{P}_{lk} \alpha_{p4} (x_4 - x_4^s) \frac{dv_{p4}}{dt} - \frac{1}{2} \bar{Q}_{04} \alpha_{q4} (\bar{V}_4^2 - \bar{V}_4^{s2}) \frac{dv_{q4}}{dt} \\
 & + \frac{1}{2} \bar{P}_{m3} \alpha_3 (\gamma_3 \psi_3)^2 + \frac{1}{2} \bar{P}_{l4} \alpha_{p4} (\gamma_{p4} \psi_{p4})^2 + \frac{1}{2} \bar{Q}_{l4} \alpha_{q4} (\gamma_{q4} \psi_{q4})^2 \leq 0
 \end{aligned}$$

Eq. 4-567

If replacing the scaling factor with

$$\begin{aligned}
 L u(x, t) = & -\frac{D_2}{\omega_0} \left(\frac{dx_2}{dt} \right)^2 - c_k \left(\frac{dx_4}{dt} \right)^2 - \frac{\bar{P}_{m3} \alpha_3}{\psi_3} \left(\frac{dv_3}{dt} \right)^2 - \frac{\bar{P}_{lk} \alpha_{p4}}{\psi_{p4}} \left(\frac{dv_{p4}}{dt} \right)^2 - \frac{\bar{Q}_{l4} \alpha_{q4}}{\psi_{q4}} \left(\frac{dv_{q4}}{dt} \right)^2 \\
 & - f_1(x_3, x_4, y_3) \left(\frac{d(x_3 - x_4)}{dt} \right) + f_2(x_3, x_4, y_3) \frac{dy_3}{dt} - f_3(x_3, x_4, y_3) \frac{d\bar{V}_4}{dt} + \lambda_k \left(\frac{d\bar{V}_4}{dt} \right)^2 \\
 & - \bar{P}_{m3} \alpha_3 (x_3 - x_3^s) \frac{dv_3}{dt} - \bar{P}_{lk} \alpha_{p4} (x_4 - x_4^s) \frac{dv_{p4}}{dt} - \frac{1}{2} \bar{Q}_{04} \alpha_{q4} (\bar{V}_4^2 - \bar{V}_4^{s2}) \frac{dv_{q4}}{dt} \\
 & + \frac{1}{2} \alpha_3^3 \bar{P}_{m3}^3 \left(\frac{\psi_3}{M_3} \right)^2 + \frac{1}{2} \alpha_{p4}^3 \bar{P}_{l4}^3 \left(\frac{\psi_{p4}}{c_k} \right)^2 + \frac{1}{2} \alpha_{q4}^3 \bar{Q}_{l4}^3 \left(\frac{\psi_{q4}}{\lambda_k V_4} \right)^2 \leq 0
 \end{aligned}$$

Eq. 4-568

Where

$$\begin{aligned}
 f_1(x_3, x_4, y_3) = & \frac{1}{2} M_3 k_b V_{s3} k_a \cos(k_a (x_3 - x_4) + c_a) (y_3 - y_3^s) \\
 & + \frac{1}{2} M_3 \omega_0 k_d k_p k_m \frac{(y_3 - y_3^s)}{(y_3 + 1)} (\bar{V}_3 \bar{V}_4 B_{34} \cos(x_3 - x_4)) \\
 & - \frac{1}{2} M_3 \omega_0 k_d k_{c2} \bar{V}_{s3} k_a \sin(k_a (x_3 - x_4) + c_a) y_3 (y_3 - y_3^s)
 \end{aligned}$$

Eq. 4-569

$$f_3(x_3, x_4, y_3) = \frac{1}{2} M_3 \omega_0 k_d k_p k_m \frac{(y_3 - y_3^s)}{(y_3 + 1)} \bar{V}_3 B_{34} \sin(x_3 - x_4)$$

Eq. 4-570

$$\begin{aligned}
f_2(x_3, x_4, y_3) = & \frac{1}{2} k_b V_{s3} \left(\sin(k_a(x_3 - x_4) + c_a) - \sin(k_a(x_3^s - x_4^s) + c_a) \right) \\
& + \frac{1}{2} \omega_0 k_d k_p k_m \bar{V}_3 \bar{V}_4 \bar{B}_{34} \left(\frac{\sin(x_3 - x_4)(2y_3 - y_3^s + 1)}{(y_3 + 1)^2} - \frac{\sin(x_3^s - x_4^s)}{(y_3^s + 1)} \right) \\
& + \frac{1}{2} \omega_0 k_d k_{c2} \bar{V}_{s3} \left(\begin{array}{c} \cos(k_a(x_3 - x_4) + c_a) \\ -\cos(k_a(x_3^s - x_4^s) + c_a) \end{array} \right) y_3^s
\end{aligned} \tag{Eq. 4-571}$$

Since the first two terms on the right of Lu are the same with the derivative of the energy of the deterministic system (pU), the Lu has the concept similar to the derivative of the stochastic energy function. However, it can definitely prove that pU is less than or equal to zero but not for Lu .

CHAPTER 5

RESULTS AND DISCUSSION PART 1

From the scopes and methodologies, the results have 2 parts. The first part consists of the characteristics of wind power, characteristics of power system incorporating wind power, effects of wind power on the small signal stability using eigenvalue method, and effects of wind power on the small signal stability using stochastic stability method: the mean first passage time (MFPT).

The second part focuses on the stochastic stability, which consists of the study of the effects of wind power on the small signal stability using new stochastic stability method: the stochastic stability index (SSI), the study of effects of wind power on the voltage stability using new stochastic stability method, the study of effects of wind power on voltage variation using probabilistic method.

This chapter focuses only on the first part of the results.

5.1 The characteristics of wind speed and wind power

The wind speed data, which is used in this section, is collected from the monitoring stations in Thailand and from modeling. The wind power is estimated using power curves from the manufacturers and the provided wind speed. There are two main types of characteristic of wind speed, which are, the slow variation and the fast variation characteristics.

Slow and fast variation components of wind speed can be determined using spectral analysis of measurement wind data. They can be separated at a cycle time about 10 minutes or 1.67 mHz. Faster than 10 minutes is a type of fast variation and slower is for slow variation wind speed [42].

For wind data from two monitoring stations in Thailand, the first station is located in Chumporn Province (CHMP1) in the South of Thailand, and the other station is located at Bangkhuntian Campus (BKT1) of King Mongkut's University of Technology Thonburi (KMUTT) in Bangkok. Wind speed data is recorded every minute during October 2011 – March 2012. The power spectral density (PSD) of wind speeds are shown in the following figures.

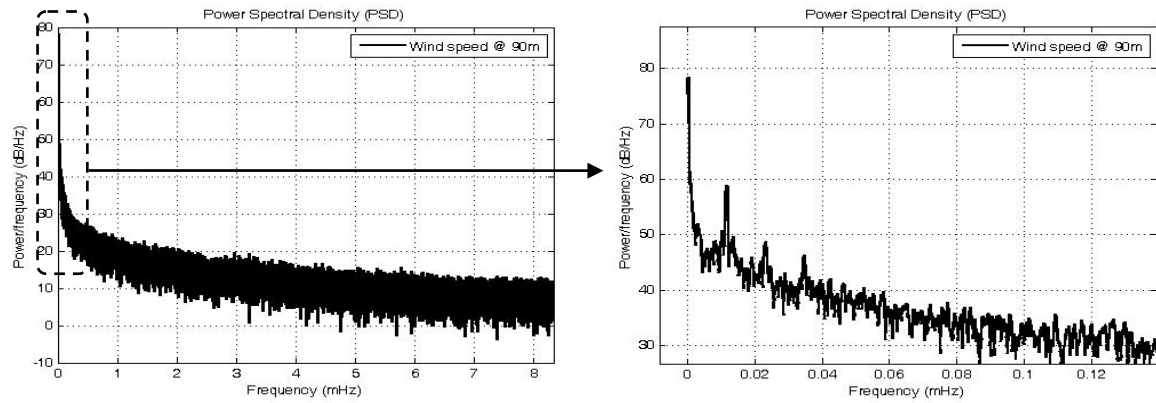


Figure 5.1 PSD of wind speed data from BKT1 station with frequency range of 0 - 8.3 mHz or ~2 minutes/cycle (left) and 0 - 0.14 mHz or ~120 minutes/cycle (right)

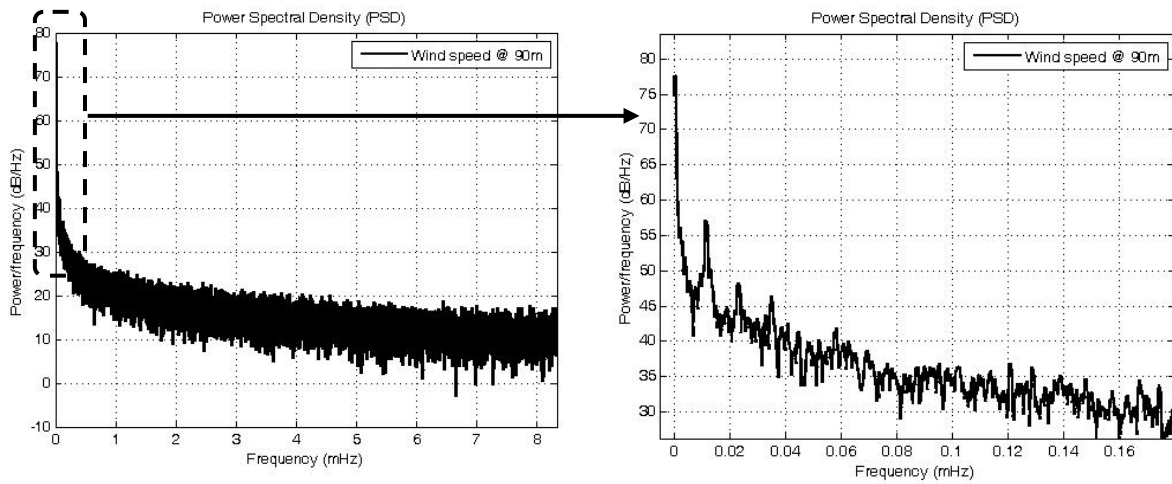


Figure 5.2 PSD of wind speed data from CHMP1 station with frequency range of 0 - 8.3 mHz or ~2 minutes/cycle (left) and 0 - 0.18 mHz or ~92 minutes/cycle (right)

In the above figures, significant parts of wind speed occur at frequency about 0.012 mHz (about 24 hours per cycle), 0.023 mHz (about 12 hours per cycle), and 0.035 mHz (about 8 hours per cycle). These cycles are influenced from the diurnal effect. Higher than 1 mHz, PSD decrease slowly and quite flat at frequency higher than 8.4 mHz (about 120 seconds per cycle). The 0 mHz component is neglected due to there is no data exist at that frequency. The fast variation components of wind speed have quite the same power and can be called turbulence wind speed.

5.1.1 Variation of wind speed

5.1.1.1 Slow variation wind speed

Slow variation wind speed can be considered the when wind speed has a cycle slower than 10 minutes. Therefore, 10-min data is an averaging interval which is used generally to record wind speed data [42]. Generally, slow variation wind speed characteristics can be characterized using variation and probabilistic behaviors in the long term. For time variation characteristics, wind speed can change slowly due to diurnal effects and seasonal effects. For example, hourly average and monthly average of wind speed of BKT1 and CHMP1 stations.

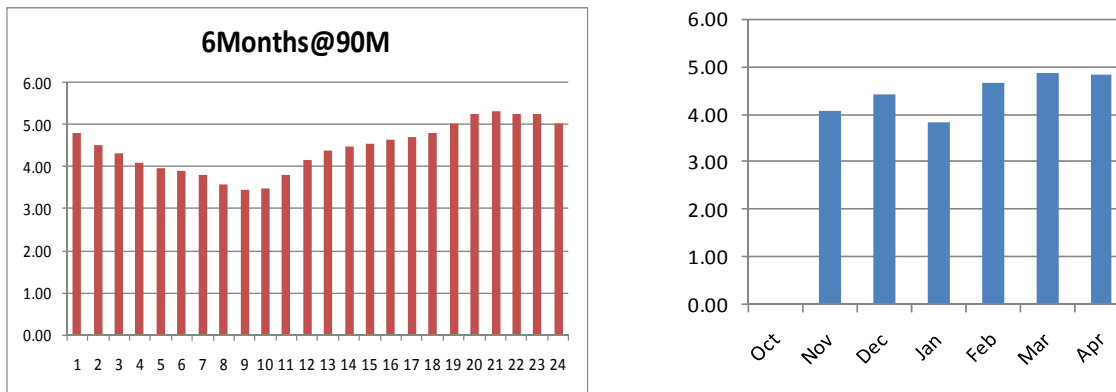


Figure 5.3 Hourly average (left) and monthly average (right) of wind speed of BKT1 station

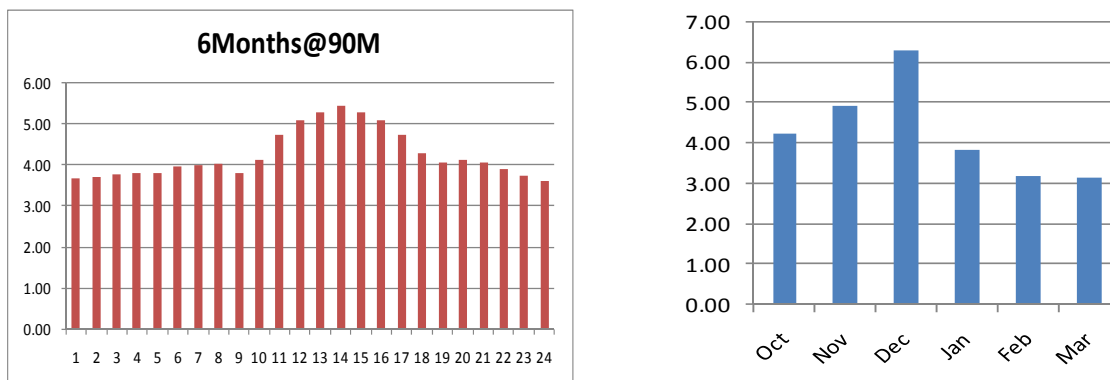


Figure 5.4 Hourly average (left) and monthly average (right) of wind speed of CHMP1 station

For probabilistic behaviors of long term wind speed, the distribution function of wind speed is generally determined. The level of fluctuation of wind speed can be

determined by the standard deviation of wind speed. The distribution data of standard deviation can also be considered to represent the long term deviation of data. The following figures show an example of the distribution of wind speed and standard deviation.

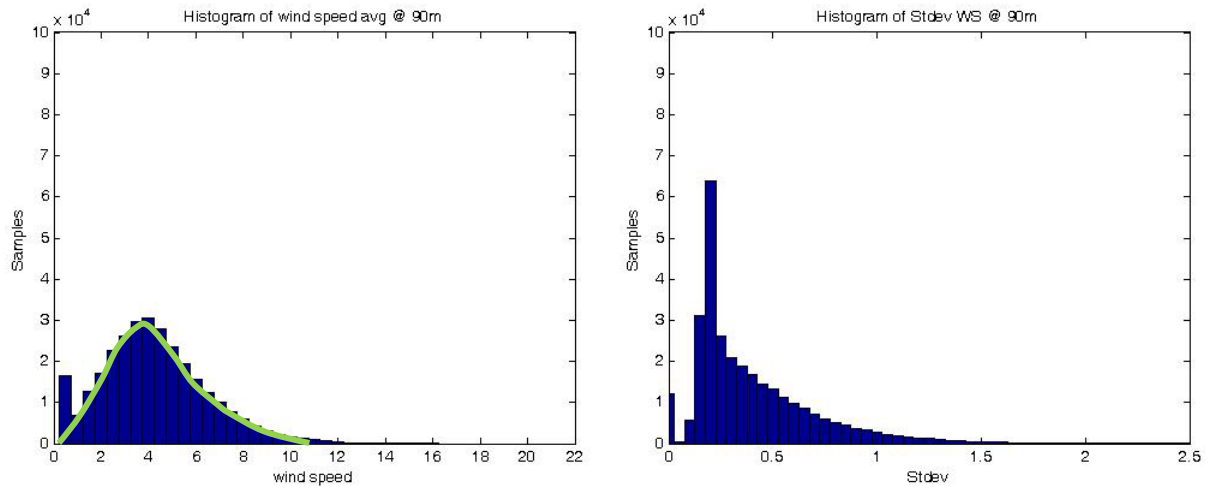


Figure 5.5 Distribution of wind speed (left) and standard deviation (right) of 1-min data of 130,000 samples at CHMP1 station at 90 m-height

This wind speed distribution can be approximated using the Weibull distribution function with scale parameter is 4.77 and shape parameter is 1.96 . For these samples, maximum standard deviation of wind speed can reach about 1.94. The standard deviation of 1-min wind data varied between 0.1 – 2.0 . The standard deviation within a range 0.5 – 2.0 will be used in the power system modeling of this thesis.

The formation of the probability distribution of wind speed is also investigated in this section. The frequency distribution of measured wind speed data are estimated using Matlab. To understand its distribution type, one-sample Kolmogorov-Smirnov method is used to compare the measured wind speed data with the six types of distribution. This is called hypothesis test. The six distribution types are Weibull distribution, Exponential distribution, Normal distribution, Log-normal distribution, Generalized-extreme value distribution, and Extreme value distribution. The resulting p-value which greater than significant value of 0.05 is an acceptable case or can be said that it cannot reject the hypothesis that this data is such kind of distribution function.

The sample wind data consist of three cases. The 1-sec data run from 10 to 900 seconds which the hypothesis is computed every 10 seconds. The 1-min data run from 10 to 800 minutes which the hypothesis is computed every 10 minutes. The 1-hour data run

from 10 to 800 hours which the hypothesis is computed every 10 hours. For each step of computation, the p-value was reported and compared.

For the 1-sec wind speed, the hypothesis test result is presented in Figure 5.6. From the result, when time increase with increasing sample, the p-value seems high for the starting run but all fall to zero after 350 seconds. Therefore, it is possible to reject the hypothesis that the distribution function matches with the measured wind speed data.

For the 1-min wind speed, the result of hypothesis test shown in Figure 5.7 is the same with the 1-sec data. The p-value seems high for the starting run but most cases fall to zero after 350 minutes except the case of Generalized-extreme distribution which fall after 600 minutes.

For the 1-hour data, the result of the hypothesis test is shown in Figure 5.8 is different from the previous two cases. The p-value seems high for the starting run but most cases fall to zero after 350 minutes, except for the case of Generalized-extreme distribution and Weibull distribution which increases continuously. Therefore, for this case, it cannot reject the hypothesis that the 1-hour data distribution can be approximated by Generalized-extreme distribution and Weibull distribution. The number of sample of 1-hour wind speed which is enough to represent Weibull distribution should be larger than 100 hours.

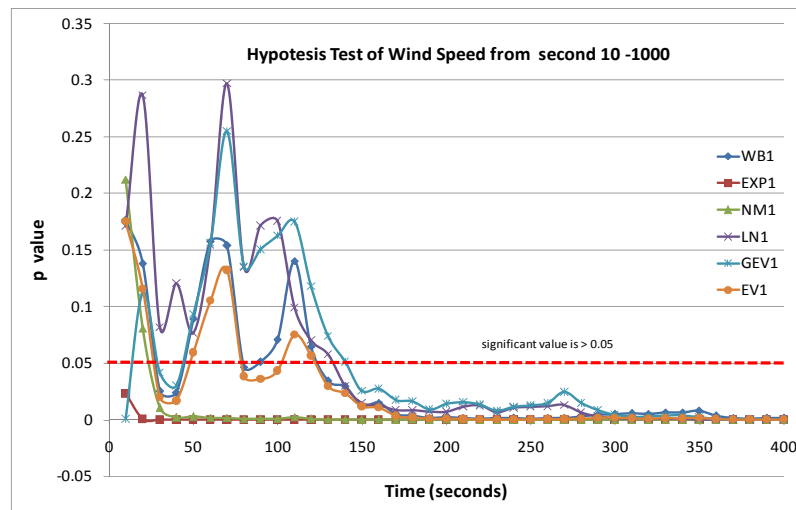


Figure 5.6 Hypothesis test of every second wind speed data

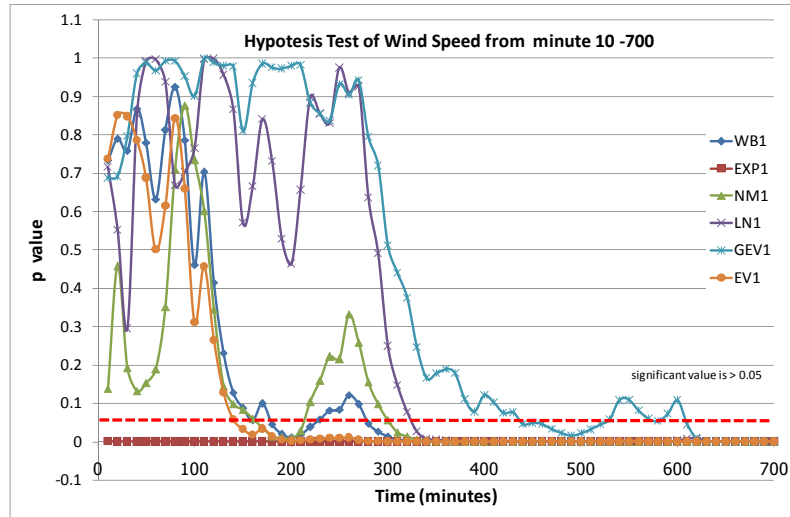


Figure 5.7 Hypothesis test of every minute wind speed data

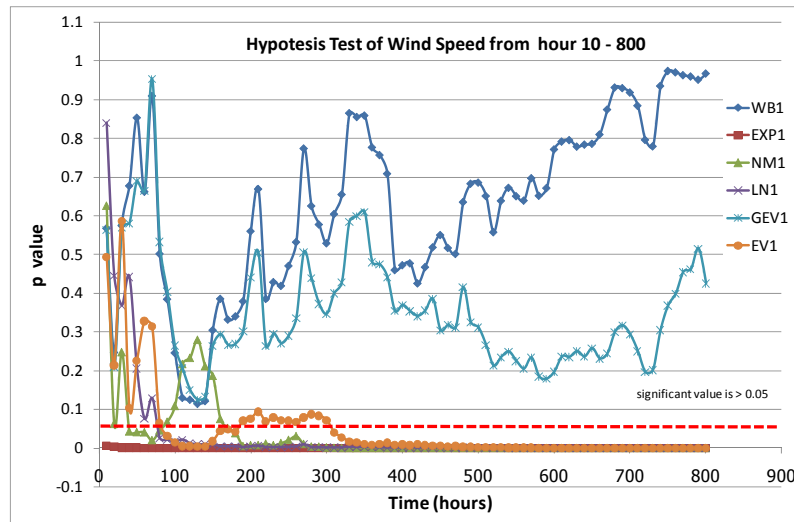


Figure 5.8 Hypothesis test of every hour wind speed data

5.1.1.2 Fast variation wind speed

The fast variation characteristics of wind speed are from the interactions between wind speed, terrain, land cover and other obstacles. Generally, fast variation characteristics are studied with a short time scale from a millisecond to several ten minutes.

Examples of wind speed at time scale in seconds and minutes are represented in Figure 5.9 and 5.10. For Figure 5.9, a short term wind speed data is recorded every second for about one day and represented here only 600 samples. This 1-sec data is averaged every 60 samples (or 1 minute) to show as mean parts surrounding by fluctuating parts.

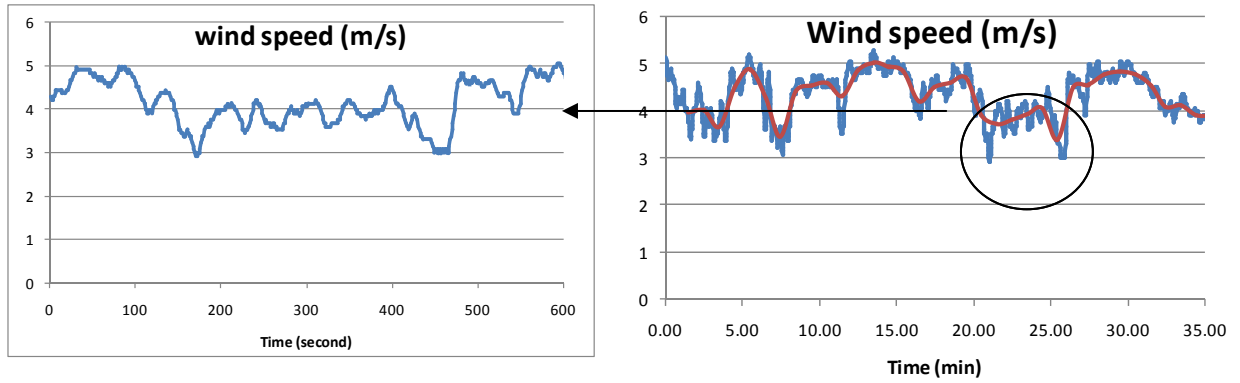


Figure 5.9 Wind speed at 90 m heights of BKT1 station with second (left) and minute (right) time scale.

In Figure 5.10, the fast variation data is represented in the long term period. The 1-minute data for 10,000 samples show highly fluctuation both wind speed data and standard deviation data. The cycle of deviation data occurs obviously due to diurnal effects.

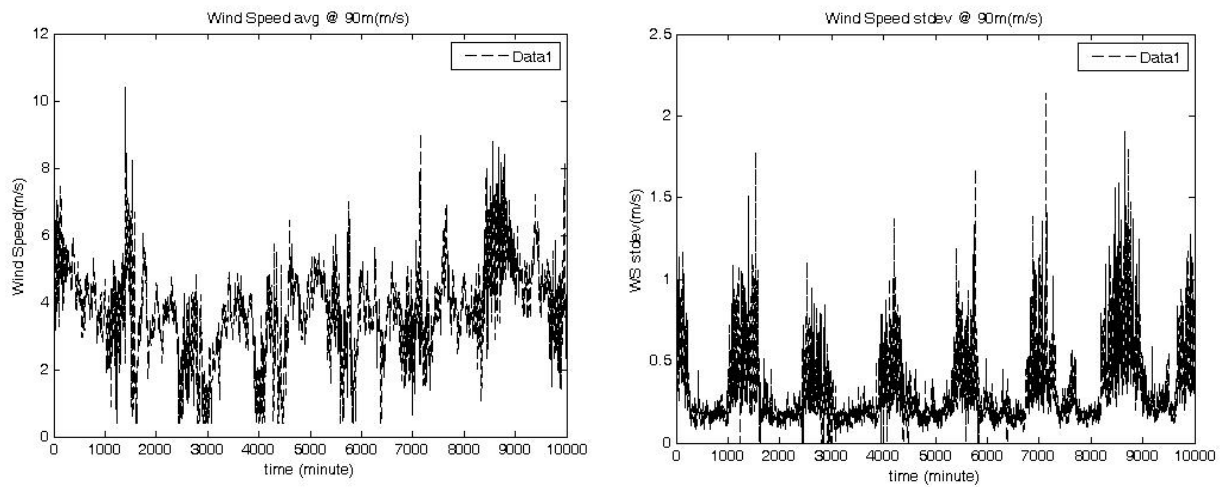


Figure 5.10 Wind speed (left) and its standard deviation (right) at 90 m heights of CHMP1 station

It is well known that fast variation wind speed, which is called turbulence, can be approximated using zero average normal distribution [42]. However, we found that measurement data of turbulence wind speed is quite different. Figure 5.11 shows the PSD and data distribution of 1-sec wind speed at 90 m heights of BKT1 station for 2000 samples. Since it is too short a time, the wind speed cannot be approximated by the Weibull distribution. At this level of frequency, the PSD is very small with less than zero dB.

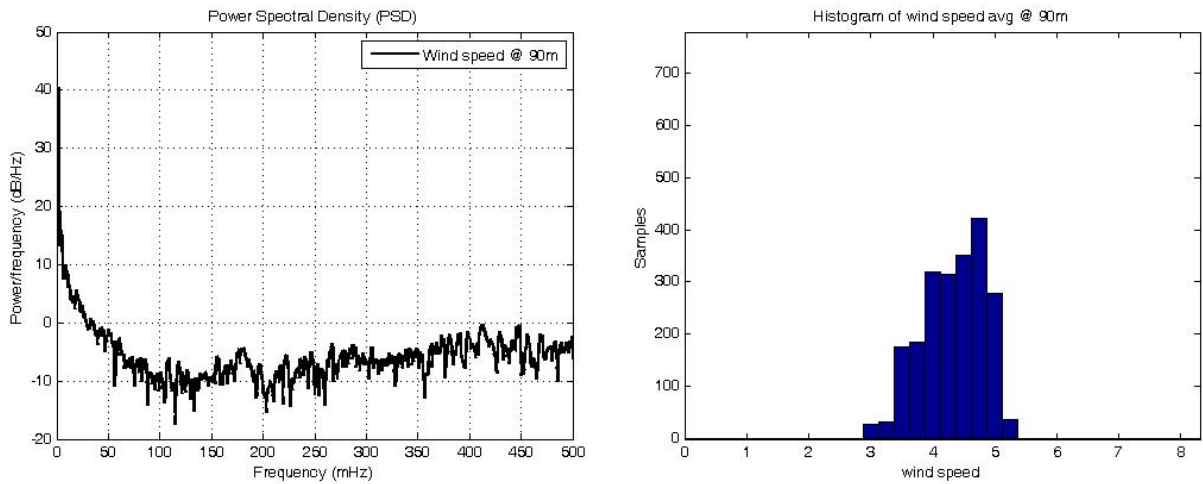


Figure 5.11 PSD (left) and histogram (right) of 1-sec wind speed at 90m heights of BKT1 station for 2,000 samples

To represent the turbulence more clearly, the 1-sec wind speed data is subtracted by 60-sec average wind speed to reveal only the turbulence part. The results are noise wind speed and its distribution, which are shown in Figure 5.12.

$$\text{Noise wind speed (turbulence)} = \text{wind speed} - \text{average wind speed every 60 samples}$$

Eq.5-1

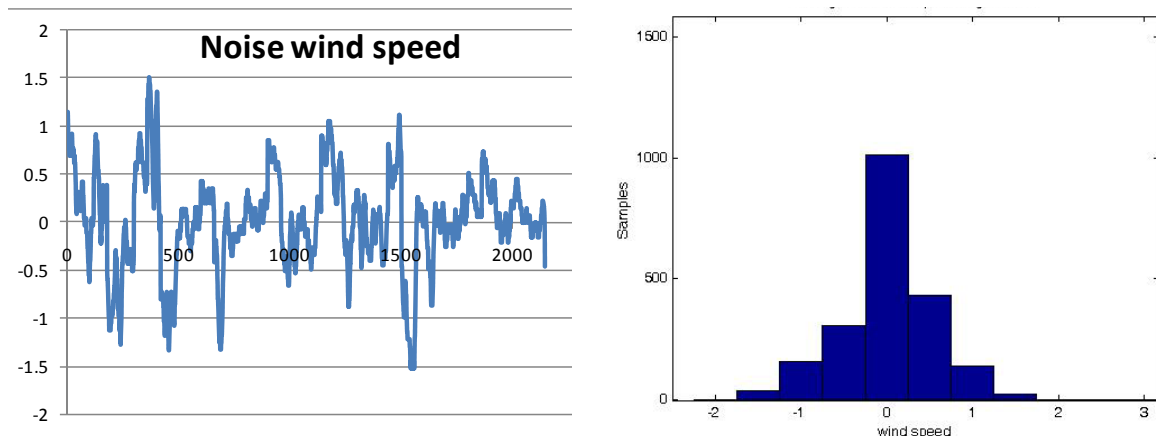


Figure 5.12 Noise wind speed 1-sec data 2,000 samples (left) and its histogram (right)

Figure 5.13 represent the turbulence term of wind speed but with 1-min data for 26,000 samples. For this figure, turbulence term seems not a type of zero average normal distribution, but look like Generalized Gaussian Distribution (GGD) instead. Therefore, the modeling of turbulence wind speed using Gaussian distribution may stimulate significance error.

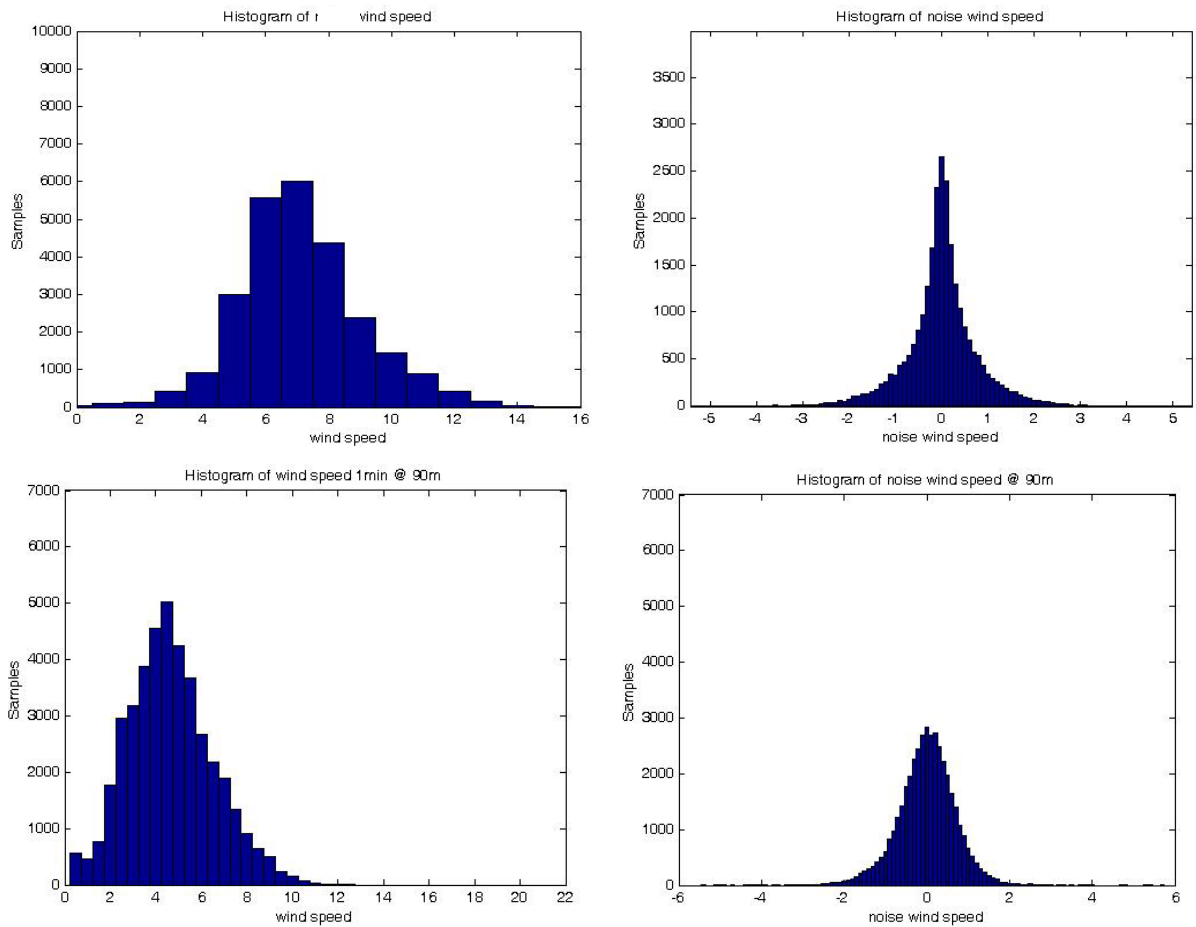


Figure 5.13 Wind speed distribution (left) and turbulence or noise wind speed distribution (right) of 1-min data for 26,000 samples at CHMP1 station (upper) and BKT1 station (lower)

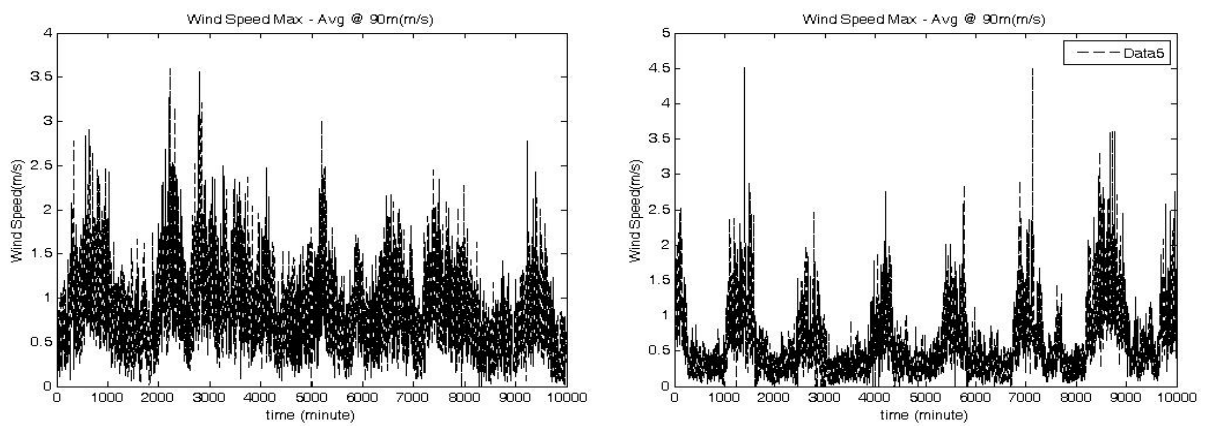


Figure 5.14 Example of gust wind speed of 1-min data for 10,000 minutes at BKT1 station (left) and CHMP1 station (right)

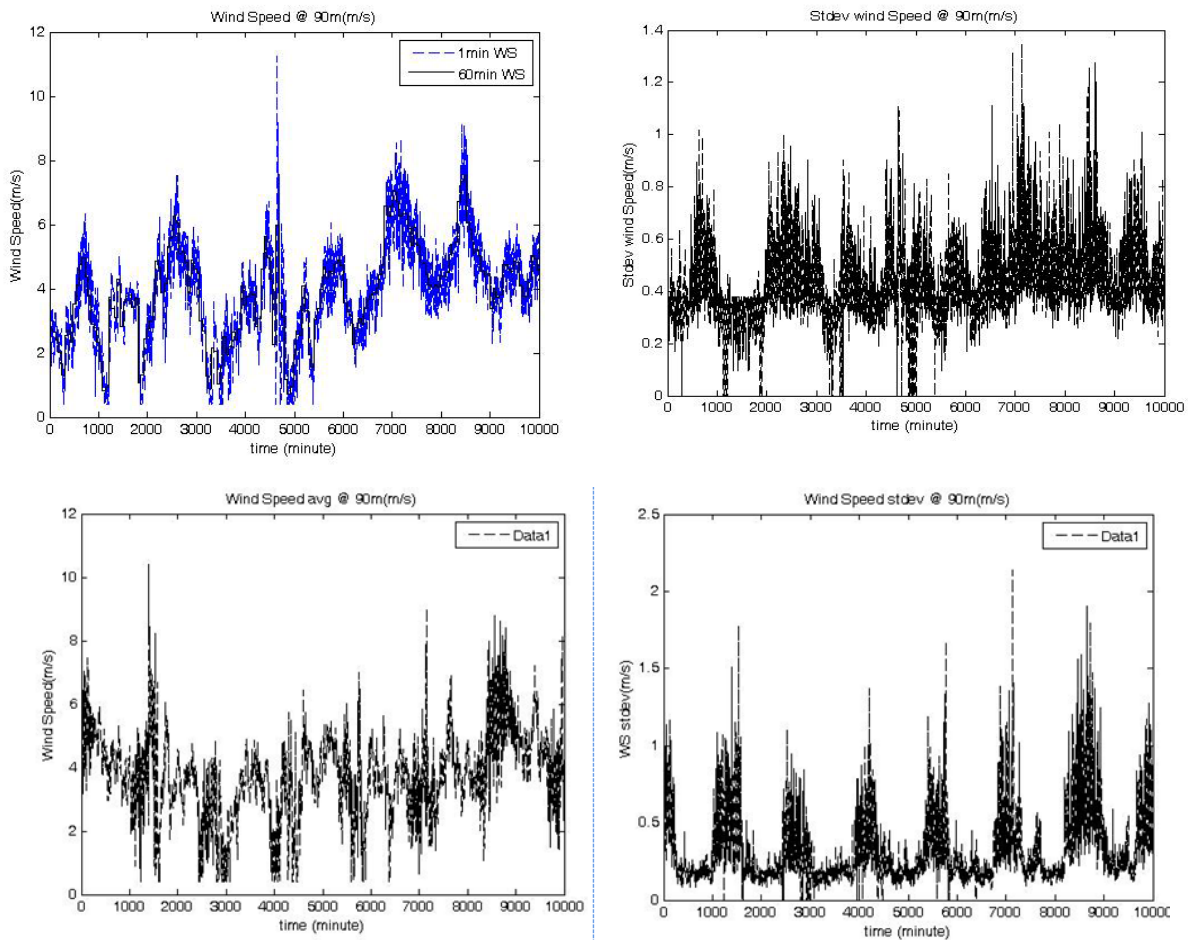


Figure 5.15 Wind speed (left) and its standard deviation (right) of 1-min data for 10,000 minutes at BKT1 station (upper) and CHMP1 station (lower)

The other case of fast variation of wind speed is the transient characteristic from gust wind speed, which is an abrupt change of wind speed within a short time. Gust wind speed can be estimated by the difference between maximum and average wind speed within 1 minute or less. The level of gust wind power can be estimated by the different of maximum and average power of wind (W/m^2) at standard air density (1.225 kg/m^3) within 1 minute or less. Examples of gust wind speed and wind power are represented in above figures.

For example, if the 1.6MW wind turbine (with swept area about $2,000 \text{ m}^2$) has an alert level of wind power change at 50% of rated within 1 minute. Therefore, the serious level of gust wind power should be within a range of $600 - 800 \text{ W/m}^2$ or larger. However, the transient phenomena are not considered yet because it is out of the scope of the thesis and does not occur frequently in nature.

5.1.2 Variation of wind power

In this section, characteristics of wind power are studied, which consider three main affecting factors, namely wind speed, wind farm modeling, and power system conditions. The wind turbine technology is the other important factor. However, since the measurement wind power data is not available, the simulation or modeling wind power will be used instead for every cases of study.

5.1.2.1 Characteristics of estimated wind power

From the previous section, wind speed can be considered to have slow and fast variation characteristics. Therefore, wind power in this case should be studied in term of slow and fast variation too.

For slow variations of wind speed and without dynamic behaviors, the output wind power (P_w) is calculated using Eq.3-1 to Eq.3-4 .

For example, hourly average wind data for 7,000 hours during August 2008 – July 2009 at coastal site in the South of Thailand are represented in Figure 5.16.

From this figure, the maximum, minimum, and fluctuation of wind power can be noticed. More than a half of time, wind power normally varies within a range 100 – 800 kW. However, it can reach as much as 1,000 – 1,200 kW (rated of wind turbine) during the stormy season in the South of Thailand.

The distribution of wind speed and wind power data at the coastal site in the South of Thailand are represented in Figure 5.17. These results can be used to compare with wind speed and wind power data at BKT1 station as shown in Figure 5.18 – 5.20.

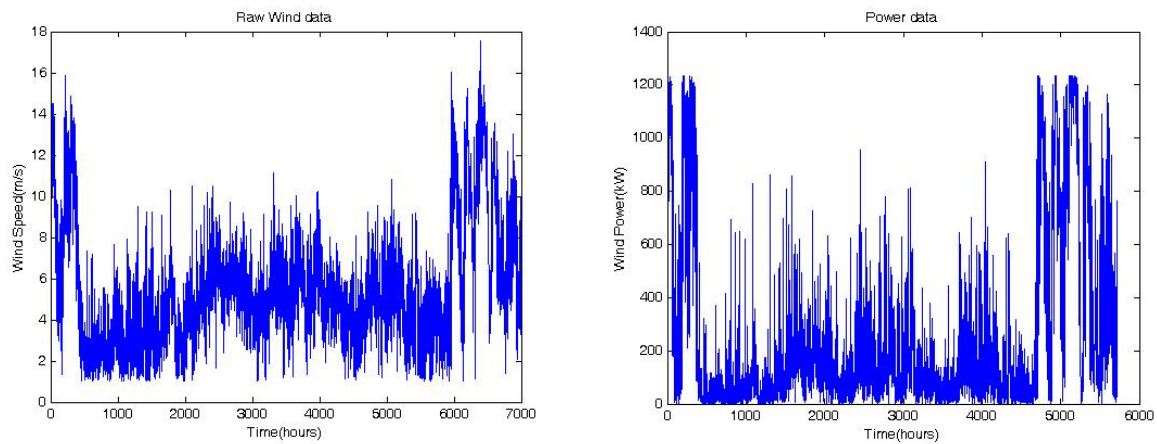


Figure 5.16 Hourly average wind speed (left) and wind power (right) from Eq.3-3 and 3-4 at the coastal site in the South of Thailand

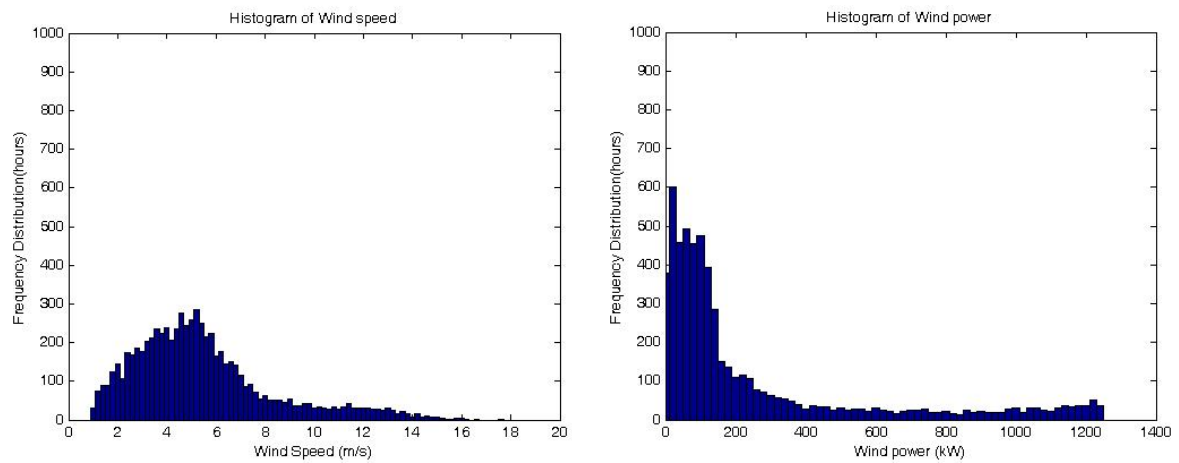


Figure 5.17 Histogram of 7,000 hours wind speed (left) and calculated wind power (right) at the coastal site in the South of Thailand

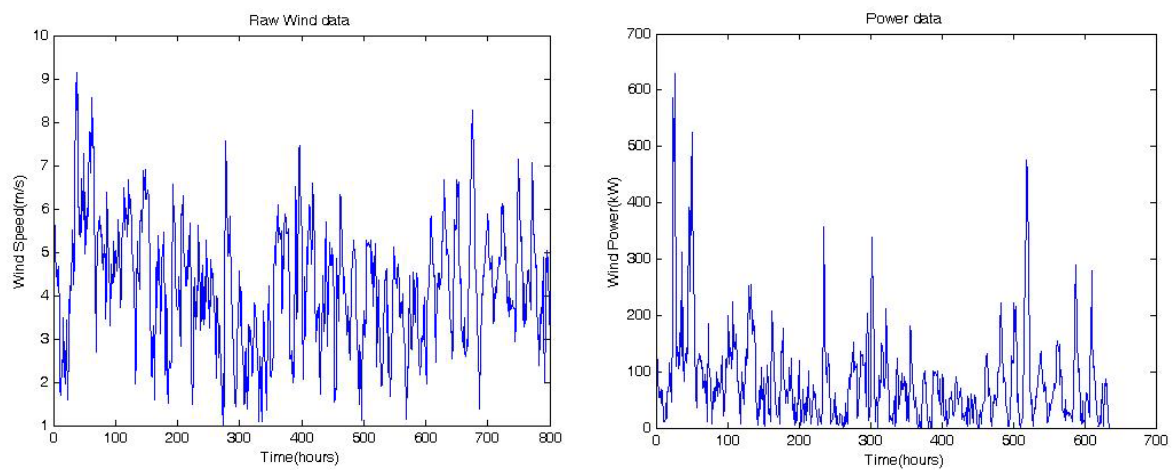


Figure 5.18 Hourly average wind speed (left) and calculated wind power (right) at BKT1 station

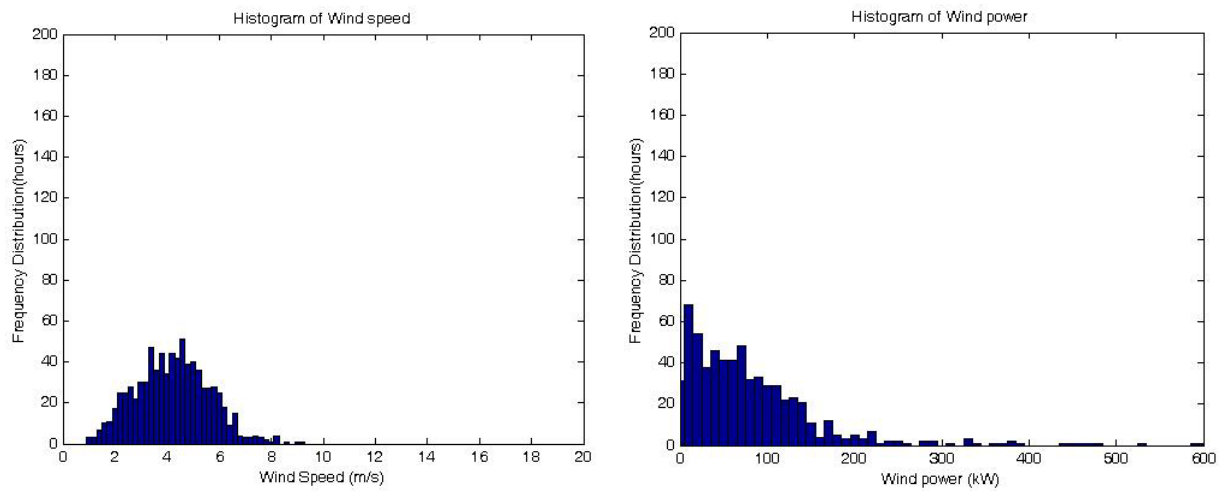


Figure 5.19 Hourly average wind speed (left) and calculated wind power (right) at BKT1 station

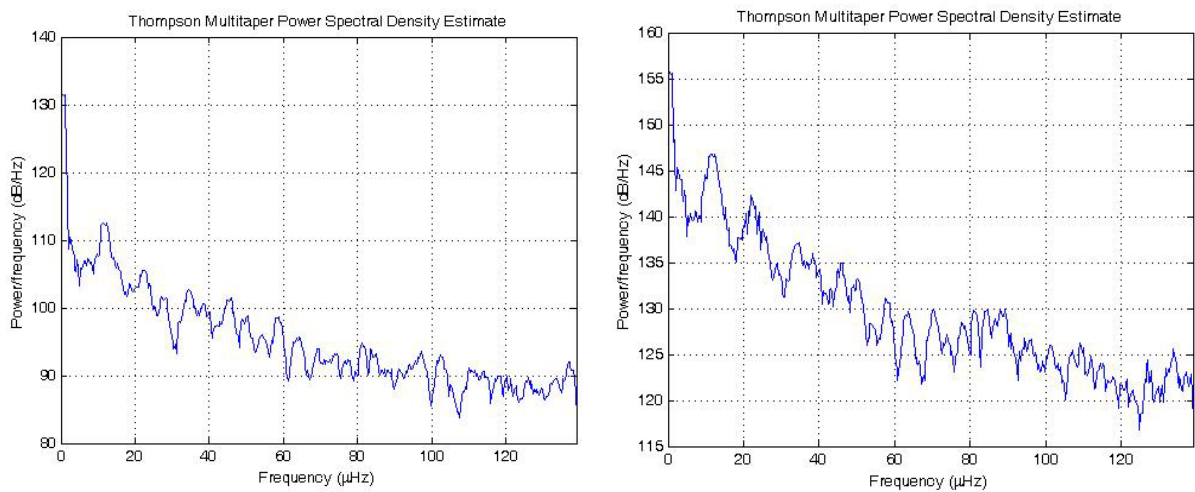


Figure 5.20 PSD of 800 hours wind speed (left) and calculated wind power (right) at BKT1 station

For Figure 5.20, at frequencies of about 12 μHz and 22 μHz show significant level of PSD. These frequencies refer to the time cycle of about 24 hours and 12 hours respectively. Therefore, it is again an influence of diurnal effect.

The following figure can represent the formation of probability distribution of wind power for 800 hours samples. From this figure, it is possible to approximate probability distribution of wind power by Weibull distribution and generalized extreme value distribution.

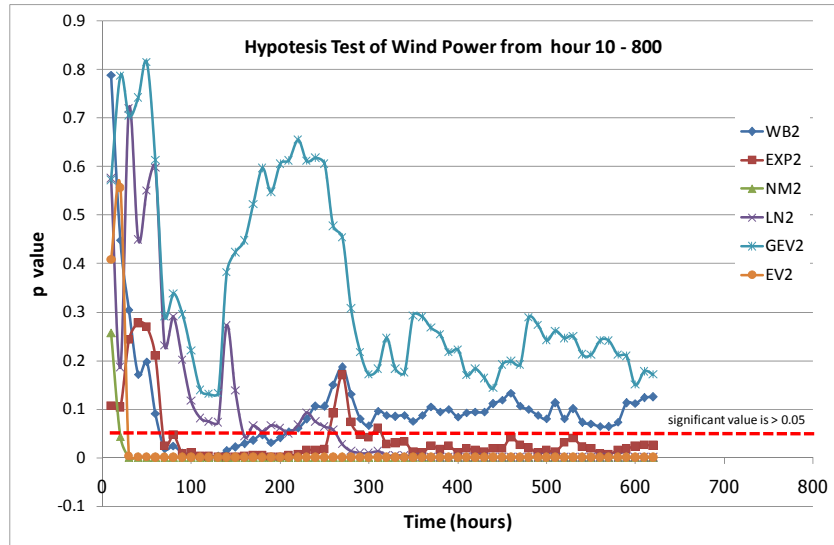


Figure 5.21 Hypothesis test of hourly averaged wind power

5.1.3 The probability distribution function of wind power

The study of probability distribution characteristics of wind power can be influenced by many factors, such as wind turbine model, power system model, wind speed model and noise model. Therefore, testing with many conditions is listed in Table 5.1.

Table 5.1 Testing conditions for the study of probability distribution of wind power

	Wind turbine model	Power system model	Wind speed model	Other conditions
Case A1	1x2MVA SCIG	1 AC source without load	Weibull distribution using inverse CDF	2 values of Weibull scale parameter, 100x2 runs
Case A2	2x2MVA SCIGs	1 AC source without load	Independent 2 wind sources with Weibull distribution	Weibull scale parameter = 10, for 10,000 runs
Case A3	5x10x2MVA SCIGs	1 AC source without load	Independent 5 wind sources with Weibull distribution	Weibull scale parameter = 10, 100 runs
Case A4	2x2MVA SCIGs	1 AC source without load	The same wind source with Weibull distribution	Add Gaussian random noise to WT2, 100 runs
Case A5	2x2MVA SCIGs	1 AC source without load	Constant wind speed = 6, 9, and 10 m/s for both WT	Add Gaussian random noise to WT2, 400, 1600 runs
Case A6	1x50x2MVA SCIG	SMIB system with load	Weibull distribution using inverse CDF	2 values of Weibull scale parameter, 200x2 runs
Case A7	1x50x2MVA SCIG	SMIB system with load	Weibull distribution using inverse CDF	WS noise using inverse CDF numerical method, 100 runs

Case A1 Single wind turbine connecting AC voltage source power system without noise

The one-line diagram of case A1 is represented in Figure 5.22. In this case, wind speed signal is generated from the inverse CDF method considering Weibull distribution.

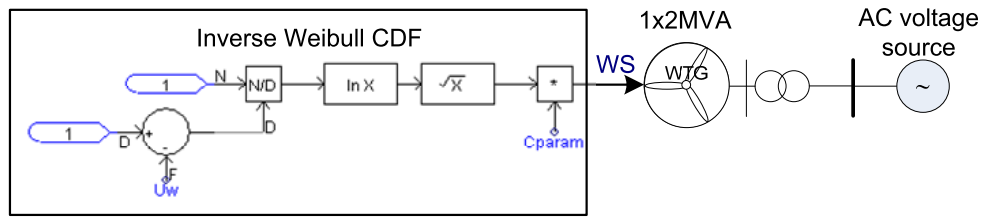


Figure 5.22 One-line diagram of test system of case A1

Where U_w is the uniform random number between 0 – 1 and C_{param} is the scale parameter. In this case, the Weibull shape parameter = 2 or called Rayleigh distribution.

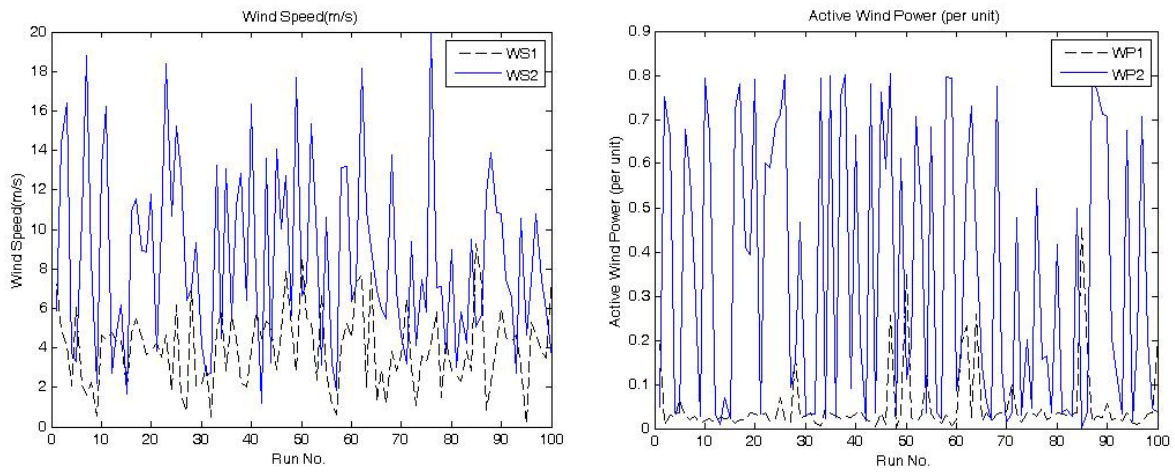


Figure 5.23 Wind speed (left) and wind power (right) of case A1 (WS1 and WP1 use $C_{param} = 5$, WS2 and WP2 use $C_{param} = 10$)

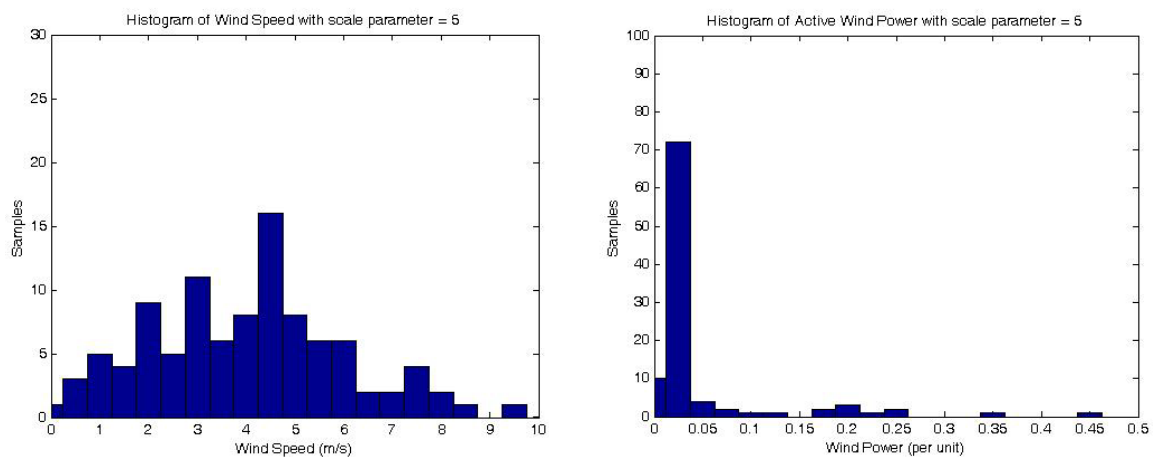


Figure 5.24 Histogram of wind speed (left) and wind power (right) of case A1 ($C_{param} = 5$)

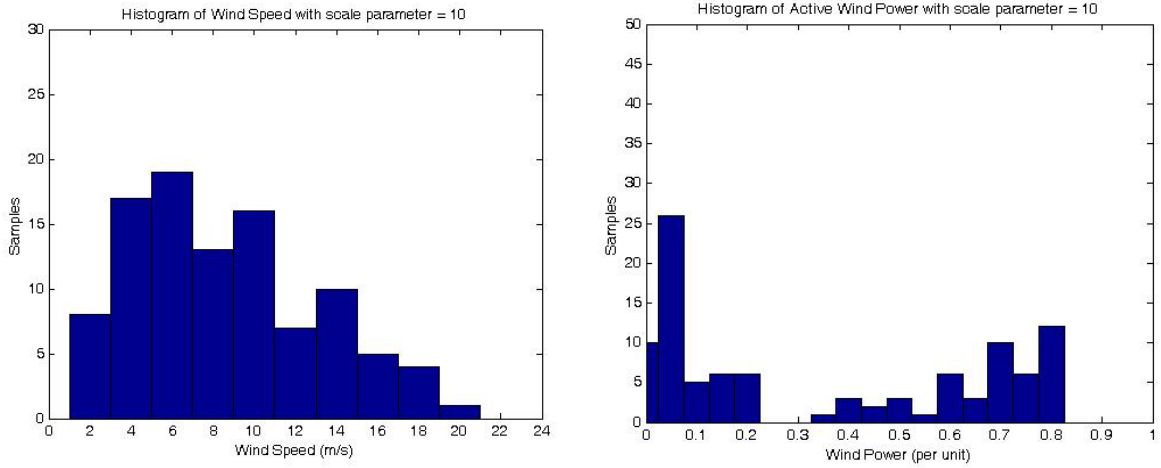


Figure 5.25 Histogram of wind speed (left) and wind power (right) of case A1 ($C_{\text{param}} = 10$)

It can be noticed in Figure 5.23 that at $C_{\text{param}} = 5$, wind power is very low or cannot generate electrical power. In Figure 5.24, the wind power distribution is again reveal that wind speed is too low to start generate power. When C_{param} increase to be 10 in Figure 5.25, the wind power distribution show large share of wind power greater than 0.3 pu.

Case A2 Two wind turbines connecting AC voltage source power system without noise

The one-line diagram of case A2 is represented in Figure 5.26. Wind speed is generated from the inverse CDF method considering Weibull distribution for both wind turbines. Wind speed and wind power of case A2 are represented in Figure 5.27. Figures 5.28 and 5.29 reveal that wind speed with large samples can be exactly approximated by the Weibull distribution, but wind power cannot. It can be concluded from these figures that, the data distribution of wind power of single wind turbine cannot be approximated using general probability distribution functions. It depends on the characteristics of wind speed and the power curve of wind turbine including cut-in speed and rated speed.

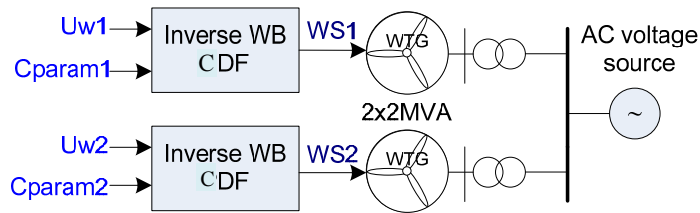


Figure 5.26 One-line diagram of test system of case A2

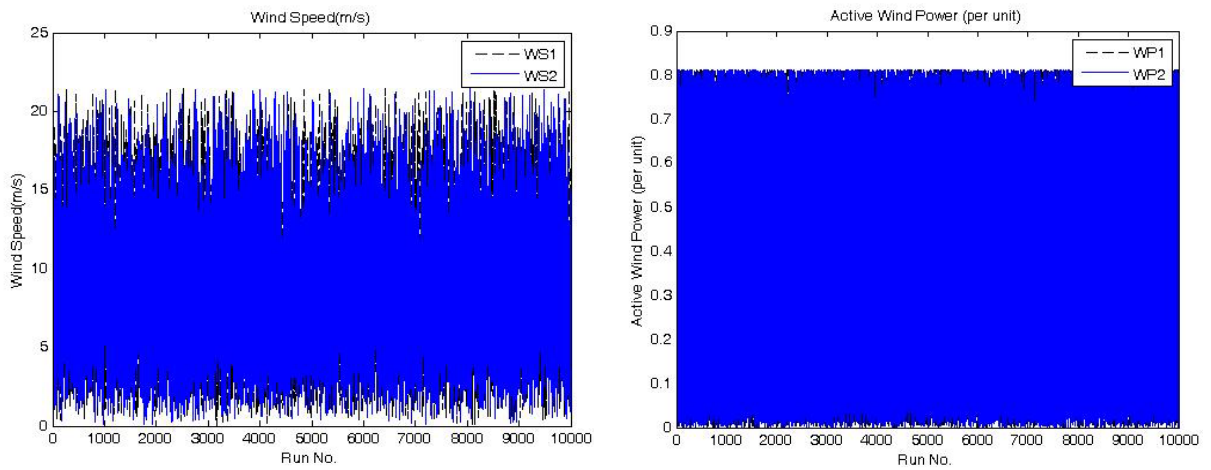


Figure 5.27 Wind speed (left) and wind power (right) of case A2 (WS1 and WP1 from WTG1, WS2 and WP2 from WTG2)

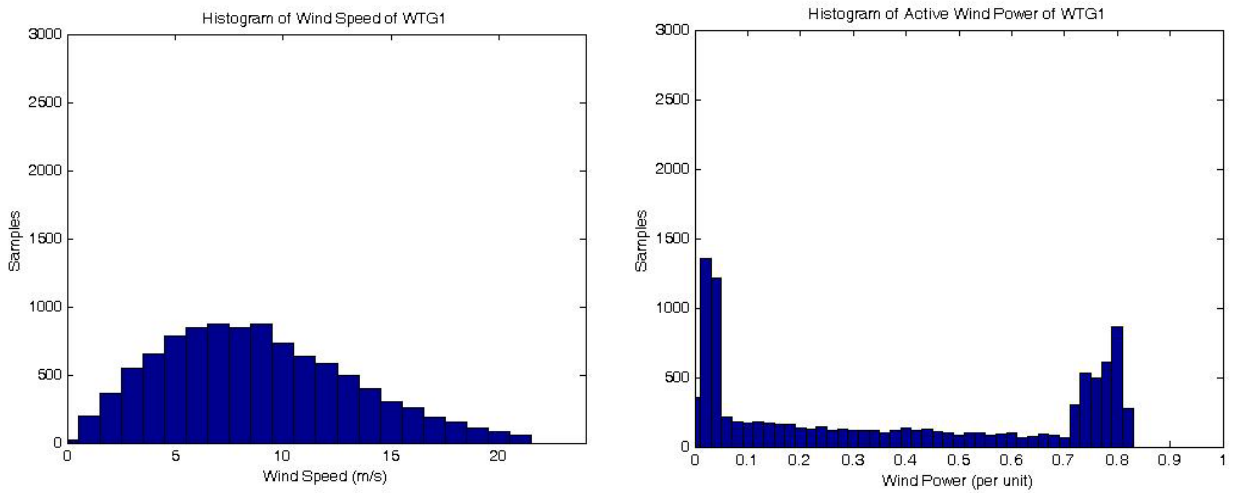


Figure 5.28 Histogram of wind speed (left) and wind power (right) of case A2 (from WTG1)

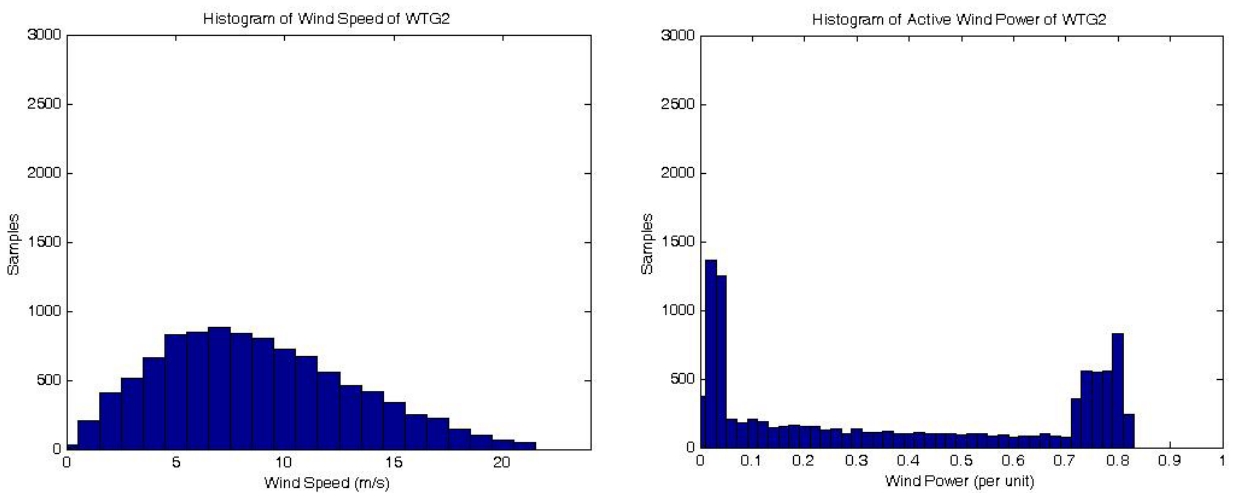


Figure 5.29 Histogram of wind speed (left) and wind power (right) of case A2 (from WTG2)

Case A3 Five aggregated wind farms connecting AC voltage source power system without noise

The one-line diagram of case A3 is represented in Figure 5.30. Wind speed is generated from the inverse CDF method considering Weibull distribution for all five aggregated wind farms. Each wind farm represent 10 coherently wind turbines of capacity 2MVA each. The total wind power (P_{wind}) is then compared with the individual wind power from each windfarm.

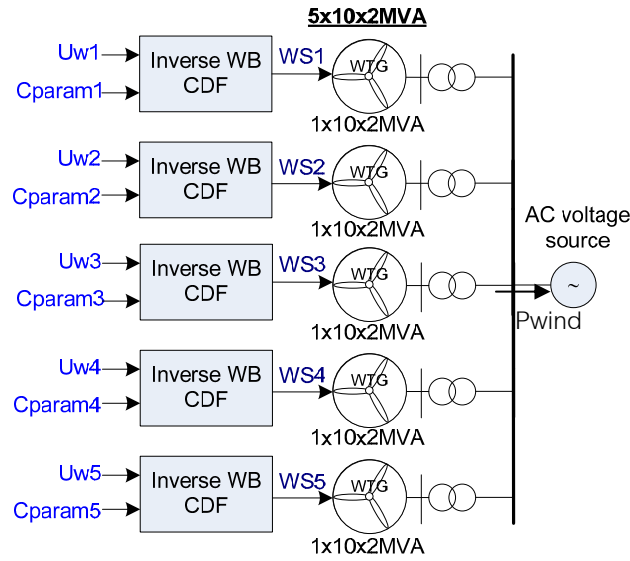


Figure 5.30 One-line diagram of test system of case A3

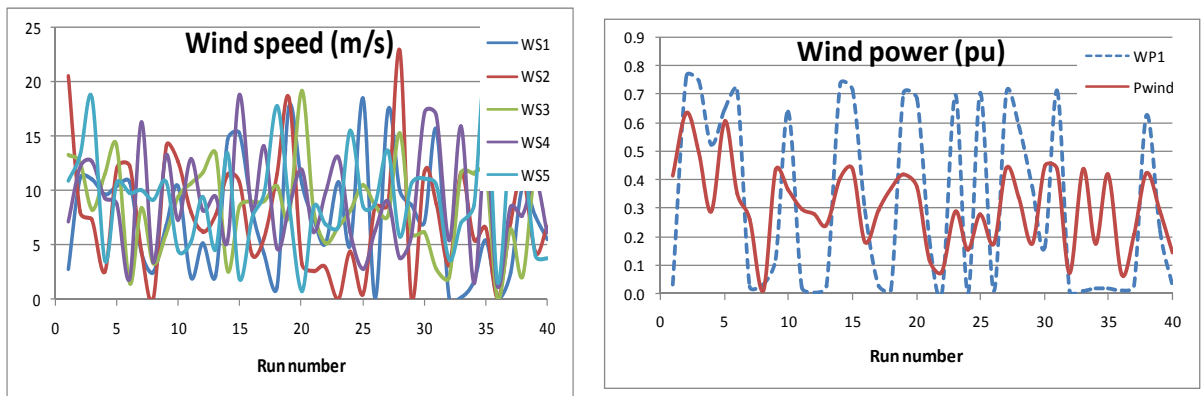


Figure 5.31 Sample of wind speed (left) and wind power (right) of case A3

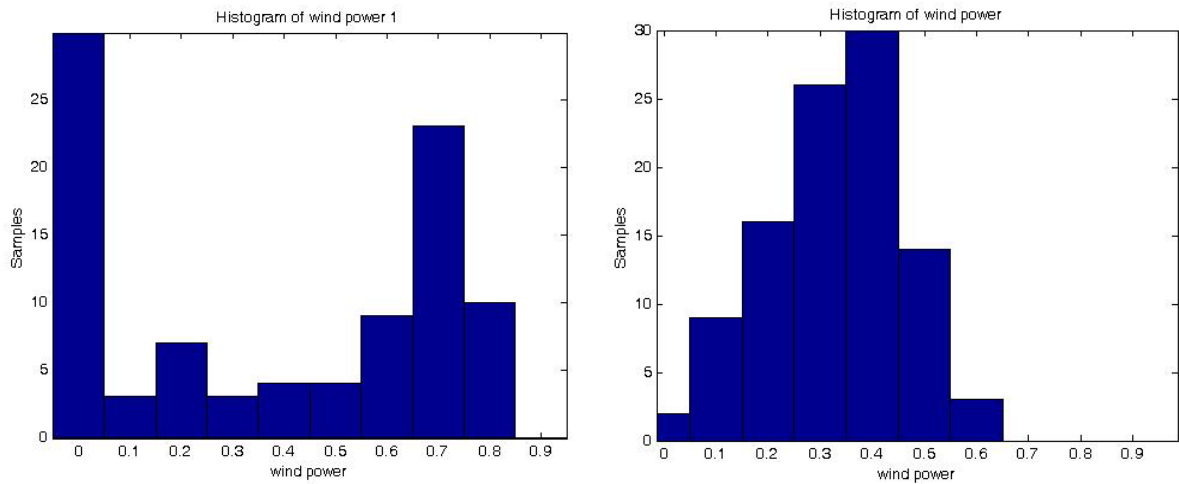


Figure 5.32 Histogram of wind power of WTG1 (left) and total wind power (right) of case A3

In Figure 5.31, for random and independent wind speed, total wind power seems smoother than individual wind power. Moreover, Figure 5.32 reveals that the total wind power can be approximated by normal distribution while the individual wind power cannot.

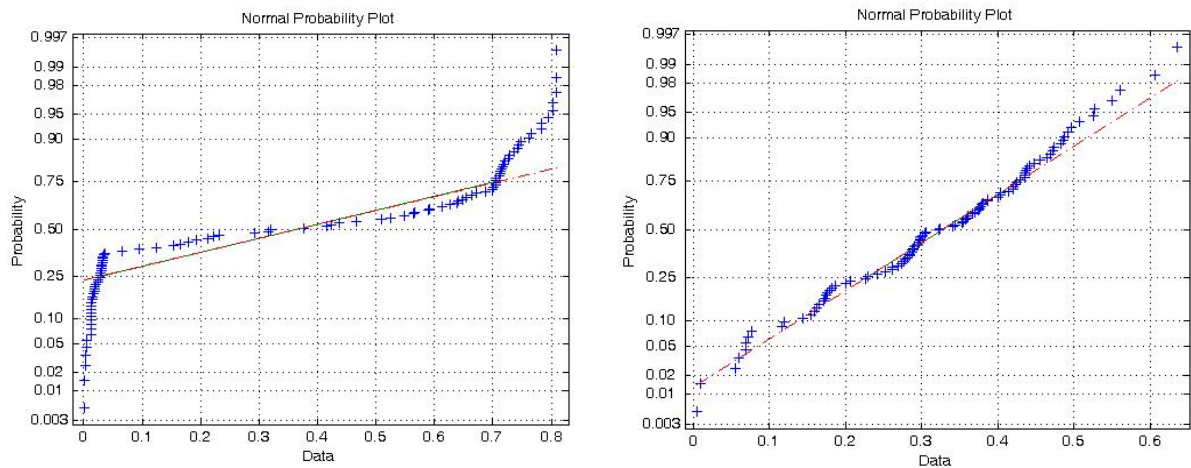


Figure 5.33 PSD of wind power of WTG1 (left) and total wind power (right) of case A3

In Figure 5.33, the normal probability plot represents again that the total wind power can be approximated by the normal distribution. This is because when the random signal mixing together, the convolution of many sources can results to converge to normal distribution.

Case A4 Two wind turbines connecting AC voltage source power system with normal random noise wind speed for one wind turbine

The one-line diagram of case A4 is represented in Figure 5.34. Wind speed is generated from the inverse CDF method considering Weibull distribution for both wind turbine (Cparam1 = 10). However, wind turbine number two has normal random noise wind speed add.

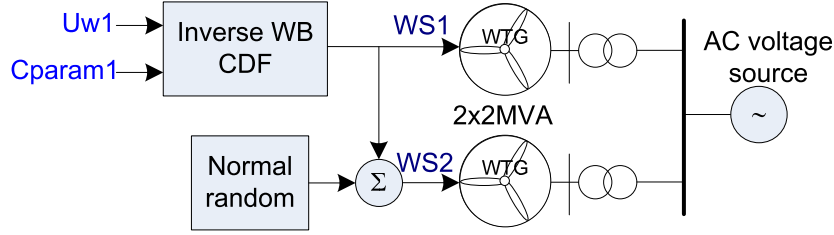


Figure 5.34 One-line diagram of test system of case A4

Since the wind power distribution cannot be approximated by any standard probability distribution, the noise wind power is then considered. The noise wind power is calculated by the difference between wind power from wind turbine number one and number two. Figure 5.35 shows that noise wind power have close to zero mean distribution. In Figure 5.36, the noise wind speed seems like normal distribution. In Figure 5.37, noise wind power distribution is very different from normal distribution. The result of normal plot in Figure 5.38 reveals that noise wind speed distribution is close to normal distribution, but noise wind power is not.

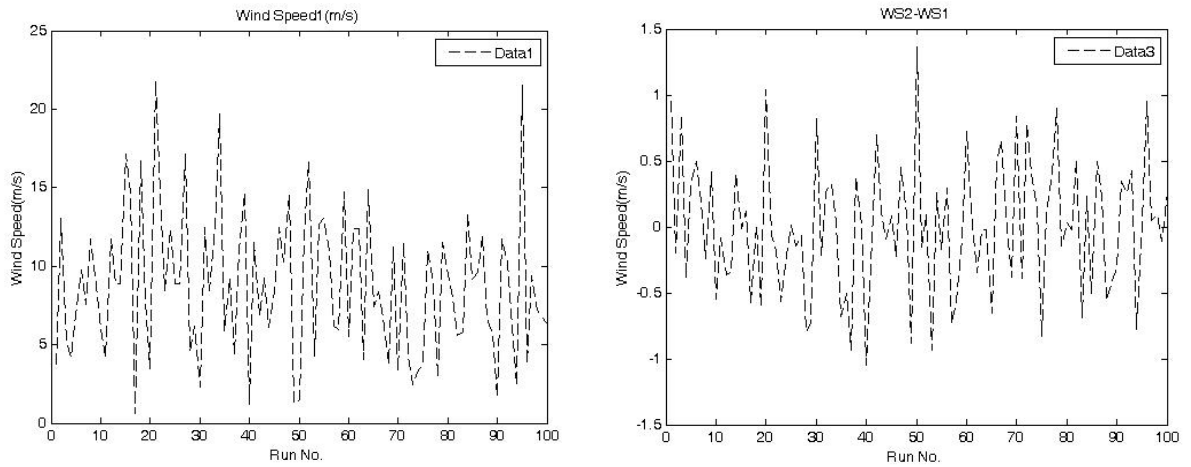


Figure 5.35 Wind speed (left) and different wind speeds (WS2-WS1) (right) of case A4

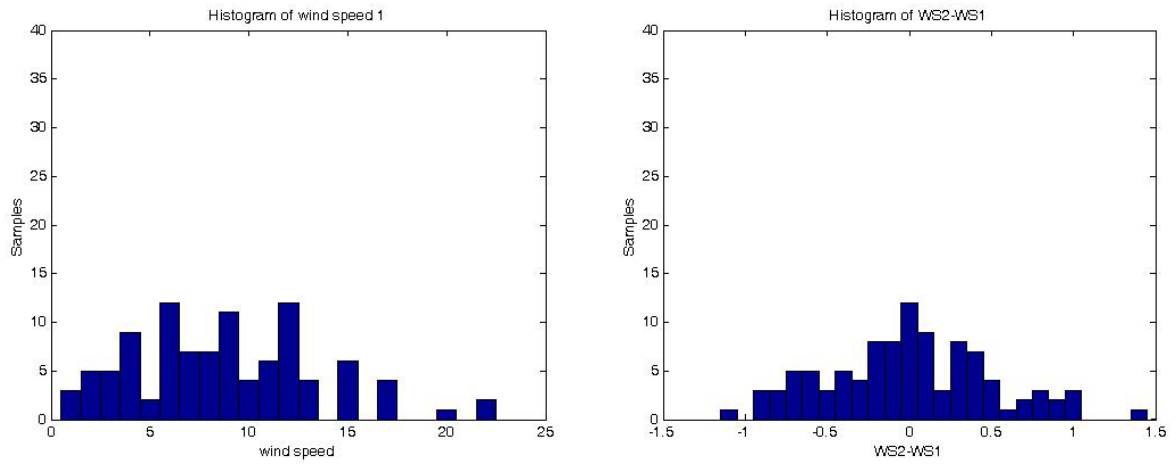


Figure 5.36 Histogram of wind speed (left) and different wind speeds ($WS2-WS1$) (right) of case A4

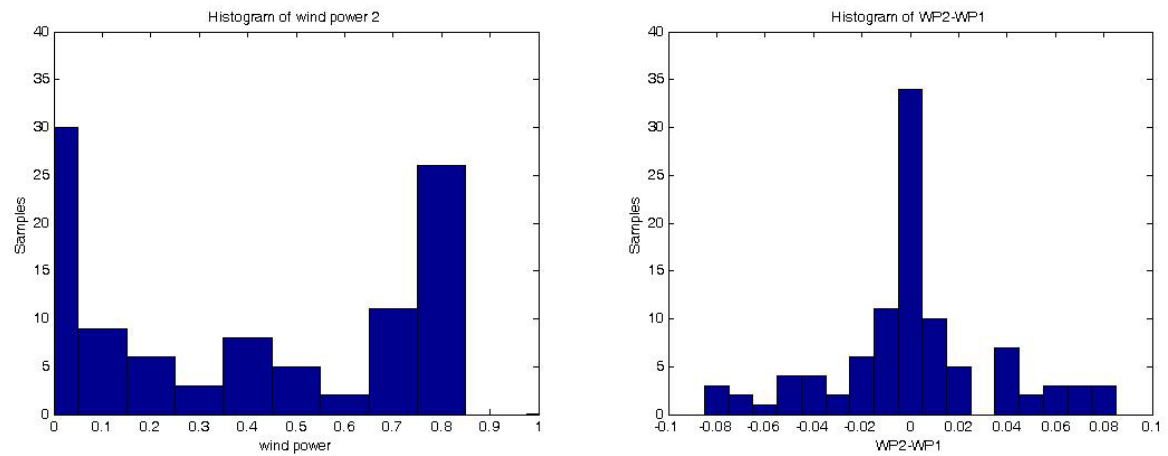


Figure 5.37 Histogram of wind power of WTG2 (left) and different wind powers ($WP2-WP1$) (right) of case A4

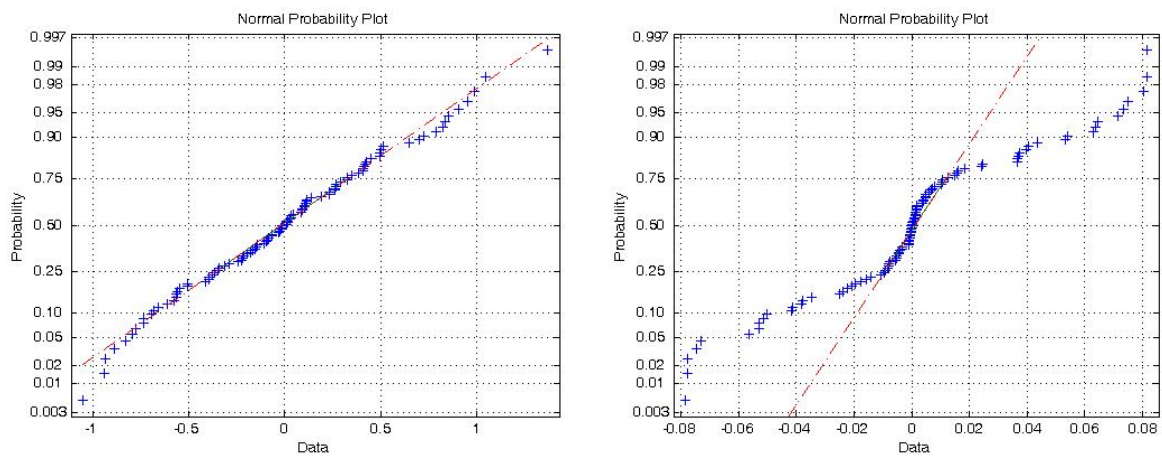


Figure 5.38 Normal probability plot of different wind speeds ($WS2-WS1$) (left) and different wind power ($WP2-WP1$) (right) of case A4

Case A5 Two wind turbines connecting AC voltage source power system with constant mean wind speed and add normal random noise wind speed for one wind turbine

The one-line diagram of case A5 is represented in Figure 5.39. Wind speed in this case is fixed for both wind turbine ($k = 6, 9, 10$ m/s). However, wind turbine number two has normal random noise wind speed added.

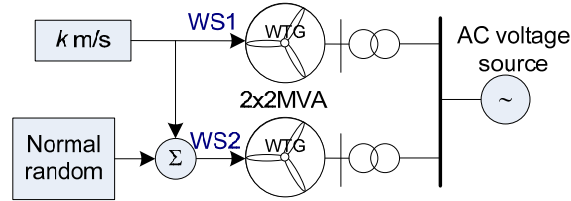


Figure 5.39 One-line diagram of test system of case A5

This testing condition interests an influence of mean wind speed on the distribution characteristics of wind power. Figure 5.40 represent that there is specific mean wind speed that can make wind power distribution symmetry. In this case is 9 m/s.

This is true also in the case of noise wind power as presented in Figure 5.41. For both wind power and noise wind power, at mean wind speed fix at 9 m/s, the normal distribution can be used to approximate its distribution. Figure 5.42 can confirm this agreement.

It can be noticed that the distribution characteristics of noise wind power in this case is different from the case A4. The difference between these two cases is the wind speed model. However, wind speed model of case A4 is more close to the nature of wind speed.

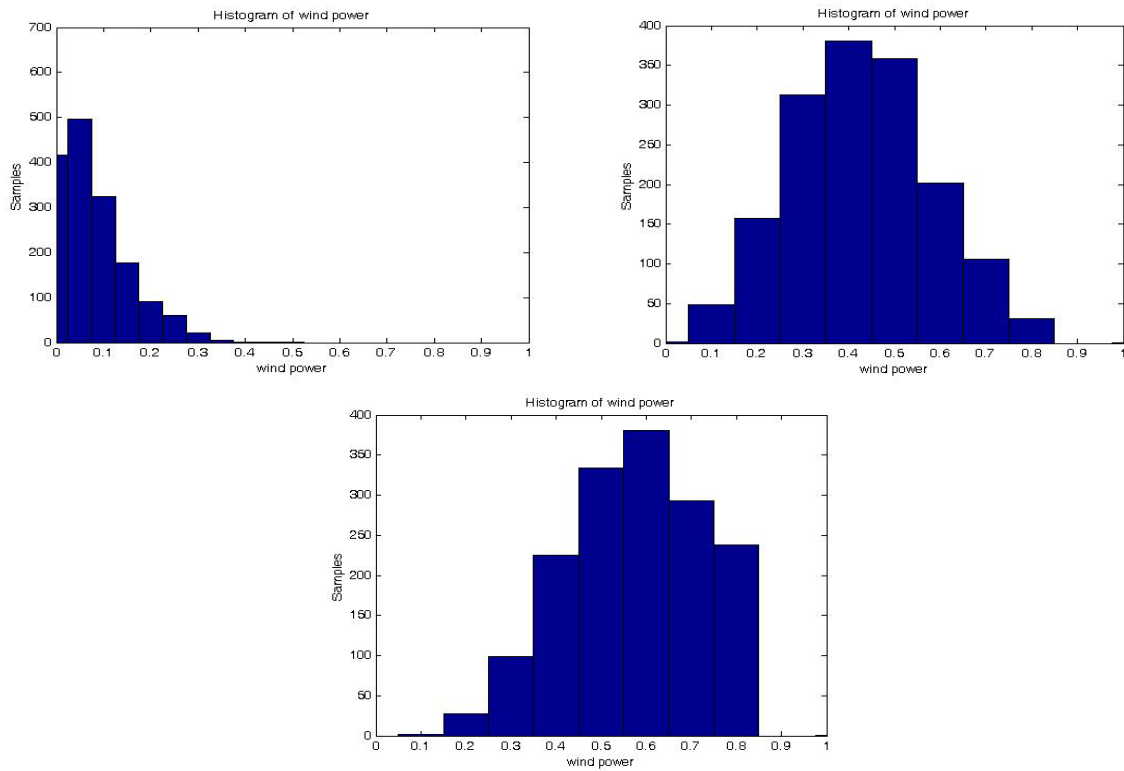


Figure 5.40 Histogram of wind powers for the case wind speed, $k = 6\text{m/s}$ (upper left), 9m/s (upper right), and 10m/s (lower)

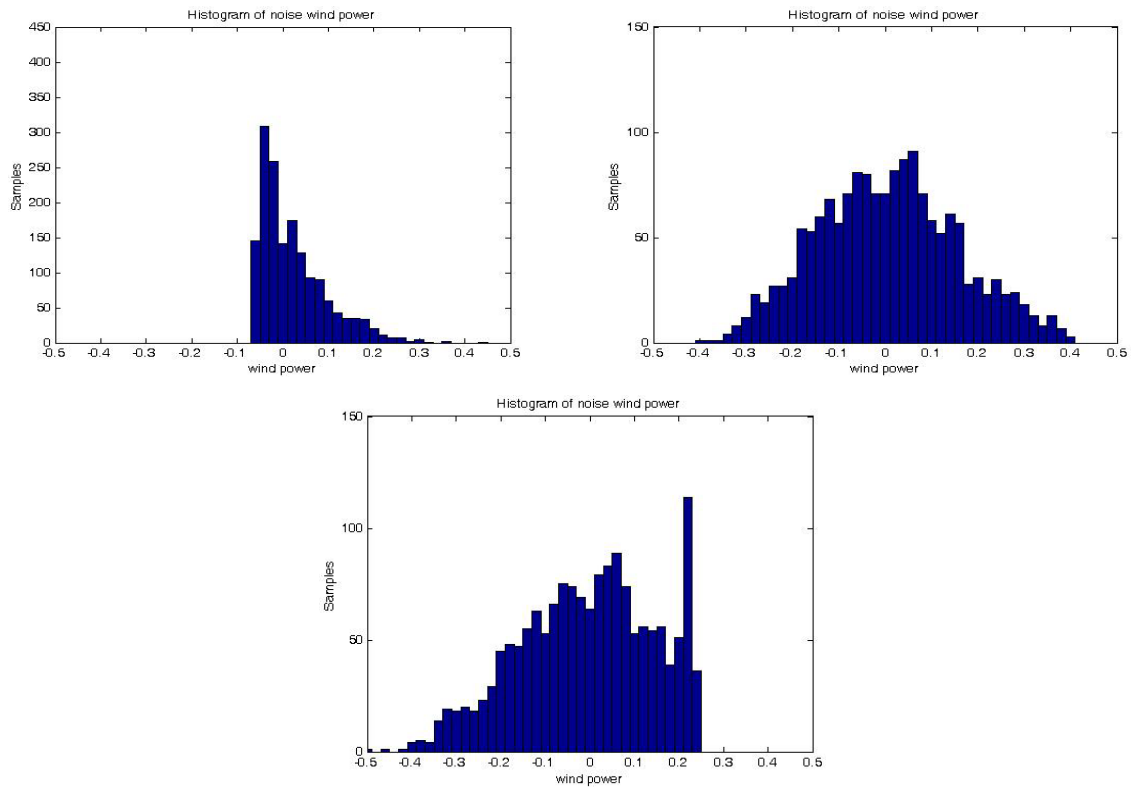


Figure 5.41 Histogram of different wind powers (WP2-WP1) for the case wind speed, $k = 6\text{m/s}$ (upper left), 9m/s (upper right), and 10m/s (lower)

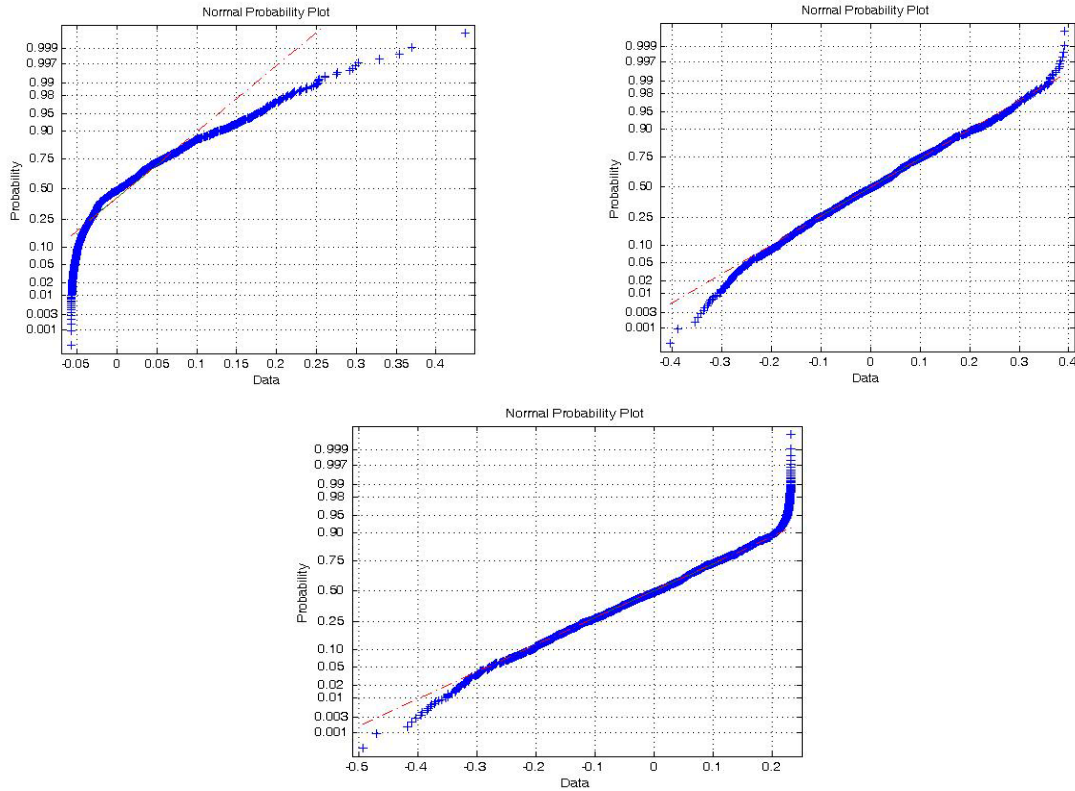


Figure 5.42 Normal probability plot of different wind powers (WP2-WP1) for the case of wind speed, $k = 6\text{m/s}$ (upper left), 9m/s (upper right), and 10m/s (lower)

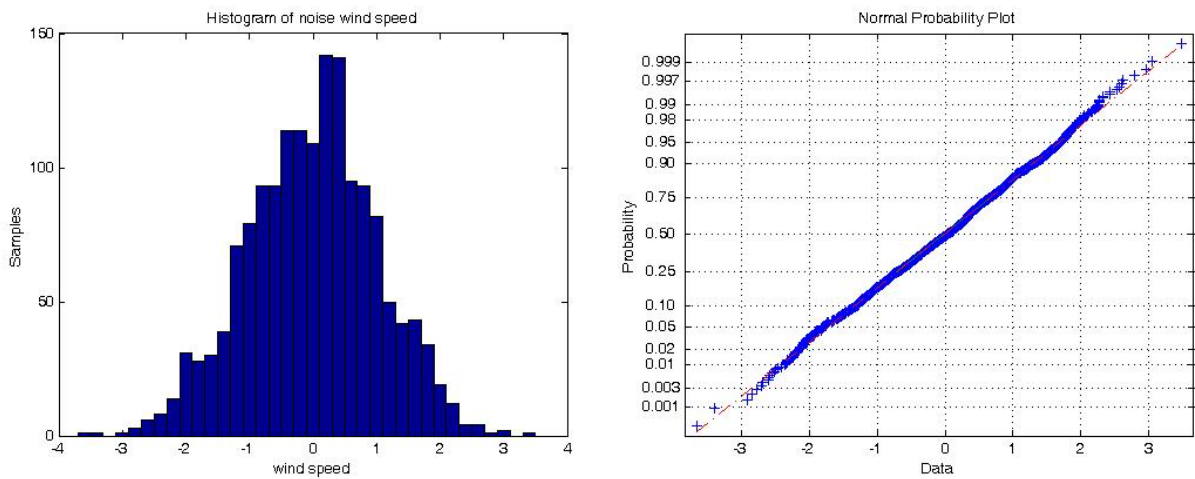


Figure 5.43 Different wind speed (WS2-WS1) for all k

Case A6 Aggregated wind farm connecting Single Machine Infinite Bus (SMIB) power system without noise

The one-line diagram of case A6 is represented in Figure 5.44. Wind speed is generated from the inverse CDF method considering the Weibull distribution. However, the power system is different from the previous cases. The single machine infinite bus system is

used to represent an influence of more complex power system on the distribution characteristics of wind power.

In Figure 5.45, the $C_{param} = 5$ is the case that wind power cannot be generated. The distribution data in Figure 5.47 is in agreed with this conclusion. For $C_{param} = 10$, the results from Figure 5.47 can be compared with Figure 5.24 and 5.25 of the case A1. It can be noticed that the distribution characteristics of wind power is very similar for these two cases. For this condition, the power system may has less influence on the distribution of wind power.

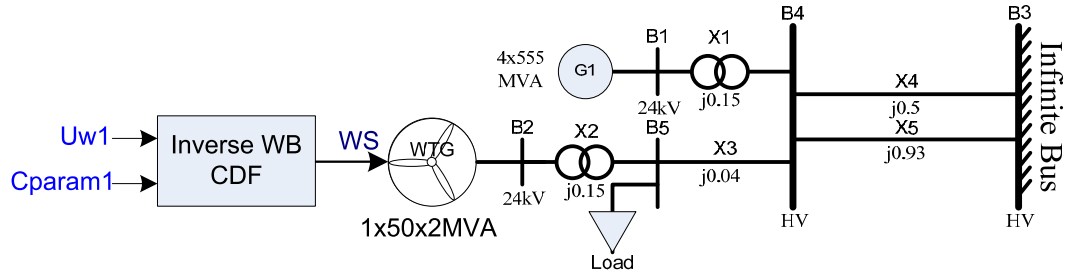


Figure 5.44 One-line diagram of test system of case A6

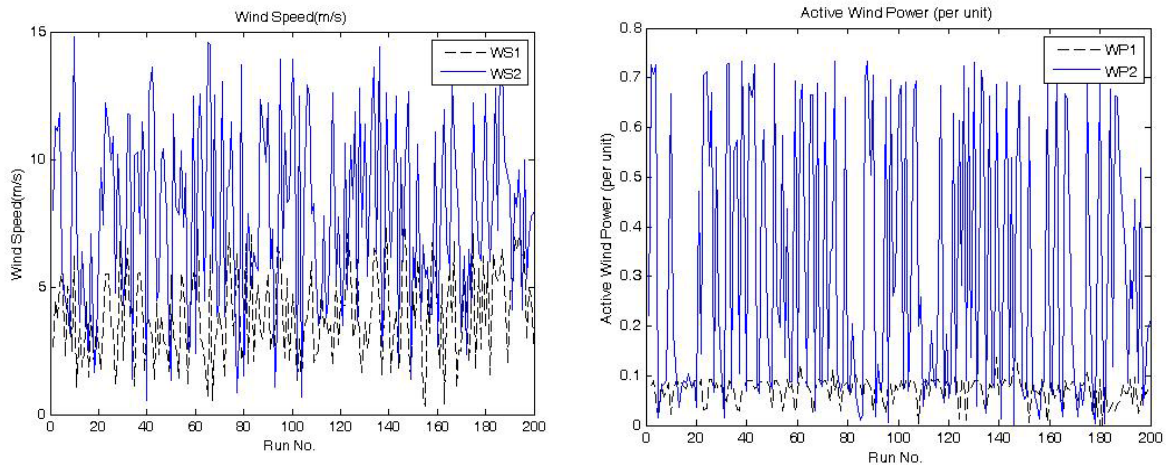


Figure 5.45 Wind speed (left) and wind power (right) of case A6
(WS1 and WP1 use $C_{param} = 5$, WS2 and WP2 use $C_{param} = 10$)

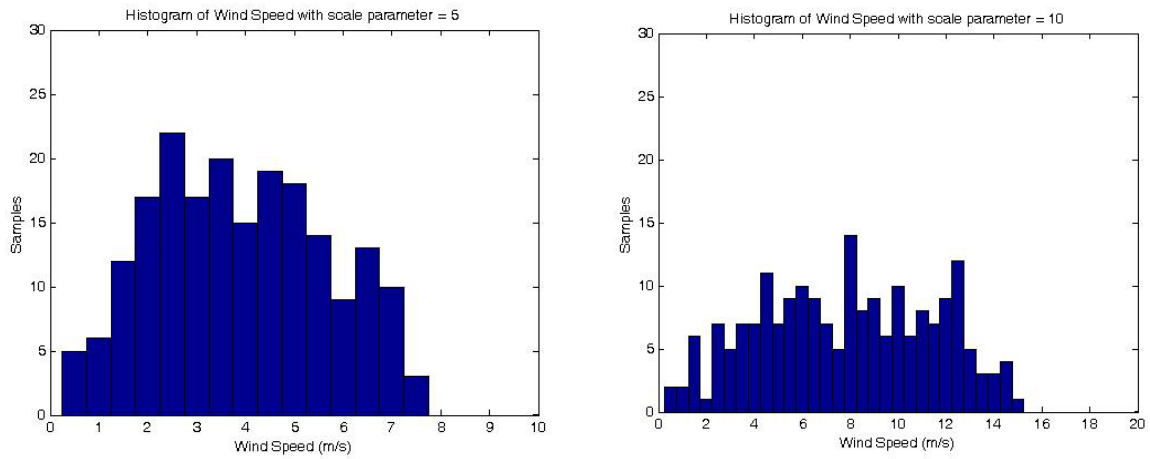


Figure 5.46 Histogram of wind speed of case A6 for $C_{\text{param}} = 5$ (left) and $C_{\text{param}} = 10$ (right)

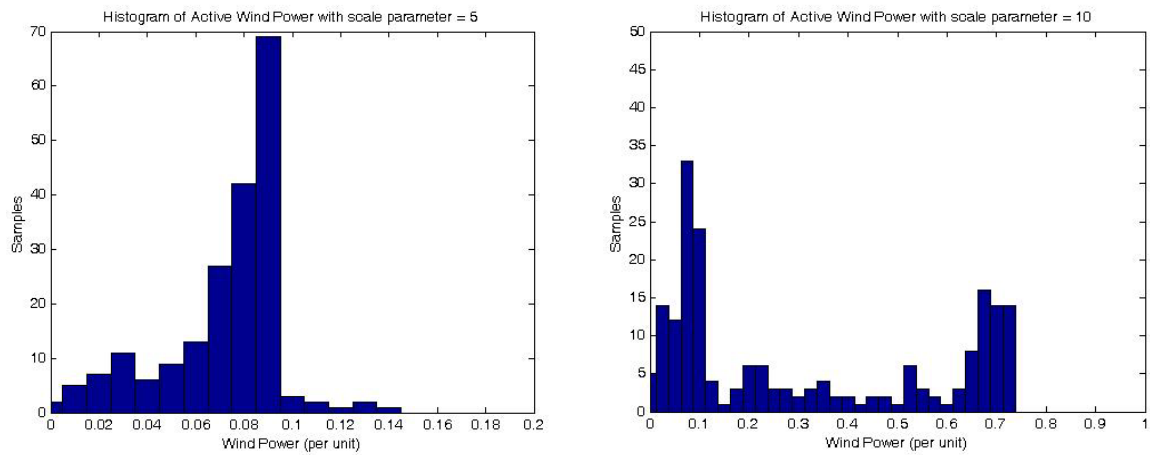


Figure 5.47 Histogram of wind power of case A6 for the case $C_{\text{param}} = 5$ (left) and $C_{\text{param}} = 10$ (right)

Case A7 Two aggregated wind farm connecting Single Machine Infinite Bus (SMIB) power system with constant mean wind speed and add normal random noise wind speed for one wind turbine

The one-line diagram of case A7 is represented in Figure 5.48. Wind speed is fixed at 10 m/s with normal random noise is added and the power system is SMIB system.

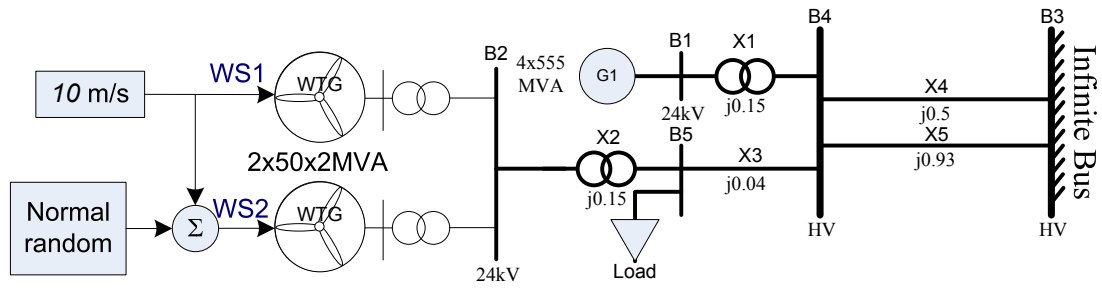


Figure 5.48 One-line diagram of test system of case A7

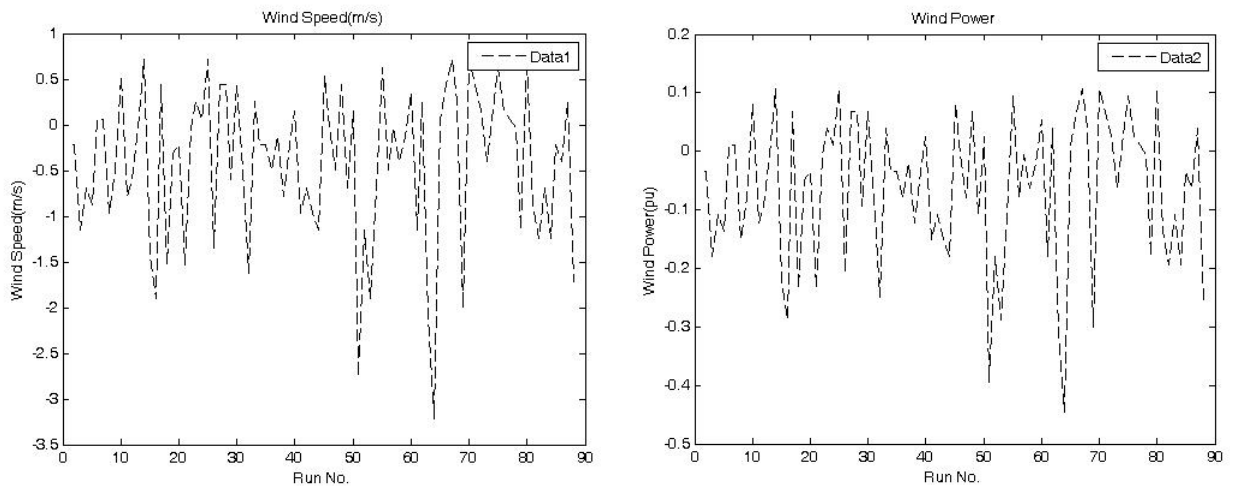


Figure 5.49 Noise wind speed (left) and noise wind power (right) of WTG2 of case A7

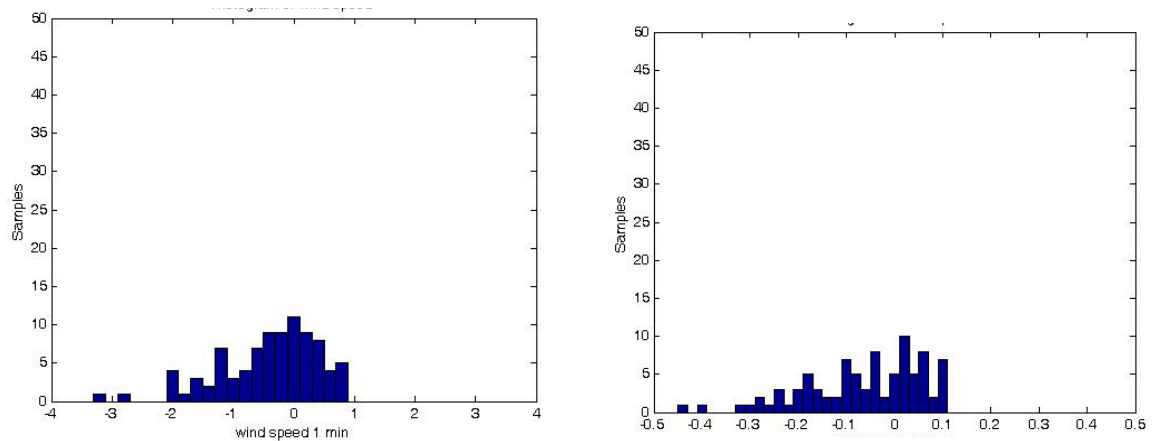


Figure 5.50 Histogram of noise wind speed (left) and wind power (right) of WTG2 of case A7

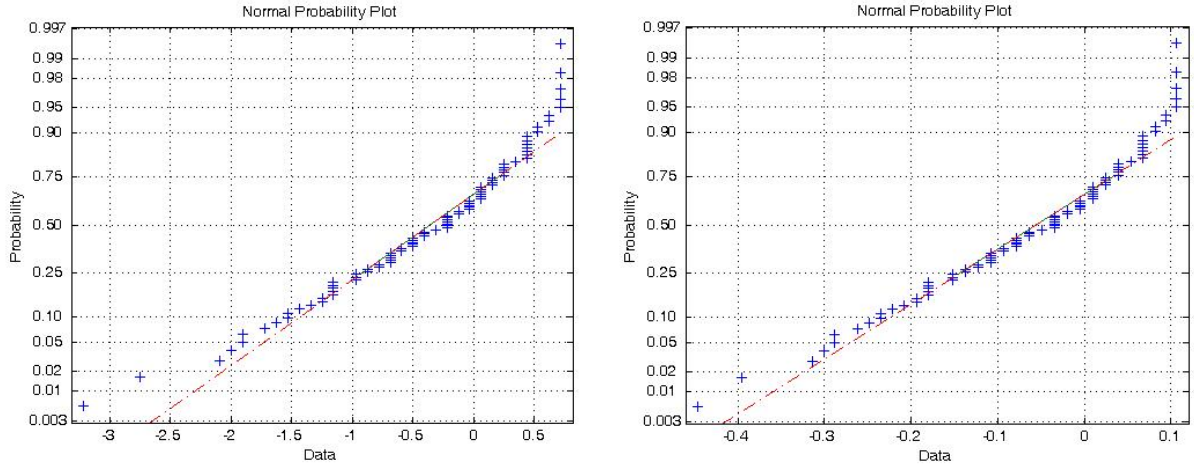


Figure 5.51 Normal probability plot of noise wind speed (left) and noise wind power (right) of WTG2 of case A7

In Figures 5.50 and 5.51, both noise wind speed and noise wind power can be approximated by normal distribution. This result agrees with the result of case A5.

5.1.4 The stochastic wind power simulation

The DFIG wind turbine model is simplified and represented by the two-order model consisting of two differential equations. From the rotor dynamic equation, when applying colored noise into the mechanical wind power (P_m), we will get the stochastic differential equation (SDE) as follows:

$$-ps_w = \frac{1}{M}(P_{ms} - P_e) + \frac{1}{M}P_{ms}\alpha_w v_w \quad \text{Eq.5-2}$$

$$p v_w = -\psi_w v_w + \gamma_w \psi_w pW \quad \text{Eq.5-3}$$

where pW is a zero-mean Gaussian distributed white noise [9], and α_w is noise intensity of the wind power with its standard deviation divided by mean value. v_w is colored noise parameter. γ_w and ψ_w are scaling parameter and bandwidth of wind power, respectively.

The power test system is a single machine infinite bus power system (SMIB). The system parameters and equations are provided in Section 4.2. The single line diagram of the power test system is represented in Figure 5.52. The simulation is done using Matlab to characterize the variations in wind power and the state variables (speed and angle) when applying colored noise. The stochastic wind power is simulated by vary bandwidths, noise intensities, and scaling parameters. Furthermore, the probability distributions of wind power

at different conditions are also determined. The results of the simulation are represented in following figures.

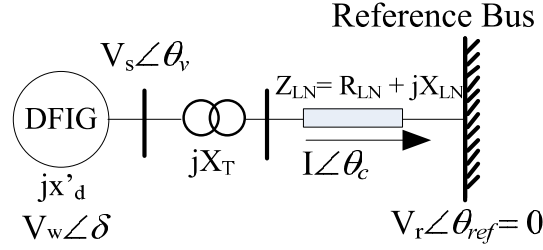


Figure 5.52 Single line diagram of SMIB with DFIG wind turbine

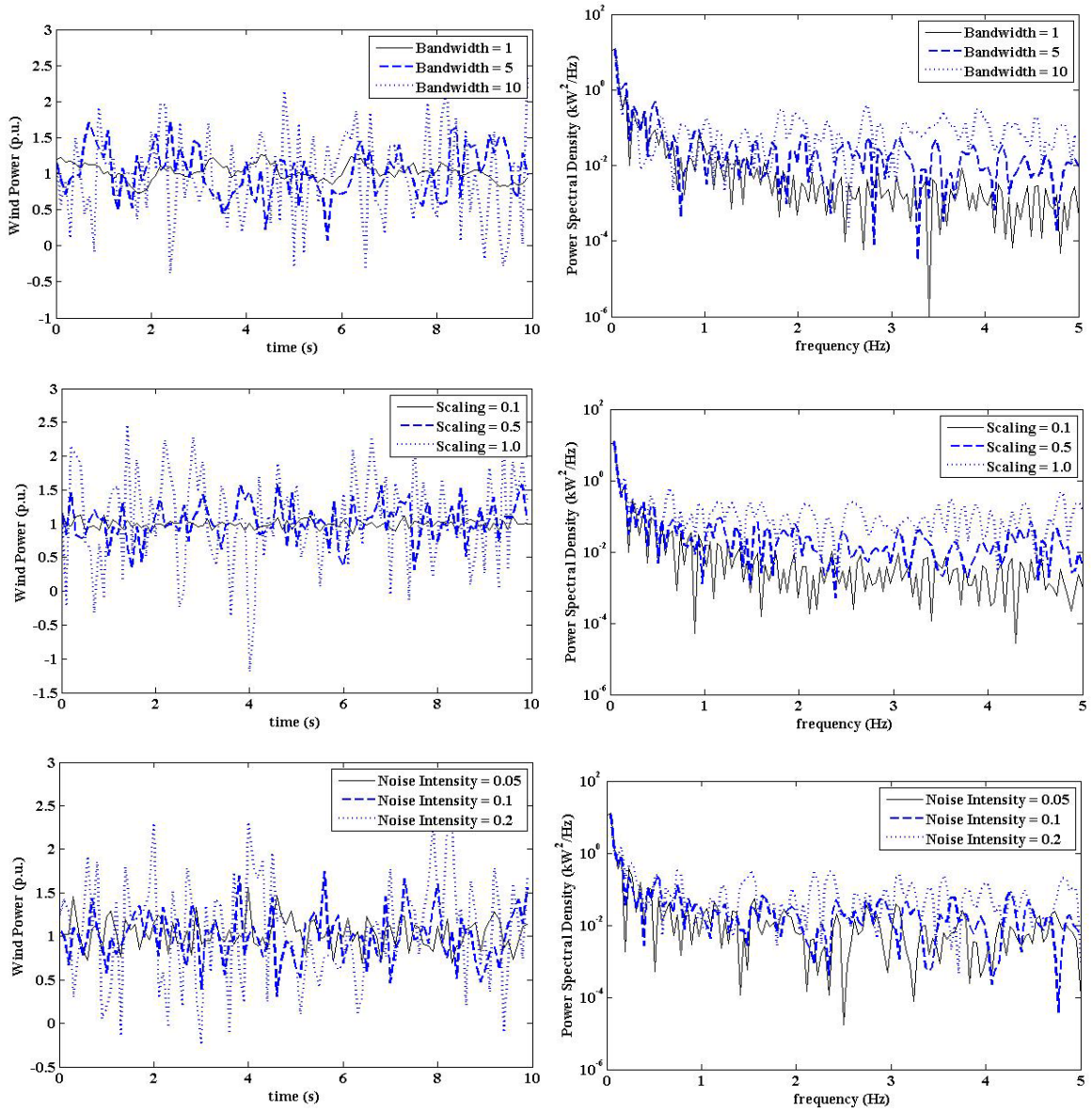


Figure 5.53 The variation of wind power (left) and its power spectral density (right) when varying bandwidth (upper), scaling factor (middle), and noise intensity (lower)

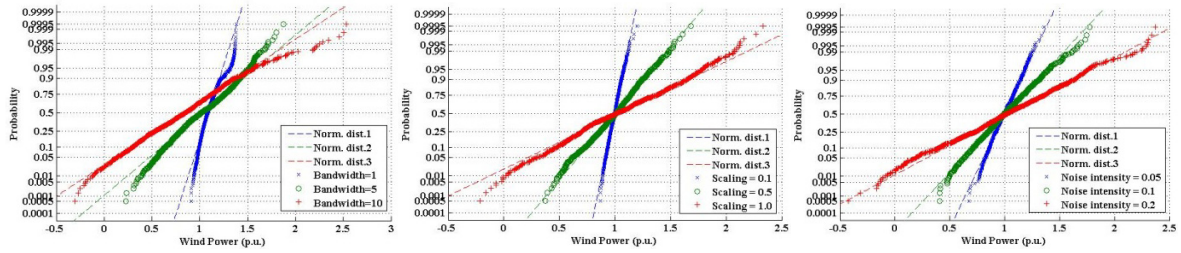


Figure 5.54 The normal curve of wind power when varying bandwidth (left), scaling factor (middle), and noise intensity (right)

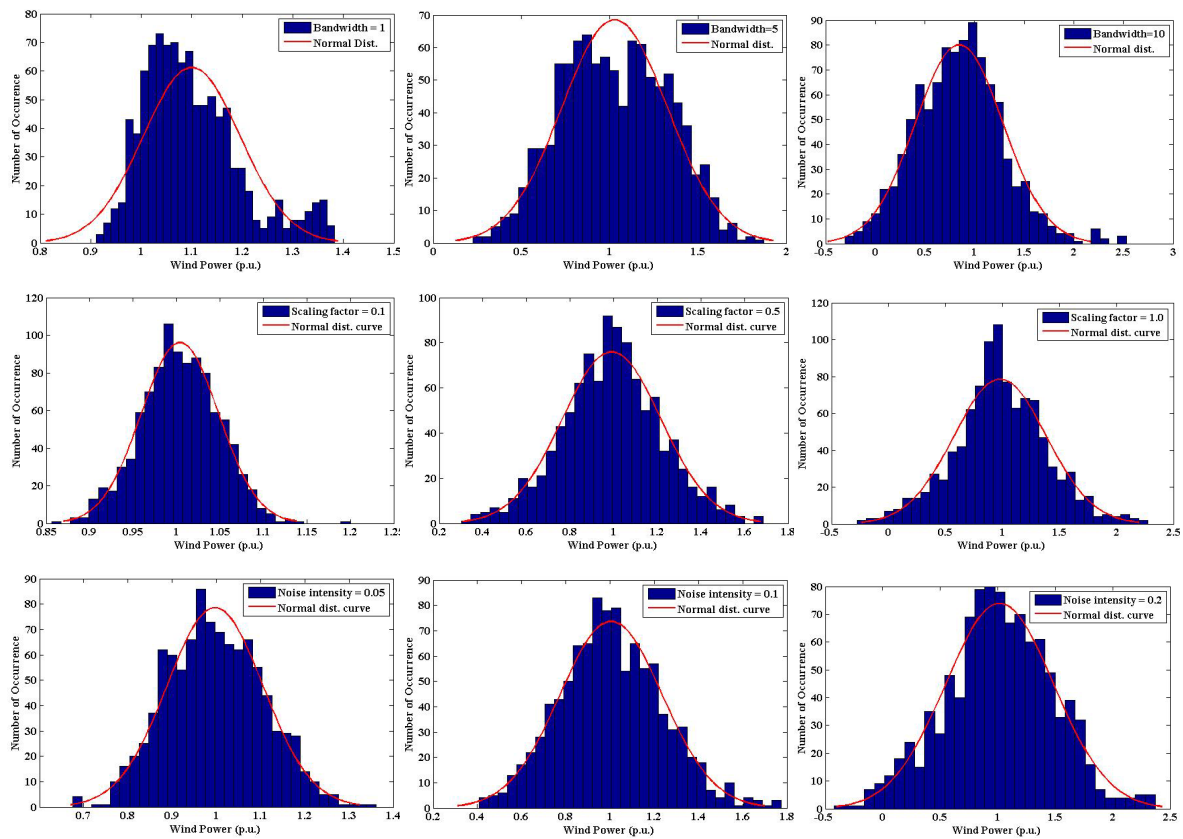


Figure 5.55 The data distribution of wind power when varying bandwidth (upper), scaling factor (middle), and noise intensity (lower)

The simulation results using Matlab can be represented in the following figures.

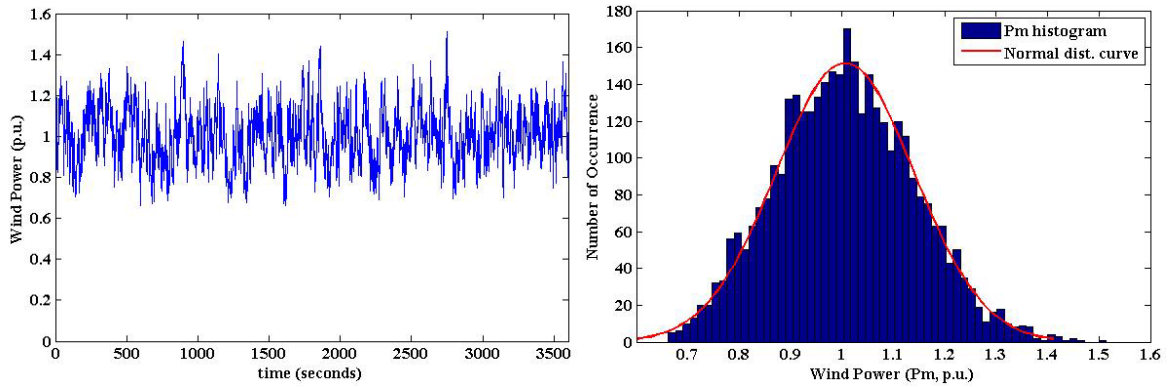


Figure 5.56 The variation (left) and data distribution (right) of wind power

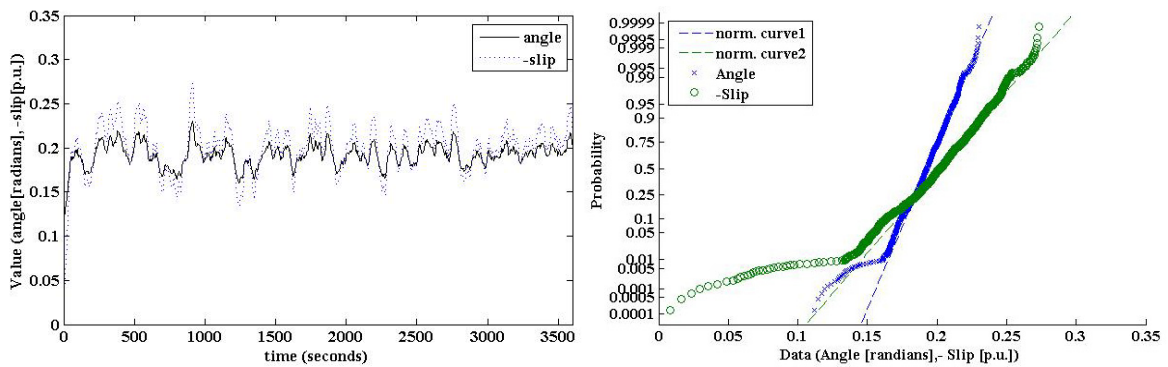


Figure 5.57 The variation (left) and normal curve (right) of angle and speed deviation (-slip)

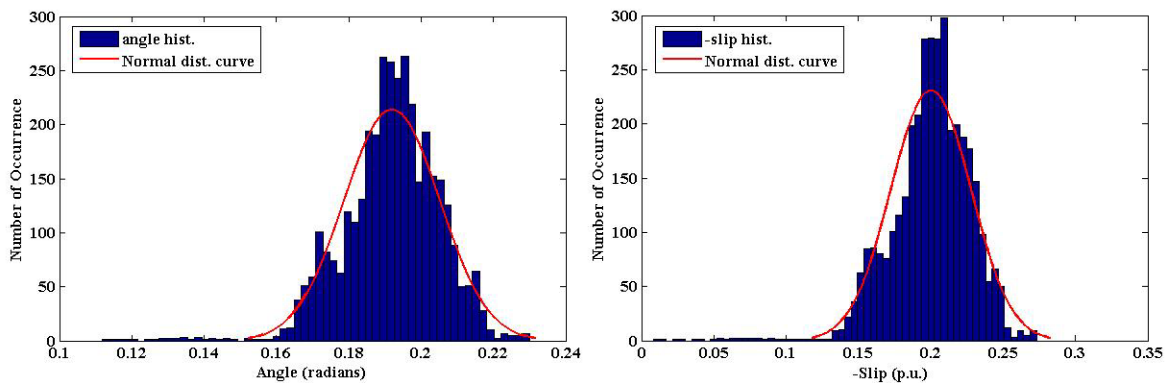


Figure 5.58 The data distribution of angle (left) and speed deviation or -slip (right)

5.2 The characteristics of power system incorporating wind power

5.2.1 Power-Angle and Power-Load on Steady State Analysis

5.2.1.1 Power-Angle Characteristic Analysis

The single machine infinite bus system (SMIB) is used in this section. The infinite bus voltage is fixed at 1.0. To investigate the power-angle characteristics of the generator, two assumptions should be considered. First is the active/reactive power-angle characteristic of the single machine power system with varying voltages and second is the

active/reactive power-angle characteristic of the single machine power system with varying line reactance. Both cases use equations in Section 3.2 (Eqs. 3-7 – 3-8) to model using Matlab. Models and equations for this case study are stated again in the following figures:

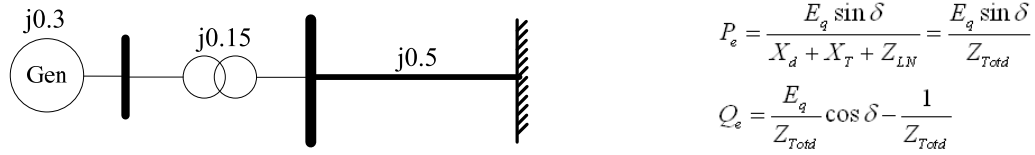


Figure 5.59 Schematic diagram of SMIB and equations

From the above figure, total impedance $Z_{Tot} = j0.3 + j0.15 + j0.5 = j0.95$. The results are presented as follows.

1) Active/reactive power-angle characteristic with varying voltage

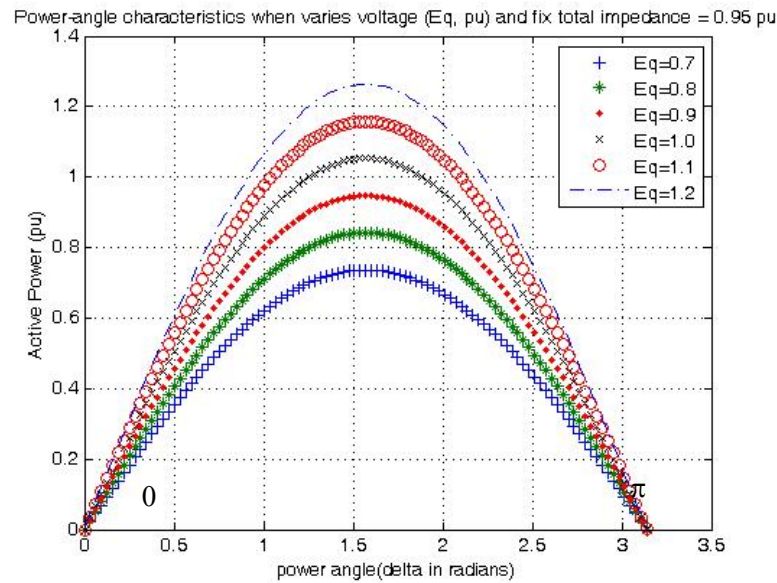


Figure 5.60 Active power-angle characteristics of SMIB system when varying voltage

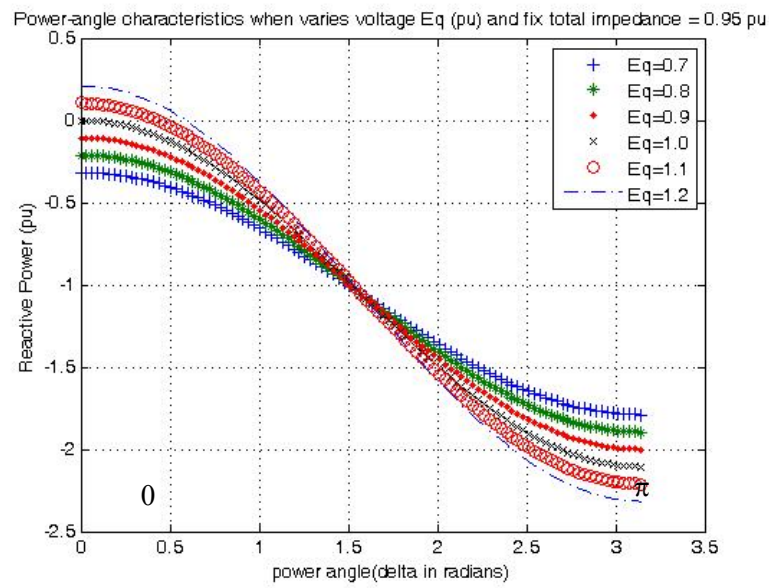


Figure 5.61 Reactive power-angle characteristics of SMIB system when varying voltage

2) Active/reactive power-angle characteristic with varying line reactance

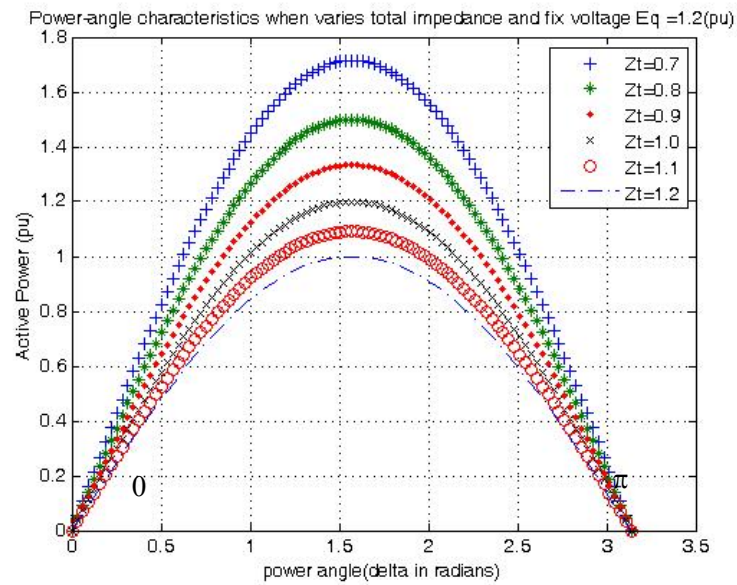


Figure 5.62 Active power-angle characteristics of SMIB system when varying total impedance

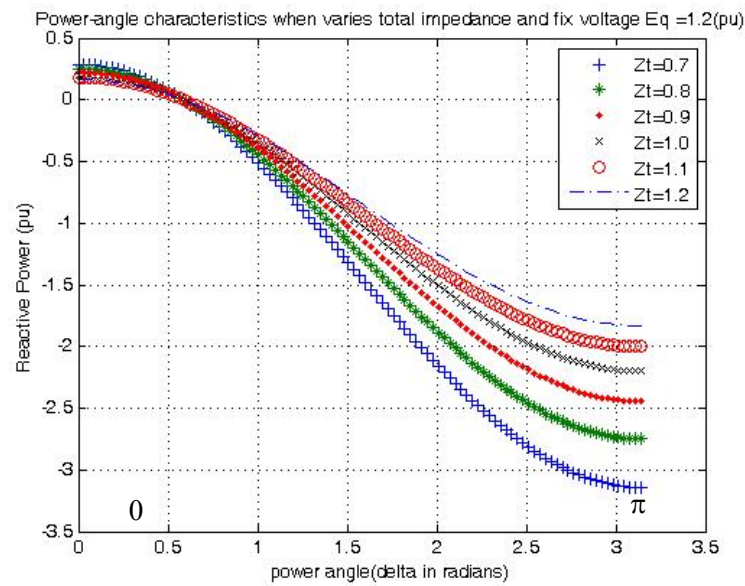


Figure 5.63 Reactive power-angle characteristics of SMIB system when varying total impedance

In Figure 5.60, since the equation has the sine function of angle varying between 0 to π , that is the reason for the shape of active power-angle characteristic having such a form. The peak value of power is when angle is 0.5π or $\sin 0.5\pi$ is equal to 1.0. This point is called *critical point*. Beyond this point, generator cannot control power by normal operation and lost synchronization finally. Furthermore, if infinite bus voltage is fixed, the higher internal voltage, the larger active power can generate from machine.

In Figure 5.61, the reactive power-angle characteristic has a different shape from the active power. However, it is clear that reactive power always has negative value. This is due to the stator winding of generator is an inductive element. The larger angle, more power is generated with increasing current, and therefore, the larger minus reactive power. Before critical point is reached, the higher internal voltage causes the smaller minus reactive power. But inversely, away from critical point, the higher internal voltage causes the larger minus reactive power.

In Figure 5.62, if internal voltage is fixed, active power increases with decreasing total impedance. For example, shorter transmission line (smaller impedance) can improve power transfer from generator to the grid.

In Figure 5.63, when internal voltage is fixed at 1.2 (larger than infinite bus voltage), reactive power is positive when power angle less than 0.5 radians. Reactive

power is a little bit larger with smaller total impedance. If power angle larger than 0.5 radians, reactive power is negative and decrease with decreasing total impedance.

3) Reactive power-voltage characteristics

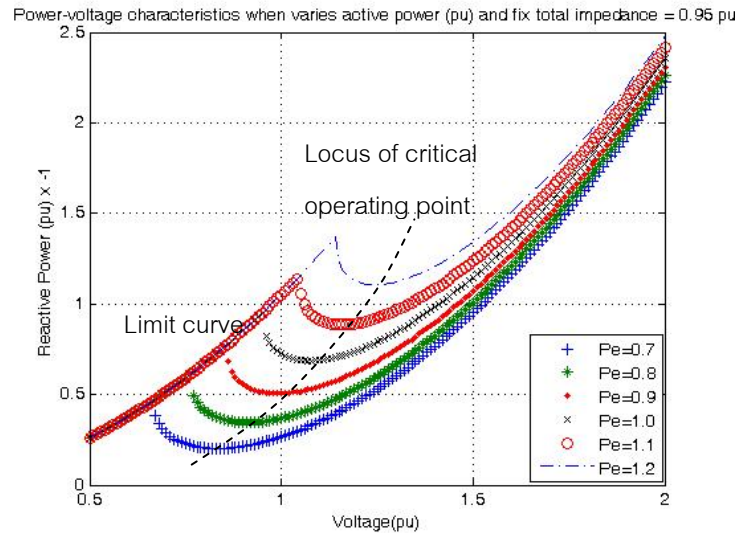


Figure 5.64 Reactive power-voltage characteristics of SMIB system with varying active power

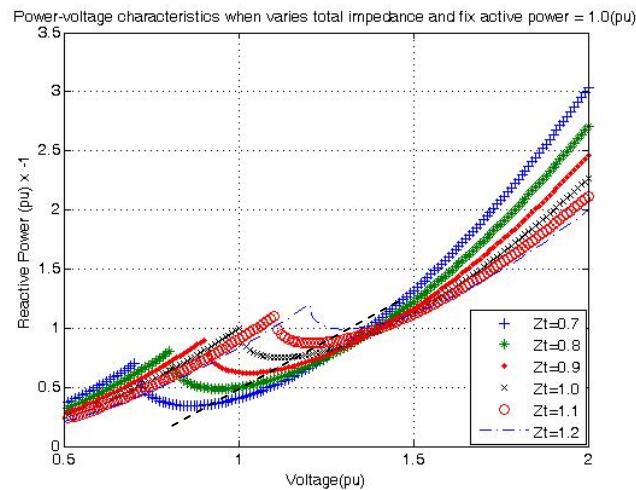


Figure 5.65 Reactive power-voltage characteristics of SMIB system with varying line reactance

In Figure 5.64, at voltages less than the locus of critical operating point (LCOP) and larger than the limit curve, voltage decreases with increasing absolute reactive power. If higher than LCOP, voltage increases with increasing reactive power. This power-voltage

characteristic is used for regulating voltage of the power system. Normal operating condition always set voltage to larger than LCOP for the reactive power compensators can control the system voltage possibly. The voltage drop, loss of compensators, and/or excess negative reactive power will reduce capability of the system to control system voltage. This is called voltage instability. With increasing active power, the system voltage (for example at 1.5 p.u.) is closer to LCOP and become instability finally.

In Figure 5.65, when active power is fixed while total impedance varies, the larger total impedance cause voltage closer to the LCOP and instability state. Beside, the limit curves are different for different total impedance.

5.2.1.2 Power-Load Characteristics Analysis

The Power-Load Characteristics of power systems lead to understanding in constraints of the system influenced by the load impedance, line impedance, load angle, and line angle. Following section is the result of analysis basing on simple one machine power system with one load and one line impedance. Testing conditions are listed in Table 5.2 .

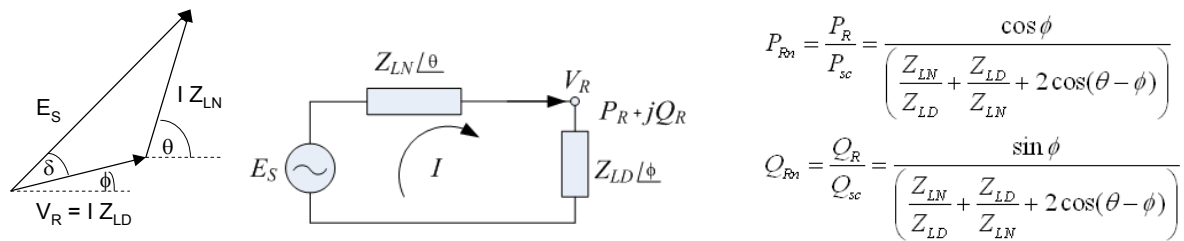


Figure 5.66 Phasor diagram, circuit diagram, and equations of power test system

Table 5.2 Testing conditions for power-load characteristic analysis

Power vs Load	Theta (θ°)	Phi (ϕ°)	$\theta - \phi^\circ$	Load (Z_{LN} / Z_{LD})
Case1 (P_{Rn} , Q_{Rn})	65:5:90	0	65:5:90	0.1:0.02:10
Case2 (P_{Rn} , Q_{Rn})	65:5:90	0:5:25	65	0.1:0.02:10

1) Active/Reactive power-Load characteristics when varying Theta and fix Phi

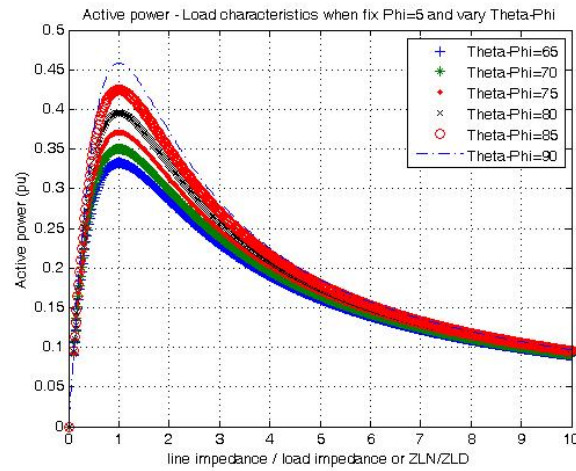


Figure 5.67 Active power-load characteristics when varying Theta and fix Phi

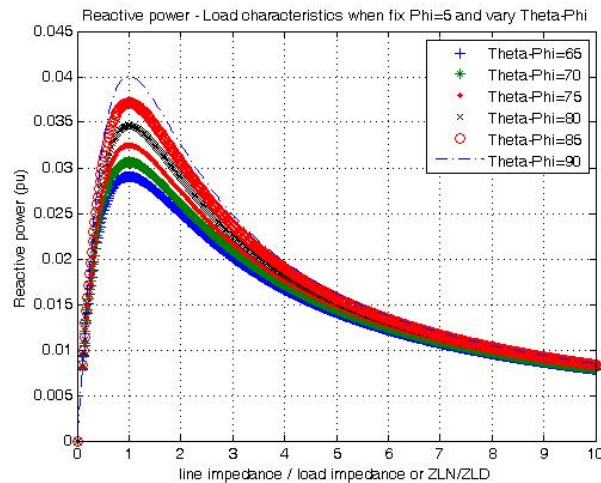


Figure 5.68 Reactive power-load characteristics when varying Theta and fix Phi

In Figures 5.67 and 5.68, active power and reactive power-load characteristics have the same shape of the curve, but with different magnitudes. For $Z_{LN} / Z_{LD} < 1$ which is normal operating condition, increasing Z_{LN}/Z_{LD} can increase both active and reactive power. At $Z_{LN} / Z_{LD} = 1$, active and reactive power reach the maximum or critical value. For $Z_{LN} / Z_{LD} > 1$, increasing of Z_{LN} / Z_{LD} result in decreasing of active and reactive power. The larger Theta-Phi, the higher active and reactive power to be consumed.

2) Active/Reactive power-Load characteristics when varying Phi and fix Theta –Phi

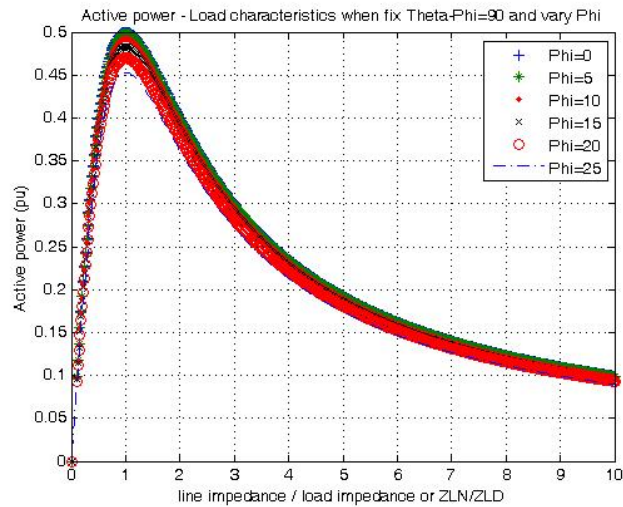


Figure 5.69 Active power-load characteristics when varying Phi and fix Theta –Phi

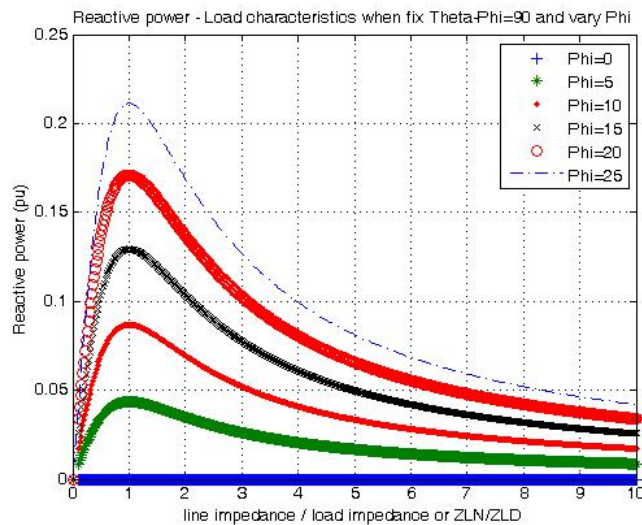


Figure 5.70 Reactive power-load characteristics when varying Phi and fix Theta –Phi

In Figures 5.69 and 5.70, when varying load angle (Phi) and fix Theta –Phi, increasing Phi causes decreasing of active power, but in contrast, increasing of reactive power. Active and reactive power reach the maximum or critical value when line impedance is equal to load impedance or $Z_{LN} = Z_{LD}$. It is important that, the reactive power is strongly depends on load angle (Phi). An increasing of load angle for 5 degrees can increase reactive power nearly 5% of base value.

Moreover, it was found that the load voltage was influenced by Theta-Phi, not by only Phi as shown in Figure 5.71.

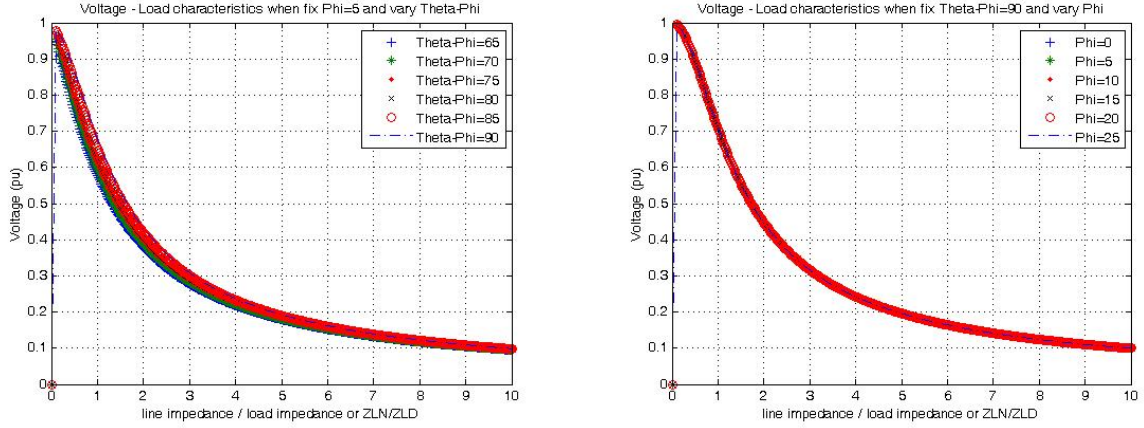


Figure 5.71 Voltage-Load characteristics when fix Phi varying Theta-Phi (left) and when fix Theta-Phi varies Phi (right)

5.2.2 Power-angle and speed characteristics of simple power system

5.2.2.1 Steady state modeling with conventional generators

Using the SMIB model and steady state models, we can draw simple schematic diagrams and phasor diagrams, as presented in Figure 5.72.

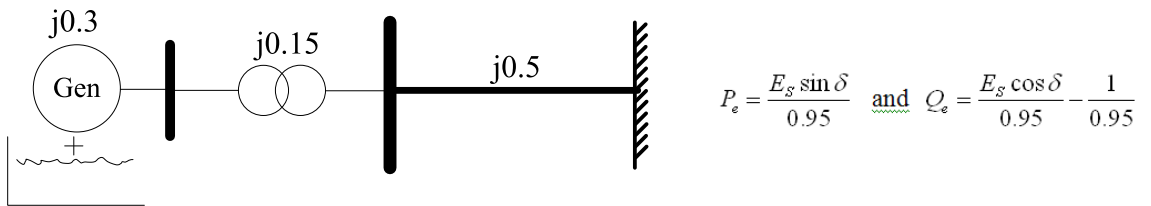


Figure 5.72 One line diagram and testing equations of SMIB power system

This simple model is used, coupled with the mathematical models in Section 3.2, to explain the relationship between electrical power and power angle, electrical power and voltage, and electrical power and load. In case of round rotor machine SMIB system, E_B is assumed constant at 1.0 p.u.

P_e and Q_e strongly depend on the internal voltage of the generator and power angle. For convenience, the external dynamic sources (from wind power and load) are not directly modeled because these effects are included in the generator voltage and power angle

In Eq.3-30, by varying δ and E_s , the power-angle characteristics can be analyzed using following conditions.

Table 5.3 Testing conditions for power-angle characteristic analysis

$P_e \& Q_e$	Power angle, δ (rad)	Voltage of Generator, E_s (p.u.)
Case 1	linearly increase 0.0314 rad/s from 0 to π within 100 seconds	constant 0.95 p.u. + sin signal 7rad/s +/- 0.05 p.u.
Case 2	linearly increase 0.0314 rad/s from 0 to π within 100 s	constant 0.9 p.u. + sin signal 7rad/s +/- 0.1 p.u.
Case 3	linearly increase 0.0314 rad/s + sin 0.1 rad/s +/- 0.5 rad within 100 s	constant 0.9 p.u. + sin signal 7rad/s +/- 0.1 p.u.
Case 4	linearly increase 0.0314 rad/s + sin 0.2 rad/s +/- 0.5 rad within 100 s	constant 0.9 p.u. + sin signal 7rad/s +/- 0.1 p.u.
Case 5	linearly increase 0.0314 rad/s + sin 0.1 rad/s +/- 0.5 rad within 100 s	constant 0.9 p.u. + Band-limited white noise PSD 0.1, sample time 0.1s
Case 6	linearly increase 0.0314 rad/s + sin 0.2 rad/s +/- 0.5 rad within 100 s	constant 0.9 p.u. + Band-limited white noise PSD 0.3, sample time 0.1s.

The results of the simulation are represented in Figures 5.74 – 5.76. Figure 5.74 shows Power angle, δ and Voltage of Generator, E_s for 6 cases of testing condition. Figures 5.75 and 5.76 represent active and reactive power-angle characteristics, respectively.

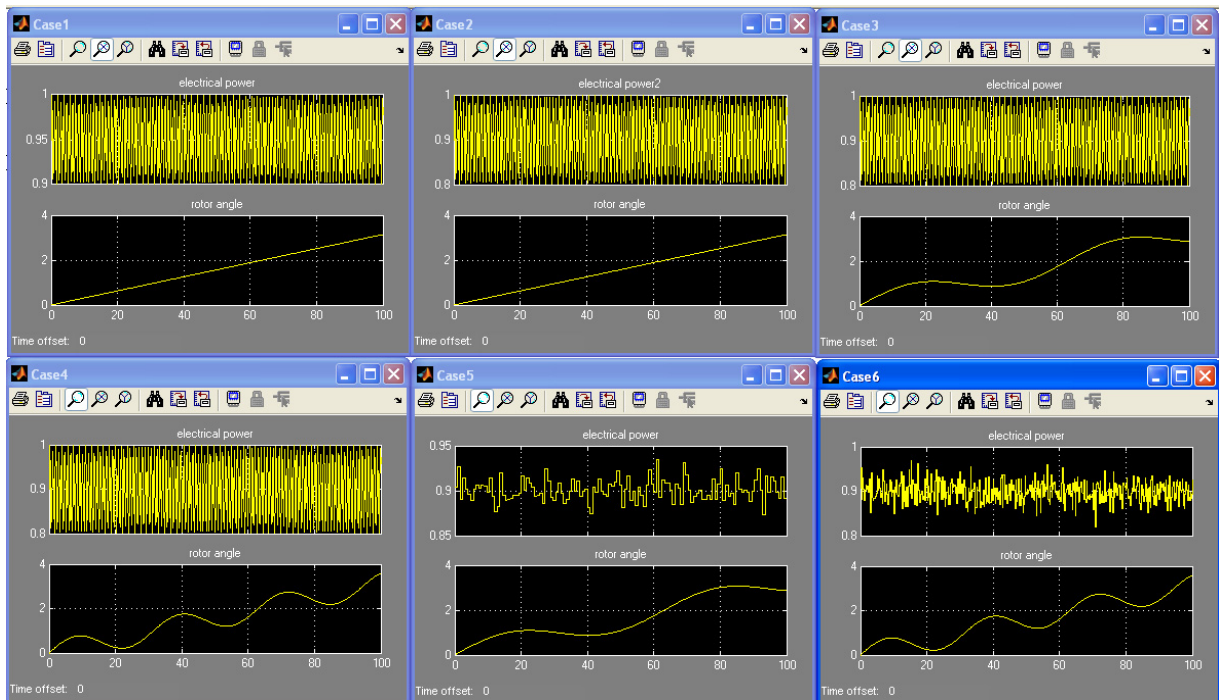


Figure 5.74 Electrical power (p.u.) and power angle (rad) of the case 1 (upper left) to case 3 (upper right) and case 4 (lower left) to case 6 (lower right).

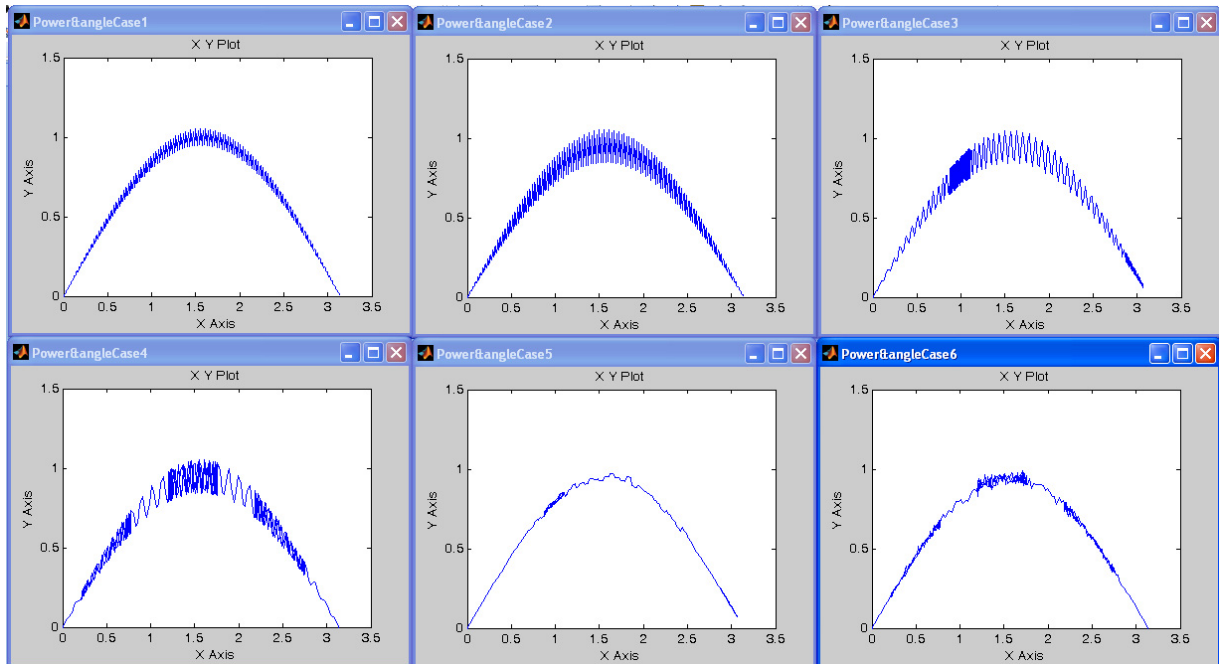


Figure 5.75 Active Power-angle characteristics for case 1 (upper left) to case 3 (upper right) and from case 4 (lower left) to case 6 (lower right).

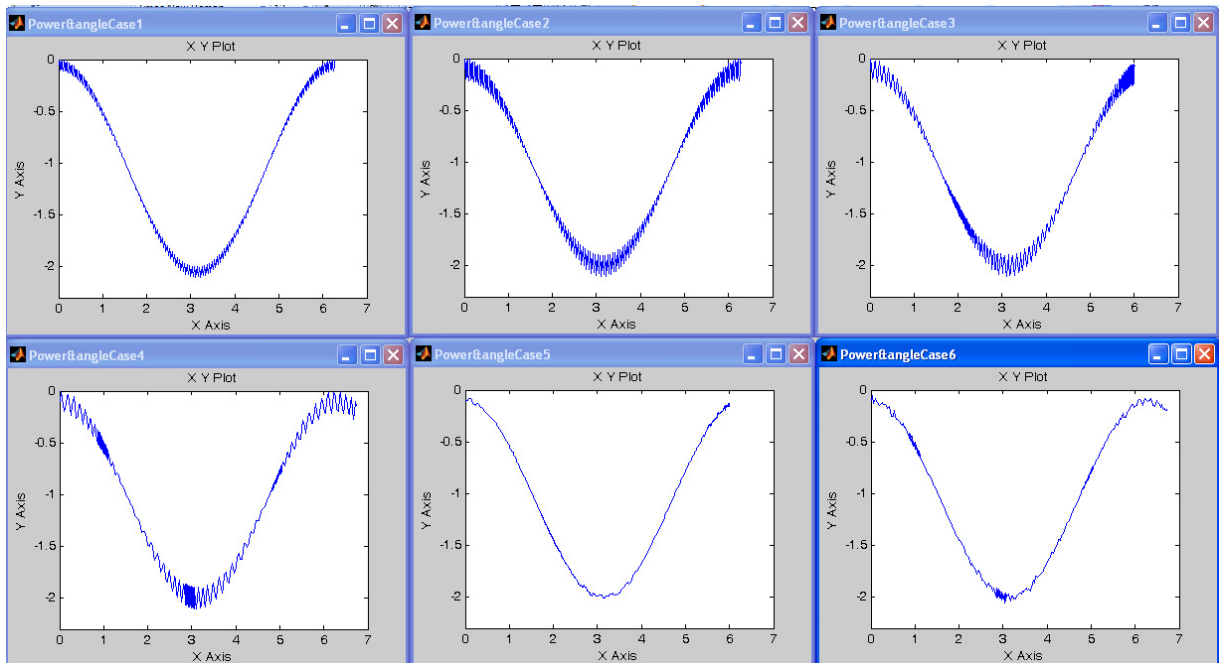


Figure 5.76 Reactive Power-angle characteristics for case 1 (upper left) to case 3 (upper right), and from case 4 (lower left) to case 6 (lower right).

In Figure 5.75, Case 1 and Case 2 represent power-angle change with variation of voltage but power angle is fixed. Interesting characteristics are Case 3 – Case 6 when power angle is varied sinusoidal. The dark-blue strip occurs when the slope of power angle is

negative. Therefore, higher frequency of power angle causes more dark-blue strips on power-angle curve (for example, Case 4 and Case 6 have negative slope of power angle for three ranges).

For all cases, Case 6 is closest to the real situation in the power system when operating under wide range of power angle. For the occurring of dark-blue strip, if we slowly replay the simulation, we will see the slowly increase and decrease of power when the slope of power angle is positive and negative, respectively.

The same description is used for reactive power but with the different shape of power-angle curve as shown in Figure 5.76.

For the real situation, operating point is fluctuated at some range when power angle is quite far from the critical point to avoid instability occurring in the system. Therefore, the generator is fixed to operate at some range, but not reach the maximum capacity.

5.2.2.2 Dynamic modeling with wind turbine generator

This section represents the result of simulation of power system using dynamics models when includes small signal from external sources such as wind power. The schematic diagram and one line diagram of power test system is represented in Figure 5.77. The model is simulated using PSCAD as described in Section 4.2.

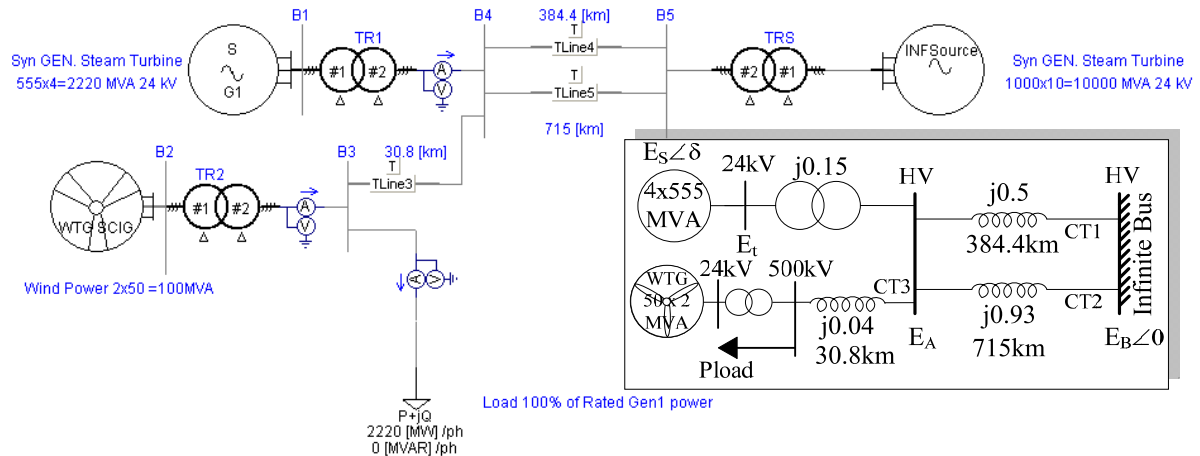


Figure 5.77 Schematic diagram and one line diagram of power test system connecting to an infinite bus and including wind power and load

There are two cases for the simulation conditions. First is the case when wind speed is zero at the first 30 seconds and is increased to be constant 10m/s for next 30 seconds.

Second is the case when constant wind speed 10m/s has ramp winds of 1m/s 4Hz to be as small signal.

For both cases, load is set as resistive load to fix value at 50% of rated capacity of synchronous generator. Wind power is injected to the grid starting at the 30th second.

Therefore, it can be seen that, for the first 30 seconds, the state parameters of the system reach the steady state since 20 seconds.

For the first case with constant wind speed, the value of wind speed, power load angle, rotor speed, active/reactive power, and voltage of generator bus are represented in Figures 5.78, 5.80, 5.82, 5.84, 5.86, and 5.88, respectively. For the second case with ramp wind speed, the value of state parameters are represented in Figures 5.79, 5.81, 5.83, 5.85, 5.87, and 5.89, respectively.

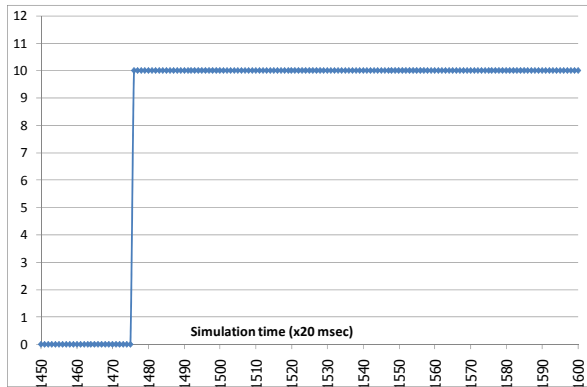


Figure 5.78 Wind speed 10m/s constant

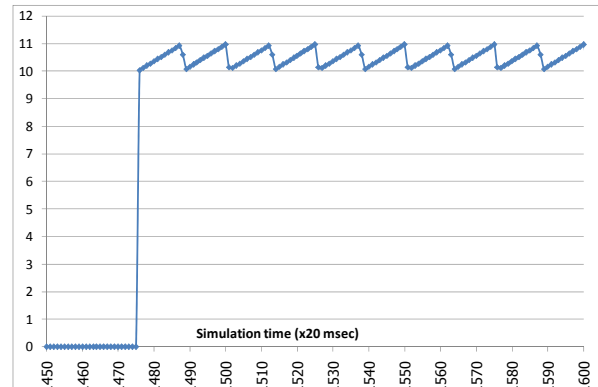


Figure 5.79 Wind speed 10m/s + ramp
1m/s4Hz

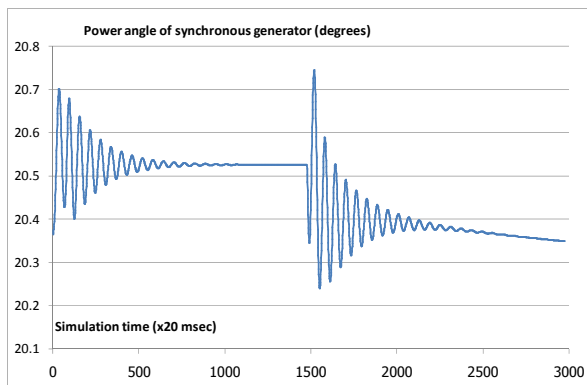


Figure 5.80 Power angle of constant wind

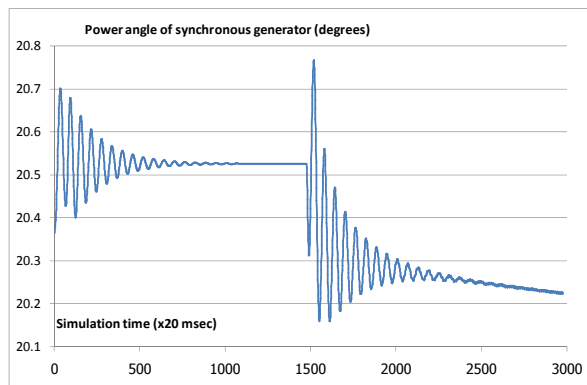


Figure 5.81 Power angle of case small
signal

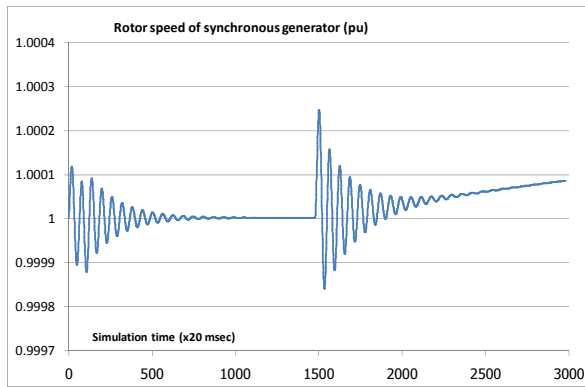


Figure 5.82 Rotor speed of constant wind

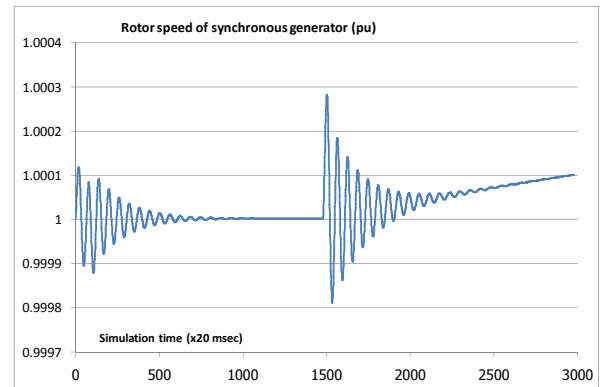


Figure 5.83 Rotor speed of case small signal

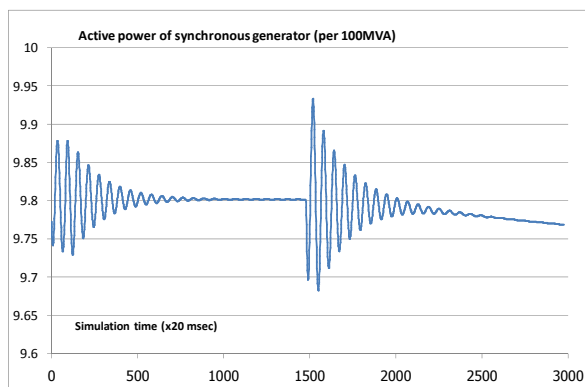


Figure 5.84 Active power of constant wind

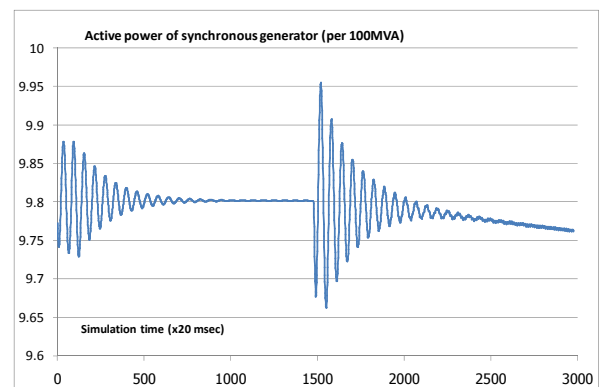


Figure 5.85 Active power of case small signal

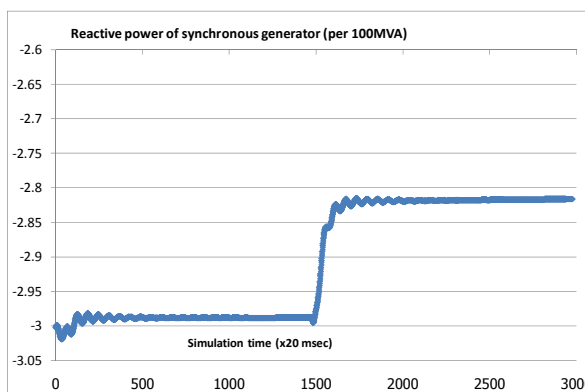


Figure 5.86 Reactive power of constant wind

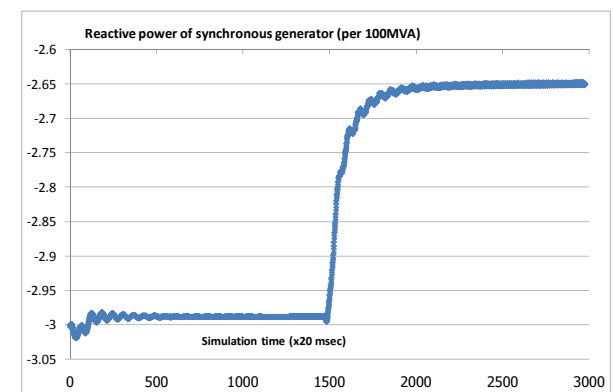


Figure 5.87 Reactive power of case small signal

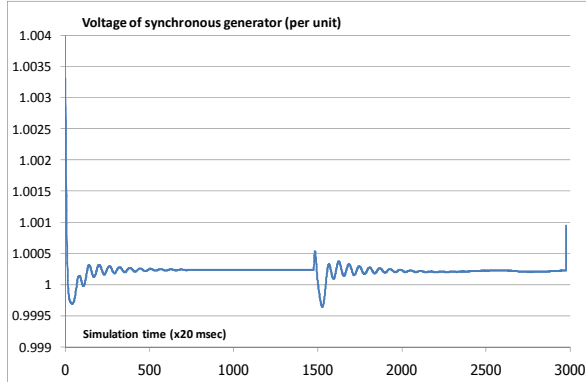


Figure 5.88 Voltage of constant wind

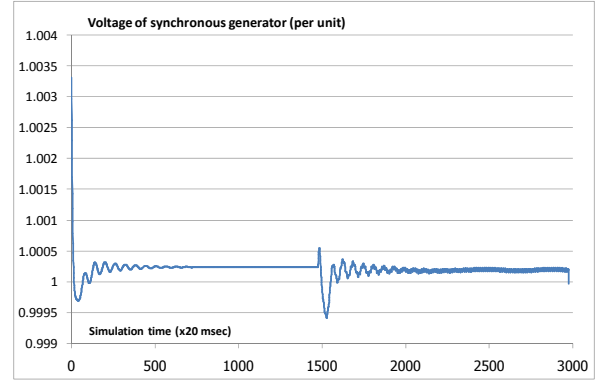


Figure 5.89 Voltage of case small signal

In Figures 5.78 to 5.89, for the first 30 seconds, the steady state values of power angle, rotor speed, active power, and reactive power are 20.525 degrees, 1.0 p.u., 980.2 MW, and -298.8MVar, respectively.

The power angle of generator without and with wind power is considered, respectively. The power angle of base case swings at first 20 seconds and then reaches the steady state at 20.525 degrees. For wind power case, the power angle swing seems to cease before 20 seconds but replacing by decrease of power angle continuously.

5.2.3 Characteristics of the power system under different testing conditions

In this section, the single machine infinite bus power system is used. The power system, including fluctuating wind power, leads to the higher degree of complexity. This situation may affect the ac power system synchronization differently depending on characteristics of wind power. Therefore, the power angle and rotor speed of synchronous generator with various characteristics of wind power are investigated.

The system voltage is 500kV with load power 50% of 2220 MVA synchronous generator. The simulation duration time is 100 seconds, which is enough for the system to reach a steady state at about 20 seconds (without wind power). The time step of the simulation is 50 micro seconds.

The synchronous generator model is IEEE generic steam turbine model supported by PSCAD (www.pscad.com). The wind power model consists of wind source model and wind turbine model with pitch control. The wind source model generates mean wind speed with noise. For wind turbine model, the 50x2 MVA squirrel cage induction generator (SCIG) is used in this study. For noise wind speed (V_n) model, seven parameters are used to define its characteristics, which are [46]:

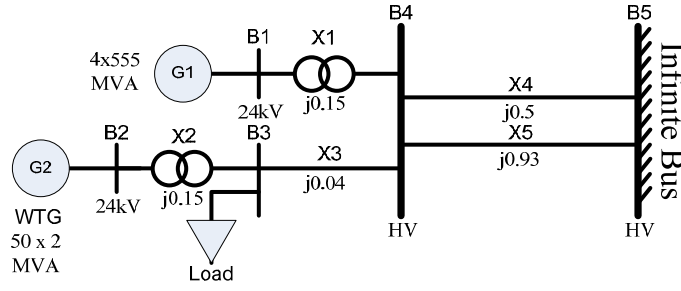


Figure 5.90 Test power system including wind power and load

The PSCAD provides the 2MW wind turbine model (separate from 2 MVA squirrel cage induction generator), as presented in Figure 5.90.

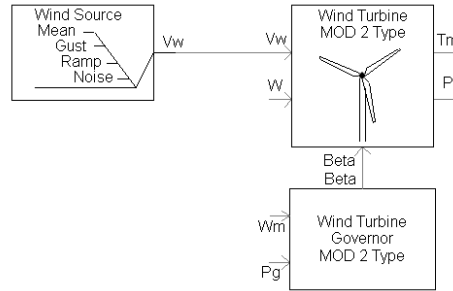


Figure 5.91 Wind turbine model in PSCAD

For the wind turbine model, the wind speed (V_w , m/s), mechanical speed of generator (ω , rad/s), and pitch angle (β , °) are input while mechanical torque (T_m) and power of turbine (P) are the output. The wind turbine has torque- ω characteristics (or equation of power coefficient) vary with V_w using standard model of wind turbine.

For synchronization system stability, important parameters to be studied are rotor speed and power angle (use power angle, δ , instead of actual rotor angle). The sources of small signal are from the different characteristics of wind speed. The 11 testing conditions with different characteristics of wind speed are represented in Table 5.4.

Table 5.4 Testing conditions for the study of characteristics of the power system incorporating wind power

	Wind turbine	Wind speed	Noise conditions	Load	Base voltage
CaseB1	No wind power	10 m/s	-	1100 MW	500 kV
CaseB2	50x2MVA	10 m/s	-	1100 MW	500 kV
CaseB3	50x2MVA	10 m/s	-	1100 MW	230 kV
CaseB4	50x2MVA	10 m/s	Stdev 0.19 m/s, frequency 1 rad/s	1100 MW	500 kV
CaseB5	50x2MVA	10 m/s	Stdev 1.86 m/s, frequency 1 rad/s	1100 MW	500 kV
CaseB6	50x2MVA	10 m/s	Stdev 1.52 m/s, frequency 0.5 rad/s	1100 MW	500 kV
CaseB7	50x2MVA	10 m/s	Stdev 1.52 m/s, frequency 2 rad/s	1100 MW	500 kV
CaseB8	50x2MVA	10 m/s	Ramp ± 1 m/s, 0.5 Hz	1100 MW	500 kV
CaseB9	50x2MVA	10 m/s	Ramp ± 1 m/s, 0.75 Hz	1100 MW	500 kV
CaseB10	50x2MVA	10 m/s	Ramp ± 1 m/s, 1.0 Hz	1100 MW	500 kV
CaseB11	50x2MVA	10 m/s	Ramp ± 1 m/s, 4.0 Hz	1100 MW	500 kV

Case B1 Base case without wind power

For the base case, the wind turbine does not generate power to the power system. The power angle and rotor speed are represented in Figure 5.92. The power angle reaches steady state of 23.14 degrees after 20 seconds. The steady state rotor speed is 1.0 pu. In this figure, PSD of both cases are quite flat for wide range except at frequency 0.75Hz which periodical fluctuation occurs and at very low frequency which the steady state component occurs.

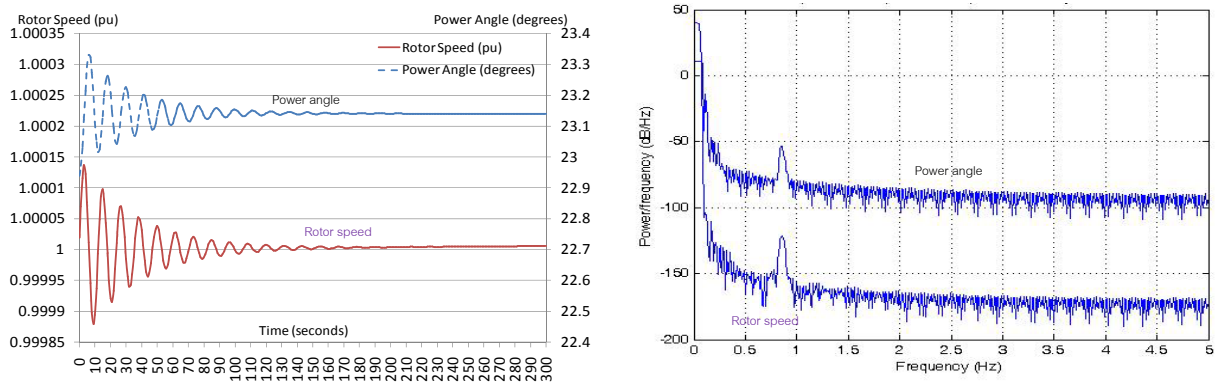


Figure 5.92 The power angle and rotor speed for base case and PSD of power angle (black) and rotor speed (blue) for base case in dB/Hz

Case B2 Aggregated wind farm with constant wind speed

In Case B2, the wind power is applied. The power angle is used instead of different rotor angle for convenience and is presented in Figure 5.93. The rotor speed of generator during 40 seconds of simulation is presented also in this figure.

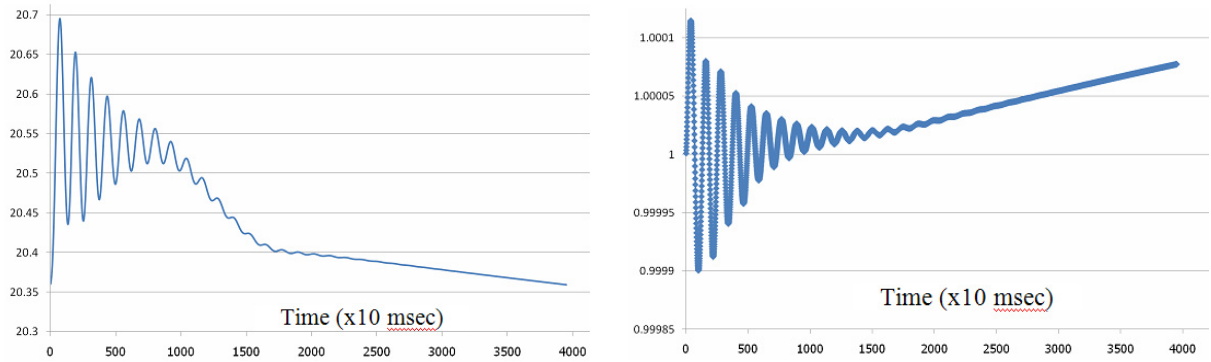


Figure 5.93 The power angle of generator for Case B2 in degrees (left) and the rotor speed of generator for Case B2 in per unit (right).

In Figure 5.93, the oscillation ceases after 20 sec with decreasing power angle. However, the rotor speed is increase continuously which may reach the steady state depending on operating conditions. It is found that steady state can be reached after the 250 seconds of simulation depending on the capacity and configuration setting of infinite bus.

Case B3 Aggregated wind farm with constant wind speed incorporate in 230kV power system

For Case B3, wind power 100MVA is connected to the power system with constant wind speed 10m/s, and the system voltage is reduced to be 230kV. The load resistance is the same with the other case. The power angle of synchronous generator is presented in Figure 5.94. The rotor speed of generator during 40 seconds of simulation is also presented in this figure.

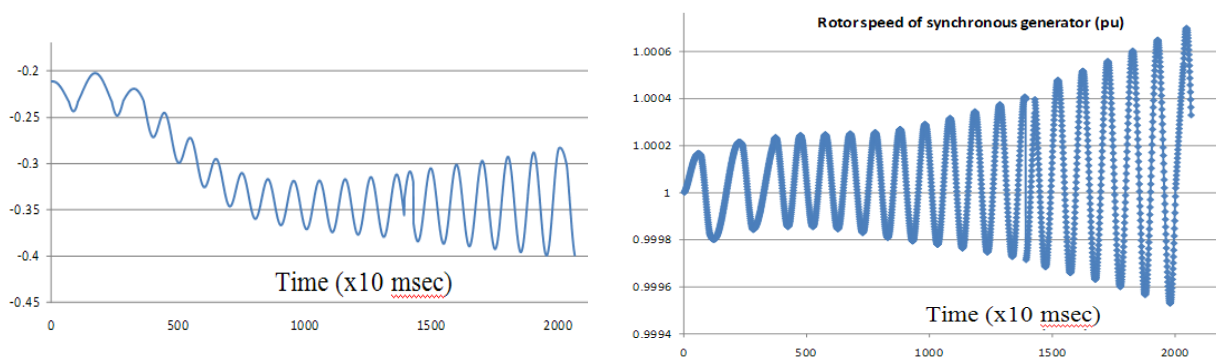


Figure 5.94 The power angle of generator for Case B3 in degrees and the rotor speed of the generator for Case B3 per unit

In Figure 5.94, both power angle and rotor speed are oscillated and increase in magnitude continuously. In terms of stability, this could be the undamped mode of oscillation or instability. This instability causes from the losses in the very long

transmission line with unsuitable system voltage. The i^2R loss can reduce damping torque and cause oscillation while i^2X loss can reduce synchronizing torque and causes continuously increase of rotor angle and speed [44].

For the cases B4 – B7, noise wind speed model is added into wind turbine model. The default of noise model consists of $N = 50$, $cd = 0.0192$, $L = 600$, $k = 50$, and $time_interval = 0.4$. The mean wind speed is 10 m/s which enough for the wind turbine to operate continuously.

The standard deviation of case B5 is from the maximum of standard deviation of measured wind speed data. The standard deviation of case B4 is set to be 10% of case B5 for comparison. The standard deviations of case B6 and case B7 are the median values of measured wind data. For $\Delta\omega$, both case B4 and case B5 use the default value while case B6 and case B7 use the possible minimum and maximum value of 0.5 and 2.0, respectively.

For 100 seconds of simulation, before second 30th, the wind turbine generator is connected to the power system but with zero wind speed. After second 30th, the fluctuating characteristics of wind speed are defined by mean value, standard deviation, and noise amplitude, as shown in Table 5.4.

The simulation results are analyzed using Matlab to investigate how power angle and rotor speed changing with different testing conditions comparing Case B4 with Case B5, and Case B6 with Case B7. The modified periodogram or Thomson multitaper method (www.mathworks.com) is used to estimate the PSD in this thesis.

CaseB4 Vs. CaseB5: Different fluctuation deviation, the same noise frequency amplitude

For Case B4 and Case B5, with the same mean wind speed and the same frequency base noise amplitude, the standard deviations of wind speed are different. The results of wind power simulation are represented in Figure 5.95. From the simulation using PSCAD, the power angle and its PSD of the synchronous generator are represented in Figure 5.96.

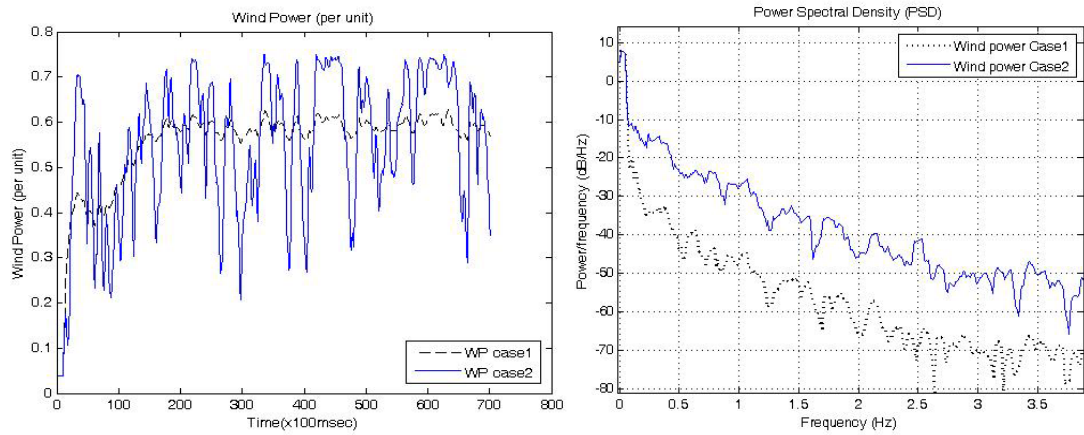


Figure 5.95 The wind power (left) of Case B4 (case1) compared with Case B5 (case2) and its PSD (right)

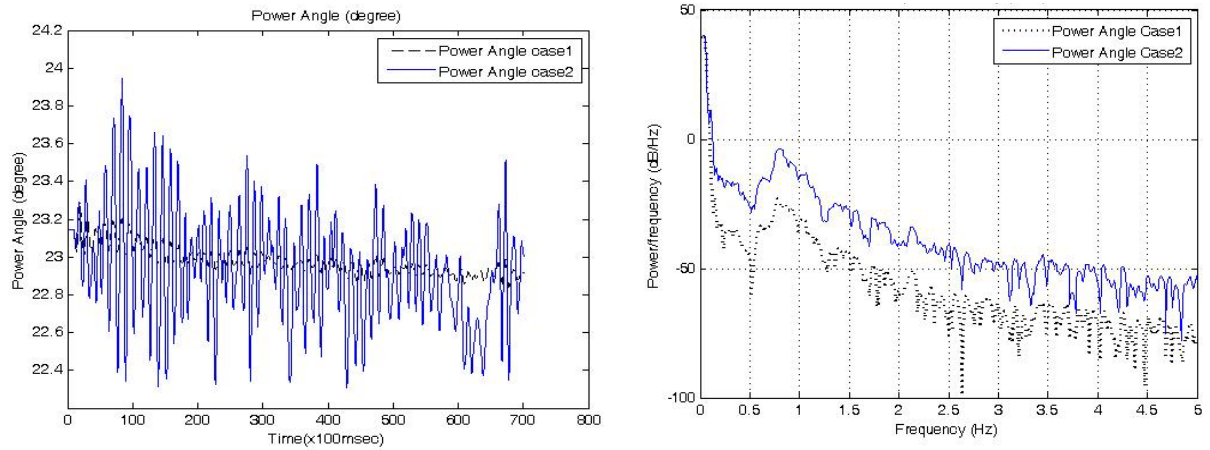


Figure 5.96 The power angle of synchronous generator of Case B4 (case1) compared with Case B5 (case2, left) and its PSD of Case B4 compare with Case B5 (right)

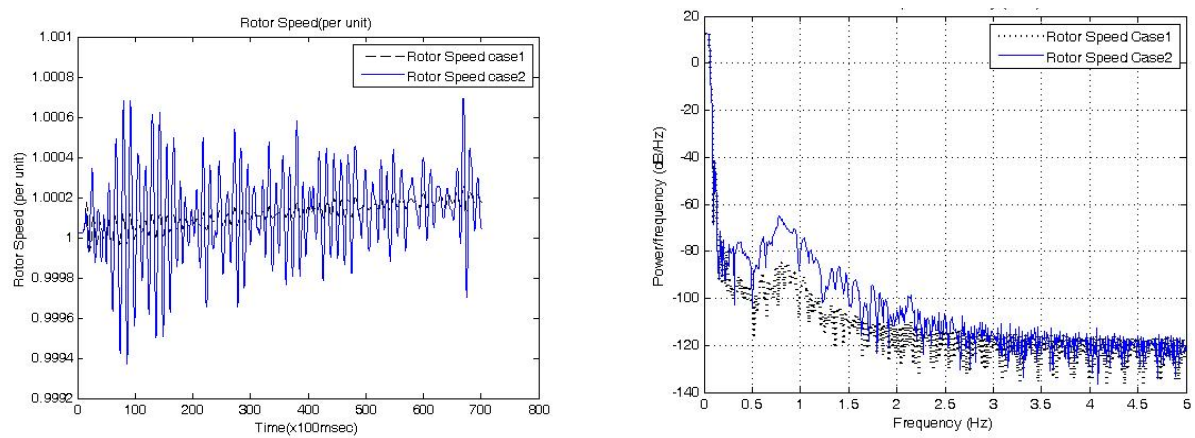


Figure 5.97 The rotor speed of synchronous generator of Case B4 (case1) compared with Case B5 (case2, left) and its PSD of Case B4 compare with Case B5 (right)

In Figure 5.96, the power angles are oscillated obviously with frequency about 0.75Hz. The amplitude of oscillation is larger for Case B5 at frequency range from 0-5Hz. However, shapes of PSD curve are comparable for both cases. Power angle of both cases decrease with time which means wind power can share load from synchronous generator but excite oscillated fluctuation.

From the rotor speed of the synchronous generator and its PSD in Figure 5.97, the rotor speed increases with time and with the oscillated fluctuation frequency about 0.75Hz. At frequency lower than 2.5Hz, rotor speed of Case2 has larger PSD than Case B4. Therefore, rotor speed is sensitive to the different deviation of small signal at frequency lower than 2.5Hz.

Case B6 Vs. CaseB7: Different frequency base noise amplitude, the same fluctuation deviation

For Case B6 and Case B7, the standard deviation of wind speed is the same but frequency base noise amplitudes are 0.5 rad/s and 2.0 rad/s, respectively. The results of wind power simulation are represented in Figure 5.98. The wind power varies in a range of ± 0.2 p.u.

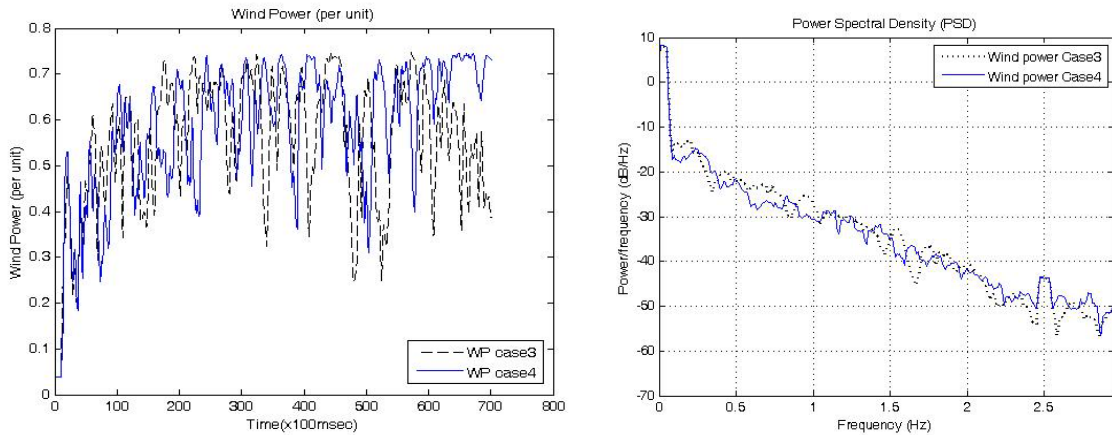


Figure 5.98 The wind power (left) and its PSD (right) of Case B6 (case 3) and Case B7 (case 4)

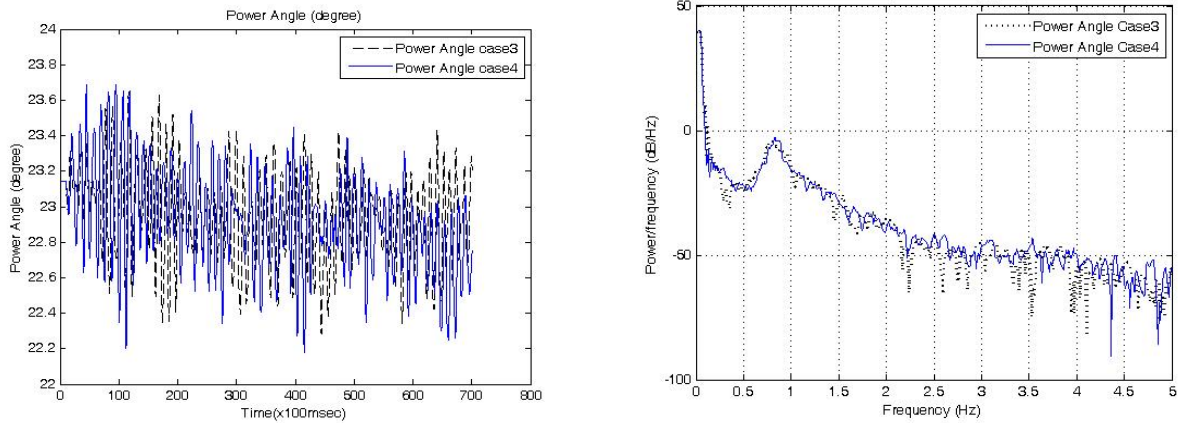


Figure 5.99 The power angle of synchronous generator of Case B6 (case 3) compare with Case B7 (case 4, left) and its PSD of Case B6 compared with Case B7 (right)

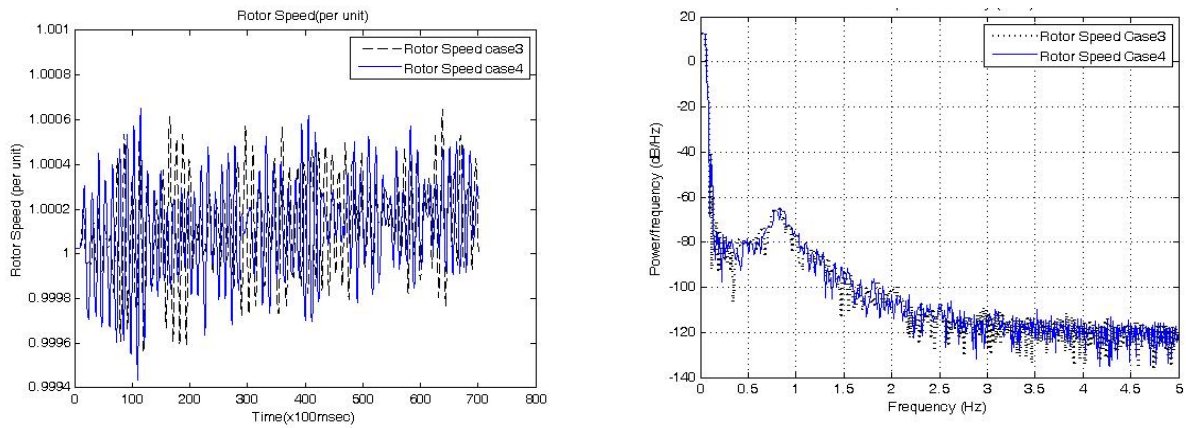


Figure 5.100 The rotor speed of synchronous generator of Case B6 (case 3) compare with Case B7 (case 4, left) and its PSD of Case B6 compared with Case B7 (right)

The simulation results of power angle and its PSD are represented in Figure 5.99. The power angle decreases with time and oscillatory fluctuates within a small range of 22.2 - 23.7 degrees. In Figure 5.99 (right), PSD is almost the same for both cases. The small difference occurs at frequency about 0.3Hz, and 4.75Hz which Case 4 has more influence. Therefore, the power angle in this simulation is not sensitive for different frequency base noise amplitude.

The rotor speed and its PSD from simulation results are represented in Figure 5.100. The rotor speed increase with time and oscillatory fluctuate in extremely small range of 0.9994 -1.0006 per unit. From Figure 5.100 (right), PSD is the same for both cases. There is no significant different between these two cases. Therefore, the power angle in this simulation is not sensitive for different frequency base noise amplitude.

The standard deviation of fluctuating wind power has influence on power angle and rotor speed of synchronous generator more than frequency base noise amplitude. Fluctuating wind power cause power angle decrease, but increases rotor speed. For this case, power generation of synchronous generator is shared partially by wind power, therefore, its power angle reduce. An increasing of rotor speed is due to unbalance between mechanical torque and electrical torque.

It is obvious that the deviation of wind power fluctuation has more influence to synchronous generator than frequency of fluctuation. However, for rotor speed, only frequency lower than 2.5Hz that deviation of wind power is significant.

For the future studies in the effects of wind power on the power system, the results of the simulation should in agree with the measurement data. Many assumptions in mathematical modeling may stimulate high magnitude of error

Case B8 – Case B11 Effects of ramp wind speed with different frequency

For cases B8 – B11, noise wind speed model is replaced by ramp wind speed model to represent an influence of frequency of small signal on the power system parameters. The four cases have ramp wind speed with amplitude 1 m/s and ramp frequency 0.5, 0.75, 1.0, and 4.0 Hz for case B8 to B11, respectively. There are five variables which are compared: wind speed, active and reactive power of wind turbine, power load angle of synchronous generator, and rotor speed of synchronous generator.

In Figure 5.101, the ramp wind speed is applied after the 30th second with the same magnitude. The mean wind speed is 10 m/s for all cases.

In Figure 5.102, active and reactive powers of wind turbine are represented. The fluctuating signal or noise over the mean value is look different from the ramp wind speed. For the case 4 Hz of ramp frequency, active and reactive powers almost never see the noise.

However, the mean values of active and reactive powers are the same for all cases.

Wind speed

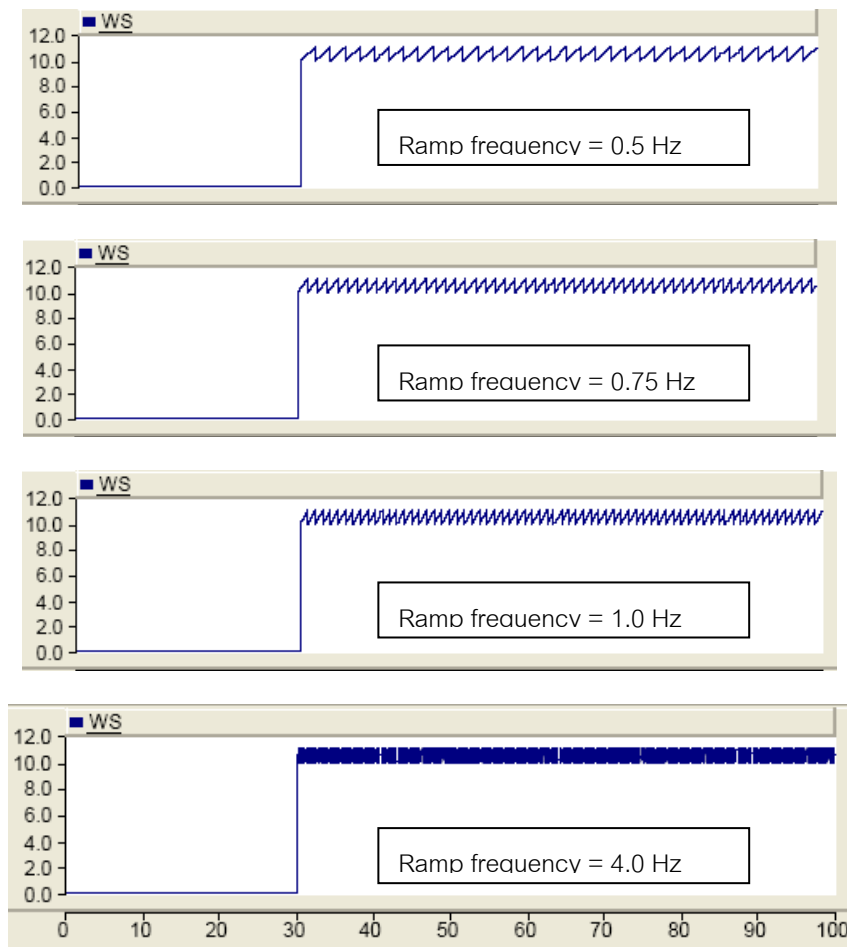


Figure 5.101 Wind speed (m/s) of the cases B8 – B11

Active and reactive power of wind turbine

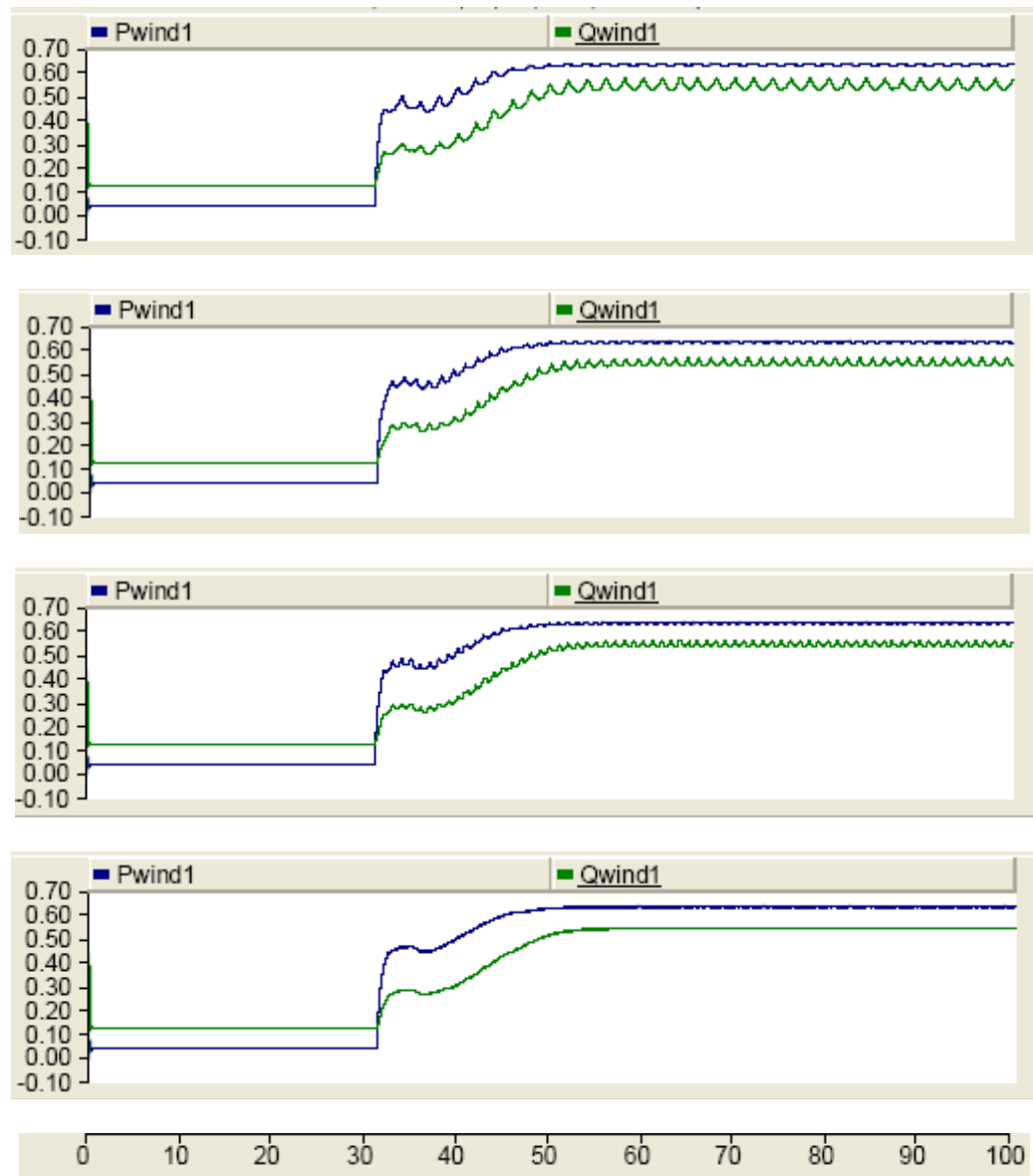


Figure 5.102 Wind power (per unit) of the cases B8 – B11

Power angle of synchronous generator

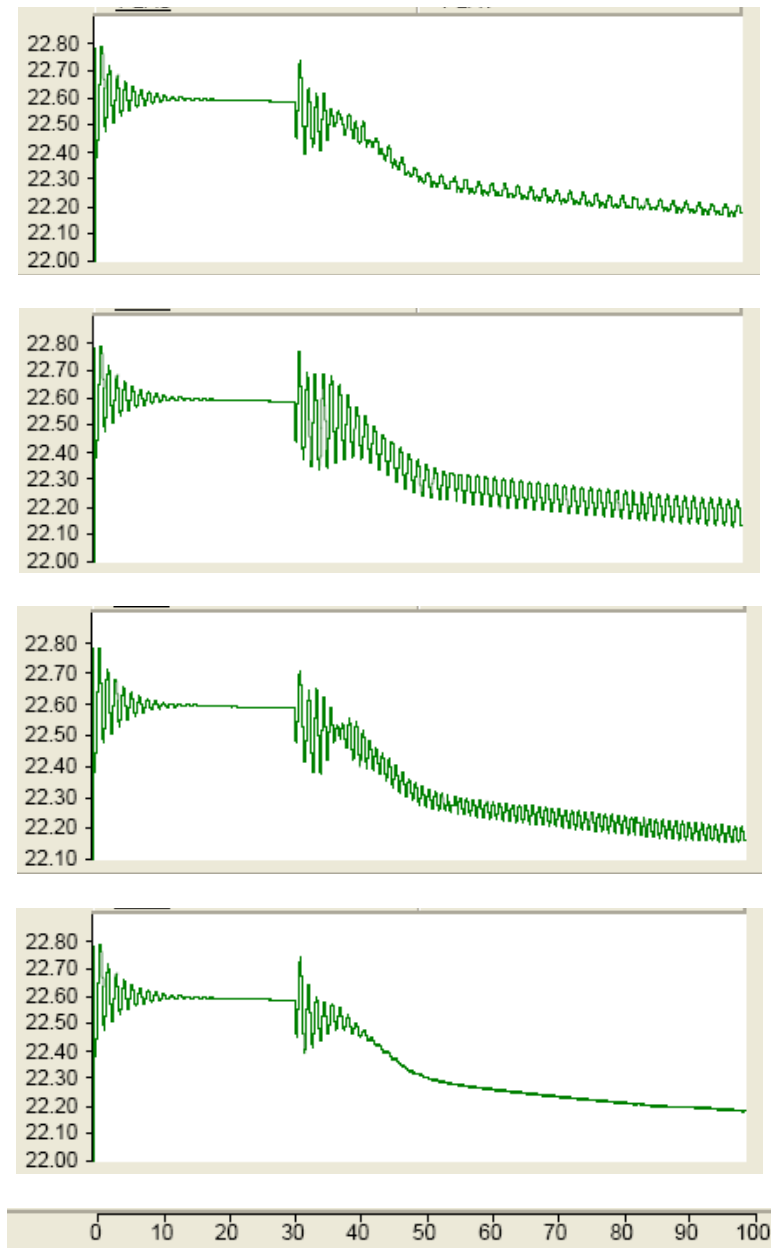


Figure 5.103 Power angle (degrees) of synchronous generator of the cases B8 – B11

In Figure 5.103, it can be noticed that the largest amplitude of oscillation occurs at the ramp frequency of 0.75 Hz. It can be concluded that around 0.75Hz is the natural frequency of the test system, because the largest response occurs at this frequency. The resonance phenomena will occur when wind power fluctuate with the same frequency as the natural frequency of the system represented by the state variables.

Rotor speed of synchronous generator

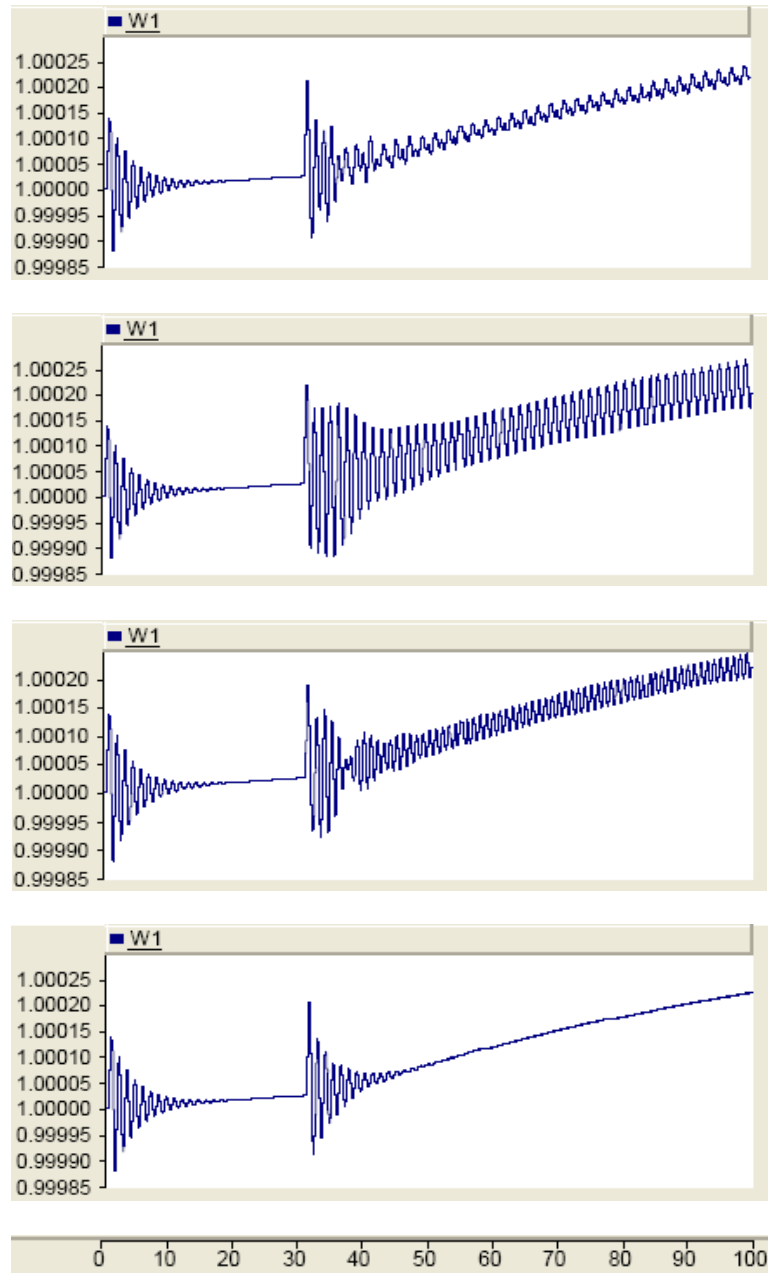


Figure 5.104 Rotor speed (per unit) of synchronous generator of the cases B8 – B11

In Figure 5.104, this result agrees with the power angle case in Figure 5.103. In terms of power system stability, if wind power has large share of this natural frequency components, the power system is possibly become unstable within a finite time. From the results of cases B4 – B7, the 0.75Hz frequency components of wind power are very small as

compared with its mean part. However, it has been found that PSD increases with increasing standard deviation of wind power. Therefore, understanding the characteristics of wind power is an important issue for the power system to incorporate large scales of intermittent power sources, such as wind power.

5.2.4 Characteristics of energy and critical energy of the power system

When applying approximated unstable equilibrium points (i.u.e.p.) using the method of Ribbens, the result of the energy values are represented in the next table.

Table 5.5 Energy of the test system at interested unstable equilibrium points

Case1	Energy at i.u.e.p.
$\mathbf{x} = \{\pi - x_1^s, x_2^s, x_3^s, x_4^s, x_5^s\}$	2.3500
$\mathbf{x} = \{x_1^s, \pi - x_2^s, x_3^s, x_4^s, x_5^s\}$	20.8935
$\mathbf{x} = \{x_1^s, x_2^s, \pi - x_3^s, x_4^s, x_5^s\}$	8.9975
$\mathbf{x} = \{x_1^s, x_2^s, x_3^s, \pi - x_4^s, x_5^s\}$	129.6840
$\mathbf{x} = \{x_1^s, x_2^s, x_3^s, x_4^s, \pi - x_5^s\}$	157.7753
Case2	
$\mathbf{x} = \{-\pi - x_1^s, x_2^s, x_3^s, x_4^s, x_5^s\}$	61.4748
$\mathbf{x} = \{x_1^s, -\pi - x_2^s, x_3^s, x_4^s, x_5^s\}$	24.1985
$\mathbf{x} = \{x_1^s, x_2^s, -\pi - x_3^s, x_4^s, x_5^s\}$	15.9153
$\mathbf{x} = \{x_1^s, x_2^s, x_3^s, -\pi - x_4^s, x_5^s\}$	129.6840
$\mathbf{x} = \{x_1^s, x_2^s, x_3^s, x_4^s, -\pi - x_5^s\}$	89.7535
Case3	
$\mathbf{x} = \left\{ \begin{array}{l} \pi - x_1^s, \pi - x_2^s, \\ \pi - x_4^s, \pi - x_5^s \end{array} \right\}$	14.7185
Case4	
$\mathbf{x} = \left\{ \begin{array}{l} -\pi - x_1^s, -\pi - x_2^s, \\ -\pi - x_4^s, -\pi - x_5^s \end{array} \right\}$	16.0443

Therefore, the minimum energy value is 2.35, which will be approximated to be the critical energy of the unperturbed system. This result can be implied that loss of synchronization of generator at bus 1 (G1) cause more serious than the other machines. It can be noticed that G1 share most of load at about 86.9% while infinite bus generator (at bus 3) and wind power (at bus 2) share only 10.2% and 4.9%, respectively.

Since wind power is naturally inconsistent, fluctuations of wind power can lead the total energy of the system to vary. The critical energy also varies depending on level of small disturbance from wind power. The previous topic reveals characteristics of wind power when wind speed fluctuates with low and high frequency. In term of data distribution characteristics, the low frequency wind speed can be approximated by the Weibull frequency distribution. In the other hand, the high frequency wind speed can be

approximated by Gaussian normal distribution. Therefore, this topic will investigate the characteristics of total energy and critical energy of the system when incorporate wind power variations.

5.2.4.1 Initial relative energy of the power system

The result of the base case is shown in Figures 5.105 and 5.106. In Figure 5.105, the total energy is close to zero when the system reaches steady state or stable equilibrium state. It is obvious that the system is larger than zero at the beginning and then reduces to be zero after a specific time. In Figure 5.106, the derivative of the total energy at the stable equilibrium state is very much close to zero. These two figures confirm an existence of the energy function, which is used in this study. The critical energy is shown in a previous table.

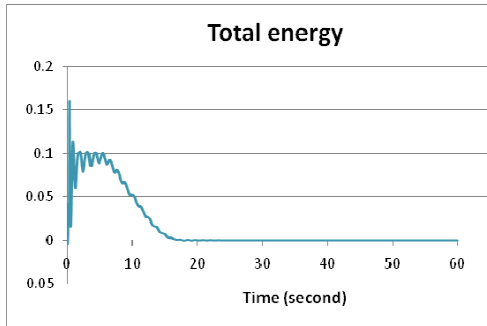


Figure 5.105 Total energy of the test system

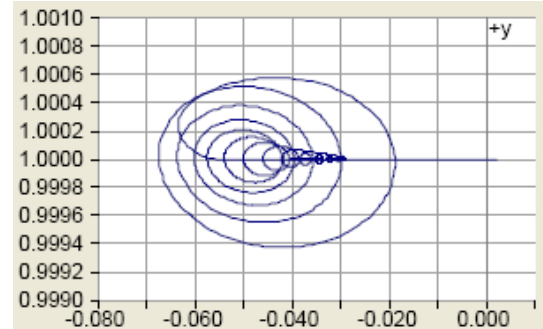


Figure 5.106 Phase portrait plot of voltage phase angle (x-axis) and rotor speed (y-axis)

5.2.4.2 The energy of the power system when varying wind speed

When wind speed varies between 6 m/s, 8 m/s, and 12 m/s, the stable equilibrium points can be presented in Table 5.6. Shares of power of each machine to the load are shown in Table 5.7.

In Table 5.7, when wind speed increases, shares of G1 have a small change, while share of infinite bus generator (at bus 3) decrease and wind power (at bus 2) increase. It can be implied that, wind power has significant impact on external infinite bus more influence than a nearby generator.

Table 5.6 Variables at stable equilibrium point of the test system with different wind speeds

Case wind speed 6 m/s			
V1 = 0.998 p.u.	x1= 0.330 rad	P _{e1} = 9.410 p.u.,	Q _{e1} = -1.416 p.u.
V2 = 1.000 p.u.	x2= -0.454 rad	P _{e2} = 0.002 p.u.,	Q _{e2} = -0.100 p.u.
V3 = 1.002 p.u.	x3= 0.000 rad	P _{e3} = 1.606 p.u.,	Q _{e3} = -4.200 p.u.
V4 = 1.011 p.u.	x4= -0.073 rad	P _{e4} = 0 p.u. ,	Q _{e4} = 0 p.u.
V5 = 0.992 p.u.	x5= -0.455 rad	P _{e5} = 10.786 p.u.	Q _{e5} = 0 p.u.
Case wind speed 8 m/s			
V1 = 0.998 p.u.	x1= 0.340 rad	P _{e1} = 9.410 p.u.,	Q _{e1} = -1.539 p.u.
V2 = 0.996 p.u.	x2= -0.375 rad	P _{e2} = 0.219 p.u.,	Q _{e2} = -0.134 p.u.
V3 = 1.002 p.u.	x3= 0.000 rad	P _{e3} = 1.436 p.u.,	Q _{e3} = -4.216 p.u.
V4 = 1.012 p.u.	x4= -0.066 rad	P _{e4} = 0 p.u. ,	Q _{e4} = 0 p.u.
V5 = 0.995 p.u.	x5= -0.440 rad	P _{e5} = 10.841 p.u.	Q _{e5} = 0 p.u.
Case wind speed 12 m/s			
V1 = 1.001 p.u.	x1= 0.366 rad	P _{e1} = 9.410 p.u.,	Q _{e1} = -1.635 p.u.
V2 = 0.939 p.u.	x2= -0.194 rad	P _{e2} = 0.674 p.u.,	Q _{e2} = -0.385 p.u.
V3 = 1.005 p.u.	x3= 0.000 rad	P _{e3} = 0.866 p.u.,	Q _{e3} = -4.209 p.u.
V4 = 1.015 p.u.	x4= -0.063 rad	P _{e4} = 0 p.u. ,	Q _{e4} = 0 p.u.
V5 = 0.988 p.u.	x5= -0.418 rad	P _{e5} = 10.747 p.u.	Q _{e5} = 0 p.u.

Table 5.7 Shares of generating power from synchronous generator, infinite bus generator, and wind turbine generator at different wind speeds

Gen. to load share	Generator 1	infinite bus generator	wind power
Case1 WS = 6 m/s	87.2%	14.9%	0.0%
Case2 WS = 8 m/s	86.8%	13.2%	2.0%
Case3 WS = 10 m/s	86.9%	10.2%	4.9%
Case4 WS = 12 m/s	87.6%	8.1%	6.3%

The total energy of the test system at interested unstable equilibrium points with different wind speeds are shown in Table 5.8. From this table, the critical energy can be estimated using the minimum value for each case of wind speed. As a result, the critical energy increases with increasing mean wind speed. When wind speed increase, the wind power can share more load from the other generator and make the system more stable. For wind speed 6 m/s and 8 m/s, total energy and its derivative are almost the same with 5.2.4.1.

Table 5.8 The critical values at different wind speeds

Unstable condition 1	Energy (WS6m/s)	Energy (WS8m/s)	Energy (WS10m/s)	Energy (WS12m/s)
$\mathbf{x} = \{\pi - x_1^s, x_2^s, x_3^s, x_4^s, x_5^s\}$	2.0361	2.1734	2.3500	2.5761
$\mathbf{x} = \{x_1^s, \pi - x_2^s, x_3^s, x_4^s, x_5^s\}$	21.3480	21.3974	20.8935	19.8076
$\mathbf{x} = \{x_1^s, x_2^s, \pi - x_3^s, x_4^s, x_5^s\}$	7.3817	7.9341	8.9975	9.8015
$\mathbf{x} = \{x_1^s, x_2^s, x_3^s, \pi - x_4^s, x_5^s\}$	127.6626	128.6871	129.6840	129.2386
$\mathbf{x} = \{x_1^s, x_2^s, x_3^s, x_4^s, \pi - x_5^s\}$	154.9043	156.7525	157.7753	156.3999
Unstable condition 2				
$\mathbf{x} = \{-\pi - x_1^s, x_2^s, x_3^s, x_4^s, x_5^s\}$	61.1608	61.2982	61.4748	61.7009
$\mathbf{x} = \{x_1^s, -\pi - x_2^s, x_3^s, x_4^s, x_5^s\}$	21.3605	22.7734	24.1985	24.0425
$\mathbf{x} = \{x_1^s, x_2^s, -\pi - x_3^s, x_4^s, x_5^s\}$	17.4725	16.9568	15.9153	15.2427
$\mathbf{x} = \{x_1^s, x_2^s, x_3^s, -\pi - x_4^s, x_5^s\}$	127.6626	128.6871	129.6840	129.2386
$\mathbf{x} = \{x_1^s, x_2^s, x_3^s, x_4^s, -\pi - x_5^s\}$	87.1339	88.6365	89.7535	88.8745
Unstable condition 3				
$\mathbf{x} = \left\{ \begin{matrix} \pi - x_1^s, \pi - x_2^s \\ \pi - x_4^s, \pi - x_5^s \end{matrix} \right\}$	15.2953	15.0710	14.7185	14.9734
Unstable condition 4				
$\mathbf{x} = \left\{ \begin{matrix} -\pi - x_1^s, -\pi - x_2^s \\ -\pi - x_4^s, -\pi - x_5^s \end{matrix} \right\}$	16.7530	16.4784	16.0443	16.2489

5.2.4.3 The energy of the power system when varying noise wind speed

Since wind speed consists of mean part (slow variation) and turbulence part (fast variation), the wind noise model is simulated to represent turbulence. Theoretically, turbulence or noise wind speed can be approximated using Gaussian distribution random noise. Two important parameters which will be varied are the standard deviation of noise and the sampling frequency of noise.

An experiment assumes that mean part of wind speed is 10 m/s. This value is suitable for wind power in the model to be varied without limit. The noise wind speed is modeled using inverse probability distribution function method. The two conditions are examined. First, the standard deviation 0.5, 1.0, and 2.0 are applied with constant sampling frequency at 0.5Hz. Second, the sampling frequency is varied to be 0.1, 0.5, and 2 Hz with constant standard deviation at 1.0. For these two cases, the phase portrait of machine speed and voltage angle is investigated together with the total energy.

To compute the total energy of the system, the stable equilibrium points from the previous study at wind speed 10m/s are used. The figure below shows noise wind speed model in PSCAD.

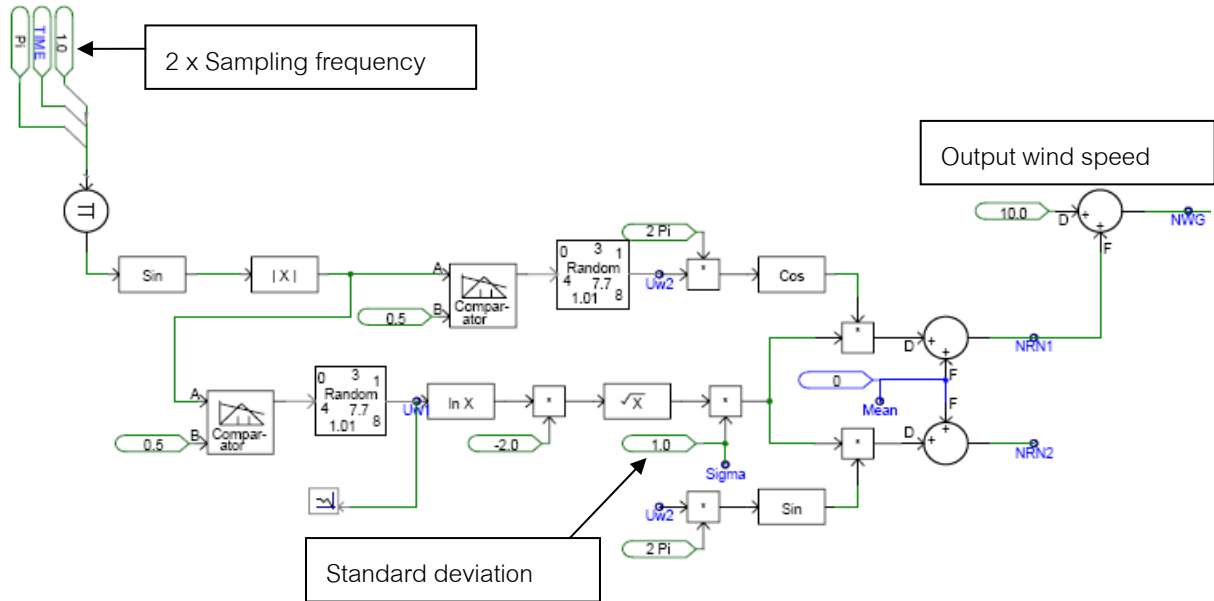


Figure 5.107 Block diagrams of wind speed model, including normal random noise wind speed

1) Varying standard deviation

The results of the standard deviations of wind speed of 0.5, 1.0, 2.0 are represented in Figures 5.108, 5.109, and 5.110, respectively. In Figure 5.108, after 20th second, the total energy fluctuate varies around zero. The maximum energy is less than 0.1 after 20th second. Rotor speed and voltage phase angle vary within a particular region, which is called region of attraction. It can be concluded that this system is stable within the region of attraction whenever total energy is not beyond the critical value.

In Figure 5.109, fluctuations of wind speed and total energy are larger than the case in Figure 5.108. The region of attraction is also larger than the case in Figure 5.108 due to the larger standard deviation of wind speed.

In Figure 5.110, it can be noticed that after about the 48th second, total energy increase continuously. The phase portrait of wind turbine show the state variable goes out of the region of attraction. The wind turbine is unstable for this situation. However, since total energy is still less than the critical energy, the system still stable and can operate normally.

If we extend the value of total energy, it will found that the maximum of total energy in this case is about 2 – 3. Therefore, since the critical energy for this case is about 20.89, the system is still far from an unstable situation.

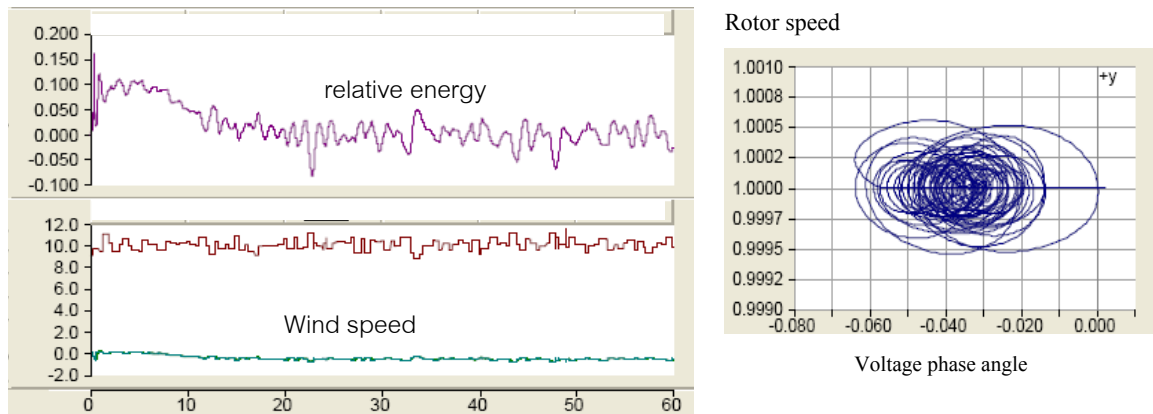


Figure 5.108 Total energy (upper left), wind speed (lower left), and phase portrait plot (right) of synchronous generator when the standard deviation of wind speed is 0.5

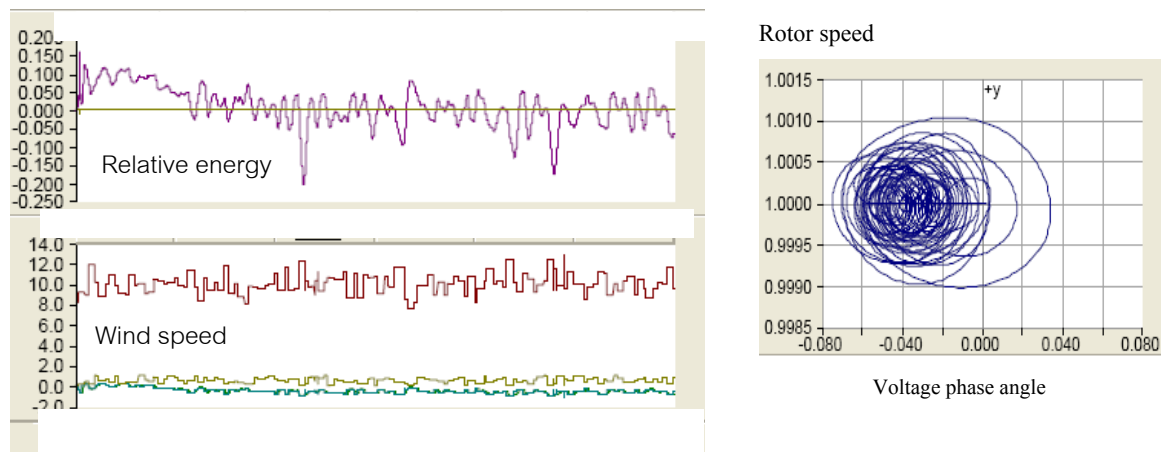


Figure 5.109 Total energy (upper left), wind speed (lower left), and phase portrait plot (right) of synchronous generator when standard deviation of wind speed is 1.0

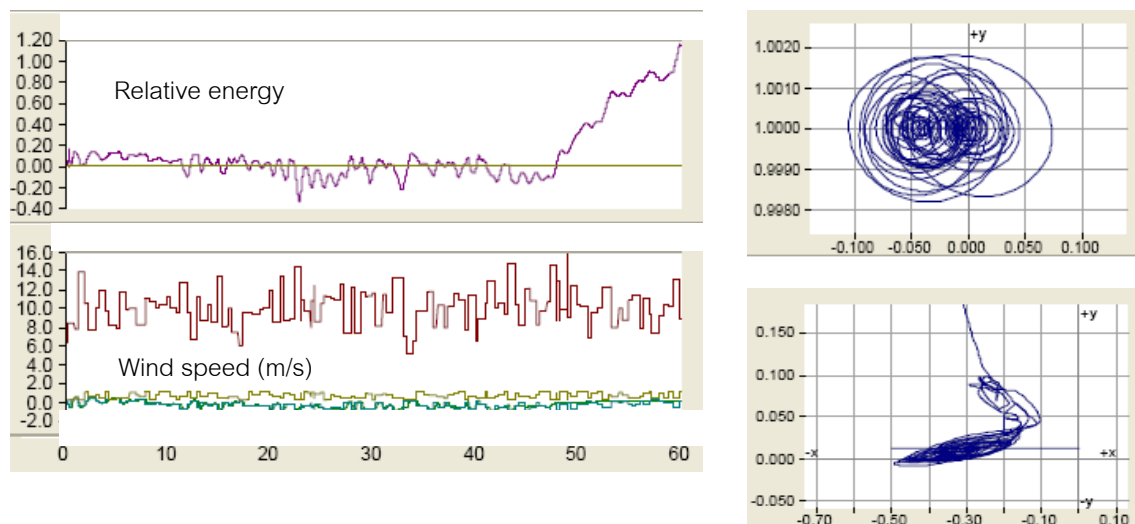


Figure 5.110 Total energy (upper left), wind speed (lower left), and phase portrait plot of synchronous generator (upper right) and phase portrait plot of wind turbine generator (lower right) when standard deviation of wind speed is 2.0

2) Vary sampling frequency

The sampling frequency of noise wind speed is the measure of how frequently the signal changes. This experiment assumes that noise wind speed change (with the same standard deviation of 1.0) every 2 seconds (0.5Hz), 0.5 second (2Hz), and 10 seconds (0.1Hz) which are presented in Figures 5.111, 5.112, and 5.113, respectively.

In Figure 5.111, the 2 seconds cycle of noise wind speed result in variation of total energy not beyond ± 0.2 and the system still stable. In Figure 5.112, when frequency increases, the total energy varies not beyond ± 0.15 which is smaller than the previous case.

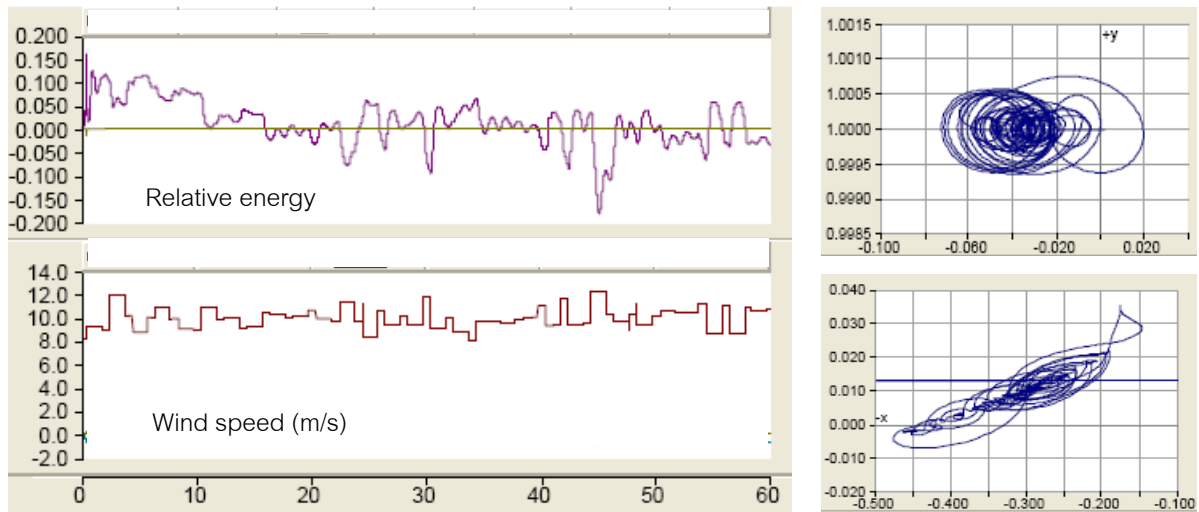


Figure 5.111 Total energy (upper left), wind speed (lower left), and phase portrait plot of synchronous generator (upper right) and phase portrait plot of wind turbine generator (lower right) when sampling frequency of wind speed is 0.5Hz

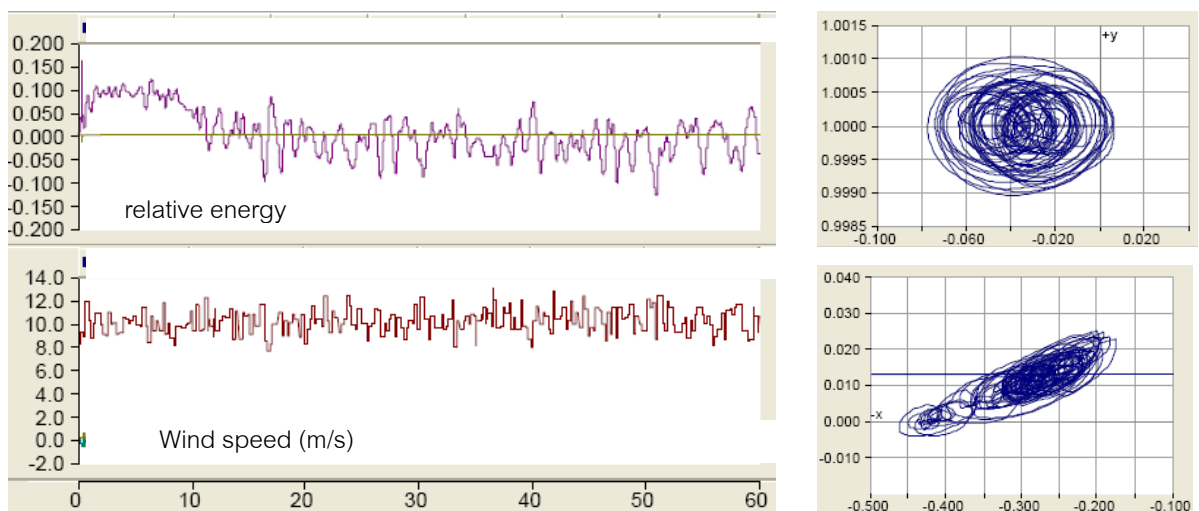


Figure 5.112 Total energy (upper left), wind speed (lower left), and phase portrait plot of synchronous generator (upper right) and phase portrait plot of wind turbine generator (lower right) when sampling frequency of wind speed is 2.0 Hz

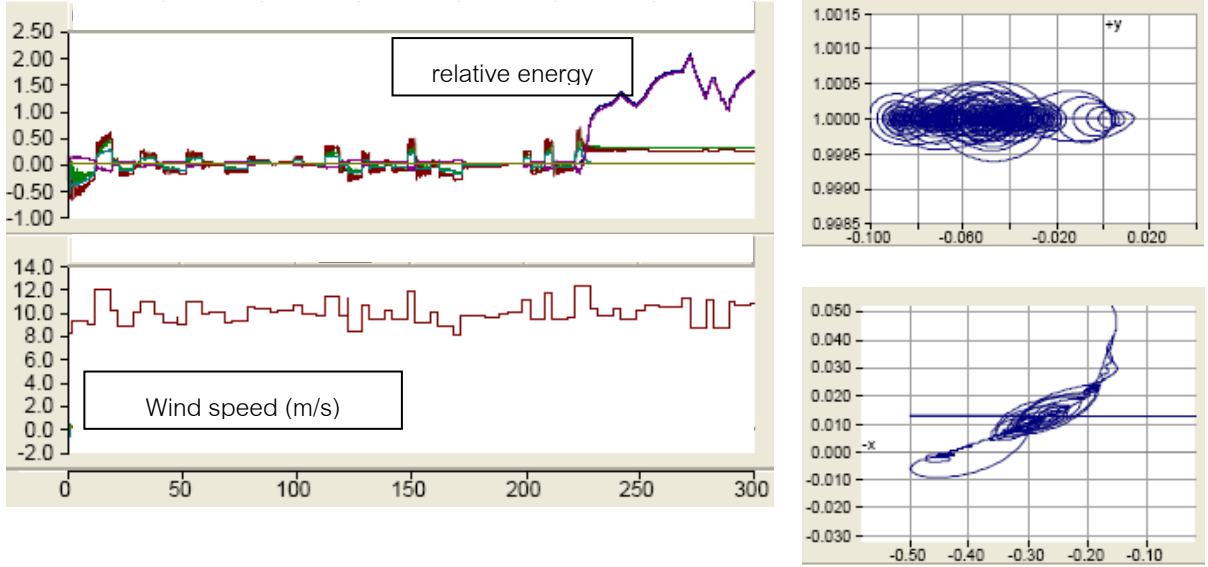


Figure 5.113 Total energy (upper left), wind speed (lower left), and phase portrait plot of synchronous generator (upper right) and phase portrait plot of wind turbine generator (lower right) when sampling frequency of wind speed is 0.1 Hz

In Figure 5.113, when sampling frequency of noise wind speed is very low, the system becomes unstable after about 230 seconds. The rotor speed of wind turbine increase continuously and go out of the region of attraction.

In conclusion, the stability of wind turbine generator is influenced by the standard deviation and sampling frequency of noise wind speed or turbulence. Larger standard deviations and lower sampling frequencies cause the state variables of wind turbine to go out of the region of attraction and become unstable. However, in this experiment, the system is robust enough to withstand such disturbances when wind power is lost from the system.

5.2.5 The stochastic power system simulation

When applying the colored noise wind power into the power test system, the system equations will become the dynamic perturbed system in a matrix form as follows:

$$\frac{d}{dt} \begin{bmatrix} x_i \\ x_w \\ x_k \\ y_i \\ y_w \\ v_w \\ v_k \end{bmatrix} = \begin{bmatrix} \omega_0 (y_i - y_0) \\ \omega_0 (y_w - y_0) + \varphi_{df}(\mathbf{V}, \mathbf{x}) \\ \varphi_k(\mathbf{V}, \mathbf{x}) + \bar{P}_{lk} \alpha_k v_k / c_k \\ \varphi_i(\mathbf{V}, \mathbf{x}) - \beta_i y_i \\ \varphi_w(\mathbf{V}, \mathbf{x}) + P_{mw} \alpha_w v_w / M_w \\ -\psi_w v_w \\ -\psi_k v_k \end{bmatrix} + \begin{bmatrix} 0 \\ 0 \\ 0 \\ 0 \\ 0 \\ \gamma_w \varepsilon_w \\ \gamma_k \varepsilon_k \end{bmatrix} \frac{dW}{dt} \quad \text{Eq.5-4}$$

$$\left. \begin{aligned} \varphi_{df}(\mathbf{V}, \mathbf{x}) &= \omega_0 k_d \bar{V}_{rq} - k_b \bar{V}_{s3} \sin(k_a (x_w - x_{ref}) + c_a) \\ \varphi_k(\mathbf{V}, \mathbf{x}) &= -\frac{1}{c_k} (\bar{P}_{lk} + \bar{P}_{ek}) - \omega_0 \gamma_0 \\ \varphi_i(\mathbf{V}, \mathbf{x}) &= \frac{1}{M_i} (\bar{P}_{mi} - \bar{P}_{ei}) \\ \varphi_w(\mathbf{V}, \mathbf{x}) &= \frac{1}{M_w} (\bar{P}_{mw} - \bar{P}_{ew}) \end{aligned} \right\} \quad \text{Eq.5-5}$$

where $\beta_i = D_i/M_i$. It can be represented in the standard stochastic differential equation as

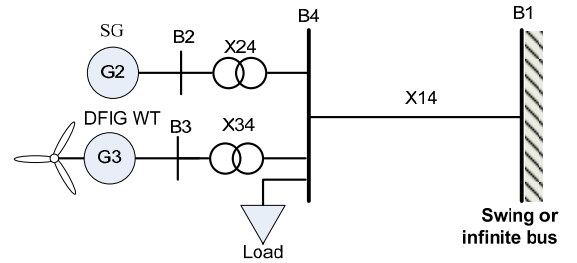
$$p\mathbf{X} = \mathbf{f}(\mathbf{X}, t) + \mathbf{g}(\mathbf{X}, t) pW, \quad \mathbf{x}(t_0) = \mathbf{x}_0, \quad t \geq t_0 \quad \text{Eq.5-6}$$

where $\mathbf{f}(\mathbf{X}, t)$ is a nonlinear drift function, $\mathbf{g}(\mathbf{X}, t)$ is a diffusion function in matrix form.

From the one line diagram in the below figure, there are aggregated synchronous generators (G2) and aggregated DFIG wind turbines (G3), connecting on bus B2 and B3, respectively. Bus B1 is an infinite bus and B4 is a load bus. The per unit base power is 100 MVA. The system is assumed lossless which the line resistance can be neglected. X_{14} is a line reactance (tie line) connecting between bus B1 and B4. X_{24} and X_{34} are line reactances including transformer's reactance. The electric load is a dynamic load which has c_k at about 0.05. The other values of system parameters and constants are listed in Table 5.9.

Table 5.9 System Parameters and Constants

$M = 7.0$ sec	$\omega_0 = 314.2$ rad/sec	$L_m = 3.95279$ p.u.
$L_r = 0.09955$ p.u.	$L_s = 0.09241$ p.u.	$T_0 = 2.343$ p.u.
$X = 4.0$ p.u.	$X' = 0.1$ p.u.	$X_T = 0.5$ p.u.
$k_d = 0.8868$	$k_b = 7.372$	$k_a = 0.274 P_m + 0.346$
$k_p = 1.0$	$k_{op} = 0.56$	$c_a = -0.022 P_m + 0.006$
$ E' = V_w = 1.05$ p.u.	$k_{c1} = 0.97396$	$k_{c2} = 1.90308$
$V_s = 1.0$ (p.u.)	$V_0 = 1.0$ (p.u.)	$k_m = 1.017$
$X_{14} = 0.75$ p.u.	$X_{24} = 0.2$ p.u.	$X_{34} = 0.2$ p.u.



When applying noise intensity 0.1, bandwidth 1.0, scaling factor 1.0, mean wind power 1.0, power load 4.0, power of G2 1.78 p.u., the simulation period is 60 seconds and 4 trials, the results of simulation are represented in Figures 5.114 - 5.117 .

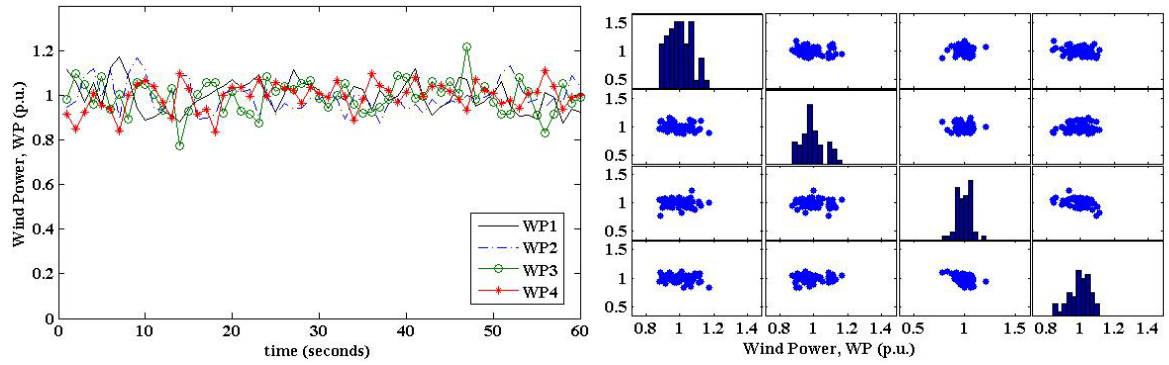


Figure 5.114 Wind power variation (left) and its distribution (right) of 4 trials of simulation

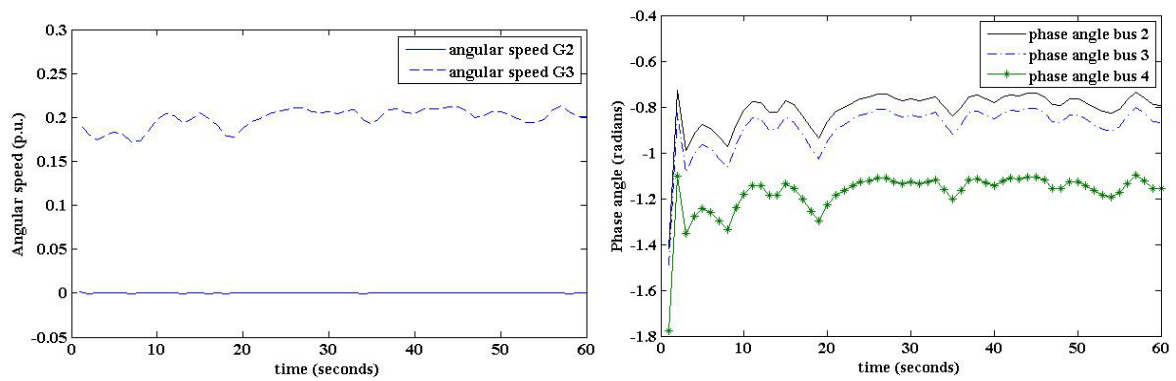


Figure 5.115 Angular speed (left) of generator no.1-2 and phase angle (right) of bus no. 2-4 of stochastic system simulation during 60 seconds of trial no.1.

After 3600 seconds of simulation period for 10 trials, the first exit-times are 500, 3542, 2589, 11, 2910, and 452 seconds. The mean first passage (or exit) time is 1544.5 seconds.

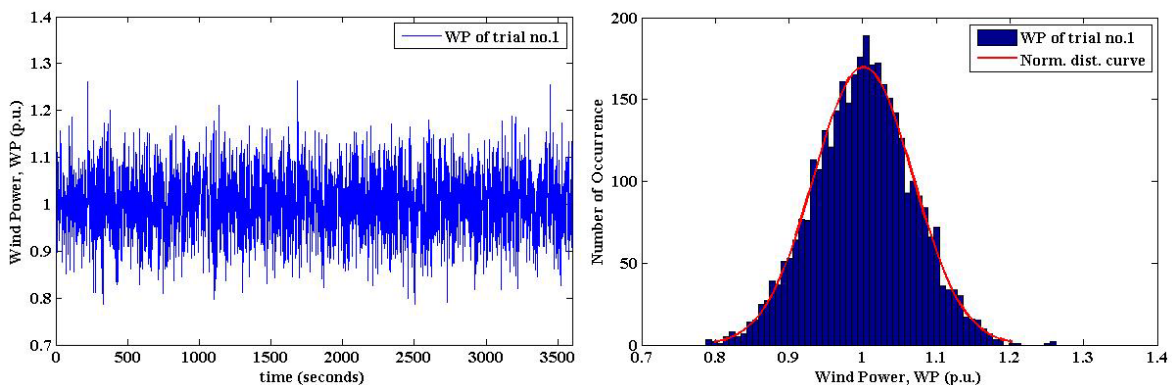


Figure 5.116 Example of wind power variation during 3600 seconds (left) and its distribution (right) of simulation trial no.1

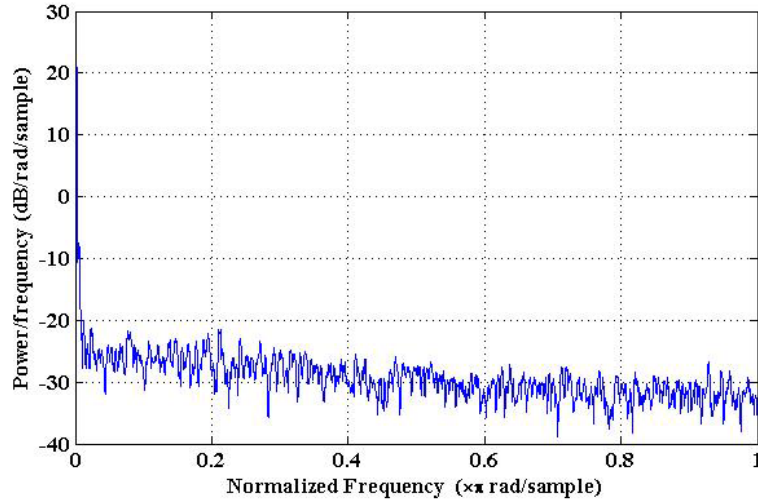


Figure 5.117 Power spectral density of wind power variation during 3600 seconds of trial no.1

5.3 A study of effects of wind power on the small signal stability using the eigenvalue method

5.3.1 Eigenvalues of single machine power system

5.3.1.1 Wind turbine with squirrel cage induction generator (SCIG)

To analyze the small signal stability of induction generator wind turbine, the state space equation will be represented in a new form as follows:

$$\begin{bmatrix} \Delta \dot{x}_w \\ \Delta \dot{y}_w \end{bmatrix} = \begin{bmatrix} -K_E & \omega_0 \\ -K_S/M & -K_D/M \end{bmatrix} \begin{bmatrix} \Delta x_w \\ \Delta y_w \end{bmatrix} + \begin{bmatrix} 0 \\ 1/M \end{bmatrix} \Delta \bar{P}_{mw} \quad \text{Eq.5-7}$$

Where $K_S = \frac{\partial \bar{P}_e}{\partial x}$ is synchronizing power coefficient, and $K_D = \frac{\partial \bar{P}_e}{\partial y}$ is damping power coefficient of induction generator.

$$K_S = \frac{\partial \bar{P}_e}{\partial x_w} = \bar{V}_w \sum_{j=1, j \neq w}^n \bar{V}_j \bar{B}_{wj} \cos(x_w^s - x_j^s) \quad \text{and} \quad K_D = \frac{\partial \bar{P}_e}{\partial y} = 0 \quad \text{Eq.5-8}$$

$$K_E = k_b \bar{V}_{sw} k_a \cos(k_a x_w^s + c_a) \quad \text{Eq.5-9}$$

magnitude of damping power coefficient (K_D) and synchronizing power coefficient (K_S).

Eq.5-8 and Eq.5-9 can be represented using a block diagram as in following figure.

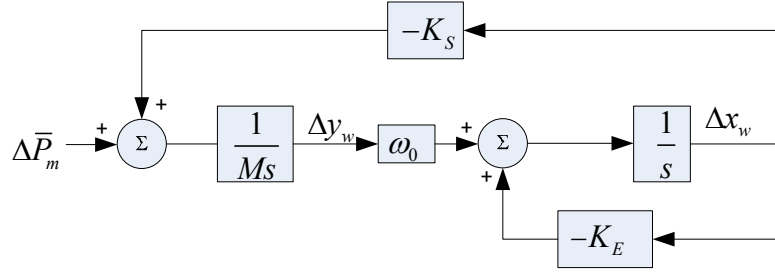


Figure 5.118 Block diagram representing state space equation of the SCIG wind turbine

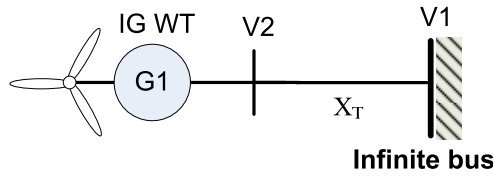


Figure 5.119 Single machine infinite bus (SMIB) power system

The induction machine parameters are as follows [45]. Given:

$$\begin{array}{llllll}
 M = 7.0 \text{ sec} & \omega_0 = 314.2 \text{ rad/sec} & L_m = 3.95279 \text{ p.u.} & L_r = 0.09955 \text{ p.u.} & L_s = 0.09241 \text{ p.u.} & \\
 X = 4.0 \text{ p.u.} & X' = 0.2 \text{ p.u.} & T_0 = 2.343 & |E'| = 1.05 \text{ p.u.} & = V_w & \eta_c = 0.95 \\
 k_d = 0.8868 & k_b = 7.372 & k_a = 0.61 & c_a = -0.05 & X_T = 0.5 \text{ p.u.} &
 \end{array}$$

$$K_S = \frac{1.05 \bar{V}_1}{(\bar{X}' + \bar{X}_T)} \cos(x_w^s) \quad \text{Eq.5-10}$$

$$K_E = 4.497 \bar{V}_{sw} \cos(0.61 x_w^s - 0.05) \quad \text{Eq.5-11}$$

Table 5.10 The testing conditions of SCIG wind turbine for SMIB power system

Parameters Variables	Case 1 Base case	Case 2 Reduce V_s	Case 3 Increase V_0	Case 4 Increase X_T	Case 5 Increase x_w
V_s (p.u.)	1.00	0.50	1.00	1.00	1.00
V_0 (p.u.)	1.0	1.0	0.5	1.0	1.0
$ X_T $ (p.u.)	0.75	0.75	0.75	1.5	0.75
x_w^s (rad)	0.5	0.5	0.5	0.5	1
K_S	0.970	0.970	0.485	0.542	0.597
K_E	4.352	2.176	4.352	4.352	3.810

In this table, when wind speed increase, speed deviation, power output, current and power factor increase, but voltage decreases. These results agree with the torque-slip, voltage-slip, and reactive power-slip characteristics of the induction generator [45].

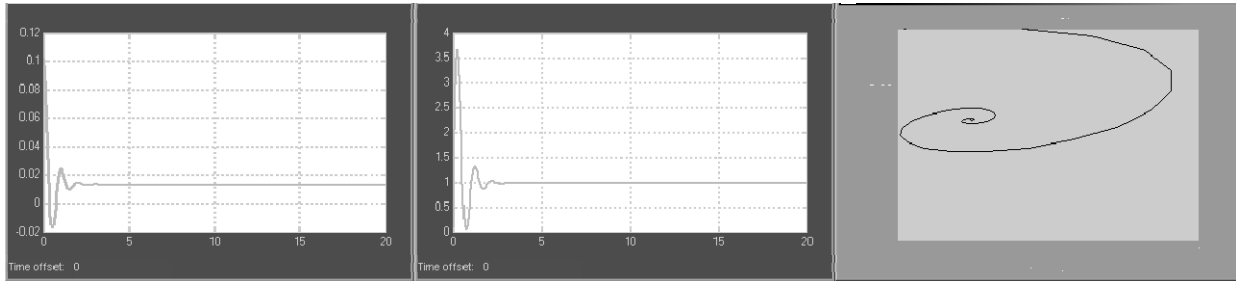


Figure 5.120 Results of simulation case 1. (base case) : Speed (left), angle (middle), and phase protrait of speed (y-axis) and angle (x-axis).

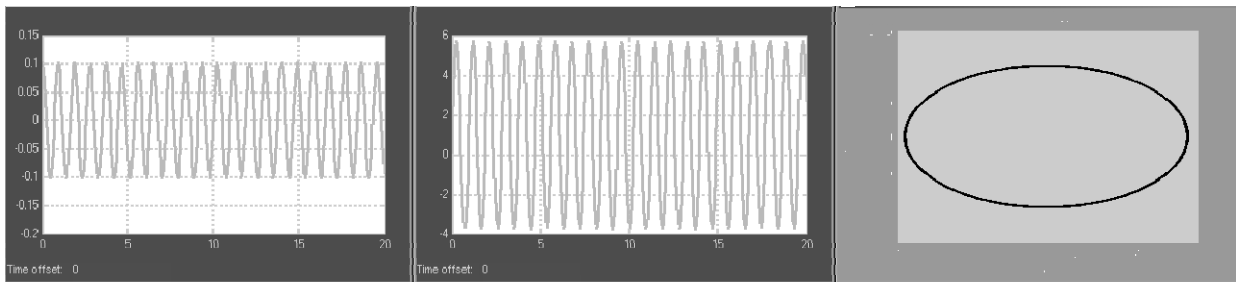


Figure 5.121 Results of simulation case 2. (reduce stator voltage of SCIG) : Speed (left), angle (middle), and phase protrait of speed (y-axis) and angle (x-axis).

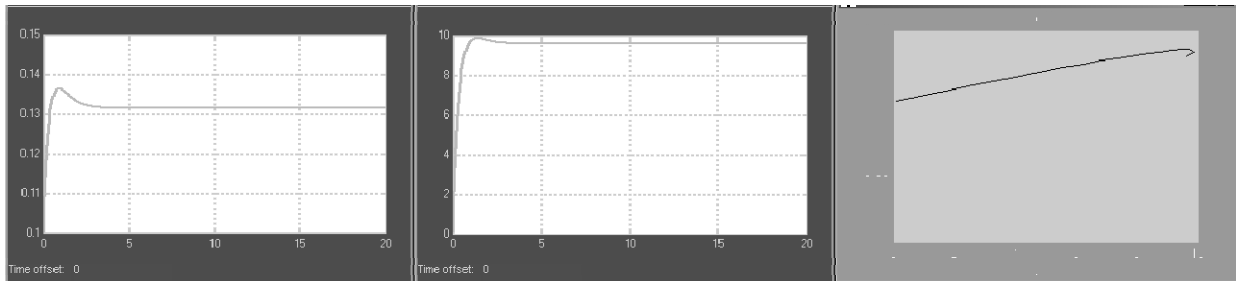


Figure 5.122 Results of simulation case 3. (increase reference voltage) : Speed (left), angle (middle), and phase protrait of speed (y-axis) and angle (x-axis).

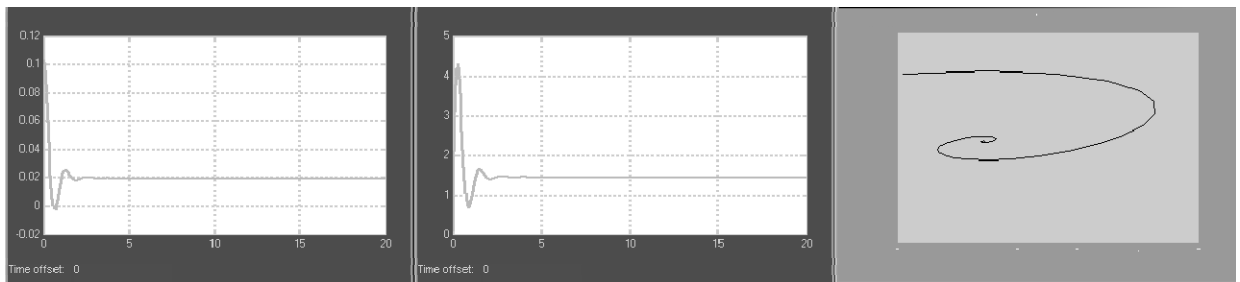


Figure 5.123 Results of simulation case 4. (increase transmission reactance) : Speed (left), angle (middle), and phase protrait of speed (y-axis) and angle (x-axis).

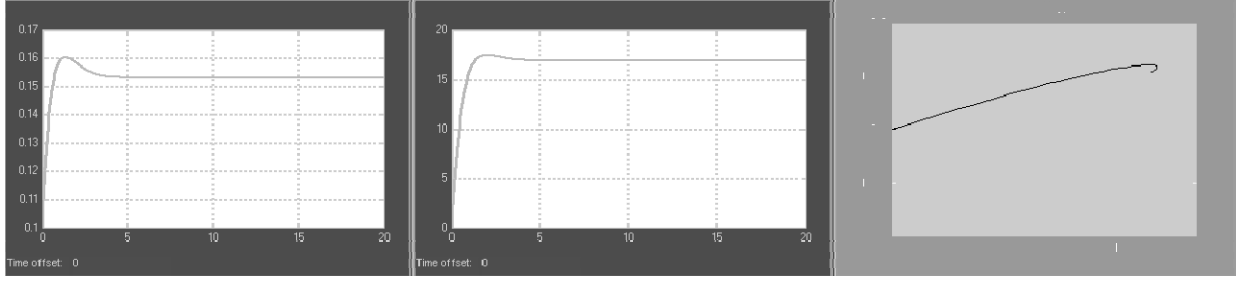


Figure 5.124 Results of simulation case 5. (increase stator reactance of SCIG) : Speed (left), angle (middle), and phase protrait of speed (y-axis) and angle (x-axis).

Table 5.11 The results of eigenvalue analysis of SCIG wind turbine

Parameters Variables	Case 1 Base case	Case 2 Reduce V_s	Case 3 Increase V_0	Case 4 Increase X_T	Case 5 Increase x_w
K_S	0.970	0.970	0.485	0.542	0.597
K_E	4.352	2.176	4.352	4.352	3.810
ω_n (rad/s)	6.598	6.598	4.666	4.933	5.177
ζ	0.330	0.165	0.466	0.441	0.368
σ	-2.18	-1.09	-2.18	-2.18	-1.91
ω (rad/s)	6.23	6.51	4.13	4.43	4.81
s	$-2.18 \pm j6.23$	$-1.09 \pm j6.51$	$-2.18 \pm j4.13$	$-2.18 \pm j4.43$	$-1.91 \pm j4.81$
Natural freq.	1.05	1.05	0.74	0.79	0.82
Frequency (Hz)	0.99	1.04	0.66	0.70	0.77

5.3.1.2 Wind turbine with doubly-fed induction generator (DFIG)

To analyze the small signal stability of an induction generator wind turbine, the state space equation is represented in a new form as follows:

$$\begin{bmatrix} \Delta \dot{x}_w \\ \Delta \dot{y}_w \end{bmatrix} = \begin{bmatrix} K_{E1} & K_{E2} \\ -K_S/M & -K_D/M \end{bmatrix} \begin{bmatrix} \Delta x_w \\ \Delta y_w \end{bmatrix} + \begin{bmatrix} 0 \\ 1/M \end{bmatrix} \Delta \bar{P}_{mw} \quad \text{Eq.5-12}$$

Where K_S is the synchronizing power coefficient and K_D is the damping power coefficient of DFIG:

$$\begin{aligned} K_{E1} &= \omega_0 k_d \frac{\partial \bar{V}_{rq}}{\partial x_w} - k_b \bar{V}_{sw} k_a \cos(k_a x_w^s + c_a) \\ &= -\omega_0 k_d k_a y_w^s k_{c2} \bar{V}_{sw} \sin(k_a x_w^s + c_a) - k_b k_a \bar{V}_{sw} \cos(k_a x_w^s + c_a) \end{aligned} \quad \text{Eq.5-13}$$

$$K_{E2} = \omega_0 + \omega_0 k_d \left[(k_{c2} \bar{V}_{sw} \cos(k_a x_w^s + c_a) - k_{c1} \bar{V}_w) + 2k_{vrq} k_{op} \frac{(1 + y_w^s)}{\bar{V}_{sw}} \right] \quad \text{Eq.5-14}$$

$$K_S = \frac{\partial \bar{P}_{ew}}{\partial x_w} + \frac{\partial \bar{P}_{sw}}{\partial x_w} y_w^s = \bar{V}_w \sum_{j=1, j \neq w}^n \bar{V}_j \bar{B}_{wj} \cos(x_w^s - x_j^s) + \frac{\bar{V}_w \bar{V}_0}{(\bar{X}'_w + \bar{X}_T)} \cos(x_w^s) y_w^s \quad \text{Eq.5-15}$$

$$K_D = \bar{P}_{sw} = \frac{\bar{V}_w \bar{V}_0}{(\bar{X}'_w + \bar{X}_T)} \sin(x_w^s) \quad \text{Eq.5-16}$$

$$k_d = \bar{L}_m / (\bar{L}_{rr} \bar{V}_w) \text{ and } k_b = (\bar{X}_w - \bar{X}'_w) / (\bar{T}_0 \bar{X}'_w \bar{V}_w) \quad \text{Eq.5-17}$$

$$\bar{T}_0 = \frac{\bar{L}_{rr}}{\omega_0 \bar{r}_r} = \frac{\bar{L}_r + \bar{L}_m}{\omega_0 \bar{r}_r} \quad \text{Eq.5-18}$$

$$\bar{X} = \bar{\omega}_s \bar{L}_{ss} = \bar{\omega}_s (\bar{L}_s + \bar{L}_m) \quad \text{Eq.5-19}$$

$$\bar{X}' = \bar{\omega}_s \left(\bar{L}_{ss} - \frac{\bar{L}_m^2}{\bar{L}_{rr}} \right) \quad \text{Eq.5-20}$$

Eqs.5-21 – 5-24 can be represented using block diagrams as in following figure.

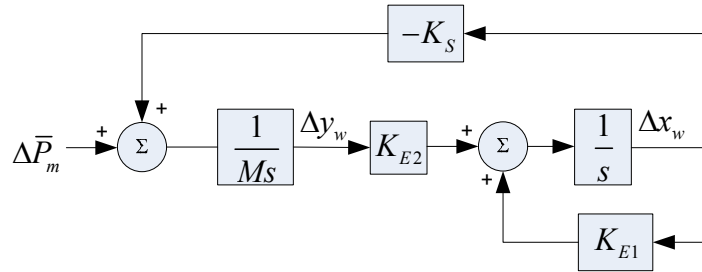


Figure 5.125 Block diagram representing state space equation of the DFIG wind turbine

The induction machine parameters for computation are as follows [45]

Given

$M = 7.0 \text{ sec}$	$\omega_0 = 314.2 \text{ rad/sec}$	$L_m = 3.95279 \text{ p.u.}$	$L_r = 0.09955 \text{ p.u.}$	$L_s = 0.09241 \text{ p.u.}$
$X = 4.0 \text{ p.u.}$	$X' = 0.2 \text{ p.u.}$	$T_0 = 2.343 \text{ p.u.}$	$ E' = V_w = 1.05 \text{ p.u.}$	$\eta_c = 0.95$
$k_d = 0.8868$	$k_b = 7.372$	$k_a = 0.61$	$c_a = -0.05$	$X_T = 0.5 \text{ p.u.}$
$k_{vrq} = 0.0056$	$k_{op} = 0.56$	$k_{c1} = 0.97396$	$k_{c2} = 1.90308$	

$$K_{E1} = \omega_0 k_d \left(\partial \bar{V}_{rq} / \partial x_w \right) - 4.49692 \bar{V}_{sw} \cos(0.61 x_w^s - 0.05) \quad \text{Eq.5-21}$$

$$K_{E2} = 42.82303 + 530.26 \bar{V}_{sw} \cos(0.61 x_w^s - 0.05) + 1.7476 \frac{(1 + y_w^s)}{\bar{V}_{sw}} \quad \text{Eq.5-22}$$

$$K_S = \frac{\bar{V}_w \bar{V}_0}{(\bar{X}'_w + \bar{X}_T)} \cos(x_w^s) + \frac{\bar{V}_w \bar{V}_0}{(\bar{X}'_w + \bar{X}_T)} \cos(x_w^s) y_w^s = \frac{\bar{V}_w \bar{V}_0}{(0.2 + \bar{X}_T)} \cos(x_w^s) (1 + y_w^s) \quad \text{Eq.5-23}$$

$$K_D = \frac{\bar{V}_w \bar{V}_0}{(0.2 + \bar{X}_T)} \sin(x_w^s) \quad \text{Eq.5-24}$$

Table 5.12 The parameters of DFIG wind turbine under different conditions

Parameters	Case 1	Case 2	Case 3	Case 4	Case 5	Case 6
Variables	Base case	Reduce V_s	Increase V_0	Increase X_T	Increase x_w	Increase y_w
V_s (p.u.)	1.00	0.50	1.00	1.00	1.00	1.00
V_0 (p.u.)	1.0	1.0	0.5	1.0	1.0	1.0
$ X_T $ (p.u.)	0.75	0.75	0.75	1.5	0.75	0.75
x_w^s (rad)	0.5	0.5	0.5	0.5	1	0.5
y_w^s (p.u.)	0.05	0.05	0.05	0.05	0.05	0.1

For DFIG, when the controlled voltage on the q-axis of rotor (V_{rq}) is not dependent on the angle of internal voltage ($\partial \bar{V}_{rq} / \partial x_w \approx 0$), the results are represented in the following table.

Table 5.13 The results of eigenvalue computations of DFIG wind turbine

Parameters Variables	Case 1 Base case	Case 2 Reduce V_s	Case 3 Increase V_0	Case 4 Increase X_T	Case 5 Increase x_w	Case 6 Increase y_w
K_{E1}	-4.375	-2.187	-4.375	-4.375	-3.762	-4.375
K_{E2}	514.503	435.565	514.503	472.285	584.762	522.604
K_S	1.229	1.229	0.614	0.614	0.756	1.229
ω_n (rad/s)	9.503	8.743	6.720	6.438	7.949	9.577
ζ	0.230	0.125	0.326	0.340	0.237	0.228
σ	-2.19	-1.09	-2.19	-2.19	-1.88	-2.19
ω (rad/s)	9.25	8.67	6.35	6.05	7.72	9.32
s	-2.19±j9.25	-1.09±j8.67	-2.19±j6.35	-2.19±j6.05	-1.88±j7.72	-2.19±j9.32
Natural freq.	1.51	1.39	1.07	1.02	1.27	1.52
Frequency (Hz)	1.47	1.38	1.01	0.96	1.23	1.48
$\partial \bar{V}_{rq} / \partial x_w$	0	0	0	0	0	0
$\partial \bar{V}_{rq} / \partial y_w$	0.7188798	0.4355719	0.7188798	0.5673586	0.9710362	0.7479535

In the above table, it is clear that the real part of eigenvalue increases (moves from negative to close to zero) with increasing angles of internal voltage and decreasing stator voltage. The imaginary part of eigenvalue decreases with increasing of reference voltage, transmission line reactance, and angle of internal voltage and decreasing of stator voltage.

When V_{rq} depends partly on an angle of internal voltage ($\partial \bar{V}_{rq} / \partial x_w \approx -0.01$), the results are represented in the following table.

Table 5.14 The results of eigenvalue computation for DFIG when V_{rq} depends partly on x_w

Parameters Variables	Case1 Base case	Case2 Reduce V_s	Case3 Increase V_0	Case4 Increase X_T	Case5 Increase x_w	Case6 Increase y_w
K_{E1}	-7.161	-4.974	-7.161	-7.161	-6.548	-7.161
K_{E2}	514.503	435.565	514.503	472.285	584.762	522.604
K_S	1.229	1.229	0.614	0.614	0.756	1.229
ω_n (rad/s)	9.503	8.743	6.720	6.438	7.949	9.577
ζ	0.377	0.284	0.533	0.556	0.412	0.374
σ	-3.58	-2.49	-3.58	-3.58	-3.27	-3.58
ω (rad/s)	8.80	8.38	5.69	5.35	7.24	8.88
s	-3.58±j8.80	-2.49±8.38	-3.58±5.69	-3.58±5.35	-3.27±j7.24	-3.58±j8.88
Natural freq.	1.51	1.39	1.07	1.02	1.27	1.52
Frequency (Hz)	1.40	1.33	0.90	0.85	1.15	1.41
$\partial \bar{V}_{rq} / \partial x_w$	-0.01	-0.01	-0.01	-0.01	-0.01	-0.01
$\partial \bar{V}_{rq} / \partial y_w$	0.7188798	0.4355719	0.7188798	0.5673586	0.9710362	0.7479535

It was found that the eigenvalue of the base case increases with decreasing $\partial \bar{V}_{rq} / \partial x_w$. The sensitivity of V_{rq} to x_w (or $\partial \bar{V}_{rq} / \partial x_w$), which is influenced by the controlled parameters affecting the small signal stability significantly. If $\partial \bar{V}_{rq} / \partial x_w$ is positive, the eigenvalues become positive and the system is unstable as a result. However, sensitivity of V_{rq} to speed deviation (y_w) or $\partial \bar{V}_{rq} / \partial y_w$ is not affect to real part of eigenvalue but significantly influence to imaginary part or frequency.

Table 5.15 The results of eigenvalue computation for DFIG when V_{rq} not depends on x_w, y_w

Parameters Variables	Case 1 Base case	Case 2 Reduce V_s	Case 3 Increase V_0	Case 4 Increase X_T	Case 5 Increase x_w	Case 6 Increase y_w
K_{E1}	-4.375	-2.187	-4.375	-4.375	-3.762	-4.375
K_{E2}	314.200	314.200	314.200	314.200	314.200	314.200
K_S	1.229	1.229	0.614	0.614	0.756	1.229
ω_n (rad/s)	7.426	7.426	5.251	5.251	5.827	7.426
ζ	0.295	0.147	0.417	0.417	0.323	0.295
σ	-2.19	-1.09	-2.19	-2.19	-1.88	-2.19
ω (rad/s)	7.10	7.35	4.77	4.77	5.51	7.10
s	-2.19±j7.10	-1.09±j7.35	-2.19±j4.77	-2.19±j4.77	-1.88±j5.51	-2.19±j7.10
Natural freq.	1.18	1.18	0.84	0.84	0.93	1.18
Frequency (Hz)	1.13	1.17	0.76	0.76	0.88	1.13
$\partial \bar{V}_{rq} / \partial x_w$	0	0	0	0	0	0
$\partial \bar{V}_{rq} / \partial y_w$	0	0	0	0	0	0

The real part of the eigenvalue (σ) is used to describe the stability condition of the system. If the σ is on the left side of complex plain (negative value), then the system is stable but if it is on the right side (positive value), then the system is unstable. The zero σ represents the critical condition of the system. From above table, conditions that can cause σ move from the left side of complex plain to the right side are the reducing of terminal voltage, speed, and reference voltage and an increasing of angle of internal voltage and line impedance.

When comparing between the eigenvalues of SCIG and DFIG, the real part of the eigenvalue of SCIG and DFIG are not much different, except when an angle of internal voltage increases. It is clear that imaginary parts of eigenvalue of DFIG are larger than of SCIG.

5.3.2 Eigenvalues of multi-machine power system including wind power

In this section, wind power is modeled using a doubly fed induction generator (DFIG) which the swing equation and voltage behind transient reactance are focused regarding the synchronization stability problem. The difference between the synchronous generator and induction generator is the slip (s_w) which is the difference between the angular speed of the rotor and the electrical field at the stator of the induction generator.

The system equations can be represented in the form of a matrix as follows:

$$\dot{\mathbf{X}} = \mathbf{A}\mathbf{X} + \mathbf{B}\mathbf{U} \quad \text{Eq.5-25}$$

or

$$\begin{bmatrix} \Delta \dot{x}_i \\ \Delta \dot{x}_w \\ \Delta \dot{x}_k \\ \Delta \dot{y}_w \\ \Delta \dot{y}_i \end{bmatrix} = \begin{bmatrix} 0 & 0 & 0 & 0 & \omega_0 \\ 0 & K_{Ew1} & K_{Ew2} & K_{Ew3} & 0 \\ -K_{Ski} & -K_{Skw} & -K_{Skk} & 0 & 0 \\ -K_{Swi} & -K_{Sww} & -K_{Swk} & -K_{Dw} & 0 \\ -K_{Sii} & -K_{Siw} & -K_{Sik} & 0 & -K_{Di} \end{bmatrix} \begin{bmatrix} \Delta x_i \\ \Delta x_w \\ \Delta x_k \\ \Delta y_w \\ \Delta y_i \end{bmatrix} + \begin{bmatrix} 0 \\ 0 \\ -\Delta \bar{P}_{lk}/c_k \\ \Delta \bar{P}_{mw}/M \\ \Delta \bar{P}_{mi}/M \end{bmatrix} \quad \text{Eq.5-26}$$

For example, the two-machine infinite bus power system can be modeled as follows:

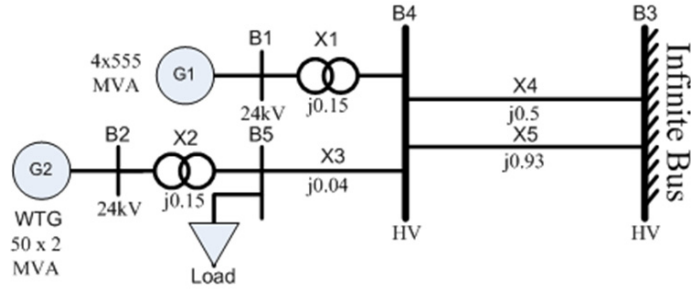


Figure 5.126 Two-machine infinite bus power system, including wind power and load

The system equations become

$$\begin{bmatrix} \Delta \dot{x}_2 \\ \Delta \dot{x}_3 \\ \Delta \dot{x}_4 \\ \Delta \dot{y}_3 \\ \Delta \dot{y}_2 \end{bmatrix} = \begin{bmatrix} 0 & 0 & 0 & 0 & \omega_0 \\ 0 & K_{Ew1} & K_{Ew2} & K_{Ew3} & 0 \\ -K_{S42} & -K_{S43} & -K_{S44} & 0 & 0 \\ 0 & -K_{S33} & -K_{S34} & -K_{D3} & 0 \\ -K_{S22} & 0 & -K_{S24} & 0 & -K_{D2} \end{bmatrix} \begin{bmatrix} \Delta x_2 \\ \Delta x_3 \\ \Delta x_4 \\ \Delta y_3 \\ \Delta y_2 \end{bmatrix} + \begin{bmatrix} 0 \\ 0 \\ -\Delta \bar{P}_{l4}/c_k \\ \Delta \bar{P}_{m3}/M_3 \\ \Delta \bar{P}_{m2}/M_2 \end{bmatrix} \quad \text{Eq.5-27}$$

5.3.2.1 Eigenvalue analysis of two-machine infinite bus power system, including wind power

In Eq.5-27, rearranging using the following form and taking Laplace transformation, yields

$$\mathbf{X}(s) = (s\mathbf{I} - \mathbf{A})^{-1} \mathbf{B}\mathbf{U}(s) \quad \text{Eq.5-28}$$

$$\text{Or } \begin{bmatrix} \Delta x_2(s) \\ \Delta x_3(s) \\ \Delta x_4(s) \\ \Delta y_3(s) \\ \Delta y_2(s) \end{bmatrix} = \begin{bmatrix} s & 0 & 0 & 0 & -\omega_0 \\ 0 & s - K_{Ew1} & -K_{Ew2} & -K_{Ew3} & 0 \\ K_{S42} & K_{S43} & s + K_{S44} & 0 & 0 \\ K_{S32} & K_{S33} & K_{S34} & s + K_{D3} & 0 \\ K_{S22} & K_{S23} & K_{S24} & 0 & s + K_{D2} \end{bmatrix}^{-1} \begin{bmatrix} 0 \\ 0 \\ -\Delta \bar{P}_{l4}(s)/c_k \\ \Delta \bar{P}_{m3}(s)/M \\ \Delta \bar{P}_{m2}(s)/M \end{bmatrix} \quad \text{Eq.5-29}$$

$$(s\mathbf{I} - \mathbf{A})^{-1} = \frac{1}{\det(s\mathbf{I} - \mathbf{A})} (s\mathbf{I} - \mathbf{A})^T \quad \text{Eq.5-30}$$

The solutions of $\det(s\mathbf{I} - \mathbf{A}) = 0$ are the eigenvalues of this state space equation, therefore

$$\det(s\mathbf{I} - \mathbf{A}) = s(s - K_{Ew1})(s + K_{S44})(s + K_{D3})(s + K_{D2}) - \omega_0(s + K_{S44})K_{S22}K_{S33}K_{Ew3} = 0 \quad \text{Eq.5-31}$$

Therefore, the results of eigenvalue analysis are represented in the following tables.

Table 5.16 Testing conditions and steady state values of speeds and angles

Variables	Case 1	Case 2	Case 3	Case 4	Case 5	Case 6
Power Load or P_L (p.u.)	4	4	4	4	4	4
P_{m3} of G_3 (p.u.)	1	1	1	0.4	0.6	0.8
P_{m2} of G_2 (p.u.)	3	4	2	3.6	3.4	3.2
Exchanged power (P_{mG})	0	-1	1	0	0	0
x_{2s}	0.64284	1.56986	-0.23281	0.79943	0.74450	0.69287
x_{3s}	0.28896	0.93253	-0.35487	0.10764	0.16780	0.22856
x_{4s}	-0.00053	0.64301	-0.64434	-0.00469	-0.00302	-0.00138
y_{2s}	0.00000	0.00000	0.00000	0.00000	0.00000	0.00000
y_{3s}	0.19987	0.19987	0.19988	-0.10627	0.02582	0.12358

Table 5.17 The results of eigenvalue analysis for six testing conditions

Conditions	Eig 1	Eig 2	Eig 3	Eig 4	Eig 5
Case 1	-860.1000	-101.9051	-0.6267 + 7.2810i	-0.6267 - 7.2810i	-0.3572
Case 2	-857.5000	-77.9554	-0.6043 + 6.4559i	-0.6043 - 6.4559i	-0.3573
Case 3	-860.6000	-106.1014	-0.7538 + 6.8096i	-0.7538 - 6.8096i	-0.3573
Case 4	-1163.8000	-94.8657	-0.5632 + 7.1263i	-0.5632 - 7.1263i	-0.1969
Case 5	-1017.4000	-97.4260	-0.5883 + 7.1882i	-0.5883 - 7.1882i	-0.2583
Case 6	-926.2000	-99.7705	-0.6090 + 7.2388i	-0.6090 - 7.2388i	-0.3110

In Table 5.17, it is found that eigenvalues Eig 5 are most significant due to they are closer to zero which represents the critical value of small signal stability. For Cases 4-6 when wind power increase, the significant eigenvalues are decrease. For Cases 1-3, when exchanged power ($P_L - P_{m2} - P_{m3}$) are varied, the significant eigenvalues (Eig 5) are not different but the other eigenvalues (Eig 1 – Eig 4) are increase with decreasing of exchanged power. Furthermore, from Table 5.18 for all 6 conditions, it is found that the significant eigenvalues are most influenced by the speed deviation (or slip) of wind turbine. The subsequent significant eigenvalues (Eig4) are influenced by the speed deviation of synchronous generator.

Table 5.18 The participation factors

Case 1	Eig1	Eig2	Eig3	Eig4	Eig5	Case 4	Eig1	Eig2	Eig3	Eig4	Eig5
x2	0.000	0.235	0.005	0.000	0.000	x2	0.000	0.248	0.004	0.000	0.000
x3	0.008	0.023	0.001	0.000	0.000	x3	0.011	0.018	0.001	0.000	0.000
x4	0.616	0.153	0.005	0.000	0.000	x4	0.735	0.169	0.005	0.000	0.000
y3	0.362	0.087	0.036	0.000	1.000	y3	0.248	0.054	0.021	0.000	1.000
y2	0.014	0.503	0.954	1.000	0.000	y2	0.007	0.512	0.969	1.000	0.000
Case 2	Eig1	Eig2	Eig3	Eig4	Eig5	Case 5	Eig1	Eig2	Eig3	Eig4	Eig5
x2	0.000	0.201	0.004	0.000	0.000	x2	0.000	0.240	0.004	0.000	0.000
x3	0.011	0.019	0.001	0.000	0.000	x3	0.010	0.020	0.001	0.000	0.000
x4	0.607	0.133	0.005	0.000	0.000	x4	0.684	0.161	0.005	0.000	0.000
y3	0.371	0.095	0.037	0.000	1.000	y3	0.297	0.067	0.026	0.000	1.000
y2	0.011	0.552	0.954	1.000	0.000	y2	0.010	0.513	0.964	1.000	0.000
Case 3	Eig1	Eig2	Eig3	Eig4	Eig5	Case 6	Eig1	Eig2	Eig3	Eig4	Eig5
x2	0.000	0.246	0.004	0.000	0.000	x2	0.000	0.237	0.004	0.000	0.000
x3	0.009	0.022	0.001	0.000	0.000	x3	0.009	0.022	0.001	0.000	0.000
x4	0.614	0.153	0.006	0.000	0.000	x4	0.646	0.156	0.005	0.000	0.000
y3	0.359	0.083	0.042	0.000	1.000	y3	0.333	0.077	0.031	0.000	1.000
y2	0.017	0.496	0.948	1.000	0.000	y2	0.012	0.508	0.959	1.000	0.000

5.4 A study of effects of wind power on the small signal stability using stochastic stability method: the mean first passage time (MFPT)

The mean first passage time (MFPT) is the performance index to quantify the average time a state-space trajectory takes to change from a given operating point to the boundary of its domain of attraction under the influence of small perturbations [9][2]. MFPT can be used to evaluate the small signal stability of the power system when incorporating stochastic wind power. This section represents the results of mean first passage time (MFPT) computation according to different testing conditions. From Chapter 3, the MFPT is a solution of the following problem

$$\left. \begin{aligned} \varepsilon C_1^* W \tau_0''(W) + [\varepsilon C_2 - C_3^* W] \tau_0'(W) &= -1 \\ \tau_0(W_C) &= 0, \quad \tau_0(0) < \infty \end{aligned} \right\} \quad \text{Eq.5-32}$$

The solution is

$$\tau_0(0) \approx \frac{1}{C_3^*} (W_C)^{-C_2/C_1^*} \left[\int_0^{W_C} t^{(C_2/C_1^*)-1} \cdot e^{-(C_3^* t / \varepsilon_l C_1^*)} dt \right] e^{(C_3^* W_C / \varepsilon_l C_1^*)} \quad \text{Eq.5-33}$$

$$\text{Or} \quad \tau(0) \approx \frac{1}{\beta C_3^*} (W_C)^{-C_2/C_1^*} \left[\int_0^{W_C} t^{(C_2/C_1^*)-1} \cdot e^{-(C_3^* t / \varepsilon_l C_1^*)} dt \right] e^{(C_3^* W_C / \varepsilon_l C_1^*)} \quad \text{Eq.5-34}$$

Where

$$\left. \begin{aligned} C_1(W) &= \frac{1}{T(W)} \oint_W \varepsilon_2 \left(\frac{\partial W}{\partial x_2} \right)^2 ds_c \\ C_2(W) &= \frac{1}{T(W)} \oint_W \varepsilon_2 \frac{\partial^2 W}{\partial x_2^2} ds_c \\ C_3(W) &= \frac{1}{T(W)} \oint_W \left(y_1 \frac{\partial W}{\partial y_1} + y_2 \alpha \frac{\partial W}{\partial y_2} + y_3 \frac{\partial W}{\partial y_3} \right) ds_c \end{aligned} \right\} \quad \text{Eq.5-35}$$

Where critical energy (W_c) computation technique is presented in the previous Chapter and coefficients C_1^* , C_2 , and C_3^* are stated in Appendix A.

Since the energy function cannot be used directly for the solution of the problem in Eq.5-34, thus an approximate energy function based on an ellipsoidal surface is represented instead. This takes [9]:

$$W = \sum_{i=1}^{n+m-1} \sum_{j=i+1}^{n+m} \left[\frac{1}{2} \frac{M_i M_j}{M_T} (y_i - y_j)^2 + \frac{1}{2} \cos(x_i^s - x_j^s) V_i V_j B_{ij} (z_i - z_j)^2 \right] \quad \text{Eq.5-36}$$

where $M_T = \sum_{i=1}^n M_i$ and $z_i = x_i - x_i^s$ if $i = 1, 2, \dots, n+m$

From Chapter 3 and Appendix A, MFPT can be calculated using the following steps

- S1) Stable equilibrium points and critical energy are computed as represented in previous topics.
- S2) Matrix **H** can be constructed using Eqs. A-3 to A-6 in Appendix A.
- S3) Find eigenvalues and eigenvectors of matrix **H**. After matrix **H** is constructed explicitly, software *Matlab* can possibly be used to find eigenvalues and eigenvectors.
- S4) Construct set of matrix **D** and matrix **F** using Eqs. A-29 to A-33 in Appendix A.
These matrixes will be used in the formulation of MFPT.
- S5) Compute C coefficient using Eqs. A-25 to A-28 in Appendix A.
- S6) Compute MFPT using Eq.5-34. Every step from S1 – S5 is done completely.
- S7) Change condition of wind power, such as, wind speed and noise intensity and repeat S1 – S6 again to see the variation of MFPT.

To compute MFPT, several processes have to be done consisting of the determination of steady state variables, estimation of critical energy, and formulation of stochastic differential equations. Energy function method, based on Lyapunov function, is

used to determine the region of attraction of stable equilibrium points and the critical values. Beyond these values, the system become unstable.

The critical energy can be estimated using the minimum value for each case of wind speed. As a result, the critical energy increases with increasing mean wind speed. When the wind speed increases, the wind power can share more load from the other generators and make the system more stable. At mean wind speeds of 6, 8, 10, and 12 m/s, the critical energies of the test system are 2.04, 2.17, 2.35, and 2.58, respectively. The total wind power from several wind farms can be comparable with white noise. Therefore, the Gaussian distribution of noise signal from wind power can be reasonably assumed for such case.

The asymptotic method is applied to the solution of MFPT. Only the first order of scale factor (β) is used to estimate MFPT. Since energy function cannot be used directly for the solution of MFPT, therefore, an approximate energy function basing on ellipsoidal surface is represented instead. The characteristic matrix of ellipsoidal surface has eigenvalues and eigenvector, which are used for the computation of MFPT.

Finally, the MFPT is computed with the variation of wind speed and noise intensity. MFPT is significantly low especially when wind speed higher or equal to 8 m/s. The lower MFPT means the higher risk of power system instability.

To implement MFPT to the practical use, the test power system is modified and the measurement data of wind power (or wind speed) is provided. After modification of the test power system, the process of MFPT computation is done. There are several steps to implement MFPT as follows

- First, measurement of wind power every 1 or 10 minutes of recording time interval is used. In the case measurement data is not available, wind power simulation using measurement wind speed data can be applied instead.
- Second, use moving average technique to compute average noise intensity and wind speed. The time interval of averaging can be considered from the ability of power system which can operate without regulation. For example, the reasonable regulation which can possibly or significantly occur at every 10 minutes.
- Third, the results of mean wind speed and noise intensity of wind power from moving average technique can be used to judge the possibility of instability of the power system under different conditions of wind power. For example in the above table, if the average wind speed is larger than 10 m/s while noise intensity is higher

than 0.25, the MFPT will be less than or equal to 10 minutes. This is the situation that should be avoided.

When varying wind speed and its noise intensity, the results of MFPT are represented in the following figures and table.

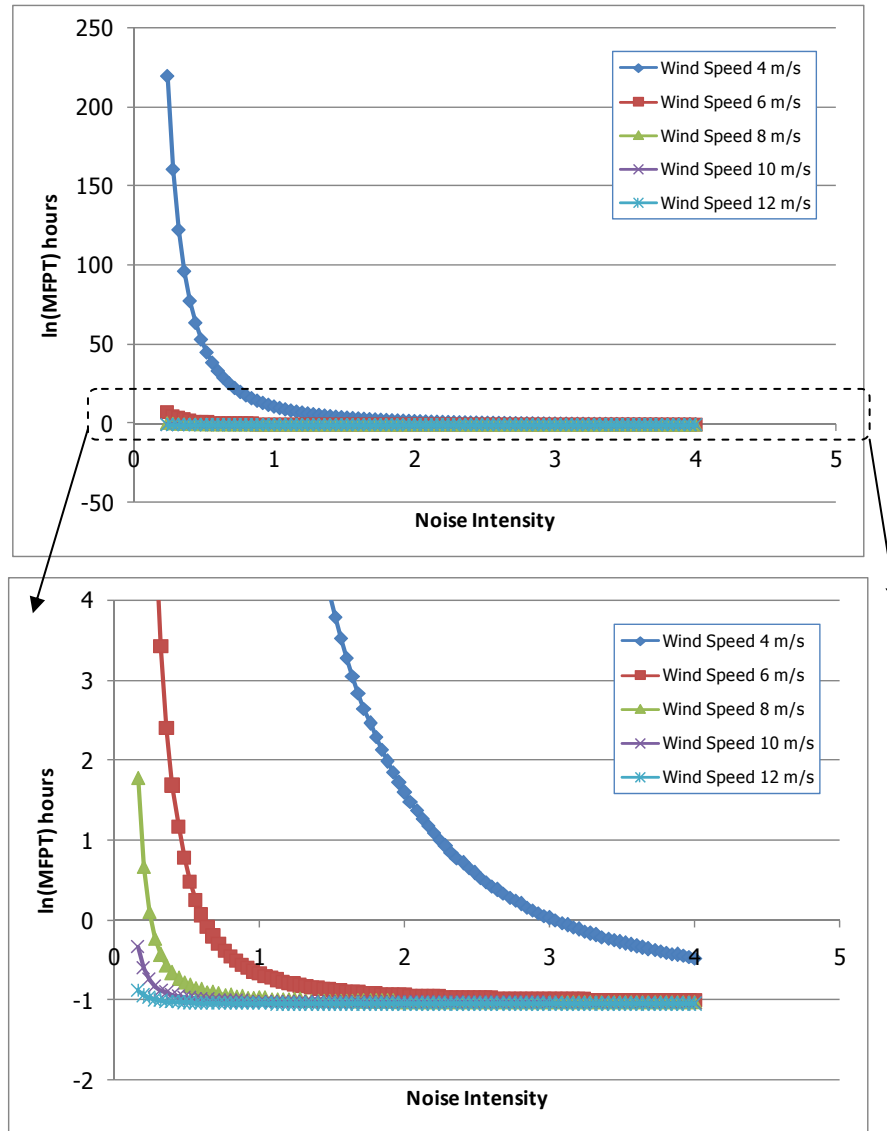


Figure 5.127 Log-scale of MFPT at different wind speeds and noise intensity

The results in Figure 5.127 and Table 5.19 show that MFPT decreases with increasing noise intensity of wind power and mean wind speed. Noise intensity is larger than 3.4, 0.88, 0.38, 0.24, and 0.18 with mean wind speed at least 4, 6, 8, 10, and 12 m/s, respectively, are seriously considerable and can lead the system to be unstable within a short time (less than 10 minutes).

Table 5.19 MFPT at different wind speeds and noise intensity

noise intensity	MFPT (hours) at mean wind speed					noise intensity	MFPT (hours) at mean wind speed				
	4 m/s	6 m/s	8 m/s	10 m/s	12 m/s		4 m/s	6 m/s	8 m/s	10 m/s	12 m/s
0.04	65535	3.2E+202	6.35E+34	3.77E+11	7677328	2.04	0.605985869	0.09941	0.090767	0.089748	0.089615
0.08	65535	7.97E+48	21983425	55.44486	4.568147	2.08	0.558612984	0.098979	0.090699	0.089726	0.089612
0.12	65535	4.13E+20	257.0525	1.172062	0.43399	2.12	0.517539572	0.098574	0.090635	0.089706	0.089611
0.16	4.0682E+186	6.28E+10	5.792008	0.346039	0.207364	2.16	0.481711836	0.098194	0.090575	0.089687	0.089613
0.2	3.5077E+118	2011752	1.10842	0.205336	0.150636	2.2	0.45028328	0.097835	0.090518	0.089669	0.089618
0.24	4.05638E+81	7869.855	0.476175	0.156892	0.127488	2.24	0.422568533	0.097498	0.090464	0.089654	0.089625
0.28	2.3031E+59	294.1306	0.293715	0.134123	0.11557	2.28	0.398008549	0.097179	0.090414	0.089639	0.089635
0.32	8.77701E+44	36.33701	0.217452	0.121428	0.10855	2.32	0.376144121	0.096878	0.090365	0.089626	0.089648
0.36	1.18259E+35	8.94814	0.178129	0.113551	0.104036	2.36	0.356595563	0.096593	0.09032	0.089614	0.089665
0.4	1.05819E+28	3.366507	0.154996	0.108293	0.100949	2.4	0.339046979	0.096323	0.090277	0.089603	0.089684
0.44	6.59911E+22	1.664309	0.140117	0.104593	0.098739	2.44	0.323234002	0.096068	0.090236	0.089594	0.089708
0.48	7.39249E+18	0.987714	0.129919	0.101883	0.097099	2.48	0.308934153	0.095825	0.090197	0.089586	0.089735
0.52	6.32629E+15	0.664913	0.122588	0.099834	0.095847	2.52	0.295959222	0.095595	0.09016	0.089579	0.089767
0.56	2.36049E+13	0.489405	0.117121	0.098246	0.094869	2.56	0.284149187	0.095376	0.090125	0.089573	0.089803
0.6	2.62565E+11	0.384311	0.112922	0.096988	0.094091	2.6	0.273367356	0.095168	0.090091	0.089569	0.089843
0.64	6679110727	0.316596	0.109621	0.095974	0.093461	2.64	0.263496431	0.094969	0.090059	0.089566	0.089889
0.68	321502762.5	0.270412	0.106974	0.095144	0.092943	2.68	0.254435331	0.09478	0.090029	0.089565	0.08994
0.72	25503572.6	0.23746	0.104816	0.094456	0.092513	2.72	0.246096594	0.0946	0.089999	0.089565	0.089997
0.76	3008347.051	0.213079	0.103031	0.09388	0.092152	2.76	0.238404247	0.094428	0.089972	0.089566	0.09006
0.8	488223.2844	0.194494	0.101537	0.093392	0.091846	2.8	0.231292055	0.094264	0.089945	0.089569	0.09013
0.84	102702.2931	0.179973	0.100272	0.092975	0.091584	2.84	0.224702064	0.094107	0.08992	0.089573	0.090207
0.88	26735.03873	0.168388	0.099193	0.092616	0.091358	2.88	0.218583401	0.093957	0.089896	0.089579	0.090291
0.92	8303.824468	0.158982	0.098262	0.092305	0.091162	2.92	0.212891262	0.093813	0.089873	0.089587	0.090384
0.96	2989.294566	0.151226	0.097455	0.092033	0.090991	2.96	0.207586063	0.093676	0.08985	0.089596	0.090486
1	1218.499628	0.144748	0.09675	0.091795	0.090841	3	0.202632734	0.093544	0.089829	0.089607	0.090598
1.04	551.8694178	0.139274	0.09613	0.091585	0.090708	3.04	0.198000114	0.093417	0.089809	0.089621	0.090719
1.08	273.4553054	0.134601	0.095583	0.091398	0.090591	3.08	0.193660441	0.093296	0.089789	0.089636	0.090852
1.12	146.3664073	0.130576	0.095096	0.091232	0.090486	3.12	0.189588915	0.09318	0.089771	0.089653	0.090997
1.16	83.73513745	0.127081	0.094662	0.091083	0.090393	3.16	0.185763327	0.093068	0.089753	0.089672	0.091155
1.2	50.75120579	0.124025	0.094273	0.09095	0.090309	3.2	0.182163745	0.09296	0.089736	0.089694	0.091328
1.24	32.34662103	0.121336	0.093923	0.09083	0.090233	3.24	0.178772233	0.092857	0.089719	0.089718	0.091515
1.28	21.54391028	0.118954	0.093607	0.090721	0.090165	3.28	0.175572619	0.092758	0.089703	0.089745	0.091719
1.32	14.91456046	0.116835	0.09332	0.090622	0.090103	3.32	0.172550291	0.092662	0.089688	0.089774	0.09194
1.36	10.68318965	0.114939	0.09306	0.090533	0.090047	3.36	0.169692015	0.09257	0.089674	0.089806	0.092181
1.4	7.886605914	0.113236	0.092822	0.090451	0.089996	3.4	0.166985787	0.092481	0.08966	0.089842	0.092442
1.44	5.980068156	0.1117	0.092605	0.090376	0.089949	3.44	0.164420695	0.092396	0.089646	0.08988	0.092727
1.48	4.643799946	0.110309	0.092406	0.090307	0.089907	3.48	0.161986801	0.092313	0.089634	0.089922	0.093035
1.52	3.683687624	0.109044	0.092224	0.090244	0.089868	3.52	0.159675038	0.092234	0.089621	0.089967	0.093371
1.56	2.978279295	0.107892	0.092055	0.090186	0.089833	3.56	0.157477122	0.092157	0.08961	0.090016	0.093735
1.6	2.449474388	0.106838	0.0919	0.090133	0.089801	3.6	0.155385469	0.092083	0.089598	0.090069	0.09413
1.64	2.045783234	0.105871	0.091757	0.090083	0.089772	3.64	0.153393126	0.092011	0.089588	0.090126	0.09456
1.68	1.732480636	0.104982	0.091623	0.090038	0.089745	3.68	0.151493708	0.091942	0.089577	0.090188	0.095026
1.72	1.485656487	0.104163	0.0915	0.089995	0.089721	3.72	0.149681343	0.091875	0.089568	0.090254	0.095533
1.76	1.288531316	0.103406	0.091385	0.089956	0.0897	3.76	0.147950625	0.091811	0.089558	0.090325	0.096083
1.8	1.129122125	0.102705	0.091278	0.089919	0.089681	3.8	0.146296565	0.091748	0.089549	0.090401	0.096681
1.84	0.99873242	0.102055	0.091178	0.089885	0.089664	3.84	0.14471456	0.091688	0.089541	0.090483	0.09733
1.88	0.890956333	0.10145	0.091085	0.089854	0.08965	3.88	0.14320035	0.091629	0.089533	0.090571	0.098036
1.92	0.801009942	0.100887	0.090997	0.089824	0.089638	3.92	0.141749991	0.091572	0.089525	0.090665	0.098802
1.96	0.725274755	0.100361	0.090916	0.089797	0.089628	3.96	0.140359829	0.091517	0.089518	0.090765	0.099635
2	0.660981179	0.09987	0.090839	0.089772	0.08962	4	0.139026471	0.091464	0.089511	0.090873	0.10054

An example using existing test systems with wind power is calculated from wind speed data is represented.

In Chumporn Province of Thailand, during October 2011 and May 2012, the mean wind speed at 90 meters hub-height is about 5 m/s while noise intensity of wind power is about 0.5. The wind power in this case is calculated using VESTAS V90 2000kW specification. The distributions of wind speed and its noise intensities are represented in Figure 5.128. The wind power and its noise intensities are represented in Figure 5.129. The relation between wind speed and noise intensity of wind power is shown in Figure 5.130.

If wind power is operated without regulation control, the power system may become unstable within 10 minutes under some conditions. The noise intensity larger than 3.4, 0.88, 0.38, 0.24, and 0.18 with mean wind speed at least 4, 6, 8, 10, and 12 m/s, respectively, are such critical conditions to be considered. Figure 5.130 shows that within shaded area, MFPT is less than 10 minutes. Therefore, outside a shaded area in which MFPT larger than 10 minutes are occurred especially when wind speed higher than 6 m/s. These serious conditions will occur during April – May and Nov – Dec when the monsoon has much influence in that area.

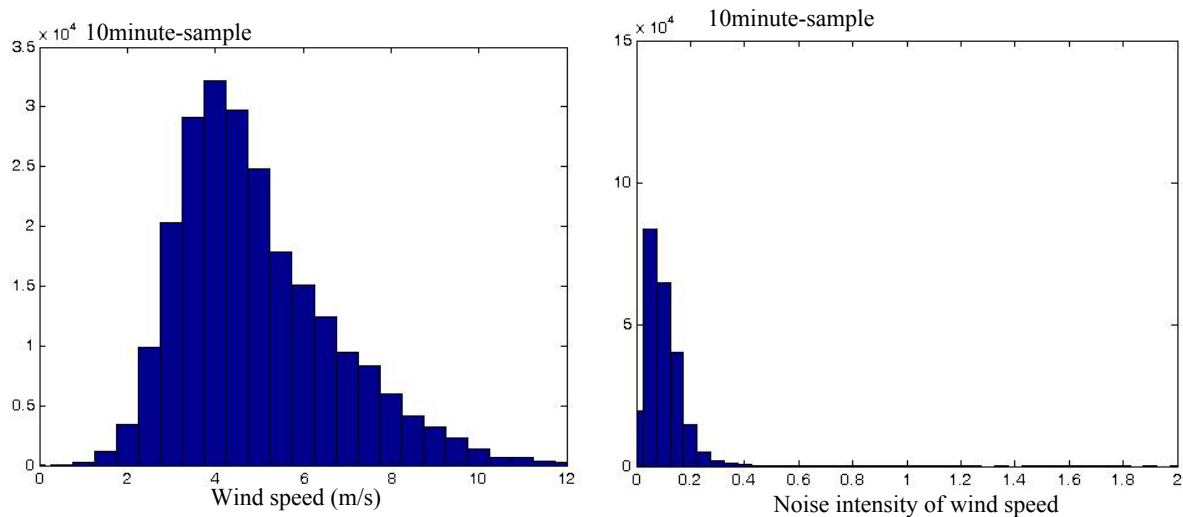


Figure 5.128 Distribution of wind speed (left) and noise intensity (right) of wind speed

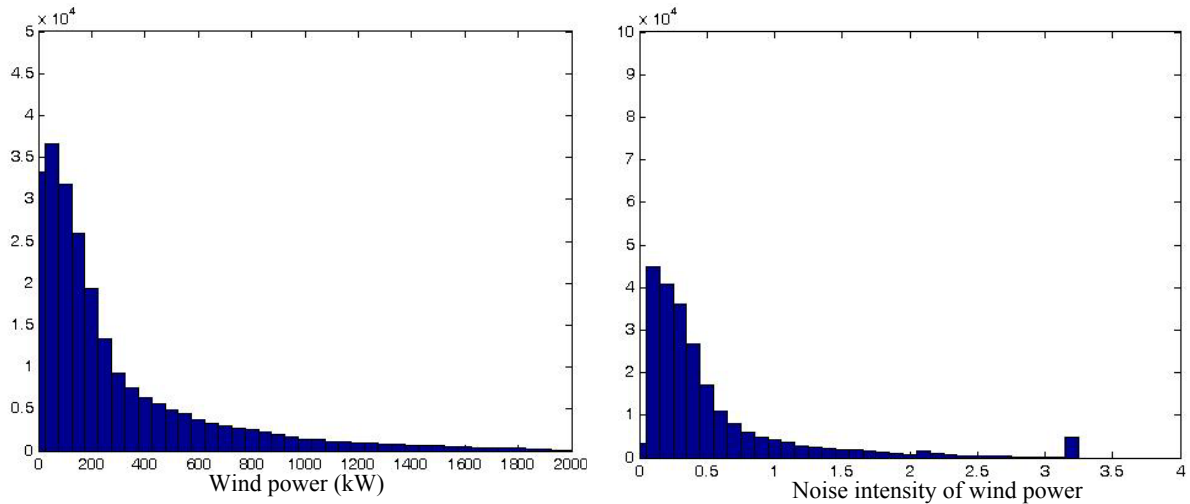


Figure 5.129 Distribution of wind power (left) and noise intensity (right) of wind power

Table 5.20 The results of MFPT implementation

Variables	Results at different wind speed				
	4 m/s	6 m/s	8 m/s	10 m/s	12 m/s
NI_{\max}	3.16	3.16	1.18	0.45	0.31
MFPT at NI_{\max} (hours)	0.18	0.09	0.09	0.1	0.1
Rt (hours)	0.167	0.167	0.167	0.167	0.167
MFPT < Rt ?	no	yes	yes	yes	yes

NI_{\max} is the maximum noise intensity of wind power occurring at each range of mean wind speed. It is found that NI_{\max} vastly decreases with increasing wind speed. R_t is an imposed constraint of the power system (for example, the constraint which are used in Area Control Error or ACE for power balancing and frequency control). In this case, R_t is assumed to be 10 minutes (0.167 hours).

In Table 5.20, the maximum noise intensity (NI_{\max}) and MFPT at NI_{\max} with different wind speeds are determined. When MFPT is less than R_t , the power system is possibly unstable before the regulation or control system can serve for any small and continuous disturbances.

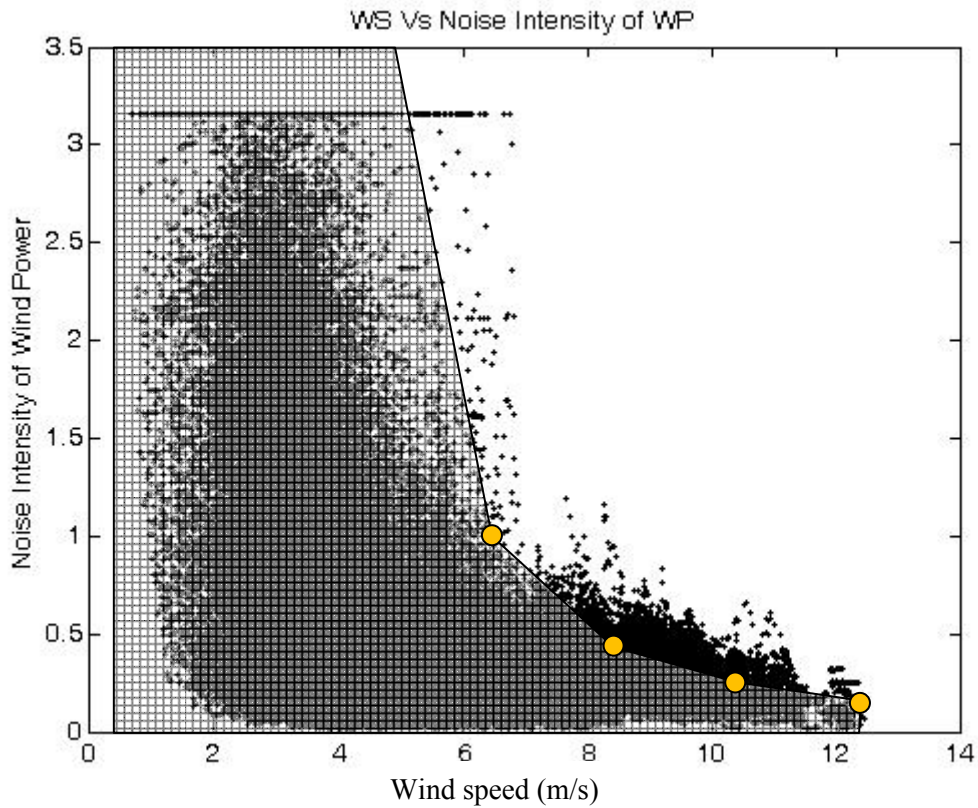


Figure 5.130 Relation between wind speed and noise intensity of wind power using the wind data of the Chumporn wind monitoring station in the South of Thailand.

In conclusion, this section can explain the main problem of the thesis. The effects of stochastic wind power on the power system stability can be determined reasonably using the stability index, namely MFPT.

Considering wind speed data from the Chumporn monitoring station, the cases when noise intensity larger than 3.4, 0.88, 0.38, 0.24, and 0.18 with mean wind speed 6, 8, 10, and 12 m/s, respectively, are seriously considerable and can possibly lead the system to be unstable within a short time (less than 10 minutes). These serious conditions will occur during April – May and Nov – Dec when the monsoon has much influence in that area.

However, this result is based on the assumption that wind power is Gaussian white noise, and the power system is unregulated, which is not practical. The dynamics with regulation system needs an improvement of the stability index. Furthermore, the energy function, using for MFPT solution, is an approximated value which has ellipsoidal surface shape. It cannot represent the complex surface problems, for example, the energy of the power system when incorporate DFIG wind turbine model. Therefore, the other methods will be developed and explained in the next chapter.

CHAPTER 6

RESULTS AND DISCUSSION PART 2

In Chapter 3 and 5, the stability index called *mean first passage time (MFPT)* was determined to evaluate the small signal stability of the power system when incorporating stochastic wind power. This method can reveal the effects of different wind power and noise intensity on the power system stability using simplified elliptic surface energy function. However, it cannot represent the complex energy function, for example, when the DFIG wind turbine model is incorporated in the power system. Therefore, to overcome this problem, a new method is developed and explained in this Chapter.

This chapter focus on the stochastic stability problems, which consist of the study of the effects of wind power on the small signal stability using a new stochastic stability method, a study of effects of wind power on the voltage stability using a new stochastic stability method, and a study of the effects of wind power on voltage variation using a probabilistic method.

6.1 The Study of Effects of Wind Power on the Small Signal Stability using New Stochastic Stability Method

6.1.1 The Derivative of Stochastic Energy (*DSE*) for Gaussian distribution white noise model

This sub-section will focus on the study of the effects of stochastic wind power and load using the stability performance index, which is called the derivative of stochastic energy (*DSE*). The wind power is modeled using Gaussian distribution white noise model. There are two kinds of effects to be studied: first is the effect of stochastic wind power and constant and second is the effect of stochastic load and constant wind power.

6.1.1.1 The effects of stochastic wind power and constant load

From Section 4.8, the *DSE* can be computed by applying the following conditions.

1) The power test system

From Sections 4.2.2 and 4.8.1, the power test system is represented in Figure 6.1.

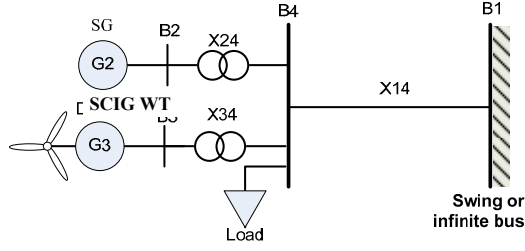


Figure 6.1 Test power system including wind power and load for *DSE*

The total n bus system consists of m bus of generation and $n-m$ bus of load and others. The bus i represents synchronous generator (SG) (total $m-p$ bus), bus w represents squirrel cage induction generator (SCIG) (total p bus) and k represents load bus. Bus no. 1 is a reference bus.

2) The stochastic differential equations (SDE)

From section 4.8.1, the matrix form of stochastic differential equations of the test system is

$$d \begin{bmatrix} x_2 \\ x_3 \\ x_4 \\ y_2 \\ y_3 \end{bmatrix} = \begin{bmatrix} \omega_0 (y_2 - y_1) \\ \omega_0 (y_3 - y_1) - k_b V_3 \sin(k_a x_3 + c_b) \\ -\frac{1}{c_k} (\bar{P}_{l4} + \bar{P}_{e4}) - \omega_0 y_1 \\ -\frac{D_2}{M_2} y_2 + \frac{1}{M_2} (\bar{P}_{m2} - \bar{P}_{e2}) \\ \frac{1}{M_3} (\bar{P}_{m3} - \bar{P}_{e3}) \end{bmatrix} dt + \begin{bmatrix} 0 \\ 0 \\ 0 \\ 0 \\ \frac{\bar{P}_{m3}}{M_3} \alpha_3 \end{bmatrix} dW \quad \text{Eq.6-1}$$

where D is damping coefficient of SG. V is terminal voltage. P_{mi} ($P_{mi} = P_{lk} - P_{mw}$) and P_{mw} are mechanical input power of SG and SCIG wind turbine, respectively. P_{lk} is a constant power load. P_{ei} , P_{ew} , and P_{ek} are electrical power at bus $i=2$, $w=3$ and $k=4$, respectively. c_k is frequency dependent coefficient of load.

3) The well-defined energy function

From section 4.4.2, the well-defined energy function of the power system and its derivative are

$$\begin{aligned}
U = & \frac{1}{2} \sum_{i=1}^{m-p} \omega_0 M_i y_i^2 + \frac{1}{2} \sum_{w=m-p+1}^m \omega_0 M_w (y_w^2 - y_w^{s2}) - \sum_{i=1}^{m-p} \bar{P}_{mi} (x_i - x_i^s) \\
& - \sum_{w=m-p+1}^m \bar{P}_{mw} (x_w - x_w^s) + \sum_{k=m+1}^n P_{lk} (x_k - x_k^s) \\
& - \sum_{w=m-p+1}^m \frac{1}{2} M_w k_b V_{sw} \left(\sin(k_a (x_w - x_{ref}) + c_a) + \sin(k_a (x_w^s - x_{ref}) + c_a) \right) (y_w - y_w^s) \\
& - \sum_{i=1}^{n-1} \sum_{j=i+1}^n \bar{V}_i \bar{V}_j \bar{B}_{ij} \left[\cos(x_i - x_j) - \cos(x_i^s - x_j^s) \right]
\end{aligned} \tag{Eq.6-2}$$

$$\dot{U} = - \sum_{i=1}^{m-p} \omega_0 D_i y_i^2 - \sum_{k=m+1}^n c_k \dot{x}_k^2 \tag{Eq.6-3}$$

4) The derivative of stochastic well-defined energy function

From section 4.8.1, the derivative of stochastic well-defined energy function (*DSE*):

$$\begin{aligned}
L u(x, t) = & -\omega_0 D_2 y_2^2 - \frac{1}{c_k} (\Delta \bar{P}_4)^2 + \omega_0 y_1 (\Delta \bar{P}_2 - \Delta \bar{P}_4) + \frac{\omega_0}{2M_3} (\bar{P}_{m3} \alpha_3)^2 \\
& - \frac{1}{2} M_3 k_a k_b V_3 (y_3 - y_3^s) \cos(k_a x_3 + c_b) \left[\omega_0 (y_3 - y_1) - k_b V_3 \sin(k_a x_3 + c_b) \right] \\
& + \frac{1}{2} k_b (\Delta \bar{P}_3) \left[\sin(k_a x_3 + c_b) - \sin(k_a x_3^s + c_b) \right] \leq 0
\end{aligned} \tag{Eq.6-4}$$

From Section 4.8.1, the *DSE* can be formulated as follows

$$DSE = - \frac{1}{c_k} (\Delta \bar{P}_4)^2 + \frac{\omega_0}{2M_3} (\bar{P}_{m3} \alpha_3)^2 \tag{Eq.6-5}$$

5) The testing conditions

The per unit base power is 100MVA, the fundamental speed, $\omega_0 = 314.159$ rad/s, an inertia constant of induction generator wind turbine (IG), $M_w = 7.0$ sec. [45], and the damping coefficient of the synchronous generator (SG), $D_i = 0.21$ [52]. The power deviation on the load bus (ΔP_4) remains constant at 0.04 throughout the simulation. The stability of this test system can be investigated by varying the noise intensity of the wind power (α_3) from 0 to 0.1 and the mechanical wind power (P_{m3}) is set to 0.5, 1.0, and 2.0. The frequency dependent coefficient of load, c_k is 0.025. The power flow of the test system with Load: Wind Power: power of SG is 4: 2: 2 p.u. .

The noise intensity (*NI*) of wind power depends generally on local wind characteristics. For example, the yearly *NI* calculated with hourly average wind power of four wind power plants in USA during 2000 – 2010 are 0.8 – 1.0 [70]. As a small signal, the noise intensity of this test system will be varied from 0 – 0.1.

6) The results

Since the stable condition of the stochastic system is $DSE < 0$, therefore, a larger DSE means that the system has higher probability to become unstable and the stability of the power system decreases. In Figure 6.2, it can be seen that the DSE gradually increases with the wind power and its noise intensity. This result indicates that the highly fluctuated wind power can reduce the rotor angle stability of the power system. When DSE is zero or critically stable condition, the critical noise intensities at wind power 0.5, 1.0, and 2.0 p.u., are about 0.09, 0.045, and 0.0225, respectively. Therefore, the critical noise intensities of wind power seem to linearly inverse to the changing of wind power. It can be implied that, to avoid system instability, the wind power should be limited by its noise intensity.

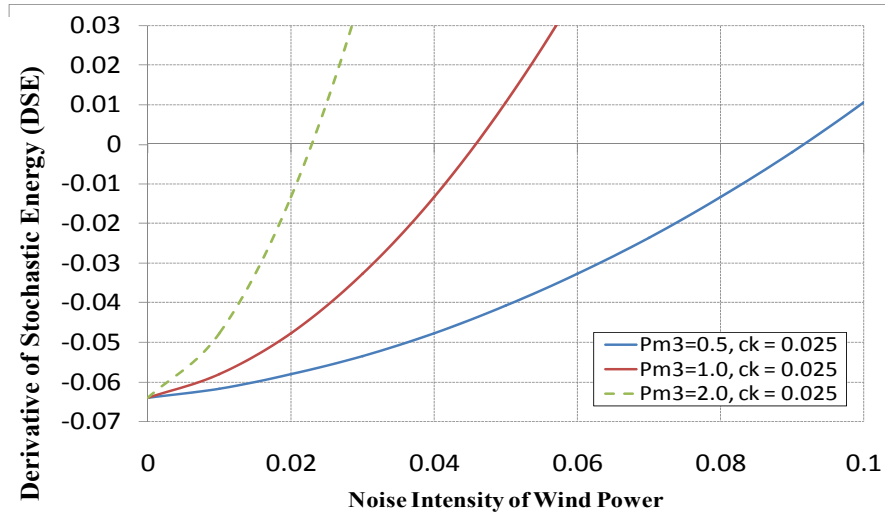


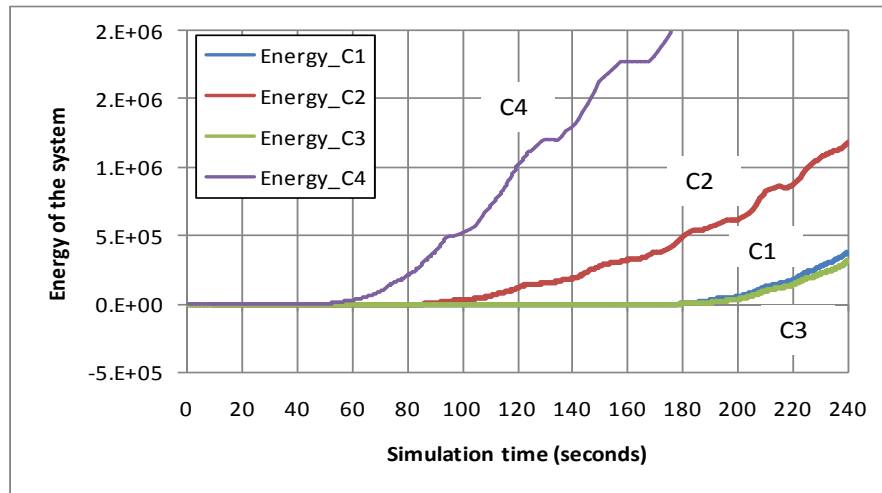
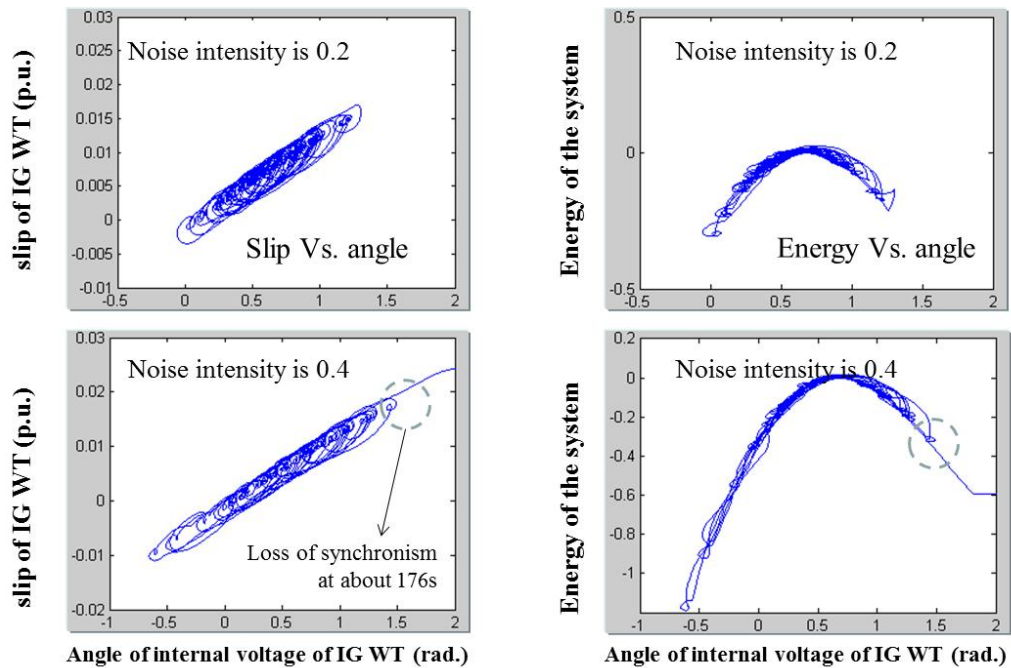
Figure 6.2 DSE compared with noise intensity of wind power (α_3) at different wind powers (P_{m3} , p.u.) when frequency dependent coefficient, $c_k = 0.025$.

7) Verification of the results

To illustrate an example of DSE , the system equations in Eq.6-1 are studied using a computer simulation. The energy in Eq.6-2 is computed and compared between 4 testing conditions (C1 to C4) with the system parameters in Table 6.1. The testing conditions and the results of the stochastic index, namely the exit time [9] (the time in which the synchronized speed increases beyond the critical value, in this case is 1.02, and results in lost synchronism) are represented in Figure 6.3.

Table 6.1 Testing conditions and results of exit times compared with *DSE*

Conditions	C1	C2	C3	C4
Noise intensity (α)	0.2	0.5	0.2	0.2
Mechanical Wind Power (P_{m3}), p.u.	2.0	2.0	2.0	3.0
frequency dependent coefficient (c_k)	0.025	0.025	0.1	0.025
Exit time (seconds)	176	85	176	47
DSE	3.67	22.75	3.72	8.24
Rate of change of Energy	6667	8750	6667	16667

**Figure 6.3** Energy of the test system under 4 test conditions C1 – C4 .**Figure 6.4** Phase portraits of slip-angle (left) and energy-angle (right) of IG wind turbine when noise intensity increase from 0.2 (upper) to 0.4 (lower).

From the results in Figure 6.3 and Table 6.1, it can be seen that the small but continuous fluctuations of wind power and state variables can finally cause the system to become unstable due to loss of synchronism. The energy of the system in Figure 6.3 increases with the different rate. If compare C1 and C2 when noise intensity increases 1.5 times, the exit time decreases 0.52 times, DSE increase 5.2 times and the rate of change of energy increase 0.3 times. For C1 as compared with C4, when wind power increases 0.5 times, the exit time decreases 0.73 times DSE increases 1.25 times and the rate of change of energy increases 1.5 times.

However, for C1 as compared with C3, the frequency dependent coefficient (c_k) has no significant effect on the exit time, whereas a small deviation on the system energy of 16.3% is observed at 240 seconds. Figure 6.4 represents the phase portrait of slip and angle of IG WT and the phase portrait of energy and angle of IG WT of the condition C1. The loss of synchronism occurs when the noise intensity of wind power increases from 0.2 to be 0.4 .

When the P_{m3} is reduced to 0.5 p.u., while the other terms remain the same with the case C1. The loss of synchronism is not observed within the simulation time period 240 seconds. Furthermore, the contribution of each term in Eq.6-4 is provided in Table 6.2. The contribution of the first (Lu_1) and the third (Lu_3) terms have shown to be more than 99.7%. This empirically justifies the formulation of the DSE in Eq.6-5.

Table 6.2 Contribution of Lu components

Conditions	% Contribution of Lu components at time 60s				
	Lu_1 (-)	Lu_2 (-)	Lu_3 (+)	Lu_4 (-)	Lu_5 (+)
Case A1	51.9%	0.0%	47.9%	0.2%	0.0%
Case C1	2.4%	0.0%	97.3%	0.3%	0.0%

8) Conclusion

The derivative of stochastic energy (DSE) proposed in this section can be used to estimate the impact of fluctuating wind power to the power system. The stochastic differential equation and the energy function of the power system are used to compute DSE . The wind turbine induction generator model (SCIG wind turbine) is included in the formulation of the energy function and to the DSE . The stability of the power system which is measured by the exit time, decreases with increasing of wind power and its noise intensity. In this study, if mean wind speed is constant while its noise intensity is varied,

the *DSE* is corresponded to the inverse of exit time. This index gives an alternative idea for power system stability analysis by stochastically incorporating the wind power.

With the stated assumptions, the *DSE* can capture the system characteristics and estimate the power system stability with less computational effort. The wind turbine model may be improved in the future work for more accurate results.

6.1.1.2 The effects of stochastic wind power and stochastic load

In this subsection, the stochastic load is applied using almost the same methods as described in the previous section. However, to focus mainly on the effects of wind power and load, this section assumes testing conditions to be different from Section 6.1.1.1 as follows:

1) The power test system

The single machine infinite bus power system is focused on the effects of wind power and electric load. The single line diagram of this test system is shown in Figure 6.5.

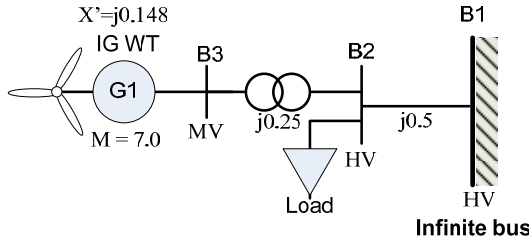


Figure 6.5 Single machine infinite bus power test system including wind power and load

2) The stochastic differential equations (SDE)

The structure preserving model power systems in this section consists of differential equations (rotor dynamics of IG of wind turbines and dynamic of load), and the algebraic equations (network equation in power balance form, and stator voltage coefficients of IG). The stochastic differential equations of the power system are applied from Section 4.8.1, which can be represented as follows:

$$d \begin{bmatrix} x_w \\ x_k \\ y_w \end{bmatrix} = \begin{bmatrix} \omega_0 (y_w - y_1) - k_b V_{sw} \sin(k_a x_w + c_b) \\ -\frac{1}{c_k} (\bar{P}_{lk} + \bar{P}_{ek}) - \omega_0 y_1 \\ \frac{1}{M_w} (\bar{P}_{mw} - \bar{P}_{ew}) \end{bmatrix} dt + \begin{bmatrix} 0 \\ 0 \\ \frac{\bar{P}_{mw}}{M_w} \alpha_w \end{bmatrix} dW \quad \text{Eq.6-6}$$

$$\left. \begin{aligned} \bar{P}_{ew} &= \bar{V}_w \sum_{j=1, j \neq w}^n \bar{V}_j \bar{B}_{wj} \sin(x_w - x_j) \\ \bar{P}_{ek} &= \bar{V}_k \sum_{j=1, j \neq k}^n \bar{V}_j \bar{B}_{kj} \sin(x_k - x_j) \\ c_b &= k_a \delta_1 + c_a \text{ and } k_b = (\bar{X}_w - \bar{X}'_w) / (\bar{T}_0 \bar{X}'_w \bar{V}_w) \end{aligned} \right\} \quad \text{Eq.6-6}$$

Where subscript n represents total number of network bus ($n = 3$), w is wind power bus (bus 3), k is load bus (bus 2). V_w is voltage behind transient reactance. V with subscript k and j are bus voltage, δ is angle of V_w and δ' is the different angle between V_w and the stator terminal voltage (V_{sw}). B_{ij} is susceptance component between bus i and j . P_{lk} is a constant power load. P_{mw} is mechanical power of IG. P_{ew} and P_{ek} are electrical power at wind power bus and load bus, respectively. c_k is frequency dependent coefficient of load. k_a and c_a are the slope and offset of the linear relationship between δ and δ' during transient. ω_0 is rated angular speed (100π). T_0 , X , and X' are transient open-circuit time constant, open-circuit reactance, and transient or short-circuit reactance, respectively [45].

3) The well-defined energy function

The well-defined energy function of the power system and its derivative are

$$\begin{aligned} U &= \frac{1}{2} \omega_0 M_w (y_w^2 - y_w^{s2}) - \bar{P}_{mw} (x_w - x_w^s) - \omega_0 M_w y_1 (y_w - y_w^s) + \bar{P}_{lk} (x_k - x_k^s) \\ &\quad - \frac{1}{2} M_w k_b V_w (\sin(k_a x_w + c_b)(y_w - y_w^s)) - \frac{1}{2} M_w k_b V_w (\sin(k_a x_w^s + c_b)(y_w - y_w^s)) \\ &\quad - \sum_{i=1}^2 \sum_{j=i+1}^3 V_i V_j B_{ij} [\cos(x_i - x_j) - \cos(x_i^s - x_j^s)] \end{aligned} \quad \text{Eq.6-7}$$

$$\dot{U} = -c_k \dot{x}_k^2 \quad \text{Eq.6-8}$$

4) The derivative of stochastic well-defined energy function

From Section 4.8.1, the derivative of the stochastic well-defined energy function is

$$\begin{aligned} L u(x, t) &= \frac{\omega_0}{2M_3} (\bar{P}_{m3} \alpha_w)^2 + \frac{1}{2} (V_1 V_2 b_{12} \cos(x_1 - x_2) + V_3 V_2 b_{32} \cos(x_3 - x_2)) \left(\frac{\bar{P}_{l2} \alpha_k}{c_k} \right)^2 \\ &\quad - \frac{1}{c_k} (\bar{P}_{l2} + \bar{P}_{e2})^2 - \frac{1}{2} M_3 k_a k_b V_3 (y_3 - y_3^s) \cos(k_a x_3 + c_b) (\omega_0 y_3 - k_b V_3 \sin(k_a x_3 + c_b)) \\ &\quad + \frac{1}{2} k_b V_3 (\bar{P}_{m3} - \bar{P}_{e3}) (\sin(k_a x_3 + c_b) - \sin(k_a x_3^s + c_b)) \leq 0 \end{aligned} \quad \text{Eq.6-9}$$

Multiplying Eq.6-9 by c_k^2/\bar{P}_{l2}^2 , the performance index, which can be called the derivative of stochastic energy (DSE), can be found as follows:

$$DSE = -c_k \left(d\bar{P}_2' \right)^2 + \frac{c_k^2 \omega_0 \alpha_w^2}{2M_3} \left(\bar{P}_{m3}' \right)^2 + \frac{1}{2} \left(V_1 V_2 b_{12} \cos(x_1 - x_2) + V_3 V_2 b_{32} \cos(x_3 - x_2) \right) \alpha_k^2 \quad \text{Eq.6-10}$$

where P_{e2} is negative which can be replaced by $-|P_{e2}|$ and $dP_2 = P_{l2} - |P_{e2}|$ is the deviation of power on load bus, $d\bar{P}_2' = d\bar{P}_2 / \bar{P}_{l2}$ and $\bar{P}_{m3}' = \bar{P}_{m3} / \bar{P}_{l2}$.

5) The testing conditions

There are mainly three cases to be examined, which are, Case #1 (base case) when wind power and power load have no stochastic part ($\alpha_w=0$ and $\alpha_k=0$), Case #2 when only power load has stochastic part ($\alpha_w=0$), and Case #3 when only wind power has stochastic part ($\alpha_k=0$).

The per unit base power is 100MVA, the fundamental speed, $\omega_0 = 314.159$ rad/s, an inertia constant of IG, $M_3 = 7.0$ s. The frequency dependent coefficient of load, $c_k = 0.05$ as the base case. Assumes V_1 , V_2 , and V_3 are close to 1.0, b_{12} is 0.5 and b_{32} is 0.25, $x_{12} = (x_1 - x_2)$ and $x_{32} = (x_3 - x_2)$ can be varied between 0.1 to 0.5 radians. P_{l2} is a real load and α_k is noise intensity of load which can be assumed to vary between 0.05 and 0.2.

The yearly noise intensity (NI) calculated with hourly average wind power of four wind power plants in USA during 2000 – 2010 are 0.8 – 1.0 [70]. The stability of this test system can be investigated by varying the noise intensity of wind power ($\alpha_w = 0.5$ and 1.0), mechanical wind power (P_{m3}), and the power deviation on the load bus (dP_2).

6) The results

For the Case #1, the terms with α_k and α_w in Eq.6-10 are zero. The DSE always less than or equal to zero and depends linearly on c_k which has the same form of dissipative energy as represented in Eq.6-8. The noise intensity when DSE is zero is called the *critical noise intensity*. Moreover, the larger c_k means the frequency deviation on load bus is less affected by the deviation of power load which cause the system damping to increase and become more stable. The results of DSE computation of Case #2 when fix wind power and Case #3 when a fixed power load are represented in Figure 6.6. This figure represents the relationship of DSE and noise intensity of power load at different bus voltage (V_2) and frequency dependent (c_k) when fixed wind power (or $\alpha_w = 0$) and noise intensity of wind

power at different penetration ratios and frequency dependent (c_k) when the power load is fixed (or $\alpha_k=0$).

For Case #2, the stochastic terms of wind power in Eq.6-10 (term with α_w) is zero. The *DSE* is affected by c_k , α_k and the variables such as bus voltage and its phase angle. If focused only on an influence of α_k at different c_k and bus voltage (V_2) as represented in Figure 6.6, the *DSE* progressively increases with increasing α_k , while linearly decreasing with decreasing bus voltage. The critical noise intensities ($DSE=0$) are 0.25, 0.2, and 0.17 when voltage increases to be 0.6, 1.0, and 1.4 p.u., respectively. The larger c_k results in the smaller *DSE* (larger critical noise intensity of power load).

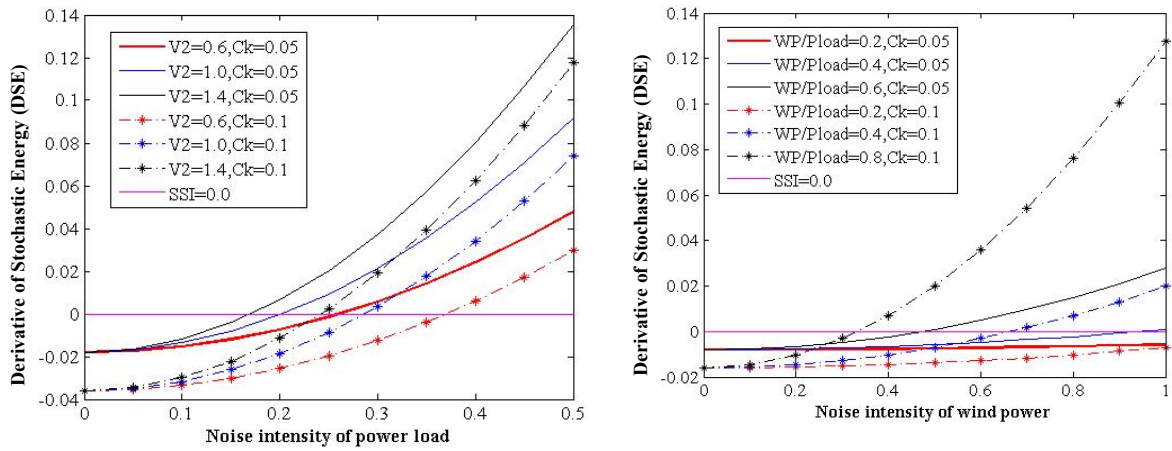


Figure 6.6 The relationship of *DSE* and the noise intensity of the power load when wind power is fixed (left) and noise intensity of wind power when power load is fixed (right)

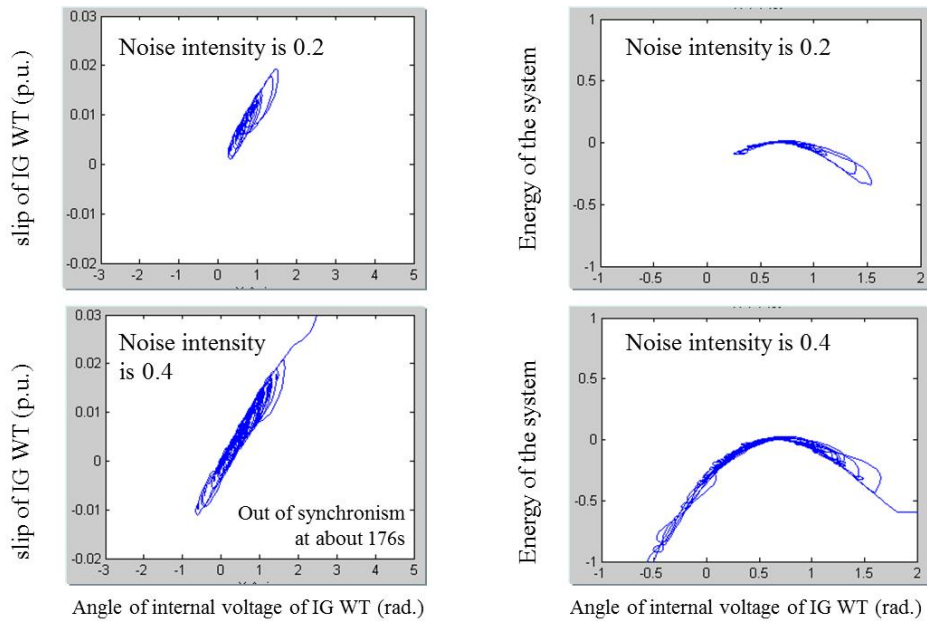


Figure 6.7 Phase portraits of slip-angle (left) and energy-angle (right) of IG wind turbine when noise intensity increase from 0.2 (upper) to 0.4 (lower) with constant load.

For Case #3, the stochastic term of the power load in Eq.6-10 (term with α_k) is zero. The DSE increase with increasing wind power (P_{m3}) and sharply increase with increasing noise intensity of wind power (α_w). The critical noise intensities ($DSE=0$) are >1.0 , 0.95 , and 0.47 when wind power penetration are 0.2 , 0.4 , and 0.6 , respectively. The effect of c_k is different from Case #2 and Case #1 such that, at small noise intensity of wind power, the larger c_k causes the smaller DSE . But for the large noise intensity, the larger c_k causes the larger DSE . Moreover, the larger c_k causes the smaller critical noise intensity.

7) Conclusion

This section applies the stochastic stability analysis method to investigate the small signal stability of the single machine infinite bus power system. The stochastic stability index is proposed to describe the effects of stochastic load and wind power.

An increase of noise intensity of both wind power and load causes the stochastic stability index to increase, and the system possibly becomes progressively unstable. When only stochastic load is represented (fix wind power), the smaller load bus voltage and the larger frequency dependent coefficient causes the lower DSE and the system possibly becomes more stable. When only stochastic wind power is represented (fix power load), the larger share of wind power leads to larger DSE and an increased in frequency dependent coefficient causes the critical noise intensity to decrease, which causes the system to be less stable.

Therefore, this method can estimate the effects of stochastic wind power and load quantitatively while the general deterministic methods cannot.

6.1.2 The Stochastic Stability Index (SSI) with Gaussian distribution of white noise

This sub-section will focus on the study of effects of stochastic wind power using the new stability performance index, which is called the stochastic stability index (SSI). For this section, the DFIG wind turbine with Gaussian distribution white noise model is applied. The following conditions are used to formulate SSI for implementation.

1) The power test system

The power test system in this section is the same as Figure 6.1 in Section 6.1.1.1, except for the SCIG wind turbine being replaced by DFIG wind turbine. The single line diagram of two machine infinite bus power system (TMIB) is represented in Figure 6.7.

In Figure 6.8, there are aggregated synchronous generators ($G2$) and aggregated DFIG wind turbines ($G3$), connecting buses $B2$ and $B3$, respectively. Bus $B1$ is an infinite

bus and B4 is a load bus. The system is assumed to be lossless for which the line resistance can be neglected. X_{14} is a line reactance (tie line) connecting between bus B1 and B4. X_{24} and X_{34} are line reactances including transformer's reactance. The electric load is a dynamic load which has c_k at about 0.05 [9]. The values of system parameters and constants are listed in Table 6.3.

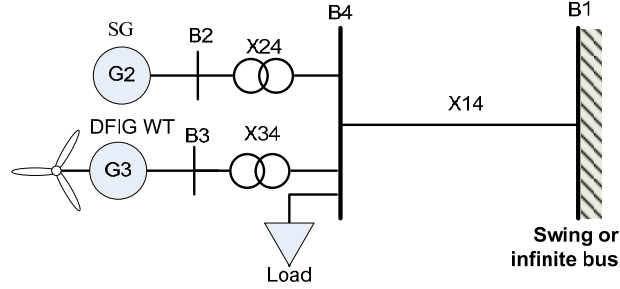


Figure 6.8 Test power system including wind power and load for DFIG WT

Table 6.3 System Parameters and Constants for TMIB

$M = 7.0$ sec	$\omega_0 = 314.2$ rad/sec	$L_m = 3.95279$ p.u.
$L_r = 0.09955$ p.u.	$L_s = 0.09241$ p.u.	$T_0 = 2.343$ p.u.
$X = 4.0$ p.u.	$X' = 0.1$ p.u.	$X_T = 0.5$ p.u.
$k_d = 0.8868$	$k_b = 7.372$	$k_a = 0.274P_m + 0.346$
$k_p = 1.0$	$k_{op} = 0.56$	$c_a = -0.022 P_m + 0.006$
$ E' = V_w = 1.05$ p.u.	$k_{c1} = 0.97396$	$k_{c2} = 1.90308$
$V_s = 1.0$ (p.u.)	$V_0 = 1.0$ (p.u.)	$k_m = 1.017$
$X_{14} = 0.5$ p.u.	$X_{24} = 0.2$ p.u.	$X_{34} = 0.2$ p.u.

2) The stochastic differential equations (SDE)

From Section 4.3.2, when the load is constant, the matrix form of stochastic differential equations will become the dynamic perturbed system in a matrix form as follows:

$$\frac{d}{dt} \begin{bmatrix} x_i \\ x_w \\ x_k \\ y_i \\ y_w \end{bmatrix} = \begin{bmatrix} \omega_0 (y_i - y_0) \\ \omega_0 (y_w - y_0) + \varphi_{df}(\mathbf{V}, \mathbf{x}) \\ \varphi_k(\mathbf{V}, \mathbf{x}) \\ \varphi_i(\mathbf{V}, \mathbf{x}) - \beta_i y_i \\ \varphi_w(\mathbf{V}, \mathbf{x}) \end{bmatrix} + \begin{bmatrix} 0 \\ 0 \\ 0 \\ 0 \\ \frac{P_{mw} \alpha_w}{M_w} \end{bmatrix} \frac{dW}{dt} \quad \text{Eq.6-11}$$

$$\left. \begin{aligned} \varphi_{df}(\mathbf{V}, \mathbf{x}) &= \omega_0 k_d \bar{V}_{rq} - k_b \bar{V}_{s3} \sin(k_a(x_w - x_{ref}) + c_a) \\ \varphi_k(\mathbf{V}, \mathbf{x}) &= -\frac{1}{c_k} (\bar{P}_{lk} + \bar{P}_{ek}) - \omega_0 y_0 \\ \varphi_i(\mathbf{V}, \mathbf{x}) &= \frac{1}{M_i} (\bar{P}_{mi} - \bar{P}_{ei}) \\ \varphi_w(\mathbf{V}, \mathbf{x}) &= \frac{1}{M_w} (\bar{P}_{mw} - \bar{P}_{ew}) \end{aligned} \right\} \quad \text{Eq.6-12}$$

Where:

$$\left. \begin{aligned} \bar{V}_{rq} &= -y_w \left(k_{c2} \bar{V}_{sw} \cos(k_a(x_w - x_{ref}) + c_a) + k_{c1} \bar{V}_w \right) + k_P \left(k_{op} (y_w + 1)^2 - k_m \bar{P}_{ew} (1 - y_w) \right) \\ \bar{P}_{ei} &= \bar{V}_i \sum_{j=1, j \neq i}^n \bar{V}_j \bar{B}_{ij} \sin(x_i - x_j) \\ \bar{P}_{ew} &= \bar{V}_w \sum_{j=1, j \neq w}^n \bar{V}_j \bar{B}_{wj} \sin(x_w - x_j) \\ \bar{P}_{ek} &= \bar{V}_k \sum_{j=1, j \neq k}^n \bar{V}_j \bar{B}_{kj} \sin(x_k - x_j) \quad \bar{P}_{ek} = \bar{V}_k \sum_{j=1, j \neq k}^n \bar{V}_j \bar{B}_{kj} \sin(x_k - x_j) \\ k_d &= \bar{L}_m / (\bar{L}_{rr} \bar{E}') \quad \text{and} \quad k_b = (\bar{X}_w - \bar{X}'_w) / (\bar{T}_0 \bar{X}'_w \bar{E}') \end{aligned} \right\} \quad \text{Eq.6-13}$$

β is a parameter to rescale the intensity of noise. For example, $\beta_i = D_i/M_i$.

3) The well-defined energy function

From Sections 4.4.3 and 4.8.2, the well-defined energy function of the power system and its derivative are:

$$\begin{aligned} U &= \frac{1}{2} \omega_0 M_2 y_2^2 - \bar{P}_{m2} (x_2 - x_2^s) - \bar{P}_{m3} (x_3 - x_3^s) + \bar{P}_{l4} (x_4 - x_4^s) \\ &+ \frac{1}{2} \omega_0 M_3 (y_3^2 - y_3^{s2}) - \frac{3}{4} M_3 k_b V_{s3} \left(\sin(k_a(x_3 - x_4) + c_a) y_3 - \sin(k_a(x_3^s - x_4^s) + c_a) y_3^s \right) \\ &+ \frac{1}{3} M_3 \omega_0 k_d k_P k_{op} \left((y_3 + 1)^3 - (y_3^s + 1)^3 \right) \\ &- \frac{1}{2} M_3 \omega_0 k_d \left[\left(k_{c2} \bar{V}_{s3} \cos(k_a(x_3 - x_4) + c_a) + k_{c1} \bar{V}_3 \right) y_3^2 - \left(k_{c2} \bar{V}_{s3} \cos(k_a(x_3^s - x_4^s) + c_a) + k_{c1} \bar{V}_3 \right) y_3^{s2} \right] \\ &- \frac{1}{4} M_3 \omega_0 k_d k_P k_m \left(\bar{P}_{e3} y_3 (3 - 2y_3) - \bar{P}_{e3}^s y_3^s (3 - 2y_3^s) \right) \\ &- \bar{V}_1 \bar{V}_4 \bar{B}_{14} \left(\cos(x_1 - x_4) - \cos(x_1^s - x_4^s) \right) \\ &- \bar{V}_2 \bar{V}_4 \bar{B}_{24} \left(\cos(x_2 - x_4) - \cos(x_2^s - x_4^s) \right) \\ &- \bar{V}_3 \bar{V}_4 \bar{B}_{34} \left(\cos(x_3 - x_4) - \cos(x_3^s - x_4^s) \right) \end{aligned}$$

Eq.6-14

$$\dot{U} = p U = - \sum_{i=1}^{m-p} \omega_0 D_i y_i^2 - \sum_{k=m+1}^n c_k \dot{x}_k^2 = -\omega_0 D_2 y_2^2 - c_k \dot{x}_4^2 \quad \text{Eq.6-15}$$

4) The derivative of a stochastic well-defined energy function

From Section 4.8.2, the derivative of a stochastic well-defined energy function is

$$\begin{aligned} Lu(x, t) = & -c_k \left(\frac{dx_4}{dt} \right)^2 - \omega_0 D_2 y_2^2 - f_1(x_3, x_4, y_3) \left(\frac{d(x_3 - x_4)}{dt} \right) \\ & + f_2(x_3, x_4, y_3) \frac{dy_3}{dt} + f_3(x_3, x_4, y_3) (P_{m3} \alpha_3)^2 \leq 0 \end{aligned} \quad \text{Eq.6-16}$$

$$\begin{aligned} f_1(x_3, x_4, y_3) = & -\frac{1}{2} M_3 \omega_0 k_d k_a k_{c2} \bar{V}_{s3} \sin(k_a (x_3 - x_4) + c_a) y_3^2 \\ & + \frac{1}{4} M_3 \omega_0 k_d k_p k_m \bar{V}_3 \bar{V}_4 b_{34} \cos(x_3 - x_4) (3y_3 - 2y_3^2) \\ & + \frac{3}{4} M_3 k_a k_b \bar{V}_{s3} \cos(k_a (x_3 - x_4) + c_a) y_3 \end{aligned} \quad \text{Eq.6-17}$$

$$\begin{aligned} f_2(x_3, x_4, y_3) = & \frac{1}{4} M_3 k_b V_{s3} \sin(k_a (x_3 - x_4) + c_a) \\ & + \frac{1}{4} M_3 \omega_0 k_d k_p k_m \bar{V}_3 \bar{V}_4 b_{34} \sin(x_3 - x_4) \end{aligned} \quad \text{Eq.6-18}$$

$$f_3(x_3, x_4, y_3) = \frac{\omega_0}{M_3} \left(\begin{aligned} & 1 + 2k_d k_p k_{op} (y_3 + 1) + k_d k_p k_m \bar{V}_3 \bar{V}_4 b_{34} \sin(x_3 - x_4) \\ & - k_d (k_{c2} \bar{V}_{s3} \cos(k_a (x_3 - x_4) + c_a) + k_{c1} \bar{V}_3) \end{aligned} \right) \quad \text{Eq.6-19}$$

It can be noticed that, the first two terms on the right of Lu in Eq.6-16 are the same with the derivative of the energy of the deterministic system (pU). Therefore, the Lu is the derivative of the stochastic energy function which can influence the system stability the same as the derivative of energy in a deterministic system. However, it can be definitely proven that the pU is less than or equal to zero, but not for Lu .

Since Lu in Eq.6-16 is quite complicate, it is assumed that the system is started from the equilibrium state in which the derivative terms are small enough and can be neglected. Therefore, Lu will be approximated by focus only on the non-derivative terms and becomes

$$Lu' \approx f_3(x_3, x_4, y_3) (P_{m3} \alpha_3)^2 \quad \text{Eq.6-20}$$

By experiment, function f_3 is always positive under normal operating conditions. Comparing with DSE in the previous section, Lu' is always positive and influences Eq.6-16 to increase Lu while DSE can probably be positive or negative.

5) The stochastic stability index (SSI)

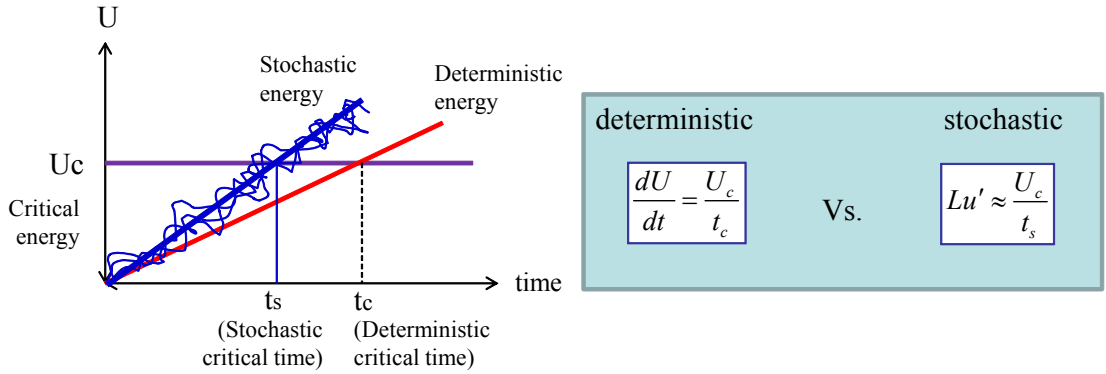
By dividing the critical energy (U_c) with the Lu' in Eq.6-20, the time that the energy takes to reach the critical value can be perceived. This conceptual time can be scaled using an appropriate parameter. For example, when Lu' is scaled by the power load term $\gamma = (c_k/P_{l4})^2$, the penetration ratio of wind power (wind power over power load) can be obtained as a result. This conceptual time is then called the *Stochastic Stability Index (SSI)* and can be computed as follows:

$$SSI = U_c / (\gamma L u') \quad \text{Eq.6-21}$$

This *SSI* is improved from the previous work in the previous section and has the same concept with the mean first passage time (*MFPT*), which is the performance index to quantify the average time that a state-space trajectory takes to change from a given operating point to the boundary of its domain of attraction under the influence of small perturbations.

Remark:

The derivative of the energy of the stochastic system can be conceptually compared with the deterministic system as follows:



The t_c is the critical time when the energy of the deterministic system increases to reach the critical value (U_c) while the t_s is for the stochastic system ($SSI = t_s$).

6) The testing conditions

The testing conditions are represented in Table 6.4. From this table, the steady state value of speed and angle are represented according to six conditions. These steady state values are from the simulation using Eqs.6-11 – 6-13. The power exchange (P_{Exchange}) is calculated from the power load (P_{load}) minus the generation power ($P_{m3} + P_{m2}$).

Table 6.4 Testing conditions for DFIG wind turbine with white noise model

Variable	Case 1 (*)	Case 2 (.)	Case 3 (+)	Case 4 (o)	Case 5 (◇)	Case 6 (□)
P_{Load}	4	4	4	4	4	4
P_{m3}	1.0	1.0	1.0	0.4	0.6	0.8
P_{m2}	3.0	4.0	2.0	3.6	3.4	3.2
$P_{Exchange}$	0.0	-1.0	1.0	0.0	0.0	0.0
y_3S	0.1129	0.1129	0.1129	-0.037	0.0174	0.0670
x_2S	0.6435	1.7754	-0.4365	0.8038	0.7478	0.6945
x_3S	0.2897	1.1385	-0.5584	0.1143	0.1723	0.2306
x_4S	0.0000	0.8480	-0.8481	0.0000	0.0000	0.0000

7) The results

The results of critical energy computation from the simulation corresponding 6 test conditions are represented in Table 6.5. The phase portraits of state variables (speed and angle) are represented in Figure 6.9. The results of Lu' and SSI computation corresponding to 6 testing conditions are represented in Figures 6.10 and 6.11, respectively.

Table 6.5 Critical energy of the test system with DFIG wind turbine and white noise model

Unstable condition 1	Case 1	Case 2	Case 3	Case 4	Case 5	Case 6
$\mathbf{x} = \{\pi - x_2^s, x_3^s, x_4^s, y_2^s, y_3^s\}$	2.44	2.75×10^{-6}	0.56	1.42	1.74	2.08
$\mathbf{x} = \{x_2^s, \pi - x_3^s, x_4^s, y_2^s, y_3^s\}$	4.95	951.06	1503.56	5.44	8.94	7.06
$\mathbf{x} = \{x_2^s, x_3^s, \pi - x_4^s, y_2^s, y_3^s\}$	803.46	1733.92	694.02	158.20	99.84	434.65
Unstable condition 2						
$\mathbf{x} = \{-\pi - x_2^s, x_3^s, x_4^s, y_2^s, y_3^s\}$	21.29	25.13	13.13	24.04	23.10	22.18
$\mathbf{x} = \{x_2^s, -\pi - x_3^s, x_4^s, y_2^s, y_3^s\}$	26.04	933.67	1519.41	0.13	14.71	21.56
$\mathbf{x} = \{x_2^s, x_3^s, -\pi - x_4^s, y_2^s, y_3^s\}$	764.83	1703.79	733.01	175.14	72.72	400.41
Unstable condition 3						
$\mathbf{x} = \{\pi - x_2^s, \pi - x_3^s, \pi - x_4^s\}$	1343.35	3811.57	24557.40	20.77	403.82	859.82
Unstable condition 4						
$\mathbf{x} = \left\{ \begin{array}{l} -\pi - x_2^s, -\pi - x_3^s \\ , -\pi - x_4^s \end{array} \right\}$	1271.75	3694.66	23482.30	36.93	337.80	789.39
Critical Energy (Minimum)	2.44	2.75×10^{-6}	0.56	0.13	1.74	2.08

From the results in Table 6.5, the critical energy has both positive and negative values. For the Case 1-3, the critical energy decreases when the magnitude of the power exchange increases, especially when export power to infinite bus. For the Case 4-6, the

critical energy increase when wind power increases. Therefore, it can be found that under steady state conditions, wind power can improve the stability of the power system.

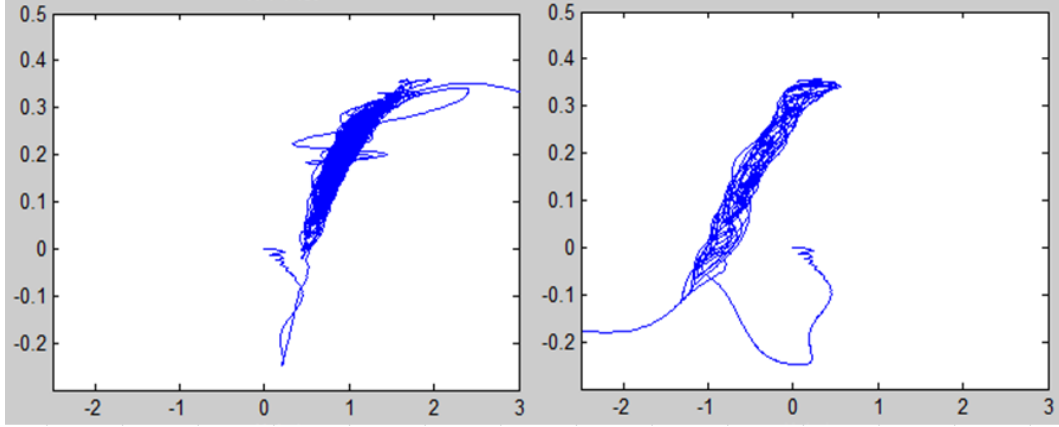


Figure 6.9 Phase portrait of speed (x-axis)-angle (y-axis) of G3 of Case 2 (left) and Case 3 (right) when noise intensity is 0.4 and 0.8, respectively

From Figure 6.10, the Lu' increases gradually with increasing noise intensity (α_3) and wind power penetration (WPP). However, Lu' cannot distinguish between Cases 1, 2 and 3 which have the same WPP but different exchanged power.

From Figure 6.11, the larger value of SSI implies that the system is possibly more stable. It can be seen from this figure that, SSI decreases with increasing of noise intensity (α_3). For the Cases 4 – 6, when WPP increase, the critical energy increase while the SSI decrease. For the deterministic method, the power system is more stable when wind power increase [45] but for this stochastic method, the power system becomes less stable at the same condition. However, for the Cases 1 – 3, the results of SSI are corresponded to the critical energy and exit time in Table 6.6. If the critical regulation time response (t_R) of the power system is 10 minutes (600 seconds), the critical noise intensities (NI_C) in which $SSI = t_R$ are 0.88, 0.67, 0.54, and 0.26 for the Cases 4, 5, 6, and 1, respectively. When noise intensity is greater than NI_C , SSI will less than t_R and the power system is possibly unstable before the regulation system can take action.

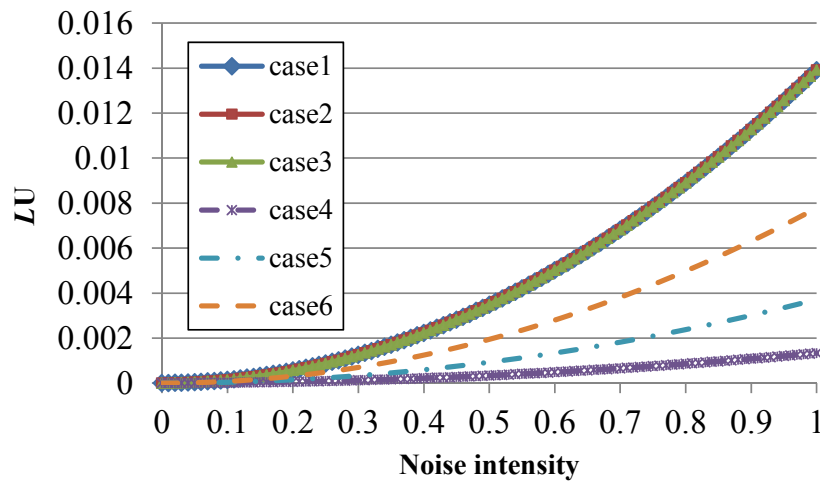


Figure 6.10 The results of Lu' computation with increasing noise intensity compared among 6 testing conditions for DFIG wind turbine with white noise model

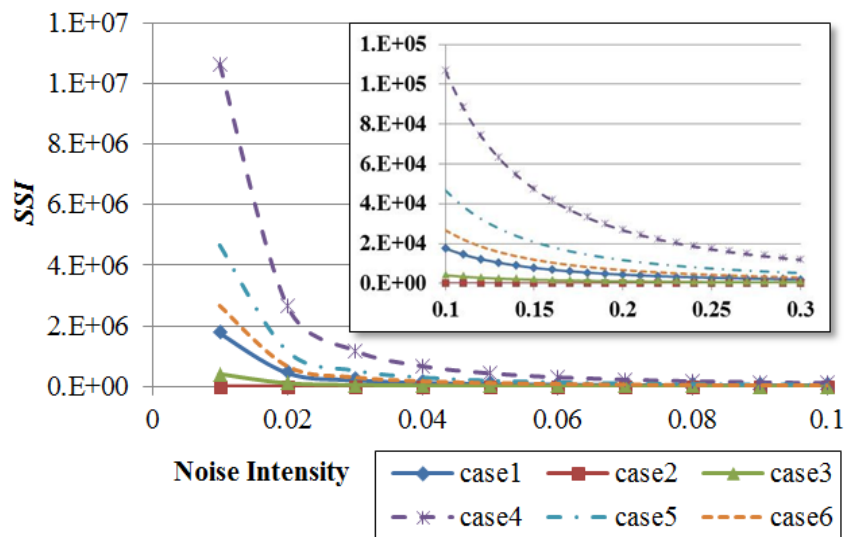


Figure 6.11 The relation of SSI (seconds) and noise intensity compared among 6 testing conditions for DFIG wind turbines with white noise model

8) Verification of the results

The results of Section (7) are verified by comparing with the averaged exit time from 20 trials of simulation. The exit times of six different conditions are shown in Table 6.6.

Table 6.6 The exit time (seconds) of six different conditions from the simulation

Variable	Case1 (*)	Case2 (.)	Case3 (+)	Case4 (o)	Case5 (◇)	Case6 (□)
P_{Load}	4	4	4	4	4	4
P_{m3}	1.0	1.0	1.0	0.4	0.6	0.8
P_{m2}	3.0	4.0	2.0	3.6	3.4	3.2
$P_{Exchange}$	0.0	-1.0	1.0	0.0	0.0	0.0
U_c	2.44	2.7E-6	0.56	1.42	1.74	2.08
ET, NI 0.4	>1000	63	>1000	>1000	>1000	>1000
ET, NI 0.6	>1000	47	321	>1000	>1000	>1000
ET, NI 0.8	>1000	46	74	>1000	>1000	>1000
SSI, NI 0.4	1097	0	252	6661	2926	1670
SSI, NI 0.6	488	0	112	2960	1300	742
SSI, NI 0.8	274	0	63	1665	731	418

* ET = Exit Time (average value of 20 trials of simulation), NI = Noise Intensity

From Case 2 and Case 3 in Table 6.6, when there is exchanged power, the exit time from the simulation decreases with increasing noise intensity. The zero values of *SSI* in Case 2 represent the close-to instability condition according to the near-zero critical energy. Furthermore, the exit time of Case 2 is less than that of Case 3, which corresponds to the value of critical energy and the *SSI*. However, for the other cases, even the simulation time is very much longer than 1000 seconds and the noise intensity is 1.0, the system still be stable and need more experiments to verify. For Case 4 (base case), 5, 6 and 1, when wind power increase 50%, 100%, and 150%, the *SSI* decrease about 56%, 75%, and 84%, respectively, comparing with base case.

9) Conclusion

This section proposes the stochastic stability analysis method, which is suitable for the study of the effects of DFIG wind turbines on power system stability, and can capture the effects of exchanged power with the infinite bus.

The wind power is modeled using aggregated DFIG wind turbines, which have the largest contribution in the market at present. The stochastic stability index (*SSI*) can quantitatively reveal the effects of increasing wind power and its noise intensity on power system stability. When the stochastic wind power increases, *SSI* will decrease and the system is less stable, especially when there is exchanged power to or from an infinite bus.

The values of *SSI* correspond to the exit times from the simulation. This stochastic stability analysis method can evaluate the nonlinear and stochastic power system stability with less time and computational effort.

6.1.3 The Stochastic Stability Index (SSI) for Gaussian distribution colored noise

In the previous section, the Gaussian distribution white noise model is an ideal noise model used in the stochastic stability analysis. However, this section will focus on the Gaussian distribution of the colored noise model, which is more practical and can be adjusted depending on bandwidth. The larger bandwidth results in being closer to the effect of white noise. The following conditions are used to formulate SSI for the study.

1) The power test system

The power test system in this section is the same as Section 6.1.2.

2) The stochastic differential equations (SDE)

The stochastic differential equations (SDE) of the power system will become the dynamic perturbed system in a matrix form as follows:

$$\frac{d}{dt} \begin{bmatrix} x_i \\ x_w \\ x_k \\ y_i \\ y_w \\ v_w \\ v_k \end{bmatrix} = \begin{bmatrix} \omega_0 (y_i - y_0) \\ \omega_0 (y_w - y_0) + \varphi_{df}(\mathbf{V}, \mathbf{x}) \\ \varphi_k(\mathbf{V}, \mathbf{x}) + \gamma_k v_k \\ \varphi_i(\mathbf{V}, \mathbf{x}) - \beta_i y_i \\ \varphi_w(\mathbf{V}, \mathbf{x}) + \gamma_k \gamma_{wk} v_w \\ -\psi_w v_w \\ -\psi_k v_k \end{bmatrix} + \gamma_k \begin{bmatrix} 0 \\ 0 \\ 0 \\ 0 \\ 0 \\ \gamma_{wk} \psi_w \\ \psi_k \end{bmatrix} \frac{dW}{dt} \quad \text{Eq.6-22}$$

$$\left. \begin{aligned} \varphi_{df}(\mathbf{V}, \mathbf{x}) &= \omega_0 k_d \bar{V}_{rq} - k_b \bar{V}_{s3} \sin(k_a (x_w - x_{ref}) + c_a) \\ \varphi_k(\mathbf{V}, \mathbf{x}) &= -\frac{1}{c_k} (\bar{P}_{lk} + \bar{P}_{ek}) - \omega_0 y_0 \\ \varphi_i(\mathbf{V}, \mathbf{x}) &= \frac{1}{M_i} (\bar{P}_{mi} - \bar{P}_{ei}) \\ \varphi_w(\mathbf{V}, \mathbf{x}) &= \frac{1}{M_w} (\bar{P}_{mw} - \bar{P}_{ew}) \end{aligned} \right\} \quad \text{Eq.6-23}$$

where $\beta_i = D_i/M_i$. $P_{ml} = \alpha P_{ms} v$, v_w represents colored noise applying to wind power, α_w and ψ_w are noise intensity (the standard deviation divided by mean value) and bandwidth of low frequency component of wind power. P_{lk} ($1 - \alpha_k v_k$) is stochastic power load, v_k represents colored noise applying to power load, α_k and ψ_k are noise intensity and bandwidth of power load.

$$\left. \begin{aligned}
\bar{V}_{rq} &= -y_w \left(k_{c2} \bar{V}_{sw} \cos \left(k_a (x_w - x_{ref}) + c_a \right) + k_{c1} \bar{V}_w \right) + k_P \left(k_{op} (y_w + 1)^2 - k_m \bar{P}_{ew} (1 - y_w) \right) \\
\bar{P}_{ei} &= \bar{V}_i \sum_{j=1, j \neq i}^n \bar{V}_j \bar{B}_{ij} \sin(x_i - x_j) \\
\bar{P}_{ew} &= \bar{V}_w \sum_{j=1, j \neq w}^n \bar{V}_j \bar{B}_{wj} \sin(x_w - x_j) \\
\bar{P}_{ek} &= \bar{V}_k \sum_{j=1, j \neq k}^n \bar{V}_j \bar{B}_{kj} \sin(x_k - x_j) \quad \bar{P}_{ek} = \bar{V}_k \sum_{j=1, j \neq k}^n \bar{V}_j \bar{B}_{kj} \sin(x_k - x_j) \\
k_d &= \bar{L}_m / (\bar{L}_{rr} \bar{E}') \quad \text{and} \quad k_b = (\bar{X}_w - \bar{X}'_w) / (\bar{T}_0 \bar{X}'_w \bar{E}')
\end{aligned} \right\}$$

Eq.6-24

Where γ_w is scaling factor of wind power noise which is formulated using the method by C.O. Nwankpa and S.M. Shahidehpour (1991) as follows:

$$\gamma_w = \frac{P_{ms} \alpha_w}{M_w} = \sqrt{2\beta \varepsilon_{lw} \varepsilon_w} \quad \text{Eq.6-25}$$

$$\sqrt{\varepsilon_{lw}} = \inf \left\{ \frac{P_{ms} \alpha_w}{M_w \sqrt{2\beta}} \middle| \alpha_w > 0 \right\} \quad \text{and} \quad \sqrt{\varepsilon_w} = \frac{P_{ms} \alpha_w}{M_w \sqrt{2\beta \varepsilon_{lw}}} \quad \text{Eq.6-26}$$

Where ε_{lw} is the noise scaling factor of wind power bus which has lowest value and ε_w is the noise scaling factor of wind power bus w . β is a parameter to rescale the intensity of noise for mathematical convenience. The γ_k is scaling factor of power load as follows:

$$\gamma_k = \frac{P_{lk} \alpha_k}{c_k} = \sqrt{2\beta \varepsilon_{lk} \varepsilon_k} \quad \text{Eq.6-27}$$

$$\sqrt{\varepsilon_{lk}} = \inf \left\{ \frac{P_{lk} \alpha_k}{c_k \sqrt{2\beta}} \middle| \alpha_k > 0 \right\} \quad \text{and} \quad \sqrt{\varepsilon_k} = \frac{P_{lk} \alpha_k}{c_k \sqrt{2\beta \varepsilon_{lk}}} \quad \text{Eq.6-28}$$

Where ε_{lk} is the noise scaling factor of load bus which has lowest value and ε_k is the noise scaling factor of load bus k . β is a parameter to rescale the intensity of noise for mathematical convenience.

Furthermore, it is assumed that

$$\gamma_{wk} = \frac{\gamma_w}{\gamma_k} = \frac{\sqrt{\varepsilon_{lw} \varepsilon_w}}{\sqrt{\varepsilon_{lk} \varepsilon_k}} = \frac{\bar{P}_{wm} \alpha_w}{\bar{P}_{lk} \alpha_k} \frac{c_k}{M_w} = \bar{P}'_{wm} \frac{\alpha_w c_k}{\alpha_k M_w} \quad \text{Eq.6-29}$$

3) The well-defined energy function

From Sections 4.4.3 and 4.8.2, the well-defined energy function of the power system and its derivative are:

$$\begin{aligned}
 U = & \frac{1}{2} \omega_0 M_2 y_2^2 + \frac{1}{2} \omega_0 M_3 (y_3^2 - y_3^{s2}) - \bar{P}_{m2} (x_2 - x_2^s) - \bar{P}_{m3} (x_3 - x_3^s) + \bar{P}_{l4} (x_4 - x_4^s) \\
 & - \frac{1}{2} M_3 k_b V_{s3} \left(\sin(k_a (x_3 - x_4) + c_a) + \sin(k_a (x_3^s - x_4) + c_a) \right) (y_3 - y_3^s) \\
 & + \frac{1}{3} M_3 \omega_0 k_d k_p k_{op} \left((y_3 + 1)^3 - (y_3^s + 1)^3 \right) \\
 & - \frac{1}{2} M_3 \omega_0 k_d k_p k_m \bar{V}_3 \bar{V}_4 \bar{B}_{34} \left(\frac{\sin(x_3 - x_4)}{(y_3 + 1)} + \frac{\sin(x_3^s - x_4^s)}{(y_3^s + 1)} \right) (y_3 - y_3^s) \\
 & - \frac{1}{2} M_3 \omega_0 k_d k_{c1} \bar{V}_3 (y_3^2 - y_3^{s2}) \\
 & - \frac{1}{2} M_3 \omega_0 k_d k_{c2} \bar{V}_{s3} \left(\cos(k_a (x_3 - x_4) + c_a) y_3 + \cos(k_a (x_3^s - x_4^s) + c_a) y_3^s \right) (y_3 - y_3^s) \\
 & - \bar{V}_1 \bar{V}_4 \bar{B}_{14} \left(\cos(x_1 - x_4) - \cos(x_1^s - x_4^s) \right) \\
 & - \bar{V}_2 \bar{V}_4 \bar{B}_{24} \left(\cos(x_2 - x_4) - \cos(x_2^s - x_4^s) \right) \\
 & - \bar{V}_3 \bar{V}_4 \bar{B}_{34} \left(\cos(x_3 - x_4) - \cos(x_3^s - x_4^s) \right) \\
 & - \bar{P}_{m3} \alpha_3 v_3 (x_3 - x_3^s) - P_{l4} \alpha_4 v_4 (x_4 - x_4^s) + \frac{1}{2} \bar{P}_{m3} \alpha_3 (v_3^2 - v_3^{s2}) + \frac{1}{2} \bar{P}_{l4} \alpha_4 (v_4^2 - v_4^{s2})
 \end{aligned}$$

Eq.6-30

$$\frac{dU}{dt} = -\omega_0 D_2 y_2^2 - c_k \dot{x}_4^2 - \frac{1}{\psi_w} \bar{P}_{m3} \alpha_3 \dot{v}_3^2 - \frac{1}{\psi_k} \bar{P}_{l4} \alpha_4 \dot{v}_4^2$$

Eq.6-31

4) The derivative of stochastic well-defined energy function

From Section 4.8.2 and operating points are not close to the steady state values, the derivative of stochastic well-defined energy function is:

$$\begin{aligned}
 L u(x, t) = & -\frac{D_2}{\omega_0} \left(\frac{dx_2}{dt} \right)^2 - c_k \left(\frac{dx_4}{dt} \right)^2 - \frac{1}{\psi_3} \bar{P}_{m3} \alpha_3 \left(\frac{dv_3}{dt} \right)^2 - \frac{1}{\psi_4} \bar{P}_{l4} \alpha_4 \left(\frac{dv_4}{dt} \right)^2 \\
 & - f_1(x_3, x_4, y_3) \left(\frac{d(x_3 - x_4)}{dt} \right) + f_2(x_3, x_4, y_3) M_3 \frac{dy_3}{dt} - \bar{P}_{m3} \alpha_3 (x_3 - x_3^s) \frac{dv_3}{dt} - \bar{P}_{l4} \alpha_4 (x_4 - x_4^s) \frac{dv_4}{dt} \\
 & + \frac{1}{2} (\bar{P}_{m3} \alpha_3)^3 \left(\frac{\psi_3}{M_3} \right)^2 + \frac{1}{2} (\bar{P}_{l4} \alpha_4)^3 \left(\frac{\psi_4}{c_k} \right)^2 \leq 0
 \end{aligned}$$

Eq.6-32

$$\begin{aligned}
f_1(x_3, x_4, y_3) = & \frac{1}{2} M_3 k_b V_{s3} k_a \cos(k_a(x_3 - x_4) + c_a)(y_3 - y_3^s) \\
& + \frac{1}{2} M_3 \omega_0 k_d k_p k_m \bar{V}_3 \bar{V}_4 \bar{B}_{34} \cos(x_3 - x_4)(y_3 + 1)^{-1}(y_3 - y_3^s) \\
& - \frac{1}{2} M_3 \omega_0 k_d k_{c2} \bar{V}_{s3} k_a \sin(k_a(x_3 - x_4) + c_a) y_3 (y_3 - y_3^s)
\end{aligned} \tag{Eq.6-33}$$

$$\begin{aligned}
f_2(x_3, x_4, y_3) = & \frac{1}{2} k_b V_{s3} \left(\sin(k_a(x_3 - x_4) + c_a) - \sin(k_a(x_3^s - x_4^s) + c_a) \right) \\
& + \frac{1}{2} \omega_0 k_d k_p k_m \bar{V}_3 \bar{V}_4 \bar{B}_{34} \left(\frac{\sin(x_3 - x_4)(2y_3 - y_3^s + 1)}{(y_3 + 1)^2} - \frac{\sin(x_3^s - x_4^s)}{(y_3^s + 1)} \right) \\
& + \frac{1}{2} \omega_0 k_d k_{c2} \bar{V}_{s3} \left(\frac{\cos(k_a(x_3 - x_4) + c_a)}{-\cos(k_a(x_3^s - x_4^s) + c_a)} \right) y_3^s
\end{aligned} \tag{Eq.6-34}$$

5) The stochastic stability index (SSI) formulation

By dividing the critical energy (U_c) with the LU in Eq.6-32, the time that the system takes to reach the critical energy can be perceived. This time can be scaled using an appropriate parameter. This conceptual exit time is then called the *Stochastic Stability Index (SSI)* and can be computed as follows:

$$SSI = U_c / (Lu) \tag{Eq.6-35}$$

This *SSI* is improved from the work in the previous section and has the same concept with the mean first passage time (*MFPT*), which is the performance index to quantify the average time a state-space trajectory takes to change from a given operating point to the boundary of its domain of attraction under the influence of small perturbations.

6) The testing conditions

The testing conditions are the same as in Section 6.1.2. From Table 6.7, the steady state value of speed and angle are represented according to six conditions. These steady state values are from the simulation using Eqs. 6-22 – 6-24. The power exchange (P_{Exchange}) is calculated from the power load (P_{load}) minus the generation power ($P_{m3} + P_{m2}$). The power load is assumed to be constant. Therefore, the terms which have stochastic load are zero. The bandwidth is assumed to be fixed at 1.0. However, the variation of bandwidth will also be analyzed.

Table 6.7 Testing conditions for DFIG wind turbine with colored noise model

Variable	Case 1 (*)	Case 2 (.)	Case 3 (+)	Case 4 (o)	Case 5 (◇)	Case 6 (□)
P_{Load}	4	4	4	4	4	4
P_{m3}	1.0	1.0	1.0	0.4	0.6	0.8
P_{m2}	3.0	4.0	2.0	3.6	3.4	3.2
$P_{Exchange}$	0.0	-1.0	1.0	0.0	0.0	0.0
x_{2S}	0.64284	1.56986	-0.23281	0.79943	0.74450	0.69287
x_{3S}	0.28896	0.93253	-0.35487	0.10764	0.16780	0.22856
x_{4S}	-0.00053	0.64301	-0.64434	-0.00469	-0.00302	-0.00138
y_{2S}	0.00000	0.00000	0.00000	0.00000	0.00000	0.00000
y_{3S}	0.19987	0.19987	0.19988	-0.10627	0.02582	0.12358

7) The results

7.1) The results of critical energy computation

The critical energy computation corresponding to the 6 test conditions are represented in Tables 6.8 and 6.9 for the case when X_{14} is 0.6 and 0.5, respectively.

Table 6.8 Critical energy of the test system with DFIG wind turbine and colored noise model when $X_{14} = 0.6$

Unstable condition 1	Case 1	Case 2	Case 3	Case 4	Case 5	Case 6
$\mathbf{x} = \{\pi - x_2^s, x_3^s, x_4^s, y_2^s, y_3^s\}$	2.436	0.000	0.575	1.417	1.735	2.075
$\mathbf{x} = \{x_2^s, \pi - x_3^s, x_4^s, y_2^s, y_3^s\}$	7.500	3.725	4.031	9.266	8.666	8.078
$\mathbf{x} = \{x_2^s, x_3^s, \pi - x_4^s, y_2^s, y_3^s\}$	33.962	15.085	36.047	33.271	33.576	33.805
Unstable condition 2						
$\mathbf{x} = \{-\pi - x_2^s, x_3^s, x_4^s, y_2^s, y_3^s\}$	21.286	25.133	13.141	24.037	23.098	22.182
$\mathbf{x} = \{x_2^s, -\pi - x_3^s, x_4^s, y_2^s, y_3^s\}$	13.783	10.008	10.314	11.779	12.436	13.104
$\mathbf{x} = \{x_2^s, x_3^s, -\pi - x_4^s, y_2^s, y_3^s\}$	8.829	-10.048	10.914	8.138	8.444	8.673
Unstable condition 3						
$\mathbf{x} = \{\pi - x_2^s, \pi - x_3^s, \pi - x_4^s\}$	179.851	1469.099	7002.342	71.448	107.288	143.577
Unstable condition 4						
$\mathbf{x} = \left\{ \begin{array}{l} -\pi - x_2^s, -\pi - x_3^s \\ , -\pi - x_4^s \end{array} \right\}$	146.416	1399.267	7132.752	49.226	79.703	112.291
Critical Energy (Minimum)	2.436	0.000	0.575	1.417	1.735	2.075

Table 6.9 Critical energy of the test system with DFIG wind turbine and colored noise model when $X_{14} = 0.5$

Unstable condition 1	Case 1	Case 2	Case 3	Case 4	Case 5	Case 6
$\mathbf{x} = \{\pi - x_2^s, x_3^s, x_4^s, y_2^s, y_3^s\}$	2.436	0.077	1.874	1.417	1.735	2.075
$\mathbf{x} = \{x_2^s, \pi - x_3^s, x_4^s, y_2^s, y_3^s\}$	7.500	4.733	5.236	9.266	8.666	8.078
$\mathbf{x} = \{x_2^s, x_3^s, \pi - x_4^s, y_2^s, y_3^s\}$	33.962	18.548	37.094	33.271	33.576	33.805
Unstable condition 2						
$\mathbf{x} = \{-\pi - x_2^s, x_3^s, x_4^s, y_2^s, y_3^s\}$	21.286	25.209	14.441	24.037	23.098	22.182
$\mathbf{x} = \{x_2^s, -\pi - x_3^s, x_4^s, y_2^s, y_3^s\}$	13.783	11.016	11.520	11.779	12.436	13.104
$\mathbf{x} = \{x_2^s, x_3^s, -\pi - x_4^s, y_2^s, y_3^s\}$	8.829	-6.585	11.961	8.138	8.444	8.673
Unstable condition 3						
$\mathbf{x} = \{\pi - x_2^s, \pi - x_3^s, \pi - x_4^s\}$	178.492	1408.681	7172.596	71.172	106.741	142.669
Unstable condition 4						
$\mathbf{x} = \left\{ \begin{array}{l} -\pi - x_2^s, -\pi - x_3^s \\ , -\pi - x_4^s \end{array} \right\}$	145.302	1340.025	7262.738	49.041	79.296	111.578
Critical Energy (Minimum)	2.436	0.077	1.874	1.417	1.735	2.075

From Tables 6.8 and 6.9, the critical energy increases with increasing wind power. Furthermore, when X_{14} decreases (or shorter transmission line), almost the conditions are unchanged except in Case 2 and Case 3 in which the critical energy increases. The critical energy of Case 2 is less than Case 3, therefore, the power when is transferred to infinite bus has more influence to power system stability than when receive from infinite bus.

7.2) The results of *SSI* and *Lu* computation

When assuming all the derivative terms in *Lu* are very small and be negligible, the *Lu* becomes *Lu'* and can be computed using non-derivative terms (such as the last two terms in Eq.6-32) and be represented in Figures 6.12 and 6.13, respectively.

In Figure 6.12, *Lu'* increase gradually with increasing of wind power and its noise intensity. However, *Lu'* of the Case1, Case2, and Case3 are not different according to the same values of wind power.

In Figure 6.13, for Case 1 – Case 3, the *SSI* of Case 2 is the lowest, followed by Case 3 and Case 1, respectively which are agree with the critical energy in Tables 6.8 and 6.9. For the Case 4 – Case 6, the *SSI* decreases gradually with increasing of wind power and its noise intensity. These results conform to the results in Section 6.1.2 (when applying white noise models), but with the different values of *SSI*. For this section (colored noise with bandwidth 1.0), the critical noise intensities (NI_C) in which $SSI = t_R$ (regulation time

response is 10 minutes or 600 seconds) are >1.0 , >1.0 , 0.87 , and 0.74 for the Case 4, 5, 6, and 1, respectively.

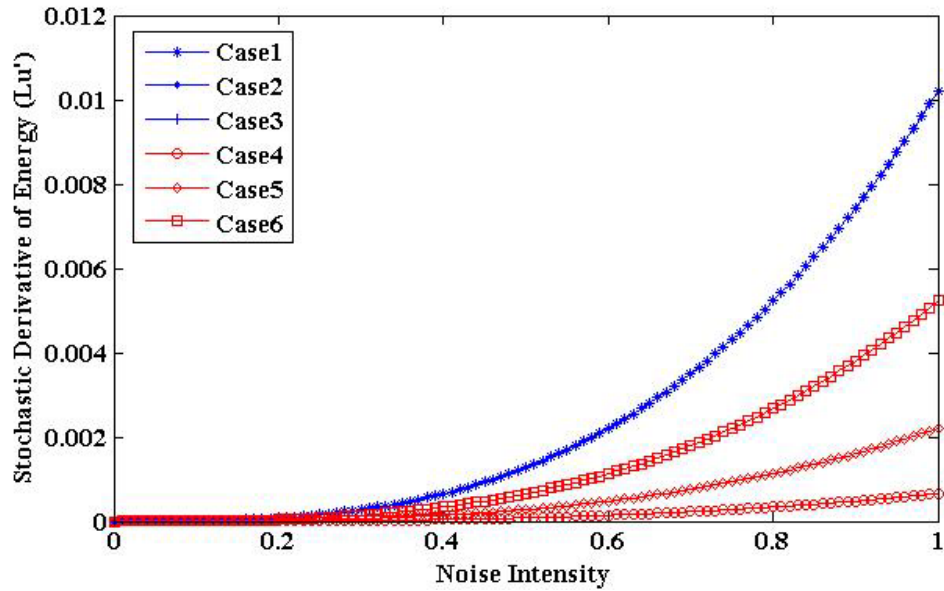


Figure 6.12 The results of Lu' computation with increasing noise intensity under 6 testing conditions for DFIG wind turbine with colored noise model

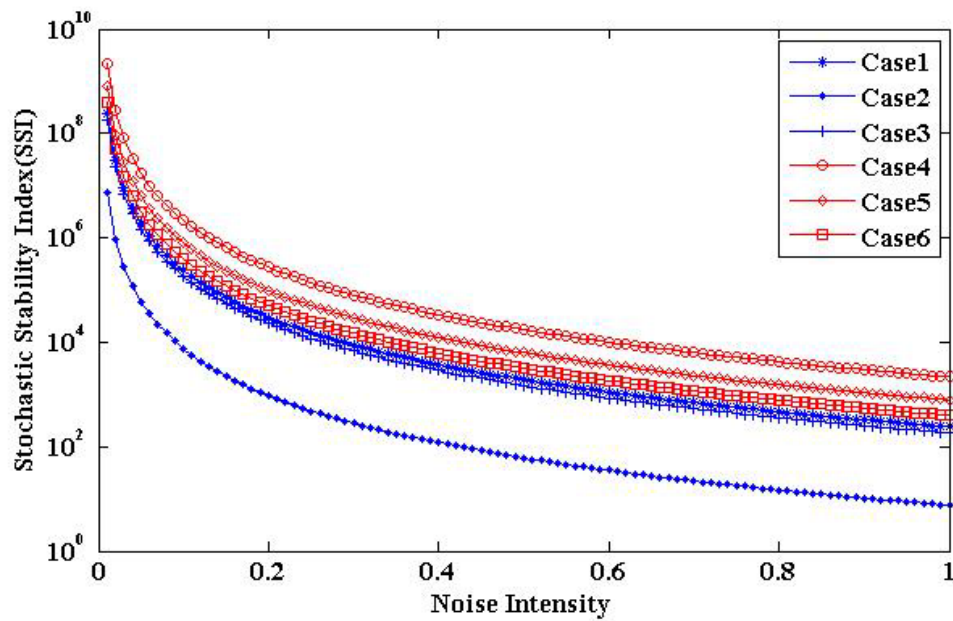


Figure 6.13 The log-scale SSI (y-axis, seconds) with increasing of noise intensity (x-axis) under 6 testing conditions for DFIG wind turbine with colored noise model

7.3) Investigation of state variables, energy, and Lu from the simulation

For Case 2 with noise intensity 0.3, bandwidth 10, and Trial no. 1, the 600 seconds of simulation reveals that the exit time is about 318 seconds. The mechanical wind power is represented in Figure 6.14. The phase angle of synchronous generator (G2), DFIG wind turbine (G3), and load are represented in Figure 6.15. The angular speed of synchronous generator (G2) and DFIG wind turbine are represented in Figure 6.16.

In Figure 6.14, it can be seen that the wind power is decreases a lot at about 315 - 316 seconds. During this time, all phase angles are decrease vastly while angular speed of G2 is increase gradually as be represented in Figure 6.15. Consequently in Figure 6.16, the angular speed of G2 increases continuously until beyond the limit value at 0.02 p.u. (unstable).

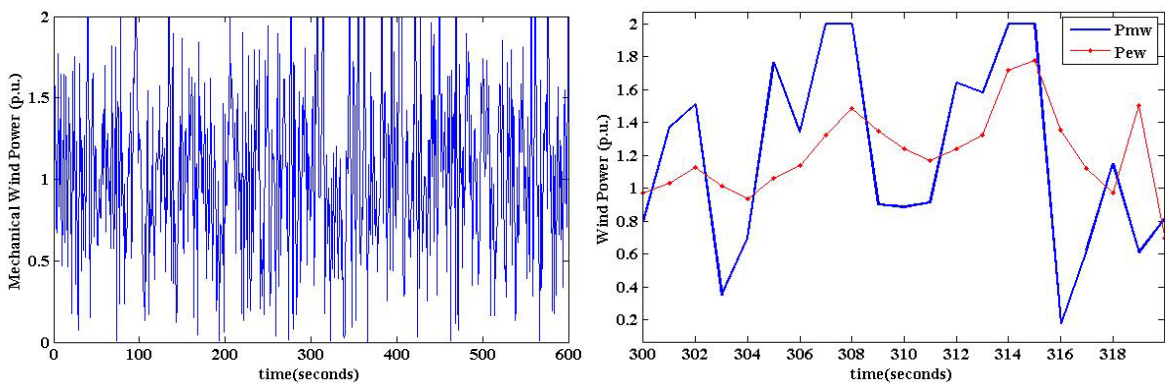


Figure 6.14 The variation of mechanical wind power during 600 seconds of simulation

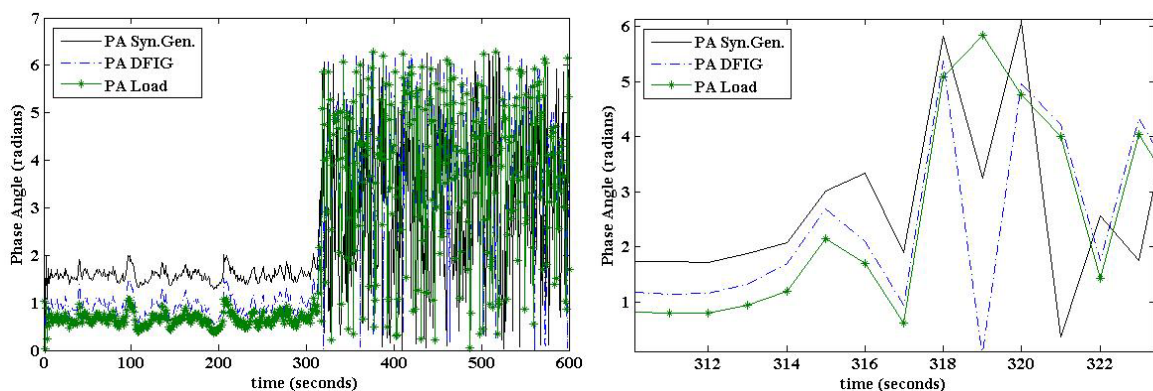


Figure 6.15 The variation of phase angle of G2 (PA Syn.Gen.), G3 (PA DFIG), and load (PA Load) during 600 seconds of simulation (left) and 311 – 323 seconds (right).

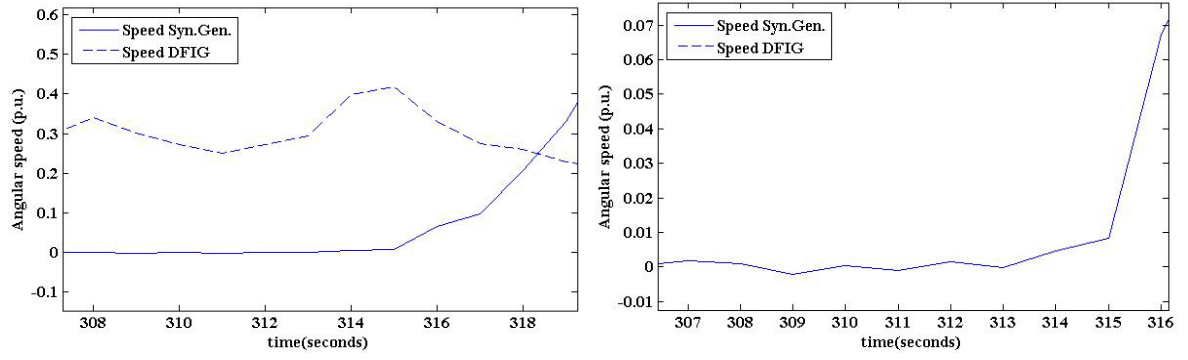


Figure 6.16 The variation of angular speed of G2 (Speed Syn.Gen.) and G3 (Speed DFIG) during 307 – 319 seconds (left) and 306 – 316 seconds (right).

During 0 – 318 seconds, the phase portrait of phase angle and angular speed of G2 and G3 are represented in Figure 6.17. From this figure, the trajectory (operating point) seems to out of bound and back again during 314 – 317 seconds. After that, the trajectory is completely out of bound.

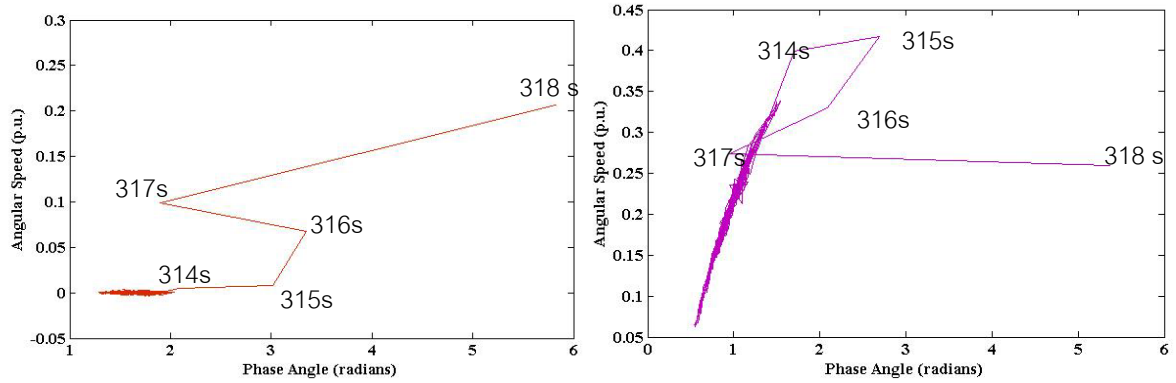


Figure 6.17 The phase portrait of phase angle and angular speed of G2 (left) and G3 (right) during 0 – 318 seconds

For the energy of the system in Figure 6.18, the energy ($ET = U$ from Eq. 6-30) increases continuously corresponding to the energy component no.1 (or $E(1) = U(1)$ in Eq.6-30). Before 318 seconds, the energy component no. 9 ($E(9) = U(9)$) and no.7 ($E(7) = U(7)$) are most influenced, respectively. After that, the $E(1)$ has more influence and increases continuously due to an increasing speed of synchronous generator G2.

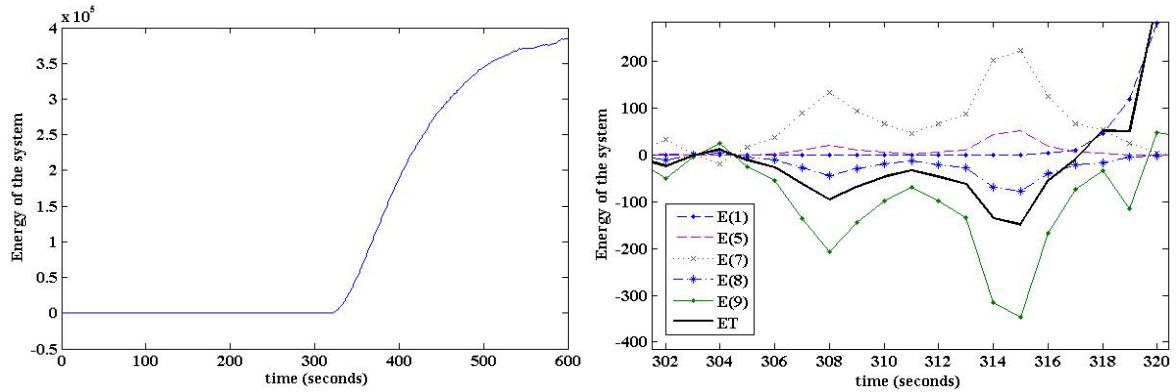


Figure 6.18 The energy of the power system during 600 seconds of simulation (left) and 302 – 320 seconds (right).

For the derivative of stochastic energy (LUT) in Figure 6.19, the most influential LU components are LU(5) and LU(6) in Eq.6-32, respectively. Comparing between Figures 6.19 and 6.15, the variation of LU is corresponded to the variation of phase angle of wind turbine (PA DFIG). It can be seen that, LU(5) in Eq.6-32 consist of the derivative of phase angle PA DFIG and phase angle of load. It can be noticed that, LU(9) is constant and always positive while the other components fluctuates alternatively.

The derivative of deterministic energy (pU) in Figure 6.20 is always negative and decreases continuously at 138 seconds which causes the trend of LUT to decrease. It can be noticed that even though the pU is negative, the power system can be unstable due to the variation of wind power.

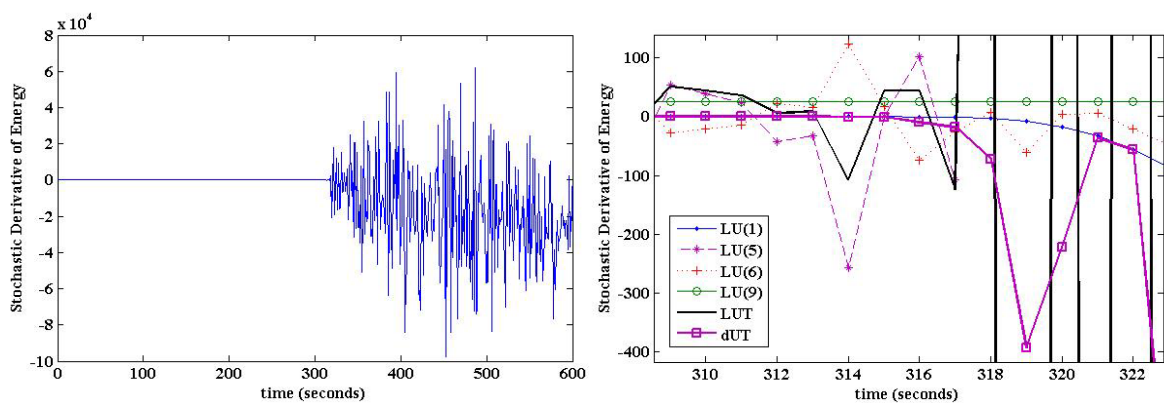


Figure 6.19 The derivative of stochastic energy of the power system (LU) during 600 seconds of simulation (left) and 308 – 323 seconds (right).

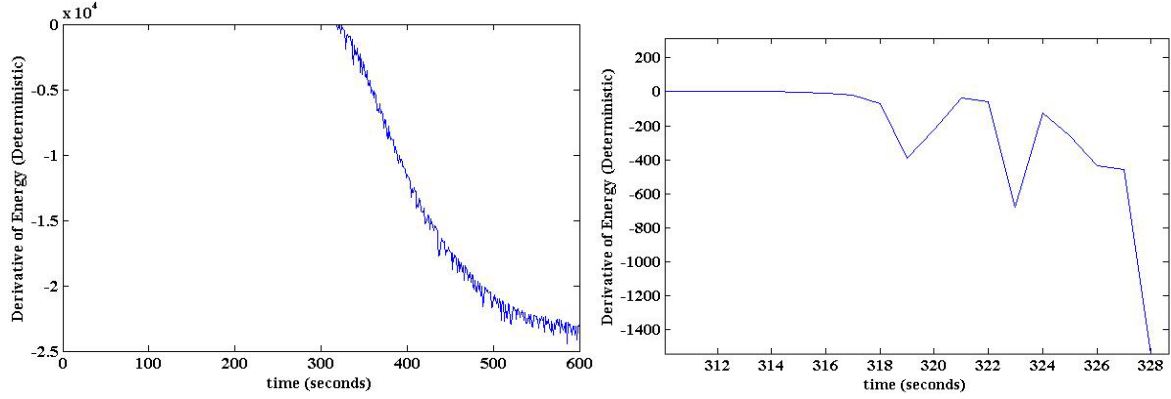


Figure 6.20 The derivative of deterministic energy of the power system (pU) during 600 seconds of simulation (left) and 310 – 329 seconds (right).

7.4) An investigation of variation and distribution of Lu

Theoretically, the positive value of Lu means the system will become unstable within a finite time. From (7.3), the component Lu (9) is investigated due to it always being positive and constant throughout the simulation period. Moreover, the Lu (9) consists of the deterministic variables which are more convenient for the power system stability analysis.

To investigate Lu (9), the three cases of testing conditions are examined in which the Lu (9) has the same value at 25.0 but Lu (5), Lu (6), and total Lu is different depending up on the noise intensity (NI) and bandwidth (BW) of wind power. The Lu (9) is represented as follows:

$$Lu(9) = 0.5 \times P_{mw} \times NI \times (BW)^2 \quad \text{Eq.6-36}$$

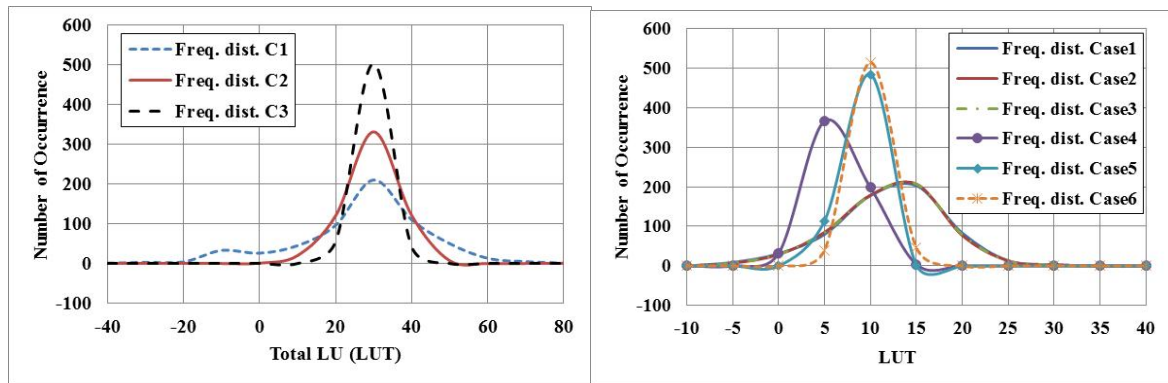
The simulation is done for 600 seconds with different conditions. From the results of simulation, the mean and standard deviation of Lu are determined and compare with the computation of Lu (9) using Eq.6-36. The testing conditions and the results are represented in Table 6.10 . From this table, for the cases C1 – C3, the mean Lu corresponds to the Lu (9) while the standard deviation of Lu corresponds to noise intensity. For Case1 – Case6, the mean Lu still corresponds to the Lu (9).

However, it was found that the standard deviation of Lu (Std Lu) does not correspond to the noise intensity or even Lu (9). Therefore, it can be concluded that the standard deviation of Lu is not clearly related to the variation of wind power.

Table 6.10 The testing conditions and results of simulation to investigate Lu

Case	Wind Power (Pmw)	Noise Intensity(NI)	Bandwidth (BW)	Mean Lu	Stdev Lu	Lu (9)
C1	1.0	0.5	10	22.76	17.47	25
C2	1.0	0.25	Sqrt(200)	24.46	7.34	25
C3	1.0	0.125	Sqrt(400)	24.84	3.65	25
Case1	1.0 (Exc. P. = 0)	0.2	10	9.69	5.83	10
Case2	1.0 (Exc. P. = 1)	0.2	10	9.69	5.76	10
Case3	1.0 (Exc. P. = -1)	0.2	10	9.69	5.78	10
Case4	0.4 (Exc. P. = 0)	0.2	10	3.94	2.35	4
Case5	0.6 (Exc. P. = 0)	0.2	10	5.92	1.28	6
Case6	0.8 (Exc. P. = 0)	0.2	10	7.84	1.77	8

Exc. P. = Exchange Power between load bus and infinite bus

**Figure 6.21** Data distribution of Lu for the case C1 – C3 (left) and Case 1 – Case 6 (right)

Data distribution of Lu for the cases C1 – C3 and Case1 – Case6 are compared as represented in Figure 6.21. The variation and data distribution of Lu for the case C1 (upper), C2 (middle), and C3 (lower) are also represented in Figure 6.22. From these figures, the mean values of Lu are always positive which imply that the system will become unstable within finite time.

In conclusion, the dominant components of Lu are component numbers 5, 6, and 9. Since the state variables of the system are varied randomly, the Lu comparing with the deviation of state variable is also random. The mean of total Lu is close to the value of Lu component number 9. However, the standard deviation of Lu is not clearly related to the standard deviation of mechanical wind power. It is found that, Lu cannot capture the different of Cases 1-3 when the exchange power between load bus and infinite bus is changed.

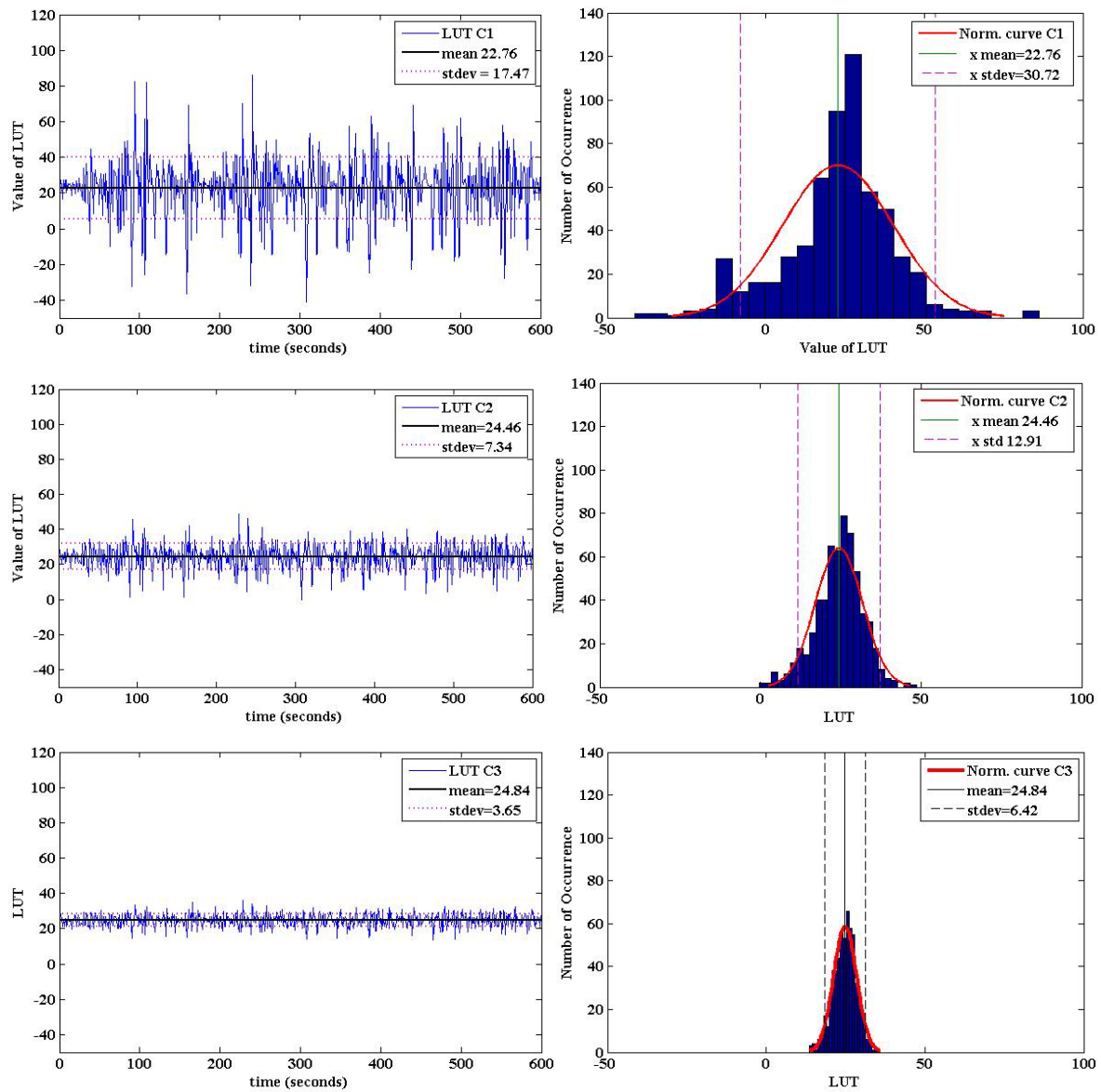


Figure 6.22 The variation (left) and data distribution (right) of Lu for the cases C1 (upper), C2 (middle), and C3 (lower)

8) Verification of the results

The results of section (7) are verified by comparing with the mean exit time from 20 trials of simulation. The exit time of 6 different conditions are shown in Table 6.11. It can be found from Table 6.11 that from Case 2 and Case 3, the exit time decreases with increasing noise intensity. Furthermore, exit time of Case 2 is less than of Case 3 which is correspond to the value of critical energy and the SSI in Figure 6.13. However, for the other cases, the exit time is longer than 3600 seconds and need more experiments to verify. For

Cases 4 (base case), 5, 6 and 1 in this section, when wind power increase 50%, 100%, and 150%, the *SSI* decrease about 64%, 82%, and 89%, respectively, comparing with base case. The *SSIs* in this section are larger than the values in Section 6.1.2, but however, the percentage of decrease in *SSI* is larger.

Table 6.11 The exit time (seconds) of six different conditions for DFIG WT with colored noise

Variable	Case 1 (*)	Case 2 (.)	Case 3 (+)	Case 4 (o)	Case 5 (◇)	Case 6 (□)
P_{Load}	4	4	4	4	4	4
P_{m3}	1.0	1.0	1.0	0.4	0.6	0.8
P_{m2}	3.0	4.0	2.0	3.6	3.4	3.2
$P_{Exchange}$	0.0	-1.0	1.0	0.0	0.0	0.0
Critical E (Uc)	2.436	0.077	1.874	1.417	1.735	2.075
ET*, NI = 0.3	>3600	227.3	943.8	>3600	>3600	>3600
ET, NI = 0.4	>3600	65.3	86.9	>3600	>3600	>3600
ET, NI = 0.5	>3600	29.1	73.6	>3600	>3600	>3600
<i>SSI</i> , NI = 0.3	8842	279.5	6802	80360	29150	14710
<i>SSI</i> , NI = 0.4	3730	117.9	2870	33900	12300	6206
<i>SSI</i> , NI = 0.5	1910	60.4	1469	17360	6297	3177

* ET = Exit Time (average value of 20 trials of simulation), NI = Noise Intensity

6.2 The Study of Effects of Wind Power on the Voltage Stability using New Stochastic Stability Method

The voltage stability is the ability of the power system to control voltage when perturbed by any disturbances. For the dynamic power system, the deviation of voltage is related to the variation of reactive power depending on the characteristic and type of electric load as be described in Section 4.1.4. This section will apply the dynamic load model including voltage deviation equation for the power system incorporating DFIG wind turbine. The colored noise of wind power and load are also modeled to represent the effects with more applicable than white noise model.

6.2.1 The Stochastic Stability Index (*SSI*) applying for voltage stability analysis

1) The power test system

The power test system in this section is the same as Section 6.1.2.

2) The stochastic differential equations (SDE)

From Section 4.3.3, the stochastic differential equations of the power system in matrix form is

$$\frac{d}{dt} \begin{bmatrix} x_i \\ x_w \\ x_k \\ y_i \\ y_w \\ V_k \\ v_w \\ v_{pk} \\ v_{qk} \end{bmatrix} = \begin{bmatrix} \omega_0 (y_i - y_0) \\ \omega_0 (y_w - y_0) + \varphi_{df}(\mathbf{V}, \mathbf{x}) \\ \varphi_{xk}(\mathbf{V}, \mathbf{x}) + \gamma_{pk} v_{pk} \\ \varphi_i(\mathbf{V}, \mathbf{x}) - \beta_i y_i \\ \varphi_w(\mathbf{V}, \mathbf{x}) + \gamma_k \gamma_{wk} v_w \\ \varphi_{vk}(\mathbf{V}, \mathbf{x}) + \gamma_{qk} v_{qk} \\ -\psi_w v_w \\ -\psi_{pk} v_{pk} \\ -\psi_{qk} v_{qk} \end{bmatrix} + \gamma_{pk} \begin{bmatrix} 0 \\ 0 \\ 0 \\ 0 \\ 0 \\ 0 \\ \gamma_{wpk} \psi_w \\ \psi_{pk} \\ \gamma_{qpk} \psi_{qk} \end{bmatrix} \frac{dW}{dt} \quad \text{Eq.6-37}$$

$$\left. \begin{aligned} \varphi_{df}(\mathbf{V}, \mathbf{x}) &= \omega_0 k_d \bar{V}_{rq} - k_b \bar{V}_{s3} \sin(k_a (x_w - x_{ref}) + c_a) \\ \varphi_{xk}(\mathbf{V}, \mathbf{x}) &= -\frac{1}{c_k} (\bar{P}_{lk} + \bar{P}_{ek}) - \omega_0 y_0 \\ \varphi_i(\mathbf{V}, \mathbf{x}) &= \frac{1}{M_i} (\bar{P}_{mi} - \bar{P}_{ei}) \\ \varphi_w(\mathbf{V}, \mathbf{x}) &= \frac{1}{M_w} (\bar{P}_{mw} - \bar{P}_{ew}) \\ \varphi_{vk}(\mathbf{V}, \mathbf{x}) &= \frac{1}{\lambda_k \bar{V}_k} (-\bar{Q}_{lk} + \bar{Q}_{ek}) \end{aligned} \right\} \quad \text{Eq.6-38}$$

$$\left. \begin{aligned} \bar{V}_{rq} &= -y_w \left(k_{c2} \bar{V}_{sw} \cos(k_a (x_w - x_{ref}) + c_a) + k_{c1} \bar{V}_w \right) + k_p \left(k_{op} (y_w + 1)^2 - k_m \bar{P}_{ew} (1 - y_w) \right) \\ \bar{P}_{ei} &= \bar{V}_i \sum_{j=1, j \neq i}^n \bar{V}_j \bar{B}_{ij} \sin(x_i - x_j) \\ \bar{P}_{ew} &= \bar{V}_w \sum_{j=1, j \neq w}^n \bar{V}_j \bar{B}_{wj} \sin(x_w - x_j) \\ \bar{P}_{ek} &= \bar{V}_k \sum_{j=1, j \neq k}^n \bar{V}_j \bar{B}_{kj} \sin(x_k - x_j) \quad \bar{P}_{ek} = \bar{V}_k \sum_{j=1, j \neq k}^n \bar{V}_j \bar{B}_{kj} \sin(x_k - x_j) \\ k_d &= \bar{L}_m / (\bar{L}_{rr} \bar{E}') \quad \text{and} \quad k_b = (\bar{X}_w - \bar{X}'_w) / (\bar{T}_0 \bar{X}'_w \bar{E}') \end{aligned} \right\}$$

Eq.6-39

Where Q_{lk} ($1 - \alpha_{qk} v_{qk}$) is the stochastic reactive power load, v_{qk} represents the colored noise applying to Q_{lk} , α_{qk} and ψ_{qk} are noise intensity and bandwidth of reactive power load, γ_{qk} is scaling factor of power load which is formulated using the method by C.O. Nwankpa and S.M. Shahidehpour (1991) as follows:

$$\gamma_{qk} = \frac{Q_{lk} \alpha_{qk}}{\lambda_k V_k} = \sqrt{2\beta \varepsilon_{lqk} \varepsilon_{qk}} \quad \text{Eq.6-40}$$

$$\sqrt{\varepsilon_{lqk}} = \inf \left\{ \frac{Q_{lk} \alpha_{qk}}{\lambda_k V_k \sqrt{2\beta}} \middle| \alpha_{qk} > 0 \right\} \quad \text{and} \quad \sqrt{\varepsilon_{qk}} = \frac{Q_{lk} \alpha_{qk}}{\lambda_k V_k \sqrt{2\beta \varepsilon_{lqk}}} \quad \text{Eq.6-41}$$

Furthermore, it is assumed that:

$$\gamma_{wpk} = \frac{\gamma_w}{\gamma_{pk}} = \frac{\sqrt{\varepsilon_{lw} \varepsilon_w}}{\sqrt{\varepsilon_{lpk} \varepsilon_{pk}}} = \frac{\bar{P}_{wm} \alpha_w}{\bar{P}_{lk} \alpha_{pk}} \frac{c_k}{M_w} = \bar{P}'_{wm} \frac{\alpha_w c_k}{\alpha_{pk} M_w} \quad \text{Eq.6-42}$$

$$\gamma_{qpk} = \frac{\gamma_{qk}}{\gamma_{pk}} = \frac{\sqrt{\varepsilon_{lqk} \varepsilon_{qk}}}{\sqrt{\varepsilon_{lpk} \varepsilon_{pk}}} = \frac{\bar{Q}_{lk} \alpha_{qk} c_k}{\bar{P}_{lk} \alpha_{pk} \lambda_k V_k} = \bar{Q}'_{lk} \frac{\alpha_{qk} c_k}{\alpha_{pk} \lambda_k V_k} \quad \text{Eq.6-43}$$

3) The well-defined energy function

From Sections 4.4.4 and 4.8.3, the well-defined energy function of the power system and its derivative are:

$$\begin{aligned} U = & \frac{1}{2} \omega_0 M_2 y_2^2 + \frac{1}{2} \omega_0 M_3 (y_3^2 - y_3^{s2}) - \bar{P}_{m2} (x_2 - x_2^s) - \bar{P}_{m3} (1 + \alpha_3 v_3) (x_3 - x_3^s) \\ & + \bar{P}_{l4} (1 - \alpha_{p4} v_{p4}) (x_{p4} - x_{p4}^s) + \frac{1}{2} \bar{Q}_{04} (1 - \alpha_{q4} v_{q4}) (\bar{V}_4^2 - \bar{V}_4^{s2}) \\ & - \frac{1}{2} M_3 k_b V_{s3} \left(\sin(k_a (x_3 - x_4) + c_a) + \sin(k_a (x_3^s - x_4^s) + c_a) \right) (y_3 - y_3^s) \\ & + \frac{1}{3} M_3 \omega_0 k_d k_p k_{op} \left((y_3 + 1)^3 - (y_3^s + 1)^3 \right) - \frac{1}{2} M_3 \omega_0 k_d k_{c1} \bar{V}_3 (y_3^2 - y_3^{s2}) \\ & - \frac{1}{2} M_3 \omega_0 k_d k_{c2} \bar{V}_{s3} \left(\cos(k_a (x_3 - x_4) + c_a) y_3 + \cos(k_a (x_3^s - x_4^s) + c_a) y_3^s \right) (y_3 - y_3^s) \\ & - \frac{1}{2} M_3 \omega_0 k_d k_p k_m \left(\frac{\bar{P}_{e3}}{(y_3 + 1)} + \frac{\bar{P}_{e3}^s}{(y_3^s + 1)} \right) (y_3 - y_3^s) \\ & + \frac{1}{2} \bar{P}_{m3} \alpha_3 (v_3^2 - v_3^{s2}) + \frac{1}{2} \bar{P}_{l4} \alpha_{p4} (v_{p4}^2 - v_{p4}^{s2}) + \frac{1}{2} \bar{Q}_{04} \alpha_{q4} (v_{q4}^2 - v_{q4}^{s2}) \\ & - \bar{V}_1 \bar{V}_4 \bar{B}_{14} \left(\cos(x_1 - x_4) - \cos(x_1^s - x_4^s) \right) - \bar{V}_2 \bar{V}_4 \bar{B}_{24} \left(\cos(x_2 - x_4) - \cos(x_2^s - x_4^s) \right) \\ & - \bar{V}_3 \bar{V}_4 \bar{B}_{34} \left(\cos(x_3 - x_4) - \cos(x_3^s - x_4^s) \right) - \frac{1}{2} B_{44} (\bar{V}_4^2 - \bar{V}_4^{s2}) \end{aligned} \quad \text{Eq.6-44}$$

$$\frac{dU}{dt} = -\omega_0 D_2 y_2^2 - c_k \dot{x}_4^2 - \lambda_4 \dot{\bar{V}}_4^2 - \frac{1}{\psi_3} \bar{P}_{m3} \alpha_3 \dot{v}_3^2 - \frac{1}{\psi_{p4}} \bar{P}_{l4} \alpha_{p4} \dot{v}_{p4}^2 - \frac{1}{\psi_{q4}} \bar{Q}_{04} \alpha_{q4} \dot{v}_{q4}^2 \quad \text{Eq.6-45}$$

4) The derivative of stochastic well-defined energy function

From Section 4.8.3 and operating points are not close to the steady state values, the derivative of stochastic well-defined energy function is:

$$\begin{aligned}
Lu(x, t) = & -\frac{D_2}{\omega_0} \left(\frac{dx_2}{dt} \right)^2 - c_k \left(\frac{dx_4}{dt} \right)^2 - \frac{1}{\psi_3} \bar{P}_{m3} \alpha_3 \left(\frac{dv_3}{dt} \right)^2 - \frac{1}{\psi_{p4}} \bar{P}_{lk} \alpha_{p4} \left(\frac{dv_{p4}}{dt} \right)^2 - \frac{1}{\psi_{q4}} \bar{Q}_{l4} \alpha_{q4} \left(\frac{dv_{q4}}{dt} \right)^2 \\
& - f_1(x_3, x_4, y_3) \left(\frac{d(x_3 - x_4)}{dt} \right) + f_2(x_3, x_4, y_3) \frac{dy_3}{dt} - f_3(x_3, x_4, y_3) \frac{d\bar{V}_4}{dt} + \lambda_k \left(\frac{d\bar{V}_4}{dt} \right)^2 \\
& - \bar{P}_{m3} \alpha_3 (x_3 - x_3^s) \frac{dv_3}{dt} - \bar{P}_{lk} \alpha_{p4} (x_4 - x_4^s) \frac{dv_{p4}}{dt} - \frac{1}{2} \bar{Q}_{04} \alpha_{q4} (\bar{V}_4^2 - \bar{V}_4^{s2}) \frac{dv_{q4}}{dt} \\
& + \frac{1}{2} \alpha_3^3 \bar{P}_{m3}^3 \left(\frac{\psi_3}{M_3} \right)^2 + \frac{1}{2} \alpha_{p4}^3 \bar{P}_{lk}^3 \left(\frac{\psi_{p4}}{c_k} \right)^2 + \frac{1}{2} \alpha_{q4}^3 \bar{Q}_{l4}^3 \left(\frac{\psi_{q4}}{\lambda_k V_4} \right)^2 \leq 0
\end{aligned}$$

Eq.6-46

Where

$$\begin{aligned}
f_1(x_3, x_4, y_3) = & \frac{1}{2} M_3 k_b V_{s3} k_a \cos(k_a (x_3 - x_4) + c_a) (y_3 - y_4^s) \\
& + \frac{1}{2} M_3 \omega_0 k_d k_p k_m \frac{(y_3 - y_3^s)}{(y_3 + 1)} (\bar{V}_3 \bar{V}_4 B_{34} \cos(x_3 - x_4)) \\
& - \frac{1}{2} M_3 \omega_0 k_d k_{c2} \bar{V}_{s3} k_a \sin(k_a (x_3 - x_4) + c_a) y_3 (y_3 - y_3^s)
\end{aligned}$$

Eq.6-47

$$\begin{aligned}
f_2(x_3, x_4, y_3) = & \frac{1}{2} k_b V_{s3} \left(\sin(k_a (x_3 - x_4) + c_a) - \sin(k_a (x_3^s - x_4^s) + c_a) \right) \\
& + \frac{1}{2} \omega_0 k_d k_p k_m \bar{V}_3 \bar{V}_4 \bar{B}_{34} \left(\frac{\sin(x_3 - x_4) (2y_3 - y_3^s + 1)}{(y_3 + 1)^2} - \frac{\sin(x_3^s - x_4^s)}{(y_3^s + 1)} \right) \\
& + \frac{1}{2} \omega_0 k_d k_{c2} \bar{V}_{s3} \left(\frac{\cos(k_a (x_3 - x_4) + c_a)}{-\cos(k_a (x_3^s - x_4^s) + c_a)} \right) y_3^s
\end{aligned}$$

Eq.6-48

$$f_3(x_3, x_4, y_3) = \frac{1}{2} M_3 \omega_0 k_d k_p k_m \frac{(y_3 - y_3^s)}{(y_3 + 1)} \bar{V}_3 B_{34} \sin(x_3 - x_4)$$

Eq.6-49

5) The stochastic stability index (SSI)

By dividing the critical energy (U_c) with Lu' (last three components of Lu) in Eq.6-46, the time that the energy takes to reach the critical value can be perceived. This conceptual time is then called the *Stochastic Stability Index (SSI)*:

$$SSI = U_c / (Lu')$$

Eq.6-50

6) The testing conditions

The testing conditions are the same as in Section 6.1.2. From Table 6.12, the steady state value of speed and angle are represented according to 6 conditions. These steady state values are from the simulation using Eqs. 6-37 – 6-39. The power exchange (P_{Exchange}) is

calculated from the power load (P_{load}) minus the generation power ($P_{m3} + P_{m2}$). The active power load is assumed constant. The bandwidth is assumed to be fixed at 1.0.

Table 6.12 Testing conditions for voltage stability analysis

Variable	Case 1 (*)	Case 2 (.)	Case 3 (+)	Case 4 (o)	Case 5 (◇)	Case 6 (□)
P_{Load}	4	4	4	4	4	4
P_{m3}	1.0	1.0	1.0	0.4	0.6	0.8
P_{m2}	3.0	3.5	2.5	3.6	3.4	3.2
P_{Exchange}	0.0	-0.5	0.5	0.0	0.0	0.0
x_2S	0.587117	1.017949	0.239299	0.777726	0.702494	0.64083
x_3S	0.280651	0.552676	0.046355	0.117212	0.171878	0.22612
x_4S	-2.7E-17	0.250562	-0.2265	-9.8E-17	-1.3E-16	-9.2E-17
y_2S	4.01E-14	-2.2E-14	-1.6E-18	4.86E-09	1.39E-10	1.91E-11
y_3S	0.199901	0.200094	0.199831	-0.03097	0.05714	0.132831

7) The results

7.1) The results of critical energy computation

In Table 6.13, the critical energy increases with increasing wind power. The critical energy of Case 2 is less than the other cases. However, the critical energy of Case 3 in this case is larger than Case 1 which is different from the results in previous section.

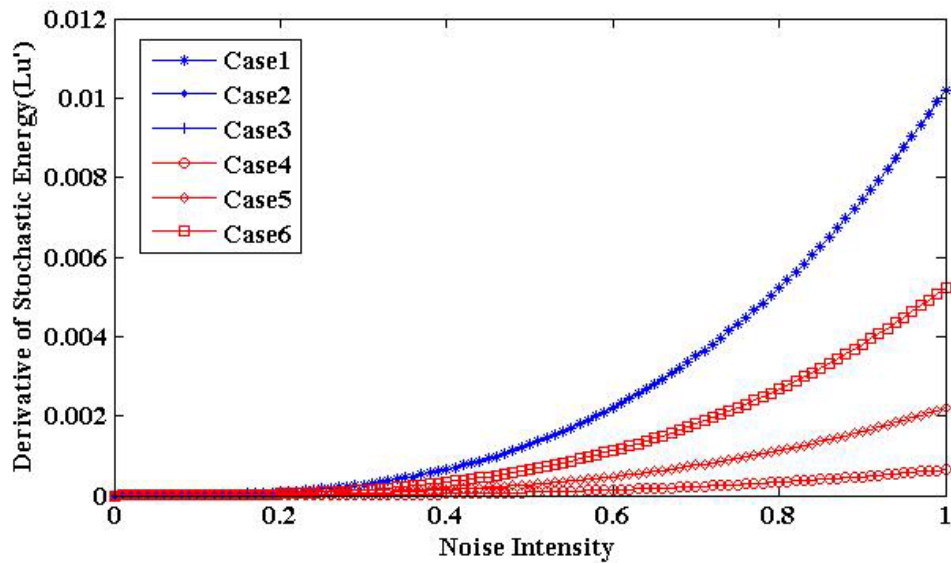
7.2) The results of SSI and Lu computation

When assuming that all the derivative terms in Lu are very small and close to zero, the Lu and SSI can be computed from non-derivative terms and represented in Figures 6.23 - 6.25, respectively. From Figure 6.23, it can be seen that, Lu increase gradually with increasing of wind power and its noise intensity. However, Lu of the Cases 1, 2, and 3 (with the same wind power) are not different. From Figures 6.24 and 6.25, for the Cases 4 – 6, the SSI decrease gradually with increasing of wind power and its noise intensity. For the Cases 1 – 3, the SSI of Case 2 is lowest, follows by Case 1 and Case 3, respectively. The $SSIs$ in this section are agreed with the results in previous section but with the different scale of SSI . For this section, the critical noise intensities (NI_C) in which $SSI = t_R$ (regulation time response is 10 minutes or 600 seconds) are >1.0 , >1.0 , 0.94 , and 0.86 for the Cases 4, 5, 6, and 1, respectively.

Table 6.13 Critical energy of the test system for voltage stability analysis

Unstable condition 1	Case 1	Case 2	Case 3	Case 4	Case 5	Case 6
$\mathbf{x} = \{\pi - x_2^s, x_3^s, x_4^s, y_2^s, y_3^s\}$	3.115219	1.259305	3.881501	1.601228	2.128044	2.6292
$\mathbf{x} = \{x_2^s, \pi - x_3^s, x_4^s, y_2^s, y_3^s\}$	4.357902	3.506202	4.175423	5.631103	5.234121	4.803396
$\mathbf{x} = \{x_2^s, x_3^s, \pi - x_4^s, y_2^s, y_3^s\}$	32.64797	24.95465	36.27428	30.58077	31.52095	32.18026
Unstable condition 2						
$\mathbf{x} = \{-\pi - x_2^s, x_3^s, x_4^s, y_2^s, y_3^s\}$	21.96478	23.25045	19.58946	24.2207	23.49087	22.73539
$\mathbf{x} = \{x_2^s, -\pi - x_3^s, x_4^s, y_2^s, y_3^s\}$	10.64109	9.789388	10.45861	8.144377	9.004032	9.829945
$\mathbf{x} = \{x_2^s, x_3^s, -\pi - x_4^s, y_2^s, y_3^s\}$	7.515232	-	11.14154	5.448024	6.38821	7.047518
Unstable condition 3						
$\mathbf{x} = \{\pi - x_2^s, \pi - x_3^s, \pi - x_4^s\}$	22.47461	584.002	-	29.21134	27.91522	25.66381
Unstable condition 4						
$\mathbf{x} = \begin{Bmatrix} -\pi - x_2^s, -\pi - x_3^s \\ -\pi - x_4^s \end{Bmatrix}$	-	-	-	-	-	-
Critical Energy (Minimum)	3.115219	1.259305	3.881501	1.601228	2.128044	2.6292

* the negative

**Figure 6.23** The results of Lu computation with increasing noise intensity comparing between 6 testing conditions for voltage stability analysis

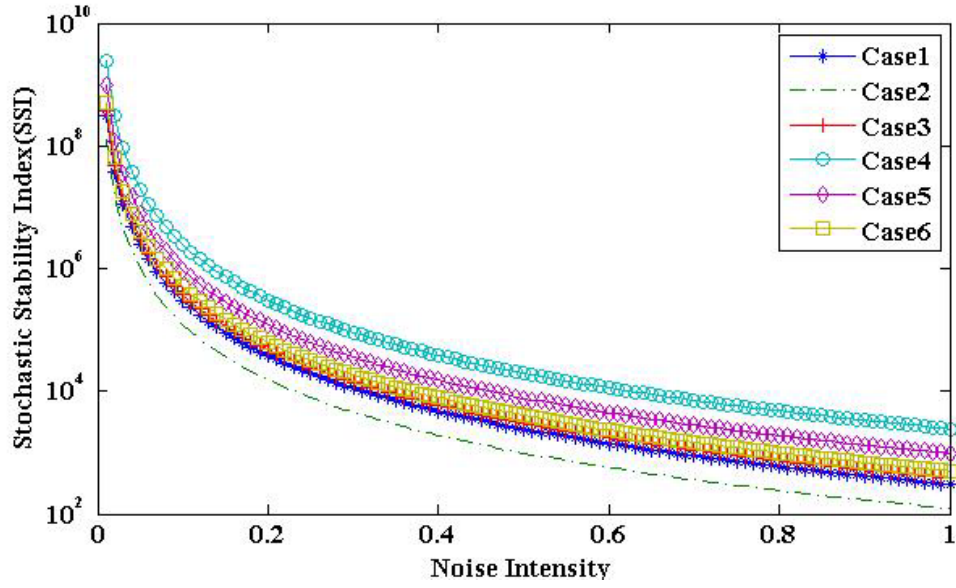


Figure 6.24 The results of log-SSI computation with increasing noise intensity (0-1.0) under 6 testing conditions for voltage stability analysis

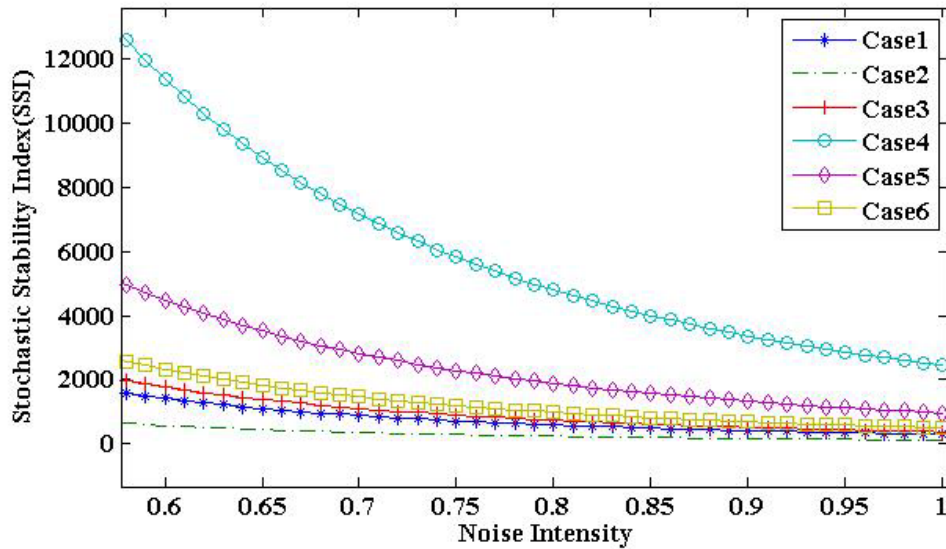


Figure 6.25 The results of SSI computation with increasing noise intensity (0.6-1.0) under 6 testing conditions for voltage stability analysis

7.3) An investigation of state variables, energy, and Lu from simulation

For Case 2, noise intensity 0.8, bandwidth 10, and Trial no. 1, the 200 seconds of simulation reveals that the exit time is at the 148th seconds. The electrical active and reactive power are represented in Figure 6.26. The phase angle of synchronous generator (G2), DFIG wind turbine (G3), and load are represented in Figure 6.27. The angular speed of synchronous generator (G2) and DFIG wind turbine are represented also in Figure 6.27.

From Figure 6.26, at 69th second, the active wind power increases while the others decrease. The reactive powers are increase except the exchanged reactive power.

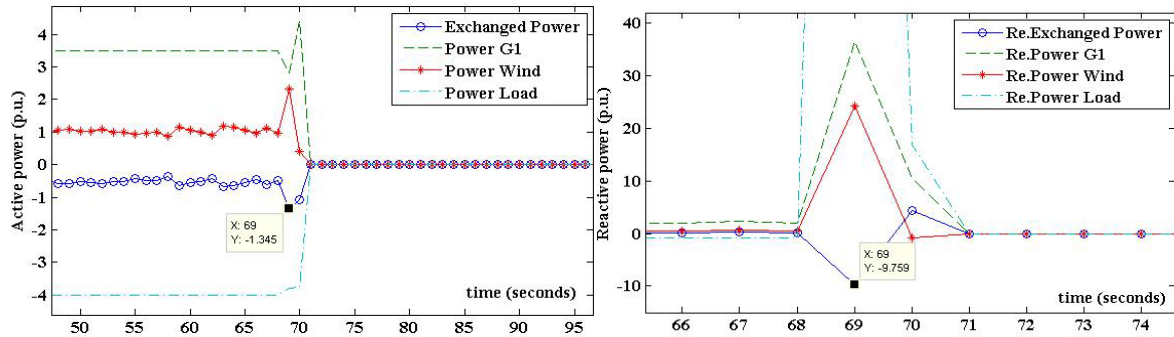


Figure 6.26 Active power (y-axis, left) and reactive power (y-axis, right).

For Figure 6.27, the phase angles are fluctuated and instantaneously reduce to zero within a few seconds. The angular speed of synchronous generator (Speed Syn. Gen.) is gradually jumped to reach maximum value and then back to zero while the angular speed of DFIG is suddenly decrease to become zero. However, an increase of Speed Syn. Gen. is beyond the limit at 0.02 p.u.

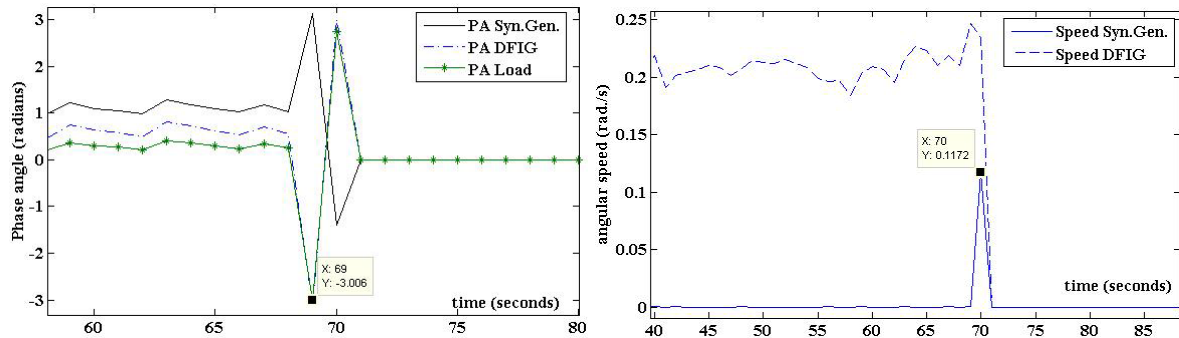


Figure 6.27 Phase angle (y-axis, left) and angular speed (y-axis, right).

Figure 6.28 represents the relative energy with its components and the derivative of stochastic energy (or Lu). For relative energy, the component numbers 10, 7, and 8 are the most significant, respectively. For the derivative of stochastic energy, the component numbers 6, 2, and 13 are most significant, respectively. It can be seen that, during 147th – 148th seconds, Lu is clearly fluctuated and swing back to zero state within a few seconds.

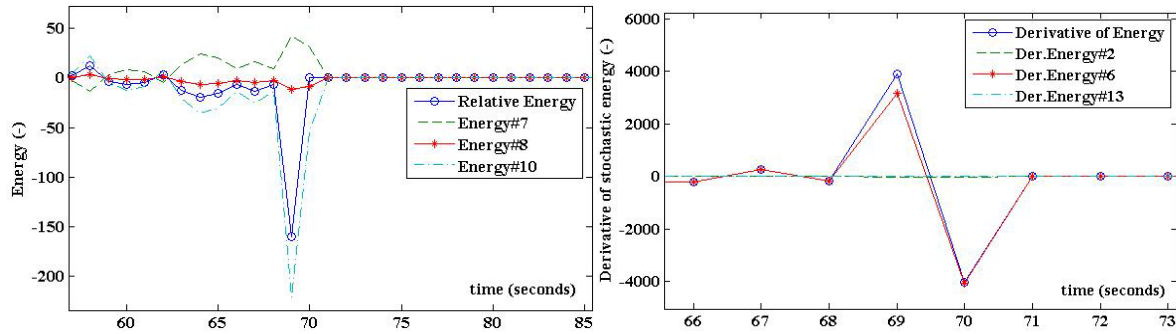


Figure 6.28 Relative energy (y-axis, left) and derivative of stochastic energy or Lu (y-axis, right).

For Figure 6.29, during 147th – 148th seconds, the voltage on load bus decrease gradually and swing back until reach zero within a few seconds. At that time, the reactive power load increase vastly and then return back to zero finally. This situation is called *Voltage Instability*.

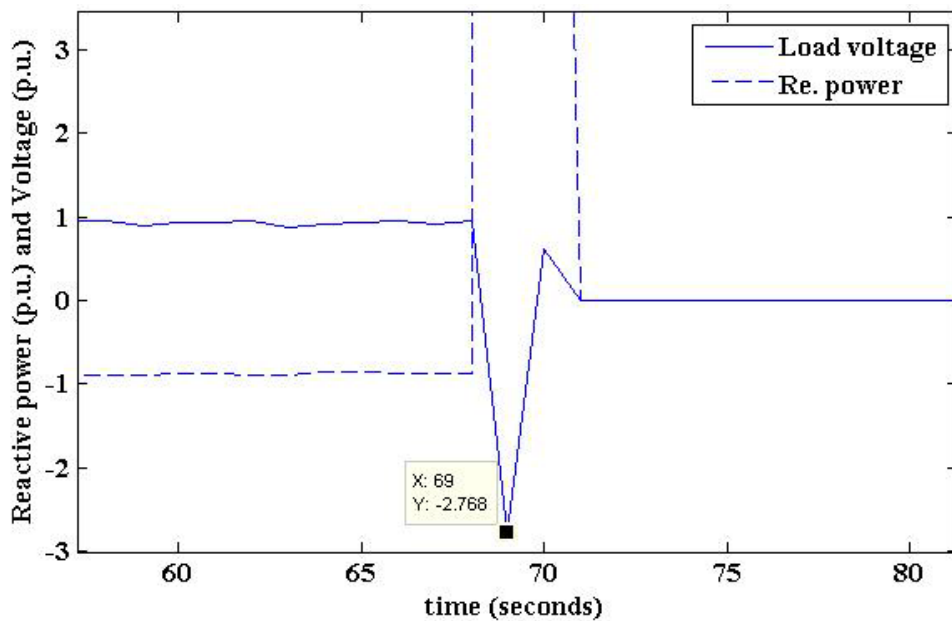


Figure 6.29 Load voltage (p.u.) and reactive power (p.u.) on load bus

8) Verification of the results

The results of section (7) are verified by comparing with the averaged exit time from 20 trials of simulation. The exit time of six different conditions are shown in Table 6.14 . It can be found from Table 6.14 that from Case 2, the exit time decrease with increasing of noise intensity. However, for the other cases, the exit time is longer than 3600 seconds and need more experiments to verify. For Cases 4 (base case), 5, 6 and 1 in this

section, when wind power increase 50%, 100%, and 150%, the *SSI* decrease about 61%, 79%, and 84%, respectively, comparing with base case. The *SSIs* and the percentage of decreasing of *SSI* in this section are less than the values in Section 6.1.3. However, the exit times are larger than the values in Section 6.1.3 which conflict with the results of *SSI*.

Table 6.14 The exit times (ET) and *SSI* for DFIG wind turbine with colored noise

Variable	Case 1 (*)	Case 2 (.)	Case 3 (+)	Case 4 (o)	Case 5 (◇)	Case 6 (□)
P_{Load}	4	4	4	4	4	4
P_{m3}	1.0	1.0	1.0	0.4	0.6	0.8
P_{m2}	3.0	3.5	2.5	3.6	3.4	3.2
$P_{Exchange}$	0.0	-0.5	0.5	0.0	0.0	0.0
Critical E. (Uc)	3.115219	1.259305	3.881501	1.601228	2.128044	2.6292
ET (s), NI = 0.6	>3600	2523.3	>3600	>3600	>3600	>3600
ET (s), NI = 0.8	>3600	699.4	>3600	>3600	>3600	>3600
ET (s), NI = 1.0	>3600	79.1	>3600	>3600	>3600	>3600
<i>SSI</i> (s), NI = 0.6	1761	571.4	1413	11350	4470	2330
<i>SSI</i> (s), NI = 0.8	742.9	241	596.3	4789	1886	982.9
<i>SSI</i> (s), NI = 1.0	380.4	123.4	305.3	2452	965.5	503.2

ET is Exit Times which are averaged from 20 trials of simulation

6.3 The Study of Effects of Wind Power on Voltage Variation using Probabilistic Method

The effects of wind power on the power quality, especially voltage, will be determined using the probabilistic method called Monte Carlo Simulation (MCS). There are two main topics that are studied: (1) the effects of wind power with stochastic noise on load voltage, and (2) the effects of different noises on load voltage.

6.3.1 The effects of wind power with colored noise on load voltage

1) Testing conditions

The testing conditions in this section are the same as in Section 6.2 in Table 6.12. The additional conditions are the three cases of colored noise conditions. First, the noise intensity (*NI*) 0.6 and bandwidth (*BW*) 10. Second, *NI* 0.3 and *BW* 10. Third, *NI* 0.3 and *BW* 1.0.

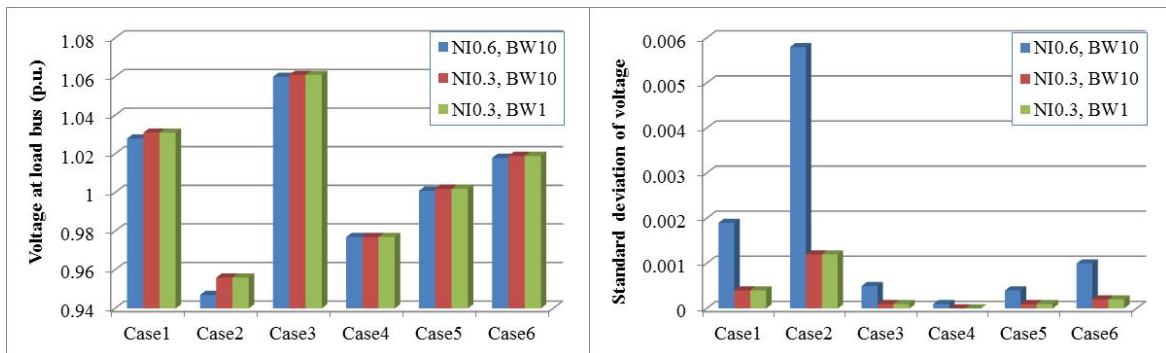
2) The stochastic differential equations (SDE)

The SDEs in this section are the same as Eqs. 6-37 to 6-39.

3) The results

Table 6.15 The statistical results of voltage on load bus

Variable	Case 1	Case 2	Case 3	Case 4	Case 5	Case 6
Load	4	4	4	4	4	4
P_{m3}	1.0	1.0	1.0	0.4	0.6	0.8
G2	3.0	3.5	2.5	3.6	3.4	3.2
balance (P_{mG})	0.0	-0.5	0.5	0.0	0.0	0.0
x_2S	0.587117	1.017949	0.239299	0.777726	0.702494	0.64083
x_3S	0.280651	0.552676	0.046355	0.117212	0.171878	0.22612
x_4S	-2.7E-17	0.250562	-0.2265	-9.8E-17	-1.3E-16	-9.2E-17
y_2S	4.01E-14	-2.2E-14	-1.6E-18	4.86E-09	1.39E-10	1.91E-11
y_3S	0.199901	0.200094	0.199831	-0.03097	0.05714	0.132831
NI 0.6	BW 10					
V_{load} Avg	1.028	0.947	1.060	0.977	1.001	1.018
V_{load} Max	1.032	0.958	1.061	0.977	1.002	1.020
V_{load} Min	1.021	0.927	1.058	0.976	1.000	1.014
V_{load} Stdev	0.0019	0.0058	0.0005	0.0001	0.0004	0.0010
NI 0.3	BW 10					
V_{load} Avg	1.031	0.956	1.061	0.977	1.002	1.019
V_{load} Max	1.032	0.959	1.061	0.977	1.002	1.020
V_{load} Min	1.030	0.952	1.060	0.977	1.002	1.019
V_{load} Stdev	0.0004	0.0012	0.0001	0.0000	0.0001	0.0002
NI 0.3	BW1					
V_{load} Avg	1.031	0.956	1.061	0.977	1.002	1.019
V_{load} Max	1.032	0.959	1.061	0.977	1.002	1.020
V_{load} Min	1.030	0.952	1.060	0.977	1.002	1.019
V_{load} Stdev	0.0004	0.0012	0.0001	0.0000	0.0001	0.0002

**Figure 6.30** The average (left) and standard deviation (right) of voltage on load bus

From Table 6.15 and Figure 6.30, for Cases 4 – 6, averaged voltage and its standard deviation increase with increasing wind power. The average value of voltage seems to rarely relate to noise intensity and bandwidth of wind power. However, the standard

deviation of voltage is clearly related to the noise intensity of wind power. The bandwidth has no effect on both average and standard deviation of voltage.

For Cases 1 – 3, the voltage is dropped when power is transfer to infinite bus while increase when power transfer from infinite bus. It is found that, the standard deviation act in the opposite way of the average voltage. The standard deviation of voltage, for this case, is strongly related to the noise intensity of wind power. The bandwidth of wind power has no effect on both average and standard deviation of voltage.

6.3.2 The effects of various noise conditions on load voltage

For the 200 trials of simulation, the testing conditions and statistical results of voltage on load bus are represented in Table 6.16. The wind power and power load are in Figure 6.31.

Table 6.16 The testing conditions for the effects of various noise conditions on load voltage

Variable	Case T1	Case T2	Case T3	Case T4	Case T5	All 1	All 2
P_{Load}	4	4	4	4	4	4	4
P_{mw}	1.0	1.0	1.0	1.0	0-1	0-1	1.0
P_{mi}	3.0	3.0	3.0	3.0	3.0	3.0	3.0
$P_{exchange}$	0.0	0.0	0.0	0.0	0.0	0.0	0.0
Q_{Load}	1.0	1.0	1.0	1.0	1.0	1.0	1.0
NI,BW P_{mw}	0.1,10	-	-	0.1,0.1	-	0.1,10	0.1,10
NI,BW P_{Load}	-	0.025,0.1	-	-	-	0.025,0.1	0.025,0.1
NI,BW Q_{Load}	-	-	0.1,0.1	-	-	0.1,0.1	0.1,0.1
Weibull WS	-	-	-	-	yes	yes	-
V_{load} Avg	1.0320	1.0303	1.0319	1.0320	1.0252	1.0228	1.0303
V_{load} Max	1.0322	1.0320	1.0336	1.0322	1.0388	1.0482	1.0332
V_{load} Min	1.0318	1.0151	1.0299	1.0318	1.0156	0.8954	1.0150
V_{load} Stdev	71×10^{-6}	2466×10^{-6}	710×10^{-6}	68×10^{-6}	8398×10^{-6}	20415×10^{-6}	2503×10^{-6}

The Weibull WS is the case when wind power is not constant, but varied by wind speed. The wind speed is modeled using the Weibull distribution with scale parameter 8.0 and shape parameter 2.0 . The wind power is computed using this wind speed and the power curve from manufacturer as represented in section 3.1.1 . The system equations are the same as previous section for Eqs.6-37 to 6-39.

From Table 6.16 and Figure 6.32, for the cases T2, T3 and T4, the standard deviation of three cases are not different. However, the variation of power load of the case T2 is most influence to the voltage on load bus. When Weibull wind speed is applied in

case T5, the deviation of voltage become much more significant. When all noises are applied, the voltage is deviated seriously with the value between 0.895 – 1.048 p.u. From the case T1 and T4, the bandwidth of wind power noise has no significant effect on the voltage of the load bus.

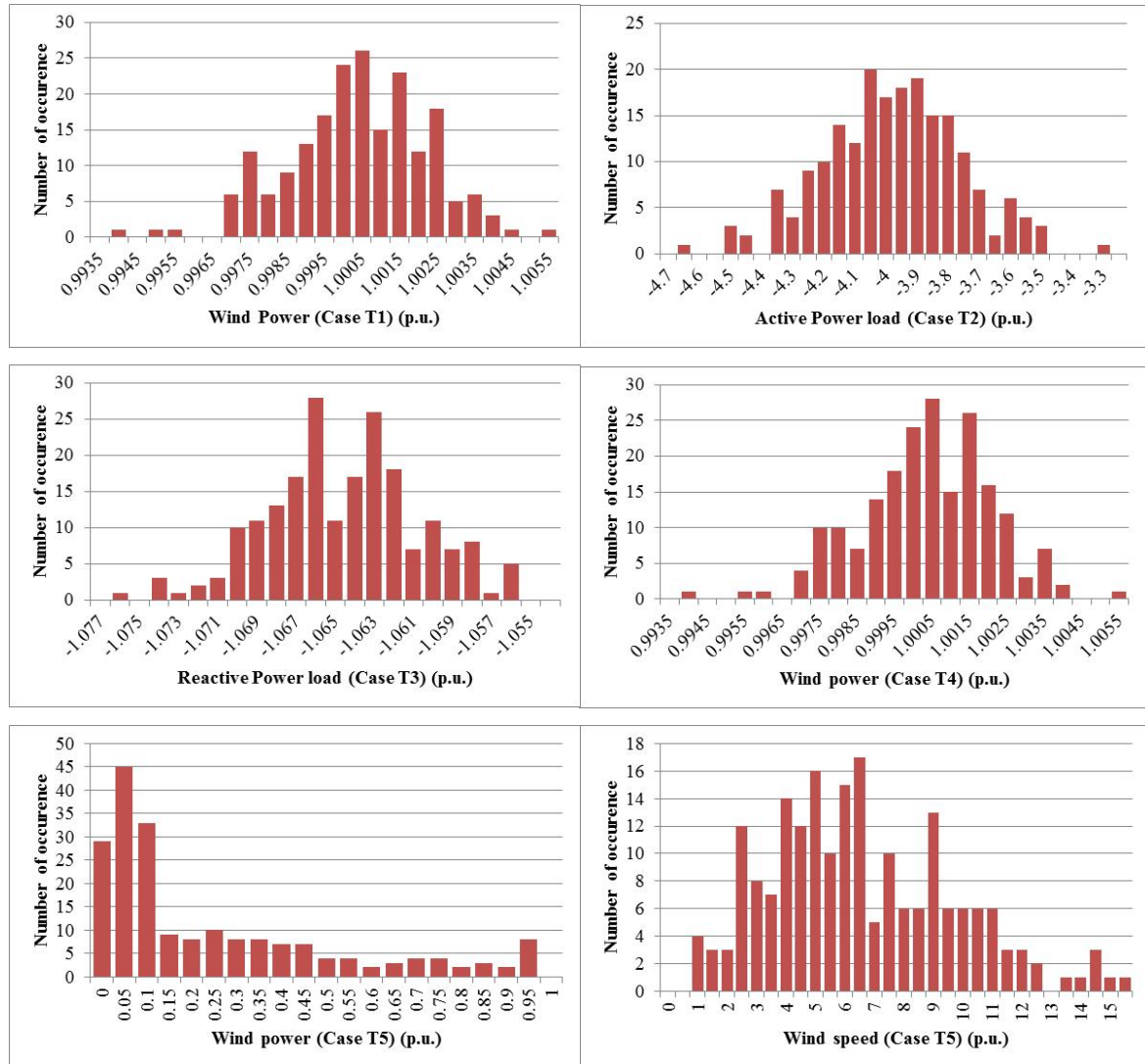


Figure 6.31 The data distributions of wind power, active and reactive power loads, and wind speed for the cases T1 – T5

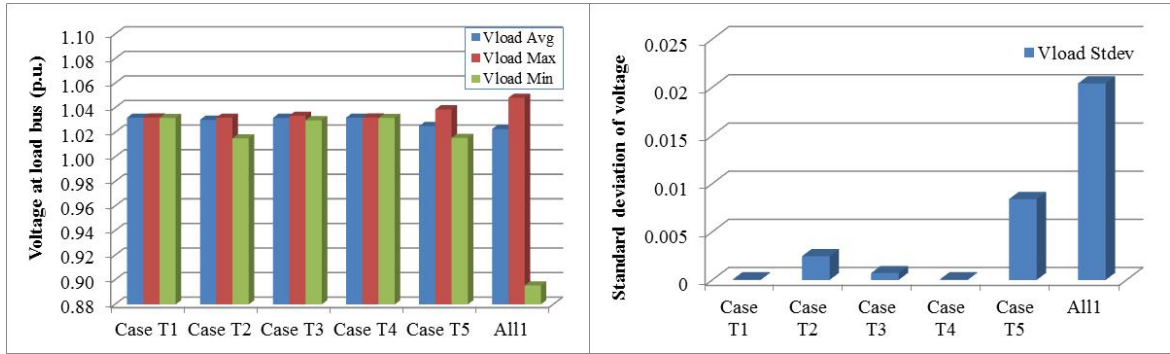


Figure 6.32 The data distribution of voltage for the cases T1 – T5 (left) and All 1 (right)

The data distributions of voltage on load bus are represented in Figure 6.33 .

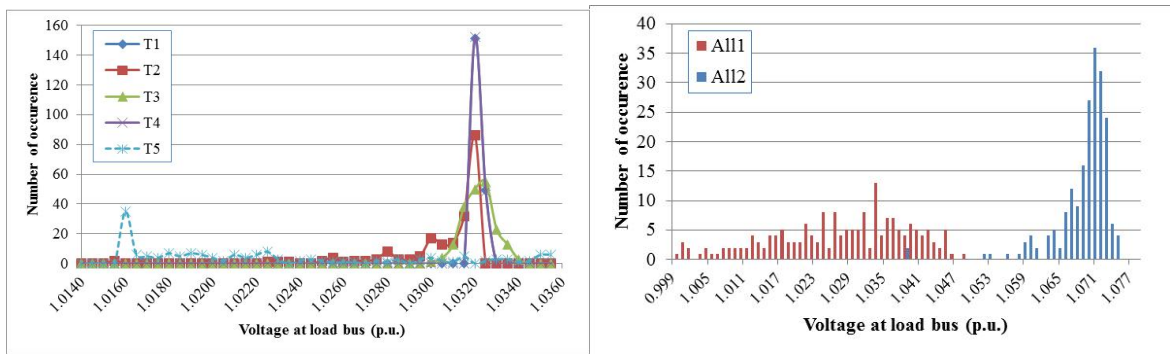


Figure 6.33 The data distribution of voltage for the cases T1 – T5 (left) and cases All 1 – All 2 (right)

In conclusion, when the power load is constant, the variation of wind power has significant effect on the voltage of load bus. The voltage increases with increasing wind power but decrease with increasing of power transfer to infinite bus. However, when power load is not constant, the variation of power load has more influence to voltage than wind power even at the same scale of fluctuation.

CHAPTER 7

CONCLUSION AND FUTURE WORK

7.1 Conclusions

This thesis can quantitatively assess the effects of stochastic wind energy on the stability of the power system using stochastic analytical method. The performance index, called the *stochastic stability index (SSI)*, is developed in this thesis based on the theory of stochastic stability. To determine *SSI*, several processes have to be done consisting of the determination of steady state variables, estimation of well-defined energy function and critical energy, and formulation of stochastic differential equations.

Characteristics of wind speed and wind power

From the measured wind speed data in Thailand, it was found that the wind speed distribution can be approximated by Weibull's distribution and noise wind speed (instantaneous – mean value) can be approximated by Generalized Gaussian Distribution (GGD). The wind power distribution of one turbine cannot be classified into any type of distribution. However, for many turbines with diversity of geographical area, the wind power distribution can be approximated using Normal distribution. The power spectral densities (PSD) of wind speed and wind power decrease with increasing of frequency. The majority parts of PSD occur within 0-500 mHz (the low frequency). The wind power with frequencies higher than 500 mHz have small contribution. Therefore, it is possible to approximate the wind power of many turbines using Gaussian distribution white noise and colored noise models.

The characteristics of power system incorporating wind power

The simulation of two machines infinite bus power system (TMIB) incorporating aggregated wind turbine is done in this section using PSCAD. It was found that when wind power increased without noise, the power angle of the nearby synchronous generator (SG) decreased, while the rotor speed increased with oscillation (frequency about 750 mHz) until reaching new steady state values. When the voltage of transmission line decrease from 500kV to be 230 kV, the oscillations of power angle and rotor speed are diverge continuously which is the condition of instability. When noise of wind power is applied, the standard deviation of noise has more influence to power angle and rotor speed of nearby SG than its frequency. However, if frequency of wind power noise is close to the

hunting frequency (frequency about 750 mHz for this study) of nearby SG, the magnitude of oscillation of power angle and rotor speed will be largely due to the resonance effect.

A study of effects of wind power to the small signal stability using the eigenvalue method

For both squirrel cage induction generator (SCIG) and doubly-fed induction generator (DFIG) wind turbines, when the wind speed increases, the speed deviation, power output, current and power factor increase, but bus voltage decreases. The real parts of eigenvalues increase (move from negative to close to zero) with increasing of angle of internal voltage and decreasing of stator voltage. The imaginary parts of eigenvalues decrease with increasing of reference voltage, transmission line reactance, and angle of internal voltage and decreasing of stator voltage. Therefore, for a single wind turbine connecting to an infinite bus, when wind speed and wind power increase, the angle of internal voltage also increase causing the real parts of eigenvalues to increase and imaginary parts of eigenvalues to decrease.

For multi-machine power system, including DFIG wind turbine, the significant eigenvalues (eigenvalues that closer to zero) decrease with increasing wind power, and decreasing of main synchronous generator, which means that the wind power can improve small signal stability of the power system. Moreover, it is found that the significant eigenvalues are mostly influenced by speed deviation (or slip) of DFIG wind turbine and follows by the speed deviation of synchronous generator. It can be implied from the results that when wind power increase to substitute the power from other conventional power plants without excess power, the small signal stability of the system is improved.

A study of effects of wind power to the small signal stability using stochastic stability method: the mean first passage time (MFPT)

The mean first passage time (*MFPT*) is the performance index to quantify the average time a state-space trajectory takes to change from a given operating point to the boundary of its domain of attraction under the influence of small perturbations. To compute *MFPT*, several processes have to be done consisting of the determination of steady state variables, estimation of critical energy, and formulation of stochastic differential equations.

Considering wind speed data from the Chumporn monitoring station, the cases when noise intensity is larger than 3.4, 0.88, 0.38, 0.24, and 0.18 with mean wind speed 6, 8, 10, and 12 m/s, respectively, are seriously considerable and can possibly lead the system

to be unstable within a short time (*MFPT* less than time constraint of regulation or control system 10 minutes). These serious conditions that occur during April – May and Nov – Dec which the monsoon has much influence in that area.

However, this result is based on an assumption that wind power is a Gaussian white noise and the power system is unregulated which is not practical. The dynamics with regulation system needs an improvement of the stability index. Furthermore, the energy function, for *MFPT* solution, is an approximated value which has ellipsoidal surface shape. It cannot represent the complex surface problems, for example, the energy of the power system when incorporate DFIG wind turbine model. Therefore, an improved method is developed in this thesis to overcome these problems.

The Study of Effects of Wind Power to the Small Signal Stability using New Stochastic Stability Method

- The derivative of stochastic energy (*DSE*) with Gaussian distribution white noise model

To quantitatively evaluate the effects of stochastic wind power to the power system, the derivative of stochastic energy (*DSE*) is formulated and used as a stability performance index. The stable condition of the stochastic system is $DSE < 0$, therefore, the larger *DSE* means the system has higher probability to become unstable.

For TMIB power system incorporating aggregated SCIG wind turbines with Gaussian distribution white noise, it was found that the *DSE* gradually increases with increasing wind power and its noise intensity. For the power flow of the test system with Load: Wind Power: power from SG is 4: 2: 2 p.u., when *DSE* is zero or critically stable, the critical noise intensities at wind power 0.5, 1.0, and 2.0 p.u., are about 0.09, 0.045, and 0.0225, respectively. Therefore, the critical noise intensities of wind power are linearly inverse to the changing of wind power.

From the simulation, the small but continuous fluctuation of wind power can finally cause the system to become unstable due to loss of synchronism. For example, if noise intensity increases 1.5 times, the exit time (the time when the rotor speed increase beyond the limited value and the system become unstable) decreases 0.52 times and *DSE* increase 5.2 times. If wind power increases 0.5 times, the exit time decreases 0.73 times and *DSE* increase 1.25 times. The *DSE* is corresponded to the inverse of exit time. Therefore, the stability of the power system, which is measured by the exit time and *DSE*, decreases with increasing of wind power and its noise intensity.

- The study of the effects of stochastic wind power and stochastic load using *DSE*

For the SMIB (single machine infinite bus) power system with SCIG wind turbine, an increasing of noise intensity of both wind power and load causes the *DSE* to increase and the system possibly becomes progressively unstable. When only stochastic load is represented (fix wind power), the larger load voltage and smaller frequency dependent coefficient causes the larger *DSE*. When only stochastic wind power is represented (fix power load), the larger share of wind power leads to larger *DSE* and an increasing of frequency dependent coefficient causes the critical noise intensity to decrease which causes the system less stable.

From these studies, the *DSE* gives an alternative idea for the stability analysis of the power system incorporating stochastic wind power without computational effort. Furthermore, it can be implied that, to avoid system instability, the mechanical wind power should be limited by its noise intensity using *DSE* to be as a stability performance evaluation index.

- The stochastic stability index (*SSI*) with Gaussian distribution white noise model

In this section, a new stability performance index is formulated from the critical energy divided by the non-derivative components of the derivative of stochastic energy (which is not dependent on state variables) and is called the Stochastic Stability Index (*SSI*). This *SSI* is improved from the previous section (*DSE*), and has the same concept with the mean first passage time (*MFPT*) which is the performance index to quantify the averaged time a state-space trajectory takes to change from a given operating point to the boundary of its domain of attraction under the influence of small perturbations.

From the results, *SSI* decreases with increasing noise intensity of wind power. For the TMIB power system incorporating DFIG wind turbine with Gaussian distribution white noise, when wind power increases, the critical energy increases while the *SSI* decreases, which means that the power system becomes less stable. This result is opposite to the deterministic method (Ex. eigenvalue analysis method) in which the power system is more stable when wind power increases. For example, assumes the critical regulation time response (t_R) of the power system is 10 minutes (600 seconds), the critical noise intensities (NI_C) of wind power in which *SSI* equal to t_R are 0.88, 0.67, 0.54, and 0.26 for wind power 0.4, 0.6, 0.8, and 1.0 p.u., respectively. If noise intensity is greater than NI_C , the *SSI* will

less than t_R and the power system is possibly unstable before the regulation system can completely take action.

Compared to the exit time from the simulation, when there is exchanged power (export to or import from infinite bus), the exit time decreases with increasing of noise intensity of wind power which is corresponded to the value of SSI . Furthermore, the exit time when export power is less than when import power which is corresponded to the value of critical energy and the SSI . Moreover, when wind power increases by 50%, 100%, and 150%, the SSI decreases by about 56%, 75%, and 84%, respectively, compared with the base case where wind power is 0.4 p.u.. However, when there is no exchanged power, even the simulation time is longer than 1000 seconds and noise intensity is 1.0, the system still be stable and need more studies to verify.

- The stochastic stability index (SSI) with Gaussian distribution colored noise model

When applying the Gaussian distribution colored noise model, which is more practical and can be adjusted depending on bandwidth, the larger bandwidth results in being closer to the effect of white noise. The results conform to the case when applying the white noise model, but with the different values of SSI . For this condition (colored noise with bandwidth 1.0), the critical noise intensities (NI_C) in which SSI equal to t_R (600 seconds) are >1.0 , >1.0 , 0.87, and 0.74 for wind power 0.4, 0.6, 0.8, and 1.0 p.u., respectively. When wind power increase 50%, 100%, and 150%, the SSI decrease about 64%, 82%, and 89%, respectively, comparing with base case which wind power is 0.4 p.u. . The percentage of decreasing of SSI when apply colored noise are larger than the values when apply white noise.

Moreover, it was found that the mean value of derivative of stochastic energy (Lu) is corresponded to the non-derivative components of Lu (which is not depended on state variables and is used to compute SSI). If there is exchanged power, the standard deviation of Lu is corresponded to noise intensity of wind power but not for the case when there is no exchanged power. Therefore, it can be implied that the standard deviation of Lu is not clearly related to the variation of wind power.

Therefore, the SSI can quantitatively reveal the effects of increasing wind power and its noise intensity to the power system stability. When the stochastic wind power increase, SSI will decrease and the system is less stable, especially, when there is

exchanged power to or from an infinite bus. The results of *SSI* are corresponded to the exit time from the simulation.

The wind turbine induction generator model (using aggregated DFIG and SCIG wind turbines) is included in the formulation of the energy function and to the *SSI*. Increasing noise intensity of both wind power and load causes the stochastic stability index to increase and the system become unstable progressively.

To maintain the synchronization of the system, the wind power generation should be limited at an appropriate value for a given noise intensity. This index gives an alternative idea for power system stability analysis by stochastically incorporating the wind power. This stochastic stability analysis method can analyze the nonlinear and stochastic power system stability with less time and computational effort.

The Study of Effects of Wind Power to the Voltage Stability using New Stochastic Stability Method

In this section, the *SSI* is applied to study the effects of wind power to voltage stability of the power system. The dynamic load model with voltage deviation equation (load voltage is not constant) is included in the power system equations incorporating DFIG wind turbine using the colored noise model of wind power.

The *SSI* increases with increasing wind power and its noise intensity, which agree with the results in the previous section, but with the different values of *SSI*. For this section, the critical noise intensities (NI_C) in which *SSI* equal to t_R (600 seconds) are >1.0 , >1.0 , 0.94 , and 0.86 for wind power 0.4 , 0.6 , 0.8 , and 1.0 p.u., respectively. Moreover, the *SSI* of the case when import power from infinite bus is larger than the case when export power. It can be implied that when apply voltage deviation equation, the power system is less stable when there is excess power exported to an infinite bus.

From the simulation results, when there is excess power exported to an infinite bus, the mean exit time decrease with increasing of noise intensity which corresponds to the results of *SSI*. However, for the other cases, the exit time is longer than 3600 seconds and need more experiments to verify. Furthermore, it is found that at the exit time, the load voltage is sharply decline while the reactive power of load vastly increases and both are return to zero after that.

If wind power increase 50%, 100%, and 150%, the *SSI* decrease about 61%, 79%, and 84%, respectively, comparing with base case. The percentages of decreasing of *SSI* in this section are less than the values in previous section when the load voltage is fixed.

The Study of Effects of Wind Power to Voltage Variation using Probabilistic Method

In this section, the effects of wind power to the power quality, especially voltage, are determined using probabilistic method called Monte Carlo Simulation (*MCS*).

When there is no exchanged power, the mean load voltage and its standard deviation increase with increasing wind power, but the mean load voltage seems to rarely relate to noise intensity and bandwidth of wind power. However, the standard deviation of load voltage is clearly related to the noise intensity of wind power. The bandwidth has no effect to both average and standard deviation of voltage.

When there is exchanged power, the mean load voltage is dropped when power is transferred to infinite bus, while increasing when power is transferred from infinite bus. It was found that the standard deviation of the load voltage changes in the opposite way of the mean value. The standard deviation of voltage, for this case, is strongly related to the noise intensity of wind power. The bandwidth of wind power has no effect on both mean and standard deviation of load voltage. However, when applying Weibull wind speed instead of Gaussian distribution, the deviation of voltage become much more significant. Moreover, when the power load is not constant, the variation of power load has more influence on the voltage than does the wind power even at the same scale of fluctuation.

7.2 Future Studies

The wind turbine model may be improved in future studies for more accurate results. The following topics should also be analyzed: the voltage stability index, the power quality evaluation, the different type of wind power and noise models, the different location, and the real data of wind power and the power system.

Several results need more analysis. For example, the different between exit time and *SSI* when there is no exchanged power and the case when apply voltage deviation equation, the power system is less stable when there is excess power exported to an infinite bus. Many other variables such as bus voltage, phase angle, machine parameters, etc. should be investigated and explained physically in the future work compared with the deterministic methods.

REFERENCES

- [1] Anawach Sangswang (2003), *Uncertainty Modeling of Power Electronic Converter Dynamics*, a Thesis document, Drexel University, USA.
- [2] Anawach Sangswang and Chika O. Nwankpa (2003), Effects of Switching-Time Uncertainties on Pulsewidth-Modulated Power Converters: Modeling and Analysis, *IEEE Transaction on Circuits and System-I: Fundamental Theory and Applications*, Vol. 50, No. 8.
- [3] Angelo Baggini (2008), *Handbook of Power Quality*, John Wiley & Sons, Ltd., England.
- [4] Arthur R. Bergen (1986), *Power System Analysis*, Prentice-Hall.
- [5] Athanasios Papoulis and S. Unnikrishna Pillai (2002), *Probability, Random Variables and Stochastic Processes*, 4th edition, McGraw-Hill.
- [6] Atsushi Ishigame and Tsuneo Taniguchi (2003), Transient Stability Analysis for Power System Using Lyapunov Function with Load Characteristics, Graduate School of Engineering, Osaka Prefecture University, Japan.
- [7] B. J. Matkowsky and Z. Schuss (1977), The Exit Problem for Randomly Perturbed Dynamical Systems, *SIAM Journal on Applied Mathematics*, vol.33, pp.365-381.
- [8] C. O. Nwankpa and S.M. Shahidehpour (1989), A Probabilistic Approach to Bulk Power Transmission System Analysis, Illinois Institute of Technology.
- [9] C. O. Nwankpa and S.M. Shahidehpour (1991), A stochastic model for small disturbance stability analysis of electric power systems, *Electrical Power & Energy Systems*, Vol.13, No.3.
- [10] C. O. Nwankpa and S.M. Shahidehpour (1991), Stochastic Model for Power System Planning Studies, *IEE Proceedings*, Part C, Vol. 138, No. 4, pp. 307-320.
- [11] C. O. Nwankpa, R. Fischl and R.M. Hassan (1992), Using Stochastic Models for Analyzing Power System Dynamics, Drexel University, Philadelphia, Pennsylvania, USA.

- [12] C. O. Nwankpa, R.M. Hassan (August 1993), A Stochastic based Voltage Collapse Indicator, *IEEE Transactions on Power Systems*, Vol. 8, No. 3.
- [13] C. O. Nwankpa, S.M. Shahidehpour, and Z. Schuss (November 1992), *A Stochastic Approach to Small Disturbance Stability Analysis*, IEEE Transactions on Power Systems, Vol. 7, No. 4.
- [14] Chun-Lien Su (August 2005), Distribution Probabilistic Load Flow Solution Considering Network Reconfiguration and Voltage Control Devices, National Kaohsiung Marine University, Kaohsiung, TAIWAN.
- [15] Claudio A. Canizares (1995), On Bifurcation Voltage Collapse and Load Modeling, *IEEE Transactions on Power Systems*, Vol. 10, No. 1.
- [16] Claudio A. Canizares (1998), Applications of Optimization to Voltage Collapse Analysis, Panel Session: Optimization Techniques in Voltage Collapse Analysis, *IEEE/PES Summer Meeting*, San Diego.
- [17] Claudio A. Canizares, Antonio C. Z. de Souza, Victor H. Quintana, Comparison of Performance Indices for Detection of Proximity to Voltage Collapse, University of Waterloo, Paper 95 SM 583-5 PWRS to be published in the IEEE Transactions on Power Systems.
- [18] Claudio A. Canizares, N. Mithulananthan, Federico Milano, and John Reeve (2004), Linear Performance Indices to Predict Oscillatory Stability Problems in Power Systems, *IEEE Transactions on Power Systems*, Vol.19, No.2, p. 1104-1114.
- [19] Djemai Naimi and Tarek Bouktir (June 2008), Impact of Wind Power on the Angular Stability of a Power System, *Leonardo Electronic Journal of Practices and Technologies*, ISSN 1583-1078, Issue 12, p. 83-94.
- [20] E. Muljadi and C. P. Butterfield, J. Chacon, H. Romanowitz (June 2006), Power Quality Aspects in a Wind Power Plant, *IEEE Power Engineering Society General Meeting*, Montreal, Quebec, Canada.
- [21] Erich Zauderer (2006), *Partial Differential Equations of Applied Mathematics*, Third Edition, John Wiley & Sons.

- [22] George J. Anders (1990), *Probability Concepts in Electric Power Systems*, John Wiley & Sons, Ltd., Canada.
- [23] Glenn W. Stagg and Ahmed H. El-Abiad (1968), *Computer methods in power system analysis*, McGraw-Hill.
- [24] GWEC: Global Wind Energy Council (2014), *Global Wind Report Annual Market Update 2013*.
- [25] H. J. Hwang (August 1969), Power Density Spectrum of Surface Wind Speed on Palmyra Island, *Monthly Volume Review*, Vol.98 No.1, St. Louis University.
- [26] H. P. Geering, G. Dondi, F. Herzog, S. Keel (April 2011), *Stochastic Systems*, Measurement and Control Laboratory, Swiss Federal Institute of Technology Zurich.
- [27] Hadiza Mohammed and Chika O. Nwankpa (Dec 1998), Uncertainty Modeling and Analysis of Wind Energy Systems, the 37th *IEEE Conference on Decision & Control Tampa*, Florida USA.
- [28] Hadiza Mohammed and Chika O. Nwankpa (March 2000), Stochastic Analysis and Simulation of Grid-Connected Wind Energy Conversion System, *IEEE Transactions on Energy Conversion*, Vol. 15, No. 1.
- [29] Hannele Holttinen (2009), *Design and operation of power systems with large amounts of wind power*, Final report, IEA WIND Task 25, Phase one 2006-08.
- [30] Hsiao-Dong Chiang (2011), *Direct Methods for Stability Analysis of Electric Power Systems : Theoretical Foundation, BCU Methodologies, and Applications*, John Wiley & Sons Ltd., UK.
- [31] I. Erlich, K. Rensch, F. Shewarega (2006), Impact of Large Wind Power Generation on Frequency Stability, University of Duisburg-Essen, Germany.
- [32] Isac Van der Hoven (1956), Power spectrum of horizontal wind speed in the frequency range from 0.0007 to 900 cycles per hour, *Journal of Meteorology*, V.14, p.160-4.

- [33] J. Arrillaga and N. R. Watson (2000), *Power System Quality Assessment*, John Wiley&Sons Ltd. England.
- [34] J. Qiu, S. M. Shahidehpour, and Z. Schuss (February 1989), Effect of Small Random Perturbations on Power System Dynamics and its Reliability Evaluation, *IEEE Transactions on Power Systems*, Vol. 4, No. 1.
- [35] J. L. Rueda and F. Shewarega (2009), Small Signal Stability of Power Systems with Large Scale Wind Power Integration, *XIII ERIAC DÉCIMO TERCER ENCUESTRO REGIONAL IBEROAMERICANO DE CIGRÉ*.
- [36] J. T. Bialasiewicz and E. Muljadi (November 2006), The Wind Farm Aggregation Impact on Power Quality, *the 32nd Annual Conference of the IEEE Industrial Electronics Society (IECON '06)* Paris, France.
- [37] Jay Apt (2007), The Spectrum of Power from Wind Turbines, *Journal of Power Sources* 169 369–374 , Carnegie Mellon University.
- [38] Joaquín Mur-Amada, Ángel A. Bayod-Rújula (October 2007), Characterization of Spectral Density of Wind Farm Power Output, *9th International Conference of Electrical Power Quality and Utilization*, Barcelona.
- [39] Junji Tamura (2001), Transient Stability Simulation of Power System Including Wind Generator by PSCAD/EMTDC, Kitami Institue of Technology, Japan.
- [40] Lawrence C. Evans (2013), *An Introduction to Stochastic Differential Equations*, American Mathematical Soc.
- [41] Louie, Henry (July 2010), Characterizing and modeling aggregate wind plant power output in large systems, *Power and Energy Society General Meeting IEEE* , Vol.1, No.8, pp. 25-29.
- [42] Lulian Munteanu, Antoneta Luliana Bratcu, Nicolaoas-Antonio Cutululis, Emil Ceanga (2008), *Optimal Control of Wind Energy Systems, Advances in Industrial Control*, Springer-Verlag London Limited, UK.
- [43] M. Ribbens-Pavella, B. Lemal (1976), Fast determination of stability regions for online transient power-system studies, *PROC. IEE*, Vol. **123**, No. 7.

- [44] M. A. Pai, D. P. Sen Gupta, K.R. Padiyar (2004), *Small Signal Analysis of Power Systems*, Alpha Science International Ltd., U.K..
- [45] Olimpo Anaya-Lara, Nick Jensens, Janaka Ekanayake, Phill Cartwright, Mike Hughes (2009), *Wind Energy Generation Modeling and Control*, John Wiley & Sons Ltd., UK.
- [46] P. M. Anderson and A. Bose (1983), Stability Simulation of Wind Turbine Systems, *IEEE Transactions on Power Apparatus and Systems*, Vol.PAS-I02, No. 12.
- [47] P. Parinya, A. Sangswang, K. Kirtikara, D. Chenvidhya, S. Naetiladdanon, C. Limsakul (June 2014), A Study of Impact of Wind Power to Power System Stability using Stochastic Stability Index, *ISCAS2014*, Melbourne, Australia.
- [48] Paul-Frederik Bach (2010), Geographical Distribution and Wind Power Smoothing 2009: Observations from Denmark, Germany and Ireland. Available online: http://www.pfbach.dk/firma_pfb/wind_power_geographical_distribution_2009.pdf.
- [49] Pedro Rosas (2003), *Dynamic Influences of Wind Power on The Power System*, a Thesis document, Technical University of Denmark.
- [50] Peter W.Sauer and M.A. Pai (1998), *Power System Dynamics and Stability*, Prentice Hall, USA.
- [51] Poul Sorensen, Anca Hansen, Lorand Janosi, John Bech and Birgitte Bak-Jensen (2001), Simulation of Interaction between Wind Farm and Power System, Riso-R-1218(EN), Riso National Laboratory, Roskilde.
- [52] Prabha Kundur (1998), *Power System Stability and Control*, Electric Power Research Institute, Power System Engineering Series.
- [53] R. Billinton and W. Li (1994), Reliability assessment of electric power systems using Monte Carlo methods, New York: Plenum Press.
- [54] R. C. Burchett and G. T. Heydt (1978), Probabilistic Methods For Power System Dynamic Stability Studies, *IEEE Transactions on Power Apparatus and Systems*, Vol. PAS-97, no. 3.

- [55] R. A. Sobolewski a, A.E. Feijóo (2012), Estimation of wind farms aggregated power output distributions, *Electrical Power and Energy Systems*.
- [56] R. H. B. Exell (1981), *The Availability of Wind Energy in Thailand*, AIT Research Report No.134, Renewable Energy Resources Information Center, Asian Institute of Technology.
- [57] Roger C.Dugan (2003.), *Electrical Power System Quality*, 2nd Edition, McGraw-Hill.
- [58] Roy D. Yates and David J. Goodman (1999), *Probability and Stochastic Processes*, John Wiley&Sons, Inc..
- [59] Ryan Rutkowski (16th Jan 2010), “China's wind power has faulty connection”, Asia Times Online, Available online:
www.atimes.com/atimes/China_Business/LF16Cb03.html .
- [60] Ryan Wiser and Mark Bolinger (August 2013), *2012 Wind Technologies Market Report*, Lawrence Berkeley National Laboratory.
- [61] S. M. Shahidehpour and J. Qiu (1986), Effect of Random Perturbations on the Dynamic Behavior of Power Systems, Illinois Institute of Technology, Chicago, IL (U.S.A.), Electric Power Systems Research.
- [62] S. Q. Bu, W. Du, H. F. Wang, Z. Chen, L. Y. Xiao, and H. F. Li (2010), Probabilistic Analysis of Small-signal Stability of Large-scale Power Systems as Affected by Penetration of Wind Generation, *IEEE Transactions on Power Systems*, Seattle UniversityWA, 98122 USA.
- [63] Sherif O. Faried, R. Billinton and P.R.S. Kuruganty (2010), Probabilistic evaluation of transient stability of a power system incorporating wind farms, *IET Renewable Power Generation*.
- [64] Subramanian Chandrasekaran (2014), *Grid Connected Doubly Fed Induction Generator Based Wind Turbine under LVRT*, Ph.D. dissertation, Dept. Electric, Electronic, Information and Engineering “GUGLIELMO MARCONI”. University of Bologna., Bologna, Italy.

- [65] T. R. Ayodele , A. A. Jimoh , J. L. Munda, J. T. Agee, The Influence of Wind Power on the Small Signal Stability of a Power System, Department of Electrical Engineering, Tshwane University of Technology, Pretoria, South Africa.
- [66] T. R. Ayodele, A. A. Jimoh, J. L. Munda, J. T. Agee (2010), Impact of Variation of Wind Speed in a Wind Integrated Power System, *International Conference on Advances in Energy Engineering*, Beijing, China.
- [67] Thomas Ackermann (2005), *Wind Power in Power System*, John Wiley&Sons Ltd.
- [68] Tony Burton, David Sharpe, Nick Jenkins, Ervin Bossanyi (2001), *Wind Energy Handbook*, John Wiley & Sons.
- [69] Xiaolu Lv, Jun Liang, Feng Zhang, Bohao Sun (2013), Probability Distribution Characteristics at Longitudinal Time Points of Wind Power, *2013 10th International Conference on Fuzzy Systems and Knowledge Discovery (FSKD)*.
- [70] Y. H. Wan (January 2012), *Long-Term Wind Power Variability*, Prepared under Task No. WE11.0910, NREL.
- [71] Youjie Ma, Hulong Wen (2009), Bifurcation Analysis of Voltage Stability and Study on Power Loss for Wind Power System, *World Non-Grid-Connected Wind Power and Energy Conference, WNWEC*.
- [72] Z. Xu, Z. Y. Dong, and P. Zhang (June 2005), Probabilistic Small Signal Analysis using Monte Carlo Simulation, *Power Engineering Society General Meeting, IEEE*, vol. 2, pp. 1658 – 1664.
- [73] Zbigniew Lubosny (2003), *Wind Turbine Operation in Electric Power Systems*, Springle-Verlag Berlin Heidelberg, Germany.
- [74] Zeev Schuss (2010), *Theory and Applications of Stochastic Processes: An Analytical Approach*, New York : Springer.
- [75] Zhao Yang Dong, Chee Khiang Pang, and Pei Zhang (June 2005), Power System Sensitivity Analysis for Probabilistic Small Signal Stability Assessment in a Deregulated Environment, *International Journal of Control, Automation, and Systems*, vol. 3, no. 2 (special edition), pp. 355-362.

- [76] Zhiyuan Zeng, Xianqi Li (2009), Investigation of Wind Farm on Power System Voltage Stability Based on Bifurcation Theory, *Power and Energy Engineering Conference, APPEEC*.

APPENDIX

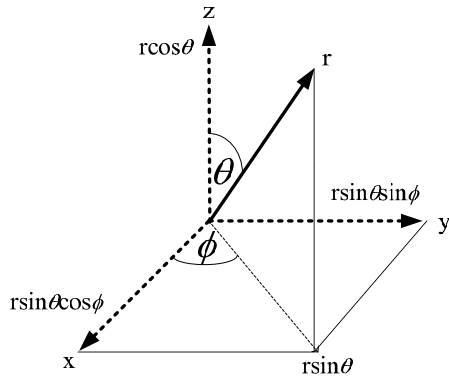
Appendix A: The identification of coefficients C_1^* , C_2 , and C_3^*

To identify C_1^* , C_2 , and C_3^* , we have to determine the coordinate system transformation, derivations of C_1^* , C_2 , and C_3^* , and finally general solution and asymptotic solution of MFPT.

A1. Coordinate system transformation

For simplicity, the integral equations of the Cartesian coordinate system of C_1 , C_2 , C_3 in Eq.2-61 will be transformed in to polar coordinate system with multiple dimensions or system variables.

For example, the transformation from Cartesian into a spherical coordinate system with 3 dimensions (variables) and 4 dimensions (variables).

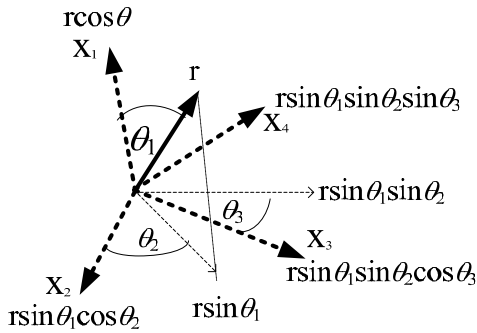


$$z = r \cos \theta$$

$$x = r \sin \theta \cos \phi$$

$$y = r \sin \theta \sin \phi$$

$$r = \sqrt{x^2 + y^2 + z^2}$$



$$x_1 = r \cos \theta_1$$

$$x_2 = r \sin \theta_1 \cos \theta_2$$

$$x_3 = r \sin \theta_1 \sin \theta_2 \cos \theta_3$$

$$x_4 = r \sin \theta_1 \sin \theta_2 \sin \theta_3$$

$$r = \sqrt{x_1^2 + x_2^2 + x_3^2 + x_4^2}$$

In the case of the system with $2n+m-1$ dimensions or variables, the coordinate transformation will become:

$$\left. \begin{aligned} x_1 &= r \cos \theta_1 \\ x_2 &= r \sin \theta_1 \cos \theta_2 \\ x_3 &= r \sin \theta_1 \sin \theta_2 \cos \theta_3 \\ &\vdots \\ x_{2n+m-2} &= r \sin \theta_1 \sin \theta_2 \cdots \sin \theta_{2n+m-3} \cos \theta_{2n+m-2} \\ x_{2n+m-1} &= r \sin \theta_1 \sin \theta_2 \cdots \sin \theta_{2n+m-3} \sin \theta_{2n+m-2} \sin \theta_{2n+m-1} \end{aligned} \right\} \quad \text{Eq. A-1}$$

The energy function from Eq.2-34 is a complicated surface function which cannot easily be used for the solution of problem in Eq.2-60. This problem can be achievable derived when the integrals terms are represented in the form of polar coordinate system. First of all, an approximate energy function basing on ellipsoidal surface is represented as in Eq.2-62 [C.O. Nwankpa, 1990].

An ellipsoidal surface energy function is then transformed into a standard form as follows:

$$W = \begin{pmatrix} \mathbf{z}^T & \mathbf{y}^T \end{pmatrix} \mathbf{H} \begin{pmatrix} \mathbf{z} \\ \mathbf{y} \end{pmatrix} \quad \text{Eq. A-2}$$

Where \mathbf{H} is a partitioned diagonal $(2n+m-1) \times (2n+m-1)$ matrix, \mathbf{y} is n vector functions of y and \mathbf{z} is $n+m-1$ vector functions of z . Thus, \mathbf{H} can be written in the form:

$$\mathbf{H} = \begin{pmatrix} \mathbf{H}_1 & 0 \\ 0 & \mathbf{H}_2 \end{pmatrix} \quad \text{Eq. A-3}$$

Where \mathbf{H}_1 is a $(n+m-1) \times (n+m-1)$ matrix and \mathbf{H}_2 is a $n \times n$ matrix as follows

$$\left. \begin{aligned} (\mathbf{H}_1)_{ii} &= \sum_{\substack{j=1 \\ j \neq i}}^{n+m} \frac{1}{2} \cos(x_i^s - x_j^s) V_{ij} \\ (\mathbf{H}_1)_{ij} &= -\frac{1}{2} V_{ij} \cos(x_i^s - x_j^s) = (\mathbf{H}_1)_{ji} \\ (\mathbf{H}_2)_{ii} &= M_i \\ (\mathbf{H}_2)_{ij} &= 0 \end{aligned} \right\} \quad \text{Eq. A-4}$$

$i, j = 1, \dots, n+m, \quad i \neq j$

If $n = 3$ and $m = 5$, therefore \mathbf{H}_1 and \mathbf{H}_2 of the energy function is

$$\mathbf{H}_2 = \begin{bmatrix} M_1 & 0 & 0 \\ 0 & M_2 & 0 \\ 0 & 0 & M_3 \end{bmatrix} \quad \text{Eq. A-5}$$

$$\mathbf{H}_1 = \begin{bmatrix} \sum_{j=2}^8 \frac{1}{2} V_{1j} \cos(x_1^s - x_j^s) & -\frac{1}{2} V_{12} \cos(x_1^s - x_2^s) & -\frac{1}{2} V_{13} \cos(x_1^s - x_3^s) & -\frac{1}{2} V_{14} \cos(x_1^s - x_4^s) & -\frac{1}{2} V_{15} \cos(x_1^s - x_5^s) & -\frac{1}{2} V_{16} \cos(x_1^s - x_6^s) & -\frac{1}{2} V_{17} \cos(x_1^s - x_7^s) \\ \sum_{j=1}^8 \frac{1}{2} V_{2j} \cos(x_2^s - x_j^s) & \sum_{j=2}^8 \frac{1}{2} V_{2j} \cos(x_2^s - x_j^s) & -\frac{1}{2} V_{23} \cos(x_2^s - x_3^s) & -\frac{1}{2} V_{24} \cos(x_2^s - x_4^s) & -\frac{1}{2} V_{25} \cos(x_2^s - x_5^s) & -\frac{1}{2} V_{26} \cos(x_2^s - x_6^s) & -\frac{1}{2} V_{27} \cos(x_2^s - x_7^s) \\ \sum_{j=1}^8 \frac{1}{2} V_{3j} \cos(x_3^s - x_j^s) & -\frac{1}{2} V_{23} \cos(x_2^s - x_3^s) & \sum_{j=3}^8 \frac{1}{2} V_{3j} \cos(x_3^s - x_j^s) & -\frac{1}{2} V_{34} \cos(x_3^s - x_4^s) & -\frac{1}{2} V_{35} \cos(x_3^s - x_5^s) & -\frac{1}{2} V_{36} \cos(x_3^s - x_6^s) & -\frac{1}{2} V_{37} \cos(x_3^s - x_7^s) \\ \sum_{j=1}^8 \frac{1}{2} V_{4j} \cos(x_4^s - x_j^s) & -\frac{1}{2} V_{24} \cos(x_2^s - x_4^s) & -\frac{1}{2} V_{34} \cos(x_3^s - x_4^s) & \sum_{j=4}^8 \frac{1}{2} V_{4j} \cos(x_4^s - x_j^s) & -\frac{1}{2} V_{45} \cos(x_4^s - x_5^s) & -\frac{1}{2} V_{46} \cos(x_4^s - x_6^s) & -\frac{1}{2} V_{47} \cos(x_4^s - x_7^s) \\ \sum_{j=1}^8 \frac{1}{2} V_{5j} \cos(x_5^s - x_j^s) & -\frac{1}{2} V_{25} \cos(x_2^s - x_5^s) & -\frac{1}{2} V_{35} \cos(x_3^s - x_5^s) & -\frac{1}{2} V_{45} \cos(x_4^s - x_5^s) & \sum_{j=5}^8 \frac{1}{2} V_{5j} \cos(x_5^s - x_j^s) & -\frac{1}{2} V_{56} \cos(x_5^s - x_6^s) & -\frac{1}{2} V_{57} \cos(x_5^s - x_7^s) \\ \sum_{j=1}^8 \frac{1}{2} V_{6j} \cos(x_6^s - x_j^s) & -\frac{1}{2} V_{26} \cos(x_2^s - x_6^s) & -\frac{1}{2} V_{36} \cos(x_3^s - x_6^s) & -\frac{1}{2} V_{46} \cos(x_4^s - x_6^s) & -\frac{1}{2} V_{56} \cos(x_5^s - x_6^s) & \sum_{j=6}^8 \frac{1}{2} V_{6j} \cos(x_6^s - x_j^s) & -\frac{1}{2} V_{67} \cos(x_6^s - x_7^s) \\ \sum_{j=1}^8 \frac{1}{2} V_{7j} \cos(x_7^s - x_j^s) & -\frac{1}{2} V_{27} \cos(x_2^s - x_7^s) & -\frac{1}{2} V_{37} \cos(x_3^s - x_7^s) & -\frac{1}{2} V_{47} \cos(x_4^s - x_7^s) & -\frac{1}{2} V_{57} \cos(x_5^s - x_7^s) & -\frac{1}{2} V_{67} \cos(x_6^s - x_7^s) & \sum_{j=7}^8 \frac{1}{2} V_{7j} \cos(x_7^s - x_j^s) \end{bmatrix}$$

Eq. A-6

From Eq. A-2, if we define
$$\begin{pmatrix} \mathbf{z} \\ \mathbf{y} \end{pmatrix} = \mathbf{R}\mathbf{v}$$
 Eq. A-7

Where \mathbf{R} is $(2n+m-1) \times (2n+m-1)$ matrix the same with \mathbf{H} and \mathbf{v} is $(2n+m-1)$ vector of new state variables. Placing Eq. A-7 into Eq. A-2, we can write

$$W = \mathbf{v}^T \mathbf{R}^T \mathbf{H} \mathbf{R} \mathbf{v} \quad \text{Eq. A-8}$$

To simplify Eq. A-8, we assume \mathbf{R} is a partitioned diagonal matrix which is the same as \mathbf{H} and \mathbf{R} is also orthogonal of \mathbf{H} . Thus $\mathbf{R}^T = \mathbf{R}^{-1}$ and from the rule of eigenvalues as a diagonal matrix, we know that

$$\mathbf{R}^T \mathbf{H} \mathbf{R} = \mathbf{R}^{-1} \mathbf{H} \mathbf{R} = \begin{bmatrix} \lambda_1 & 0 & \cdots & 0 \\ 0 & \lambda_2 & \cdots & 0 \\ \vdots & \vdots & \ddots & \vdots \\ 0 & 0 & \cdots & \lambda_{2n+m-1} \end{bmatrix} = \mathbf{N} \quad \text{Eq. A-9}$$

Where \mathbf{N} is a diagonal matrix for which elements are eigenvalue, λ_i . For this case, \mathbf{R} is a matrix consisting of a set of eigenvectors of \mathbf{H} corresponding to each λ .

If we state that $\mathbf{N} = \mathbf{N}^* \mathbf{N}^*$ when

$$\mathbf{N}^* = \begin{bmatrix} \sqrt{\lambda_1} & 0 & \cdots & 0 \\ 0 & \sqrt{\lambda_2} & \cdots & 0 \\ \vdots & \vdots & \ddots & \vdots \\ 0 & 0 & \cdots & \sqrt{\lambda_{2n+m-1}} \end{bmatrix} \quad \text{Eq. A-10}$$

Therefore, placing into Eq. A-8, we can write

$$W = \mathbf{v}^T \mathbf{N}^* \mathbf{N}^* \mathbf{v} = \mathbf{A}^T \mathbf{A} \quad \text{Eq. A-11}$$

Where $\mathbf{N}^* \mathbf{v} = \mathbf{A}$ and thus

$$\mathbf{A} = \begin{bmatrix} \sqrt{\lambda_1} & 0 & \cdots & 0 \\ 0 & \sqrt{\lambda_2} & \cdots & 0 \\ \vdots & \vdots & \ddots & \vdots \\ 0 & 0 & \cdots & \sqrt{\lambda_{2n+m-1}} \end{bmatrix} \begin{bmatrix} v_1 \\ v_2 \\ \vdots \\ v_{2n+m-1} \end{bmatrix} = \begin{bmatrix} a_1 \\ a_2 \\ \vdots \\ a_{2n+m-1} \end{bmatrix} \quad \text{Eq. A-12}$$

Where $a_i = v_i \sqrt{\lambda_i}$. The Eq. A-11 can be represented in the form as follows

$$W = \mathbf{A}^T \mathbf{A} = a_1^2 + a_2^2 + \cdots + a_{2n+m-1}^2 = \lambda_1 v_1^2 + \lambda_2 v_2^2 + \cdots + \lambda_{2n+m-1} v_{2n+m-1}^2 \quad \text{Eq. A-13}$$

From Eq. A-1, if we replace x_i with a_i from Eq. A-13, then

$$r = \sqrt{a_1^2 + a_2^2 + \dots + a_{2n+m-1}^2} = \sqrt{W} \quad \text{Eq. A-14}$$

Thus, the polar coordinate system can be constructed as follows:

$$\left. \begin{aligned} a_1 &= \sqrt{W} \cos \theta_1 \\ a_2 &= \sqrt{W} \sin \theta_1 \cos \theta_2 \\ a_3 &= \sqrt{W} \sin \theta_1 \sin \theta_2 \cos \theta_3 \\ &\vdots \\ a_{2n+m-2} &= \sqrt{W} \sin \theta_1 \sin \theta_2 \cdots \sin \theta_{2n+m-3} \cos \theta_{2n+m-2} \\ a_{2n+m-1} &= \sqrt{W} \sin \theta_1 \sin \theta_2 \cdots \sin \theta_{2n+m-3} \sin \theta_{2n+m-2} \sin \theta_{2n+m-1} \end{aligned} \right\} \quad \text{Eq. A-15}$$

The Jacobian matrix of multi-variables polar coordinate system can be computed as [Wendell Fleming, 1977]:

$$J = \left(\sqrt{W} \right)^{2n+m-2} \left(\sin^{2n+m-3} \theta_1 \right) \left(\sin^{2n+m-4} \theta_2 \right) \dots \left(\sin \theta_{2n+m-3} \right) \quad \text{Eq. A-16}$$

Then, the surface elements of this multi-variables polar coordinate system is given by:

$$ds = J d\theta_1 d\theta_2 \dots d\theta_{2n+m-2} \quad \text{Eq. A-17}$$

Furthermore, \mathbf{z} and \mathbf{y} in Eq. A-7 can be transformed into \mathbf{A} by this following step:

From Eq. A-11, multiply by $(\mathbf{N}^*)^{-1}$ to become

$$\mathbf{v} = (\mathbf{N}^*)^{-1} \mathbf{A} \quad \text{Eq. A-18}$$

If we multiply Eq. A-12 by \mathbf{R} and use the result of Eq. A-18, we will get:

$$\mathbf{Rv} = \mathbf{R}(\mathbf{N}^*)^{-1} \mathbf{A} = \begin{pmatrix} \mathbf{z} \\ \mathbf{y} \end{pmatrix} \quad \text{Eq. A-19}$$

Since \mathbf{H} is a partitioned diagonal $(2n+m-1) \times (2n+m-1)$ matrix, thus \mathbf{R} and \mathbf{N} are also partitioned diagonal matrix in the form:

$$\mathbf{R} = \begin{pmatrix} \mathbf{R}_1 & 0 \\ 0 & \mathbf{R}_2 \end{pmatrix} \text{ and } \mathbf{N} = \begin{pmatrix} \mathbf{N}_1 & 0 \\ 0 & \mathbf{N}_2 \end{pmatrix} \quad \text{Eq. A-20}$$

Where \mathbf{R}_1 and \mathbf{N}_1 are $(n+m-1) \times (n+m-1)$ matrix while \mathbf{R}_2 and \mathbf{N}_2 are $n \times n$ matrix.

From Eq. A-19, the standard form of \mathbf{z} and \mathbf{y} in Eq. A-7 can be represented in the following form

$$\left. \begin{aligned} \mathbf{z} &= \mathbf{R}_1 (\mathbf{N}_1^*)^{-1} \mathbf{A}_1 \\ \mathbf{y} &= \mathbf{R}_2 (\mathbf{N}_2^*)^{-1} \mathbf{A}_2 \end{aligned} \right\} \quad \text{Eq. A-21}$$

A2. Derivations of C_1^* , C_2 , and C_3^*

To determine

$$\left. \begin{aligned} \varepsilon C_1^* W \tau_0''(W) + [\varepsilon C_2 - C_3^* W] \tau_0'(W) &= -1 \\ \tau_0(W_c) &= 0, \quad \tau_0(0) < \infty \end{aligned} \right\} \quad \text{Eq. A-22}$$

$$\tau_0(0) \approx \frac{1}{C_3^*} (W_c)^{-C_2/C_1^*} \left[\int_0^{W_c} t^{(C_2/C_1^*)-1} e^{-(C_3^* t / \varepsilon_l C_1^*)} dt \right] e^{(C_3^* W_c / \varepsilon_l C_1^*)} \quad \text{Eq. A-23}$$

$$\tau(0) \approx \frac{1}{\beta C_3^*} (W_c)^{-C_2/C_1^*} \left[\int_0^{W_c} t^{(C_2/C_1^*)-1} e^{-(C_3^* t / \varepsilon_l C_1^*)} dt \right] e^{(C_3^* W_c / \varepsilon_l C_1^*)} \quad \text{Eq. A-24}$$

where

$$C_2(W) = \frac{1}{T(W)} \oint_W \varepsilon_2 \frac{\partial^2 W}{\partial x_2^2} ds_c = \varepsilon_2 \frac{\partial^2 W}{\partial x_2^2} \frac{1}{T(W)} \oint_W ds_c = \varepsilon_2 \frac{\partial^2 W}{\partial x_2^2} \quad \text{Eq. A-25}$$

$$C_2(W) = \varepsilon_2 \sum_{\substack{r=1 \\ r \neq 2}}^{n+m} \cos(x_2^s - x_r^s) V_2 V_r B_{2r} \quad \text{Eq. A-26}$$

$$C_1 = C_1^* W = \frac{1}{2(n+m)} \sum_{i=1}^{n+m-1} (\mathbf{F}_1)_{ii} W \quad \text{Eq. A-27}$$

$$C_3 = C_3^* W = \frac{1}{2n} \sum_{i=1}^n (\mathbf{F}_3)_{ii} W \quad \text{Eq. A-28}$$

$$\mathbf{F}_1 = (\mathbf{N}_1^*)^{-1} \mathbf{R}_1^T \mathbf{D}_1 \mathbf{R}_1 (\mathbf{N}_1^*)^{-1} \quad \text{Eq. A-29}$$

$$\mathbf{F}_3 = (\mathbf{N}_2^*)^{-1} \mathbf{R}_2^T \mathbf{D}_3 \mathbf{R}_2 (\mathbf{N}_2^*)^{-1} \quad \text{Eq. A-30}$$

$$\left. \begin{aligned} (\mathbf{D}_1)_{kj} &= \varepsilon_{kj} V_k V_j \sum_{r=1}^{n+m} \sum_{h=1}^{n+m} \cos(x_k^s - x_r^s) \cos(x_j^s - x_h^s) V_r V_h B_{kr} B_{jh} \\ &+ V_k V_j \sum_{r=1}^{n+m} \sum_{h=1}^{n+m} \varepsilon_{rh} \cos(x_k^s - x_r^s) \cos(x_j^s - x_h^s) V_r V_h B_{kr} B_{jh} \\ &- V_k V_j \sum_{h=1}^{n+m} \varepsilon_{kh} \sum_{r=1}^{n+m} \cos(x_k^s - x_r^s) \cos(x_j^s - x_h^s) V_r V_h B_{kr} B_{jh} \\ &- V_k V_j \sum_{r=1}^{n+m} \varepsilon_{rj} \sum_{h=1}^{n+m} \cos(x_k^s - x_r^s) \cos(x_j^s - x_h^s) V_r V_h B_{kr} B_{jh} \end{aligned} \right\} \quad \text{Eq. A-31}$$

$$\left. \begin{aligned}
 (\mathbf{D}_1)_{kj} = & \varepsilon_2 V_2 V_2 \sum_{r=1}^{n+m} \sum_{h=1}^{n+m} \cos(x_2^s - x_r^s) \cos(x_2^s - x_h^s) V_r V_h B_{2r} B_{2h} \\
 & + V_k V_j \varepsilon_2 \cos(x_k^s - x_2^s) \cos(x_j^s - x_2^s) V_2 V_2 B_{k2} B_{j2} \\
 & - V_2 V_j \varepsilon_2 \sum_{r=1}^{n+m} \cos(x_2^s - x_r^s) \cos(x_j^s - x_2^s) V_r V_2 B_{2r} B_{j2} \\
 & - V_k V_2 \varepsilon_2 \sum_{h=1}^{n+m} \cos(x_k^s - x_2^s) \cos(x_2^s - x_h^s) V_2 V_h B_{k2} B_{2h}
 \end{aligned} \right\} \quad \text{Eq. A-32}$$

$$(\mathbf{D}_3)_{ij} = \begin{cases} D_i M_w, & i = j, i = 1, \dots, n; \\ 0, & i \neq j, i, j = 1, \dots, n. \end{cases} \quad \text{Eq. A-33}$$

A3. General solution and asymptotic solution of MFPT

```

clear all
close all
clc;

t = 10;
nim = 0.2;
a = 0;

%%% Case1 WS = 6 m/s Vary NI
V = [0.998 1.000 1.002 1.011 0.992 0.998 1.000 1.002]; %%%% Assume
Internal voltage is the same with terminal voltage %%%%
P = [9.410 0.05 1.606 0 10.786];
xs = [0.330 -0.454 0.0 -0.073 -0.455 0.330 -0.454 0.0]; %%%% Assume
internal angle is not affected by internal impedance of machine %%%%
Wc = 2.036 ; %%%% Critical energy from simulation and calculation
for i = 1:1:t
NI(i) = (nim*(a+(t-a)*i/t))/t ; %%%%%%%%%%%%% Noise intensity
%%%%%%%%%%%%%%%%%%%%%%%%%%%%%%%%%%%%%%%%%%%%%%%%%%%%%%%%%%%%%%%%%%%%%%%%
MFPTc1(i) = MFPT2(xs,V,P,Wc,NI(i));
end
%%%%%%%%%%%%%%%%%%%%%%%%%%%%%%%%%%%%%%%%%%%%%%%%%%%%%%%%%%%%%%%%%%%%%%%%

%%% Case2 WS = 8 m/s Vary NI
V = [0.998 0.996 1.002 1.012 0.995 0.998 0.996 1.002]; %%%% Assume
Internal voltage is the same with terminal voltage %%%%
P = [9.410 0.219 1.436 0 10.841];
xs = [0.340 -0.375 0.0 -0.066 -0.440 0.340 -0.375 0.0]; %%%% Assume
internal angle is not affected by internal impedance of machine %%%%
Wc = 2.173 ; %%%% Critical energy from simulation and calculation
for i = 1:1:t
NI(i) = (nim*(a+(t-a)*i/t))/t ; %%%%%%%%%%%%% Noise intensity
%%%%%%%%%%%%%%%%%%%%%%%%%%%%%%%%%%%%%%%%%%%%%%%%%%%%%%%%%%%%%%%%%%%%%%%%
MFPTc2(i) = MFPT2(xs,V,P,Wc,NI(i));
end
%%%%%%%%%%%%%%%%%%%%%%%%%%%%%%%%%%%%%%%%%%%%%%%%%%%%%%%%%%%%%%%%%%%%%%%%

%%% Case3 WS = 10 m/s Vary NI
V = [0.998 0.969 1.002 1.012 0.994 0.998 0.969 1.002]; %%%% Assume
Internal voltage is the same with terminal voltage %%%%
P = [9.410 0.526 1.101 0 10.826];

```

```

xs = [0.356 -0.248 0.0 -0.051 -0.413 0.356 -0.248 0.0]; %%% Assume
internal angle is not affected by internal impedance of machine %%%
Wc = 2.35 ; %%% Critical energy from simulation and calculation
for i = 1:1:t
NI(i) = (nim*(a+(t-a)*i/t))/t ; %%% Noise intensity
%%%%%%%%%%%%%%%%%%%%%%%%%%%%%%%%%%%%%%%%%%%%%%%%%%%%%%%%%%%%%%%%%%%%%%%%
MFPTc3(i) = MFPT2(xs,V,P,Wc,NI(i));
end
%%%%%%%%%%%%%%%%%%%%%%%%%%%%%%%%%%%%%%%%%%%%%%%%%%%%%%%%%%%%%%%%%%%%%%%%

%% Case4 WS = 12 m/s Vary NI
V = [1.001 0.939 1.005 1.015 0.988 1.001 0.939 1.005]; %%% Assume
Internal voltage is the same with terminal voltage %%%
P = [9.410 0.674 0.866 0 10.747];
xs = [0.366 -0.194 0.0 -0.063 -0.418 0.366 -0.194 0.0]; %%% Assume
internal angle is not affected by internal impedance of machine %%%
Wc = 2.576 ; %%% Critical energy from simulation and calculation
for i = 1:1:t
NI(i) = (nim*(a+(t-a)*i/t))/t ; %%% Noise intensity
%%%%%%%%%%%%%%%%%%%%%%%%%%%%%%%%%%%%%%%%%%%%%%%%%%%%%%%%%%%%%%%%%%%%%%%%
MFPTc4(i) = MFPT2(xs,V,P,Wc,NI(i));
end
%%%%%%%%%%%%%%%%%%%%%%%%%%%%%%%%%%%%%%%%%%%%%%%%%%%%%%%%%%%%%%%%%%%%%%%%
xlswrite('MFPT_varyWS.xls',[NI(:),MFPTc1(:),MFPTc2(:),MFPTc3(:),MFPTc4(:)])
;

```

```

function [MFPT] = MFPT2(xs,V,P,Wc,NI)

```

```

%NI = Noise intensity
%V = Assume Internal voltage is the same with terminal voltage
%P = is active power of the system
%Q = is reactive power of the system
%xs =Assume internal angle is not affected by internal impedance of machine
%ys = [0 0 0]; in steady state rotor speed
%Wc = Critical energy from simulation and calculation

```

```

%% 1. Case 1 Wind Power Incorporating SMIB
%% 1.1 System data and configuration
M = [3.117 5 1000]; %%% Inertia of Machine %%%
D = [0.03*M(1) 0 0.03*M(3)]; %%% Damping part of Machine %%%
cf = 0.05 ; % frequency coefficient
Pbs = 100 ; % Base power 100MVA
Vbs = 500 ; % Base Voltage 500 kV
n = 3 ; % Number of Generation Machine = 3
m = 5 ; % Number of all bus = 5
B = zeros([n+m n+m]); % Susceptance matrix
H1 = zeros([n+m-1 n+m-1]); % Susceptance matrix
H2 = zeros([n n]); % Susceptance matrix
H01 = zeros([n+m-1 n]);
H02 = zeros([n n+m-1]);
D1 = zeros([n+m-1 n+m-1]);
D3 = zeros([n n]);
R1 = zeros([n+m-1 n+m-1]);
R2 = zeros([n n]);
N1 = zeros([n+m-1 n+m-1]);
N2 = zeros([n n]);
B(1,4) = 6.667;
B(2,5) = 6.667;
B(3,4) = 3.075;

```

```

B(4,5) = 25.0;
B(4,1) = B(1,4);
B(5,2) = B(2,5);
B(5,4) = B(4,5);
B(4,3) = B(3,4);
B(1,1) = -6.667;
B(2,2) = -6.667;
B(3,3) = -3.075;
B(4,4) = -34.78;
B(5,5) = -31.67;
B(1,6) = 0.3; %%%%%%%%% Internal Susceptance of Machine 1 %%%%%%%%%
B(2,7) = 0.03; %%%%%%%%% Internal Susceptance of Machine 2 %%%%%%%%%
B(3,8) = 0.6; %%%%%%%%% Internal Susceptance of Machine 3 %%%%%%%%%
B(6,1) = B(1,6);
B(7,2) = B(2,7);
B(8,3) = B(3,8);
D11 = 0;
D12 = 0;
D13 = 0;
D14 = 0;
C1 = 0;
C2 = 0;
C3 = 0;
intgl = 0;
ns = P(2)*NI/sqrt(2*M(2)) ; % noise scale

%%% 1.2 Find stable equilibrium points %%%

%%% 1.3 Construct matrix H
% For H1
for i = 1:1:m+n-1
    for j = i:1:m+n-1
        if i==j
            for k = 1:1:m+n
                if i ~= k
                    H1(i,j) = H1(i,j)+0.5*cos(xs(i)-xs(k))*V(i)*V(k)*B(i,k);
                end
            end
        else
            H1(i,j) = -0.5*cos(xs(i)-xs(j))*V(i)*V(j)*B(i,j);
            H1(j,i) = H1(i,j);
        end
    end
end
% For H2
for i = 1:1:n
    for j = i:1:n
        if i==j
            H2(i,j) = M(i);
        else
            H2(i,j) = 0;
            H2(j,i) = H1(i,j);
        end
    end
end
H = [H1 H01
     H02 H2];

%%% 1.4 Find eigenvalues & eigenvectors of matrix H
[R N] = eig(H);

```

```

for i = 1:1:m+n-1
    for j = i:1:m+n-1
        R1(i,j) = R(i,j);
        N1(i,j) = sqrt(N(i,j));
    end
end

for i = 1:1:n
    for j = i:1:n
        R2(i,j) = R(i+n+m-1,j+n+m-1);
        N2(i,j) = sqrt(N(i+n+m-1,j+n+m-1));
    end
end

%%% 1.5 Construct matrix D
% For D1
for i = 1:1:n+m-1
    for j = i:1:n+m-1
        for r = 1:1:n+m
            for h = 1:1:n+m
                D11 = D11 + cos(xs(2)-xs(r))*cos(xs(2)-
xs(h))*V(r)*V(h)*B(2,r)*B(2,h) ;
            end
        end
        D11 = D11*ns*V(2)*V(2) ;

        D12 = ns*V(i)*V(j)*cos(xs(i)-xs(2))*cos(xs(j)-
xs(2))*V(2)*V(2)*B(i,2)*B(j,2) ;

        for r = 1:1:n+m
            D13 = D13 + cos(xs(2)-xs(r))*cos(xs(j)-
xs(2))*V(r)*V(2)*B(2,r)*B(j,2) ;
        end
        D13 = D13*ns*V(2)*V(j) ;

        for h = 1:1:n+m
            D14 = D14 + cos(xs(i)-xs(2))*cos(xs(2)-
xs(h))*V(2)*V(h)*B(i,2)*B(2,h) ;
        end
        D14 = D14*ns*V(i)*V(2) ;

        D1(i,j) = D11 + D12 - D13 - D14 ;

    end
end
% For D3
for i = 1:1:n
    for j = i:1:n
        if i==j
            D3(i,j) = D(i)*M(2);
        else
            D3(i,j) = 0;
            D3(j,i) = D3(i,j);
        end
    end
end

%%% 1.6 Construct matrix F

```

```

F1 = inv(N1)*transpose(R1)*D1*R1*inv(N1);

F3 = inv(N2)*transpose(R2)*D3*R2*inv(N2);

%%% 1.7 Compute C
for i = 1:1:n+m-1
    C1 = C1 + F1(i,i);
end
C1 = 0.5/(n+m)*C1 ;

for i = 1:1:n
    C3 = C3 + F3(i,i);
end
C3 = 0.5/n*C3 ;

for r = 1:1:n+m
    if r~= 2
        C2 = C2 + cos(xs(2)-xs(r))*V(2)*V(r)*B(2,r) ;
    end
end
C2 = C2*ns ;

%%% 1.8 Compute MFPT
a = C2/C1-1;
b = C3/C1/ns;
delt = 1/1000;
for i = 1:1:Wc*1000
    intgl = intgl + ((i/1000)^a)/exp(b*(i/1000))*delt;
end

MFPT = M(2)/C3*(Wc^(-C2/C1))*exp(C3*Wc/C1/ns)*intgl/60/60/24 ; %%%% unit in
days %%%%

```